Bulletin of the Fisheries Research Board of Canada

SEISMIC SEA WAVES
TSUNAMIS

T.S.Murty



BULLETIN 198
Ottawa 1977

Fisheries and Environment Canada
Fisheries and Marine Service

Pêches et Environnement Canada
Service des pêches et de la mer

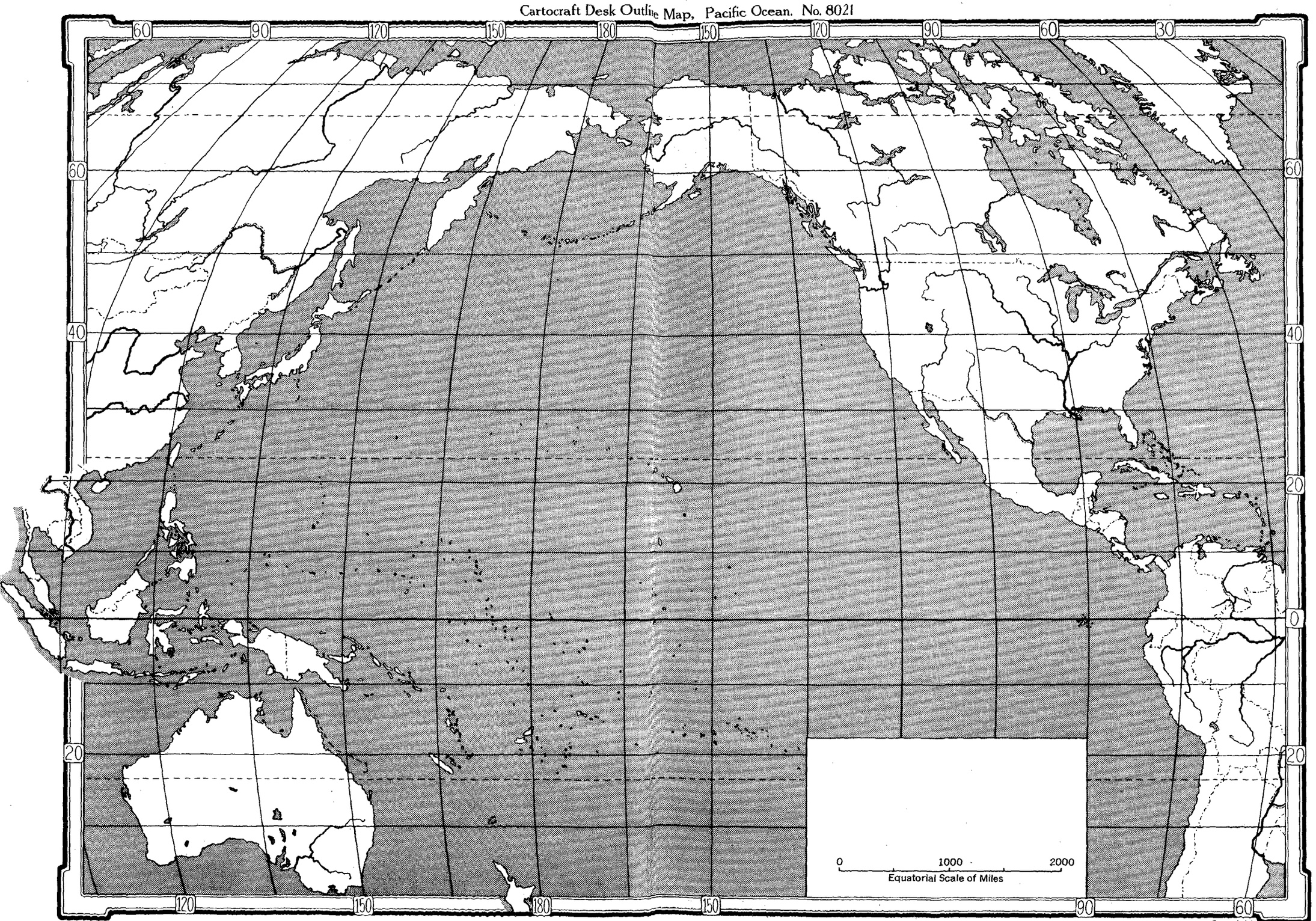
About the Book

Seismic sea waves — tsunamis represents eight years of research, detailed studies, and analysis by the author. Current knowledge of tsunami propagation; tsunami generation by earthquakes, volcanic eruptions, and nuclear explosions; laboratory experiments on tsunami generation, and propagation are included. The various coastal phenomena associated with tsunamis have been considered in detail. Descriptions of tsunamis in various regions from 1400 B.C. to 1975 are supported by detailed tables and illustrations.

Catalog No. Fs 94-198
ISBN 0-660-00565-4
ISSN 0068-7537

Canada $10.00
Other countries $12.00

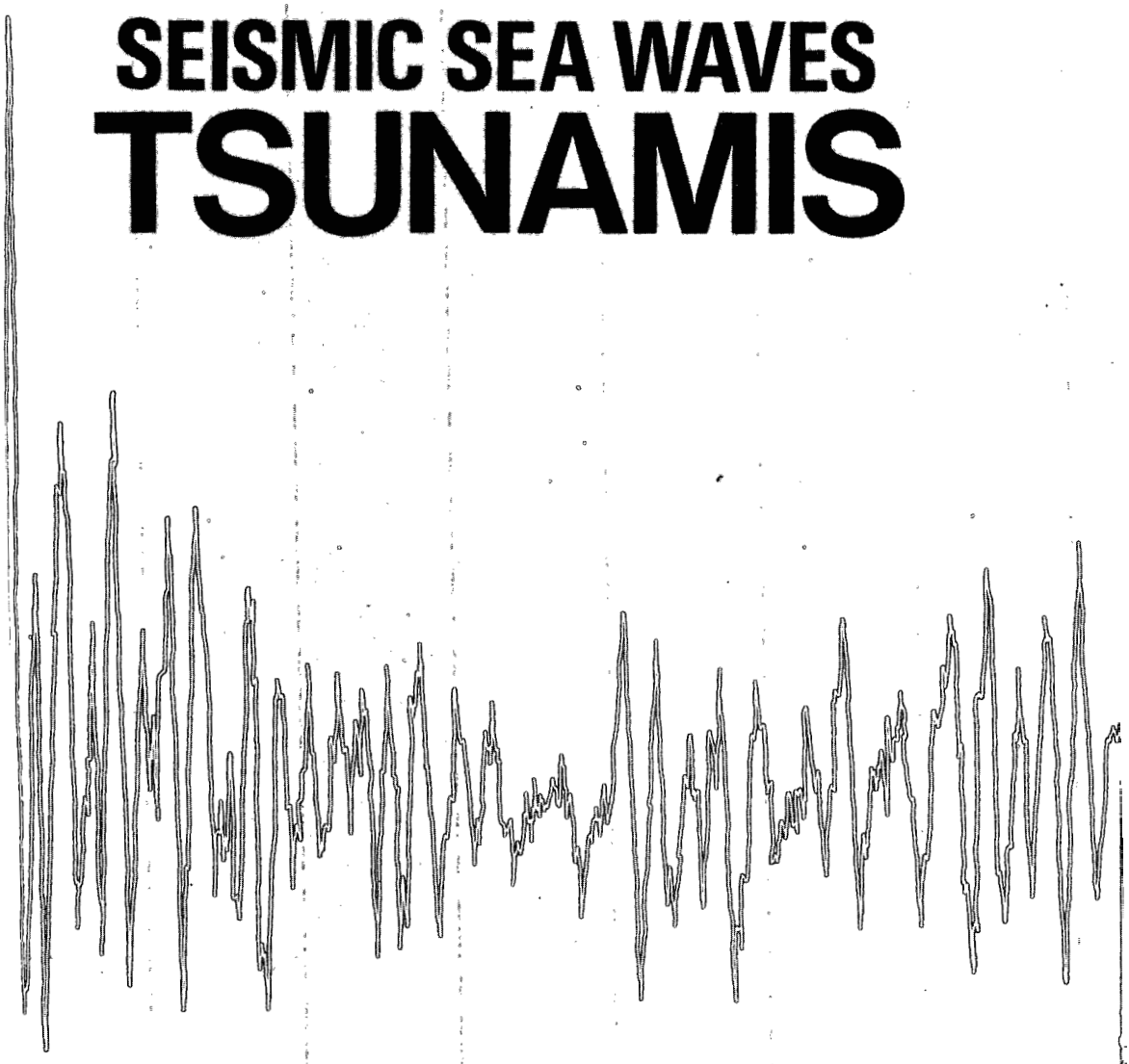
Cartocraft Desk Outline Map, Pacific Ocean. No. 8021



Reproduced by permission from Denoyer-Geppert Co., Chicago, Illinois

Copyright

SEISMIC SEA WAVES
TSUNAMIS



Bulletins are designed to interpret current knowledge in scientific fields pertinent to Canadian fisheries and aquatic environments.

The *Journal of the Fisheries Research Board of Canada* is published in annual volumes of monthly issues and *Miscellaneous Special Publications* are issued periodically. These series are for sale by Supply and Services Canada, Printing and Publishing, Ottawa, K1A 0S9. Remittances must be in advance, payable in Canadian funds to the order of the Receiver General for Canada.

Editor and Director of Scientific Information	J. C. STEVENSON, PH.D.
Deputy Editor	J. WATSON, PH.D.
Assistant Editors	JOHANNA M. REINHART, M.SC. D. G. COOK, PH.D.
Production-Documentation	J. CAMP G. J. NEVILLE MONA SMITH MICKEY LEWIS

Department of Fisheries and the Environment
Fisheries and Marine Service
Scientific Information and Publications Branch
Ottawa, Canada
K1A 0E6

BULLETIN 198

(La version française est en préparation)

SEISMIC SEA WAVES
TSUNAMIS

T. S. MURTY[1]

Marine Environmental Data Services Branch
Fisheries and Marine Service
Department of Fisheries and the Environment
Ottawa, Canada

DEPARTMENT OF FISHERIES AND THE ENVIRONMENT
FISHERIES AND MARINE SERVICE
Ottawa 1977

[1] Vice-chairman, Tsunami Committee, International Union of Geodesy and Geophysics

© Minister of Supply and Services Canada 1977

Available by mail from:

Printing and Publishing
Supply and Services Canada
Ottawa, Canada K1A 0S9

or through your bookseller

A deposit copy of this publication is also available
for reference in public librairies across Canada

Canada: $10.00
Other countries: $12.00

Catalog No. Fs 94-198
ISBN 0-660-00565-4
ISSN 0068-7537

Price subject to change without notice

Ottawa

Dust jacket and cover designed by Christine Rusk

Printed by D. W. Friesen & Sons Ltd.
Altona, Manitoba, Canada

Contract No. 0KX6-0982

Printed in Canada 1977

Contents

PREFACE vii

ABSTRACT/RÉSUMÉ ix

INTRODUCTION 1

CHAPTER 1. DISPERSION AND INITIAL VALUE PROBLEM

1.1 Dispersion 3

1.2 The Cauchy–Poisson problem 14

CHAPTER 2. TSUNAMI GENERATION

2.1 Tsunami–earthquake energy relations, source areas 31

2.2 Tsunami generation by earthquakes 42

2.3 Tsunami generation by nonseismic causes 47

2.4 Inverse tsunami problem 58

2.5 Laboratory experiments 63

CHAPTER 3. TSUNAMI PROPAGATION

3.1 Refraction, diffraction, and scattering 75

3.2 Trapping wave energy 94

3.3 Tsunami propagation 117

3.4 Laboratory experiments 139

CHAPTER 4. COASTAL PROBLEMS

4.1 Resonance 145

4.2 Coastal phenomena 167

4.3 Tsunami response and inundation of specific water bodies 189

4.4 Laboratory experiments 201

CHAPTER 5. GLOBAL TSUNAMIS

5.1 Tsunamis in Japan, USSR, Australia, and New Zealand 215

5.2 Tsunamis in the Pacific Islands, Aleutians, and Alaska 235

5.3 Tsunamis in South and North America (excluding Alaska) 259

5.4 Tsunamis in the Atlantic Ocean, Europe, Middle East, and Asia 268

CHAPTER 6. TSUNAMI WARNING SYSTEMS PAST, PRESENT, AND FUTURE

6.1 Seismic and tsunami instrumentation 281

6.2 Tsunami protection measures 286

6.3 Tsunami warning systems of the past and present 289

6.4 Acoustic and internal gravity waves in the atmosphere 302

6.5 Atmospheric nuclear explosions 308

6.6 Atmospheric disturbances generated by earthquakes and volcanic explosions 312

Contents (*concluded*)

REFERENCES 319

APPENDIX A. SEISMOLOGY (microfiche in pocket)

A.1 Structure of the earth and the new global tectonics 1
A.2 Seismic waves and concepts of intensity and magnitude 4
A.3 Epicenter determination and travel-time curves 10
A.4 Earthquake mechanism 19
A.5 Regional seismicity 29
A.6 Earthquake prediction and control 35

Preface

This book represents my attempt to synthesize current knowledge on tsunamis. To keep it small, it was necessary to omit most of the early work on tsunamis. The book is written primarily for oceanographers and assumes a knowledge of hydrodynamics, especially water waves. I attempted to utilize a uniform mathematical notation throughout but some repetition of English and Greek symbols was unavoidable. Because of this repetition, it was felt that inclusion of a table of mathematical symbols would serve no purpose and the symbols, where they appear, are fully explained.

The introduction gives a brief nonmathematical description of the various aspects of the tsunami problem. Section 1.1 introduces the so-called "Ursell parameter" to determine under what conditions phase and amplitude dispersions are important. In Section 1.2 the classical Cauchy–Poisson problem in dealing with water waves generated from an initial perturbation is introduced. Chapter 2 discusses the tsunami generation by earthquakes, volcanic eruptions, and nuclear explosions. In Chapter 3 problems related to the propagation of tsunamis in the oceans, trapping of long waves by islands, and related problems such as refraction, diffraction, and scattering, are discussed. Chapter 4 deals with the coastal aspects of tsunamis, namely tsunami forerunner, tsunami bore, initial withdrawal of water, secondary undulation, tsunami response and inundation, and such related topics as resonance, Helmholtz mode, and radiation stress. The laboratory experiments on tsunami generation, propagation, and coastal problems have been included in Chapters 2, 3, and 4, respectively.

Chapter 5 describes tsunamis in various regions on the globe: Japan, USSR, Australia, New Zealand, Hawaii, other Pacific Islands, Aleutians, Alaska, South and North America, Atlantic Ocean, Europe, Middle East, and Asia. Seismic and tsunami instrumentation is described in Section 6.1. Tsunami protection measures and warning systems of the past and present and sociological problems are treated, respectively, in Sections 6.2 and 6.3. Sections 6.4 to 6.6 deal with the concept of acoustic and internal gravity waves in the atmosphere, and disturbances in the atmosphere generated by earthquakes, tsunamis, volcanic explosions, and nuclear tests. The concept of the ionospheric detection of tsunamis is fairly new, looks promising, and is included.

Required background information on seismology appears in the Appendix (in microfiche form). In this, topics such as structure of the earth, new global tectonics, concepts of earthquake intensity and magnitude, epicenter determination, travel-time curves, regional seismicity, and earthquake prediction and control are briefly discussed.

I thank Drs N. J. Campbell and J. R. Wilson of the Marine Sciences and Information Directorate, Fisheries and Marine Service, Department of Fisheries and the Environment, for providing the facilities to carry out this work, and my colleague Mr F. G. Barber for his help and guidance throughout. Professor Paul H. Leblond of the University of British Columbia reviewed the manuscript and offered many constructive suggestions. Mrs R. Chawla helped with the library research and Mrs Margaret Johnstone did all the necessary typing, including the equations.

I thank the following societies and associations for granting me permission to reproduce material from their publications: American Geophysical Union; American Institute of Physics; American Mathematical Society; American Association for the Advancement of Science; American Journal of Science; American Society of Civil Engineers; Cambridge University Press, New York; Clarendon Press, Oxford, U.K.; D. Reidel Publishing Company, Dordrecht, Netherlands; Earthquake Research Institute, Tokyo; East-West Center Press, Honolulu; European Seismological Commission; Geophysics – Journal of the Society of Exploration Geophysicists; Hawaii Institute of Geophysics; Horace Lamb Centre, Flinders University of South Australia, Adelaide; International Tsunami Information Center, Honolulu; Imperial Academy of Japan; International Union of Geodesy and Geophysics; Japan Society of Civil Engineers; Japan Meteorological Society; Journal of Applied Physics; Journal of Fluid Mechanics; Journal of Marine Research; Laboratoire De Geophysique, Tahiti; MacMillan Educational Corporation, New York; McGraw-Hill, Inc., New York; Massachusetts Institute of Technology Press, Cambridge, Massachusetts; Nagoya University, Japan; National Research Council of Canada; National Research Council, USA; New Zealand Journal of Geology and Geophysics; New Zealand Journal of Science and Technology; New Zealand National Commission for UNESCO; Pacific Science; Pergamon Press, Inc., New York; Physico-Mathematical Society of Japan; Prentice-Hall Inc., Englewood Cliffs, New Jersey; Royal Society of New Zealand; Royal Society, London; Seismological Society of America; Soviet Academy of Sciences; Swedish Geophysical Society; St. Louis University Press, St. Louis, Missouri; Sears Foundation for Marine Research, Connecticut; Tetra Tech Corporation, Pasadena, California; The Japanese Committee for Field Investigation of Chilean Tsunami of 1960; Thomas Murphy and Co. Ltd., London; University of Washington Press, Seattle, Washington; and University of Michigan, Great Lakes Division, Ann Arbor, Michigan.

Finally, I thank the authors of various technical reports and unpublished manuscripts for permitting me to use their information.

T. S. Murty

Abstract

MURTY, T. S. 1977. Seismic sea waves – tsunamis. Bull. Fish. Res. Board Can. 198: 337 p.

This Bulletin is an attempt to synthesize current knowledge of tsunamis. Although it is directed primarily to oceanographers, other disciplines are not excluded. The book deals with phase and amplitude dispersion problems and the "Ursell" parameter, which delineates various regimes of dispersion. The classical Cauchy–Poisson problem is also introduced and the subsequent developments in the field of water-wave generation due to explosions is discussed. Tsunami generation by earthquakes and seismic sources such as volcanic explosions and nuclear explosions is considered. Some related phenomena such as landslides and turbidity currents are also included. The propagation of tsunamis across the oceans is discussed. The influences of refraction, diffraction, and scattering is examined, and the problem of trapping tsunami energy by islands and shoals is examined in detail. The coastal tsunami problems such as forerunner, initial withdrawal of water, secondary undulations, and tsunami bore are included, as well as the influence of resonance on tsunamis. Tsunamis in various parts of the world are described. Tsunami warning systems of the past, present, and future are discussed, as well as tsunami instrumentation and protection measures. Background information on seismology is in the Appendix (in microfiche form).

Résumé

MURTY, T. S. 1977. Seismic sea waves – tsunamis. Bull. Fish. Res. Board Can. 198: 337 p.

Ce Bulletin tente de synthétiser nos connaissances actuelles sur les tsunamis. Bien que préparé surtout à l'intention des océanographes, il n'exclut pas les autres disciplines. Le volume traite des problèmes de dispersion de phase et d'amplitude, et du paramètre d'«Ursell», qui définit les divers régimes de dispersion. On introduit également le problème classique de Cauchy–Poisson ainsi que les développements qui se sont produits par la suite dans le domaine de la génération des vagues causées par des explosions. Nous examinons la formation de tsunamis par tremblements de terre et à la suite de phénomènes séismiques tels qu'éruptions volcaniques et explosions nucléaires. On y inclut certains phénomènes connexes tels que les glissements de terrain et les courants de turbidité. On discute de la propagation des tsunamis dans les océans. L'influence de la réfraction, de la diffraction et de la dispersion est étudiée, de même que le problème du harnachement de l'énergie des tsunamis par les îles et les hauts-fonds, qui est examiné en détail. Ce Bulletin couvre également les problèmes des tsunamis côtiers, entre autres l'onde montante, le retrait initial de l'eau, les ondulations secondaires, les mascarets, ainsi que l'influence de la résonnance sur les tsunamis. Nous décrivons les tsunamis dans diverses parties du monde. Nous discutons des systèmes d'alerte passés, présents et futurs, de même que l'instrumentation et les mesures de protection relatives aux tsunamis. L'Annexe (sous forme de micro-fiche) contient une information de base sur la séismologie.

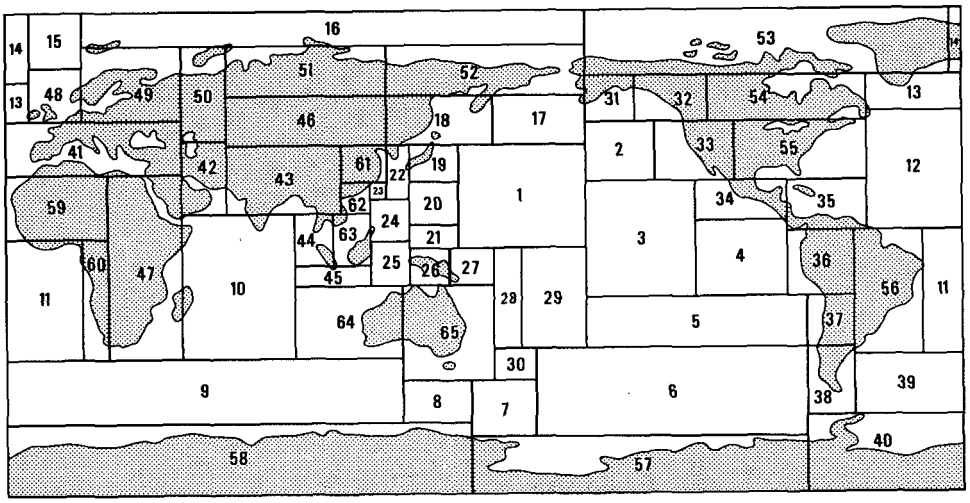
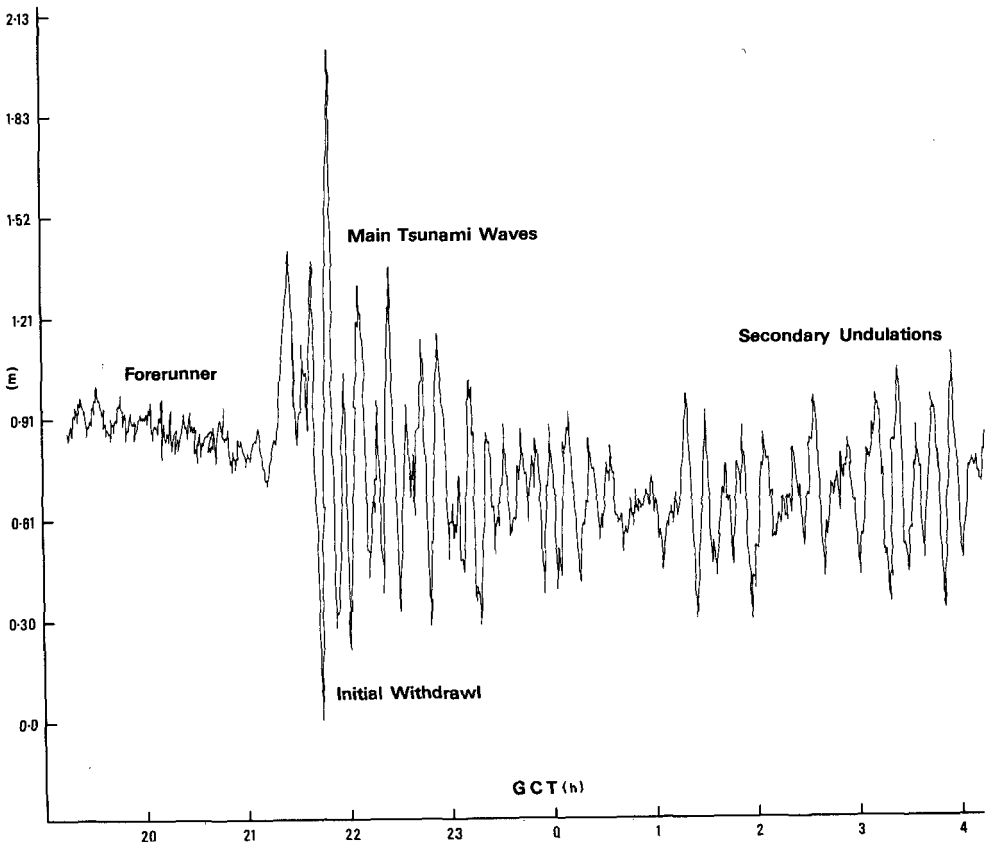


FIG. A. (*above*) Global Seismicity. Oceanic stable regions, 1–3; oceanic seismic regions, 4–16 (except 7); circumpacific seismic regions, 17–40 and 7; Alps-Himalayan seismic regions, 41–45; continental seismic regions, 46–47; and continental stable regions, 48–65. (Mizoue 1967)
FIG. B. (*below*) Tide-gage record showing tsunami at Midway Island, Nov. 4–5, 1952. (Zerbe 1953)



Introduction

Origin of the Word "Tsunami"

"Tsunami" is a Japanese word meaning harbor wave. It is now used to describe gravity waves in water bodies mainly due to earthquakes or events connected with them (e.g. landslides) and to volcanic island explosions or man-made nuclear explosions. In the past these were called "tidal waves," which is incorrect because tsunamis are not caused by tides. Another widely used term is "seismic sea wave," but this excludes gravity waves due to volcanic island eruptions and man-made nuclear explosions. Here I will use Van Dorn's (1968a) definition: "Tsunami is the Japanese name for the gravity wave system formed in the sea following any large-scale, short duration disturbance of the free surface." By this definition, storm surges (wind tides) and the seiches associated with them are excluded. The Japanese sometimes spell the word "tunami" but pronounce it as "tsunami." To avoid confusion, in the English literature only the latter form has been used.

Definitions of some Seismological Terms

The Greek root of the word "seismic" means earthquake, hence, *seismology* is the study of earthquakes. *Fault* is a break in the earth's structure that may or may not be visible at the surface but could extend to great depths. *Focus* or *hypocenter* is the point in the earth where rupture first occurs. *Depth of focus* is the vertical distance between the focus and the earth's surface. *Epicenter* is the location on the earth's surface directly above the focus. *Foreshocks* and *aftershocks* are minor, accessory earthquakes that precede and follow an earthquake. *Dip-slip* and *strike-slip* faulting refer to vertical and horizontal displacement between the two portions of the fault.

Jacobs et al. (1959) used the following classification of earthquakes: shallow (0–70 km), intermediate (70–300 km), and deep (300–700 km).

Global Seismicity

Figure A shows the distribution of seismic and nonseismic regions (also referred to as stable regions). About 90% of the world's large, shallow earthquakes occur in the circumpacific belt on the periphery of the Pacific Ocean. The percentage is even higher for intermediate earthquakes and this zone accounts for almost all deep earthquakes. There are usually around a million earthquakes per year but most cause no damage.

Tsunami Prone Areas

The following regions are tsunami prone: Japan, the Asian coast of the Soviet Union (Kamchatka, Sakhalin, Kuril Islands), Aleutian Islands, Alaska, Hawaii, west coast of South America, west coasts of USA and Canada, east coast of Canada, New Zealand, Australia, French Polynesia, Puerto Rico, Virgin Islands, Dominican Republic, Costa Rica, Azores, Portugal, Italy, Sicily, Aegean Sea Coast, Adriatic Sea Coast, Ionian Sea Coast, Greece, eastern Mediterranean Coast of North Africa, Ghana, Middle East, India, Indonesia, and Philippines. The severity and frequency of tsunami damage varies from place to place.

Generation of Tsunamis by Earthquakes

Current thinking is that tsunamis are generated by a sudden dip-slip motion along faults during major earthquakes. Although earthquakes that occur along strike-slip faults sometimes generate tsunamis, they are local and generally do not propagate long distances. Isacks et al. (1968) pointed out that major earthquakes along large strike-slip faults near the coasts of Alaska and British Columbia generated tsunamis that were observable at distances no greater than 100 km.

Tsunamis usually occur following a large shallow earthquake under the sea. However, there are a number of instances when the earthquake (that produced the tsunami) occurred inland. Hence, one must deduce that tsunamis can be generated either by changes of sea bottom (i.e. faulting) or by the seismic surface waves passing across the shallow continental shelf. The long-period, surface earthquake waves (the so-called Rayleigh waves) have a vertical component and transmit a fair share of the earthquake energy.

Tsunami Generation by Nonseismic Causes

Probably the best example is the tsunami in the Sunda Strait (between Java and Sumatra), caused by the eruption of the volcanic island Krakatoa on Aug. 27, 1883. Although turbidity currents and landslides are not directly related to tsunamis, studies on these topics are considered part of the tsunami literature. A well-known case of turbidity currents occurred following the Grand Banks earthquake of Nov. 18, 1929, which broke several transatlantic cable lines.

An example of water waves generated by landslides is Lituya Bay, Alaska. On July 9, 1958, part of a mountain broke (following an earthquake) and fell into the bay, and the water splashed to a height of about 500 m. In Italy on Oct. 9, 1963, a rockslide into a reservoir from an altitude of about 160 m generated a water wave that killed about 3000 people.

Properties of Tsunami Waves

Tsunamis fall under the general classification of long waves. Length of the waves is of the order of several hundred kilometers, although their amplitude over the deeper part of the oceans is usually of the order of a meter. Hence, it is difficult to detect them either from the air or from ships. The waves travel with a speed proportional to the square root of the water depth. In the deep ocean their speed can be several hundred km/h.

As the tsunami waves enter the continental shelf, they slow down considerably, but wave height increases. The arrival of a tsunami is sometimes indicated by a withdrawal of water (see Fig. B), which might be preceded by short-period, low-amplitude oscillations, known as forerunners. A tsunami consists of a series of waves that approaches the coast with periods usually ranging from 5 to 90 min. The wave of greatest height is not usually the first (in Fig. B the third wave is highest), but mostly occurs among the first 10 or so. The main tsunami waves are followed by secondary undulations that are mainly due to resonance effects in the bays that receive energy input from the main tsunami waves. Sometimes these secondary oscillations are also referred to as tsunami coda.

Chapter 1 Dispersion and Initial Value Problem

1.1 Dispersion

Amplitude and phase dispersion relations relevant for long gravity waves, and the theory of generation of gravity waves by deformation at the bottom (e.g. earthquake), or deformation at or near the surface (e.g. explosions), will be discussed.

Under the assumption that depth is small compared to a horizontal length scale, there are three regions of approximation for the long-wave theory (Chen et al. 1975): (a) linear equations, (b) finite-amplitude equations, and (c) Boussinesq or Kortweg-de-Vries (KdV) type equations. Three characteristic lengths determine which equation is most appropriate: water depth, D, wave length, λ, and wave amplitude, η.

Three nondimensional parameters can be defined:

$$\epsilon \equiv \frac{\eta}{D}; \mu \equiv \frac{D^2}{\lambda^2}; U \equiv \frac{\epsilon}{\mu} = \frac{\eta\lambda^2}{D^3} \tag{1.1}$$

U is generally referred to as the "Ursell parameter" and expresses the relative significance of amplitude and phase dispersion.

In the linear periodic wave theory (see Lamb 1945) the frequency, ω, is given by:

$$\omega^2 = gk \tanh (KD) \tag{1.2}$$

where g is gravity, K is wave number, and the phase velocity, C, is given by:

$$C = \frac{\omega}{K} \tag{1.3}$$

For very long waves, tanh (KD) can be approximated by the leading term in its expansion. Then from (1.2) and (1.3):

$$C = \sqrt{gD}\left\{1 - \frac{2\pi^2}{3}\frac{D^2}{\lambda^2}\right\} \tag{1.4}$$

where the wave number, K, is $2\pi/\lambda$.

From (1.4) it can be seen that long waves travel with a speed mainly determined by water depth but subject to a small negative correction proportional to μ. Two wave components with a slightly different value of μ will tend to separate as they progress; then μ is a measure of "frequency dispersion."

To understand the second type of dispersion, consider the formula for the celerity of a solitary wave (see Equation (1.39)).

$$C \simeq \sqrt{gD}\ (1 + \frac{\epsilon}{2}) \tag{1.5}$$

The celerity is approximately $\sqrt{gD}$ but is subject to a small positive correction proportional to the relative amplitude. Thus, ϵ is a measure of the amplitude dispersion.

One can distinguish among the following three regimes of U:

U
- $\ll 1$ Amplitude dispersion can be ignored. Linear long-wave theory is valid.
- $0(1)$ Both amplitude and phase dispersions are important. The Boussinesq equations (to be introduced later) are appropriate. Under certain conditions these equations reduce to the KdV equations.
- $\gg 1$ Amplitude dispersion dominates. Finite-amplitude, nonlinear, long-wave theory is appropriate.

In tsunami studies, both linear and nonlinear long-wave equations have been utilized. However, for tsunami travel over the continental shelf, neither the linear nor nonlinear cases might be relevant; indeed, one might have to use the intermediate type, e.g. Boussinesq-type equations.

LeMéhauté (1969) pointed out that the Ursell parameter is not wholly satisfactory in delineating the different regimes. He agrees that when $U \ll 1$ the linear small-amplitude wave theory applies. However, for very long waves in shallow water (flood waves, bore, nearshore tsunami) the value of U (supposed to be $\gg 1$) depends on the interpretation given to λ. (For very long waves the concept of wavelength loses its meaning because the wavelength of a solitary wave is ∞, but the flow curvature under the crest is that of a cnoidal wave for which a finite wavelength can be defined.) The relative amplitude, η/D, is then more relevant than U for interpreting the importance of nonlinear terms.

Following Broer (1964), the Ursell parameter will be formally developed, and the problem of treatment of interaction of nonlinearity (or amplitude dispersion) and dispersion (i.e. phase dispersion) in wave propagation will be discussed. The Boussinesq Equation (1.6) approximately describes the unidirectional propagation of finite-amplitude waves on a water layer of uniform depth, when the ratio of depth to wavelength, although small, is not negligible as in the theory of tides. The classical form of this equation is:

$$\frac{\partial^2 h}{\partial t^2} - gD\,\frac{\partial^2 h}{\partial x^2} = \tfrac{3}{2}\,g\,\frac{\partial^2}{\partial x^2}\,(h-D)^2 + \tfrac{1}{3}\,gD^3\,\frac{\partial^4 h}{\partial x^4} \tag{1.6}$$

where t is time and x is the horizontal direction of wave propagation. In this equation, the first term on the right is the nonlinear term due to finite wave amplitude, and the second term represents the dispersion due to finite depth to wavelength ratio. Here $h(x,t)$ is the local wave height above the horizontal bottom.

Assuming irrotational flow, the velocity components, u and w, are given in terms of the velocity potential, $\Phi(x,z,t)$, by:

$$u = \frac{\partial \Phi}{\partial x};\; w = \frac{\partial \Phi}{\partial z} \tag{1.7}$$

The potential, Φ, satisfies Laplace's equation

$$\frac{\partial^2 \Phi}{\partial x^2} + \frac{\partial^2 \Phi}{\partial z^2} = 0 \tag{1.8}$$

The boundary condition at the bottom is no flow normal to it, i.e.

$$\frac{\partial \Phi}{\partial z} = 0 \text{ for } z = 0 \tag{1.9}$$

There are two surface boundary conditions. The kinematic condition is (e.g. Lamb 1945):

$$\frac{\partial h}{\partial t} + \frac{\partial \Phi}{\partial x}\frac{\partial h}{\partial x} = \frac{\partial \Phi}{\partial z} \text{ for } z = h(x,t) \tag{1.10}$$

The dynamic condition is:

$$gh + \frac{\partial \Phi}{\partial t} + \tfrac{1}{2}\left[\left(\frac{\partial \Phi}{\partial x}\right)^2 + \left(\frac{\partial \Phi}{\partial z}\right)^2\right] = g\mathrm{D} \text{ for } z = h \tag{1.11}$$

Assuming that Φ is analytical in x and z (i.e. no singularities), equations (1.8) (1.9) are satisfied by writing:

$$\Phi(x,z,t) = \phi(x,t) - \frac{z^2}{2!}\frac{\partial^2 \phi}{\partial x^2} + \frac{z^4}{4!}\frac{\partial^4 \phi}{\partial x^4} - \cdots \tag{1.12}$$

where $\phi(x,t)$ is the potential at the bottom. From (1.10) (1.11) after using (1.12), two simultaneous equations for $\phi(x,t)$ and $\eta(x,t)$ are obtained.

These differential equations will be of infinite degree in η and infinite order in $\partial/\partial x$. To obtain an equation similar to (1.6), one has to truncate equations (1.10) (1.11).

However, before this truncation, it is convenient to work with dimensionless variables. Choose dimensionless variables (denoted by prime) such that:

$$x \equiv \mathrm{L}x'; z = \mathrm{D}z'; t = \frac{\mathrm{L}t'}{\sqrt{g\mathrm{D}}}; \phi = \phi' \epsilon \mathrm{L}\sqrt{g\mathrm{D}} \tag{1.13}$$

Also write

$$h = \mathrm{D}(1+\epsilon\eta') \tag{1.14}$$

where ϵ is the relative wave amplitude defined in (1.1) and $\eta'(x',t')$ is so chosen that its maximum value is unity for some initial or boundary value. This means the dimensionless slope $\partial\eta'/\partial x'$ is of the order of unity provided L is chosen appropriately.

Suppose the dominant wavelength, λ, is chosen for L, and noting the definition of μ from (1.1) and from (1.10) (1.11) (1.12), retaining terms of order zero and one only, then:

$$\frac{\partial \eta}{\partial t} + \frac{\partial^2 \phi}{\partial x^2} = -\epsilon\left[\eta\frac{\partial^2 \phi}{\partial x^2} + \frac{\partial \eta}{\partial x}\frac{\partial \phi}{\partial x}\right] + \tfrac{1}{6}\mu\frac{\partial^4 \phi}{\partial x^4} \tag{1.15}$$

and

$$\eta + \frac{\partial \phi}{\partial t} = -\tfrac{1}{2}\epsilon\left(\frac{\partial \phi}{\partial x}\right)^2 + \tfrac{1}{2}\mu\frac{\partial^3 \phi}{\partial x^2\,\partial t} \tag{1.16}$$

From (1.15) (1.16) the solutions will depend on the ratio ϵ/μ, the Ursell parameter defined earlier in (1.1).

Lighthill (1958) appears to be the first to coin the words "frequency dispersion" and "amplitude dispersion." Other authors used the terms "dispersion" to refer to "frequency dispersion" and "nonlinear effects" to refer to amplitude dispersion. Frequency dispersion means wave components of different frequencies propagate with different velocities whereas amplitude dispersion refers to the situation where greater values of surface elevation propagate with greater velocities to cause steepening of the waves. Situations when phase and amplitude dispersions tend to balance each other will be discussed.

First, consider the case when the terms with ϵ are ignored in (1.15) (1.16). The equations then become linear and on eliminating η between them, one obtains:

$$\frac{\partial^2\phi}{\partial x^2} - \frac{\partial^2\phi}{\partial t^2} = \tfrac{1}{6}\,\mu\,\frac{\partial^4\phi}{\partial x^4} - \tfrac{1}{2}\,\mu\,\frac{\partial^3\phi}{\partial x^2\partial t} \tag{1.17}$$

$$\text{express } \phi = \exp i\,(\mathrm{K}x - \omega t) \tag{1.18}$$

where $i = \sqrt{-1}$, the following dispersion equation is obtained:

$$\frac{\omega^2}{\mathrm{K}^2} = \frac{1 + \frac{1}{6}\mu\mathrm{K}^2}{1 + \frac{1}{2}\mu\mathrm{K}^2} \simeq 1 - \tfrac{1}{3}\,\mu\mathrm{K}^2 \tag{1.19}$$

To this order, the exact dispersion relation is in the units used so far. (Gravity is contained in the nondimensionalization of t).

$$\omega^2 = \frac{\mathrm{K}}{\sqrt{\mu}}\,\tanh\left(\mathrm{K}\sqrt{\mu}\right) \tag{1.20}$$

Next, in (1.15) (1.16) ignore the terms with μ and define:

$$u = \frac{\partial\phi}{\partial x} \tag{1.21}$$

the velocity at the bottom in the x direction. Then (1.15) (1.16) become:

$$\frac{\partial\eta}{\partial t} + \frac{\partial}{\partial x}\left\{(1+\epsilon\eta)\,u\right\} = 0 \tag{1.22}$$

$$\frac{\partial\eta}{\partial t} + \frac{\partial u}{\partial t} + \epsilon u\,\frac{\partial u}{\partial x} = 0 \tag{1.23}$$

In these equations there is no restriction on ϵ because if the expansions leading to (1.15) (1.16) are continued the terms with ϵ^2 and higher powers occur always with μ, and these terms drop out when terms with μ are ignored.

When terms with both ϵ and μ are ignored in (1.15) (1.16), linear equations without dispersion are obtained. For waves traveling to the right, the solution is:

$$\eta = u = \eta\,(x - t) \tag{1.24}$$

Hence:

$$\frac{\partial \eta}{\partial x} + \frac{\partial \eta}{\partial t} = \frac{\partial u}{\partial x} + \frac{\partial u}{\partial t} = 0 \tag{1.25}$$

REDUCED FORM OF THE BOUSSINESQ EQUATION

In this nondimensional notation, the Boussinesq Equation (1.6) becomes:

$$\frac{\partial^2 \eta}{\partial t^2} - \frac{\partial^2 \eta}{\partial x^2} = \tfrac{3}{2}\,\epsilon\,\frac{\partial^2}{\partial x^2}(\eta)^2 + \tfrac{1}{3}\,\mu\,\frac{\partial^4 \eta}{\partial x^4} \tag{1.26}$$

However, the left side of (1.26) can be deduced from (1.15) (1.16) and this gives:

$$\frac{\partial^2 \eta}{\partial t^2} - \frac{\partial^2 \eta}{\partial x^2} = \epsilon\left\{\frac{\partial^2}{\partial x^2}\left(\frac{u^2}{2}\right) - \frac{\partial^2}{\partial x \cdot \partial t}(\eta u)\right\} - \tfrac{1}{3}\,\mu\,\frac{\partial^4 u}{\partial x^3 \partial t} \tag{1.27}$$

It is clear that Equation (1.27) is not the same as (1.26) but will reduce to (1.26) provided (1.24) (1.25) are valid. Actually, due to the approximate nature of (1.15) (1.16) all one has to assume, instead of (1.24) (1.25) are $\eta - u = O(\epsilon,\mu)$ and

$$\frac{\partial}{\partial x} + \frac{\partial}{\partial t} = O(\epsilon,\mu) \tag{1.28}$$

The significance is that solutions of (1.15) (1.16) (where the main part is waves traveling to the right, assuming these exist at least during some time interval) could be found from the simpler Equation (1.26) under the present approximation. For waves propagating to the left, the signs in (1.28) can be changed; then also Equation (1.26) can be obtained from (1.27). Thus, provided (1.28) holds, Boussinesq's equation is equivalent to (1.15) (1.16) for unidirectional waves only and not for more general solutions.

As the principle of superposition cannot be used for the nonlinear equations dealt with here, it will be useful to at least simplify Equation (1.26) by ignoring the waves traveling to the left. Provided (1.28) holds and assuming (1.21) throughout, (1.15) (1.16) become:

$$\frac{\partial \eta}{\partial t} + \frac{\partial u}{\partial x} = -\,\epsilon\,\frac{\partial}{\partial x}(\eta u) + \tfrac{1}{6}\,\mu\,\frac{\partial^3 u}{\partial x^3} \tag{1.29}$$

$$\frac{\partial \eta}{\partial x} + \frac{\partial u}{\partial t} = -\,\epsilon\,\frac{\partial}{\partial x}\left(\frac{u^2}{2}\right) + \tfrac{1}{2}\,\mu\,\frac{\partial^3 u}{\partial x^2 \partial t} \tag{1.30}$$

From (1.28) one can write:

$$\frac{\partial \eta}{\partial t} + \frac{\partial \eta}{\partial x} - \frac{\partial u}{\partial t} - \frac{\partial u}{\partial x} = 0 \tag{1.31}$$

Take (1.29) + (1.30) - (1.31) and use (1.28) for the right side to give:

$$\frac{\partial \eta}{\partial t} + \frac{\partial \eta}{\partial x} + \tfrac{3}{4}\,\epsilon\,\frac{\partial}{\partial x}(\eta^2) + \tfrac{1}{6}\,\mu\,\frac{\partial^3 \eta}{\partial x^3} = 0 \tag{1.32}$$

This is the reduced equation (from Boussinesq's equation) that can be used to understand the interaction between amplitude and phase dispersions.

Cnoidal Waves

Solitary wave – To examine the properties of the reduced equation following Broer (1964), drop the numerical factors in (1.32) and write:

$$\frac{\partial \eta}{\partial t} + \frac{\partial \eta}{\partial x} + \epsilon \eta \frac{\partial \eta}{\partial x} + \mu \frac{\partial^3 \eta}{\partial x^3} = 0 \tag{1.33}$$

This equation is suitable for initial value problems in which:

$$\eta (x,0) = \mathrm{F}(x) \tag{1.34}$$

is given.

Both amplitude and phase dispersions will tend to distort the wave forms; however, there might be situations when both effects cancel each other for special wave forms. In this case, the solution is simply:

$$\eta = \mathrm{F}(x - at) \tag{1.35}$$

where a is the speed of propagation of the waves. From (1.33) (1.35) after introducing $t = 0$ and integrating with respect to x one gets:

$$(1-a)\,\mathrm{F} + \tfrac{1}{2}\epsilon \mathrm{F}^2 + \mu \frac{\partial^2 \mathrm{F}}{\partial x^2} = 0 \tag{1.36}$$

Multiply this with $\partial \mathrm{F}/\partial x$ and integrating again leads to:

$$\tfrac{1}{2}(1-a)\,\mathrm{F}^2 + \tfrac{1}{6}\epsilon \mathrm{F}^3 + \tfrac{1}{2}\mu \left(\frac{\partial \mathrm{F}}{\partial x}\right)^2 = b \tag{1.37}$$

where b is a constant of integration.

Equation (1.37) can be solved in terms of the elliptic functions. As these are represented by "cn," the name "cnoidal waves" was coined to refer to solutions of (1.37). For $b = 0$, the simple solution is:

$$\mathrm{F} = \frac{p}{\cosh^2 (qx)} \tag{1.38}$$

where

$$p \equiv \frac{3(a-1)}{\epsilon} \quad \text{and} \quad q \equiv \tfrac{1}{2}\sqrt{\frac{a-1}{\mu}}$$

This is the solution for the so called "solitary wave" and the Ursell parameter becomes $\epsilon/(\frac{3}{2}\mu)$ and is independent of a and p.

The speed of the solitary wave is from (1.36)

$$a = 1 + \tfrac{1}{2}\epsilon \eta + \frac{\mu}{\eta}\frac{\partial^2 \eta}{\partial x^2} \tag{1.39}$$

If the third term is ignored, and it is taken into consideration that (1.39) is in nondimensional units, then (1.39) reduces to (1.5).

Before going into some detail of cnoidal waves, solitary waves, and Stokes finite-amplitude waves (to be introduced later), it is worthwhile to indicate the relevance to tsunamis of the various waves and approximations to the theories discussed so far. In deep water, especially in the near-field of tsunami generation, the linear theory (phase dispersion alone is relevant) is probably adequate; on

the continental shelf both phase and amplitude dispersions will be important, thus, cnoidal waves and solitary waves are relevant. In the very shallow coastal areas (bays, harbors, inlets) the amplitude dispersion dominates.

Both amplitude and phase dispersions will tend to cause a gradual distortion of the waves. The nature of the distortion produced by amplitude and phase dispersions need not be the same. The reduced form of Boussinesq Equation (1.33) will be used to examine this problem. Consider a frame of reference that moves with unit speed (in nondimensional units). For this define:

$$S = x - t \tag{1.40}$$

Then (1.33) becomes:

$$\frac{\partial \eta}{\partial t} + \epsilon \eta \frac{\partial \eta}{\partial S} + \mu \frac{\partial^3 \eta}{\partial S^3} = 0 \tag{1.41}$$

The effects of amplitude and phase dispersions will be estimated qualitatively by integrating (1.41) with respect to S. However, solutions will be restricted to those where η is either periodic or of the nature of a solitary wave, so that η and its derivatives tend to zero for large $|S|$. In both cases, the integrated terms can be discarded after integrating by parts.

Integration of (1.41) gives:

$$\frac{d}{dt}\int \eta \, dS = 0 \tag{1.42}$$

Multiply (1.41) by η, η^2, η^n gives the following relations after integration:

$$\frac{d}{dt}\int \tfrac{1}{2} \eta^2 \, dS = 0 \tag{1.43}$$

$$\frac{d}{dt}\int \tfrac{1}{3} \eta^3 \, dS = -\mu \int \left(\frac{\partial \eta}{\partial S}\right)^3 dS \tag{1.44}$$

and the general relation is:

$$\frac{d}{dt}\int \eta^{n+1} \, dS = -\tfrac{1}{2} n(n+1)(n-1)\mu \int \left(\frac{\partial \eta}{\partial S}\right)^3 \eta^{n-2} \, dS \tag{1.45}$$

Differentiate (1.41) with respect to S, multiply by $\partial\eta/\partial S$ and integrate to give:

$$\frac{d}{dt}\int \left(\frac{\partial \eta}{\partial S}\right)^2 dS = -\epsilon \int \left(\frac{\partial \eta}{\partial S}\right)^3 dS \tag{1.46}$$

The integrals on the right sides of (1.44) to (1.46) can be considered as expressing the asymmetry of the waves. For waves with steep fronts the integrals will be negative. Thus, these equations show that phase dispersion will tend to heighten the crests and flatten the troughs. Equation (1.46) shows that the amplitude dispersion will increase the averaged square of the slope of the waves.

Small-Amplitude Wave Theories

The classical, linear, small-amplitude wave theory was originally developed by Airy (1845) and the main assumption is that the amplitude of the wave is

small compared to water depth. Another assumption is $\frac{a}{\lambda} << \left(\frac{D}{\lambda}\right)^2$. Consider a two-dimensional vertical plane, xZ. The equations of motion with the neglect of rotation are:

$$\frac{\partial u}{\partial t} + u\,\frac{\partial u}{\partial x} + w\,\frac{\partial u}{\partial Z} = -\frac{1}{\rho}\,\frac{\partial p}{\partial x} \tag{1.47}$$

$$\frac{\partial w}{\partial t} + u\,\frac{\partial w}{\partial x} + w\,\frac{\partial w}{\partial Z} = -g - \frac{1}{\rho}\,\frac{\partial p}{\partial Z} \tag{1.48}$$

The continuity equation is:

$$\frac{\partial u}{\partial x} + \frac{\partial w}{\partial Z} = 0 \tag{1.49}$$

and the condition of irrotationality is:

$$\frac{\partial u}{\partial Z} - \frac{\partial w}{\partial x} = 0 \tag{1.50}$$

The Bernoulli equation for this situation of uniform density of fluid and irrotationality is:

$$-\frac{\partial \phi}{\partial t} + \tfrac{1}{2}(u^2+w^2) + \frac{p}{\rho} + gZ = 0 \tag{1.51}$$

Because of the small amplitude assumption, the velocity head $\frac{1}{2}(u^2+w^2)$ can be ignored compared to the pressure. Hence, the convective acceleration terms $u\frac{\partial u}{\partial x}$, $w\,\frac{\partial u}{\partial Z}$ in (.47), and $u\,\frac{\partial w}{\partial x}$ and $w\,\frac{\partial w}{\partial Z}$ in (1.47) can be ignored. The boundary conditions are:

$$\text{At the surface } Z = 0\,,\ w = \partial\eta/\partial t \tag{1.52}$$

$$p = p_a$$

$$\text{At the bottom } Z = -D,\ w = 0 \tag{1.53}$$

Here p_a is the atmospheric pressure acting on the water surface and the origin of the coordinate system was taken at the undisturbed level of the free surface.

For simple harmonic progressive waves, the solution is:

$$\eta\,(x,t) = a\cos\,(Kx-\omega t) \tag{1.54}$$

where a is the wave amplitude, K is the wave number, and ω is the frequency. The solutions for u, w, and p are:

$$u = a\omega\,\frac{\cosh\,[K(Z+D)]}{\sinh\,(KD)}\cos\,(Kx-\omega t) \tag{1.55}$$

$$w = a\omega\,\frac{\sinh\,[K(Z+D)]}{\sinh\,(KD)}\sin\,(Kx-\omega t) \tag{1.56}$$

$$p = p_a - \rho g Z + \rho g a \frac{\cosh [K(Z+D)]}{\cosh (KD)} \cos (Kx - \omega t) \qquad (1.57)$$

$$\text{Here } \omega^2 = gK \tanh (KD) \qquad (1.58)$$

Because the phase velocity, C, is ω/K one can write:

$$C^2 = \frac{g}{K} \tanh (KD) \qquad (1.59)$$

For KD either large or small the above expressions reduce to simpler forms.

For deepwater (short) waves, D/λ is greater than $\frac{1}{2}$. Here D is the water depth and λ is the wavelength. For this case tanh (KD) is of the order of unity and (1.59) becomes:

$$C^2 = \frac{g}{K} = \frac{g\lambda}{2\pi} \qquad (1.60)$$

The particle velocities, u and w, and the pressure field, p, reduce to the following forms from (1.55) to (1.57):

$$u = a\,\omega\, e^{KZ} \cos (Kx - \omega t) \qquad (1.61)$$

$$w = a\,\omega\, e^{KZ} \sin (Kx - \omega t) \qquad (1.62)$$

$$p - p_a = -\rho g Z + \rho g a\, e^{KZ} \cos (Kx - \omega t) \qquad (1.63)$$

The particle orbits are closed circles with radius, a, and frequency, ω. The radius of the orbits decreases with depth. Other important properties of deepwater waves are the pressure decays with depth, and at some depth the second term on the right side of (1.63) can be ignored and then the pressure distribution is approximately hydrostatic; (1.60) shows that the phase velocity of deepwater waves depends on wavelength, thus, phase dispersion is an important property of deepwater waves.

For shallow-water (long) waves $\frac{D}{\lambda} < \frac{1}{20}$; then tanh (KD) becomes approximately equal to KD, so that the phase velocity is given from (1.59) by:

$$C = \sqrt{gD} \qquad (1.64)$$

Because the phase velocity is independent of the wavelength or wave period, long waves are nondispersive. From (1.55) to (1.57) the particle velocities and pressure field reduce to:

$$u = \frac{aC}{D} \cos (Kx - \omega t) \qquad (1.65)$$

$$w = \frac{aC}{D} K(Z+D) \sin (Kx - \omega t) \qquad (1.66)$$

$$p - p_a = \rho g Z + \rho g a \cos (Kx - \omega t) \qquad (1.67)$$

As Z does not enter the expression for u in (1.65), u is the same at all depths. However, w is dependent of Z. Due to this, the particle orbits are ellipses (not

circles) with the major axis horizontal. The length of the major axis is the same at all levels and is equal to $2a/(KD)$. The length of the minor axis decreases with depth and is given by $2a(Z+D)/D$. Close to the bottom the ellipse almost becomes a straight line.

Equation (1.67) shows that the time-varying component of pressure is also independent of the depth. The two conditions that must be satisfied for the shallow-water approximation to be valid are $a/D \ll 1$ and the Ursell parameter $U \ll 1$. As $D/\lambda < \frac{1}{20}$ for long waves, a/D has to be less than $1/(20)^2$.

Finite-Amplitude Waves

The small-amplitude theory is convenient because the surface elevation can be considered zero, i.e. the motion takes place within boundaries of known positions. Also, the assumption of linearity allows the determination of complex wave motions by superposition of elementary wave motions.

Stokes (1847) showed that periodic wave trains are possible in nonlinear dispersive systems. For the finite-amplitude case, the convective terms cannot be ignored and the relevant equations are (1.47) to (1.50). The free surface is defined by:

$$P(x,\eta,t) = p_a = \text{constant} \tag{1.68}$$

and the nonlinear free surface boundary condition is:

$$\frac{\partial p}{\partial t} + u\,\frac{\partial p}{\partial x} + w\,\frac{\partial p}{\partial Z} = 0 \tag{1.69}$$

Because of the nonlinear terms, closed-form solutions are difficult to obtain and Stokes used the method of successive approximations to obtain solutions for waves (now referred to as Stokes waves). Wiegel (1964) approached this problem somewhat differently. Equations (1.47) (1.48) together were written in the form of the integrated Bernoulli equation for unsteady flow:

$$\frac{p}{\rho} = gZ + \frac{\partial \phi}{\partial t} - \tfrac{1}{2}\left\{\left(\frac{\partial \phi}{\partial t}\right)^2 + \left(\frac{\partial \phi}{\partial Z}\right)^2\right\} \tag{1.70}$$

The condition of irrotationality can be written as:

$$\frac{\partial^2 \phi}{\partial x^2} + \frac{\partial^2 \phi}{\partial Z^2} = 0 \tag{1.71}$$

For solutions for the velocity potential, ϕ, wave amplitude, η, particle velocities, u and w, and the pressure field, p, see Muga and Wilson (1970). Other useful references are Whitham (1974) and Kinsman (1965). These can be viewed as some solutions for the first order (which gives the small-amplitude waves) and a second order correction term. The expressions reduce to simpler forms for deep and shallow-water waves. Solutions for higher orders are now available. For example, Skjelbreia (1959) gave solutions for the third order and Skjelbreia and Hendrickson (1962) for the fifth order.

Based on the second order solution the following conclusions can be drawn (Muga and Wilson 1970): the surface profile is not sinusoidal but is an elongated trochoid and the amplitude of the crest is greater than that of the trough. The

particle orbits are noncircular and do not close. Thus, there is a net forward displacement of the particles.

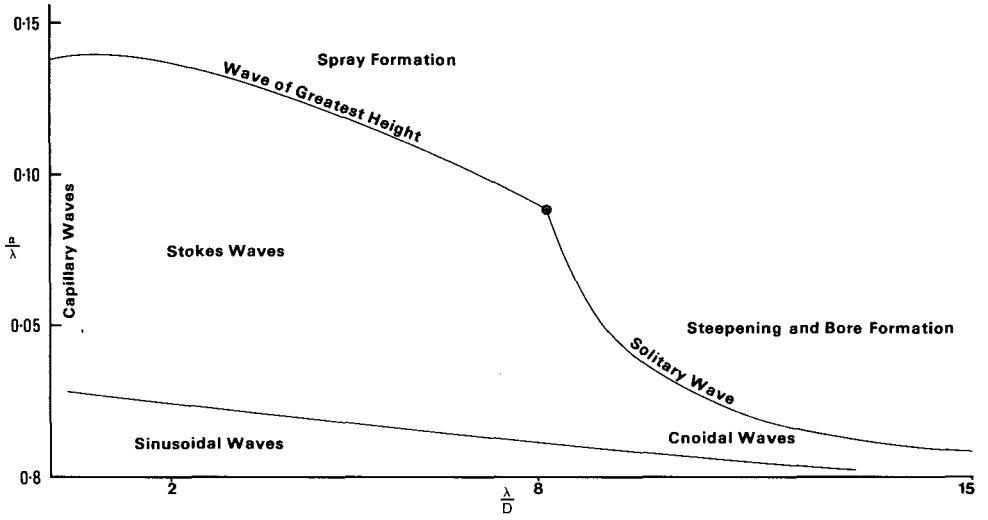


FIG. 1.1. Amplitude–wavelength diagram for water waves. (Modified from diagram 4 Lighthill 1958)

Figure 1.1 shows the abscissa is λ/D and the ordinate is a/λ where a is taken as the vertical height between the crest and the trough. Two kinds of breaking can limit the possible existence of periodic waves. At the deepwater end of the scale, the wave of greatest height might form which, when it occurs as a stationary wave on a stream, brings the water locally to rest at its wedge-shaped crest (originally predicted by Stokes). The waves of intermediate height for which Stokes already calculated the wave forms are now called Stokes waves.

On the other hand, at the long-wave end of the scale, say for $\lambda > 8D$, the existence of periodic waves is limited by amplitude dispersion. That is, there is a tendency for each value of η to propagate with speed $\sqrt{g\eta}$ appropriate to the local depth than the speed $\sqrt{gD}$ appropriate to the mean depth. This dispersion, and the fact that the particle velocity is forward when η is greatest and backward when η is least, will lead to steepening of the wave until it becomes a hydraulic jump or bore.

If the amplitude is not too large, amplitude dispersion may be balanced exactly by frequency dispersion in such a way that periodic waves are possible. These are the cnoidal waves whose existence depends on the fact that the higher harmonics in the wave travel somewhat slower than the fundamental, which, for particular wave forms, can just balance the steepening caused by amplitude dispersion. Modifications of the wave form because of frequency dispersion are proportional to D^2/λ^2, whereas the changes due to amplitude dispersion are proportional to a/D. Hence, any given cnoidal wave is possible for a fixed ratio $a/\lambda : D^2/\lambda^2$. The limiting case is the solitary wave for which $a\lambda^2/D^3 \sim 25$. Russel (1844) identified the solitary wave in laboratory experiments.

For amplitudes above that of solitary wave, steepening and bore formation occurs, whereas for amplitudes just below, cnoidal wave train starts to degenerate into a sequence of isolated solitary waves. The two curves in Fig. 1.1 for the different kinds of breaking meet at a point representing the solitary wave of greatest height computed by McCowan (1894). For recent work on solitary waves see Longuet-Higgins (1974) and Longuet-Higgins and Fenton (1974).

1.2 The Cauchy–Poisson Problem

The Classical Problem

The Cauchy–Poisson (C–P) problem is the initial value problem for surface waves. The classical C–P problem as described by Lamb (1945) deals with one-dimensional standing waves in an ocean of infinite depth. Although the classical problem is hardly suitable for tsunami studies, it is simple and can be used to introduce certain concepts. Two different initial states are considered: initial elevation of the free surface with no motion, and a horizontal surface with an initial distribution of surface impulse.

First consider initial elevation. Taking the origin at the undisturbed level of the surface, the water level, η, and the velocity potential, ϕ, can be written for simple harmonic standing waves:

$$\eta = \cos(\omega t)\cos(kx) \tag{1.72}$$

$$\phi = \frac{g \sin(\omega t)}{\omega} e^{kz} \cos(kx) \tag{1.73}$$

$$\text{where } \omega^2 = gk \tag{1.74}$$

The initial state is given by:

$$\eta = f(x),\ \phi_0 = 0 \tag{1.75}$$

The Fourier double integral representation is:

$$f(x) = \frac{1}{\pi}\int_0^\infty dk \int_{-\infty}^\infty f(\alpha)\cos k\,(x-\alpha)\,d\alpha \tag{1.76}$$

From (1.72), (1.73, (1.75), (1.76)

$$\eta = \frac{1}{\pi}\int_0^\infty \cos(\omega t)\,dk \int_{-\infty}^\infty f(\alpha)\cos k\,(x-\alpha)\,d\alpha \tag{1.77}$$

$$\phi = \frac{g}{\pi}\int_0^\infty \frac{\sin(\omega t)}{\omega} e^{kz}\,dk \int_{-\infty}^\infty f(\alpha)\cos k\,(x-\alpha)\,d\alpha \tag{1.78}$$

Lamb assumed that the initially elevated region is small in extent and is confined to the immediate vicinity of the origin, so that $f(\alpha)$ is nonzero for infinitesimal values of α. Lamb expressed ϕ and η in a series as well as in another form involving Fresnel's integrals.

For initial impulse, the initial conditions are:

$$\begin{aligned} \rho\phi_0 &= f(x) \\ \eta &= 0 \end{aligned} \tag{1.79}$$

A similar procedure was followed as above.

For large $gt^2/(4x)$, the following expressions hold approximately. For initial elevation:

$$\eta = \frac{g^{\frac{1}{2}}\, t}{2^{\frac{3}{2}}\, \pi^{\frac{1}{2}}\, x^{\frac{3}{2}}} \left[\cos\left(\frac{gt^2}{4x}\right) + \sin\left(\frac{gt^2}{4x}\right)\right] \tag{1.80}$$

and for initial impulse:

$$\eta = \frac{g^{\frac{1}{2}}\, t^2}{2^{\frac{5}{2}}\, \pi^{\frac{1}{2}}\, \rho x^{\frac{5}{2}}} \left[\cos\left(\frac{gt^2}{4x}\right) - \sin\left(\frac{gt^2}{4x}\right)\right] \tag{1.81}$$

One drawback of these solutions is that as the origin is approached the wavelength decreases monotonically, whereas the wave height increases asymptotically.

Kelvin's Method of Stationary Phase and Airy Integral

Kelvin (1877) suggested that the C–P problem can be studied by more simple methods than were adopted by Cauchy and Poisson.

Consider the integral:

$$\int_a^b \phi(x)\, e^{if(x)}\, dx$$

and assume that $f(x)$ varies much more rapidly than in a periodic manner. Kelvin's method uses the fact that the various elements of the integral will for the most part cancel by annulling interference except in the neighborhood of x, if any, for which $f(x)$ is stationary. For details on Kelvin's method of stationary phase see Jeffreys and Jeffreys (1946) and Stoker (1957).

Consider one-dimensional propagation of a disturbance due to an initial elevation over the water surface. Following Jeffreys and Jeffreys represent the disturbance as:

$$f(x) = \int_0^\infty f(\mathrm{K}) \cos(\mathrm{K}x - \omega t)\, d\mathrm{K} \tag{1.82}$$

Then at point x_0, at time t_0, the disturbance can be asymptotically represented by Kelvin's method of stationary phase as:

$$f(x_0, t_0) \approx \frac{f(\mathrm{K}_0)}{\left[\frac{1}{2}\pi\, t \left| \frac{d\mathrm{C}_g}{d\mathrm{K}} \right|\right]^{\frac{1}{2}}} \cos\left(\mathrm{K}_0 x - \omega t \mp \frac{\pi}{4}\right) \tag{1.83}$$

Here the subscript 0 signifies that the function has to be evaluated for the wave number, K_0. Also C_g is the group velocity and the $\mp$ sign should be taken when $d\,\mathrm{C}_g/d\mathrm{K}$ is positive or negative.

However, Equation (1.83) is not valid in the following two cases: (a) when the group velocity is stationary or (b) at the head of a wave train where the long-wave formula (1.64) holds. In these situations the method of stationary phase should be carried out to a higher approximation. Then the disturbance could be expressed,

instead of Equation (1.82), in terms of the Airy integral given by:

$$A_i(\alpha) = \frac{1}{\pi} \int_0^\infty \cos\left(\frac{t^3}{3} + \alpha t\right) dt \tag{1.84}$$

where α is some variable.

If one approximates

$$\tanh(KD) \sim KD - \tfrac{1}{6}(KD)^3 \tag{1.85}$$

The group velocity of tsunami waves arriving at any point is:

$$C_g = \sqrt{gD}\left(1 - \tfrac{1}{2}K^2D^2\right) \tag{1.86}$$

Let the initial form of the surface be such that: $\eta = 1$ in the region $-L < x < L$ and $\eta = 0$ elsewhere. If α is identified with the phase velocity of a long wave, $\sqrt{gD}$, the asymptotic form of η near $x = \alpha t$ is:

$$\eta \sim L\left(\frac{2}{\alpha t D^2}\right)^{\frac{1}{3}} A_i\left\{\frac{2(x-\alpha t)^3}{\alpha t D^2}\right\}^{\frac{1}{3}} \tag{1.87}$$

The form of the Airy function is such that it increases monotonically to a maximum and then oscillates with decreasing amplitude. For positive α, $A_i(\alpha)$ can be expressed in terms of the Bessel functions of imaginary argument, whereas for negative α, it can be expressed in terms of the Bessel function, J. Based on the behavior of $A_i(\alpha)$ one can deduce that at any given point after the passage of the head of the wave train succeeding waves must be of the form of a dispersive wave train. The following asymptotic form is valid for η after the initial few oscillations.

$$\eta = L\left(\frac{2}{\alpha t D^2}\right)^{\frac{1}{3}} \frac{1}{\pi^{\frac{1}{2}}(\alpha t - x)^{\frac{1}{4}}} \left(\frac{\alpha t D^2}{2}\right)^{\frac{1}{12}} \times \sin\left[\tfrac{2}{3}(\alpha t - x)^{\frac{3}{2}} \left(\frac{2}{\alpha t D^2}\right)^{\frac{1}{2}} + \frac{\pi}{4}\right] \tag{1.88}$$

Kranzer and Keller Theory for Radial Symmetry

Kranzer and Keller (1959) developed a theory for water waves produced by explosions either above or below the water surface and assumed a water body of finite depth. They gave explicit formulae for the height of waves produced by an arbitrary axially symmetric initial disturbance which could be of any one form or combination of different forms such as an impulse, an initial elevation, or depression of the surface. Where the form of the initial disturbance was known only approximately, upper bounds on the heights of the waves were given.

The analysis was based on the linear theory for surface waves in water of uniform but finite depth, D. Symmetry was assumed about the initial disturbance and, because of this, polar coordinates were used. The surface elevation, η, due to an initial impulsive force distributed over the surface is: (See Krazer and Keller (1959) for details.)

$$\eta(r,t) \sim \frac{I_0\sqrt{R}}{\rho\sqrt{g}\,r} A \sin 2\pi\left(\frac{t}{T} - \frac{r}{\lambda}\right) \text{ for } r >> R \tag{1.89}$$

where r is the radial coordinate and denotes the distance from the origin, t is time, I_0 is the initial impulse at the origin, R is the effective radius of the initial impulse defined through (1.90), A is the amplitude, T is the period, and λ is the length of the waves.

$$R^2 = \frac{\int_0^\infty r\,|I(r)|}{\frac{1}{2}|I_0|}\,dr \tag{1.90}$$

The total initial impulse is $\pi|I_0|R^2$.

It can be seen from (1.89) that η decreases proportional to the distance, r. A given portion of the wave pattern travels with a constant speed but different parts travel with different speeds, with the outer parts traveling faster than the inner parts. The parameters A, T, λ, were expressed in terms of an auxiliary variable defined as:

$$\sigma \equiv \frac{2\pi D}{\lambda} \tag{1.91}$$

which is a function of $r/(t\sqrt{gD})$ and is defined as the unique nonnegative root of the equation.

$$F(\sigma) \equiv \frac{1}{2}\left(\frac{\tanh\sigma}{\sigma}\right)^{\frac{1}{2}} + \frac{1}{2(\cosh\sigma)^{\frac{3}{2}}}\left(\frac{\sigma}{\sinh\sigma}\right)^{\frac{1}{2}} = \frac{r}{t\sqrt{gD}} \tag{1.92}$$

Equation (1.91) essentially defines λ in terms of σ. The expression for T is:

$$T = \frac{2\pi}{\sqrt{\frac{g\sigma}{D}\tanh\sigma}} \tag{1.93}$$

The amplitude, A, is 0 for $r > t\sqrt{gD}$ and nonzero for $r < t\sqrt{gD}$, and is given in terms of the zero order Hankel transform $\bar{I}(\sigma/D)$ of the initial impulse distribution $I(r)$.

$$\bar{I}\left(\frac{\sigma}{D}\right) = \int_0^\infty I(r)\,J_0\left(\frac{\sigma r}{D}\right) r\,dr \tag{1.94}$$

For a given value of $r/(t\sqrt{gD})$, σ can be found from the transcendental Equation (1.92) and λ, T, A can be computed knowing σ. However, because of the difficulty associated with transcendental equations, it will be easier to choose

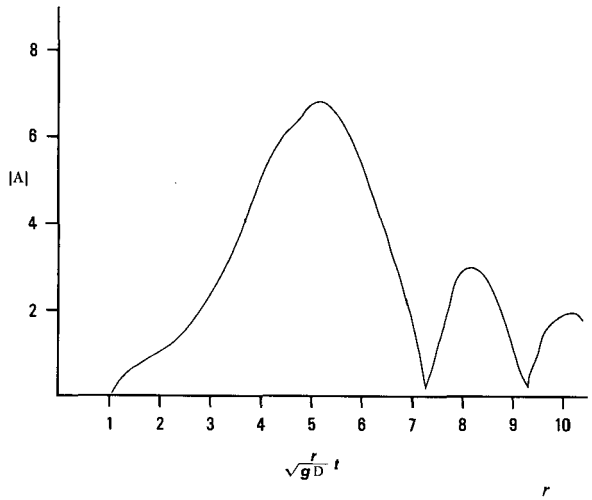


FIG. 1.2. The wave amplitude $|A|$ as a function of $\frac{r}{\sqrt{gD}}\,t$. Waves are due to the parabolic impulse distribution $I(r) = 10\left\{1-\frac{1}{2}(\frac{r}{R})^2\right\}$ for $r \leq \sqrt{2}R$ and $I(r) = 0$ for $r > \sqrt{2}\,R$ with $R = \frac{2}{7}D$. (Kranzer and Keller 1959)

values of σ and compute $r/(t\sqrt{gD})$. Figure 1.2 shows that the amplitude, A, is zero for $r > t\sqrt{gD}$ and is continuous at $r = t\sqrt{gD}$ although its first derivative is discontinuous. An important feature of the amplitude curve is the location and magnitude of the maxima of $|A|$ which depend on the initial impulse distribution. The following upper bound was put on $|A|$ for any initial shape.

$$|A| < 1.40 \text{ for } \frac{R}{D} < 2 \tag{1.95}$$

In table 1 of their paper, Kranzer and Keller (1959) gave the maximum amplitude A_{max}, group velocity $C_{g_{max}}$, wavelength λ_{max}, and period T_{max} at the maximum and the total energy for five different impulse distributions $I(r)$. They also gave diagrams of the wave height, η, as a function of t for a given r, and as a function of r for a given t.

For an initial elevation or depression of the free surface, the wave height is given by:

$$\eta(r,t) \sim \eta_0 \frac{R}{r} B \cos 2\pi\left(\frac{t}{T} - \frac{r}{\lambda}\right) \text{ for } r >> R \tag{1.96}$$

where η_0 is the initial elevation at the origin. The effective radius, R, of the initial displacement is defined as:

$$R^2 \equiv \frac{\int_0^\infty E(r) r\, dr}{\frac{1}{2}|\eta_0|} \tag{1.97}$$

where $E(r)$ is the initial elevation and $\pi R^2|\eta_0|$ is the volume of water initially displaced. The amplitude, B, is expressed similar to A in zero order Hankel Transform (of the initial elevation $E(r)$ for this case). An upper bound on B valid for any shape is:

$$|B| < 1.16 \text{ for } \frac{R}{D} < 1.64 \tag{1.98}$$

Although, in general, the wave features of this case (i.e. initial elevation or depression) are similar to those of initial impulse, important differences exist. In this case the wave amplitude, B, is not continuous at $r = t\sqrt{gD}$ and a bore precedes the waves. The dimensionless amplitude and duration of the bore are given by:

$$B_{bore} = \pm \frac{R'}{2D} \frac{R'}{R} \tag{1.99}$$

and

$$T_{bore} = \frac{1.4 D^{\frac{1}{6}} r^{\frac{1}{3}}}{g^{\frac{1}{2}}} \tag{1.100}$$

where

$$R' \equiv \frac{\left| \int_0^\infty r E(r)\, dr \right|}{\frac{1}{2}|\eta_0|} \tag{1.101}$$

The amplitude may increase a little behind the bore but falls off gradually to zero at $t = \infty$.

In reality, because of the presence of viscosity, the amplitude is continuous at $r = t\sqrt{gD}$ and is not exactly zero for $r > t\sqrt{gD}$. Actually, the bore represents a rapid change in B from zero to the value given by (1.98). However, with increase of time it becomes steeper and tends to resemble a discontinuity. If the volume of the fluid above the undisturbed water surface is exactly equal to the volume of fluid removed from below it, i.e. if $\bar{E}(0) = 0$, then a bore does not occur.

To calculate the actual wave forms produced by explosions, the initial impulse distribution for the first case and the initial surface displacement for the second case must first be determined. It is relatively easy to compute the initial impulse distribution for an explosion above the surface from the shock wave or pressure pulse, but the initial displacement of the water surface (for the second case) can only be estimated. For details on providing the initial conditions, see Kranzer and Keller (1959). Kranzer and Keller's theory is not valid for short distances from the origin, due to use of the method of stationary phase.

Whalin (1965) developed a technique to compute the wave motion close to the source which he took as a parabolic impulse of radius, 2R. His results showed that indeed, for $t < r/\sqrt{gD}$ and for $r > 10R$ the initial motion is negligible. Thus, for such distances the method of stationary phase requiring less computation can be used. For $r < 10R$, Whalin's method is desirable. However, he cautioned that

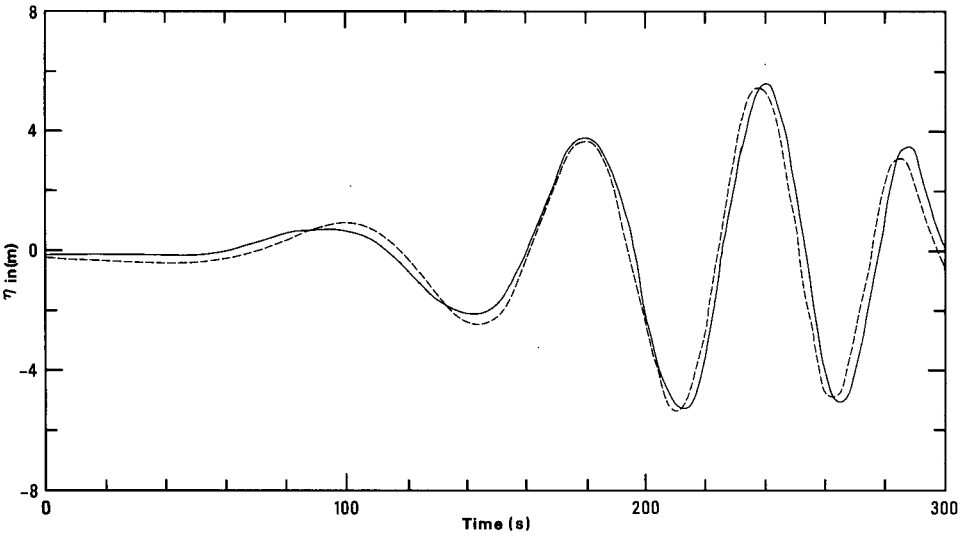


FIG. 1.3. Wave amplitude as a function of time 10 km from source for a parabolic impulse. Method of stationary phase (solid line), Whalin's method (broken line). (Whalin 1965)

for $r < 3R$, the linear theory used by him breaks down. Figure 1.3 shows the wave form computed by Whalin at a point 10 km from the origin, as a function of time.

THE THEORY OF KAJIURA

Kajiura (1963) critized Kranzer and Keller (1959) because of their incorrect application of the method of stationary phase up to the wave where the Airy integral should be considered. He considered the problem of surface waves generated by an arbitrary but localized disturbance of the free surface and gave a solution that included the effects of initial displacement, velocity, pressure, and bottom motion.

The problem was formulated in the following manner. In a water body of infinite extent but finite depth, D, the origin of a Cartesian coordinate system, x, y, z, was taken at the undisturbed level of the water surface and irrotational motion was assumed. The variables were nondimensionalized through defining.

$$x^* \equiv \frac{x}{D} \qquad t^* \equiv \left(\frac{g}{D}\right)^{\frac{1}{2}} \qquad \phi^* \equiv \frac{\phi}{D(gD)^{\frac{1}{2}}}$$

$$y^* \equiv \frac{y}{D} \qquad \eta^* \equiv \frac{\eta}{D} \qquad p^* \equiv \frac{p}{\rho g D} \tag{1.102}$$

$$z^* \equiv \frac{z}{D}$$

Here η is the deviation of the water level from its equilibrium position, ϕ is the

velocity potential, ρ is density of water, and p is the deviation of the atmospheric pressure at the sea surface from its mean value.

Kajiura made the linear approximation, thereby treating the surface elevation and bottom deformation small compared to the water depth, D, and the wavelength, λ. The joint condition is that the Ursell parameter defined in Equation (1.1) has to be less than one.

The governing equation is Laplace's equation and there are two conditions at the surface and one at the bottom. The water level is now referred to as η, the boundary conditions are applied at the undisturbed level of the free surface, and the asterisks have been dropped for convenience, so the kinematic condition (1.10) at the surface reduces for this case to:

$$\frac{\partial \phi}{\partial z} = \frac{\partial \eta}{\partial t} \tag{1.103}$$

The dynamic condition (1.11) at the free surface becomes:

$$\frac{\partial \phi}{\partial t} = -\eta - p \tag{1.104}$$

The condition (1.9) at the bottom becomes:

$$\frac{\partial \phi}{\partial z} = w_B \tag{1.105}$$

where w_B is the velocity (prescribed) of the bottom deformation.

Kajiura approached the solution to this problem through a time-dependent Green's function, G, which is harmonic in x, y, z with a singularity at some point (x_0, y_0, z_0) introduced at time, $t = \tau$. This Green's function satisfies Laplace's equation:

$$\nabla^2 G = 0 \text{ for } 0 > z > -1 \text{ and } t \geq \tau \tag{1.106}$$

In the nondimensional notation, $z = 0$ is the undisturbed surface and $z = -1$ is the bottom. The two surface conditions (1.103) (1.104) become:

$$\frac{\partial^2 G}{\partial t^2} + \frac{\partial G}{\partial z} = 0 \text{ at } z = 0 \tag{1.107}$$

and the bottom condition (1.105) becomes:

$$\frac{\partial G}{\partial z} = 0 \text{ at } z = -1 \tag{1.108}$$

Initially, at $t = \tau$ it is assumed that:

$$G = \frac{\partial G}{\partial \tau} = 0 \text{ at } z = 0 \tag{1.109}$$

The following conditions on boundedness should be satisfied: (a) for x and y tending to ∞, G and $\partial G/\partial \tau$ and their first derivatives with respect to x and y must be uniformly bounded for all t, and (b) at the point (x_0, y_0, z_0), $(G - \frac{1}{R})$ must

be bounded, where:

$$R \equiv \left[(x-x_0)^2 + (y-y_0)^2 + (z-z_0)^2\right]^{\frac{1}{2}} \tag{1.110}$$

When these conditions are satisfied, G can be determined uniquely.

Following Stoker (1957), Kajiura wrote Green's function in terms of Bessel functions and hyperbolic functions. Ultimately he arrived at the following expression:

$$\eta + p = \frac{1}{4\pi}\iint_s (F_1 + F_2 + F_3)\, ds \tag{1.111}$$

where $ds = dx \cdot dy$, and F_1, F_2, F_3 have the following meanings: F_1 expresses the contribution from the initial velocity and elevation of the water surface, F_2 shows the effect of surface pressure, and F_3 gives the contribution from the bottom deformation.

Kajiura (1963) considered five cases of source conditions and in each expressed the forcing function suitably: (a) an initial elevation, (b) a pressure applied impulsively, (c) the bottom deformed instantaneously, (d) the bottom deformation during a time interval, and (e) the bottom moved impulsively but no net deformation of the bottom. In all cases, the water was initially assumed to be devoid of motion.

Kajiura's results can be summarized in the following table taken from his work.

Nature of source	Initial surface elevation or sudden bottom deformation		Surface impulse	
	$q > 3$	$q < 1$	$q > 3$	$q < 1$
One dimensional propagation	0	$-\frac{1}{3}$	$-\frac{1}{3}$	$-\frac{2}{3}$
Two dimensional propagation	$-\frac{2}{3}$	-1	-1	$-\frac{4}{3}$

The numerals show the power of the radial distance, r, that gives the loss of decay with distance of the leading wave of the tsunami. The source is assumed to be rectangular with major and minor axes, $2x_a$ and $2x_b$. The parameter, q, is defined as:

$$q \equiv \left\{\frac{6\sqrt{D/g}}{t}\right\}^{\frac{1}{3}} \frac{x_a}{D} \tag{1.112}$$

If the wave is in the direction of the minor axis of the source, x_a should be replaced by x_b.

Practical Simplifications Based on Kajiura's (1963) Work

LeMéhauté (1971) showed that Kajiura's theory can be simplified for application to practical problems. LeMéhauté considered water waves generated by explosions at or near the surface and the term F_3 in (1.111) is not relevant for his study. He found that for practical use, the generality of Kajiura's theory is not

necessary and one can include the effects of initial velocity and pressure into a fictitious initial surface deformation, chosen in such a way that the predicted waves are essentially the same as would be found by actual velocity, deformation, and pressure.

LeMéhauté starts with the following expression, generally referred to as the Kranzer–Keller solution:

$$\eta(r,t) = \int_0^\infty k \cos(\omega t)\, J_0(kr) \left\{ \int_0^\infty \eta_0(r_0)\, J_0(kr_0)\, r_0 dr_0 \right\} dk \qquad (1.113)$$

where $\eta_0(r_0)$ is the initial deformation. For large r and t, $J_0(kr)$ is replaced by an asymptotic form and the resulting integral is approximated by the method of stationary phase. Then

$$\eta(r,t) \approx \frac{1}{r} \left[\frac{kC_g}{-\left(\frac{dC_g}{dk}\right)} \right]^{\frac{1}{2}}_{k=k_p} \bar{\eta} \cos \left[\lambda r - t\,(\lambda \tanh \lambda)^{\frac{1}{2}} \right] \qquad (1.114)$$

where

$$\bar{\eta} = \int_0^\infty \eta_0(r_0)\, J_0(kr_0)\, r_0\, dr_0 \qquad (1.115)$$

and the group velocity C_g is given by:

$$C_g = \frac{1}{2k}(k \tanh k)^{\frac{1}{2}} + \frac{K}{2\cosh^2(k)(k \tanh k)^{\frac{1}{2}}} \qquad (1.116)$$

and k_p is the particular value of K for given values of r and t found from:

$$C_g = \frac{r}{t} \qquad (1.117)$$

The problem now is to choose $\eta_0(r_0)$ in such a way, depending on water depth and explosion characteristics, that (1.114) can accurately predict such a wave train.

In (1.114) the cosine term represents the individual waves, whereas the remainder of the expression represents their varying amplitude or envelope, given by:

$$A = \frac{\bar{\eta}}{r} \left\{ \frac{kC_g}{-\left(\frac{dC_g}{dK}\right)} \right\}^{\frac{1}{2}} \qquad (1.118)$$

where K is the root of (1.117). It can be seen from (1.118) that for any fixed value of r, the least nonzero value of K, for which $dA/dK = 0$, is independent of r. The significance of this is that the maximum of the first wave envelope where $dA/dK = 0$ is associated with a constant value of K (hence a constant value of wavelength and period) throughout its propagation. This constant value of K at

the first envelope maximum, K_{max}, depends only on the nature of the source disturbance, $\eta_0(r_0)$, through the factor, $\overline{\eta}(K)$. Evaluating A at K_{max} one can write:

$$A_{max}\, r = \left\{ \overline{\eta} \left[\frac{K C_g}{-\frac{dC_g}{dK}} \right]^{\frac{1}{2}} \right\}_{K = K_{max}} = \text{constant} \tag{1.119}$$

for a particular source deformation $\eta_0(r_0)$ which means that the amplitude of the maximum waves is inversely proportional to r.

LeMéhauté (1971, p. 9) gives the justification for replacing A_{max} by η_{max}. The two constraints he imposed on a choice for $\eta_0(r_0)$ are: (a) the resulting wave envelope shape be quite similar to observed shapes that some fudging of the numerical coefficients will give an accurate fit, (b) the Hankel Transform of $\eta_0(r_0)$ could be obtained in a closed form. The following form was chosen for $\eta_0(r_0)$:

$$\eta_0(r_0) = \begin{cases} \eta_{0_{max}} \left[2 \left(\frac{r_0}{R} \right)^2 - 1 \right] & \text{for } r_0 \leq R \\ 0 \text{ for } r_0 > R \end{cases} \tag{1.120}$$

where $\eta_{0_{max}}$ is a coefficient that appears in the following relation:

$$\eta\,(r,t) = -\frac{\eta_{0_{max}} R}{r} \left[\frac{C_g}{k\left(-\frac{dC_g}{dK}\right)} \right]^{\frac{1}{2}} J_3(KR) \cos \left[k - t(k \tanh k)^{\frac{1}{2}} \right] \tag{1.121}$$

Thus, the two cavity parameters, η_{0max} and R, enter into the expression for the envelope amplitude, A. It is through the empirical determination of these two parameters that LeMéhauté correlated the theory with experiments (Chapter 2).

Other Effects in the C-P Problem

Braddock and Van Den Driessche (1971) developed a theory for the C–P problem when the source is asymmetric with reference to the axis (of a cylindrical polar coordinate system) with the origin placed at the bottom. The ocean bottom is assumed to move with the velocity

$$F(x,y,t) = X(x)\, Y(y)\, T(t) \tag{1.122}$$

Although this separation of variables is somewhat simplistic, some generality is achieved by expanding $X(x)$, $Y(y)$, $T(t)$, in series of orthogonal functions. This

type of bottom motion is more general than in the theory of Kajiura.

$$X(x) = \sum_{m=0}^{\infty} \alpha_n H_m(x) \exp\left(-\frac{x^2}{2}\right) \text{ for } -\infty < x < \infty$$

$$Y(y) = \sum_{n=0}^{\infty} \beta_n H_n(y) \exp\left(-\frac{y^2}{2}\right) \text{ for } -\infty < y < \infty \qquad (1.122a)$$

$$T(t) = \sum_{p=0}^{\infty} \gamma_p L_p(t) \exp\left(-\frac{t^2}{2}\right) \text{ for } 0 < t < \infty$$

Here $H_m(x)$ is the Hermite polynomial of degree, m, and $L_p(t)$ is the Laguerre polynomial of degree, p.

The coefficients α_m, β_n, and γ_p can be written as follows:

$$\alpha_m = \frac{1}{2^m m! \sqrt{\pi}} \int_{-\infty}^{\infty} X(x) \exp\left(-\frac{x^2}{2}\right) H_m(x)\, dx$$

$$\beta_n = \frac{1}{2^n n! \sqrt{\pi}} \int_{-\infty}^{\infty} Y(y) \exp\left(-\frac{y^2}{2}\right) H_n(y)\, dy \qquad (1.123)$$

$$\gamma_p = \frac{1}{p!} \int_{-\infty}^{\infty} T(t) L_p(t) \exp\left(-\frac{t}{2}\right) dt$$

Because of the presence of factors 2^m, $m!$, $n!$, $p!$ in the denominators of (1.123), the coefficients $\alpha_m, \beta_n, \gamma_p$ decrease rapidly as m, n, p increase. Hence, in practice only a few terms will be necessary.

It is possible that the source area for a tsunami could be very close to the shore such as a shallow submarine earthquake or an underwater nuclear explosion. In this case, the effect of the sloping nature of the bottom on the tsunami generated has to be taken into account. Slatkin (1971) used a three-dimensional model to study this problem.

The origin of a Cartesian coordinate system, x, y, z, is taken at the equilibrium position of the free surface with the Z-axis pointing upward. Then the bottom is given by $Z = -D(x,y,t)$ and the free surface perturbation is $\eta(x,y,t)$. In the linear shallow-water theory for the nonrotating case, the wave equation is (see Lamb 1945):

$$g\left\{\nabla \cdot (D \nabla \eta)\right\} - \frac{\partial^2 \eta}{\partial t^2} = -\frac{\partial^2 D}{\partial t^2} \qquad (1.124)$$

where ∇ is the gradient operator. Let the bottom profile be specified as:

$$D(x,y,t) = D_0(y) + D_1(x,y,t) \qquad (1.125)$$

where $D_1 \ll D_0$ and $D_0(y)$ is the bottom profile in the equilibrium state, assumed to be prescribed in $0 \leq y < \infty$. The shore and the infinite extent of the ocean are represented by $y = 0$ and ∞, respectively.

From (1.124) (1.125) the wave equation to the lowest order is:

$$g \frac{\partial}{\partial y}\left\{D_0(y) \frac{\partial \eta}{\partial y}\right\} + g D_0 \frac{\partial^2 \eta}{\partial x^2} - \frac{\partial^2 \eta}{\partial t^2} = -\frac{\partial^2 D_1}{\partial t^2} \qquad (1.126)$$

The following boundary conditions must be satisfied at $y = 0$

$$\left(\frac{\partial \eta}{\partial y}\right)_{y=0} = 0 \text{ if } D_0(0) \neq 0 \text{ or } (\eta)_{y=0} \text{ is finite if } D_0(0) = 0 \tag{1.127}$$

Take the Laplace Transform in t and the Fourier Transform in x of (1.126) and define:

$$\bar{\eta}(K,y,S) = \int_{-\infty}^{\infty} e^{ikx} \int_0^{\infty} e^{-St}\, \eta(x,y,t)\, dt \cdot dx \tag{1.128}$$

Then:

$$g \frac{d}{dy}\left\{D_0(y) \frac{d\bar{\eta}}{dy}\right\} - (gD_0k^2 + S^2)\bar{\eta} = F(k,y,S) \tag{1.129}$$

where:

$$F(k,y,S) = -\int_{-\infty}^{\infty} e^{ikx} \int_0^{\infty} e^{-St} \frac{\partial^2 D_1}{\partial t^2}\, dt \cdot dx + S\bar{\eta}(k,y,t=0) + \frac{\partial \bar{\eta}}{\partial t}(k,y,t=0) \tag{1.130}$$

The equivalence of the effects of ground motion of finite duration and initial surface displacement (Hwang and Tuck 1970b) makes the method of solution somewhat independent of the exact nature of the source.

The following form was assumed for $D_0(y)$:

$$D_0(y) = D_0(1 - e^{-\alpha y}) \tag{1.131}$$

where D_0 and α are prescribed. This is finite at ∞ and is analytic in the range $0 < y < \infty$. Define:

$$V \equiv e^{-\alpha y} \tag{1.132}$$

Then (1.129) becomes:

$$\begin{aligned} &V^2(1-V)\frac{\partial^2 \bar{\eta}}{\partial V^2} + V(1-2V)\frac{\partial \bar{\eta}}{\partial V} \\ &- \left\{\frac{S^2}{\alpha^2 g D_0} + \frac{K^2}{\alpha^2}(1-V)\right\}\bar{\eta} \\ &= \frac{1}{\alpha^2 g D_0} F\left(K, \frac{1}{\alpha}\ell n \frac{1}{V}, S\right) \\ &\equiv G(K,V,S) \end{aligned} \tag{1.133}$$

Thus, the problem reduces to solving (1.133) under the following conditions: (a) η is finite at $V = 0$, (b) η is finite $V = 1$, and (c) the radiation condition.

Slatkin (1971) determined the eigenfunctions (different possible wave modes) of the homogeneous part of (1.133) to solve this problem, and then expanded G

in terms of these functions. One result is that long waves can be trapped along the coast and can travel with deep-water wave speed, $\sqrt{gD}$, and that the energy in these waves decays as $x^{-\frac{1}{2}}$ rather than as x^{-1}, so that more energy would be observed on this coast than is expected on the basis of deep-water wave amplitudes. The application of this theory to the Alaskan earthquake tsunami of 1964 will be discussed in Chapter 2.

THE C-P PROBLEM INCLUDING VISCOSITY

Sretenskiy (1941) considered the transient development of one-dimensional surface waves on a viscous fluid. Basset (1888) and Lamb (1945) studied the basic motions and classified them in three categories: (a) damped gravity waves which represent mainly a balance between gravitational and inertial forces, but with modification by viscous forces, (b) a diffusive motion which represents a primary balance between viscous and inertial forces, and (c) a creep wave, which represents a primary balance between gravitational and viscous forces. The relative importance of the three types of motion for any initial state depends on the viscous length:

$$\ell \equiv g^{-\frac{1}{3}} \nu^{\frac{2}{3}} \tag{1.134}$$

where ν is the kinematic viscosity.

Miles (1968) developed a theory for the C-P problem, including viscosity, with the aim of applying it to examine a suggestion made by Van Dorn (1968b) regarding the origin of the concentric circular ridges that surround the crater orientale on the moon. Miles considered an ocean of infinite depth and took the vertical axis, z, of the coordinate system pointing downward. The ocean is initially at rest and is subject to an impulse, $\rho\phi\,(r)$, and an initial free surface displacement, $\eta_0(r)$, at $t = 0$. The pressure, p, and the potential, ϕ, are related through:

$$p\,(r,z,t) = \rho\,\frac{\partial\phi}{\partial t}\,(r,z,t) \tag{1.135}$$

where r is the radial coordinate.

Let $r\,\psi(r,z,t)$ be the Stokes stream function (see Lamb 1945). The radial and downward components of the particle velocity, W, are:

$$\begin{aligned} u &= -\frac{\partial\phi}{\partial r} + \frac{\partial\psi}{\partial z} \\ w &= -\frac{\partial\phi}{\partial z} - \frac{1}{r}\frac{\partial}{\partial r}\,(r\psi) \end{aligned} \tag{1.136}$$

Under the assumption of infinitesimal disturbances, the linearized form of the Navier-Stokes (N-S) equations in vector form and the continuity equation are, respectively,

$$\frac{\partial \mathrm{W}}{\partial t} = -\nabla\left(\frac{p}{\rho}\right) + \nu\,\nabla^2\,\mathrm{W} \tag{1.137}$$

and

$$\nabla \cdot \mathrm{W} = 0 \tag{1.138}$$

From the above equations:

$$\frac{\partial^2 \phi}{\partial r^2} + \frac{1}{r}\frac{\partial \phi}{\partial r} + \frac{\partial^2 \phi}{\partial z^2} = 0 \tag{1.139}$$

and

$$\frac{\partial^2 \psi}{\partial r^2} + \frac{1}{r}\frac{\partial \psi}{\partial r} - \frac{1}{r^2}\psi + \frac{\partial^2 \psi}{\partial z^2} = \frac{1}{\nu}\frac{\partial \psi}{\partial t} \tag{1.140}$$

The initial conditions are:

$$\begin{aligned} \phi(r,0,0) &= \phi_0(r) \\ \eta(r,0) &= \eta_0(r) \end{aligned} \tag{1.141}$$

The total impulse acting on the surface at $t = 0$ is:

$$I = 2\pi \rho \int_0^\infty \phi_0(r)\, r\, dr \tag{1.142}$$

The potential energy associated with the initial displacement is:

$$p_{E_0} = \pi \rho g \int_0^\infty \eta_0^2(r)\, r\, dr \tag{1.143}$$

where $\eta_0(r)$ satisfies the condition

$$\int_0^\infty \eta_0(r)\, r\, dr = 0 \tag{1.144}$$

provided the displaced volume is zero.

The kinematic and dynamic boundary conditions (1.10) and (1.11) at the surface assume the following forms for this situation:

$$\frac{\partial \eta}{\partial t} = w \tag{1.145}$$

$$\frac{\partial \phi}{\partial t} + g\eta - 2\nu \frac{\partial w}{\partial z} = 0 \tag{1.146}$$

$$\nu \left(\frac{\partial u}{\partial z} + \frac{\partial w}{\partial r} \right) = 0 \tag{1.147}$$

Although, strictly speaking, these conditions should be satisfied at $z = \eta$, rather than at $z = 0$, the second alternative is taken because of its simplicity, with the understanding that the error caused is no more than the linearization of the equations of motion.

Miles (1968) used Laplace and Hankel transforms to obtain a formal solution to this problem. He considered two cases: (a) point-impulse problem and (b) initial cavity problem. In the first problem, it is assumed that the radius of the area over which the impulse is applied is negligible compared with the viscous length,

ℓ, defined in (1.134), and that the initial displacement vanishes identically. In the case of the initial cavity, a nonzero initial displacement is prescribed. Results for both cases are similar, in that the three different regimes discussed above exist. Nikitin and Potetyunko (1967) studied the C-P problem with the inclusion of viscosity, for a water body of finite depth (unlike Miles' study for infinite depth).

Chapter 2 Tsunami Generation

2.1 Tsunami-Earthquake Energy Relations, Source Areas

Tsunami Magnitude in Relation to Other Parameters

Iida (1970) followed the earlier work by Imamura (1949) to define tsunami magnitude, m, in reference to Japan, as:

$$m = \log_2 \eta_{max} \tag{2.1}$$

where η_{max} is the maximum height in meters measured at a coast 10–300 km from the tsunami origin. Iida (1956) gave the tsunami grade scale based on η (Table 2.1). Iida (1970) cataloged the earthquakes of magnitude, M, greater than 5.8 accompanied by tsunamis, in and near Japan from 1900 to 1968. The geographic distribution of the epicenters of the tsunamigenic earthquakes (classified according to tsunami magnitude, m) shows that most epicenters lie on the Pacific Ocean side of Japan (not in the Sea of Japan).

Table 2.1. Tsunami grade scale of Iida and Imamura. Depending on the requirement, this scale has been extended occasionally from -3 to 5. (Iida 1956)

Grade scale	Significance
-1	Minor tsunami with max. wave height (h) less than $\frac{1}{2}$ m
0	h is of the order of 1 m; no damage
1	h is of the order of 2 m; house damage along coast; ships washed ashore
2	h is of the order of 4–6 m; some destruction of houses; considerable loss of life
3	h is of the order of 10–20 m; damaged area along coast about 400 km
4	h is greater than 50 m; damaged area along coast more than 500 km

Iida (1963b) studied about 100 tsunamigenic earthquakes that occurred from 1700 to 1960 and produced a diagram (not shown here) showing the relation between tsunami magnitude, m, and water depth, D, at the epicenter. From this diagram, the following upperbound on tsunami magnitude can be expressed:

$$m = 1.66 \log D - 1.62 \tag{2.2}$$

where D is expressed in meters.

Iida (1963b) also investigated the relation between m and log S where S is the ratio of the water depth at the epicenter to the distance between the epicenter and the point on the coast where m is determined. This is expressed as:

$$\log S = 0.12\, m + 2.12 \tag{2.3}$$

or inversely

$$m = 8.33 \log S - 17.0 \tag{2.4}$$

These relations show that tsunami magnitude is proportional to the slope, S, of the sea bottom at the epicenter and that the water depth, D, at the epicenter has more influence on m than the distance of the epicenter to the coast.

The tsunami grade magnitude scale discussed above was originally devised for tsunamis with sources within 600 km of the Sanriku coast. This scale is not linear, even after the logarithmic transformation. Adams (1974) devised a new tsunami magnitude scale, based on the logarithm to the base of 2, of the run-up expected at 1000 km from the epicenter. He called this the "logarithmically linear scale" of tsunami magnitude. This scale is better than the tsunami grade magnitude scale, because data are reduced to a fixed epicentral distance, even if not observed there. The linearly logarithmic scale also includes a correction for geometrical spreading.

The Concept of "Tsunami Intensity"

Soloviev (1970, p. 152) pointed out the inappropriateness of the usage "tsunami magnitude." He stated:

> "If seismological terminology is applied to description of tsunamis, the grades of the Imamura–Iida scale must be designated as the intensity of the tsunami and not its magnitude. This is because the latter value must characterize dynamically the processes in the source of the phenomenon and the first one must characterize it at some observational point ... the nearest point to the source included."

Another important point made by Soloviev was the distinction between the mean height, $\bar{\eta}$, and the maximum height, η_{max}, of tsunami inundation. This distinction is necessary because, although it is the mean height that is relevant for the estimation of tsunami energy, in older descriptions of tsunamis emphasis was given to the maximum height. The differences between mean height and maximum height could be mostly attributed to topography. Figure 2.1 shows the relation between $\bar{\eta}$ and η_{max} for different tsunamis.

Soloviev defined tsunami intensity, i, as:

$$i = \log_2 (\sqrt{2}\, \eta) \tag{2.5}$$

Compared to (2.1), (2.5) differs in three respects. First, instead of magnitude, m, intensity, i, appears. Second, the maximum height, η_{max}, is replaced by the average height, $\bar{\eta}$. Third, the factor, $\sqrt{2}$, was introduced to account for the average difference in the maximum and mean heights of tsunamis of different intensities.

Tsunamigenic and Nontsunamigenic Earthquakes

Iida (1970) studied the relation between earthquake magnitude, M, and focal

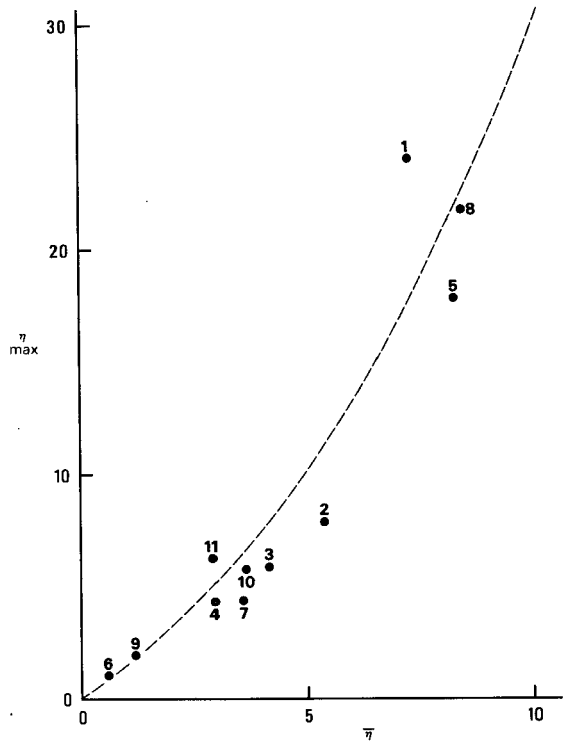


FIG. 2.1. Correlation between maximum η and mean $\bar{\eta}$ heights of tsunamis (m). **1.** Sanriku, 1933; **2.** Tonankaido, 1944; **3.** Nankaido, 1946; **4.** Tokachi-Oki, 1952; **5.** Kamchatka, 1952; **6.** Boso, 1953; **7.** Iturup, 1958; **8.** Chile, 1960; **9.** Urup, 1963; **10.** Alaska, 1964; **11.** Niigata, 1964. (Soloviev 1970)

depth, H, of submarine earthquakes that occurred from 1926 to 1968 in and near Japan (Fig. 2.2). The solid line represents the boundary between tsunamigenic and nontsunamigenic earthquakes, i.e. tsunamigenic earthquakes occur to the right side of this line. This (lower) limiting magnitude for tsunamigenic earthquakes is expressed as:

$$M = 6.3 + 0.005\ H \tag{2.6}$$

where the focal depth, H, is expressed in km. However, there are three tsunamigenic earthquakes to the left of the solid line (not shown here). If these are included then the smallest magnitude of a tsunamigenic earthquake is given by:

$$M = 5.6 + 0.01\ H \tag{2.7}$$

Iida (1970) also gave the following relation for the lower limit for the magnitude of earthquakes which have generated disastrous tsunamis (i.e. tsunamis of magnitude > 2):

$$M = 7.7 + 0.05\ H \tag{2.8}$$

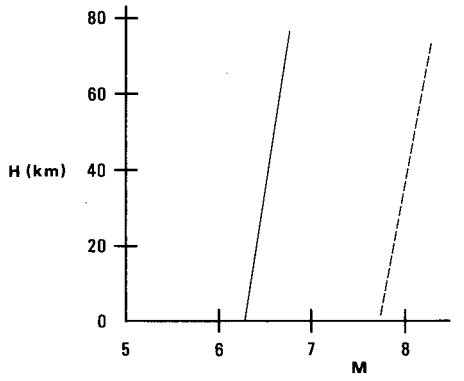


FIG. 2.2. Relation between earthquake magnitude and focal depth of submarine earthquakes, 1926–68. (Iida 1970)

This limit is shown by the dashed line in Fig. 2.2.

In the data represented in Fig. 2.2, there were 79 earthquakes with magnitudes greater than given by (2.6) and yet they were not followed by tsunamis. Of these, 32 were aftershocks and 15 were relatively deep-focus shocks. Both types are unlikely to produce tsunamis. Iida used the concept of faulting to explain the fact that the remaining 32 earthquakes were nontsunamigenic.

For these 32 earthquakes, Iida considered focal-plane solutions. Radiation patterns from both P and S waves were used, and faulting along the nodal plane was assumed, to calculate the dip and strike components of the unit vector of motion because of faulting. The faulting is classified as dip-slip type if the dip component exceeds the strike component. The reverse situation is called strike-slip. Iida found that for more than 60% of the tsunamigenic earthquakes studied, faulting was the dip-slip type.

Iida (1970) investigated the relation between earthquake magnitude and tsunami magnitude classified according to the type of faulting. He concluded that tsunami magnitude is proportional to earthquake magnitude and that most large tsunamis result from earthquakes associated with dip-slip faulting. For other detailed studies on Japanese tsunamis see Hatori (1970) and Watanabe (1970). For the source mechanism of tsunamigenic and nontsunamigenic earthquakes in the northwest part of the Pacific Ocean see Balakina (1970).

SEISMIC ENERGY VERSUS TSUNAMI ENERGY

Iida (1963b) gave the following relation between earthquake magnitude, M, and tsunami magnitude, m:

$$m = (2.61 \pm 0.22)\,M - (18.44 \pm 0.52) \tag{2.9}$$

Gutenberg and Richter (1956) gave the following relation between M and seismic energy, E_s (expressed in ergs):

$$\log E_s = 11.8 + 1.5\,M \tag{2.10}$$

From these two equations, one can write:

$$\log E_s = 22.4 + 0.6\, m \tag{2.11}$$

or

$$E_s = E_0 \times 10^{0.6m}$$

with

$$E_0 = 2.5 \times 10^{22} \text{ ergs} \tag{2.12}$$

Takahasi (1951) gave the following relation between tsunami magnitude, m, and tsunami energy, E_t:

$$E_t = E_0' \times 10^{0.6m} \tag{2.13}$$

with

$$E_0' = 2.5 \times 10^{21} \text{ ergs}$$

In Takahasi's method, the tsunami energy is estimated from the following relation (based on symmetry, for example Equation (1.143)):

$$E_t = \pi\, \rho\, g\, r \sqrt{gD}\ (\bar{\eta})^2 \tau \tag{2.14}$$

where g is gravity, ρ is water density, r is the distance between the observation location and tsunami source, D is the water depth at the observation point, $\bar{\eta}$ is the average observed height of tsunami, and τ is the duration of tsunami.

From (2.9) and (2.13)

$$\log E_t = 21.4 + 0.6\, m = 10.3 + 1.5\, M \tag{2.15}$$

Hence, comparing (2.11) with (2.15)

$$\frac{E_s}{E_t} = \frac{E_0}{E_0'} = 10 \tag{2.16}$$

Thus, about a tenth of the seismic wave energy appears as tsunami energy. Table 2.2 supports this statement quite well (actually E_s/E_t has been observed to vary over a substantial range with an average value of about 10).

TABLE 2.2. Tsunami energy, E_t, versus seismic wave energy, E_s. (Iida 1963a)

Earthquake	Magnitude (M)	Seismic wave energy (E_s) 10^{23} *ergs*	Tsunami energy (E_t) 10^{23} *ergs*
Chile, May 22, 1960	8.5	35.5	3.0
Sanriku, Mar. 2, 1933	8.3	17.8	1.7
Nankaido, Dec. 20, 1946	8.1	8.9	0.8
Tokachi, Mar. 4, 1952	8.1	8.9	0.8
Tonankai, Dec. 7, 1944	8.0	6.3	0.79
Aomori, Feb. 10, 1945	7.3	0.56	0.004

Iida (1963a) gave the following empirical relation between earthquake magnitude, M, and the area, A, of aftershock activity (expressed in km^2).

$$\log A = 0.9\,M - 3.0 \tag{2.17}$$

He also deduced that the area over which crustal deformation occurs (which might lead to tsunami generation) is equal to the area of aftershock activity. However, care should be taken to treat this as a specific rather than as a universal result.

For Pacific Ocean tsunamis, Soloviev (1970) gave the following relation between τ (duration of tsunami), its intensity, i, and earthquake magnitude, M:

$$\log \tau = -0.6 + 0.12\,i + 0.24\,M \tag{2.18}$$

Soloviev also deduced the following relation between tsunami frequency, n, and tsunami intensity, i:

$$\log n = k_1 - k_2\,i \tag{2.19}$$

where $k_2 = 0.31$. He prepared a table (Table 2.3) and listed the coefficients a and b (for different geographic regions on the globe) of the following formula which expresses the relation between earthquake magnitude, M, and earthquake frequency, N.

$$\log N = a - bM \tag{2.20}$$

TABLE 2.3. Data on recurrence of earthquakes and tsunamis in the Pacific Ocean. (Soloviev 1970)

Zone	a	b	T
Aleutian Is. & southwest Alaska	8.43	0.92	-0.15
Kamchatka & Kuril Is.	8.72	0.96	-0.2
Hokkaido	8.90	0.82	-0.1
East Honshu	9.21	1.08	-0.4
South Japan	6.80	0.80	-0.1
Japan Sea	7.07	0.86	+0.1
Ryukyu Is.	7.68	0.92	-0.4
Taiwan	8.24	1.20	-0.6
Luzon	7.84	0.96	0.0
Southwest Philippines	5.27	0.60	+0.1
Philippine Deep	7.05	0.80	-0.1
Talaud & Sangihe Is.	5.52	0.60	-0.1
Banda Sea	6.06	0.70	+0.2
Sulawesi & Kalimantan	7.86	1.00	+0.4
Djawa & Lesser Sunda Is.	8.63	1.10	-0.1
Sumatera	6.23	0.68	0.0
Irian	5.75	0.68	+0.1
New Britain & North Solomon Is.	7.35	0.80	-0.3
South Solomon Is.	6.67	0.75	-0.1
Santa Cruz & New Hebrides Is.	8.04	0.90	-0.2
Fiji Is.	7.00	0.84	0.0
Samoa, Tonga, Kermadec Is.	10.70	1.30	-0.45
New Zealand, North Is.	7.58	0.94	0.0
Chile & Peru	7.67	0.85	+0.15
Central America & Mexico	7.85	0.84	-0.35
California	7.20	0.90	0.0
Canada	7.94	1.00	0.0
Hawaiian Is.	7.00	0.92	+0.5

Soloviev also defined the following parameter:

$$T = \frac{\log n(0)}{N(7\frac{1}{2})} \tag{2.21}$$

where $n(0)$ is the frequency of tsunamis with zero intensity, and $N(7\frac{1}{2})$ expresses the frequency of earthquakes with magnitude $7\frac{1}{2}$. Soloviev interpreted the parameter, T, as the ability of earthquakes in a given region to generate tsunamis. Table 2.3 lists values of T for various regions.

According to Soloviev, the difference in tsunami probability among different regions can probably be accounted for by the peculiarity of tectonics of zones. In zones of block tectonics with rigid superficial layers and superficial seismic activity, the probability of an earthquake exciting a tsunami is higher than in zones of so-called arc tectonics with relatively mild superficial layers and somewhat buried seismic activity.

Methods of Estimating Tsunami Energy

Generally speaking there are four methods to estimate tsunami energy: (1) based on propagation of tsunami waves from the generation area, (2) knowing the vertical displacement at the generation area, (3) from the empirical relation between earthquake and tsunami magnitude, and (4) knowing the maximum predominant period of a tsunami.

The first (Takahasi) method has been described earlier. In the second method, the principle that the earthquake causes the sea bottom to move vertically is used, and the work partly goes into increasing the potential energy of sea water while the rest goes into generation of tsunami. The work done against the hydrostatic bottom pressure, $\rho g D$, is:

$$E_1 = \rho g \sum_S b D \, dS \tag{2.22}$$

where D is the water depth, b is the vertical displacement of a small portion, dS, of the sea bottom. The work done that goes into increasing the potential energy of the water is:

$$E_2 = \rho g \sum_S b\left(D - \frac{b}{2}\right) dS \tag{2.23}$$

Hence, the energy, E, transformed into tsunami is:

$$E = E_1 - E_2 = \tfrac{1}{2} \rho g \sum_S b^2 \, dS \tag{2.24}$$

observations showed that E determined from (2.24) is probably an overestimate.

In an average sense, one can write:

$$\sum_S b^2 \, dS = b_m^2 \, A \tag{2.25}$$

where b_m is the average vertical displacement and A is the area of dislocation at the tsunami origin. From (2.24) (2.25)

$$E = \tfrac{1}{2} \rho g b_m^2 \, A \tag{2.26}$$

At this stage, Iida (1963a) assumed that the area, A, of bottom dislocation is approximately equal to the area, A_s, of aftershock activity, which of course is a highly questionable assumption. He gave the following relation between A and earthquake magnitude, M:

$$\log A = 0.9\ M - 7 \tag{2.27}$$

This formula disagrees with the relation he gave in his 1963b paper (Equation (2.17)). From (2.26) (2.27):

$$\log E = 9.69 + 0.9\ M + 2 \log b_m \tag{2.28}$$

Here b_m is expressed in cm. Table 2.4 lists tsunami energy computed from this formula.

TABLE 2.4. Tsunami energy estimated from vertical displacement. (Iida 1963a)

Earthquake			Vertical displacement (m)	Tsunami energy (10^{22} $ergs$)
	Location	Magnitude (M)		
Mar. 3, 1933	off Sanriku	8.3	6.5	18
Nov. 4, 1952	Kamchatka	8.2	10.7	14
Dec. 21, 1946	off Nankaido	8.1	9.5	8
Mar. 2, 1952	off Tokachi	8.1	6.5	4
Dec. 7, 1944	off Tonankai	8.0	10.0	8
Nov. 3, 1936	off Sanriku	7.7	7.1	2.1

In the third method, the empirical relations between earthquake energy and tsunami energy were used to estimate the latter (Equation (2.13)).

In the fourth method, the empirical relation between the predominant period, T_p, of a tsunami and tsunami energy, E_t, is used:

$$\log E_t = 11.7 + 6.8 \log T_p \tag{2.29}$$

The predominant period, T_p, of a tsunami is defined by Iida (1963a) as that period with the maximum spectral intensity which can be determined from tide-gage records. Table 2.5 compares energy of different tsunamis determined by the four methods.

Grigorash and Korneva (1970) studied the effect of refraction to estimate tsunami energy based on tide-gage records. The tsunami they studied was in the Black Sea after the earthquake at Anapa July 12, 1966. The small tsunami caused by this earthquake was recorded at several tide gages on the Crimean and Caucasian Black Sea coasts. In their analysis, the tidal record from Gelendzhik was mainly used. They assumed that the average speed of the tsunami was 180 km/h^{-1} and the period of the tsunami was 38 min. When refraction near the epicenter was ignored, the energy, E_t, of the tsunami was estimated to be 6.5×10^{20} ergs, whereas

when refraction is included, the energy was estimated as 2×10^{19} ergs. Thus, ignoring refraction, one can overestimate the energy by 30 times.

TABLE 2.5. Comparison of tsunami energy from five earthquakes. (Iida 1963a)

Earthquake		Tsunami energy (10^{22} *ergs*) estimated from			
	Location	Tsunami waves	Earthquake magnitude	Tsunami magnitude	Maximum period
Mar. 3, 1933	off Sanriku	17	20	16	18
Dec. 7, 1944	off Tonankai	8	8	16	6
Dec. 21, 1946	off Nankaido	8	11	16	6
Mar. 2, 1952	off Tokachi	8	11	4	0.2
Nov. 4, 1952	Kamchatka	13	16	16	13

TSUNAMI SOURCE MOTION

Adams and Furumoto (1970) recognized the binary relation between earthquakes and tsunamis. "...either a very large tsunami is generated or none at all...."

Japanese tsunamists have paid significant attention to the association in the area of tsunami generation and area of aftershock activity (e.g. Hatori 1963). One important point made by Hatori is that the tsunami-generating areas are usually elliptical. Hatori (1970) found that the features of tsunami sources for northeastern and southwestern Japan are different. In the northeast, sources of small tsunamis are mostly located in the sea, at depths shallower than 2 km, and sources of large tsunamis lie on the steep continental slope near the trench. In southwestern Japan, sources of large tsunamis lie near the coast. The major axes of source areas are parallel to the island arcs. The dimension of the source area of a tsunami generated by a deep earthquake is considerably smaller than that from a shallow earthquake. Watanabe (1970) studied the tsunamigenic earthquakes in and near Japan for 1900–68 and placed special emphasis on the tsunami source, area of aftershocks, magnitude of earthquakes, and type of faulting.

Van Dorn (1964) determined the source mechanism of the Alaskan earthquake tsunami of March 1964, based on crustal dislocation following the earthquake, the behavior of the water immediately following the earthquake, and the tsunami record at Wake Island. He found that enormous areas have undergone relatively large vertical changes in elevation relative to sea level. Virtually the entire Kenai Peninsula, from the Turnagain Arm of Cook Inlet, including the Kenai–Kodiak Ridge, and Kodiak Island itself, appears to have subsided by 0.6–1.8 m (Fig. 2.3). At the same time, most land areas along the sea coast from the Yakutat area to the center of Prince William Sound have been elevated by similar amounts. The axis about which this dipolar movement occurred is shown in Fig. 2.3.

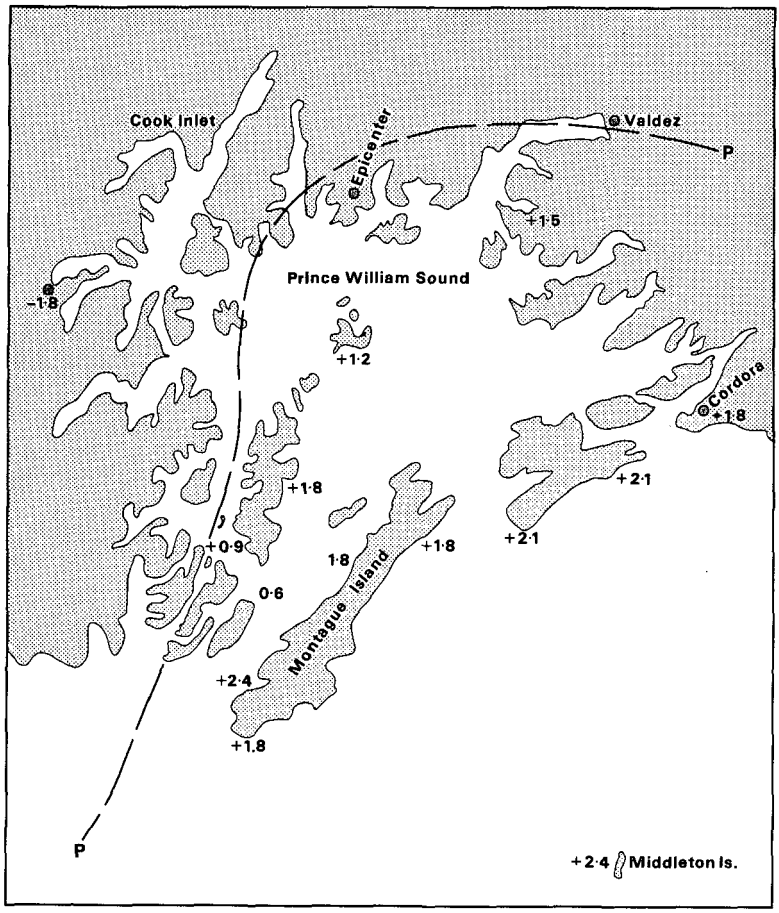


FIG. 2.3. Land elevation changes near the epicenter following 1964 Alaska earthquake. (Van Dorn 1964)

Regarding the pattern of water movement, Van Dorn stated that there was relatively little exchange of energy between Prince William Sound and the Gulf of Alaska, because the Sound is virtually cut off from the Gulf by a group of islands. Van Dorn analyzed the tsunami record at Wake Island (6052 km from the epicenter) and concluded that a large fraction of the tsunami energy was contained in a solitary wave formed in the Gulf of Alaska.

Pararas-Carayannis (1967) studied the source mechanism of the 1964 Alaskan earthquake tsunami somewhat along the same lines as Van Dorn (1964). Although his results generally agree with those of Van Dorn, there are some differences. He estimated the total area of displacement by the earthquake to be 215,000 km^2. Van Dorn has not given any corresponding value, at least explicitly. The energies of the tsunami were estimated by the authors as 5.88×10^{21} ergs (Pararas-Carayannis) and 2.3×10^{21} ergs (Van Dorn).

Pararas-Carayannis also supported the contention of the Japanese tsunamists that the area of major aftershock activity and the generation area of tsunamis roughly agree. To support this, he stated that about 52 aftershocks occurred following the 1964 Alaskan earthquake, the areas agreeing with tsunami source area.

Van Dorn attributed the tsunami to the tectonic movement caused by the earthquake, but Pararas-Carayannis, although agreeing with Van Dorn about the tsunami in the Gulf of Alaska, argued that in Prince William Sound waves were generated by slumping and landslides, in addition to the tectonic mechanism. He reasoned that if the tsunami was only generated by tectonic movement, then the first wave would be the highest. However, observations showed that at Uzinki, Kodiak City, Women's Bay, and other places on Kodiak Island, the third and fourth waves were highest. In fact, Pararas-Carayannis identified two different major tsunamis in Prince William Sound, one at Montague Island and the other at Port Valdez.

Pararas-Carayannis (1967, p. 308), however, was careful not to attach too much importance to the second mechanism. He stated:

> "Slumps or avalanches, similar to the ones that occurred in Prince William Sound, are usually localized; they can produce no large tsunamis that would travel across wide portions of the ocean. According to Wiegel (1954), not more than 2% of the potential energy of a falling or sliding body is converted into wave energy. In Prince William Sound however, slumping and sliding when added to tectonic movements created tsunami waves of very large energy, but their effect was catastrophic only locally; very little of the energy escaped the Sound."

Van Dorn (1963) determined the source mechanism of the tsunami caused by the Aleutian earthquake of Mar. 9, 1957. The principle used was to take the wave record at Wake Island and calculate its spectrum. By inversion of the Kanzer–Keller solution (Chapter 1) the spectrum at the source was obtained. He found that the tsunami source was a circular depression and had displaced a total volume of 2.3×10^{10} m^3. About 4% of the seismic energy had gone into tsunami energy.

Sokolowski and Miller (1970) developed a simple technique for identification of tsunami source region from a single seismic record. Although this method might not work universally, it has the merit that (where it works) it can be used in real time prediction. Sokolowski and Miller (1970, p. 135) described the principle of their method:

> "In selected cases, there appears to be a similarity between seismic records of earthquakes which occur within a small source region. This similarity exists only between the record of a given seismograph station, not between the records of earthquakes recorded at different stations. If this similarity is consistent, it may be possible to identify in real time the particular fault system in which an earthquake occurs, assuming a sufficient amount of reference data exists. As the net ground motion along a given fault is typically consistent, it should be possible to improve the estimation of tsunami generation."

In Chapter 3, the T-waves produced by an earthquake will be considered. Johnson (1970) proposed a method to determine the rupture length following an earthquake, by T-phase data. Johnson believed that rupture length is better than

earthquake magnitude as an indicator of the tsunami-generating potential of an earthquake. Certainly this presents a different viewpoint and should be seriously considered.

Johnson and Norris (1968), during their study of a series of Aleutian earthquakes starting Feb. 4, 1965, showed that T-phase source solutions appeared in groups about some points along the Aleutian ridge. These cluster points were referred to as T-phase radiators and, according to the authors, a major earthquake will excite T-phase radiators in a sequence as the rupture progresses along the fault. Eaton et al. (1961) proposed that the duration of the T-phase can be used to estimate the rupture length.

Johnson and Norris (1968) studied the Fox Island earthquake swarm of Dec. 21, 1962, and showed, through study of the T-phases, that each earthquake in the swarm affected the same region of the ocean floor, but with differing strengths. They concluded that the region affected was too confined and could not generate a tsunami and their surmise proved to be correct.

It might not be feasible to collect the T-phase from different stations and coordinate it properly for practical prediction in the short time available. To overcome this difficulty, Johnson (1970) proposed that an array of hydrophones be used at a single station and the azimuth of the signal received could be calculated through cross-correlation analysis.

There might be some difficulty in determining precisely the duration of the T-phase (defined as the time between the arrivals of the T-phase from the first and last radiator excited by the main shock) when aftershocks are present. Johnson proposed to rectify this by a correlogram that would show a monotonic variation in the azimuth of the peaks.

Ionospheric recording of Rayleigh waves due to earthquakes (e.g. Yuen et al. 1969) can be used to determine the source mechanism. This method will be especially advantageous for the real time tsunami prediction problem, because other seismic methods of determining the source mechanism through P or S wave analysis might be impractical in the short time available.

Furumoto (1970) proposed that Rayleigh waves recorded by ionospheric Doppler effects could be studied through the surface wave analysis technique developed by Brune et al. (1960), to yield information on the source mechanism. The success of this method will depend on a prior knowledge of the dispersive properties of the medium between the epicenter and the seismic recording station. For details of the surface wave analysis see Brune et al. (1960).

2.2 Tsunami Generation by Earthquakes

In Section 1.2 the classical C-P problem and the theories of Kranzer and Keller, and Kajiura were considered. In this section, the application of the C-P problem to tsunami generation following occurrence of an earthquake will be discussed. Special emphasis will be given to numerical models that simulate tsunami generation much more realistically than analytical models.

Analytical Models

Modifications to the classical C–P problem — Carrier (1971) developed an analytical theory for the generation and propagation of tsunamis and applied this to the 1964 Alaskan earthquake tsunami. Two important results emerged: (1) for tsunami source areas of considerable breadth dispersion is not important, whereas for narrow initial displacements it is extremely important; (2) if the statement that the second or third crest is higher than the first is valid, then the ground displacement must consist of elevation and subsidence and not just elevation.

Podyapolsky (1970) developed a theory for tsunami generation by treating the crust of the earth as an elastic solid half-space and treating the ocean as an elastic liquid in a uniform field of gravity. Displacement of the ocean bottom following the earthquake was considered small compared to the uniform depth of the ocean. He concluded that the differences between his theory and the relatively simpler classical theory are insignificant for periods of the order of 10^4 s, but for tsunamis with periods up to 10^3 s, the classical theory is adequate.

Cherkesov (1965, 1966a, 1968) and Fedosenko and Cherkesov (1968) studied the effect of inhomogeneity of the ocean on tsunami waves. They showed that the effect of stratification on tsunamis is not significant. One interesting conclusion of Cherkesov's 1965 paper is that secondary tsunamis could be caused by nonuniformity such as depth discontinuities, when a density discontinuity occurs simultaneously. Cherkesov (1970) investigated the effect of viscosity on tsunami generation and propagation and showed that viscosity reduces the maximum wave amplitude at some point far from the source area; this reduction factor depends on shallow-water and deepwater depths. Also, viscosity influences low water after the arrival of the main crest of the tsunami.

Numerical Models for Tsunami Generation

Compared to analytical theories available for tsunami generation, numerical models aimed at simulating tsunami generation are few. Aida (1969a, b) used numerical modeling to study the tsunamis caused by the 1964 Niigata and 1968 Tokachi-Oki earthquakes. The computed water levels at two stations agreed reasonably well with observed levels (Fig. 2.4). Aida (1969a) assumed instantaneous deformation of the bottom, whereas in his 1969b paper he considered progressive deformation. These numerical experiments threw some light on the important question of directivity coefficient, defined as the ratio of the heights of the waves radiated in opposite directions. The directivity coefficient depends on the speed of the bottom deformation in the horizontal plane. If the depth decreases in the direction of progress of the bottom deformation, then the directivity coefficient increases in that direction.

Hwang and Divoky (1970, 1971, 1972) numerically simulated the tsunami generation and propagation following the 1964 Alaskan earthquake. Hwang et al. (1970a) performed numerical experiments to simulate the tsunami generation caused by the underground nuclear explosions "Milrow" and "Cannikan" and the Rat Island earthquakes. Hwang et al. (1970b; 1972a, b) simulated the tsunamis due to the Alaskan earthquake of March 1964, the Chilean earthquake of May 1960,

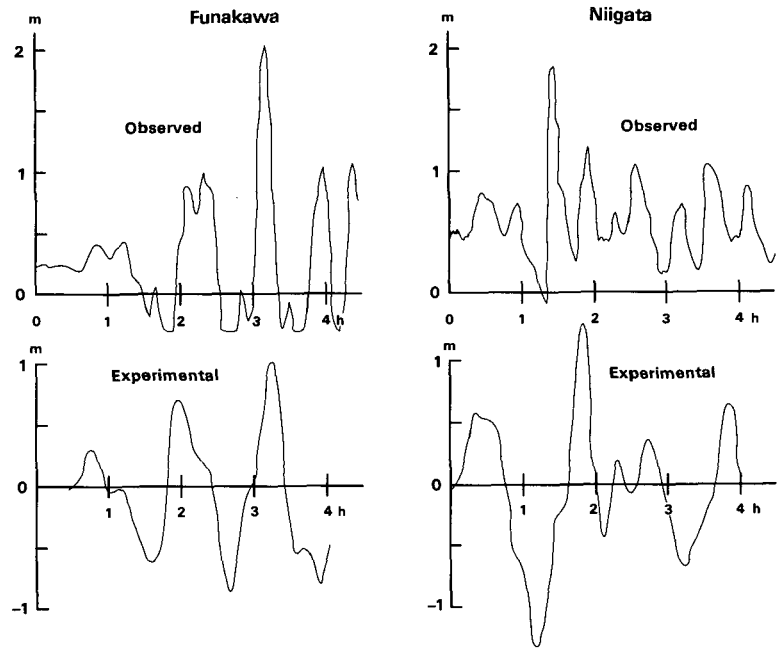


FIG. 2.4. Comparison between observed and computed wave forms of the Funakawa and Niigata tsunamis. (Aida 1969a)

and the Andreanof earthquake of 1957.

Hwang et al. (1970a) assumed that a portion of the sea bottom moves as:

$$Z = -\xi(x,y,t) \tag{2.30}$$

The continuity equation is:

$$\left(\frac{\partial \eta}{\partial t} - \frac{\partial \xi}{\partial t}\right) + \frac{\partial}{\partial x}\left\{(D - \xi + \eta)\, U\right\} + \frac{\partial}{\partial y}\left\{(D - \xi + \eta)\, V\right\} = 0 \tag{2.31}$$

where U and V are the vertically averaged velocity components in the x and y directions, D is the water depth, η is the water level relative to its equilibrium position, and ξ is the displacement of the ocean bottom. The horizontal equations of motion, with the inclusion of the convective acceleration terms but the neglect of friction and Coriolis terms (in later models they included Coriolis terms and spherical polar coordinates), along with the continuity equation, form a set of three equations for the three variables U, V, and η.

The finite difference forms of these equations, suitable for numerical integration in time, were adapted from Leendertse (1967). Each time step was split in half. In the first half step, η and U were computed implicitly whereas V was computed explicitly and this process goes from time step $n\,\Delta t$ *to* $(n+\frac{1}{2})\,\Delta t$. During the progression to $(n+1)\,\Delta t$, η and V are computed implicitly and U is computed explicitly. Inclusion of the Coriolis terms needs special attention because U term occurs in the V momentum equation and vice versa.

Hwang and Divoky (1970) numerically simulated the tsunami created by the 1964 Alaskan earthquake and prescribed the following bottom displacement: let (a,b) and (i,j) denote the coordinates (with reference to a Cartesian system) of the epicenter of the main shock and some point in the source region. Then the vertical motion at (i,j) is assumed to start at time

$$t_{i,j} = \frac{\Delta x}{V_p}\left\{(a-i)^2 + (b-j)^2\right\}^{\frac{1}{2}} \tag{2.32}$$

where Δx is the grid spacing and V_p is the velocity with which the rupture propagates. Plafker and Savage (1970) estimated V_p to be 3–4 km/s.

The bottom displacement is prescribed as follows:

$$\xi_{i,j}(t) = \begin{cases} 0 \text{ for } t \leq t_{i,j} \\ \xi'_{i,j} \sin^2 \left\{\dfrac{\pi(t-t_{i,j})}{2\tau}\right\} \text{ for } t_{i,j} \leq t \leq t_{i,j} + \tau \\ \xi'_{i,j} \text{ for } t \geq t_{i,j} + \tau \end{cases} \tag{2.33}$$

Here τ is a characteristic time scale of ground motion. Berg and Housner (1961) estimated $\tau \sim 10$ s generally. The parameter $\xi'_{i,j}$ is the permanent displacement at i,j following the earthquake.

Figure 2.5 shows the positions of the leading wave of the tsunami at successive times (in seconds). The dotted area represents the tsunami source region. For large travel distances, instead of a Cartesian system, spherical polar coordinates were used (Hwang and Divoky 1975).

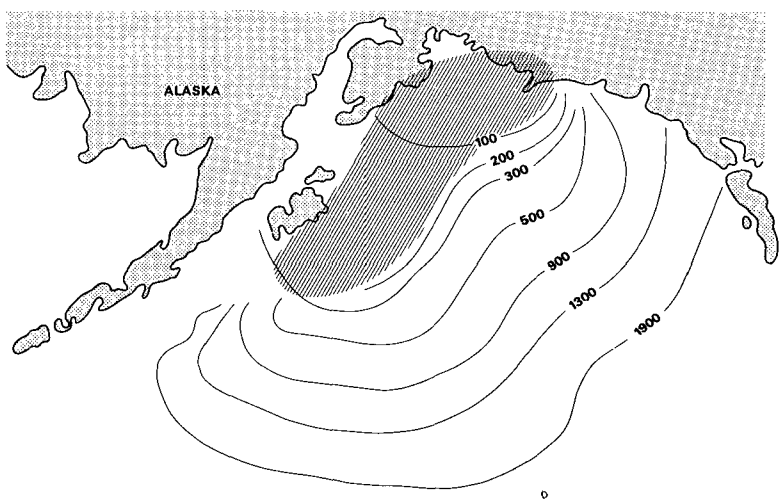


FIG. 2.5. Position of leading disturbance of the Alaskan tsunami at successive times (in seconds) (region of ground motion shaded). (Hwang et al. 1970b)

Although use of a spherical polar coordinate system makes the model more sophisticated, nevertheless, there are some uncertainties in the boundary conditions. Usually, a condition of complete reflection is adopted at closed boundaries, mainly for simplicity. This is not a good assumption because limited evidence indicates tsunami energy is lost at a rate of roughly 60% per shoreline interaction (Munk et al. 1962). A better condition should incorporate such a dissipative factor into the model. The condition at open boundaries is more difficult to specify. The physical requirement is that the wave be totally transmitted through the boundary, but this cannot be achieved without computation beyond the boundary. An artifice sufficiently accurate is to assume that the wave profile travels without change of form across the final space grid point. Figure 2.6 shows the position of the leading wave of the tsunami at several times, following the Chilean earthquake of May 1960. The dotted area shows the tsunami source region.

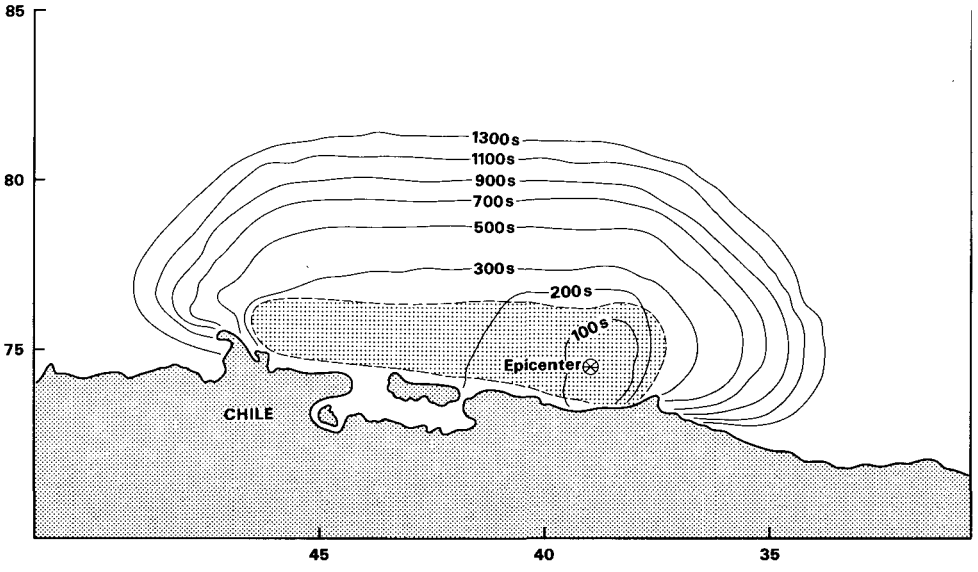


FIG. 2.6. Computed position of leading disturbance at various times, Chile 1960; region of ground displacement shaded. (Hwang and Divoky 1975)

These numerical experiments also confirmed the phenomenon of energy radiation preferentially directed normal to the major axis of the source. This directivity of radiation is dependent on the elongation of the source region. It appears that sources for large tsunamis are typically quite elongated with major axes paralleling the local coast, trench, or island arc so that generally the dominant flow of energy is seaward.

Garcia (1972) studied the generation of tsunamis due to motion on the eastern end of the Mendocino Escarpment near California. He used the complete Navier–Stokes equations and restricted his study to the first 200 s after generation. An initial single crest split in two and moved in opposite directions. He verified his numerical results against his laboratory experiment which will be briefly discussed later.

2.3 Tsunami Generation by Nonseismic Causes

Tsunami generation caused by sources other than earthquakes (such as volcanic eruptions, nuclear explosions, and landslides) will be considered.

Application of C-P Problem to Explosions at or Near the Water Surface

Terazawa (1915) studied an extended initial disturbance below the surface to simulate an underwater explosion. He assumed that the water body had infinite horizontal dimensions and infinite depth. Two different forms of initial conditions were made: he allowed first an initial surface displacement without an initial velocity, and second, an initial surface impulse without an initial surface displacement. Terazawa (1917) also considered the case when an explosion occurred below the free surface at a finite depth. However, he made at least two unrealistic assumptions: first, that either the explosion took place at such great depth or was so weak that it would not break the water surface by ejecting a column of water upward; and second, that the pressure pulse generated by the explosion was assumed to travel with infinite speed. The second assumption enabled him to use the method of images, widely used in electrostatics.

Nomura (1938) extended Terazawa's work to include water of finite depth. Unoki and Nakano (1953a, b) applied the C–P problem to the tsunamis generated by the Myojin volcanic explosions. Keller (1963) showed that a displacement at the surface is more efficient in producing water waves than an identical displacement at the ocean bottom. Levy and Keller (1963) considered instantaneous vs. noninstantaneous sources, point sources vs. extended sources, and symmetric vs. asymmetric sources.

Tsunamis Due to Volcanic Eruptions

The volcanic Myojin Reef (32°N,140°E) erupted several times in September 1952, and generated three different tsunamis (Nakano et al. 1954). The first tsunami occurred Sept. 16; the second, Sept. 24, and was probably responsible for the destruction of the survey ship *Kaiyo-Maru No. 5,* belonging to the Hydrographic Service of Japan. A third tsunami occurred Sept. 26. Lane (1965, p. 252) stated that the tsunamis attained maximum heights of 7 m.

When the volcano Sakurajima erupted in January 1914, it proved to be one of the largest volcanic eruptions in the history of Japan. The tsunami following the major eruption attained a height of about 3 m. There appears to be an association between volcanic eruptions and earthquake swarms. One example is the Ebino earthquake swarm in 1968 and its relation to the Kirisima volcanoes. These swarms generated tsunamis that caused some damage to the coasts of Miyazaki and Kooti prefectures.

The volcanic Mount St. Augustin, Alaska, erupted on Oct. 6, 1883, at about 0800 h (local time). Twenty five min after the eruption, a tsunami 7.6 ± 0.9 m high invaded Port Graham (Davidson 1884). Two waves 5.5 and 4.6 m high followed at 5 min intervals.

One of the most powerful volcanic eruptions appears to have occurred around 1450 B.C. (suggested through radio carbon dating). The volcanic island Santorin

(now called Thera) in the Aegean Sea erupted. The tsunami generated was estimated to have been over 100 m high and inundated the shorelines of the eastern Mediterranean Sea (Marinatos and Imboden 1972). According to the authors, the Santorin eruption was more violent than that of Krakatoa (83 km^2 of erupted island vs. 21 km^2).

A most devastating tsunami due to nonseismic causes occurred when the volcano Krakatoa (in the Sunda Strait between Java and Sumatra) erupted in August 1883. The major eruption occurred at 1055 h (Batavia time) on Aug. 27, and was the largest explosion in recorded history. The tsunamis following this underwater eruption were up to 30 m high and caused extensive damage on the coasts of Java and Sumatra (Lane 1965). About 36,000 people died, 295 villages and towns were inundated, and 5000 ships were destroyed. The tsunami appears to have traveled at speeds from 560 to 640 km/h. The tsunami was noticed at Port Elizabeth (Gill 1883) in South Africa (8045 km away) and there are indications that it might have arrived in the English Channel (17,700 km from Krakatoa). For details on the tsunami heights at various locations see Verbeek (1884). The period of the tsunami varied from 75 min at Negapatam (on the southeast coast of India) to 24 min at Aden. The wave amplitude varied from 0.56 m at Negapatam to 0.23 m at Aden. No tide-gage disturbances were observed at Singapore, only one-third the distance of Negapatam. There appears to be two reasons for this. First, the directivity of the tsunami was such that its energy was concentrated toward the Indian Ocean (and not toward Singapore) and second, many shallow areas and islands between Krakatoa and Singapore could have dissipated the tsunami.

The tsunami was also recorded (Boutelle 1884) at Kodiak, Alaska, and at Saucelito, near San Francisco. One curious result was that, although Kodiak is 2370 km closer to Krakatoa than San Francisco, it felt less impact of the tsunami. Also, the tsunami appeared to have arrived earlier at San Francisco than at Kodiak, which probably can be explained by the different paths traveled by the tsunami.

Earlier explanations of the tide-gage disturbances following the Krakatoa eruption were based on the travel of the tsunami as a long gravity wave, whereas later theories also included the important phenomenon of atmospheric–oceanic coupling. The Royal Society prepared an extensive report on the various aspects of the Krakatoa eruption (Symons 1888) and this report formed the basis for several investigations.

Ewing and Press (1953, 1955) explained the tide-gage disturbances through the concept of coupling between the atmosphere and the ocean. In their 1953 paper (p. 3) they described some important consequences of the eruption. A barometric disturbance traveled outward from the volcano and was recorded at many stations on at least three passages around the earth. Ewing and Press specifically examined the following conclusions arrived at by Captain W. J. L. Wharton (in the Royal Society Report) on the tsunami following the eruption: (1) to the north and east in the Java Sea the waves could be traced for 724 km, then were reduced to small amplitudes; (2) to the south and east the propagation was limited, not extending beyond the west coast of Australia; (3) to the west the waves traveled over great distances, reaching Cape Horn and possibly the English Channel; and (4) distur-

bances in the Pacific and Caribbean had no connection with Krakatoa, but were the results of some seismic activities.

Ewing and Press concluded that, whereas the tide-gage disturbances in the Indian Ocean could be explained as due to the tsunami, disturbances in the other oceans could be accounted for by the coupling of the barometric disturbance to the ocean. This latter assumption was based on the fact that the times of tide-gage disturbances correlated well with arrival times of either the first or second airwave.

Ewing and Press (1953) gave a table listing some stations outside the Indian Ocean where the tide-gage disturbances were observed, with the local times of arrival of the airwave, and the expected arrival time of the tsunami generated by atmospheric coupling. A correction (based on Wharton's work) was applied to the travel times to take into account the shallow region near the tide-gage station. The differences between the observed time of tide-gage disturbance and expected time of occurrence based on atmospheric coupling were generally less than 1 h. Only at St. Paul (Kodiak Island) was the difference as large as 4.5 h. Ewing and Press hypothesized that the Alaskan Peninsula and the mainland of North America, respectively, could have blocked the first and second waves.

Although Ewing and Press (1953, 1955) proposed the mechanism of air coupling they did not resolve the subsequent problems their hypothesis raised. They mentioned they were investigating whether a free wave in the ocean with a phase speed of 1100 km/h (the phase speed of the Krakatoa airwave) is possible and whether significant coupling of atmosphere to ocean could occur even though there is no resonance.

Press and Harkrider (1966) considered this problem and calculated the acoustic-gravity modes (described in Chapter 6) for an ocean of uniform depth of 5 km, underlying an atmosphere with many isothermal layers. This calculation (Press and Harkrider 1962; Harkrider 1964) revealed that free waves with phase velocities close to long gravity waves in the ocean do exist in the atmosphere and these could efficiently transfer energy to the oceanic modes.

To prove that the atmospheric mode did excite the ocean mode, Press and Harkrider (1966) plotted the ratio of the water level deviation to the atmospheric pressure at sea level as a function of the phase velocity, and found resonant peaks corresponding to all gravity modes.

Garrett (1970), although agreeing with Harkrider and Press (1966, 1967) on some counts, disagreed on others and offered, in my opinion, a correct explanation. Garrett (1970, p. 44) questioned the possibility of the airwave having the same phase speed as the ocean wave generated by the Krakatoa eruption, and elaborated on his skepticism as follows:

> "There are certain difficulties associated with the mechanism proposed by Harkrider and Press, notably those connected with the difference between the phase and group velocities of the atmospheric gravity wave, and with horizontal variations in ocean depth, but it suffices to point out that their theory is inconsistent with many of the observations."

Garrett proposed that free ocean waves are produced by the atmospheric pressure pulse at any abrupt change in the depth of the ocean (e.g. the continental slope), and he satisfactorily accounted for the observed tide-gage disturbances.

According to the inverse barometer effect, 1 millibar (mb) of surface pressure corresponds to an amplitude of about 1 cm. The atmospheric pressure wave from Krakatoa was probably a few mb, but as the tide gages are situated usually in shallow water, the forced displacement of the sea surface due to the pressure wave would be much less than 1 cm, and undetectable.

Garrett then considered free waves generated at a depth discontinuity. Compared to the wavelength of the airwaves from the Krakatoa eruption, the continental slope can be treated as an abrupt depth discontinuity, rather than a gradual variation of depth. Thus, in the course of traveling over the ocean to the coast with an amplitude of a few mb, a pressure pulse can produce a transmitted free wave with an amplitude of several cm and can be detected. Shallowing and resonance, could amplify this even further.

Before comparison with observed data, the highlights of Garrett's theory will be briefly summarized. The atmospheric pressure pulse from Krakatoa could generate at the continental slope free ocean waves of sufficient amplitude to be detectable by coastal tide gages. When the airwave arrives from the ocean to the land, the first sea wave could be thought of as a free wave generated at the continental slope, but when the airwave travels from the land to the ocean, the sea wave is hardly detectable (available data indicate this). Sea waves arriving at later stages may be explained as free waves generated either at the opposite side of the ocean or at some other major depth changes in the ocean so these depth changes may focus the long waves at certain places, enhancing their amplitude.

Let t_o, t_s, and t_a, respectively, be the times when the airwaves pass the tide gage, the travel time of the sea wave from the continental slope to the tide gage, and the travel time of the airwave from the continental slope to the tide gage. Then the expected time of the sea wave at the tide gage is $t_o + t_s - t_a$ which is strictly true only for normal incidence. But as $t_a << t_s$, the sea wave is expected approximately at time, t_s, after the arrival of the airwave. This agrees with the conclusions arrived at by Ewing and Press (1953) based on Wharton's data, bearing in mind that Ewing and Press considered only the first arrivals. Also, some identifications of the disturbances by Wharton on the tide-gage records are open to doubt, according to Garrett.

Garrett (1970) was surprised that the extensive Royal Society Report by Symons (1888) contained no information on the pressure amplitude of the airwaves. However, Scott (1883) showed that in Europe the first two airwaves (one direct and the other through antipodes) had an average range of 3 mb. As Europe is roughly 90° from Krakatoa, the airwave was not the largest. It is quite possible that, with pressure amplitudes in excess of 3 mb, the airwaves could have caused the observed tide-gage disturbances.

Another conclusion of Ewing and Press (1953) was that no tide-gage disturbances were observed when the airwave traveled from the continents to the oceans. This is in agreement with Garrett's theory, because the sea wave in this case should only have $\frac{1}{5}$ the amplitude of the reverse situation, at least for normal incidence. According to Garrett, this wave should disturb the tide gage at $t_s + t_a$ after the passage of the airwave over the gage.

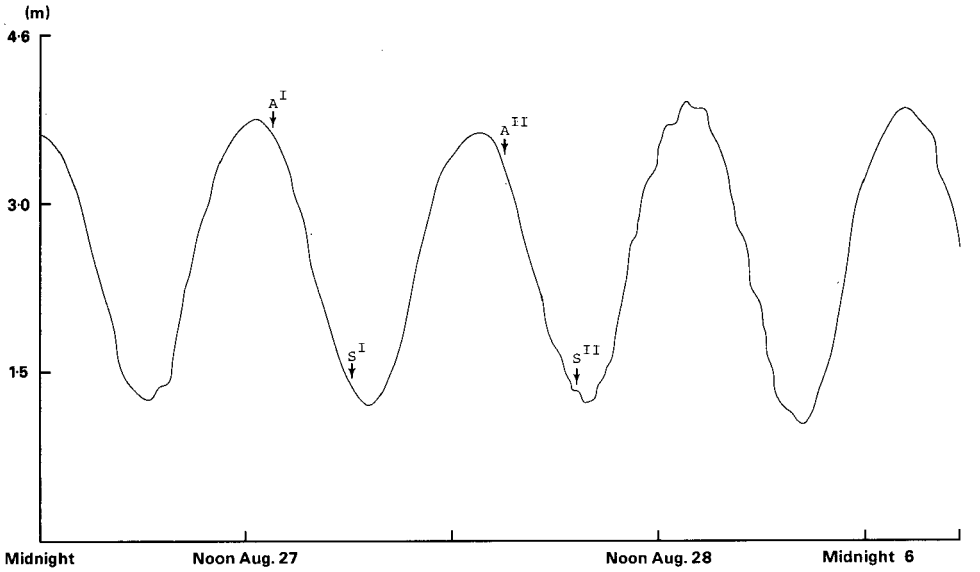


FIG. 2.7. The Devonport tide record following Krakatoa eruption. (Garrett 1970)

Figure 2.7 shows the tidal record for Devonport where the generated sea wave (when the airwaves traveled from land to ocean) was detectable. In this diagram, A^{I} and A^{II} are the arrival times of the direct airwave and the airwave through the antipodes. A^{I} is offshore and A^{II} is onshore and both were approximately normal to the continental slope. The first arriving sea wave associated with A^{II} is marked S^{II} whereas S^{I} is the first arriving sea wave associated with A^{I}. Garrett explained that the sea wave at San Francisco which arrived $5\frac{1}{2}$ h after the first (onshore airwave) probably was generated either near the Philippines, or as the airwave was passing over the Mariana Ridge south of Japan. Some contribution to the San Francisco record might have come from the refracted free waves generated by airwaves traveling over the Hawaiian Ridge and the Aleutians. The main sea wave at St. Paul (Kodiak) arrived some 13 h after the arrival of the first wave and 2 h before the arrival of the second. This sea wave might have been generated at the Philippines and then reflected off North America.

TSUNAMIS DUE TO NUCLEAR EXPLOSIONS

Garrett (1969, 1970) tried to detect the sea waves arising from the atmospheric pressure pulse caused by the large Soviet nuclear test on Oct. 30, 1961, over Novaya Zemlaya, when a 5.7×10^{10} kg bomb was detonated. No significant sea waves were detected either associated with this test or any other atmospheric nuclear test (underground nuclear tests will be considered later). To understand the energies involved in nuclear explosions and volcanic eruptions, according to Press and Harkrider (1966), a surface explosion of $100–150 \times 10^{10}$ kgm would be required to duplicate the pressure pulses generated by the Krakatoa eruption.

Van Dorn (1961) made wave measurements at Eniwetok Atoll, Wake Island, and Johnston Island during the underground nuclear explosions "Cherokee," "Zuni,"

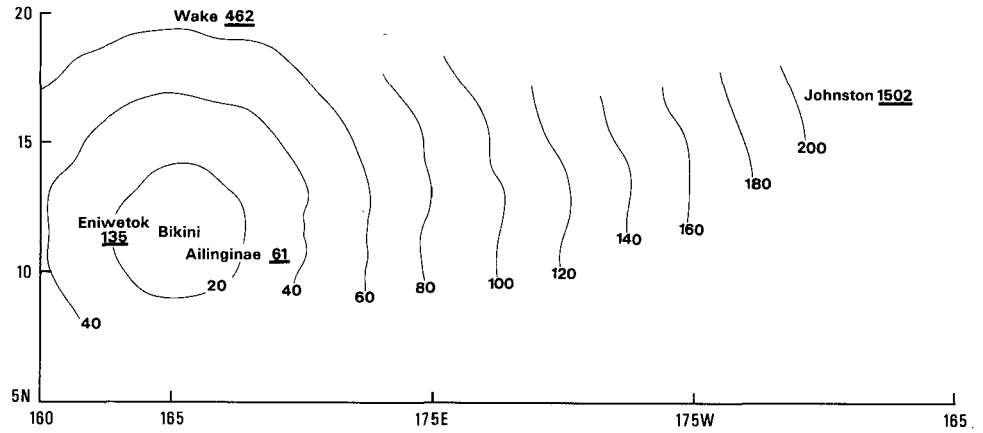


FIG. 2.8. Distribution of wave recording stations and great circle distances in kilometers from Bikini Atoll. Contours give instantaneous positions of wave front originating at Bikini at 20-min intervals. (Van Dorn 1961)

"Navaho," and "Tewa" conducted at Bikini Atoll in 1956. Figure 2.8 shows locations of the tests and observing stations, and the number below the names of observing stations are the great circle distances between that station and Bikini Atoll in nautical miles.

From the analysis of his data, Van Dorn found that the linear theory was adequate to account for the observed dispersion of these gravity waves as well as their decay with increasing distance. Van Dorn also studied the dispersion of the tsunami of Mar. 9, 1957, and it was quite similar to that of the explosion-generated waves. Thus, Van Dorn's study gave support to the contention that for a centered wave system phase dispersion does not depend on the nature of the source. Another interesting result from Van Dorn's study is that even small islands can effectively scatter the waves and a correction has to be applied in calculating

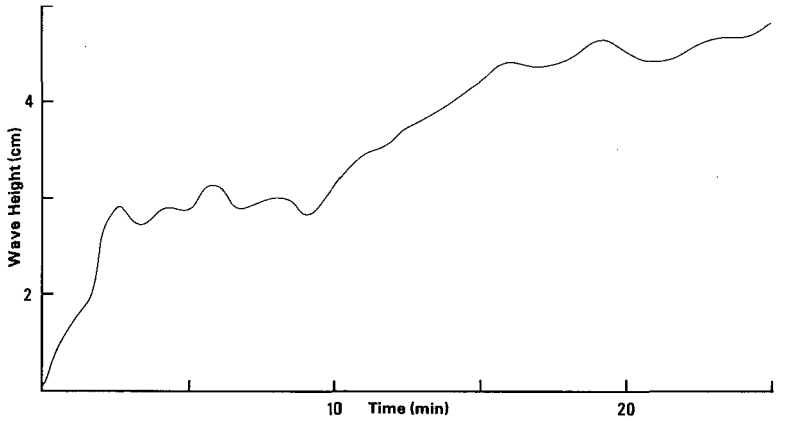


FIG. 2.9. Waves generated by the underground nuclear test Oct. 1969, Amchitka Island. (Vitousek and Miller 1970)

the rate of amplitude decay. For details on the scattering correction see Van Dorn (1961, fig. 15).

Vitousek and Miller (1970) described an instrumentation system that could be used to measure tsunami waves in the open ocean. They claimed this system is capable of functioning to a depth of 6 km. Here, only the measurements made by this system on the tsunami due to the "Milrow" underground nuclear explosion on Amchitka Island, Oct. 2, 1969, will be briefly discussed. Figure 2.9 shows the envelope of waves generated. This test, which had a yield of about 10^9 kg, produced waves only with amplitudes of a few cm. The "Cannikan" explosion on Amchitka Island in 1971, with a yield of about .5 x 10^{10} kg, did not create a significant tsunami.

Hwang et al. (1970a) performed numerical experiments to simulate the tsunamis generated by the underground nuclear explosions "Milrow" and "Cannikan." Figure 2.10 shows the contours of the water level of the tsunami generated by the Milrow

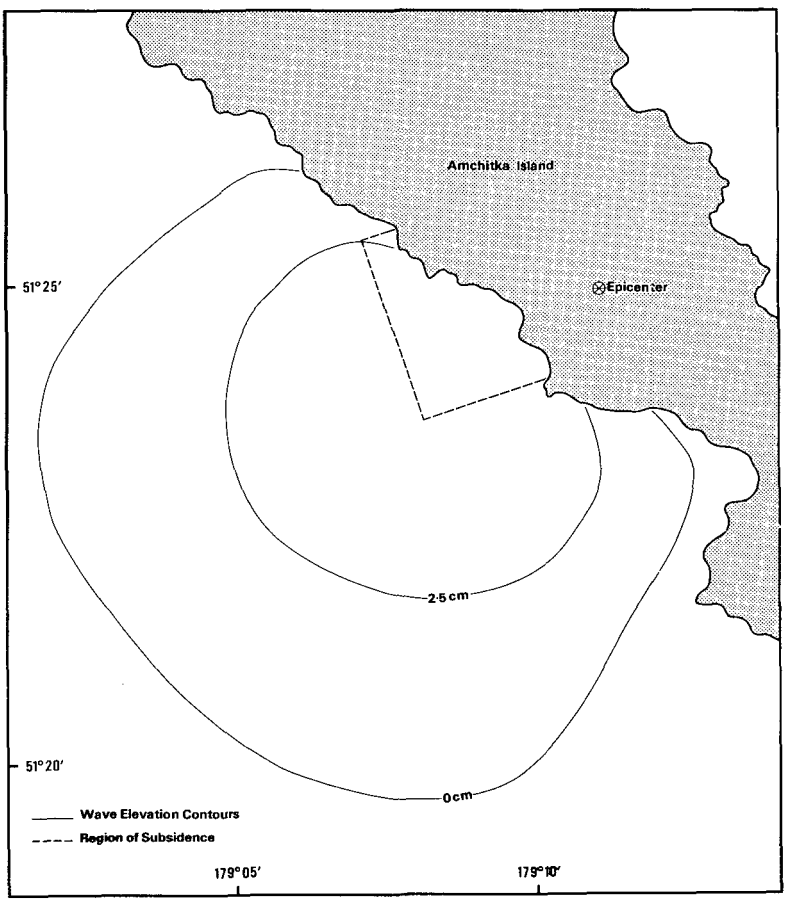


FIG. 2.10. Surface displacement contours (in cm) resulting from nuclear test on Amchitka Island. (Hwang et al. 1970a)

test, as simulated by a numerical experiment. In this diagram, the epicenter refers to the site of the explosion.

Turbidity Currents and Landslides

Although turbidity currents and tsunamis are not directly related, nevertheless, both could be caused by earthquakes such as the 1929 Grand Banks earthquake. This topic is included because it is considered part of the tsunami literature. Turbidity currents and tsunamis could also be generated by landslides whether or not an earthquake occurred.

Most submarine telegraph cables from North America to Europe pass south of Newfoundland (Heezen and Ewing 1952). At about 2032 h GCT, Nov. 18, 1929, an earthquake of magnitude 7.2 occurred on the continental slope southeast of the Cabot Trench. This generated a tsunami that caused considerable property damage and loss of life along the shores of Placentia Bay.

Another important consequence occurred during the 13 h and 17 min following the earthquake. An orderly sequence of breaks occurred in the telegraph cables to 483 km south of the epicenter. According to Heezen and Ewing (1952), although all cables along the continental slope and on the floor of the ocean south of the epicenter were broken, none on the continental shelf were disturbed. The exact times and locations of the cable breaks were known, respectively, from the telegraph records and resistance measurements.

Bucher (1940) hypothesized that erosion in the submarine canyons caused by the tsunami left the cables unsupported, thus leading to breakage. Heezen and Ewing (1952) criticized Bucher's explanation on the grounds that the cable breaks were too regular in time and the cables were of different ages and breaking strengths. In turn, they offered the following explanation (Heezen and Ewing, p. 864):

> "A severe shock jarred the continental slope and shelf, setting landslides and slumps in motion. These virtually instantaneous movements affected an area 129 by 241 km along the continental slope. These mass movements, starting on the relatively steep continental slope, raced downward, and by the incorporation of water, the moving sediment was transformed from sliding masses into turbidity currents. Undoubtedly the pattern of canyons and tributaries caused initial concentrations of the flow, but as the canyons joined the currents grew larger, quickly becoming so large that they were not restricted by the submarine canyons and eventually covered the bottom of the 322-km wide bight which lies between the southern Grand Banks and the continental slope off Sable Island. The currents had many times the force necessary to break the cables, and snapped each cable shortly after reaching it."

Plapp and Mitchell (1960, p. 983) defined a turbidity current as follows:

> "A turbidity current occurs along a sloping bottom in a large body of liquid when liquid adjacent to the bottom contains suspended sediment that causes the average density of the mixture to be greater than the density of the surrounding clear water. The current flows down the slope and may continue to flow for a long distance after it reaches a relatively level section of the bottom."

Calculations of the progress of the turbidity current following the 1929 Grand Banks earthquake was based on the orderly breaks in the cables. The first cables to break were on the continental slope. In the literature, many more details are given of this particular turbidity current and the cable breaks.

A schematic representation of a turbidity current with low and high velocity is shown in Fig. 2.11.

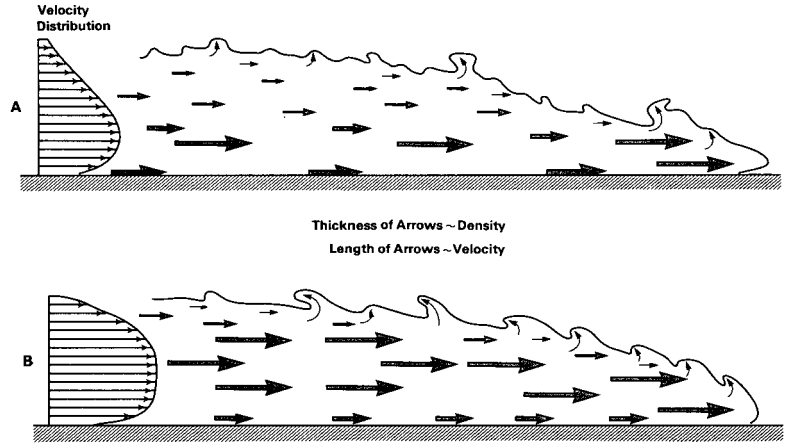


FIG. 2.11. Diagrammatic section of turbidity currents. (A) current with relatively coarse suspended load (or small velocity), (B) current with relatively fine-grained suspended load (or high velocity). (Kuenen 1956)

Heezen and Ewing (1952) showed rather convincingly that the successive series of breaks in the telegraph cables following the Grand Banks earthquake of 1929 were caused by the turbidity current generated. Heezen et al. (1954) presented additional evidence.

Kuenen (1952) agreed that turbidity currents broke the cables, nevertheless, he wondered whether velocities of up to 100 km/h are possible over hundreds of kilometers of level ground. The following estimate made by him shows that these velocities are not unreasonable.

He estimated the size, V, of the turbidity current from the relation:

$$V = C\sqrt{msd} \tag{2.34}$$

where C is a constant, s is the slope of the ground on which the current is flowing, d is the effective density, and m is a hydraulic mean depth. Actually this formula is normally used to calculate the velocity of flow in a river. As is obvious, the constant, C, which depends on friction, must be larger for the turbidity current than for river flow.

According to Kuenen, C could have maximum values to 700 or 800 cgs. He gave tables of the velocity of the turbidity current for different slopes with C = 400 and d = 0.6. He also varied C from 200 to 600 and d from 0.3 to 0.8. The maximum velocity of the turbidity current was calculated to be 101 km/h.

Heezen and Ewing (1952) estimated that the velocity of the turbidity current at the first breaking point was about 101 km/h whereas Kuenen's (1952) estimate gave an average velocity of 143 km/h. The initial slide was estimated to be 50 m thick, but the thickness of the turbidity current was estimated at 270 m, and the

average thickness of the deposited bed was 1 m. According to Kuenen, these values are reasonable and the hypothesis of turbidity current causing the breaks is sound.

Heezen and Ewing (1955) and Heezen (1963) provided some data on the break of submarine cables in the Mediterranean Sea following an earthquake in Orleansville, Algeria. The cable breaks occurred mainly in the Balearic abyssal plain.

Plapp and Mitchell (1960) developed a steady state theory for turbidity currents based on the concepts of boundary-layer flow. The driving force for the turbidity current is the excess density of the fluid in motion over that of the surroundings. In this situation the Reynolds Number will be such that the flow would be turbulent and this turbulence keeps the sediment particles suspended.

Plapp and Mitchell identified the following as the important parameters of the problem: ocean bottom slope, thickness, velocity, and density of the turbidity current.

Benjamin (1968) presented a theory of gravity currents under rather ideal conditions. He presented schematically a gravity current (also called a density current) consisting of a head wave followed by a turbulent zone where a heavy fluid flows along a horizontal bottom (Fig. 2.12A). As the density of the surrounding fluid is less than the density of the current, the piezometric pressure gradient provides the motive force.

Benjamin referred to the work of Prandtl (1952), who assumed that the velocity of the mean flow is greater than that of the front so that a portion of the stream is deflected up near the front. Benjamin also referred to the work of Von Kármán (1940) (see Fig. 2.12B) where the coordinate system is moving with the denser fluid (density, ρ_1). Von Kármán used Bernouilli's theorem for steady irrotational flows to get the following results: (a) at the forward stagnation point, the angle between the bottom and the interface is 60°, and (b) the flow velocity is given by:

$$c_1 = \sqrt{\frac{2gH(\rho_1 - \rho_2)}{\rho_2}} \tag{2.35}$$

where H is the asymptotic height of the interface above the bottom as shown in Fig. 2.12B.

Benjamin argued that although (2.35) is essentially correct, the arguments of Von Kármán leading to it are not, because energy conservation is not possible in this case. A more appropriate condition is the overall balance of momentum fluxes against the fluid forces.

Benjamin also made an analogy to the flow past a cavity shown in Fig. 2.12C. In this setup, a long rectangular box is filled with liquid, then one end is opened; as the liquid flows out the air cavity travels along the length of the box.

Benjamin gave the following expression for c_1, to compare the theory with Keulegan's (1958) experimental measurements on density currents involving the movement of saline water into fresh water:

$$c_1 = C_1 \sqrt{\frac{gH\Delta\rho}{\rho_2}} \tag{2.36}$$

where p_2 is the density of the lighter fluid. Benjamin's theoretical estimate for C_1

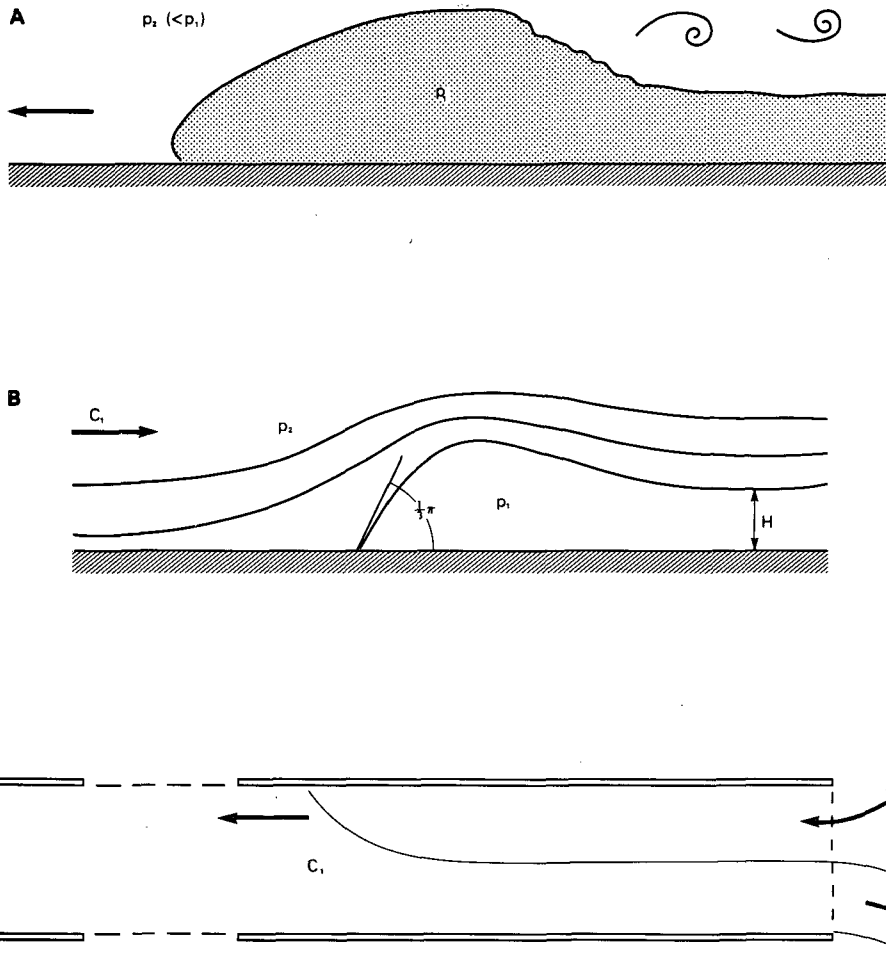


FIG. 2.12. (A) Observed from gravity current, (B) theoretical model proposed by Von Kármán, (C) illustration of motion when liquid flows from a long horizontal box. (Benjamin 1968)

is 1.414 and Keulegan's value is 1.20. Benjamin attributed the influence of the upper boundary to this discrepancy. He also mentioned that Keulegan gave a universal value of 1.07 for C_1 applicable for Reynolds numbers larger than 500; the Reynolds Number being defined as:

$$R_e \equiv \frac{c_1 H}{\nu} \tag{2.37}$$

where ν is the kinematic viscosity of the stream.

WATER WAVES GENERATED BY LANDSLIDES

There have been numerous instances of very large water waves generated by huge rock falls and landslides. On July 9, 1958, following an earthquake, a portion of a mountain fell into Lituya Bay, Alaska, causing an upsurge of water over 518 m (Miller 1960). Submarine landslides following the 1964 Alaskan earthquake caused

huge waves with amplitudes to 30.5 m in several places on the coast of Alaska (Kachadoorian 1965). On Oct. 9, 1963, a great rock slide fell 175 m into a reservoir in the Vaiont Valley in Italy and crested a wave that wiped out a town and killed 3000 people (Wiegel et al. 1970). In Norwegian fiords there have been numerous instances of landslides followed by huge water waves (see Miller 1960; Muller 1964).

Noda (1970) developed a theory for water waves generated by landslides. He made a distinction between vertical and horizontal landslides: the vertical landslide could be thought of as a two-dimensional box falling to the bottom at one end of a semi-infinite channel whereas the horizontal landslide could be modeled by making a two-dimensional wall move into the fluid.

Noda established the region of validity of his asymptotic solution by comparison with the solution from a direct numerical integration of the governing equations. He compared his theoretical results with results from the experiments of Wiegel et al. (1970). The theoretical results deviate more and more from experimental values with increasing B/D (where B is thickness of the slide and D is water depth). This means the linearization used by him is not satisfactory. Based on the analysis of the experimental data, Noda identified the different regions of wave characteristics as shown in Fig. 2.13.

Noda applied this theory to waves generated by the vertical landslide in Lituya Bay, Alaska, on July 9, 1958, and Miller (1960) gave the following data for this incident: thickness of slide $= \lambda \sim 91.5$ m, height of fall ~ 610 m, depth of water ~ 122 m, height of largest wave generated ~ 61 m, calculated velocity of free fall 109 m/s, and B/D equal to 0.75. The relevant value of V for this case is 3.16 and this puts the wave in the solitary wave region, D, shown in Fig. 2.13. The solution for this case gives a maximum wave height of 91.5 m.

If friction is included and the geometry of the problem might make V = 1.0, the same solution will be valid and η_{max} would be 76.9 m.

Noda essentially proceeded along analogous lines for the horizontal slide problem, and used the method of stationary phase to approximate the velocity time-history of the wall, by means of N straight lines. However, there were no experimental data in the linear range to compare with Noda's theory, and in the nonlinear range he compared his theory with the experimental results of Miller and White (1966) discussed in Section 2.5.

2.4 Inverse Tsunami Problem

Reid and Knowles (1970) and Knowles and Reid (1970) are probably the first to use the terminology "inverse tsunami problem" to mean the determination of the deepwater signature of a tsunami based on records made at or near an island station. The significance of this terminology will be broadened to include determinations in the deeper water of such parameters as source region, tsunami signature, and tsunami energy based on recordings made near land, whether a mainland coast or an island.

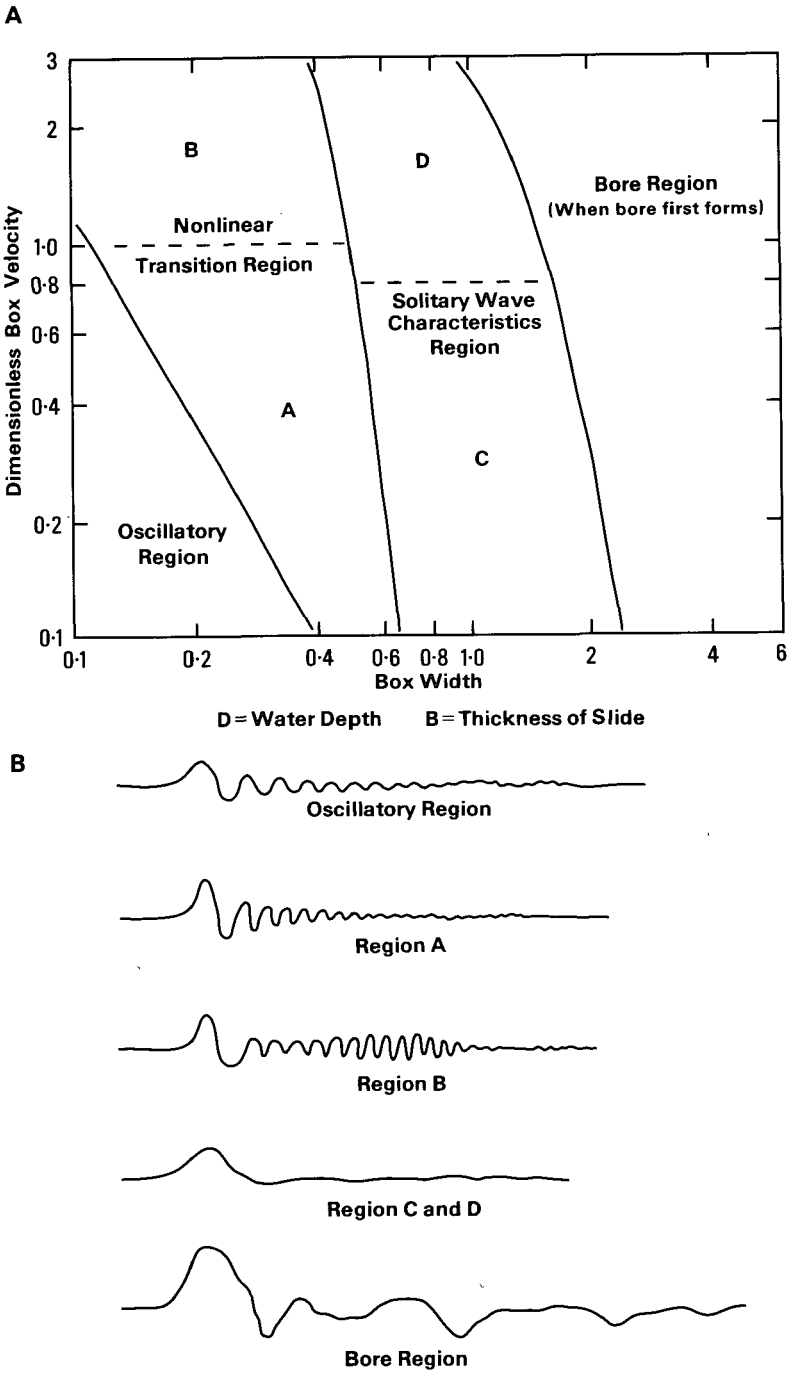


FIG. 2.13. (A) Box-drop problem; regions of wave characteristics, (B) wave characteristics for box-drop problem. (Noda 1970)

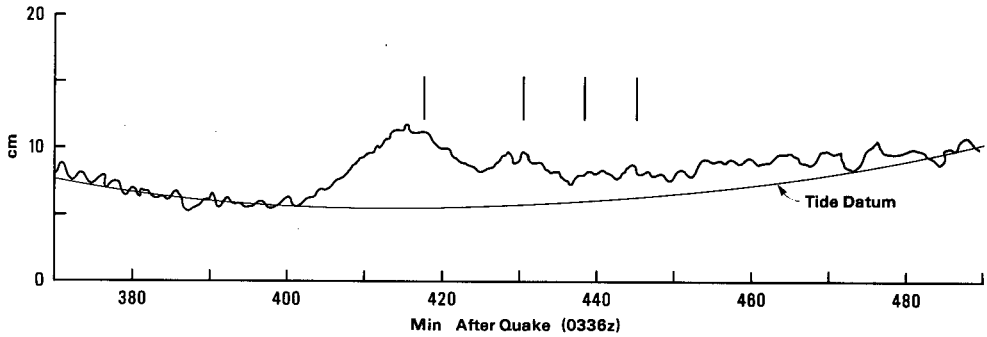


FIG. 2.14. Tide-gage recording at Wake Island for 1964 Alaskan earthquake. Verticle lines over the trace show arrival times of first 4 crests. (Van Dorn 1970a)

Van Dorn (1970a) determined the source mechanism for the 1964 Alaskan earthquake tsunami based on the water-level record at Wake Island (Fig. 2.14). This diagram shows the first crest is the highest of the whole wave train. This observation led Van Dorn to assume that the displacement caused by the earthquake was a long-line source. The tsunami wave train generated was distorted subsequently by refraction.

Van Dorn theoretically (using Airy integral, see Section 1.2) determined the wave form for three different types of sources: (1) abrupt monopolar uplift, (2) dipolar motions with zero net displacement, and (3) impulsive sources initiated from rest. The wave form shown in Fig. 2.14 resembles more the wave form obtained from source one. However, at the outset this result appears to be in disagreement with other deductions. (Van Dorn (1964) suggested that dipolar movement occurred.) Van Dorn resolved this by arguing that "...Because most of the uplifted region was under water, while a large fraction of the depressed sector was on land, the net effect of the dipolar ground motion was to add water to the ocean. Thus the oceanic effect was essentially a modular uplift."

Reid and Knowles (1970) determined the deepwater signature of a tsunami based on its record near an island and some of their assumptions are: the tsunami in deep water can be represented by a plane wave and the distance between the epicenter and the island is much larger than the dimension of the island. Processes such as scattering, diffraction, refraction, and resonance were ignored and the linear long-wave theory was used.

Let P be the location near an island where the tsunami is recorded. Reid and Knowles defined a transfer function as the ratio of the Fourier Transform of the response at P to the Fourier Transform of the input, the deepwater signature of the tsunami. If this transfer function (generally a complex function of frequency and direction of incoming waves) is determined, then from the mareograms the deepwater signature of the tsunami can be determined.

This transfer function, P, can be determined from either observational studies, laboratory experiments, or numerical models; the topography and other conditions duplicated as closely as possible in the latter two cases. Reid and Knowles used a simple geometry for the island so that analytical solutions of the problem could

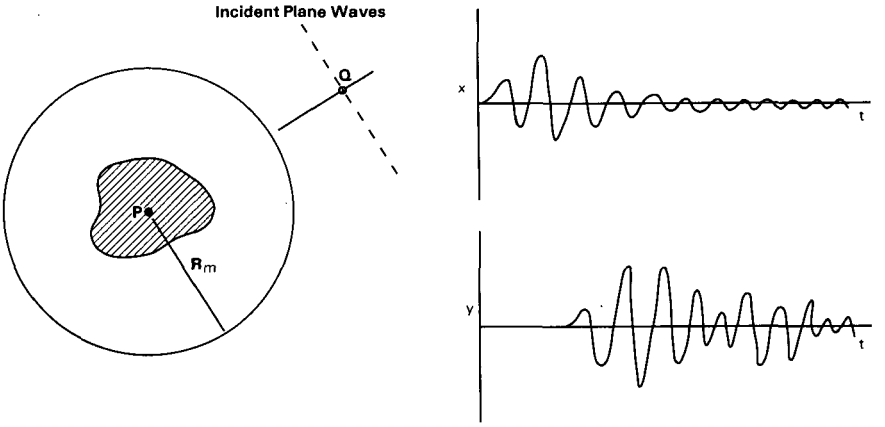


FIG. 2.15. Schematic diagram of plane-wave incident on a cylindrical island. Input is trace X, response is trace Y. (Reid and Knowles 1970)

be obtained. Then they used a numerical model to incorporate several improvements such as broad-band input spectrum, real topography of the island, and different wave directions.

With reference to Fig. 2.15 let R_m be the radius of the circle surrounding an island such that, for radii greater than R_m, the region is deep and has uniform depth. Let $X(t)$ and $Y(t)$ be the water-level records at some point slightly outside R_m and at the point, P, near the island.

Assume that at the source, Q, the wave input is of plane progressive form and that the response at P is linear, then X and Y can be expressed as convolutions of each other:

$$Y(t) = \int_{-\infty}^{\infty} K(\lambda)\, X(t-\lambda)\, d\lambda \tag{2.38}$$

and

$$X(t) = \int_{-\infty}^{\infty} G(\lambda)\, Y(t-\lambda)\, d\lambda \tag{2.39}$$

where λ is the wavelength and $K(\lambda)$ and $G(\lambda)$ are the kernel functions that depend on the bathymetry of the island, the wave propagation direction, and the location of P.

Let $F_x(f)$ and $F_y(f)$, where f is the frequency, be the Fourier transforms of $X(t)$ and $Y(t)$ and let $R(f)$ be the Fourier Transform of $K(t)$. Then the Fourier Transform of $G(t)$ is $R(f)^{-1}$. By definition, then:

$$\begin{aligned} F_x(f) &= \int_{-\infty}^{\infty} X(t) e^{i2\pi ft}\, dt \\ F_y(f) &= \int_{-\infty}^{\infty} Y(t) e^{i2\pi ft}\, dt \\ R(f) &= \int_{-\infty}^{\infty} K(t) e^{i2\pi ft}\, dt \end{aligned} \tag{2.40}$$

In general these will be complex. The Fourier Transform of (2.38) gives:

$$F_y(f) = R(f)\, F_x(f) \tag{2.41}$$

If $X(t)$ and $Y(t)$ are known then from Equation (2.41) the transfer function $R(f)$ can be determined.

Reid and Knowles (1970) used only simple island geometry (a circular cylinder) so that analytical solutions for the transfer function were known. However, they claimed that the results were encouraging enough to warrant further work involving real topography.

Aida (1972) used the "impulse response method" and the "method of characteristics," under the one-dimensional propagation assumption, to obtain the offshore form of tsunami signature based on the tide-gage record at the head of a bay. At Enoshima, he obtained satisfactory comparisons between the theoretically determined signature and observed record for the 1963 Iturup earthquake tsunami, for the 1964 Alaskan earthquake tsunami, and the 1965 Aleutian earthquake tsunami.

The work of Ben-Menahem and Rosenman (1972) is a very significant contribution to the problem of the relation between the seismic and tsunamigenic source

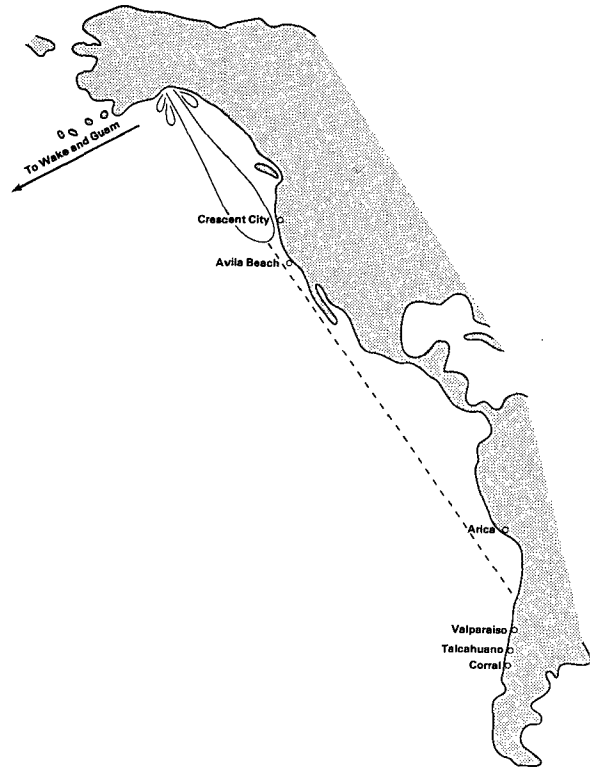


FIG. 2.16. Calculated tsunami radiation patterns for 1964 Alaskan earthquake (Ben-Menahem and Rosenman 1972)

parameters. The technique they developed is substantially different from the inverse refraction technique considered so far in this section. Indeed, their technique gave smaller tsunamigenic areas compared to those by other authors for the same earthquakes. These authors used the mantle Rayleigh and Love waves to deduce the source parameters for certain Kuril Island earthquakes and the Rat Island earthquake of Feb. 4, 1965. They derived an expression relating the tsunami amplitudes in deep water to the seismic source parameters and the topography of the propagation path. They also used the Kranzer-Keller solution.

Ben-Menahem and Rosenman used their theory to predict an amplitude ratio of 1:13 between the amplitude in the direction of the fault (i.e $\phi = 0°$), and the amplitude normal to the fault (i.e. $\phi = 90°$). This deduction is confirmed by tide-gage records, e.g. the wave amplitudes at Crescent City and Avila Beach, Calif., and at Arica, Valparaiso, Talcahuano, and Corral, Chile; all those corresponding to $\phi = 90°$ were about 15 times larger than those at Wake Island and Guam which corresponded to $\phi = 0°$ (Fig. 2.16).

The same principle can be used to account for the high directivity of the Grand Banks earthquake tsunami of 1929, toward Newfoundland (in a northerly direction) as compared to the progression of the tsunami in a westerly direction (toward Nova Scotia).

Some important results of the paper by Ben-Menahem and Rosenman are: (1) the tsunamigenic area obtained was considerably smaller than those obtained by other authors; (2) the inverse refraction technique of determining the tsunamigenic area based on coastal run up was inaccurate; and (3) there need not be any simple relation between the tsunamigenic area and the area of the aftershocks as assumed by Hatori (1970), because the mechanisms were different for the main shock and aftershocks.

2.5 Laboratory Experiments

Experiments with Generating Source at the Bottom

These experiments are relevant for tsunamis generated by earthquakes. Takahasi (1934) appears to be one of the first to conduct laboratory experiments on tsunami generation and he was concerned with the form of free surface and the nature of wave motion due to the dislocation of a portion of the sea bottom. He also used the Law of Similitude to relate his laboratory experiments to the natural situations.

Assume that a circular area, πr^2, of the sea bottom is dislocated through a vertical extent, S, in a time interval, T, in a linear fashion and let s denote the dislocation at time, t. Then

$$s = \mathrm{SF}\left(\frac{t}{\mathrm{T}}\right) \tag{2.42}$$

Let D be the ocean depth at the position of dislocation and let λ, η, ν be the length, height, and velocity of the waves following the dislocation. Let μ be the dynamic viscosity of water, ρ its density, g its gravity, and R the distance of the point of observation (where λ, η, ν are measured) from the origin. The wave motion

is determined by the following nondimensional parameters.

$$\frac{\lambda}{D}, \frac{\eta}{D}, \frac{\nu}{\sqrt{gD}}, \frac{r}{D}, \frac{s}{D}, \frac{\sqrt{g}}{\sqrt{D}} T, \frac{R}{D}, \frac{\sqrt{g}}{\sqrt{D}} t, \frac{\mu}{\rho} \frac{T}{D^2} \tag{2.43}$$

According to the Law of Similitude, these nondimensional parameters must have the same values in the model as well as in nature for the model to be truly representative of nature. An examination of (2.43) reveals the difficulties in satisfying the Law of Similitude. For example, if the space dimension is scaled down to $1/\ell$, then the time scale in the model must be $1/\sqrt{\ell}$ of that in nature. This requires the bottom dislocation to occur with a greater speed in the model than in nature. In addition, if the viscous condition has to be satisfied ($\frac{\mu}{\rho}\frac{T}{D^2}$ must be the same in the model and in nature), then a fluid with a small kinematic viscosity, μ/ρ, must be used. Indeed, the kinematic viscosity of the fluid must be $1/\ell^{\frac{5}{2}}$ that of sea water. Silicone oils probably will be suitable for this purpose, but when Takahasi performed his experiments in 1933, these oils were not commercially available and the only fluid he could use was mercury. However, use of mercury requires the ratio of the natural scale to the model scale 2.58, thus requiring an impossibly large model. For this reason, Takahasi abandoned the idea of satisfying the viscous condition.

In these experiments, Takahasi (1934) used a wooden tank 200 × 150 × 30 cm. To simulate upheaval of a portion of the sea bottom, a circular piston was fitted to the center of the tank bottom. A fine resin powder sprinkled on the water surface and photographed by an optical system provided a record of the wave forms. A total of 45 experiments were performed with different combinations of water depth, D, length, S, of the piston stroke, and velocity of the piston, with the following results: although a series of progressive waves was formed, the first appeared to be of maximum height. The front portion of the wave train (wave front) had a propagation velocity much greater than that of the first wave crest. Hence, the first wave gradually lengthened and the slope of the front part became less. Although a qualitatively similar change of form occurred with other parts of the wave train, dispersion was not as pronounced. The length of the wave train as a whole increased with travel distance. The first wave crest traveled with a velocity considerably greater than $\sqrt{gD}$ in the immediate vicinity of the piston but approached $\sqrt{gD}$ asymptotically with increasing distance from the piston. Above the piston, only stationary waves occurred and progressive waves started to form only at a distance of twice the piston's radius. The experiments also showed that heights of the circular progressive waves decreased as $1/R^{0.6}$.

Measurements on the wavelength were less certain, but indications were that the wavelength was approximately constant, except when the piston moved very slowly. In this case, the wavelength was greater.

In 1957, Takahasi performed further experiments at the University of California, and reported the results in his 1963 paper. He stated that these experiments were conducted to clarify the following features of waves produced by movement of the bottom of the sea (Takahasi 1963, p. 235): (1) wave shapes and propagation

velocity of the frontal part of the wave train in the neighborhood of the origin, (2) attenuation law of wave heights in the neighborhood of the origin, (3) directionality in the energy radiation when the original area of dislocation is extended in one direction; for this purpose, two or more circular origins were lined up very close to each other, (4) phenomena observable in the neighborhood of the origin when the origin consists of two circular areas, and (5) coupling coefficient of the bottom movement and water movement.

These experiments were conducted in a basin 19.5 × 45.7 × 0.85 m. An iron box 2.4 × 1.2 × 0.2 m was used as the wave generator. It had a lid with 10 circular openings each 0.3 m in diameter, with the idea that, by a suitable combination closing and opening, various shapes of submarine dislocations could be achieved in the experiments.

Four types of experiments were performed: in the first set a hydraulic cylinder was used in the generating mechanism; in the second, one air operated piston was used; in the third and fourth sets, two and six pistons were used, respectively. While maintaining a constant stroke of 4.4 cm, 22 runs were made with one piston, 33 with two pistons, and 14 with six pistons. Each experimental run consisted of a series of upward and downward strokes, each producing a wave train.

Based on these experiments Takahasi arrived at the following conclusions:

a) One piston

i) The front of the wave train is propagated with the velocity $\sqrt{gD}$ except within one wavelength of the origin, where the velocity is much greater.

ii) A wave train produced by the upward motion of the piston (designated upwave, hereafter) is quite different in shape from the downwave, when the water depth is small, but, as the depth becomes greater, both waves gradually become similar, except that the sense is reversed.

iii) The first trough or first crest has a velocity very close to $\sqrt{gD}$.

iv) The wave form seems to be composed of a dispersive wave train superposed on a nondispersive one.

v) The amplitude of the initial crest or trough seems to decrease roughly as $r^{-\frac{5}{6}}$.

b) Two pistons

Thirty-three runs were made with two pistons moving with the same sense and with opposing sense. E is the direction connecting the center of the pistons, and S the direction perpendicular to E. It seems that energy of the wave was emitted much more (16 times in the case of upwave and 4 times in the case of downwave) in the direction of S than in the direction of E. There seems to be a remarkable difference also in the period of the waves emitted into the two perpendicular directions.

c) Six pistons

Pistons were lined up in the direction, E. In this case, a nearly plane wave is propagated toward direction, S. The decline of the crest or trough with the distance differed with the azimuth. It was $r^{-\frac{1}{3}} \sim \frac{1}{4}$ toward S and $r^{-\frac{3}{2}}$ toward E. Superposition of the elementary waves produced by an individual piston

does not seem to be equal to the wave height produced by all pistons moving simultaneously in water 10.2 cm deep.

Finally, Takahasi estimated the tsunami energy (in the model) based on the following considerations: the energy, E, of a circular wave train at distance, r, from the origin moving with a velocity, V, with amplitude, A, and period, T, is (see also Section 2.1):

$$E = \pi\rho g r \Sigma A^2 TV \tag{2.44}$$

where g is gravity and ρ is the density of sea water. Takahasi assumed that the amplitude and periods in a wave train varied uniformily from one wave to another and wrote:

$$A = A_0 a^n; \; T = T_0 p^n; \; V = V_0 c^n \tag{2.45}$$

From these two relations and taking:

$$a = \frac{1}{1.3} = 0.77 \qquad V_0 = \sqrt{gD} \qquad T = 0.8 \text{ s}$$

$$p = \frac{1}{1.1} = 0.91 \qquad r = 1.83 \text{ m} \qquad V_0 = 70 \text{ cm}$$

$$c = \frac{1}{1.05} = 0.95 \qquad D = 5.1 \text{ cm} \qquad A_0 = 0.27 \text{ cm}$$

he estimated $E = 4.5 \times 10^6$ erg.

The work done by the piston on the water is:

$$W_p = S_p h(\rho g D + KCV\rho) \tag{2.46}$$

where D is the water depth, S_p is the area of the piston, V is the velocity with which the piston moves, h is the piston stroke, K is the coupling coefficient, and C is the speed of sound in water. Part of the work done by the piston on water increases the potential energy of water, $S_p h\rho g\,(D - \frac{h}{2})$. The energy, W_w, that could be transformed into wave energy is:

$$W_w = Sh(\tfrac{1}{2}\rho g h + KCV\rho) \tag{2.47}$$

In the laboratory experiment, the coupling coefficient, K, is very small and the second term on the right side of (2.47) can be ignored. The reason K is small is because the piston diameter is extremely small compared to the length of the sound wave emitted by the piston. Because of the large bottom displacements involved in actual tsunamis, sound waves might be transmitted significantly to cause sea shocks strong enough to rock nearby ships. However, this sound wave energy may not be efficiently transformed into tsunami energy.

Coming back to the laboratory situation, Takahasi estimated that $W_w = 4.6 \times 10^6$ ergs which agreed favorably with the wave energy estimated from the experiments. Based on this agreement, Takahasi concluded that the potential energy of sea water upheaved at the origin imparts energy to the tsunami waves.

For the Sanriku earthquake tsunami of 1933, wave energy was estimated at 1.6×10^{23} ergs. The earthquake had a magnitude of 8.3 and an estimated energy of 2.8×10^{24} ergs. This means about $\frac{1}{17.5}$ of the earthquake energy had been converted into tsunami energy (see also Section 2.1).

Improved technology has made better and more efficient tsunami generators for laboratory experiments possible since Takahasi's (1934) experiments (see Iwagaki et al. 1970). Hammack and Raichlen (1972) performed theoretical calculations as well as laboratory experiments on tsunami generation due to bottom motion and near field propagation. The experiments dealt with only two-dimensional situations whereas the theory included three-dimensional cases. The authors identified a parameter called a "time-size ratio" which is nondimensional and includes the duration of the bottom movement, the water depth, gravity, and the extent of the disturbance in the direction of wave propagation. Some features of the tsunami, such as maximum amplitude and duration of the leading wave, can be expressed as a function of this time-size ratio.

The time-size ratio has three regions: an impulsive region, where details of the bottom movement have no significant influence on the generated forms of the waves; a creeping region, which corresponds to very slow movement of the bottom when wave forms are strongly dependent on the details of the bottom motion; and an intermediate region between the two.

Hwang and Tuck (1970b) also performed laboratory experiments where a hinged plate capable of moving upward simulated ground motion. They recognized the comparison was only qualitative because of limitations of their theory as well as the experiments.

Experiments of Garcia

Reference has been made to the numerical model studies of Garcia (1972) for simulation of tsunamis caused by motion on the eastern end of the Mendocino Escarpment near California. He also performed four series of laboratory experiments and verified his numerical calculations.

The eastern end of the Mendocino Escarpment along the San Andreas Fault was modeled as the source and the experiments represented either displacement of the ocean floor or landslides. Two different sections along the eastern end of this escarpment, at 125°30′W and 128°W, were considered in detail.

In the experiments, the wall displacements were such that the boundary Froude Number $N_{F\,avg} = V_{avg}/\sqrt{gd}$ had a moderate range (Fig. 2.17). Here g is gravity, d is the water depth, and V_{avg} is the average speed with which the wall moves. The four series of experiments consisted of studies of waves produced by a moving vertical wall, moving slope walls with two different slopes of 1:1 and 1:2 vertical to horizontal, and a moving underwater step.

Figure 2.17 shows experimental results for the vertical wall. Here λ is the maximum boundary displacement and η is the height of the crest of the first wave. The diagram also includes results from the numerical calculations of Garcia (1972) and experimental results of Das and Wiegel (1972).

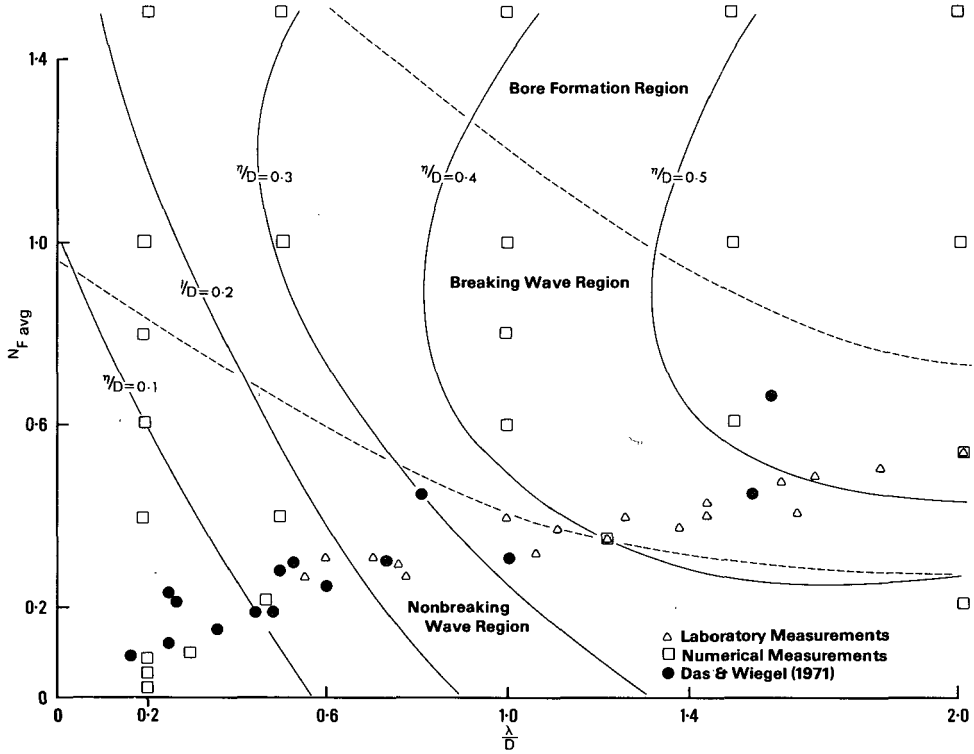


FIG. 2.17. Range of data and wave characteristics of vertical wall $N_{F\,avg} = \frac{V_{avg}}{\sqrt{gD}}$ vs. $\frac{\lambda}{D}$ for $\frac{x}{D} = 10.0$. (Garcia 1972)

EXPLOSION-GENERATED WAVES

Prins (1956, 1958a, b) studied experimentally the characteristics of waves generated by a local disturbance at or near the water surface. Usually, experiments aimed at such problems consider simulating one or more of three initial states: (a) initial elevation or depression of the surface with zero initial velocity field, (b) undisturbed surface with an initial distribution of surface impulse, or (c) undisturbed surface with an initial distribution of a submerged impulse (underwater explosion). In his 1958b paper, he dealt with condition (a).

His experiments were performed in a flume 18.3 m × 0.3 m. At one end an elevation or depression in the water could be created without disturbing the rest of the liquid; at the opposite end was a wave absorber. Vertical motion of the water was monitored at five different locations along the tank length. The important parameters in these experiments were the undisturbed water depth, D, and the height, η, of the elevations or depression. Experiments were carried out with the following values for these parameters: D = 6.1, 10.7, 15.2, and 70.1 cm; η = ± 3.0, ± 6.1, and ± 9.1 cm; and L = 10, 30.5, and 61 cm.

Experimental results were compared with values calculated from the theories of Unoki and Nakano (1953a, b) and Kranzer and Keller (1955). Although Unoki

and Nakano's two-dimensional theory is for an initial elevation of a finite area in water of infinite depth, Kranzer and Keller's three-dimensional theory is applicable for an initial elevation or depression of a finite area in water of finite depth.

Prins (1956; 1958a, b) distinguished the types of leading parts of the generated wave train as (1) leading wave with oscillatory characteristics as part of the dispersive wave pattern, (2) leading wave with solitary wave characteristics with respect to its velocity of propagation, followed by a trough connecting it with the dispersive wave pattern, (3) leading wave a single wave with solitary wave characteristics separated from the dispersive wave pattern by a more or less flat part, and (4) leading part a complex form, which, while traveling outward, breaks up into a few waves with solitary wave characteristics separated from the dispersive wave pattern.

The experiments with $\eta/D < 0.18$ and $L/D < 0.9$ gave the following results: (1) generated wave pattern was of a dispersive character, (2) variation of height and extent of the initial disturbance did not affect the phase velocities, (3) phase periods agreed with the theory of Kranzer and Keller (1955) and for deep water with the theory of Unoki and Nakano (1953a, b), (4) wave patterns showed an interference phenomenon, (5) leading part of the wave pattern for an initial elevation showed exactly the negative performance of the waves generated by an initial depression ($\eta_{elev} = -\eta_{depr}$). Probably this can account for the initial withdrawal of water that has been reported associated with several tsunamis, (6) amplitudes of the leading waves were directly proportional to the height of the initial disturbance, (7) wave amplitudes did not show a satisfactory agreement with the theoretical values of Unoki and Nakano. In general, the measured values were found to be smaller than the theoretical values. This is not surprising because the theory of Unoki and Nakano is for deep water.

Miller (1970, 1971) performed experiments on impulsively generated waves in a wave tank of uniform width with a water layer of uniform depth, to simulate waves generated by a single impulse. The nondimensional variables have been identified by Miller as the relevant parameters of the problem: (1) ratio of the piston displacement to undisturbed water depth, ℓ/D, and (2) piston Froude Number $= F_V = V/\sqrt{gD}$ where V is the piston speed. Several experiments were run with various combinations of ℓ/D and F_V.

Miller identified four possible wave modes in these experiments: sinusoid, solitary, undular bore, and fully developed bore. His results showed that: (1) the fully developed bore decays rapidly to the unbroken undular bore form, (2) the lead wave of the undular form takes on the "solitary" mode leaving behind the rest of the "undular" wave. In several cases, the second and even the third undulations in turn take on the "solitary" mode, and (3) the "sinusoid" mode generated at short piston displacements transforms gradually as the trailing trough rises to the undisturbed water level, and finally enters the solitary mode.

Williams and Jordaan (1970) constructed a laboratory model to study so-called double-humped waves, the theory developed by Butler (1967). These double-humped waves or waves with two crests could be represented by:

$$\eta = 1024\, \epsilon\, x^2(a+8x)^2\, e^{16px} \tag{2.48}$$

where the variables x and η denote the negative distance from the beach ($x=0$) and the free surface elevation, both in nondimensional form. The two parameters a and p determine the relative height and spacing of the two crests, and ϵ is a vertical scale magnification parameter which could depend on wave breaking.

The parameters a and p and the positions of the crests determined a characteristic length, ℓ_0, used to nondimensionalize x, whereas $\alpha\ell_0$ (where α is the slope of the beach) has been used to nondimensionalize η. Butler calculated the elevation as a function of time at the beach for the double-humped waves, where their leading edges were at the beach and had zero particle velocity initially.

Williams and Jordaan performed laboratory experiments to check Butler's calculations. Their wave tank, made of lucite, was 7.6 m × 0.3 m with a maximum depth of 0.46 m and a beach slope of 1/7. A wave generator constructed from several strips of lucite was dropped vertically into the water and the wave profiles thus created were recorded by resistance probes. The surface tension effects near the beach were reduced by coating the beach with a mixture of water and detergent.

The experimental results did not agree well with theoretically predicted wave forms: probably the theory is inadequate to represent double-humped waves satisfactorily. Further theoretical developments and experiments on double-humped waves could be useful to interpret coastal tsunami records.

LeMéhauté (1971) achieved some simplification of the solutions of Kajiura (1963) and Kranzer and Keller (1959) by identifying two cavity parameters, $\eta_{o_{max}}$ and R, which determine the wave envelope amplitude, A. Correlations between his simplified theory and the results from field observations involving a 4363-kgm TNT explosion, showed that, except for irregularities caused by noise (wind waves), wave refraction, and interference patterns due to wave reflection from boundaries, good agreement is indeed possible.

However, there are some limitations to the theoretical model. The bulk of data on which these correlations were based is from explosions of 0.23 to a few hundred kgm of TNT. It is not clear how reliable the extrapolation from this would be to large yields in the nuclear range (e.g. 10^{10} kgm TNT). In fact, LeMéhauté (1971, p. 18) cautioned that:

> "...similarity is never achieved so that no simple scaling law can be expected to cover the entire range of yields of interest. In particular, the transition from chemical to nuclear sources with increasing yield may be a point of similarity violation; indeed, it would be surprising if such were not the case. Extrapolation then, to large yield from small chemical yield data must be accepted with a considerable measure of caution."

Van Dorn (1966, 1970a) performed laboratory experiments to simulate the tsunami generated by the Alaskan earthquake of Mar. 28, 1964.

The experiments were performed in a wave tank 27 m long. On one end of the tank was a shallow region 5 m long and 3.3 cm deep. Over the next 3-m length the depth increased from 3.3 cm to the full depth of 31.5 cm and in the remaining 19 m the depth was uniformly 31.5 cm. According to Van Dorn (1970a, p. 40) the relevance of this model is:

> "On a scale of 1:17,000, this model represents a section of the continental shelf normal to the fault axis 90 km in half-breadth and 565 m deep, descending at the appropriate

slope to the uniform depth of 5400 meters corresponding to the effective depth computed for the travel path to Wake Island..."

The wave-generating mechanism consisted of a long plunger hinged at one end, which, when raised to its extreme position, just cleared the surface of the water, and when lowered dipped to a maximum depth of 1 cm. The 6.4-cm width of the plunger was relatively small compared to the 40-cm width of the tank. According to Van Dorn, by rapidly lowering the plunger a positive half-wave of 0.25 cm maximum amplitude and 5 m length could be produced. A displacement transducer was used to measure the motion of the plunger and pressure transducers were employed to measure wave heights at four different positions; T_1 at the shallow end of the tank, T_2 at 5 m where depth starts to increase, T_3 at 8 m where depth increased to the full value, and T_4 near the deepwater end of the tank.

Many experimental runs were made under different initial conditions and plunger speeds. Van Dorn (1970a) selected two particular runs for inclusion in his paper on the basis of close resemblance to the Wake Island record. Figure 2.18 shows the plunger (trace T_0) started from its bottom center position and cycled approximately sinusoidally to its initial position during a time interval of about 8 s, which simulated an initial depression of the sea floor accompanied by an uplift of some magnitude.

Van Dorn (1970a, p. 42) interpreted Fig. 2.18 as:

"The other traces give the time-history of surface elevation at the transducer stations, including reflections from the far end of the channel. Trace T_2 shows that the tsunami at the edge of the continental shelf consisted of a leading trough, followed by a double pulse (A). The reflected train at the same station (B) exhibits a shallower trough and a dispersive train rather like the Wake record."

Experiments by Williams and Jordaan (1970) on the so-called double-humped waves have been described. These are somewhat similar to the double-pulse waves

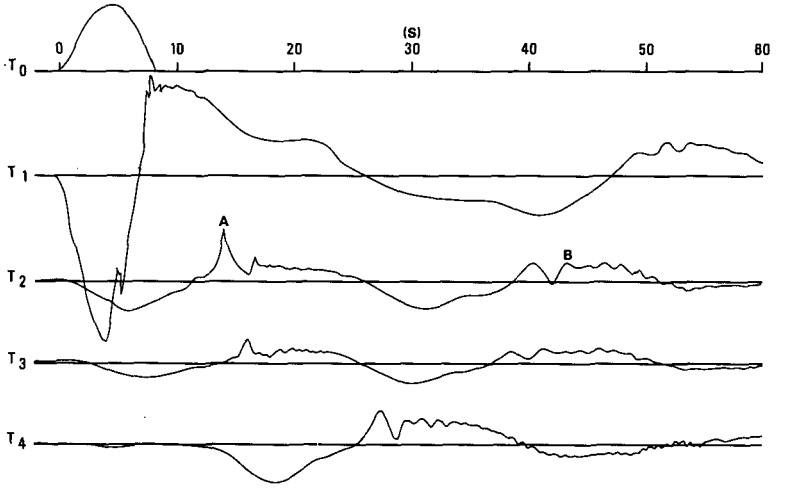


FIG. 2.18. Model experiment recording for plunger started from bottom-centered position and cycled for 8 s. (Van Dorn 1970a)

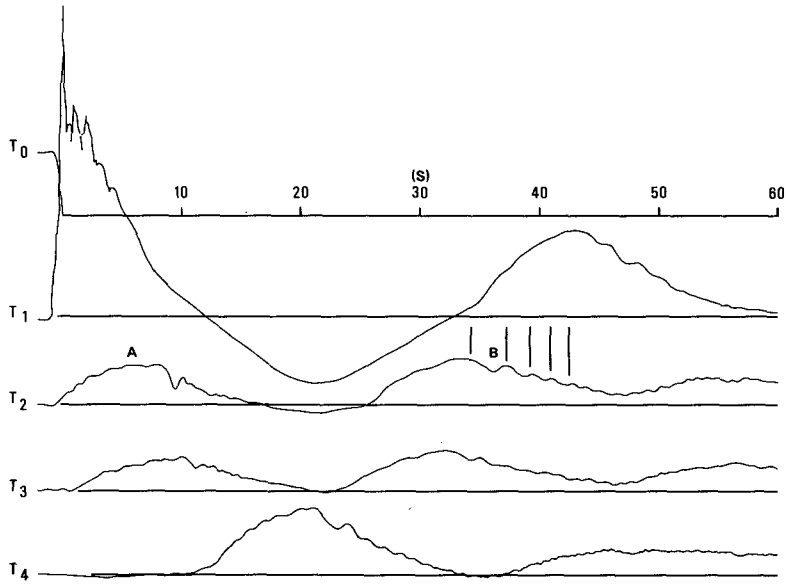


FIG. 2.19. Model experiment recording for single rapid plunger depression corresponding to a simulated shelf uplift. (Van Dorn 1970a)

that appeared in the experiments of Van Dorn. He also estimated the half-breadth of the source as follows: in Fig. 2.19, let t_1 and t_2 be the arrival times of the first crest at the shelf edge, (T_2), and at some other station, T_4 (say). The duration of the pulse at $t = t_1$ will be $2t_1$, because it consists of its direct and reflected wave from the end of the tank at station T_1. The pulse duration, Δt, at station T_4 can be represented by the following relation, using the long-wave approximation:

$$\Delta t = 2t_1 \left(\frac{t_2}{t_1}\right)^{\frac{1}{3}} \tag{2.49}$$

If a is the half-breadth of the shelf between T_1 and T_4, then:

$$t_1 = \frac{a}{\sqrt{gD_1}} \tag{2.50}$$

From (2.49) and (2.50) then:

$$a = \left(\frac{\Delta t}{2}\right)^{\frac{3}{2}} \sqrt{\frac{gD_1}{t_2}} \tag{2.51}$$

Van Dorn used the following representative values based on Fig. 2.18: Δt = 24.5 s, t_1 = 8.5 s, t_2 = 21.5 s, and D_1 = 3.3 cm. He used these in (2.51) to obtain: a = 525 cm which agreed favorably with the value of 500 cm, the shelf width in the model. For the Wake record itself, he took: Δt = 80 min, t_2 = 417 min, and D_1 = 100–200 m, which gave a = 23 km for D_1 = 100 m, and 33 km for D_1 = 200 m. These values bracketed the width of 30 km between the 200-m contour and the assumed axis of the maximum uplift.

Experiments on Underwater Slides, Landslides into Water, and Turbidity Currents

Wiegel (1955) studied through laboratory experiments the system of gravity waves generated by the movement of a submerged body, to test whether a tsunami could be caused by a dipolar disturbance such as an underwater landslide (which is unlikely according to Shepard et al. (1950)). Wiegel remarked that his experiments applied equally well to the situation when the vertical movement of a block is compensated by equal movement in the opposite direction.

The earlier work of Sauer and Wiegel (unpublished data) consisted of piling coarse gravel over a sheet metal piece at one end of a laboratory channel and suddenly pulling the sheet. However, this did not create a slide as was planned but a slump occurred. Hence, in the later experiments they used a box sliding down an inclined plane to simulate an underwater slide.

Later Wiegel (1955) performed tests where a submerged body was made to fall vertically through water of different depths from several different heights. Also, experiments were rerun with different slopes of the inclined plane for the slide experiments. Most experiments were done in a wave tank 18.3 m × 0.3 m × 0.9 m, and water depth of 0.76 m. An inclined beach was arranged at the far end of the channel to minimize reflection but some reflection occurred, and was apparent after the second wave crest.

Results of these experiments can be summarized as follows: In general, within the range of experimental conditions, dispersive waves were generated by a body either falling vertically or sliding down an incline. An exception was a flat plate falling in quite shallow water (3.0–6.1 cm) when an Airy-type wave was generated, with dispersive waves forming the tail. Surface-time histories of the disturbance measured a short distance from the source showed that a crest always formed first, followed by a trough from one to three times the amplitude of the first crest (depending on the slope of the incline primarily), followed by a crest with about the same amplitude as the trough. Due to the dispersive qualities of the waves, additional crests and troughs continued to form with increasing distance from the origin, while at the same time the amplitudes of the initial crests and trough decreased.

Magnitudes of the amplitudes depended primarily on the submerged weight of the body, but also on the depth of submergence, the water depth, and other characteristics of the generation.

The "period" associated with gravity waves of the disturbance was found to be independent of water depth, initial depth of submergence, weight of body, or time of fall. It was, however, found to be related to length of the body, with the period increasing with increasing length, and to slope of the incline, with the smaller the incline, the greater the period.

Computations of the approximate energy of the wave disturbance generated by the vertically falling body indicated that about 1% of the initial potential energy (net, submerged) of the body was transformed into wave energy. Within the band of results it was seen that for water of constant depth, the less the initial depth of submergence of the body the greater the percentage of energy transformed into

wave energy; and for constant initial depth of submergence, the smaller the water depth the greater the percentage of energy transformed into wave energy.

A landslide in Lituya Bay, Alaska, that caused a giant wave has been discussed. The landslide caused the water on the opposite side of the bay to surge upward 366 m above its mean level, and a wave almost solitary in form traveled from the bay into the ocean. Wiegel (1963a) modeled this phenomenon in the laboratory and was successful to the extent of creating a solitary wave but it was followed by "a complex tail." One interesting result of these experiments was that the crest moved with almost uniform speed across the bay even though it was much shallower near its entrance than at its center.

Earlier discussions described how turbidity currents generated by the Grand Banks earthquake of 1929 broke transatlantic cables and caused heavy damage. The work of Benjamin (1968) on turbidity currents has been briefly discussed. Some details of Middleton's (1966b) experiments will be described. According to Middleton, a turbidity current is a density current formed by sediment in suspended form. Middleton performed these experiments for a dual purpose: first, to infer the hydraulic behavior of turbidity currents; and second, to determine differences in the hydraulic behavior between turbidity currents of interest to geologists (in this case, the turbidity current carries coarse sediment in suspension) and turbidity currents of interest to engineers. By the latter, Middleton meant clay suspension turbidity currents and saltwater density currents. Harleman (1961) and Middleton (1966a) reviewed these types of currents.

Middleton (1966b) used a transparent plastic flume 500 × 15.4 × 50 cm that could be tilted when necessary. In the first set of experiments Middleton created saline density currents by pumping salt solution into the tilted flume. In the second set, he simulated turbidity currents by suddenly releasing plastic beads at one end of the flume which was kept horizontal. The results of both experiments were somewhat similar in the sense that the saline density current and the turbidity current formed a characteristic head.

Middleton's experiments showed that for slopes less than 4%, the velocity of the head of the density current more or less agrees with (2.36).

Chapter 3 Tsunami Propagation

3.1 Refraction, Diffraction, and Scattering

Some general concepts regarding refraction, diffraction, and scattering of water waves will be considered. These phenomena are important to the tsunami propagation problem.

Wave Refraction

Consider progressive waves with wavelengths much larger than the water depths over which they propagate, called shallow-water or long waves. Because the waves are long, different parts of the wave might be over widely varying depths (especially in coastal areas) at a given instant. As depth determines the phase velocity of long waves, different parts travel with different phase velocities, causing the waves to bend, and this is called wave refraction.

From an engineering point of view, Snell's Law from optics has been used in the past to study refraction of water waves:

$$\frac{\sin \alpha_2}{\sin \alpha_1} = \frac{C_2}{C_1} \tag{3.1}$$

Here α_1 and α_2 are the angles between adjacent positions of the wave front and the corresponding bottom contours. The ratio C_2/C_1 for given water depths and wave periods can be determined from tabulated wave functions.

Changes in wave height, period, and direction of travel are important for tsunami prediction as well as for many other engineering applications. A refraction diagram is a device through which wave refraction can be studied. In this diagram, positions of wave crests can be shown at a given instant, or positions of a given wave crest as it propagates can be shown at different times. A set of lines, known as orthogonals, everywhere normal to the wave crests are drawn on the same map. It is then assumed that the power transmitted between any two orthogonals is the same. Hence, changes in wave height due to refraction can be estimated. Sometimes the orthogonals are drawn directly, without drawing the wave-crest positions.

Depending on the local hydrography, adjacent orthogonals could cross in two different ways (Fig. 3.1; Wiegel 1964). In the simpler case, a given wave crest divides in two and the severed sections cross each other. In a complicated situation, the orthogonals form a caustic envelope (Fig. 3.2). Based on simple theory, the meeting of adjacent orthogonals means the wave height is infinite and the simple theory is inapplicable.

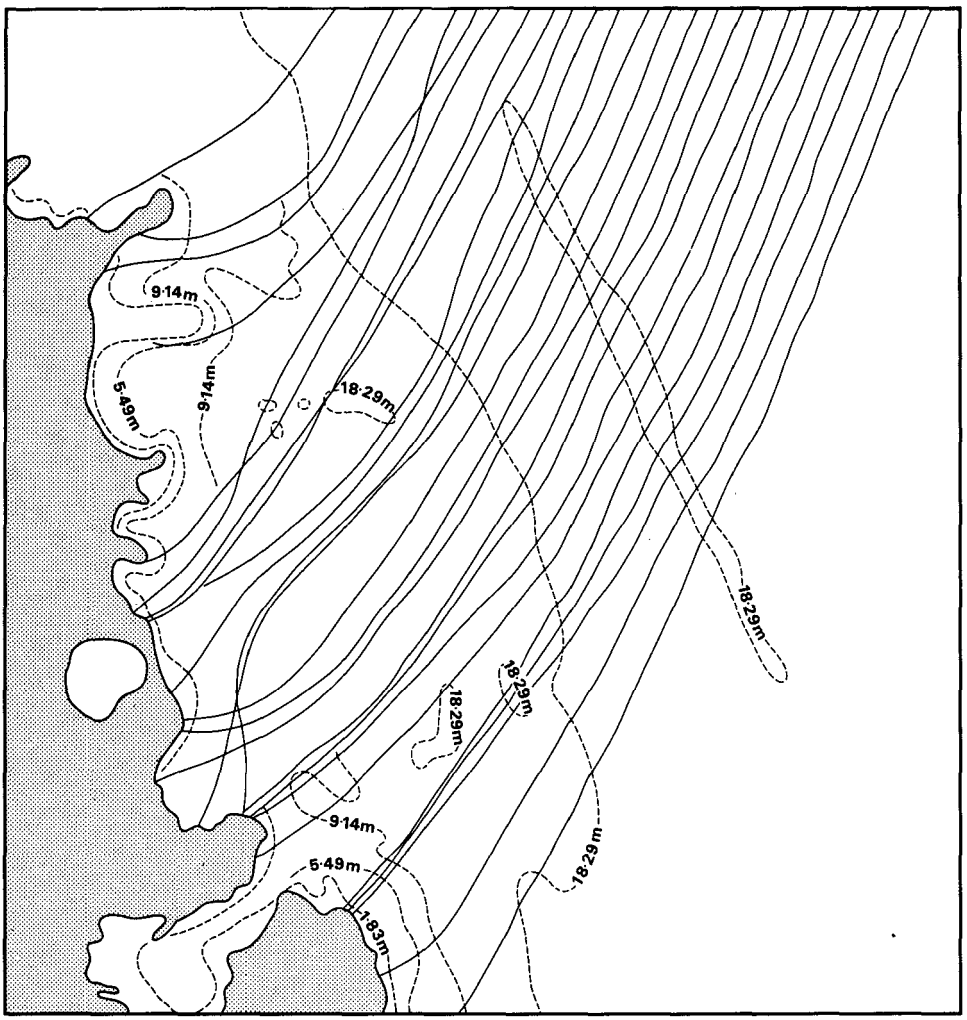


FIG. 3.1. Wave refraction diagram for the southern coast of Vieques Island, Puerto Rico. (Griswold 1963)

REFRACTION COEFFICIENT

The refraction coefficient is defined after Wiegel (1964). The linear theory gives the following expression for the power, P, transmitted by a train of long-crested sinusoidal waves:

$$P = C_g \, b \, \eta^2 \, \frac{\gamma}{8} \tag{3.2}$$

where C_g is group velocity, b is length of the crest perpendicular to the local direction of travel, η is wave height, and γ is specific weight of water. Although this formula strictly speaking does not apply to ocean waves that are not sinusoidal, nevertheless, it is useful in estimating wave heights and can be corrected usually through empirical

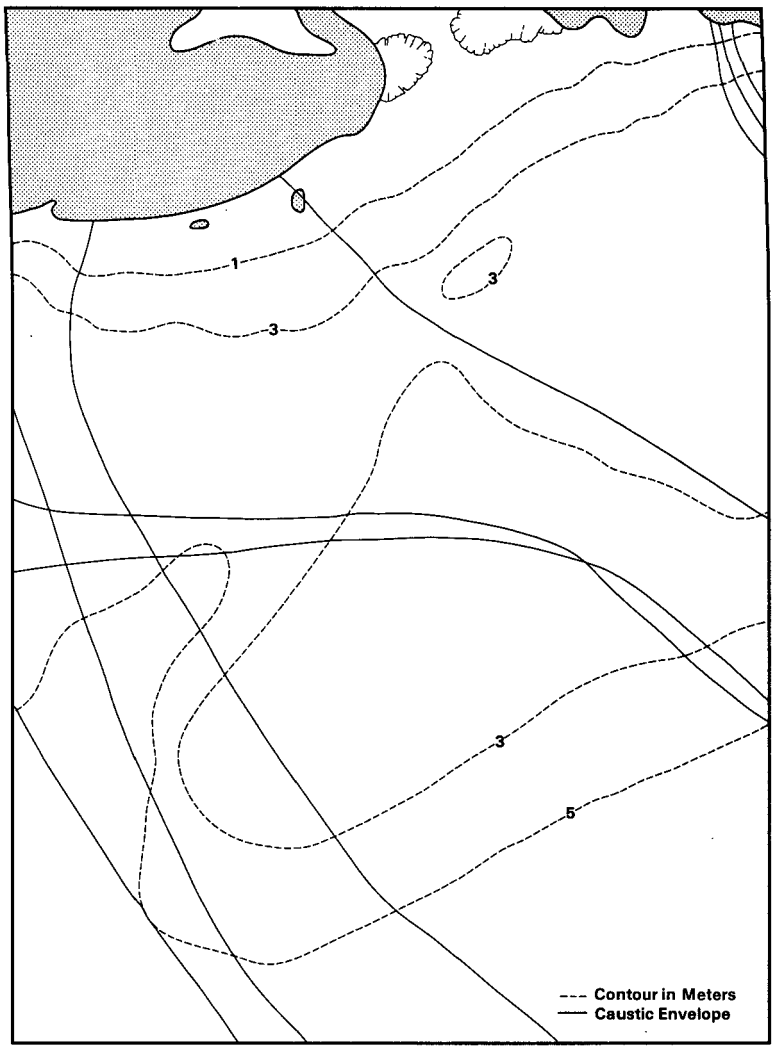


FIG. 3.2. Caustic envelope formed by 8-s waves from east-southeast on Vieques beach, Puerto Rico. (Griswold 1963)

results. Assuming that no energy flow occurs laterally along a wave crest between any two orthogonals, the same power must be transmitted past all positions. Thus, denoting the deepwater conditions through subscript 0:

$$P = P_0 \tag{3.3}$$

$$\frac{\eta}{\eta_0} = \frac{C_{g_0}}{C_g} \frac{b_0}{b} \tag{3.4}$$

The quantity b_0/b is termed the refraction coefficient and is denoted usually by K_d. The quantity C_{g_0}/C_g is called the shoaling coefficient and represents the effect of a change in depth on wave height, usually denoted by D_d.

$$\eta = \eta_0 \, D_d \, K_d \tag{3.5}$$

Wiegel presented methods to determine K_d for different situations, such as a straight shore with parallel contours, and islands and shoals with concentric circular contours. He also tabulated D_d, which depends on water depth and wavelength. Griswold (1963) presented numerical methods to calculate the refraction coefficient and constructing refraction diagrams.

Shoaling could cause wave refraction. There are other mechanisms that cause refraction of water waves even in deep water and without topographical irregularities. For example, Johnson (1947) showed that a current moving obliquely to the waves could change their direction of propagation, wavelength, and steepness. Johnson gave mathematical expressions for these modifications in terms of magnitude of the current, and wavelength and direction of the waves before they encounter the current. As this work is of interest for the tsunami problem, Johnson's paper will be discussed here.

Unna (1942) studied waves that advance directly in a current that moves either with or against the waves. In Johnson's work, the waves approach the current from a side. However, Johnson pointed out that his case does not reduce to Unna's case when the angle between the wave crests and the current becomes 90°. In this situation the condition that the waves enter the current from a side is not satisfied. Referring to the importance of refraction of waves by currents, Johnson (1947, p. 867) stated that there are at least two situations when the refraction of waves by currents may be of practical importance. At tidal entrances, ebb currents run counter to the waves and increase wave height and steepness, thus adding to the hazards of navigation, whereas flood currents flatten the waves. Major ocean currents, such as the Gulf Stream, may have an appreciable effect on the height, length, and direction of waves approaching the shore and under some circumstances may cause almost complete reflection.

Figure 3.3 shows that ABC and A′B′C′ denote the positions of the wave front at two different times, with T the elapsed time interval. Let T also be the period of the incident wave train measured with respect to a point fixed on the bottom. Because the crest has to be continuous across the discontinuity, the following relations can be written:

$$\frac{C_0}{\sin \alpha} = u + \frac{C}{\sin \beta} \tag{3.6}$$

and

$$\frac{L}{\sin \beta} = \frac{L_0}{\sin \alpha} \tag{3.7}$$

where C_0 and C are velocities of the wave at initial and final positions, L_0 and

L are the wavelengths, u is speed of the current, and α and β are the angles shown in Fig. 3.3.

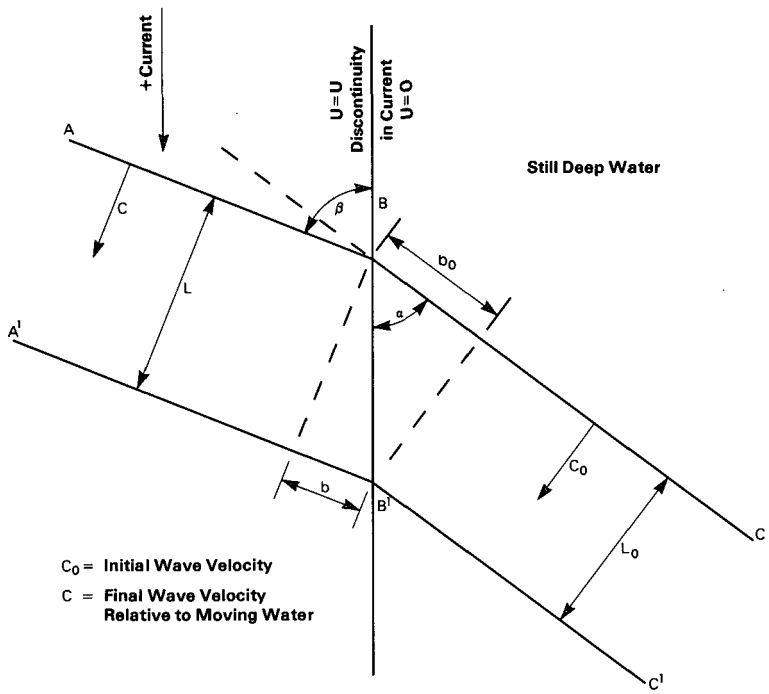


FIG. 3.3. Relative positions of wave crests before and after refraction by a current. (Johnson 1947)

For deepwater waves, writing $C = \sqrt{\frac{gL}{2\pi}}$, using (3.6) and (3.7), and defining $m \equiv \frac{u}{C_0}$ one obtains:

$$\sin \beta = \frac{\sin \alpha}{(1 - m \sin \alpha)^2} \tag{3.8}$$

Ranges of m and α are, respectively, $-\infty$ to $+\infty$ and 0 to 90°. However, for ocean waves, m is usually less than unity. The modified wavelength is given by:

$$\frac{L}{L_0} = \frac{1}{(1 - m \sin \alpha)^2} \tag{3.9}$$

Johnson presented plots of β and $\frac{L}{L_0}$ as functions of m and α.

Let b_0 and b be the lengths of the wave crest before and after refraction. These are given by:

$$\begin{aligned} b_0 &= BB' \cos \alpha \\ b &= BB' \cos \beta \end{aligned} \tag{3.10}$$

If η is wave height, then the average energy-per-unit surface area of the wave is proportional to η^2, and this total energy is equally partitioned between kinetic and potential.

The balance of energy is represented by:

$$\frac{C_0 b_0}{2} \eta_0^2 = \frac{C\, b}{2} \eta^2 + u \sin \beta\, b\, \eta^2 \tag{3.11}$$

Wave steepness, η/L, after refraction is given by:

$$\left(\frac{\eta}{L}\right)^2 = \left(\frac{\eta_0}{L_0}\right)^2 \left(\frac{L_0}{L}\right)^2 \frac{b_0}{b} \frac{C_0}{(C+2u \sin \beta)} \tag{3.12}$$

Equations (3.8), (3.9), and (3.10) give:

$$\left(\frac{\eta}{L}\right)^2 = \left(\frac{\eta_0}{L_0}\right)^2 \left(\frac{\cos \alpha}{\cos \beta}\right) \left\{\frac{(1-m \sin \alpha)^6}{(1+m \sin \alpha)}\right\}$$

From this Johnson wrote:

$$\frac{\eta}{L} = M \frac{\eta_0}{L_0} \tag{3.13}$$

where

$$M \equiv \sqrt{\frac{\cos \alpha}{\cos \beta} \frac{(1-m \sin \alpha)^6}{(1+m \sin \alpha)}}$$

He presented plots of M vs. α for different values of m, and gave the theoretical value of η/L as 0.14.

Refraction changes wave steepness in two different ways; one is a change of wavelength from L_0 to L, whereas the other involves elongation or compression of the wave crest from b_0 to b. Depending on the direction of the current, the two effects may support or oppose each other.

Determination of Refraction Coefficient of Waves at a Given Point

To determine the refraction coefficient of water waves at a given point, such as the end of a breakwater, construction of a refraction fan diagram would be useful. Dorrestein (1960) gave a simple procedure. Here it is assumed that the laws of geometric optics will hold and wave reflection at the coast or obstacles is ignored. The following notation has been used: Let θ be the azimuth of a wave ray at point P under consideration, measured either relative to north or some other specified direction, and let θ' be the azimuth of the same wave ray in deep water. Then, for waves at P and in deep water let C and C′, respectively, be phase velocities, and C_g and C'_g the group velocities, let η and η' be root mean square heights, and let e and e′ be energy flux densities. Energy flux density means the wave energy passing through a given point-per-unit width in unit time. Then for long-crested waves:

$$e = \tfrac{1}{8} \rho g \eta^2 C_g \qquad e' = \tfrac{1}{8} \rho g \eta'^2 C'_g \tag{3.14}$$

The refraction coefficient K_d is given by:

$$K_d = \sqrt{\frac{e}{e'}} \tag{3.15}$$

Dorrestein (1960) derived the following expression:

$$K_d^2 = \frac{e'}{e} \left| \frac{\delta\theta}{\delta\theta'} \right| \tag{3.16}$$

where $\delta\theta'$ is increment in θ' corresponding to an increment $\delta\theta$ in θ. The modulus of $\delta\theta/\delta\theta'$ is used to allow for the fact that an increase in θ could be accompanied by a decrease in θ'.

Starting at point P, wave rays are drawn into the ocean with an appropriate interval, say 10°. The values θ' of the azimuth in deep water are plotted against θ, and a smooth curve is drawn through these data points. Knowing the slope of this curve, the refraction coefficient at P can be determined from equation (3.16). However, in practice the procedure might not be this simple; θ' will be a single-valued function only when the bottom topography is regular. For complex topography, singularities could arise. Dorrestein (1960) considered in detail how to deal with such situations.

Brief Review of Theories for Refraction Studies

Following Beitinjani and Brater (1965), some theories used classically in refraction studies, as well as some recent developments, will be reviewed. Although some of these theories were considered earlier, refraction aspects will be the main concern. In the small-wave theory of Airy the wave height was assumed to be small compared to the wavelength, whereas Stokes studied finite-amplitude waves without assuming that their slope or steepness was small. Both Airy's and Stokes' theories were derived for water of uniform depth only, although they have been used for small slopes of the bottom.

In Airy's theory the wave celerity, C, for a simple harmonic progressive wave in water of any depth is from (1.59):

$$C = \left\{ \frac{gL}{2\pi} \tanh\left(\frac{2\pi D}{L}\right) \right\}^{\frac{1}{2}} \tag{3.17}$$

D is depth of water; L, wavelength; and g, gravity. For $D/L > 0.5$, $\tanh\left(\frac{2\pi D}{L}\right)$ is usually replaced with unity and:

$$C_0 = \left\{ \frac{gL_0}{2\pi} \right\}^{\frac{1}{2}} \tag{3.18}$$

where the subscript 0 denotes deep water. Hence:

$$\frac{C}{C_0} = \left\{ \frac{L}{L_0} \tanh\left(\frac{2\pi D}{L}\right) \right\}^{\frac{1}{2}} \tag{3.19}$$

If it is assumed that the period, T, of the wave remains constant during its propagation, then:

$$T = \frac{L_0}{C_0} = \frac{L}{C} \tag{3.20}$$

From (3.19) and (3.20) it follows that:

$$\frac{C}{C_0} = \frac{L}{L_0} = \tanh\left(\frac{2\pi D}{L}\right) \tag{3.21}$$

These relations show that $\frac{D}{L}$, $\frac{C}{C_0}$, and $\frac{L}{L_0}$ are all functions of $\frac{D}{L_0}$, and for any deepwater conditions $\frac{L}{L_0}$ can be determined for any given $\frac{D}{L}$.

The wave energy averaged over one wavelength is:

$$E = \tfrac{1}{8}\,\rho g \eta^2 \tag{3.22}$$

and the rate of transfer of energy, P, is given by:

$$P = E\,n\,C \tag{3.23}$$

where

$$n \equiv \tfrac{1}{2}\left\{1 + \frac{\left(\frac{4\pi D}{L}\right)}{\sinh\left(\frac{4\pi D}{L}\right)}\right\} \tag{3.24}$$

Recall that orthogonals are perpendicular to the wave crests and let b and b_0 be the separation between two successive orthogonals in shallow and deep water, respectively. In the classical approach to water-wave refraction, it was always assumed that no energy was dissipated or transmitted across the orthogonals, so that the same power passed all positions between two orthogonals, i.e.:

$$P_0 b_0 = P b \tag{3.25}$$

P_0 is the average value of the power transmitted in deep water. Then from (3.22), (3.23), and (3.25):

$$\frac{\eta}{\eta_0} = \left\{\frac{1}{2n}\,\frac{C_0}{C}\right\}^{\frac{1}{2}} \left(\frac{b_0}{b}\right)^{\frac{1}{2}} \tag{3.26}$$

Equation (3.26) and a refraction diagram can be used to estimate wave height at any given position. The above analysis does not include the effects of bottom friction.

Stokes (1847) did not assume small steepness and, unlike Airy in his theory, he included higher-order terms and represented the wave profile by a trigonometric series. Stokes' wave profile has sharper crests and broader troughs than those in Airy's theory. In practice, only the first three terms from Stokes' theory are used. Skjelbria's (1959) tables for the Stokes wave parameters were summarized by Beitinjani and Brater (1965).

Let L be the wavelength and η the elevation of the surface relative to the equilibrium position. Then:

$$\frac{\eta}{L} = A_1 \cos\theta + A_2 \cos 2\theta + A_3 \cos 3\theta \tag{3.27}$$

where θ is defined as:

$$\theta \equiv 2\pi \left(\frac{x}{L} - \frac{t}{T} \right) \tag{3.28}$$

The wave propagates in the x-direction, t is time, and T is the period of the wave. The coefficients A_1, A_2, A_3 are defined through the following relations:

$$\frac{\eta}{D} \equiv \frac{L}{D} \left[2A_1 + 2\pi^2 A_1^3 \left\{ \frac{\frac{3}{16} \times 8 \left(\cosh \frac{2\pi D}{L} \right)^6 + 1}{\sinh \left(\frac{2\pi D}{L} \right)} \right\} \right] \tag{3.29}$$

$$A_2 \equiv \pi A_1^2 \frac{\cosh \left(\frac{2\pi D}{L} \right) \left\{ \cosh \left(\frac{4\pi D}{L} \right) + 2 \right\}}{2 \left(\sinh \frac{2\pi D}{L} \right)^3} \tag{3.30}$$

$$A_3 \equiv \frac{3}{16} \pi^2 A_1^3 \frac{\left\{ 8 \left(\cosh \frac{2\pi D}{L} \right)^6 + 1 \right\}}{\left(\sinh \frac{2\pi D}{L} \right)^6} \tag{3.31}$$

The wave celerity, C, is given by:

$$\frac{C^2}{L} = \frac{g}{2\pi} \tanh \left(\frac{2\pi D}{L} \right) \left[1 + (2\pi A_1)^2 \frac{\left\{ \cosh \left(\frac{8\pi D}{L} \right) + 8 \right\}}{8 \left(\sinh \frac{2\pi D}{L} \right)^4} \right] \tag{3.32}$$

Equations (3.18) and (3.32) give:

$$\frac{D}{L_0} = \frac{D}{L} \tanh \left(\frac{2\pi D}{L} \right) \left[1 + (2\pi A_1)^2 \frac{\left\{ \cosh \left(\frac{8\pi D}{L} \right) + 8 \right\}}{8 \left(\sinh \frac{2\pi D}{L} \right)^4} \right] \tag{3.33}$$

L_0 is the wavelength in deep water and can be obtained from (3.18), (3.20) to give:

$$L_0 = \frac{g}{4\pi^2} T^2 \tag{3.34}$$

Equations (3.17) and (3.32) are similar except for the second term in the parenthesis

of the latter. When the wave height is small, $A_1 \to 0$ and (3.32) reduces to (3.17). Equations (3.29), (3.30), (3.31), and (3.33) show that, although D/L is only a function of D/L_0 in the small-amplitude wave theory, in Stokes' theory it is a function of η/D also. This means to calculate the wavelength, L, at a certain depth, D, the waveheight, η, must be known. Because this is not known, D/L and η have to be determined from a transcendental relation by trial and error.

Beitinjani and Brater Method for Extreme Refraction

In the determination of wave heights from refraction diagrams, it is usually assumed that no energy is transmitted across surfaces orthogonal to wave crests. Of course, this assumption is invalid for cases of extreme refraction when wave crests exhibit a significant amount of curvature and wave height varies substantially along the wave crests. Beitinjani and Brater (1965) developed a technique that can be used in such situations, and checked their theory against laboratory experiments.

They applied Stokes' theory for small-bottom slopes although, strictly speaking, it is meant for uniform depth only. Let x be direction of wave propagation and z the vertical coordinate, positive upward. Let D be water depth, H be wave height (actually maximum range of the wave in the vertical direction), and $\eta(x,t)$ deviation of water level from its equilibrium position. Let ϕ be velocity potential, ρ density of the water, and L the wavelength. Then for a progressive wave, rate of transfer of energy, P, across a fixed strip of unit width and averaged over one wavelength, L, is:

$$P = \frac{\rho}{L}\int_0^L \int_0^{D+\eta} \frac{\partial \phi}{\partial t}\,\frac{\partial \phi}{\partial x}\,dz \cdot dx \tag{3.35}$$

The velocity $\partial\phi/\partial x$ nondimensionalized with respect to C, where C is defined by Equation (3.32), is:

$$\frac{1}{C}\,\frac{\partial \phi}{\partial x} = F_1 \cosh\left(\frac{2\pi z}{L}\right)\cos\theta + F_2 \cosh\left(\frac{4\pi z}{L}\right)\cos 2\theta + F_3 \cosh\left(\frac{6\pi z}{L}\right)\cos 3\theta \tag{3.36}$$

where θ is defined in (3.28) and F_1, F_2, and F_3 have the following definitions:

$$F_1 \equiv \frac{2\pi A_1}{\sinh\dfrac{2\pi D}{L}} \tag{3.37}$$

$$F_2 \equiv \frac{\frac{3}{4}(2\pi A_1)^2}{\sinh\left(\dfrac{2\pi D}{L}\right)} \tag{3.38}$$

and

$$F_3 \equiv \tfrac{3}{64}\,(2\pi A_1)^3\,\frac{\left\{11 - 2\cosh\left(\frac{4\pi D}{L}\right)\right\}}{\sinh\left(\frac{2\pi D}{L}\right)^7} \tag{3.39}$$

Define:

$$\zeta \equiv \frac{z}{L} \qquad \xi \equiv \frac{x}{L} \tag{3.40}$$

which are the nondimensional space variables. Noting that:

$$\frac{\partial \phi}{\partial t} = -\,C\,\frac{\partial \phi}{\partial x} \tag{3.41}$$

Equation (3.35) becomes:

$$\frac{P}{C^3\,\rho L} = \int_0^{1} \int_0^{(D+\eta)/L} \frac{1}{C^2}\left(\frac{\partial \phi}{\partial x}\right)^2 d\zeta \cdot d\xi \tag{3.42}$$

The right side of this equation is a function of the dimensionless parameters, D/L and H/D.

Beitinjani and Brater (1965) reduced the double integral in (3.42) to a single integral and solved it numerically. They gave plots of $P/(C^3\rho L)$ vs. H/D with isolines of D/L shown on it. Also, from (3.32) plots of C^2/L vs. H/D were prepared with isolines of D/L.

Wave Refraction Theory when Caustics are Present

Chao (1970) developed a theory for refraction of water waves that would hold even in the presence of caustics. Caustic is defined as a smooth surface or curve forming the envelope of a family of rays. If the ray-theory approach to wave refraction is used then near a caustic infinite wave heights are obtained, which is meaningless. Chao introduced the bottom slope into the equations and solved these by an asymptotic solution in terms of the inverse of the bottom slope. In his solution, the amplitude of the wave increases monotonically and attains a maximum immediately before arriving at the caustic. On the caustic itself a phase shift of $\left|\frac{\pi}{2}\right|$ occurs and some fraction of the wave energy is diffracted onto the other side of the caustic. On the far side of the caustic, wave amplitude decreases exponentially with increasing distance from the caustic.

Chao used spherical polar coordinates so that refraction of water waves traveling over large expanses of the globe can be computed. He stated that he used the technique developed by Ludwig (1965, 1966, 1968) to solve the problem of refraction at a caustic. Ludwig's technique used a new kind of "uniform asymptotic solution" involving the Airy function. On one side of the caustic the expansion is similar to that of geometrical optics, and on the other side of the caustic an exponentially

damped solution is obtained. Near the caustic there is a smooth transition from oscillatory to exponentially damped solution and the solution is finite on the caustic itself. Although Chao's solution is elegant, because of space requirements, it will not be included (see Chao 1970).

Construction of Refraction Diagrams for Tsunamis

Several authors have developed methods suitable for digital computer to construct refraction diagrams for use with tsunami studies (e.g. Momoi 1964). Usually the input to these programs consists of water depths, direction of wave, separation angle, and ray separation between two adjacent rays. The output from the model is the path of wave orthogonals, refraction coefficients, wave heights, and travel times.

Keulegan and Harrison (1970) described a method for constructing tsunami refraction diagrams with a digital computer. These authors developed a scheme to provide input for a hydraulic model to simulate protection of Crescent City, Calif., from tsunamis by a breakwater. Compensation was also made for the distortion of the earth's surface that occurs on a Mercator map. Figure 3.4 shows the

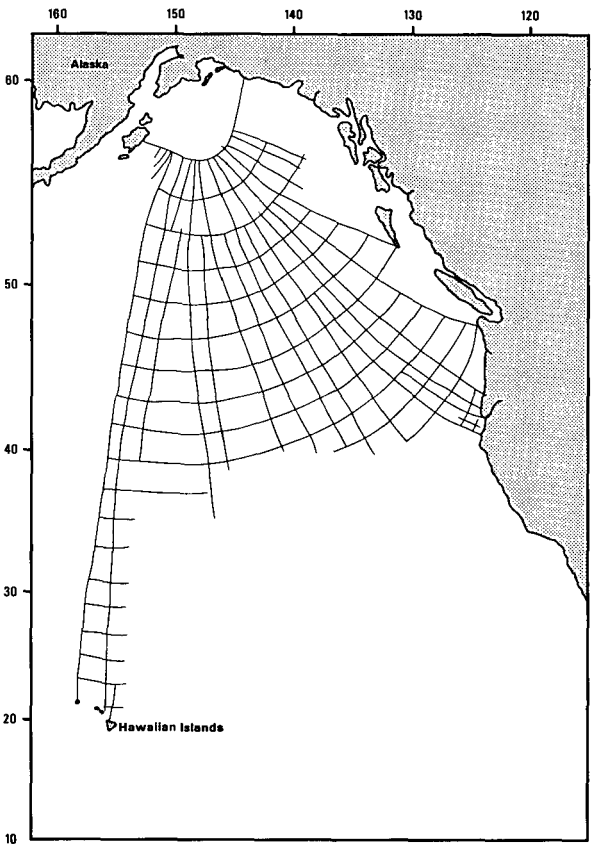


FIG. 3.4. Refraction diagram for 1964 Alaskan tsunami. (Keulegan and Harrison 1970)

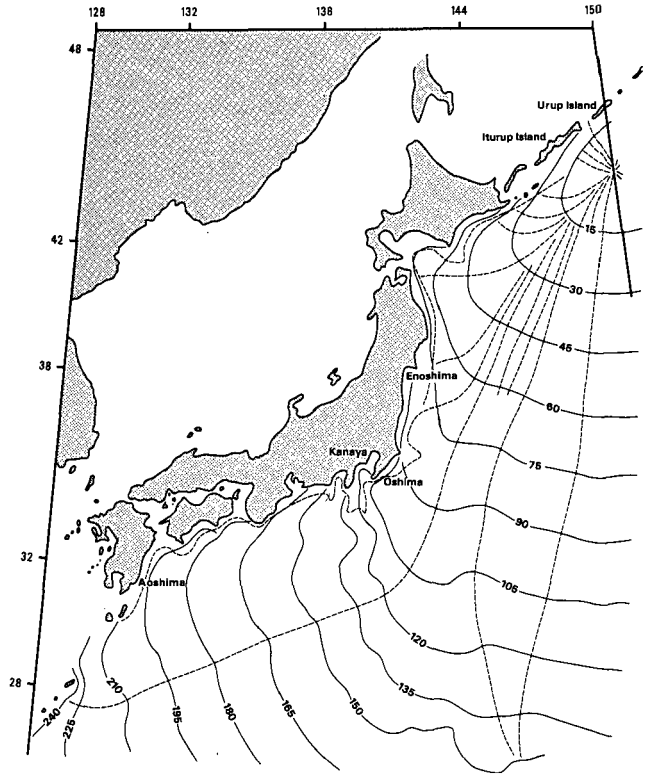


FIG. 3.5. Refraction diagram of wave fronts at 15-min intervals for the October 1963 tsunami. (Hatori and Takahasi 1964)

refraction diagram for the Alaskan earthquake tsunami of March 1964. Figure 3.5 shows the refraction diagram for the tsunami of October 1963 near Japan.

For a recent article on numerical models for wave refraction see Chu (1975), and for a good review on effects of refraction and shoaling on the propagation of explosion-generated waves see LeMéhauté (1971). Without going into detail, the approach presented by LeMéhauté (1971, p. 23) was:

> "... in addition to dispersion; reflection, refraction, shoaling, bottom friction, and nonlinear convective effects are important. Since a generalized theory for dispersive waves of finite amplitude over a complex bottom topography is beyond the present state of the art, one has to rely upon simplified theories which permit one to assess the most realistic practical approach and to determine an order of magnitude of the corrections due to secondary effects.
>
> "The fundamental approach consists of developing a numerical technique for wave shoaling and wave refraction for linear dispersive waves travelling over a one-dimensional bottom topography. The method is based on the assumption of conservation of wave energy flux as developed by Van Dorn (1964). Other effects will appear mostly as corrections to the fundamental results.... It was demonstrated that these corrections are indeed negligible in most cases. The following simplifying assumptions must be made.

"The first assumption of importance is the neglect of the dispersive effect. In the case of an explosion located at a far distance from a significant depth variation, this assumption is certainly valid if the slope is short. It is also valid in shallow water since the group velocity tends to equal the phase velocity. The wave trains can then be considered as quasi-periodic; i.e., the wave pattern is treated as a succession of periodic waves since the variation of wave period from wave to wave is indeed very small at a great distance from the explosion. The reflective effect due to a depth variation may be calculated for plane periodic waves assumed to be of small amplitude. This method is not suitable for explosions taking place on or very nearby a slope. However in this latter case the reflection coefficient may often be neglected since the waves simply tend to be shorter in length near the explosion. In shallow water, nonlinear effects of importance are due to convective inertia and quadratic bottom friction. Suitable mathematical treatments are based on steady state periodic or solitary waves.

"Free surface profile and velocity and pressure fields are then given by high-order Stokian theories or cnoidal theories valid for steady-state periodic waves. The nonlinear wave-shoaling correction is calculated by assuming conservation of energy flux for nonlinear waves. The wave damping effect due to a quadratic bottom friction is determined from a dissipation function, either for periodic long waves or solitary waves. This effect is a nonnegligible correction in the case of long shallow bottom topographies. There is presently no simple practical method to account for the possible instability of these high-peaked long waves as they arrive in shallow water even though this phenomenon should be expected."

LeMéhauté also studied nonlinear effects caused by convective inertia and bottom friction. He subdivided the influence of the convective inertia into three parts: (1) a free surface profile, pressure field, and velocity field different from those given by the linear theory; (2) a high probability of wave profile instability causing the generation of multiple undulations from each linear wave given by the Kranzer–Keller solution; and (3) a variation of wave height due to bottom-depth variation different from the one which would be given by the laws obtained by assuming conservation of energy flux for linear periodic waves. In the first and third cases, periodic, nondispersive waves can be considered. For shallow water, phase dispersive effect can be neglected because group velocity equals the phase velocity.

LeMéhauté found that the correction to the wave profile because of bottom friction somewhat balanced the correction due to nonlinear effects, thus, neglect of both effects might be justified in studying the propagation of explosion-generated waves.

Diffraction of Water Waves

Diffraction is a well-known phenomenon, especially concerning optics and acoustics. Although the same principles more or less carry over into hydrodynamics, generally speaking it will be convenient to define water-wave diffraction, as is understood in coastal engineering (Wiegel 1964, p. 180):

"Consider a wave system interrupted by an impervious structure such as a breakwater. The portion of the waves incident to the structure will be reflected, or break, or both, whereas the portion moving past the tip of the surface will be the source of a flow of energy in the direction essentially along the wave crest and into the region in the lee of the structure. The 'end' of the wave will act somewhat as a potential

source and the wave in the lee of the breakwater will spread out in approximately a circular arc with the amplitude decreasing exponentially along this arc. The same phenomenon will also occur in the reflected portion of the wave. This complicates the physical picture considerably, as part of the wave energy associated with the 'radial' wave being generated from the 'end' of the reflected wave, will move into the harbour region. The two sets of waves cylindrical and radial, reinforce and cancel each other in such a manner as to cause an irregular wave height in this region. This physical phenomenon is known as diffraction."

Sommerfield (1896), in connection with optics, solved the problem of diffraction of a plane wave by a half-plane. Penny and Price (1944) showed that Sommerfield's solution holds for diffraction of water waves also. Many papers in the literature deal with diffraction of water waves around a breakwater. But most use in some form or other Sommerfield's solution, which involves the method of separation of variables. However, this restricts these methods for very simple shapes of the breakwater.

Wada (1965) used integral equations to show that the Wiener–Hopf technique to solve more complicated diffraction problems could be successful. Momoi (1967a, b; 1968a–c; 1969a–d) considered very extensively and intensively diffraction about a breakwater.

Although it may be somewhat out of place in the sense that it does not concern diffraction, there is a useful paper by Longuet-Higgins (1967) where he derived simple formulae to deduce the wave-induced difference in mean sea level between the two sides of a submerged breakwater. This result follows from the concept of radiation stress which will be discussed in Chapter 4. When waves approach a submerged breakwater or sand bar, the water level is usually higher on the far side of the breakwater than along the wave-incident side.

Jarlan's (1965) study of perforated vertical breakwaters for shore protection introduced many analogies to acoustic wave concepts, and might prove to be practicable in certain situations. Another work of practical importance is that of Morrow (1966) where he calculated the diffraction of ocean waves about a breakwater outside a harbor (or marina) mouth.

Scattering of Water Waves

Katz (1963b) used an analogy with geometric optics to derive a ray theory for wave propagation in a nonuniform medium and applied it to tsunami propagation.

Although the medium is nonuniform it is assumed to be statistically homogeneous and the aim is to follow the trajectory of a phase point. Katz specifically examined two effects; the retardation of the phase point by the variable local wave speed along the trajectory, and the further retardation and dispersion caused by meandering. He described the retardation of the wave front and the dispersion of the phase point from the incident radiation in terms of mean and mean-squared displacements.

Katz (1963a) took 0.3 m as a typical tsunami height, 161 km as a typical length of the tsunami wave, 805 km as a typical length of the bottom irregularities, and 2.4 km as an average depth of the ocean. Based on his theory for these typical

values, he deduced that for a tsunami to travel 9654 km the variable depth will retard the tsunami by a quarter-wave period, which might amount to several minutes.

Carrier (1970) used stochastic concepts to study the scattering of tsunamis (as they travel over the irregular topography of the ocean) and concluded that scattering is not important during tsunami travel over the deep part of the ocean. Nevertheless, because of the promise of stochastic concepts to tsunami problems Carrier's paper will be considered briefly. He cautioned that at the outset reflection and scattering associated with depth variations could be considered significant, because if a one-dimensional depth distribution such as:

$$H = H_0 (1+\epsilon \cos (2k_0 x)) \tag{3.43}$$

is assumed, and $\epsilon \sim 1/50$ and $\lambda = 2\pi/k_0 \sim 161$ km is used, most energy in a spectral band $|k - k_0| < \frac{1}{2} \epsilon k_0$ would not be expected to arrive at the target. Carrier felt there was no observational evidence to support this contention and there should be a better method to estimate the strength of the reflections. He used a one-dimensional bottom topography and justified this as follows (Carrier 1970, p. 249):

> "We will treat the phenomenon as though the bottom topography were one-dimensional and as though it were one realization of a family of bottom topographies whose properties are known stochastically. We adopt this point of view not only because no precise description of the topography is available, but also because the appropriate one-dimensional 'sections' of that topography will vary from one tsunami to another in accord with their different locations. Thus, in a very real sense, we are studying an ensemble of problems characterized by an ensemble of depth distributions. The palatability of the decision to treat the problem as a stochastic one is also enhanced by the observation that the deterministic problem with a realistic depth distribution would be very difficult to solve."

Over the deep ocean the amplitude of the tsunami is at the most a few meters but its length could be several hundred kilometers. This means the surface slope is negligible and the nonlinear effects can be ignored. In this work, Carrier ignored dispersion as he had studied it in an earlier paper (Carrier 1966). Hence, in the 1970 work he studied the propagation of a monochromatic gravity wave over an ocean of variable depth and, in the mathematical formulation, used the linear shallow-water wave theory. Carrier (1970) concluded that very little tsunami energy in any spectral region is deterred from reaching any given target by the irregularities of deepwater bottom topography. This agrees with Katz (1963b).

Munk (1963) introduced several useful concepts for tsunami dissipation (in analogy with acoustics). A typical e-folding time (i.e. time taken for the initial intensity to decay to $\frac{1}{e}$ of its value) for tsunamis is $\frac{1}{2}$ day and a typical reverberation time is of the order of a week. (When a pistol is fired in an empty hall the sound echoes and reechoes from the walls, ceilings, and floors for a considerable time. Acoustical engineers call this phenomenon "reverberation time.") For Pacific Ocean tsunamis, he also considered the leakage of energy into the Atlantic and Indian oceans.

Munk estimated the circumference of the Pacific Ocean to be 45,000 km, not including the Antarctic windows of 3500 km. To estimate the circumference, all

irregularities of the coastline shorter than a wavelength were ignored. From this information, Munk estimated that roughly 1.7 reflections per day could occur in the Pacific Ocean.

Munk grouped the phenomena of geometric spreading, dispersion, reflection, and scattering under one heading, "diffusion," because all these processes diffuse the energy over the ocean basin without dissipating the tsunami energy into heat. Munk (1963, p. 55) envisaged the process as follows:

> "Initially the disturbance is confined within a circular annulus spreading from the epicenter. Its radius increases as C t, or by about 750 km/hour, and the energy density within the annulus must diminish accordingly. The initial annulus width is determined by the dimensions of the disturbance. The width increases slowly with time because of dispersion; energy associated with high frequencies spreads somewhat more slowly than that associated with lower frequencies. The variable depth of the sea (variable 'index of refraction') leads to further modifications. Shoals and deeps whose horizontal extent is large as compared to the tsunami wave length lead to refractive convergences or divergences of energy; features that are comparable in wave length are effective in scattering the energy (small features are relatively ineffective scatterers). Islands of comparable dimensions are very effective scatterers. Large islands reflect the energy. The coastline reflects and scatters the energy, again depending on the dimensions of the irregularities. Another feature is the leakage of energy into the Atlantic and Indian Oceans."

Munk concluded that the duration of the tsunami would not be significantly affected by dispersion from the following arguments. First, he wrote:

$$C = C_0 (1 - \tfrac{1}{6} \mu^2) \tag{3.44}$$

where

$$\mu(f) \equiv 2\pi f \sqrt{\frac{h}{g}}$$

$C_0 = \sqrt{gh}$ is the velocity at zero frequency and $C(f)$ is the velocity at frequency, f. As most tsunami energy is contained in frequencies less than 12 cycles/h, $f = 1/300$ cycles per s (cps). Also, taking an average depth of 4 km for the Pacific Ocean, $\mu \simeq 0.4$ and $C/C_0 \simeq 0.97$ are obtained. Thus, the dispersive delay of high frequencies is about 3% and, according to Munk, even for the most distant source the duration of the direct wave would not increase by more than 1 h, and even after 5 days of multiple reflection and scattering, the dispersive lengthening is only by as much as 4 h.

To determine the leakage of energy from the Pacific Ocean Munk assumed a highly idealized model, where he ignored variations of intensity in a given ocean. Let I_i ($i = 1,2,3$) be the intensities of the tsunami in the Pacific, Atlantic, and Indian oceans and S_i be the surface areas. The flux of energy from the Pacific Ocean into the Atlantic is: $(I_1 - I_2)\, C\, R_{12}$ where R_{12} is the width of the opening between the oceans. There are three equations of the following form, one for each ocean:

$$\frac{1}{\alpha_1} \frac{dI_1}{dt} = -I_1 - \beta_{12}(I_1 - I_2) - \beta_{13}(I_1 - I_3) \tag{3.45}$$

where α_i ($i = 1,2,3$) are constants to be determined and β_{ij} are defined:

$$\beta_{ij} \equiv \frac{C R_{ij}}{\alpha_i S_i} \tag{3.46}$$

The other two equations can be written simply by a cyclic rotation of the subscripts, noting that $\beta_{ij} \neq \beta_{ji}$.

Next Munk assumed that the energy decayed by a factor 1/e for each reflection for the three oceans. He gave for α_i

$$\alpha_i = \frac{\pi}{8} \frac{C R_i}{S_i} \tag{3.47}$$

where R_i are the circumferences of these oceans. The leakage coefficients are then given by:

$$\beta_{ij} = \frac{8}{\pi} \frac{R_{ij}}{R_i} \tag{3.48}$$

which shows that these depend only on the fractional length of the openings or windows.

The solutions for the intensities can be written as:

$$I_i = \sum_{k=1}^{3} F_i(p_k)\, e^{-p_k(t)} ; i = 1, 2, 3 \tag{3.49}$$

knowing α_i and β_{ij}, the roots, p_k, and the coefficients, $F_i(p_k)$, can be evaluated. Figure 3.6 shows the decay of the normalized intensities for the Pacific, Atlantic, and Indian oceans. Munk (1963, p. 63) interpreted this diagram as follows:

> "The Indian and Atlantic Oceans attain maximum intensity within roughly $\frac{1}{2}$ day; inasmuch as this 'leakage time' is of the same order as the absorption time, our assumption of diffuse wave energy is hardly justified. Still certain features are suggestive: the peak intensity in the Atlantic is only 5 per cent of the intial Pacific intensity; whereas for the Indian Ocean, this figure is twice as large. The corresponding ratios in rms amplitudes are 22 per cent and 31 per cent. With some careful filtering it should be possible to extract the tsunami waves from Indian and Atlantic tide gauges. The Atlantic peak is very broad, and this implies the predominant role of a delayed leakage via the Indian Ocean as compared to the direct leakage through the narrow window between the Pacific and Atlantic. Finally, the dashed curve shows the Pacific decay in the absence of a leakage, according to exp $(-\alpha, t)$. Leakage losses are an important but not a predominant factor in accounting for the decay of tsunami energy in the Pacific."

Next Munk considered the absorption problem. He referred to the work of Miller et al. (1962) who estimated the tsunami decay time to be about 12 h. They based this on the spectra of La Jolla, Calif., tidal record for the first, second, third, and fourth 12-h intervals and the third, fourth, and fifth day, and they found the decay curves were approximately exponential. Munk asked the question, "To what extent is the recorded decay the result of diffusion of an originally concentrated source and to what extent due to energy absorption?" He arrived at an upper limit for the diffusive decay as follows: if E is the total tsunami energy, then the

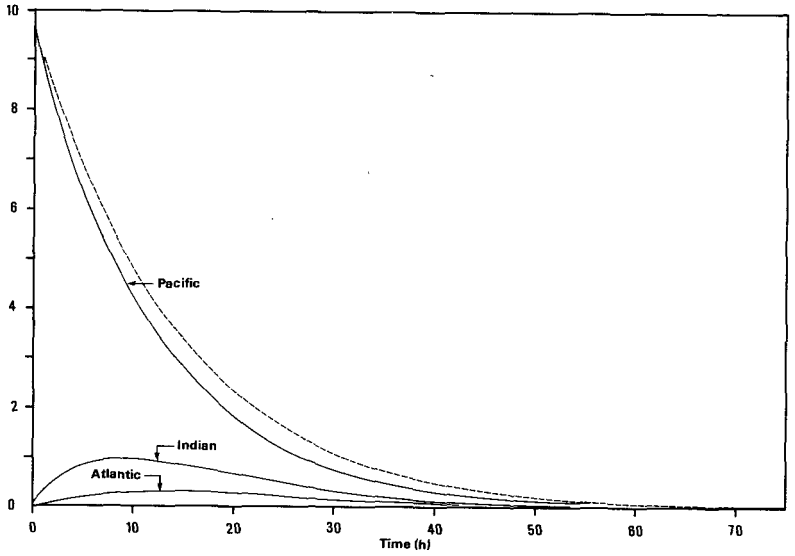


FIG. 3.6. Intensity in relative units (ordinate) in the Pacific, Indian, and Atlantic oceans. Broken curve shows Pacific decay if there were no leakages into other oceans. (Munk 1963)

intensity in the spreading annulus with width, r, is given by:

$$\frac{E}{2\pi r \cdot \Delta r} \tag{3.50}$$

which refers to the direct arrival. Because in time the energy is diffused over the area, S, of the Pacific Ocean, the intensity is E/S. Thus, the intensity decreases from the initial to the final state by the ratio $S/(2\pi r \cdot \Delta r)$. Taking typical values of $r = 8500$ km, $\Delta r = 1000$ km, and $S = 1.8 \times 10^8$, km^2 gives the reduction as 3.4 to 1. If the Atlantic and Indian oceans are included, then the reduction is about double this ratio. Even then this is insignificant compared to the observed reduction of 1000 to 1 from the first to the fifth day.

The duration of the direct signal at any given point is r/C, about $1\frac{1}{2}$ h. In the decay computation, the initial intensity used is an average value over the first 12 h and, subsequently, the same interval was used for averaging. The reflection frequency is 1.7 cycles per day, and 12 h is about the same order of magnitude as the interval between boundary reflections. This means, a time average over 12 h at a given point is approximately the same as the space average over the whole ocean. Munk (1963, p. 65) further stated:

> "If there were little diffusion, the record would consist of intermittent arrivals of the direct and reflected signals. Even then, the intensity averaged over a reflection time would be far less than that of the strong intermittent signals and not much removed from the 'diffuse intensity' E/S. In fact, the records are not characterized by the arrival of intense intermittent signals associated with well-defined reflections, and only in rare instances have there been attempts to identify 'second arrivals' due to reflections from distant coasts (Cochrane and Arthur, 1948); rather the intensity

diminishes in a reasonably smooth fashion. This appears to be typical at all stations.

"The conclusion is then that diffusion is a minor factor in the observed decay of intensity. If diffusion were so slow that for an appreciable time the record at any one station would consist of intense intermittent signals, the decay in the intensities averaged over intervals of the order of the characteristic reflection time would primarily be an indication of absorption; and this is even more true if (as appears to be the case) the signal itself is diffuse at any early stage and then is time-averaged over a reflection time."

It has been assumed that the absorption over the whole Pacific Ocean is uniform, which, of course, is highly questionable. A more realistic situation is when a few highly localized regions account for most of the absorbing. For details on this, see Munk (1963).

3.2 Trapping Wave Energy

Summerfield (1969) made a comprehensive study of the problem of wave energy trapped by bottom topography and his arguments will be followed closely. To study trapped waves, a distinction must be made between oscillations of the first class (OFC) and the oscillations of the second class (OSC) (see Platzman 1971b, for a detailed discussion of these oscillations). Oscillations of the first class are gravity waves modified by rotation, whereas OSC can exist only in the presence of rotation.

First-Class, Trapped-Wave Motions

Eckart (1950) recognized that gravity waves generated in shallow water might get totally reflected while proceeding into deep water at the continental slope. Isacks et al. (1951) used ray theory concepts to show that these waves could be captured from the open sea and guided along a long coastline by successive reflections between the shoreline and the offshore water. Snodgrass et al. (1962) showed from theory that trapped waves could exist along California's borderland, and from spectral analysis of long-wave records they pointed out that the shoreline is a good reflector for long-wave energy. Munk et al. (1964) made observations especially designed to isolate the trapped waves from other motions and concluded that trapped waves account for most low-frequency energy. The important fact that tsunamis approaching a coast can generate trapped waves has been conclusively shown with reference to the Japanese coast by Nakamura (1962), Hatori and Takahasi (1964), Nakamura and Watanabe (1966), Aida (1967), and Hatori (1967).

Consider how the topography was modeled in some studies mentioned above. Usually the continental shelf and the deep water are modeled as two different regions, each of uniform depth, with a discontinuity of depth along the straight continental slope. A straight, vertical, and perfect reflecting wall is assumed for the coastline and this one-step model is known in the literature as the straight-ledge. Munk et al. (1964) improved this model by including a steplike variation of depth between the coast and deep sea. The main defect of these models is that the shelf is assumed to be infinitely long and of uniform width. Aida et al. (1968) performed a laboratory experimental study on the effect of the one-step model of a smooth right-angled bend on the trapped waves.

Summerfield (1969) pointed out some unclear use of the terms "trapped waves" and "edge waves." To make this clear he quoted from Longuet-Higgins (1967) who described edge waves as (Summerfield 1969, p. 5): "...type of motion possible in the neighbourhood of a plane beach inclined at a constant angle α to the horizontal. The wave progresses parallel to the shoreline, its amplitude diminishing exponentially with distance seawards (measured along the bottom)."

Stokes (1846), the first to discover these theoretically, used the linearized forms of the surface-wave equations. Ursell (1952) not only found higher-order edge waves but demonstrated their existence in laboratory experiments. Munk et al. (1956), Donn and Ewing (1956), and Donn (1959) found edge waves from water level records taken during the passage of storms (see also Freeman and Murty 1972; Murty and Freeman 1973). Theoretical calculations on the edge waves have been made by Greenspan (1956), Reid (1958), Kajiura (1958), Johns (1965), Ball (1967), and Mysak (1968a, b).

Trapping gravity wave energy (caused by guiding waves along the continental shelf) is somewhat analogous to other wave guides in geophysical problems (e.g. Love waves in the earth's crust and sound waves in the Sound Fixing and Ranging (SOFAR) channel in the oceans). The following literature on the wave guide in the shallow-water region is important. Isacks et al. (1951) suggested that gravity waves might be totally reflected from the deep water on either side of a shallow-water region. Ursell (1951) showed that surface waves could be trapped along a submerged circular cylinder. Munk and Arthur (1952) used ray theory to show that gravity waves could be guided along underwater ridges. Further work on this problem has been done by Sun (1959), Garipov (1965, 1967), and Buchwald (1969).

An important paper on trapped modes is Longuet-Higgins (1967) who showed that isolated islands might trap long waves that are guided by local bathymetry. The observation that prompted Longuet-Higgins work is the long-wave records at Macquarie Island (54°30′S, 158°58′E) which clearly showed an oscillation period of 6 min and a beat period of 3 h. He showed from theoretical calculations for an idealized circular seamount or sill, that there are some oscillations or modes trapped by the mount. He showed further that waves traveling from the open sea and incident on the mount could impart sufficient energy to these modes to make them detectable in shallow-water wave records. To explain the beat period found in the Macquarie Island records, it is tempting to invoke the Coriolis force, which causes a frequency split into identical motions propagated in opposite directions around the seamount, and would appear as a low-frequency beat in the shallow-water wave records. However, the beat period arising in this manner is too large to account for that of Macquarie Island. The asymmetry of the island was pointed out by Longuet-Higgins to be the cause of this frequency split.

There are other important works on the general problem of wave motion around seamounts or islands. Arthur (1946, 1951) showed that the effect of the local bathymetry in refracting waves around an island is an important factor in creating large waves on the lee shore. The severe damage caused by tsunamis motivated several authors to calculate the response of the shallow-water region around an island to incoming long-wave radiation from the open sea. Omer and Hall (1949),

Homma (1950), Wong et al. (1963), and Webster and Perry (1966) used simple models to calculate amplitude response curves. Some laboratory experiments were done by Wong et al. (1963) and Williams and Kartha (1966). More complex and more realistic topography was included in calculations by Momoi (1967) and Vastano and Reid (1967).

Second-Class, Trapped-Wave Motions

The so-called oscillations of the second class (OSC) owe their existence to the earth's rotation. These waves also could get trapped like the gravity waves discussed earlier. Reid (1958), while studying the effect of Coriolis force on OFC, found another type of very low-frequency motions that propagate along (in the same direction as Kelvin waves) and are almost confined to the shoreline, which he called quasi-geostrophic boundary waves. For these waves, the longshore component of the fluid flow and the offshore wave slope approximately balance each other.

Two extreme cases arise: the longshore wavelength of these waves is much less or much greater than the width of the shelf. In the former case, Mysak (1968a) showed that the finite width of the shelf has no influence on the waves whereas in the latter case, Robinson (1964) showed that the waves are more or less confined to shallow water and he named these free, second-class, surface wave motions "continental shelf waves."

The concept of the inverse barometric effect will be briefly introduced. It has been observed that the sea level responds to atmospheric pressure changes in an inverse manner, about 1 cm of water level per mb of pressure change. However, there are many instances when the inverse barometric effect does not apply.

Hamon (1962, 1963, 1966) studied the sea-level data on the Australian coast and concluded that shallow water did not respond barometrically to low-frequency atmospheric pressure fluctuations. Based on the data of adjacent tide gages, he showed that a northward traveling wave existed along the east coast and a southward traveling wave on the west coast of Australia. Mooers and Smith (1968) did spectral analysis of the sea-level and atmospheric pressure data recorded along the Oregon coast and deduced the existence of free, continental shelf waves propagating northward. Mysak and Hamon (1968) showed that a similar wave traveling southward could exist along the east coast of the USA. Shoji (1955, 1961) observed similar waves along the Japanese coast and Yoshida (1960) speculated these might be surface manifestation of internal Kelvin waves.

The absence of the inverse barometer effect in the work described by Hamon was attributed by Robinson (1964) to the excitation of the fundamental shelf wave. Mysak (1966, 1967a, b) treated the continent of Australia as circular and assumed that an atmospheric pressure system propagates across it from west to east and showed that resonance coupling with this atmospheric pressure field could excite shelf waves. Adams and Buchwald (1968) showed that the longshore component of the geostrophic wind could excite horizontal, nondivergent shelf waves and these could account for the behavior of the sea level described by Hamon. Buchwald and Adams (1968) used theoretical dispersion relations to show that the quasi-geostrophic waves are similar to the Rossby or planetary waves originally introduced

in the field of meteorology. Several authors (e.g. Longuet-Higgins 1964) studied these in the context of oceanography.

Longuet-Higgins (1968) theoretically showed that for continental shelf waves to exist, the shallow-water region could have infinitesimal width. He showed that under uniform rotation, long waves could be trapped along a straight-line discontinuity separating two regions, each of uniform depth, and the trapped waves were the OSC-type and propagated along the discontinuity only in the same direction of travel as Kelvin waves in the deeper of the two regions. Buchwald and Adams (1968) extended the Longuet-Higgins (1968) study for a straight shelf of uniform width that slopes between the two regions and obtained guided motions of the nondivergent type. For these OSC, the potential vorticity is conserved under the action of conservative forces (Ball 1965).

Rhines (1969a, b) extended Buchwald and Adams (1968) study by considering an ocean on a $\beta-$ plane where β is the variation of the Coriolis parameter, f, with latitude. Although on the globe β varies with latitude, in the $\beta-$ plane approximation it is treated as uniform. His study showed that the motions are guided along coherent and closely spaced contours of the ratio, f/D, where D is the depth of the ocean.

The motions considered here under OSC have periods greater than a pendulum day, defined as the period of revolution of a Foucault's pendulum. This is given by:

$$\text{pendulum day} = 2T_p = \frac{2\pi}{\Omega \cdot \sin\theta} \tag{3.51}$$

where θ is the latitude and Ω is the angular velocity of earth's rotation. This expression shows that the pendulum day varies from place to place, depending on latitude. It is $2\pi/\Omega$ at the pole and tends to ∞ at the equator. When the rotation $\Omega \to 0$ the OSC become steady currents. Crease (1956) speculated that in a uniformly rotating ocean of uniform depth the existence of a trapped long wave along a finite length straight-line barrier is possible. The works of Chambers (1964) and Williams (1964) verified Crease's suggestion. A similar phenomenon was discovered by Sekerzh-Zen'kovich (1968) for a cylindrical island in an ocean of uniform depth. These special types of OSC propagate along the barrier or island in the same sense as a Kelvin wave. However, although the motions exist only in the presence of rotation, they have periods less than a pendulum day and in that sense do not belong strictly to OSC. After reviewing the mathematical theory and results of the trapped motions following Summerfield (1969), the developments subsequent to Summerfield's work will be considered briefly.

Mathematical Formulation of the Trapped-Wave Problem

Following Summerfield (1969), the mathematical problem for trapped waves will be formulated. Solutions for different geometries and under different conditions will be considered in subsequent subsections. Consider a right-handed Cartesian coordinate system (x,y,z) with the origin at the undisturbed position of the water surface and the vertical z-axis positive upward. Let $h(x,y)$ be the depth of water in the undisturbed state and let $\zeta(x,y,t)$ denote the deviation of the water level

from its equilibrium position, t being time. Let g be the acceleration due to gravity and U and V the x and y components of the fluid velocity. The Coriolis parameter, f, is defined as:

$$\begin{aligned} f &= 2\Omega \sin\theta \\ &= 2\Omega \cos\phi \end{aligned} \tag{3.52}$$

where θ is the latitude ($\phi = 90° - \theta$ is the colatitude) of the center of the region under consideration. The linearized shallow-water equations of motion in the x and y directions for a uniformly rotating homogeneous fluid are:

$$\begin{aligned} \frac{\partial U}{\partial t} - fV &= -g\frac{\partial \zeta}{\partial x} \\ \frac{\partial V}{\partial t} + fU &= -g\frac{\partial \zeta}{\partial y} \end{aligned} \tag{3.53}$$

The continuity equation is:

$$\frac{\partial \zeta}{\partial t} + \frac{\partial}{\partial x}(hU) + \frac{\partial}{\partial y}(hV) = 0 \tag{3.54}$$

Define:

$$\begin{aligned} \nabla^2 &\equiv \frac{\partial^2}{\partial x^2} + \frac{\partial^2}{\partial y^2} \\ \underline{\nabla} h \cdot \underline{\nabla} &\equiv \frac{\partial h}{\partial x}\frac{\partial}{\partial x} + \frac{\partial h}{\partial y}\frac{\partial}{\partial y} \\ \hat{\underline{\Omega}} \cdot \underline{\nabla} h \times \underline{\nabla} &\equiv \frac{\partial h}{\partial x}\frac{\partial}{\partial y} - \frac{\partial h}{\partial y}\frac{\partial}{\partial x} \end{aligned} \tag{3.55}$$

Then manipulation of (3.53) and (3.54) gives:

$$\left\{\nabla^2 - \frac{1}{gh}\left(\frac{\partial^2}{\partial t^2} + f^2\right) + \frac{1}{h}\underline{\nabla} h \cdot \underline{\nabla}\right\}\frac{\partial \zeta}{\partial t} + \frac{f}{h}\hat{\underline{\Omega}} \cdot \underline{\nabla} h \times \underline{\nabla}\zeta = 0 \tag{3.56}$$

Assume simple harmonic motion with respect to t:

$$\zeta(x,y,t) = e^{-i\sigma t}\zeta^*(x,y)$$

where σ denotes the frequency in radians/s.

Then (3.56) becomes:

$$\left\{\nabla^2 + \frac{(\sigma^2 - f^2)}{gh} + \frac{1}{h}\underline{\nabla} h \cdot \underline{\nabla} + \frac{if}{\sigma}\frac{1}{h}\hat{\underline{\Omega}} \cdot \underline{\nabla} h \times \underline{\nabla}\right\}\zeta^* = 0 \tag{3.57}$$

If the depth, h, is uniform, then this equation reduces to:

$$\left\{ \nabla^2 + \frac{(\sigma^2 - f^2)}{gh} \right\} \zeta^* = 0 \tag{3.58}$$

If the rotation is zero, (3.58) further reduces to:

$$\left(\nabla^2 + \frac{\sigma^2}{gh} \right) \zeta^* = 0 \tag{3.59}$$

Long waves in shallow water separated from deep water by depth discontinuities of infinitesimal width will be considered. At a depth discontinuity two conditions must be satisfied.

The volume transport is the same on either side, i.e.:

$$h \underline{U} \cdot \underline{n} \text{ is continuous} \tag{3.60}$$

and the perturbation height is the same on both sides, i.e.:

$$\zeta \text{ is continuous} \tag{3.61}$$

The notation $\underline{U} = (U,V)$ is used and $\underline{n}$ denotes the unit normal at the discontinuity in depth.

Because U and V are also simple harmonic, assume $U = e^{-i\sigma t} U^*(x,y)$ and $V = e^{-i\sigma t} V^*(x,y)$. Equations (3.53) and (3.54) give:

$$\begin{aligned} U^* &= \frac{-i\sigma g}{(\sigma^2 - f^2)} \left(\frac{\partial}{\partial x} + i \frac{f}{\sigma} \frac{\partial}{\partial y} \right) \zeta^* \\ V^* &= \frac{-i\sigma g}{(\sigma^2 - f^2)} \left(\frac{\partial}{\partial y} - \frac{if}{\sigma} \frac{\partial}{\partial x} \right) \zeta^* \end{aligned} \tag{3.62}$$

If $\sigma^2 \neq f^2$, then at the depth discontinuity, the continuity of volume transport requires that:

$$h \left(\frac{\partial}{\partial n} + i \frac{f}{\sigma} \frac{\partial}{\partial s} \right) \zeta^* \text{ be continuous} \tag{3.63}$$

Here s and n are the tangential and normal directions to the discontinuity. At a rigid boundary $\underline{U} \cdot \underline{n} = 0$ hence, the condition on ζ^* is:

$$\left(\frac{\partial}{\partial n} + i \frac{f}{\sigma} \frac{\partial}{\partial s} \right) \zeta^* = 0 \tag{3.64}$$

The problem then reduces to solving (3.57) under the above boundary conditons for wave motion propagating along a coastline of prescribed geometry. As there could be no energy source for the free modes of oscillation, ζ should either tend to zero with increasing distance from the coastline or it must correspond to a wave motion propagating away from shallow water to deep water. This is the so-called radiation condition.

SCALE CONSIDERATIONS

The OFC inertia-gravity waves have small length scales so the Coriolis parameter, f, can be treated as uniform and the curvature of the earth can be ignored. However, this is not true for OSC because these could have lengths of the order of several hundred miles. Following Longuet-Higgins (1964, 1965) Summerfield incorporated β into (3.57) after taking the y-axis in a northern direction so that $\partial f/\partial y = \beta$. The modified form of (3.57) is:

$$\left[\nabla^2 + \frac{(\sigma^2 - f^2)}{gh} + \frac{1}{h}\underline{\nabla} h \cdot \underline{\nabla} + i\frac{f}{\sigma}\frac{1}{h}\hat{\underline{\Omega}} \cdot \underline{\nabla} h \times \underline{\nabla}\right]\zeta^* + \frac{\beta}{(\sigma^2 - f^2)}\left[2f\frac{\partial}{\partial y} - i\frac{(\sigma^2 + f^2)}{\sigma}\frac{\partial}{\partial x}\right]\zeta^* = 0 \tag{3.65}$$

Let a typical length scale of OSC be 1/m and as for these motions $\sigma \simeq f$, the second term in the square brackets in (3.65) is small compared to the first term, provided:

$$\left|\frac{\beta}{mf}\right| \ll 1 \tag{3.66}$$

The following relation could be used away from the equator:

$$\frac{\beta}{mf} = \frac{\tan\phi}{m\,\mathrm{R}}$$

where ϕ is the colatitude and R is the earth's radius. This expression is invalid at the equator because $f = 0$ there.

Because R $\sim$ 6436 km, to satisfy (3.66):

$$\frac{f^2}{m^2 gh} \ll 1 \tag{3.67}$$

Hence, at the scales of motion when (3.57) adequately approximates (3.65), (3.57) can be further reduced to:

$$\left\{\nabla^2 + \frac{1}{h}\underline{\nabla} h \cdot \underline{\nabla} + i\frac{f}{\sigma}\frac{1}{h}\hat{\underline{\Omega}} \cdot \underline{\nabla} h \times \underline{\nabla}\right\}\zeta^* = 0 \tag{3.68}$$

This further reduction implies that the following simpler continuity equation $\frac{\partial}{\partial x}(h\mathrm{U}) + \frac{\partial}{\partial y}(h\mathrm{V}) = 0$ replaces the usual continuity relation (3.54). The motions are horizontally nondivergent.

TRAPPED WAVES ON A STRAIGHT LEDGE

The nonrotating case — Summerfield (1969) used the following depth distribution (Fig. 3.7):

$$h(x,y) = \begin{cases} h_1 \text{ for } -a < x < 0 \\ h_2 \text{ for } x > 0 \end{cases} \tag{3.69}$$

A rigid wall located at $x = -a$ is taken as the coast. Summerfield referred to the shallow-water region between $x = -a$ and $x = 0$ as the ledge, the depth discontinuity at $x = 0$ as the edge, and the deepwater region as the ocean. It is this simple model that Snodgrass et al. (1962) used in their study of ocean waves in the period range of 6 min to 5 h over the continental shelf off La Jolla, Calif. The authors were concerned with wave motion that had the form of a standing wave on the ledge normal to the edge and propagated along the coast. They deduced a discrete spectrum of oscillations they called "trapped modes." For these modes, the amplitude decreases with increasing distance from the edge toward the ocean and the modes have a fixed number of nodal lines parallel to the coast and the j th mode has ($j = 1,2,3,\ldots$).

Longuet-Higgins (1967) assumed that the coast was a perfect reflector and showed that trapped waves were guided along the ledge by successive reflections from the coast and by total internal reflection from the edge. Following Summerfield, for a fixed wave number, m, along the edge the behavior of the j th mode when the ledge width $a \to 0$ will be studied, after deriving the dependence of the frequency σ_j on a. One important result is a cut-off ledge width, a_j, so the following situation exists:

For $a > a_j$
- σ_j is real
- The j th mode is well trapped on the ledge
- The dependence of σ_j on a can be easily derived from an eigenvalue problem

For $a < a_j$
- σ_j is complex
- The j th mode leaks energy from the ledge to the ocean
- The dependence of σ_j on a cannot be easily deduced other than through numerical evaluation

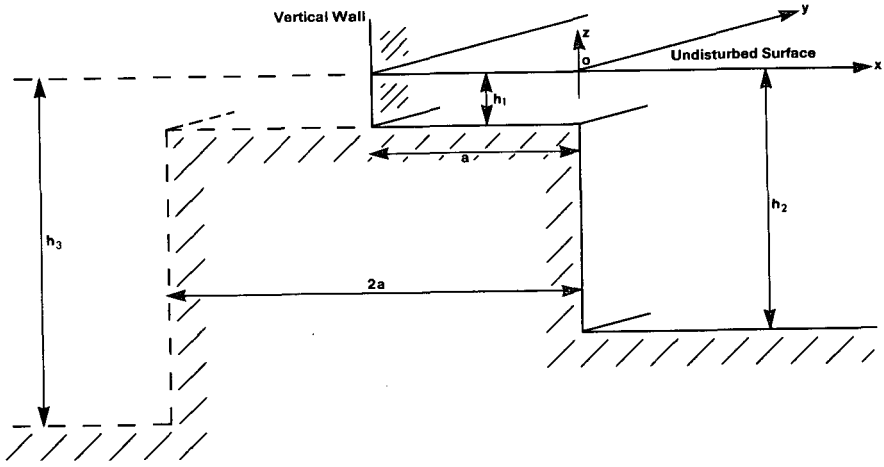


FIG. 3.7. Cross section of a ledge of uniform width a, broken line is the extension to a rectangular oceanic ridge. (Summerfield 1969)

The nonrotating case will be studied and then modification of the results when rotation is introduced will be considered. With the notation that subscript i denotes the two regions with depths h_1 and h_2 the surface elevation $\zeta^*(x,y)$ must satisfy Equation (3.59) written in compact notation as:

$$\left[\nabla^2 + \frac{\sigma^2}{gh_i}\right] \zeta_i^* = 0; i = 1, 2 \tag{3.70}$$

The following three boundary conditions have to be satisfied:

$$\frac{\partial \zeta_1^*}{\partial x} = 0 \tag{3.71}$$

At the depth discontinuity $x = 0$

$$\zeta_1^* = \zeta_2^* \tag{3.72}$$

and

$$h_1 \frac{\partial \zeta_1^*}{\partial x} = h_2 \frac{\partial \zeta_2^*}{\partial x} \tag{3.73}$$

A solution of (3.59) is: $\zeta(x,y,t) = A \cdot e^{i(\ell x + my - \sigma t)}$ where $\ell^2 + m^2 = \frac{\sigma^2}{gh}$.
The real part of this solution for ζ (with σ, m, and ℓ real) defines a simple harmonic wave of length $\lambda \equiv \frac{2\pi}{\sqrt{\ell^2 + m^2}}$ and period $\tau \equiv \frac{2\pi}{\sigma}$ which propagates along a straight line trajectory that makes an angle, ϕ, with the x-axis where:

$$\phi = \text{arc} \cdot \sin \left\{\frac{m}{\sqrt{\ell^2 + m^2}}\right\}$$

This ϕ should not be confused with the colatitude. For definiteness sake, Summerfield takes σ, m, and ℓ as positive. The wave propagates with the speed, c, shown below (the same as a long wave in shallow water):

$$c = \frac{\lambda}{\tau} = \sqrt{gh}$$

Following Longuet-Higgins (1967), Summerfield wrote the solution for the trapped waves on the ledge as the real part of:

$$\zeta(x,y,t) = A\, e^{i(my - \sigma t)} \begin{cases} R\, e^{i(\ell_1 x + \gamma)} + R\, e^{-i(\ell_1 x + \gamma)} & \text{for } -a < x < 0 \\ e^{-\ell_2 x} & \text{for } x > 0 \end{cases} \tag{3.74}$$

The parameters, ℓ_1 and ℓ_2, are defined through:

$$\begin{aligned} \ell_1^2 &\equiv \frac{\sigma^2}{gh_1} - m^2 \\ \ell_2^2 &\equiv m^2 - \frac{\sigma^2}{gh_2} \end{aligned} \tag{3.75}$$

The parameters γ and R could be expressed in terms of the other variables shown in (3.76) and (3.77) through invoking the boundary conditions (3.71), (3.72), and (3.73):

$$\gamma = \text{arc} \cdot \tan \left(\frac{h_2 \ell_2}{h_1 \ell_1} \right) \tag{3.76}$$

$$R = \tfrac{1}{2} \left\{ 1 + \left(\frac{h_2 \ell_2}{h_1 \ell_1} \right)^2 \right\}^{\frac{1}{2}} \tag{3.77}$$

and

$$\tan (a\ell_1) = \frac{h_2 \ell_2}{h_1 \ell_1} \tag{3.78}$$

If σ, m, ℓ_1, and ℓ_2 are all real, then:

$$\frac{h_1}{h_2} < \frac{m^2 g h_1}{\sigma^2} < 1 \tag{3.79}$$

Without loss of generality it can now be assumed that σ, m, and ℓ are positive. This means the wave on the ledge represented by:

$$\zeta = \text{ARe}^{i(\ell_1 x + \gamma + my - \sigma t)} \tag{3.80}$$

which travels toward the ocean, arrives at the edge at an incident angle given by arc sin $\frac{m}{\sigma} \sqrt{g h_1}$. The critical angle ϕ_c for the depth function given by (3.69) is arc sin $\sqrt{h_2/h_2}$. Hence, total internal reflection occurs at the edge and the reflected wave which travels toward the coast is represented by:

$$\zeta = \text{ARe}^{i(-\ell_1 x - \gamma + my - \sigma t)} \tag{3.81}$$

This reflected wave traveling toward the coast, gets reflected at the coast and the resulting wave travels back toward the edge. Thus, the wave motion represented by (3.74) is essentially contained on the ledge because of successive reflections from the coast and the edge, and there is only an exponentially decaying motion on the ocean side of the edge for $\ell_2 > 0$.

Longuet-Higgins (1967) suggested that the same frequency Equation (3.78) could be obtained by equating the total phase change to the wave, caused by the crossing and recrossing of the ledge in a normal direction with y and t held unchanged, to an integral multiple of 2π. For the wave motion given by Equation (3.80) this total phase change due to the total internal reflection at the ledge is -2γ. Summerfield used this method of frequency determination (described in detail in Budden (1961)) to derive the frequency equation for trapped long waves on a simple oceanic ridge. For details see Summerfield (1969, appendix 1).

Summerfield used (3.75) to rewrite the frequency Equation (3.78) as follows:

$$T(\ell_1) = E(\ell_1)$$

where

$$T(\ell_1) \equiv \ell_1 \tan (a\ell_1) \tag{3.82}$$

and

$$E(\ell_1) \equiv \frac{h_2}{h_1}\left\{\left(\frac{h_2}{h_1} - 1\right) m^2 - \ell_1^2\right\}^{\frac{1}{2}}$$

Figure 3.8 shows the plots of functions $E(\ell_1)$ and $T(\ell_1)$ vs. ℓ_1. For every nonzero value of a and m there is a discrete, but finite, number of trapped modes of wave number, m, along the ledge of width, a.

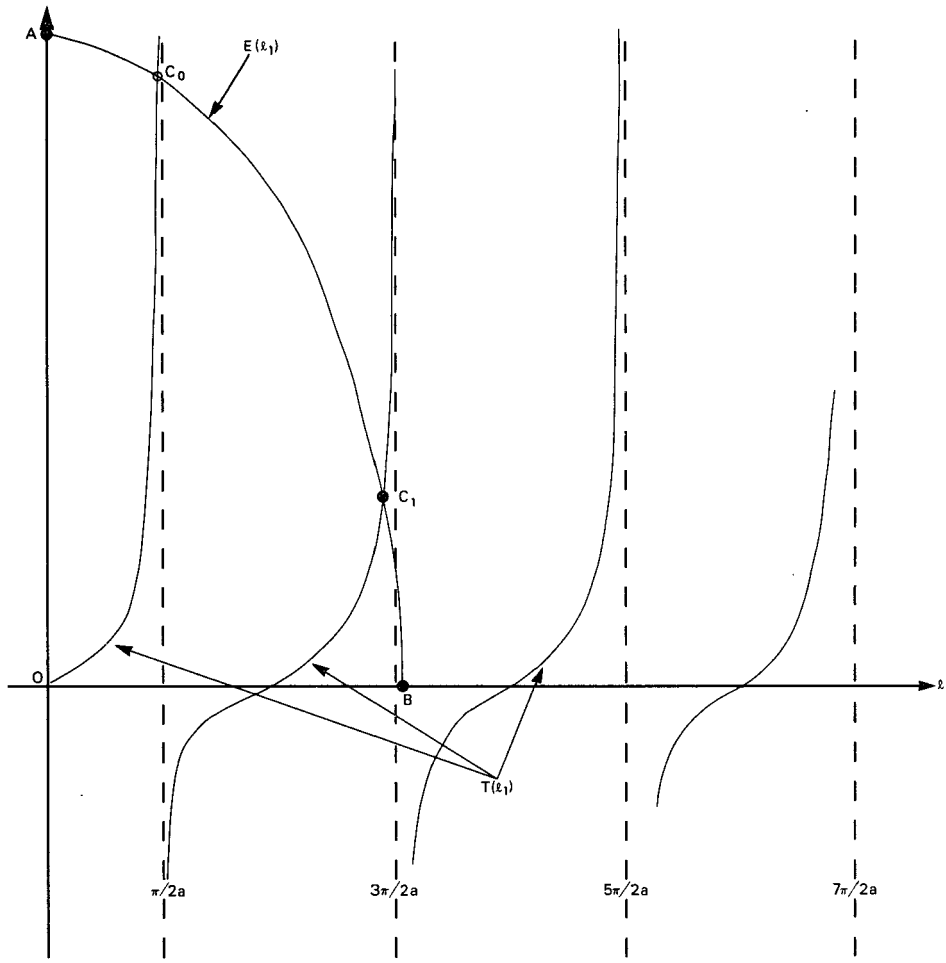


FIG. 3.8. Graphs of $T(\ell_1) = \ell_1 \tanh \ell_1$ and $E(\ell_1) = \left[\frac{h_2}{h_1}\left\{\left(\frac{h_2}{h_1} - 1\right)m^2 - \ell_1^2\right\}\right]^{\frac{1}{2}}$. Both are symmetric about $\ell_1 = 0$ and $E(\ell_1)$ intersects the axes at $A = \left(0, \left[\frac{h_2}{h_1}\left\{\left(\frac{h_2}{h_1} - 1\right)m^2\right\}^{\frac{1}{2}}\right]\right)$ and $B = \left[|m|\left(\frac{h_2}{h_1} - 1\right)^{\frac{1}{2}}, 0\right]$. (Summerfield 1969)

When root, ℓ_1, of (3.82) lies in the interval:

$$\frac{j\pi}{a} < \ell_1 < (j+\tfrac{1}{2})\,\frac{\pi}{a}; j = 0, 1, 2, 3, \ldots \tag{3.83}$$

the perfectly trapped wave is referred to as the j th mode by Summerfield. The condition for existence of the j th mode is:

$$a > a_j$$

$$a_j \equiv \frac{j\pi}{\sqrt{\left(\frac{h_2}{h_1} - 1\right)m^2}} \tag{3.84}$$

a_j being called the cut-off ledge width for the j th mode. Because the expression $\cos(\ell_1 x + \gamma)$ has γ zeros on the ledge $-a < x < 0$, the j th mode has j fixed nodal lines parallel to the coast.

The effect of the ledge width, $a \to 0$, on the j th mode can be seen partly from Fig. 3.8. If m, h_1, and h_2 are held fixed, then a_j remains unchanged, and $E(\ell_1)$ will be a fixed curve. With decreasing a, as the asymptotes $\pm\frac{\pi}{2a}, \pm\frac{3}{2}\frac{\pi}{a}, \pm\frac{5}{2}\frac{\pi}{a}$, etc., of $T(\ell_1)$ move farther away from $\ell_1 = 0$, it can be deduced that as a decreases from ∞ to a_j, ℓ_{1_j} increases monontonically from zero to $\sqrt{\left(\frac{h_2}{h_1} - 1\right)m^2}$. However, simultaneously σ_j increases monotonically from $m\sqrt{gh_1}$ to $m\sqrt{gh_2}$ (Equation (3.75)). Summerfield (1969, table 4.1) traces the corresponding variations in the other parameters.

When $a < a_j$, the wave given by (3.80) would be incident on the edge at an angle less than ϕ_c and this would create a refracted wave that propagates into the ocean away from the ledge. However, as there is no input energy into the ledge oscillation, the motion decays with time and σ_j is complex.

Summerfield verified the above conclusions by the numerical procedure where he used the following dimensionless variables:

$$\begin{aligned}
\nu &\equiv \frac{\sigma a_2}{\sqrt{gh_1}} && \text{is a dimensionless frequency} \\
\epsilon &\equiv \sqrt{h_1/h_2} && \text{is a ratio of water depths} \\
\alpha_L &\equiv \frac{a}{a_2} && \text{is a dimensionless ledge width} \\
n &\equiv m\,a_2 && \text{is a dimensionless wave number}
\end{aligned} \tag{3.85}$$

where a_2 is some positive arbitrary length. The following ranges are valid for the nondimensional parameters: $\nu > 0$, $n > 0$, $\alpha_L > 0$, and $0 < \epsilon < 1$.

Use of (3.75) and (3.85) gives $a_2 \ell_1 = \sqrt{\nu^2 - n^2}$ and $a_2 \ell_2 = \sqrt{n^2 - \epsilon^2 \nu^2}$. The non-dimensional cut-off ledge width, α_j, is given by:

$$\alpha_j = \frac{j\pi}{\left[n^2\left(\frac{1}{\epsilon^2} - 1\right)\right]^{\frac{1}{2}}} \tag{3.86}$$

The roots of the frequency Equation (3.78) give the same eigenvalues as the zeros of the function $L(\nu; \epsilon, \alpha_L, n)$ where:

$$L(\nu; \epsilon, \alpha_L, n) \equiv \epsilon^2 \sqrt{\nu^2 - n^2} \tan \alpha_L \sqrt{\nu^2 - n^2} - \sqrt{n^2 - \epsilon^2 \nu^2} \tag{3.87}$$

where ϵ, α_L, and n are fixed and ν is treated as variable. Summerfield determined these zeros numerically (see Summerfield 1969, appendix 2.1).

Thus, summarizing the results for the nonrotating case on a straight ledge as its width is decreased, it can be seen that:

$$\sigma_0 < \sigma_1 < \sigma_3 < \sigma_k < R(\sigma_{k+1}) < R(\sigma_{k+2}) < \ldots \tag{3.88}$$

The lowest order modes up to and including σ_k represent the trapped modes whereas the higher modes are the leaky modes. Here k is the largest value of j for which cut-off ledge width, a_j, is less than the actual width, a, of the ledge. As a decreases to a_j the j th mode $(0 < j \leq k)$ changes from a trapped mode to a leaky mode. For $a << a_j$, the frequency is given by:

$$\sigma_j \approx \left[\left(j - \tfrac{1}{2}\right)\pi - i \operatorname{arc} \cdot \tanh \sqrt{\frac{h_1}{h_2}}\right] \frac{\sqrt{gh_1}}{a} \; ; j \geq 1 \tag{3.89}$$

Hence, for $a < a_1$, only the fundamental trapped-wave mode may exist. This acquires the finite frequency $m\sqrt{gh_2}$ as $a \to 0$, thus this frequency depends on the wave number, m, along the edge. However, for higher modes the limiting frequency depends only on the order of the mode. Other conclusions are: if the width of the ledge is held fixed, then the number of perfectly trapped waves of prescribed wave number, m, along the edge decreases as the depth ratio, h_1/h_2, increases (Fig. 3.8). On the other hand, if the width, a, of the ledge and the depths, h_1 and h_2, are held fixed, then the number of perfectly trapped modes increases with the wave number, m. Perfectly trapped modes such as those described here, have been produced in the laboratory (Aida et al. 1968). Summerfield also showed that periodic waves impinging on the ledge traveling from the ocean could excite the leaky modes. For details on this see Summerfield (1969, appendix 4).

The rotating case — In the nonrotating case, perfectly trapped waves could propagate along the ledge in either direction. However, for the rotating case, the two waves traveling along the ledge in opposite directions have slightly differing frequencies, and another class of motions occurs that does not exist in the nonrotating case. These are OSC and have periods greater than a pendulum day and propagate along the ledge in one direction only. In the limiting case of the ledge width,

$a \to \infty$, the motions reduce to the so-called double-Kelvin waves described by Longuet-Higgins (1968).

Equation (3.58), which holds in the presence of rotation, can be rewritten as:

$$\left[\nabla^2 + \frac{(\sigma^2 - f^2)}{gh_i}\right] \zeta_i^* = 0; i = 1, 2 \tag{3.90}$$

The boundary conditions in the rotating case, corresponding to (3.71), (3.72), and (3.73) are:

$$\left(\frac{\partial}{\partial x} + i\,\frac{f}{\sigma}\,\frac{\partial}{\partial y}\right)\zeta_1^* = 0 \text{ at } x = -a \tag{3.91}$$

$$\zeta_1^* = \zeta_2^* \text{ at } x = 0 \tag{3.92}$$

$$h_1\left(\frac{\partial}{\partial x} + i\,\frac{f}{\sigma}\,\frac{\partial}{\partial y}\right)\zeta_1^* = h_2\left(\frac{\partial}{\partial x} + i\,\frac{f}{\sigma}\,\frac{\partial}{\partial y}\right)\zeta_2^* \tag{3.93}$$

The solution for the trapped waves in the rotating case can be written similar to (3.74) as the real part of:

$$\zeta(x,y,t) = Ae^{i(my-\sigma t)} \begin{cases} R_1 e^{i(\ell_1 x + \gamma_1)} + R_1 e^{-i(\ell_1 x + \gamma_1)} \text{ for } -a < x < 0 \\ e^{-\ell_2 x} \text{ for } x > 0 \end{cases} \tag{3.94}$$

The following definitions hold in the rotating case:

$$\ell_1^2 \equiv \frac{(\sigma^2 - f^2)}{gh_1} - m^2$$

$$\ell_2^2 \equiv m^2 - \frac{(\sigma^2 - f^2)}{gh_2} \tag{3.95}$$

$$\gamma_1 \equiv \text{arc} \cdot \tan\left\{\frac{h_2\ell_2 + m\,\frac{f}{\sigma}\,(h_2 - h_1)}{h_1\ell_1}\right\} \tag{3.96}$$

$$R_1 \equiv \tfrac{1}{2}\left\{1 + \left[\frac{h_2\ell_2 + m\,\frac{f}{\sigma}\,(h_2 - h_1)}{h_1\ell_1}\right]^2\right\}^{\frac{1}{2}} \tag{3.97}$$

The frequency equation in the rotating case corresponding to (3.78) is:

$$\ell_1 \tan(a\ell_1) - \frac{h_2}{h_1}\,\ell_2 = m\frac{f}{\sigma}\left\{\begin{array}{l} \dfrac{h_2}{h_1} + \dfrac{h_2\ell_2}{h_1\ell_1}\tan(a\ell_1) \\ + \dfrac{mf}{\sigma}\,\dfrac{(h_2 - h_1)}{h_1\ell_1}\tan(a\ell_1) \end{array}\right\} \tag{3.98}$$

The roots of this equation for which σ, m, ℓ_1, and ℓ_2 (taken positive) are real, gives the frequencies of the waves represented by (3.94) corresponding to perfectly

trapped modes. Summerfield confined the solution of Equation (3.98) only to the case $|f/\sigma| << 1$, because the value of this ratio deduced from observations is approximately 10^{-2}. Summerfield (1969, p. 1) observed: "Long-wave records at Macquarie Island (54°30°S, 158°58'E) display a distinctive oscillation, with a period of 6 minutes and a beat period of 3 hours. This fact has led to the suggestion that gravity waves can be trapped around islands by the form of the contours of the surrounding sea bed."

Under the approximation $|f/\sigma| << 1$, (3.98) is similar to (3.78) except for a small perturbation term:

$$m\frac{f}{\sigma}\left\{\frac{h_2}{h_1} + \frac{h_2\ell_2}{h_1\ell_1}\tan(a\ell_1)\right\}$$

The effect of this term on the real roots of (3.98) can be understood from the form of the change of ℓ_1 with f near $f = 0$. For wave motion of a fixed longshore wave number, m:

$$\left(\frac{\partial\ell_1}{\partial f}\right)_{f=0} = \frac{m}{\sigma\ell_1\left\{\frac{h_1}{h_2}\frac{1}{\ell_2} + a\left(1 + \frac{h_1}{h_2} - \frac{\sigma^2}{m^2gh_2}\right)\right\}} \tag{3.99}$$

When x is real, the function sgn (x) behaves as:

$$\text{sgn}(x) = \begin{cases} +1 \text{ for } x > 0 \\ 0 \text{ for } x = 0 \\ -1 \text{ for } x < 0 \end{cases}$$

When sgn (mf/σ) is positive, the real root of (3.98) is slightly greater than that of (3.78). On the other hand, if sgn (mf/σ) is negative, the root in the rotating case is slightly less than that for the nonrotating case. Positive sign for the sgn function means that the trapped wave is traveling along the ledge in the same direction as earth's rotation, whereas a negative sign implies travel in a direction opposite to earth's rotation. Ball (1967) called the trapped waves traveling in the same direction and opposite to earth's rotation, positive and negative, respectively. Thus, rotation causes a frequency split evaluated by Summerfield (1969).

Summerfield introduced the following dimensionless Coriolis parameter, ω:

$$\omega \equiv \frac{fa_2}{\sqrt{gh_1}} \tag{3.100}$$

Summerfield (1969, appendix 6) showed that $|\omega| < 0.1$ for typical values of f, a_2, and h_1. Equations (3.85) and (3.100) give:

$$a_2\ell_1 = (\nu^2 - \omega^2 - n^2)^{\frac{1}{2}} = \nu_A$$

$$a_2\ell_2 = \left\{n^2 - \epsilon^2(\nu^2 - \omega^2)^{\frac{1}{2}}\right\} = \nu_B$$

and

$$a_2 m\frac{f}{\sigma} = \frac{n\omega}{\nu}$$

Zeros of the following relation give the same eigenfrequencies as the roots of (3.98):

$$L(\nu;\epsilon,\alpha_L,n,\omega)=\epsilon^2\nu_A\tan\alpha_L\nu_A-\nu_B$$

$$-\frac{n\omega}{\nu}\left\{1+\frac{\nu_B\tan\alpha_L\nu_A}{\nu_A}+\frac{n\omega}{\nu}(1-\epsilon^2)\frac{\tan\alpha_L\nu_A}{\nu_A}\right\} \tag{3.101}$$

The notation $\nu_{\omega j}$ has been used to denote the root of this function corresponding to the j th mode zero, ν_{0j}, of $L(\nu;\epsilon,\alpha_L,n)$. Also, if both n and $R(\nu_{\omega j})$ are taken as positive then $\nu_{\omega j}$ gives the eigenfrequency of a positive mode when ω is positive and vice versa. For the perfectly trapped j th mode, the change in frequency caused by rotation is:

$$\Delta\nu_{\omega j}=\left(\nu_{\omega j}-\nu_{0j}\right)\operatorname{sgn}\left(\frac{n\omega}{\nu_{0j}}\right) \tag{3.102}$$

which is usually positive when $|\omega/\nu_{0j}| << 1$. Summerfield verified this by computing $\Delta\nu_{\omega j}$ for several mode orders with n = 1(1) 8 and ω = -0.3(0.05) 0.3. (The notation 1(1) 8 means from 1 to 8 in steps of 1.)

Some important deductions by Summerfield are (details are covered in various appendices in his work):

i) With a prescribed dimensionless, long shore, wave number, n, for the j th mode: $\Delta\nu_{\omega j}\approx\Delta\nu_{-\omega j}$ $\omega>0$ for α_L. slightly greater than α_j. For $\alpha_L >> \alpha_j$: $\Delta\nu_{\omega j}>\Delta\nu_{-\omega j}\simeq 0$. For the positive mode, the cut-off ledge width is slightly greater than in zero rotation and for the negative mode, is slightly less. Also, for the fundamental negative mode:

$$\nu_{\omega 0}\to\begin{cases}\dfrac{n}{\epsilon} & \text{as } \alpha_L\to 0\\ n & \text{as } \alpha_L\to\infty\end{cases}$$

and the limiting values, $\nu_{\omega 0}$, are independent of the magnitude of ω.

When $a << 1$ there is only one trapped wave along the ledge, the negative fundamental mode of wave number, m. When $a\to 0$ this mode reduces to a Kelvin wave propagating in water of depth, h_2, along the wall at $x = 0$, and Ball (1967) showed this is the only perfectly trapped mode in this case. On the other hand when $a\to\infty$, the limiting, negative, perfectly trapped wave is again a Kelvin wave propagating in water of depth, h_1. Thus, the limiting frequencies when $a\to 0$ and $a\to\infty$, are, $m\sqrt{gh_1}$ and $m\sqrt{gh_2}$, respectively, and are independent of the magnitude of f, as long as $f\neq 0$.

ii) For trapped waves with dimensionless longshore wave number, n, when $\alpha_L>\alpha_j$, the following ordering holds generally: $\Delta\nu_{\omega 0}>\Delta\nu_{\omega 1}>\ldots\Delta_{\omega j}$, but if α_L is only slightly greater than α_j: $\Delta\nu_{\omega j}>\Delta\nu_{\omega j-1}$ and when $\alpha_L >> \alpha_j$, $\Delta\nu_{\omega j}\approx\Delta\nu_{\omega j-1}$.

iii) When α_L is sufficiently greater than α_j, the value of $\Delta\nu_{\omega j}$ decreases with increasing $n(>n_0)$ for the j th mode.

iv) For $\alpha_L > \alpha_j$, and j and ω positive: $\Delta\nu_{2\omega j} > \Delta\nu_{\omega j} > \Delta\nu_{-\omega j} > \Delta\nu_{-2\omega j}$, which holds for all n.

Free Waves Around a Circular Island in an Ocean

Zero rotation – Figure 3.9a shows the following depth distribution:

$$h(r,\theta) = \begin{cases} h_1 \text{ for } a_1 < r < a_2 \\ \\ h_2 \text{ for } r > a_2 \end{cases} \tag{3.103}$$

where r, θ represent the plane polar coordinates, a_1 is the radius of the circular island, and a_2 (greater than a_1) and h_2 (greater than h_1) are constants.

The following terminology is used: the vertical-walled, perfectly reflecting coastline at $r = a_1$ is the coast; the annular-shaped shallow region between $r = a_1$ and a_2 is the shelf; the depth discontinuity at $r = a_2$ is the edge; and the deep water with $r > a_2$ is the ocean. As pointed out by Summerfield (1969) this model has at least two drawbacks: uniform width for the shelf and the perfect symmetry due to the circular shape of the island. The first drawback appears also with the straight-ledge case studied earlier. Summerfield, in an attempt to rectify the second drawback, considered an elliptic sill and deduced the frequency splitting due to the asymmetry. Although an elliptical island or sill is not truly representative of any real island, nevertheless, it is one step closer than circular shape in achieving reality.

In the limiting case when the radius, a_1, of the island is equal to zero, the geometry reduces to that of a circular sill or seamount over which lies a water column of depth, h_1. This limiting case was studied by Longuet-Higgins (1967) when he considered the resonant trapped waves of the first class. Here, the term resonant is used in the context that the phase of every free mode does not change after completing a circuit around the sill.

It has been argued (e.g. Rayleigh 1914; Longuet-Higgins 1967) that circularly symmetric bottom contours cannot trap waves perfectly. What seems to happen is that, corresponding to the leaky modes in the straight-ledge geometry, there are also leaky modes in the circular seamount geometry but they leak very little energy to the ocean. In this sense these are "almost-trapped modes" and not "perfectly trapped modes." Summerfield considered the range: $0 \leq \frac{a_1}{a_2} \leq 1$ and showed there is a single value of a_1/a_2 for which the leakage of energy is a minimum. This means the island shelf combination is a resonator for the free waves of the sill. He also showed two different systems of motions: trapped and leaky modes comprise the first, and the second corresponds to wave motions generated in the ocean.

Next, turning to the mathematical formulation and solution of the nonrotating case, the space dependent part, $\zeta^*(r,\theta)$, of the surface elevation, $\zeta(r,\theta,t)$, must satisfy the following equation:

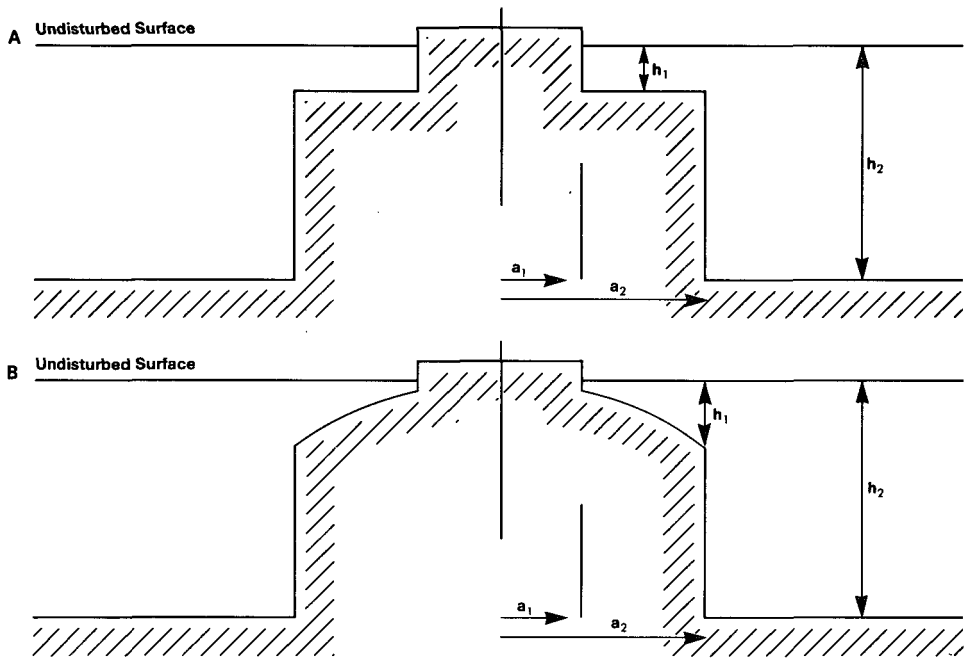


FIG. 3.9. (A) Meridional section of a uniform shelf about a circular island, (B) Meridional section of a parabolic shelf about a circular island. (Summerfield 1969)

$$\left[\nabla^2 + \frac{\sigma^2}{gh_i}\right]\zeta_i^* = 0; i = 1, 2$$
$$\text{with } \nabla^2 \equiv \frac{\partial^2}{\partial r^2} + \frac{1}{r}\frac{\partial}{\partial r} + \frac{1}{r^2}\frac{\partial^2}{\partial \theta^2} \tag{3.104}$$

The three boundary conditions, analogous to the straight-ledge case, are:

$$\frac{\partial \zeta_1^*}{\partial r} = 0 \text{ at } r = a_1 \ (a_1 \neq 0) \tag{3.105}$$

$$\zeta_1^* = \zeta_2^* \text{ at } r = a_2 \tag{3.106}$$

and

$$h_1 \frac{\partial \zeta_1^*}{\partial r} = h_2 \frac{\partial \zeta_2^*}{\partial r} \text{ at } r = a_2 \tag{3.107}$$

In addition to these, a radiation condition has to be satisfied.

Summerfield followed a procedure involving separation of variables used by Longuet-Higgins (1967) to write solutions for $\zeta(r,\theta,t)$ corresponding to the free mode in the two regions $0 < a_1 < r < a_2$ and $r > a_2$. See Summerfield (1969, p. 47)

for the solutions. The solutions are expressed in terms of Hankel functions, $H_n^{(1)}$ and $H_n^{(2)}$, defined as: $H_n^{(1)} \equiv J_n + i\,Y_n$ and $H_n^{(2)} \equiv J_n - i\,Y_n$

This solution is single valued in θ as long as n is an integer, thus, the phase of the waves remains unchanged after each complete circuit around the shelf. Without loss of generality n and $r(\sigma)$ can be taken as positive.

The solutions contain two systems of harmonic waves (at least for large values of n and the real part of σ). The waves have trajectories tangential to the circle, $r = n/k_1$, referred to as "the inner critical circle" by Longuet-Higgins (1967). Here the following definition is used:

$$k_i \equiv \frac{\sigma}{\sqrt{gh_i}} \; ; i = 1, 2 \tag{3.108}$$

The waves represented by:

$$A(\sigma)\, e^{i(n\theta - \sigma t)}\, H_n^{(1)}(k_1 r) \tag{3.109}$$

travel toward the edge, and those with:

$$B(\sigma)\, e^{i(n\theta - \sigma t)}\, H_n^{(2)}(k_1 r) \tag{3.110}$$

propagate toward the coast.

In the ocean itself, there is a system of waves traveling away from the island along straight-line trajectories that are tangential to the so-called outer critical circle, $r = n/k_2$. Longuet-Higgins (1967) showed that, in comparison with the energy of motion on the shelf, leakage of energy from the shelf into the ocean is small during time intervals of the order of one wave period. There is less leakage if there is a great separation between the edge and the outer critical circle. The components given by Equation (3.109) of the almost-trapped wave are oscillatory in the radial direction. Hence, the shelf virtually traps these waves provided:

$$k_2\left(\frac{n}{k_2} - a_2\right) >> 1 \tag{3.111}$$

and

$$\frac{n}{k_1} < a_2 \tag{3.112}$$

Equation (3.111) gives:

$$\frac{n}{k_1 a_2} > \sqrt{\frac{h_1}{h_2}} \tag{3.113}$$

Also, the component waves of the almost-trapped mode given by (3.109) arrive at the edge with an angle of incidence of $\frac{\pi}{2} - u$ where:

$$u \equiv \cos^{-1}\left(\frac{n}{k_1 a_2}\right) \tag{3.114}$$

The last two equations show that the incident angle is greater than the critical angle, ϕ_c, total internal reflection takes place at the edge, and the waves are virtually trapped on the shelf.

The following frequency equation results from the solutions in Summerfield (1969):

$$\sqrt{\frac{h_1}{h_2}}\, H_n^{(1)}(k_2a_2)\left\{H_n^{(1)'}(k_1a_1)\, H_n^{(2)'}(k_1a_2) - H_n^{(2)'}(k_1a_1)\, H_n^{(1)}(k_1a_2)\right\}$$
$$- H_n^{(1)'}(k_2a_2)\left\{H_n^{(1)'}(k_1a_1)\, H_n^{(2)}(k_1a_2) - H_n^{(2)'}(k_1a_1)\, H_n^{(1)}(k_1a_2)\right\} = 0 \tag{3.115}$$

where the prime denotes differentiation with respect to the argument. In this equation, if the four parameters, a_1, a_2, h_1, and h_2, that specify the geometry of the model are known, then the only variable is the frequency, σ, of the free waves. Summerfield argues from (3.115) that free waves that can propagate around the island in either direction are identical. When the radius, a_1, of the island is equal to zero, then the case of a sill or seamount considered by Longuet-Higgins (1967) is obtained, and the following frequency equation is relevant:

$$\sqrt{\frac{h_1}{h_2}}\, H_n^{(1)}(k_2a_2)\, J_n'(k_1a_2) - H_n^{(1)'}(k_2a_2)\, J_n(k_1a_2) = 0 \tag{3.116}$$

When $a_1 = a_2$ an island with vertical walls of radius, a_2, in an ocean depth, h_2 is obtained.

As with the straight-ledge case, Summerfield used nondimensional variables in the numerical evaluation of the frequency equation. He defined the following nondimensional parameters:

$$\nu \equiv \frac{\sigma a_2}{\sqrt{gh_1}} \text{ is a nondimensional frequency} \tag{3.117}$$

$$\epsilon \equiv \sqrt{\frac{h_1}{h_2}} \text{ is the square root of the ratio of water depths} \tag{3.118}$$

and

$$\alpha_I \equiv \frac{a_1}{a_2} \text{ is the ratio of the island to that of the shelf or underlying sill} \tag{3.119}$$

The parameter, ϵ, ranges from 0 to 1 and small values of ϵ mean that differences in water depths at the edge are large and vice versa. The range of ϵ is the same as the straight-edge case. The parameter α_I has the following range:

$$0 \leq \alpha_I \leq 1 \tag{3.120}$$

the lower and upper ends of this range correspond to the limiting circular still and isolated vertical-walled island, respectively. An important contrast between the parameters, α_I of the present case and α_L of the straight-ledge case, is that with

the increase of α_I the width of the shelf decreases in the former case, but in the latter case the width of the ledge decreases with the decrease of α_L.

In the straight-ledge case, the longshore wave number, m, has been dimensionalized by multiplication with a_2, and n has been used to denote the nondimensional form. In the present case, the corresponding parameter is the azimuthal wave number, n/r. At the edge this becomes n/a_2 and in the frequency Equation (3.115) the order n of the Hankel function, H_n, is determined by the wave number along the edge of the oscillations and n takes only integral values.

Equations (3.108), (3.117), (3.118), and (3.119) give: $k_1 a_1 = \alpha_I \nu$, $k_1 a_2 = \nu$, $k_2 a_2 = \epsilon\nu$. Hence, the nondimensional values of the eigenfrequencies can be obtained as the zeros of the following expression:

$$\begin{aligned} I(\nu; \epsilon, \alpha_I, n) \equiv \epsilon H_n^{(1)}(\epsilon\nu)\, H_n^{(1)'}(\alpha_I\nu)\, H_n^{(2)'}(\nu) - H_n^{(2)'}(\alpha_I\nu)\, H_n^{(1)'}(\nu) \\ - H_n^{(1)'}(\epsilon\nu) \left\{ H_n^{(1)'}(\alpha_I\nu)\, H_n^{(2)}(\nu) - H_n^{(2)'}(\alpha_I\nu)\, H_n^{(1)}(\nu) \right\} \end{aligned} \tag{3.121}$$

Summerfield evaluated these numerically.

To estimate frequencies of the almost-trapped modes he used the so-called method of "self-consistency," i.e. equating the total phase-change that occurs when the shelf is radially crossed and recrossed with θ and t nonvarying, to an integral multiple of 2π.

Based on his calculation of the zeros of $I(\nu; \epsilon, \alpha_I, n)$, with the α_I curve method, Summerfield (1969, p. 68) stated:

> "... the resonant 'free' wave-motions of the waters about a circular island are essentially of two types, viz., 'trapped-leaky' and 'shelf-island' wave motions. The former are the more important in the context of self-sustained oscillations, especially those which are almost trapped on the shelf. To some extent, the answer to the question whether (or not) a particular mode of along-edge wave number $\frac{n}{a_2}$ is trapped on the shelf depends on the relative magnitudes of n, ϵ and α_I; in addition, the corresponding oscillation of the limiting seamount model must also be virtually trapped. Furthermore, the α_I curve of the appropriate eigenfrequencies shows that the effect of the island on the mode is negligible, while the island's radius is less than the mode's inner critical radius ...."

When $\alpha_I > n/\xi$ where ξ is the real part of the complex conjugate of ν, the wave components that describe the motion on the shelf are reflected alternately from the coast and the edge. From the edge it is a total internal reflection and as long as $\xi > \frac{n}{\epsilon}$ the wave is leaky. For large values of α_I that correspond to narrow shelf, for the mode to be practically trapped on the shelf, n has to be large. The wave damping, given by the ratio n/ξ, is heavy when $\alpha_I \simeq 1$.

A sloping shelf – Summerfield (1969) next considered the influence of a sloping shelf on the free waves by an island-parabolic shelf model. Figure 3.9b shows the following depth distribution (a somewhat better representation of the nearshore bathymetry than the island shelf model):

$$h(r,\theta) = \begin{cases} h_1 \left(\frac{r}{a_2}\right)^2 & \text{for } a_1 < r < a_2 \\ h_2 & \text{for } r > a_2 \end{cases} \tag{3.122}$$

He defined the nondimensional parameter α_p:

$$\alpha_p \equiv \frac{a_1}{a_2} \tag{3.123}$$

as the ratio of the radii of the island to the radii of the parabolic shelf.

He proceeded in a manner similar to the island-shelf model and showed that the eigenfrequencies are the zeros of:

$$\begin{aligned} p(\nu;\epsilon,\alpha_p,n) \equiv \epsilon H_n^{(1)}(\epsilon\nu) \left\{1 - \alpha_p^{(\rho_1-\rho_2)}\right\}(n^2-\nu^2) \\ - \nu H_n^{(1)}(\epsilon\nu)\left\{\rho_1\,\alpha_p^{(\rho_1-\rho_2)} - \rho_2\right\} \end{aligned} \tag{3.124}$$

where

$$\begin{aligned} \rho_1 &\equiv -1 + (n^2 - \nu^2 + 1)^{\frac{1}{2}} \\ \rho_2 &\equiv -2 - \rho_1 \end{aligned} \tag{3.125}$$

The important results of this calculation are that when $\alpha_p \simeq 1$, i.e. when the shelf is narrow, the slope of the shelf has little effect on the motions and the zeros of $P(\nu;\epsilon,\alpha_p = \alpha_I,n)$ are approximately the same as those of $I(\nu;\epsilon,\alpha_I,n)$. However, for small values of α_1, the trapped leaky mode of the island-parabolic shelf model has a smaller frequency than the corresponding mode of the island-shelf model. Also, the damping is appreciably less in the former case than the latter.

Another result is that if a_2 and h_1 have the same numerical values, then travel times of the long waves across the shelves from the coast to the edge in the radial direction are equal for the two models when the following condition is satisfied:

$$\log\left(\frac{I}{\alpha_p}\right) = 1 - \alpha_I \tag{3.126}$$

An additional result is that, when:

$$\alpha_I + \alpha_L = 1 \tag{3.127}$$

travel times of the long waves across shallow water for the island-shelf model and straight-ledge case are the same. Finally, when $h_2 = h_1$, the parabolic-shelf model reduces to the model used by Homma (1950) in his studies of the response to incoming tsunamis of the shallow water around islands.

The rotating case – The method of incorporating rotation into the problem has been dealt with in the straight-ledge case. Summerfield (1969) followed essentially a similar procedure for this island-shelf model but details are omitted here. The important results from Summerfield's study are included. The frequencies of positive almost-trapped modes are slightly greater than those corresponding to zero

rotation, but for negative modes, the opposite is true. Summerfield referred to half the frequency change due to rotation as "frequency-split" and found that this depends significantly on the relative sizes of the island and the shelf. In the parabolic-shelf model, another factor that can influence the frequency-split is the slope of the shelf.

In addition to these modes, as with the straight ledge, there exists another class of modes belonging to the OSC that do not exist in the nonrotating case. These have periods in excess of one pendulum day and can be perfectly trapped on any isolated feature such as an island, provided it has perfectly symmetric bottom contours.

Effect of Asymmetry on Trapped Motions

Longuet-Higgins (1967) showed that any departure from the circular symmetry of the geometry could lead to a frequency split of the trapped gravity modes into two different pairs of modes. Summerfield (1969) studied this problem taking the geometry as an elliptical sill. He used elliptical coordinates and obtained solutions in terms of Mathieu and modified Mathieu functions. Of the two pairs of modes, one pair is symmetric about the major axis of the elliptic sill and the other is antisymmetric about it and, as would be expected, the two pairs have different eigenfrequency split as a function of the wave number along the edge, for prescribed dimensions of the geometry. He used this calculation to interpret some long-wave records at Macquarie Island; the same problem considered earlier by Longuet-Higgins (1967).

The island is located at 54°30′S, 158°58′E, is approximately 37 km long, and has an average width of 4.8 km. A narrow shelf surrounds the island and the water is a few hundred meters deep on the shelf. During 1965, surface waves were recorded in two bays. The records in one bay showed a regular large amplitude oscillation with a period of 6–7 min, the amplitude fluctuating with a beat period of about 3 h. Occasionally regular oscillations with two other periods of 3 and 12–13 min were also noticed.

Longuet-Higgins (1967) showed theoretically that the conspicuous periods in the records should be given by:

$$\text{conspicuous period in minutes} = \frac{42}{n} \qquad (3.128)$$

where n is the azimuthal wave number. If n were given a value of 7, then the conspicuous period should be 6 min, which agrees with the observations. The calculations of Summerfield showed that, in fact, the mode $n = 7$ could be virtually trapped about an ideal circular island.

Summerfield also studied the response of his island-shelf model to an incoming pulse of energy. He showed that, because of imparting energy to the shallow water, this pulse could excite a free mode of oscillation of the OFC type. However, the amplitude of this motion depends strongly on the time-rate decay of the mode, which is negligibly small for almost-trapped modes of lowest order, with a large wave number along the edge.

Snodgrass et al. (1962), Munk et al. (1964), and Aida (1967) considered the practical problem of separation of trapped and leaky modes. In the first two references, the area of interest was the continental shelf off California, and in the third, it was the continental shelf in the vicinity of Miyagi-Enoshima.

Murty and Wigen (1976) showed that impedement to the progress of the 1929 Grand Banks earthquake tsunami was partly because of trapping by Sable Island and the sand banks surrounding it. Brandsma et al. (1975) developed a numerical model to calculate the water level near islands associated with propagating tsunamis. Hwang and Divoky (1975) calculated the water level at Wake Island (caused by the Alaskan earthquake tsunami of March 1964) as a function of time, and compared it with the observed record (Fig. 3.10).

Lautenbacher (1970) attributed the larger wave heights observed around islands (rather than on sloping beaches) to refractive focusing. For the boundary condition, he used the usual radiation condition. His study differs from those of Vastano and Reid (1966, 1967) in that the model of the latter authors is relevant for the case of no-flow as coastal boundary condition, and the model of the former author can take into account any condition other than no-flow.

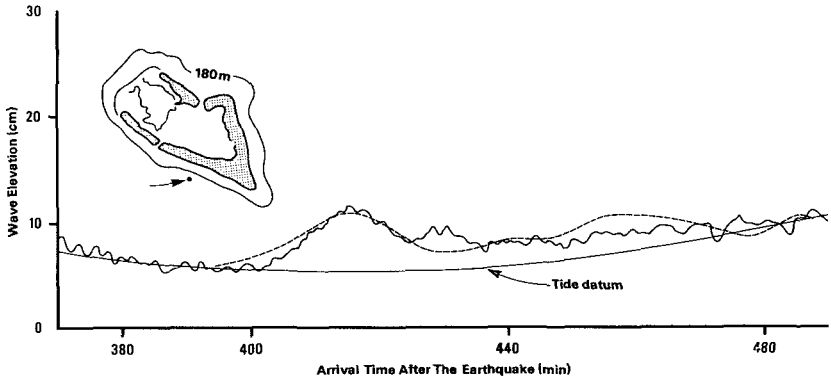


FIG. 3.10. Wake Island record of the 1964 Alaskan tsunami (Van Dorn 1969) and history computed by the present numerical model (broken line). (Hwang and Divoky 1975)

3.3 Tsunami Propagation

ANALYTICAL THEORIES

Dispersion occurs during propagation of tsunami waves, refraction is important in shallow water, and scattering by the bottom irregularities in the deep ocean is not important.

Backus (1962) considered the effect of earth's rotation on the propagation of ocean waves of small amplitude over large distances and showed that the effects are different for shallow-water and deepwater waves. In particular, he deduced

that, for shallow water, the effects are of the order of $\Omega \sqrt{\frac{D}{g}}$ and for deep water are of the order of Ω/ω where Ω is the angular velocity of earth's rotation, ω is the frequency, D is the uniform depth of the ocean, and g is gravity. The rotation effects are strongest at $kD = 1.878973$ where k is the wave number.

Backus showed that earth's rotation has no influence on the group velocity of deepwater waves, although their trajectories deviate from great circles by amounts proportional to their periods. For shallow-water waves on the other hand, rotation affects the group velocity (as well as the trajectories). However, the amount of change is independent of the wave period. If the depth is either nonuniform or smaller than the wavelength, then refraction must be taken into account.

McGoldrick's (1968) theory is probably the most comprehensive work on propagation of long waves over corrugated bottoms. When the bottom is sinusoidal in shape let D_0 be the average depth of the ocean so that the phase speed of a long gravity wave, based on average depth, is $c_0 = \sqrt{gD_0}$. When the wave is above a crest of the bottom corrugation, its speed is less than c_0 whereas when it is over a trough, its speed is greater than c_0. The wave loses more time over the crest of the bottom than it gains over the trough of the bottom and the net result is retardation of the wave. This deduction holds only when the wavelength of surface waves is much less than the length of bottom variations. Katz (1963b) also showed that the phase speed of a long wave is less in irregular depth compared to the speed based on an average depth.

It is always possible that the bottom corrugations could have length scales comparable to the wavelengths of the surface waves. To study the general problem of propagation of long waves over corrugated bottom of sinusoidal shape McGoldrick (1968) used the linearized shallow-water equations, but without any restrictions on either the wavelength of the surface waves, or on the amplitude and wavelength of the bottom corrugations. The only restriction was that when the crests of the bottom corrugations protruded above the surface of the water, the concept of progressive waves with wavelengths compared to bottom shape became rather meaningless, and the problem then became one of seiches.

The most important result of McGoldrick's study is the existance of a range of wavelengths close to that of the scale of the bottom corrugations, where the waves are not retarded but actually travel faster than the phase speed given by the average depth, because of the subharmonic resonance between the surface waves and the bottom. This range of wavelengths, L_W, of the surface waves for which the phase speed is greater than that for a flat bottom is: $\sqrt{3}\ L_B < L_W < 2L_B$ where L_B is the wavelength of the bottom corrugation.

Stoneley (1964) considered the effects of compressibility and viscosity of the water on tsunami propagation. He showed that inclusion of compressibility reduces the velocity of propagation by 1% at most and the effect of viscosity on tsunami dissipation is negligible. Cherkesov (1966b) showed that the effect of viscosity is 1.6% at most.

Kajiura (1963) studied the problem of the partial reflection of water waves traveling over a bottom of variable depth. His study showed that if the ratio of the width of a transition zone to the wavelength of incident waves is less than 0.05 the reflection coefficient is the same as that for an abrupt transition. But if this ratio is of the order of unity then the reflection coefficient is small.

Kajiura (1961) calculated the reflection coefficient of long waves at a submarine ridge for conditions typical of the southern Sea of Japan. If ℓ is half the width of the ridge and λ_∞ is the wavelength of the incoming long wave, then the reflection coefficient decreases with the increase of ℓ/λ_∞. Taking $\ell \sim 250$ km, the reflected wave has less than 10% the energy of the incident wave.

Nakamura (1961) probably gave the most concise discussion of the effects of different factors on the velocity of propagation of long gravity waves in the ocean: compressibility of the water, elasticity of the earth below the ocean, the earth's rotation, the earth's curvature, and the effect of viscosity of the water. He showed that for waves with lengths in the range of 100–10,000 km, the effects of the above factors are at most 1%.

Numerical Models and Travel-Time Curves

Ueno (1965) simulated propagation in the Pacific Ocean of the Chilean earthquake tsunami of May 22, 1960. This appears to be one of the earliest numerical models for tsunami propagation. He used a grid of 5° latitude–longitude, and initially everywhere, except the generation area, the water level and currents were set to zero. The initial elevation (following the earthquake) in the generating area is determined from:

$$\zeta_0^2 = \frac{2E}{\rho g S} \tag{3.129}$$

where ζ_0 is the initial elevation at the origin, E is the tsunami energy, ρ is the density of water, g is gravity, and S is the total area of the origin (i.e. the area of tsunami generation). The energy, E, for Chilean tsunami was estimated to be $1\text{–}3 \times 10^{23}$ ergs (from the tide records at Christmas and Johnston islands). For the grid size considered here, $S = 3 \times 10^{16}$ cm^2 and (3.129) gives $\zeta_0 = 120$ cm.

Two important results emerged from this calculation: first, the set-up caused by the first wave decreased with increasing distance from the area of generation but increased again close to the coasts of Japan and Alaska. Second, the set-up caused by the second wave was large along the coasts of Japan, Alaska, and Hawaii and somewhat smaller near Midway and Wake islands.

In Chapter 2, reference was made to the numerical models developed at the Tetra Tech Corporation. These models considered the two different aspects of the tsunami problem, generation and propagation. Because topographical effects near the coasts have not been taken into consideration (in the propagation models, e.g. Hwang and Divoky (1970)), it is not legitimate to compare coastal records of the tsunami with calculated amplitudes. These authors used only observations made at Atolls for comparison (Table 3.1).

The observed amplitude of the tsunami was about twice the calculated amplitude (except for Canton and Wake islands). This discrepancy is not unreasonable

TABLE 3.1. Comparison of predicted amplitudes and recorded amplitudes at five stations for the 1964 Alaskan earthquake tsunami. (Hwang and Divoky 1970)

	Predicted amplitude[a] (*cm*)	Recorded amplitude (*cm*)
Johnston Is. 16°45'N, 169°31'W	18.9	30.5
Midway Is. 28°13'N, 177°22'W	13.7	27.4
Wake Is. 19°17'N, 166°37'E	19.2	15.2
Canton Is. 02°49'S, 171°43'W	16.5	6.1
Kwajalein 08°44'N, 167°44'E	14.0	30.5

[a]Without consideration of local effects.

because effects due to shoaling, dispersion, dissipation, diffraction, scattering, and reflection are ignored in the theoretical computation; the only correction applied is for refraction. The reversal at Canton Island may be because the tide gage is on the lee side of the island.

Hatori and Koyama (1971) constructed tsunami travel-time diagrams (actually inverse refraction diagrams) for 19 representative Japanese stations. They considered the tsunami data for 1894–1969. Figure 3.11 shows a chart for Miyako.

The U.S. Coast and Geodetic Survey (1965) prepared a set of tsunami travel charts for 30 locations around the rim of the Pacific Ocean and these formed the basis for predicting tsunami travel times by the International Tsunami Warning Service based at Honolulu (see Chapter 6). The charts are based on the long-wave formula and are correct to ± 1.5 min for every hour traveled. The U.S. National Ocean Survey (1971) revised the earlier charts and included more stations to bring the total to 50. An example of such a chart is Fig. 3.12.

Braddock (1970) developed a grid-refinement technique to compute propagation of tsunamis over large distances, an improvement over earlier techniques. Green (1961) gave the following equation for the travel time, T(S), of a tsunami along a curve, s:

$$T(S) = \int_s \frac{dS}{c} \tag{3.130}$$

where $c = \sqrt{gD}$ is the phase speed of a long wave traveling over water of (variable) depth, D. Green evaluated (3.130) along the arcs of great circles but Braddock (1970) warned that this technique could produce wrong results in anomalous cases such as the travel time of the Apr. 1, 1946, Aleutian earthquake tsunami to Sitka.

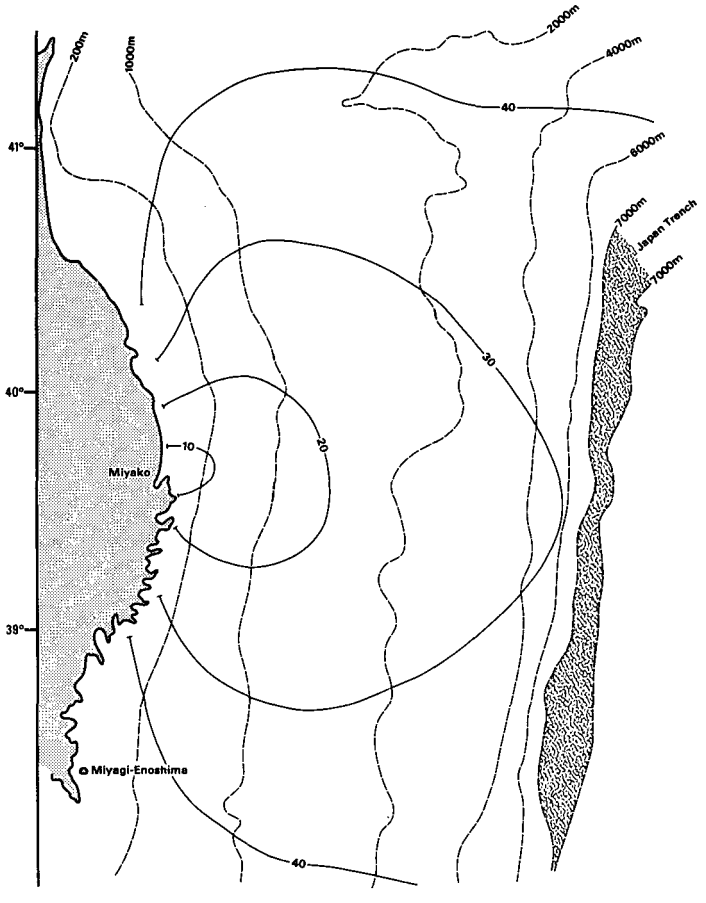


FIG. 3.11. Tsunami travel time to Miyako. Time interval is 10 min. (Hatori and Koyama 1971)

The Huygens' method of wave fronts necessitates enormous computation for accurate results. Gilmour (1961) modified the Huygens' method and calculated travel times from sets of great circle paths and joined points representing equal travel time, to provide an approximate picture of the wave fronts. Braddock again warned that if the arcs of great circles and the ray paths do not agree closely, this method will yield wrong results.

Braddock (1970) applied the grid-refinement technique to calculate travel times of the Alaskan tsunami of Mar. 28, 1964, to the west coasts of North and South America and the southwest Pacific. The calculated values agreed more closely with observed travel times for the American coasts than for the South Pacific because the wave system is dispersed by the complex bathymetry northeast of Australia. The grid-refinement technique can be explained as follows: between two points, A and B, on the globe, T_{min} and S_{min} are the optimal travel time and the corresponding travel path, and T_1 and S_1 are some first approximations to these.

Successive approximations could be obtained as follows: the path, S_1, is divided by the points, $E_j, j = 1, 2 \ldots m$, into $m - 1$ intervals of length less than, but approximately equal to, some suitable grid spacing, DS_1 (Fig. 3.13). A normal grid spacing, DN_1, is selected and a grid parameter, U, such that:

$$U \equiv \frac{DS_1}{DN_1} \tag{3.131}$$

Then at each point $E_j, j = 1, 2 \ldots m$, a normal to S_1 is constructed and nodes are marked off at intervals, DN_1, along each normal. Next a control length, DL_1, is selected such that $DL_1 \geq \max(DS_1, DN_1)$ and a second grid parameter, Q, is defined such that:

$$Q \equiv \frac{DL_1}{DS_1} \tag{3.132}$$

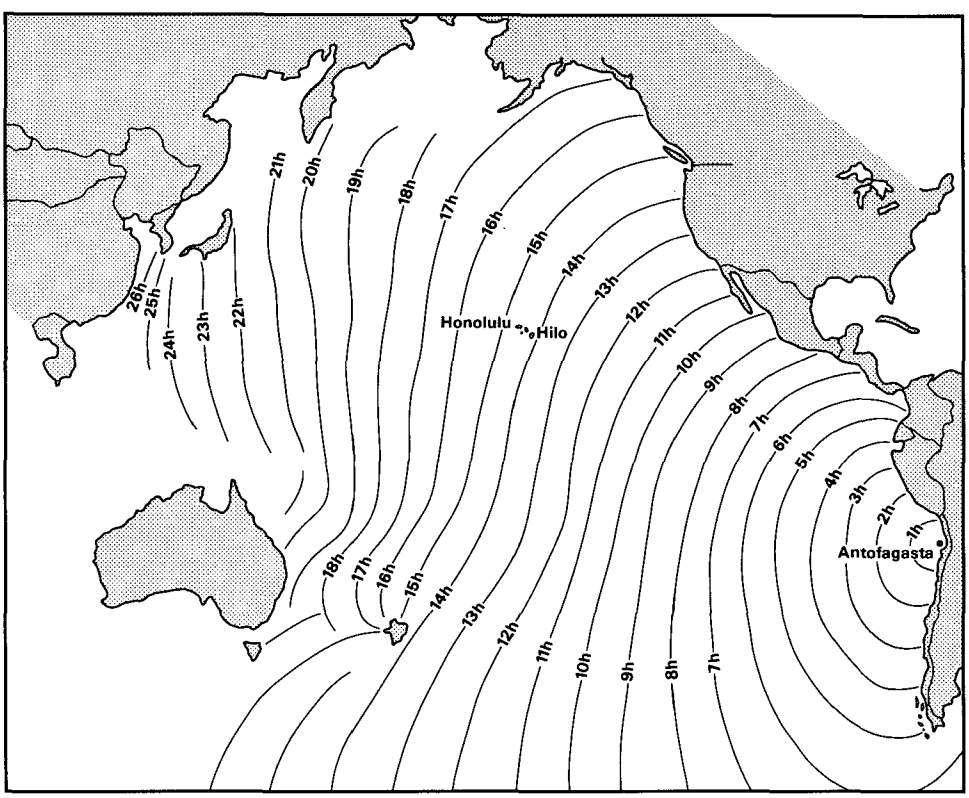


FIG. 3.12. Tsunami travel time from Antofagasta, Chile. (U.S. National Ocean Survey)

Arcs less than DL_1 long are used and links are constructed between the nodes to complete the grid. Travel time along each arc is estimated by the bathmetric data.

Braddock (1970) constructed his finite discrete network of paths in the field of travel in this manner so travel times along the individual arcs would be known. Then he used an algorithm developed by Dantzig (1960) to calculate the shortest time path, S_2, through this discrete grid along with the travel time, T_2. Next, a new tangential grid spacing, DS_2, is selected so $DS_2 \leq DS_1$ and a grid-refinement parameter, R, is defined as:

$$R \equiv \frac{DS_2}{DS_1} \tag{3.133}$$

and by interpolation, extra nodes are added to S_2 so that the maximum spacing between any two adjacent nodes which form S_2 is less than DS_2. From U and Q, DN_2 and DL_2 are obtained and a new grid is constructed about S_2 and further approximations obtained. To construct the grids, great circle arcs need not be used between the nodes because, as the refinement progresses with successive approximations, the arcs become shorter and straight-line grids are accurate enough. According to Braddock, the above process of successive approximations generates a monotically decreasing sequence of travel times, T_i, and a sequence of paths, S_i, converging to a limit curve. Actually each S_i is the centerline of the succeeding construction and a possible path through the grid. Thus, $T_i \geq T_{i+1}$ for all $i \geq 1$.

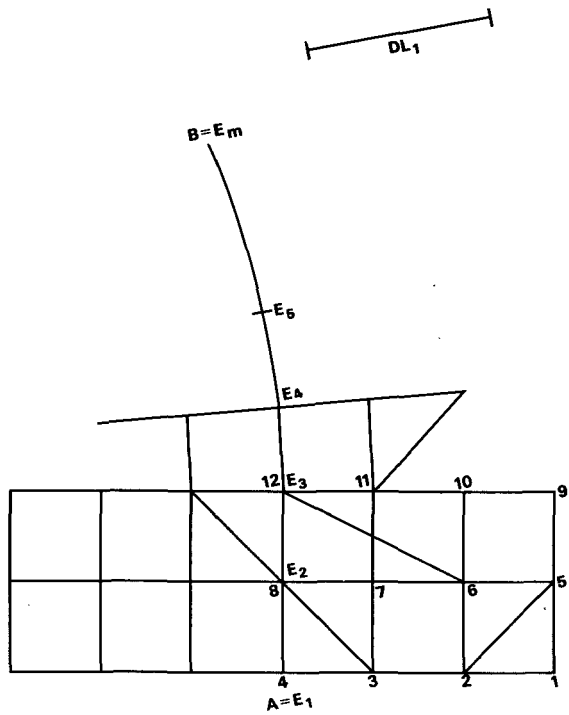


FIG. 3.13. Illustration of typical construction of finite discrete network of paths in the field of travel. (Braddock 1970)

The parameters U, Q, and R determine the extent of the computation and the accuracy attained at each step. From Equation (3.133), it follows that $0 < R \leq 1$. Braddock found that if R is small (about $\frac{1}{2}$) the tangential spacing, DS_i, decreases rapidly and a large number of nodes are required to specify the approximating paths, and this leads to storage difficulties in the computer. For large values of R (about $\frac{3}{4}$) the refinement is slow and many calculations are required, taking up computer time. In general, by controlling the value of Q, i.e. by restricting the number of arcs in each grid, the number of calculations may be reduced. From Equation (3.132) it is obvious that $Q \geq 1$, because $Q < 1$ implies that $DL_i < DS_i$, which means that S_i may not be included in the set of possible paths through the succeeding grid. Then it follows that T_i is not necessarily monotonically decreasing and may even increase. In the third parameter, U, $U = 1$ means the tangential and normal grid spacings are equal. Braddock found that greater accuracy may be obtained by selecting $U > 1$.

There is one main drawback of this grid-refinement technique. For certain bathymetric distributions, several curves yield minimum values for T(S). The optimal path is the curve, S_{min}, for which T(S) attains its minimum value, T_{min}, with respect to all possible paths between the two end points. Other curves, s_e, for which T(S) attains a minimum value with respect to the curves close to s_e are called locally optimal paths. In the grid-refinement technique it is possible that S_i and T_i may converge to a locally optimal solution. The use of large initial grids that thoroughly sample the complete velocity field will, in general, avoid this situation.

Braddock (1970) applied this technique to calculate propagation of the Aleutian earthquake tsunami of Apr. 1, 1946, to Sitka, Alaska (Fig. 3.14), and propagation of the Alaskan earthquake tsunami of Mar. 28, 1964, to the eastern and southwestern Pacific. Previously there was considerable confusion about travel times of the 1946 tsunami to Sitka, and Braddock cleared this up. The observed travel time was 2 h and 42 min whereas the computed travel time, using the great circle route and $\sqrt{gD}$ for the velocity, gave 6 h approximately. Zetler (1947) explained this discrepancy by pointing out that the great circle route passes through shallow water on the continental shelf and this makes the computed travel time very large. If the tsunami did not follow the great circle route but traveled to Sitka via some route through deep water only, then the observed travel time would, of course, be small. Zetler suggested that if the travel path from the epicentral area to Sitka were first to southeast and then along the Aleutian Trench, the computed travel time would be reduced from 6 to about 3 h.

Braddock used his grid-refinement (G-R) technique, to estimate the travel time via different paths and his final convergent values were around 2 h 42 min, somewhat less than the observed travel time of 2 h 55 min reported by Zetler. This discrepancy is attributed by Braddock to the differences in the interpretation of the Sitka record by himself and Zetler.

The Sitka record shows two small waves (travel time 2 h 42 min) followed by a larger wave train (travel time 2 h 55 min). Braddock suggested that for propagation over large distances the earlier waves are relevant (Wilson 1962).

Table 3.2 compares observed travel times with the travel times calculated by Braddock for different stations for the 1964 Alaskan earthquake tsunami. Figure 3.15 shows the calculated ray paths of the tsunami to several stations. Braddock's results showed that the travel paths to Sitka and Astoria were seaward of the great circle routes and did not pass through the shallow waters at the head of the Gulf of Alaska.

Calculations for tsunami propagation into the southwest Pacific showed many interesting results. The ice pack around Antarctica and the chain of islands and Great Barrier Reef northeast of Australia prevented the tsunami from reaching Brisbane or McMurdo Sound.

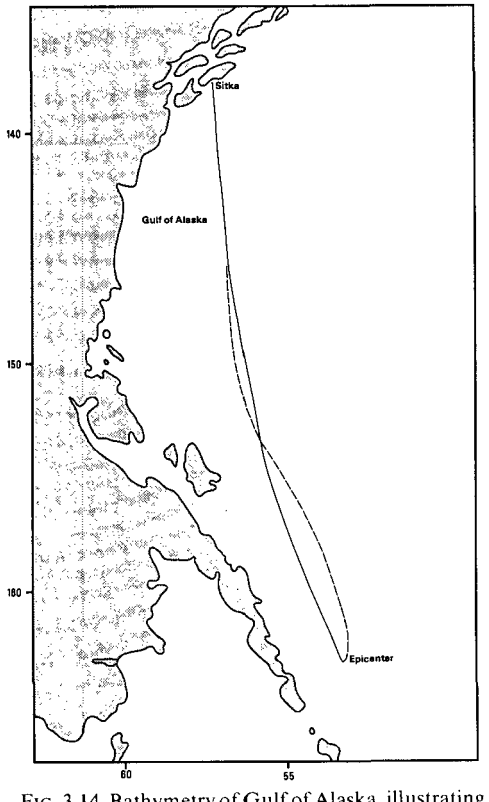


FIG. 3.14. Bathymetry of Gulf of Alaska, illustrating relative positions of the Aleutian Trench and epicenter of the Alaskan earthquake of April 1, 1946. The great circle arc and the optimal path obtained by the grid refinement technique are also shown. (Braddock 1970)

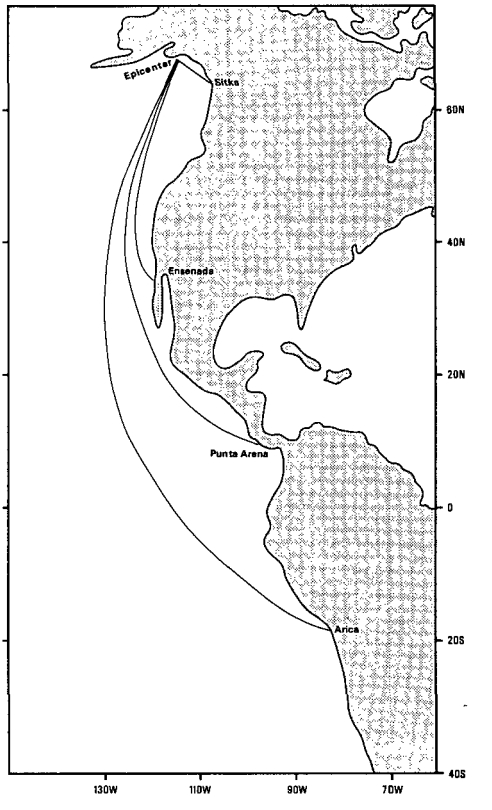


FIG. 3.15. Calculated ray paths for the Alaskan earthquake tsunami of March 1964 to Sitka, Ensenada, Punta Arenas, and Arica. (Braddock 1970)

Although stations Nelson and Greymouth are approximately the same distance from Alaska as Coff's Harbor, Sydney, and Lyttelton, the observed travel times to Nelson and Greymouth were 4–5 h longer. Also, although Coff's Harbor is closer

to Alaska than Sydney the observed travel time was longer. Figure 3.16 shows locations and reflected paths. The tide record for Macquarie Island showed recurrence of tsunamis during a time interval exceeding 7 h. Braddock stated that this recurring activity, which showed travel times of 26 h 39 min and 31 h 54 min, is incorrect in the time records.

Interpretation of the tidal record at Macquarie Island presented considerable difficulty. Table 3.3 shows the summary of the travel times for this station. Braddock used the concept of reflection of wave energy at the western edge of the Undulla Deep on the east coast of Australia to account for the observations at Macquarie Island.

Directivity of Tsunamis

The directivity of tsunamis is whether or not there are preferred directions at the epicenter, where most tsunami energy is radiated. There is little doubt that asymmetry is the rule rather than the exception. The tsunami caused by the Aleutian earthquake of Apr. 1, 1946, exhibited remarkable directivity. Maximum amplitude of the waves at Hawaii (about 3200 km south of the epicenter) was about 16.8 m. Wake Island, approximately the same distance southwest of the epicenter, was not affected. At Unimak Island, a short distance north of the epicenter, waves of 30.5-m

Table 3.2. Comparison between computed and observed travel times of the 1964 Alaskan earthquake tsunami. (Braddock 1970)

Tide Station	Travel time			
	Obs.		Calc.	
	(*h*)	(*min*)	(*h*)	(*min*)
Sitka	1	30	1	31
Astoria	4	20	4	19
Ensenada	6	6	6	11
Manzanillo	8	39	8	46
Punta Arenas	12	47	12	39
Talara	14	20	14	21
Arica	16	54	17	13
Talcahuano	18	39	18	51
Brisbane	indefinite		18	51
Coff's Hbr.	17	39	17	37
Sydney				
Camp Cove	16	54	17	7
Fort Denison	17	9	not calc.	
Hobart	20	19	20	30
Canton Is.	8	39	not calc.	
Pago Pago	10	15	not calc.	
Nelson	22	20	18	55
Greymouth	23	20	18	5
Lyttelton	18	34	17	2
McMurdo Sound	indefinite		not calc.	

Table 3.3. Comparison of observed, calculated, and corrected travel times for the arrival of the Alaskan earthquake tsunami of March 1964 at Macquarie Island. (Braddock 1970)

Path to Macquarie Is.	Travel time					
	Calc.		Obs.		Corrected	
	(*h*)	(*min*)	(*h*)	(*min*)	(*h*)	(*min*)
Via west side New Zealand	20	33	26	39	20	39
Via east side New Zealand	23	32	30	39	24	39
Indefinite	—	—	31	54	25	54

amplitude were observed. Thus, most of the energy appears to have radiated northward and southward.

Miyoshi (1955) gave two examples of tsunamis with remarkable directivity; the tsunami following the Hokkaido earthquake of Mar. 4, 1952, and another on Nov. 26, 1953. He attributed the directivity to the bottom topography at the tsunami origin (this appears to be the general consensus).

Miyoshi selected the tsunami created by the Kamchatkan earthquake of Nov. 4, 1952, as an example of nondirectivity. Although the tsunami energy appears to have been radiated in all directions, one of the maximum heights at distant stations was at Talcahuano, Chile. Miyoshi explained this was due to a convex lens effect of the Hawaiian Islands and the shallows around the islands, on the tsunami orthogonals. The lens effect could be such that Talcahuano and the tsunami origin area might be the conjugate foci of this lens.

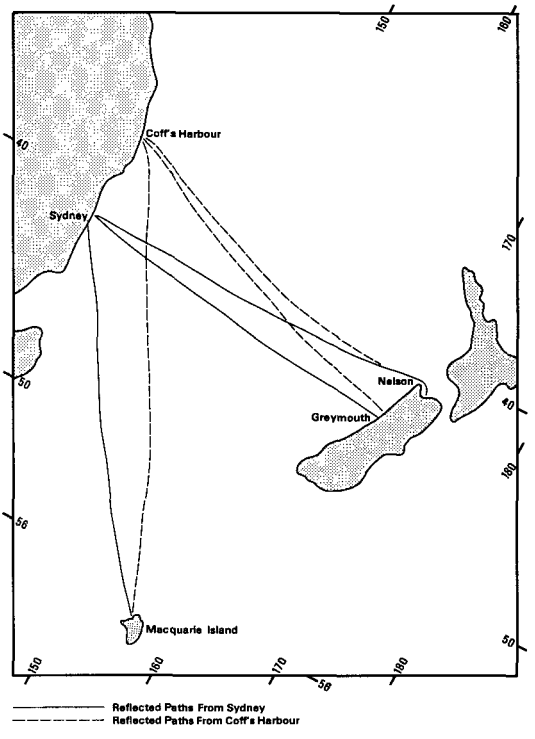


FIG. 3.16. Reflected paths from the east coast of Australia for the Alaskan earthquake tsunami of March 1964. (Braddock 1970)

TRANSOCEANIC REFLECTION OF TSUNAMIS

Cochrane and Arthur (1948) considered this problem systematically. Take the origin of a Cartesian coordinate system at the undisturbed level of the water surface

above the depth discontinuity, to the right of which is shallow water of uniform depth, D_2, and to the left deep water of uniform depth, D_1. The vertical coordinate, Z, is positive upward and the horizontal coordinates are such that x is normal to the coast and y is parallel to the coast.

Plane and sinusoidal wave motion is assumed and shallow-water theory is used. The amplitude, η, of the surface perturbation is assumed to be small compared to depths as well as to wavelength, L. The wave equation for shallower water (i.e. $x > 0$) is:

$$\frac{\partial^2 \eta_2}{\partial t^2} = c_2^2 \left(\frac{\partial^2 \eta_2}{\partial x^2} + \frac{\partial^2 \eta_2}{\partial y^2} \right) \tag{3.134}$$

where

$$c_2 = \sqrt{gD_2}$$

where subscript 2 is shallower water, t is time, and g is gravity. For deeper water (i.e. $x < 0$ and using subscript 1):

$$\frac{\partial^2 \eta_1}{\partial t^2} = c_1^2 \left(\frac{\partial^2 \eta_1}{\partial x^2} + \frac{\partial^2 \eta_1}{\partial y^2} \right) \qquad c_1 = \sqrt{gD_1} \tag{3.135}$$

The discontinuity is assumed to represent the continental slope. On the shallower water side there is a transmitted wave but on the deeper water side, there is a reflected as well as an incident wave. Let θ_1 and θ_1' be the angles between the incident wave and the negative x-axis and between the reflected wave and the negative x-axis, and θ_2 be the angle between the transmitted wave and the positive x-axis. Define:

$$\begin{aligned} \mu_1 &\equiv \cos \theta_1 \\ \mu_1' &\equiv \cos (\pi - \theta_1') = -\cos \theta_1' \\ \mu_2 &\equiv \cos \theta_2 \\ \nu_1 &\equiv \sin \theta_1 \\ \nu_1' &\equiv \sin (\pi - \theta_1') = \sin \theta_1' \end{aligned} \tag{3.136}$$

and

$$\nu_2 \equiv \sin \theta_2$$

Let T be the period and σ be the frequency.

The solutions of (3.134) and (3.135) using (3.136) are:

$$\begin{aligned} \eta_1 &= A_1 \cos \left[\sigma \left\{ t + \frac{(\mu_1 x + \nu_1 y)}{c_1} \right\} \right] + A_1' \cos \left[\sigma \left\{ t + \frac{(\mu_1' x + \nu_1' y)}{c_1} \right\} \right] \\ \eta_2 &= A_2 \cos \left[\sigma \left\{ t + \frac{(\mu_2 x + \nu_2 y)}{c_2} \right\} \right] \end{aligned} \tag{3.137}$$

The following boundary conditions must be satisfied at depth discontinuity, $x = 0$:

$$\eta_1 = \eta_2 \tag{3.138}$$

$$D_1 u_1 = D_2 u_2 \tag{3.139}$$

Where u_1 and u_2 are normal components of velocities in the two regions. Because for sinusoidal waves $u \sim \frac{\partial \eta}{\partial x}$ Equation (3.139) becomes:

$$D_1 \frac{\partial \eta_1}{\partial x} = D_2 \frac{\partial \eta_2}{\partial x} \tag{3.140}$$

From (3.137), (3.138), and (3.140) then:

$$A_1 + A_1' = A_2 \tag{3.141}$$

and

$$\frac{h_1 \mu_1 A_1}{c_1} + \frac{h_1 \mu_1' A_1}{c_1} = \frac{h_2 \mu_2 A_2}{c_2} \tag{3.142}$$

at $x = y = 0$. From Equations (3.141) and (3.142):

$$\frac{A_1'}{A_1} = \frac{c_2 \mu_2 - c_1 \mu_1}{c_1 \mu_1' \quad c_2 \mu_2} \tag{3.143}$$

and

$$\frac{A_2}{A_1} = \frac{c_1 \mu_1' - c_1 \mu_1}{c_1 \mu_1' - c_2 \mu_2} \tag{3.144}$$

Let $A_1'/A_1 \equiv r$ = amplitude coefficient of reflection and $A_2/A_1 \equiv s$ = amplitude coefficient of transmission. According to the principle of reflection $\theta_1 = \theta_1'$ or $\mu_1 = \cos \theta_1 = \cos \theta_1' = -\mu_1'$. Hence, the reflection and transmission coefficients can be written as:

$$r = \frac{c_1 \cos \theta_1 - c_2 \cos \theta_2}{c_1 \cos \theta_1 + c_2 \cos \theta_2}$$

$$s = \frac{2 c_1 \cos \theta_1}{c_1 \cos \theta_1 + c_2 \cos \theta_2} \tag{3.145}$$

Invoking Snell's law $\frac{\sin \theta_1}{c_1} = \frac{\sin \theta_2}{c_2}$,

r can be determined as a function of c_1/c_2 for a prescribed angle of incidence, θ_1. Figure 3.17 shows r as a function of c_1/c_2 for different values of θ_1 when $c_1/c_2 > 1$ for $0° < \theta_1 < 20°$, r does not change significantly. On the other hand if $c_1/c_2 < 1$ (i.e. when the incident wave travels from shallow to deeper water), total reflection occurs at some critical angle of increase (then $r = 1$).

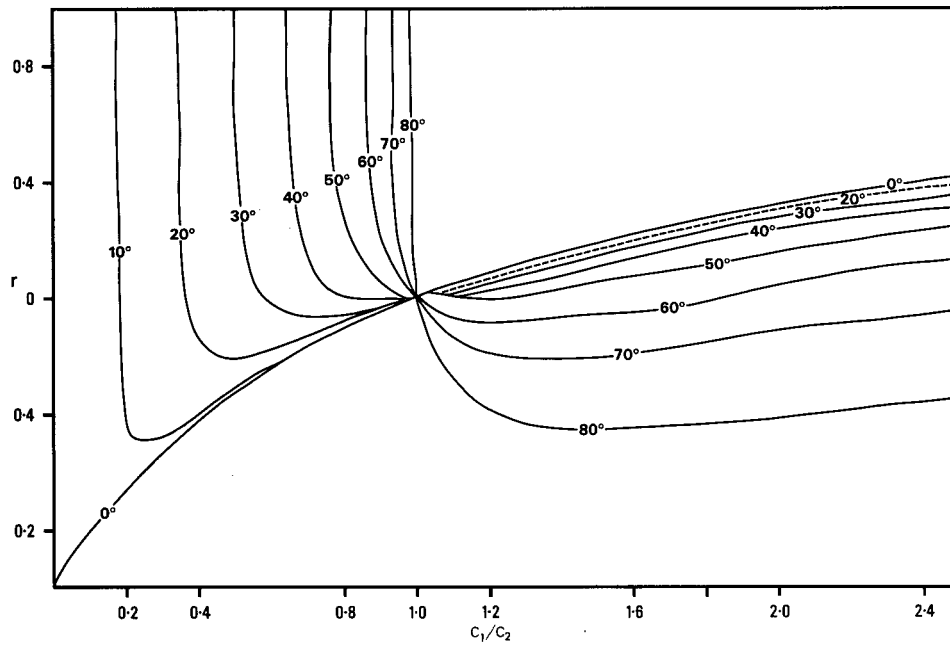


FIG. 3.17. Amplitude coefficient of reflection, r, as a function of the velocity ratio c_1/c_2 for various values of the angle of incidence. (Cochrane and Arthur 1948)

Cochrane and Arthur (1948) used an analogy from acoustics to show that, if the depth change is not discontinuous as is assumed so far but is gradual in a region of length, d, then the reflection coefficient depends on the ratio, $d/(\mathrm{L}/\sin\theta)$, where L is the wavelength and θ is the angle of incidence. If this ratio is small, r approaches the value obtained from discontinuous depth change. On the other hand, if this ratio is large, $r \simeq 0$. On the continental slope near Crescent City, Calif., the depth changes from 305 to 101 m in a distance of only 24.1 km. If the period of the tsunami is 15 min (in deeper water) then the wavelength is 186.6 km and for normal incidence

$$\frac{d}{(\mathrm{L}/\sin\theta)} = \frac{24.1}{186.6} = 0.13 \tag{3.146}$$

The possible transoceanic reflection of tsunamis could be inferred when a tide-gage record registers a significant increase in the amplitude a long time after the arrival of the initial wave train. Figure 3.18 shows such a possible reflection associated with the Aleutian earthquake tsunami of Apr. 1, 1946. According to Cochrane and Arthur, the reflection occurred near the continental slope off the south Oregon coast and the reflected wave reached Hanasaki, Japan, some 10 h after the reflection occurred.

The amplitudes of the direct waves at Hanasaki were insignificant and it was the reflected waves that showed large amplitudes. As there is no tide gage at the

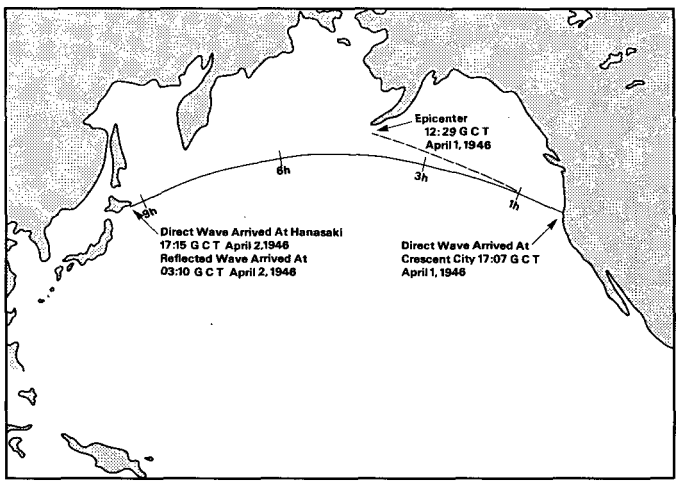


FIG. 3.18. Arrival times at Hanasaki of direct and reflected waves for tsunami April 1, 1946. Solid line indicates probable path of reflected waves reaching Japanese coast. (Cochrane and Arthur 1948)

continental slope off south Oregon, amplitude of the wave had to be estimated by the nearest tide gage at Crescent City, Calif. Green's law gave:

$$\frac{H_1}{H_2} = \left(\frac{D_2}{D_1}\right)^{\frac{1}{4}} \tag{3.147}$$

Where H_1 and H_2 were the wave amplitudes over water depths D_1 and D_2, the wave height at the continental slope could be estimated. Water depth at the Crescent City tide gage was approximately 6.1 m, water depth of the shallow side of the continental slope was 914.4 m, so the wave height $H_{914.4}$ at the continental slope was given by:

$$H_{914.4} = H_C \left(\frac{6.1}{914.4}\right)^{\frac{1}{4}} \tag{3.148}$$

where H_C was the wave height at Crescent City.

The transmission and reflection coefficients, s and r, at the continental slope (treated as a depth discontinuity) are obtained from the theory of Cochrane and Arthur (1948). Taking the angle of incidence as 10° and water depths on either side as 3017.5 m and 914.4 m, then $r = 0.27$, $s = 1 + r = 1.27$ for $\frac{c_1}{c_2} = \sqrt{\frac{3017.5}{914.4}}$ then, the height, H_R, of the wave reflected at 3017.5 m is:

$$H_R = \frac{r}{s} H_{914.4} = \frac{0.27}{1.27} H_{914.4} \tag{3.149}$$

The expression by Jeffreys and Jeffreys (1946) is used to determine the effect of distance on wave heights. This expression is valid only for the first few waves of a wave train generated impulsively:

$$\frac{H_1}{H_2} = \left(\frac{R_2}{R_1}\right)^{\frac{1}{3}} \tag{3.150}$$

Here R_1 and R_2 are the distances from the epicenter to the Oregon coast and between the Oregon coast and Hanasaki. Thus, wave height at Hanasaki at a depth of 3017.5 m is:

$$H_j = \left(\frac{3057.1}{10{,}136.7}\right)^{\frac{1}{3}} H_R \tag{3.151}$$

where R_1 and R_2 are 3057.1 and 10,136.7 km. From Green's law the wave height, H_H, at the tide-gage location at Hanasaki can be obtained (assuming water depth is 6.1 m).

$$H_H = \left(\frac{3017.5}{9.14}\right)^{\frac{1}{4}} H_j \tag{3.152}$$

From the observed wave height a Crescent City, $H_C = 85$ cm:

$$\begin{aligned} H_{914.4} &= 25 \text{ cm} \\ H_R &= 5.3 \text{ cm} \\ H_j &= 3.6 \text{ cm} \\ H_H &= 17 \text{ cm} \end{aligned} \tag{3.153}$$

The value of 17 cm for the wave height deduced from this approximate analysis agreed fairly well with observed wave heights between 9 and 11 h after the initial (but insignificant) wave train arrived at Hanasaki.

Shimozuru and Akima (1952) detected possible reflections of the tsunami from Guam Island. The south coast of Shikoku Island was affected by the earthquake that occurred Dec. 21, 1946, at 0419 h Japan standard time, with the epicenter at 33.0°N,134.8°E and magnitude 8.1. Tide-gage records at four stations, Hachinohe, Mera, Ito, and Uchiura, at the time of this tsunami showed both long- and short-period waves.

Because long-period waves suffer less dissipation during travel and get reflected more easily at abrupt depth variations, reflected waves, if they occur, could be detected more easily in the long-period waves. To get a record of long-period waves alone from the above records, the predicted tide was removed first, then short-period waves were removed through a low-pass filter. The filtered records showed long-period waves with average periods of about 80 min. The question naturally arises: were these waves due to purely local effects such as resonances in the bay where the tide gage was situated, or was their source far away? The answer is provided

by comparing the records of the Tonankai earthquake tsunami of Dec. 7, 1944, with an epicenter at 34.0°N,137.1°E and magnitude 8.3. The epicenters of the two earthquakes are close enough that travel paths to the tide gages can be considered almost identical. The records of the second tsunami were also subjected to low-pass filtering and did not show any long-period waves as in the Nankai earthquake tsunami. Hence, the authors concluded that the long-period waves accompanying the Nankai earthquake tsunami were not due to local causes but had their source near the tsunami origin.

Plots of period and amplitude of these filtered records vs. time for two stations, Hachinohe and Ito, showed that both the period and amplitude of the waves continually decreased for several hours after the initial maximum wave then suddenly picked up again. For Hachinohe the time interval between the arrivals of the direct wave and the reflected phase was 5 h 36 min, for Ito it was 6 h 10 min. As there were no significant aftershocks for this earthquake, the long-period waves could not have been caused by another tsunami generated by any of the aftershocks but must have been due to waves reflected at some distant coast or islands.

Cochrane and Arthur (1948) used the long-wave formula to draw wave fronts to determine the probable boundaries of reflection as either Guam Island or the Mariana Trench. If the reflection occurred from a trench, the phase of the reflected wave must be reversed, but as this was not observed in the records, the authors concluded that the Nankai tsunami was most probably reflected from Guam Island and its surrounding reef. However, one puzzling feature is that the amplitude of the reflected waves was greater than that of direct waves at Hachinohe and the authors have no definite answer except to speculate that the direct waves might have suffered dissipation while traveling through the sea ridges of Izu Islands.

Murty and Boilard (1970), while studying the spectra of tsunami records at Tofino on the west coast of Canada (Fig. 3.19) for the 1964 Alaskan earthquake tsunami, deduced there were some indications of transoceanic reflection of the tsunami. In general, Fig. 3.19 shows the dissipation of the tsunami energy with time. The peak at 87.3 min was stronger during the fourth interval than during the third. This might have been due to either a transoceanic reflection or an interaction between the tide and the tsunami or a combination of both.

T-Phase and Its Application to Tsunamis

The T-phase is a short-period (about 0.5 s) earthquake phase originally observed by Linehan (1940) in the seismograms from earthquakes originating in the West Indies. Ewing et al. (1950) proposed that the T-phase might be used in tsunami warning. Leet (1951) severely criticized this proposal and Ewing et al. (1952) presented additional arguments to support the earlier proposal. Probably no other topic concerned with tsunamis has generated such rival arguments and this topic deserves further attention.

The T-phase is a compressional wave propagated through the ocean with the speed of sound in seawater (Tolstoy and Ewing 1950). Ewing et al. (1950) stated that the T-phase has periods of 0.5 s or less and travels in deep water with the

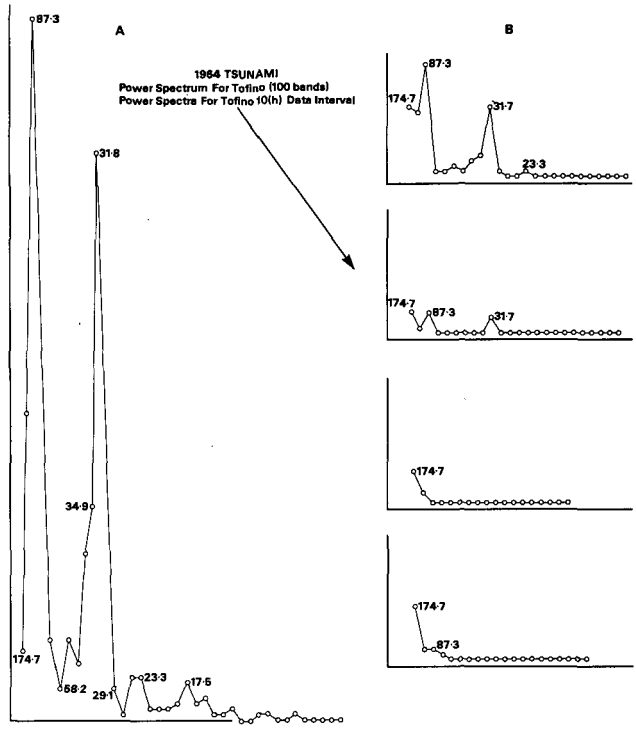


FIG. 3.19. Normalized Autospectra for Tofino (A) computed from total data record of 40 h, and (B) computed with the record divided into four equal parts, each of 10-h duration. Numerals are periods in minutes.

speed of sound in water, and in shallow water and on land with speeds ranging from 3.7 to 5.5 km s^{-1}, with amplitude decreasing rapidly over land.

Worzel and Ewing (1948) observed the propagation of high-frequency waves with the speed of sound, following shallow underwater explosions. Pekeris (1948) developed a theory for this problem that was later generalized by Press and Ewing (1948) who considered sound propagation in a liquid layer overlying an infinite solid layer.

Ewing et al. (1950) studied the T-phase on the east coast stations of the USA from epicenters of Dominican Republic earthquakes. They concluded that T-phase is produced only when the earthquake magnitude exceeds 7 and claimed a remarkable correlation between T-phase and tsunami generation. They used the work of Heck (1947) who listed 11 Pacific tsunamis from 1932 to 1947. Ewing et al. omitted six from this list because they were not expected to produce T-phases at stations in California because of intervening land barriers. Of the five tsunamis studied, four produced T-phases at Berkeley and Pasadena. The exception was the tsunami of Apr. 1, 1946.

Ewing et al. (1950) also discussed the T-phases recorded at Weston, Mass.; Fordham, N.Y.; and Ottawa, Ont., caused by Dominican Republic earthquakes

and concluded there was good correlation between T-phase generation and tsunamis. They suggested that this might be used for tsunami warning in the Atlantic Ocean.

Leet (1951) severely criticized the work of Ewing et al. (1950) on the T-phase. This criticism was probably correct and to give the full impact Leet (1951, p. 165) stated:

> "Ewing, Tolstoy, and Press of Columbia University reported that 'a striking correlation between the occurrence of a short-period earthquake phase (T-phase) travelling through the ocean with the speed of sound in sea water and the occurrence of tsunamis has been observed.'
>
> "Their statements about the characteristics of T are incorrect in every essential detail. For the Pacific Ocean, they list five tsunamis between 1933 and 1946, of which the largest, on April 1, 1946, was generated by an earthquake for which no T was recorded. They neglect to mention the earthquake of January 23, 1938, near Hawaii, which produced the largest T recorded on the Pacific coast to date, but no tsunami. The importance of these outstanding exceptions; errors in reporting the data, and uncertainty concerning the actual number of T-phases recorded on the Pacific coast combine to make the evidence for any value of T as a tsunami warning decidedly inconclusive.
>
> "In the Atlantic, the proposal that T be used as a tsunami warning reduces to an absurdity. Ewing, Tolstoy, and Press state that between 1939 and 1948, '20 Dominican Republic shocks produced T-phases' and that one of them was followed by a definite tsunami. Actually, more than 200 Dominican Republic shocks produced T within that span of years, and many in other Atlantic regions. With one minor tsunami among 200 to 250 T-phases, the correlation is not impressive."

Leet (1951) also disagreed with Ewing et al. (1950) on the range of period of the T-phase. He maintained that the range is 0.5–1.0 s generally, whereas the other authors put 0.5 s as an upper limit. The distinction is very important according to Leet (1951, p. 166) who stated:

> "A study of more than 200 records of T from the Atlantic has shown that in all cases the period ranges upward rather than downward from 0.5 sec., being for the most part between 0.5 and 1.0. This is significant, because SOFAR propagation (SOFAR stands for Sound Fixing and Ranging) along an axis of minimum velocity cannot explain transmission of waves of periods longer than 0.5 sec. carrying the greater part of the energy in T.
>
> "T does not travel with the velocity of sound in water for the part of its path crossing deep water. Its oceanic velocity ranges from 1.70 km/sec. to 2.65 km/sec. in different parts of the Atlantic, in contrast to velocities of sound in water from 1.46 to 1.53 km/sec. Its speed over land paths is 2.13 km/sec."

The Work of Ewing, Press, and Worzel

Ewing et al. (1952) presented further evidence to support the contentions put forth by Ewing et al. (1950). It appears that Leet (1951) was correct in his criticism of the 1950 paper. However, the latter paper (i.e. 1952) seems sound. In the 1952 paper, Ewing et al. ascertained that T-phase had periods in the range of 0.5–1.0 s.

Because their earlier work had applied some correction for the continental path of the T-phase and, as there is no accurate basis to determine this correction, in their 1952 paper they chose data based on locations of detectors and epicenters so that the continental path was negligible. They used seismographs at Honolulu, Kaneohe, and Point Sur SOFAR stations. In this case, no land travel was involved

and the velocity could simply be determined by dividing the distance by the time of travel. The velocities were estimated to be about 1.40 ± 0.02 km s^{-1}.

One interesting observation by Ewing et al. (1952, p. 42) was:

> "It is interesting to note that earthquakes southwest of Honolulu which produced T-phases on the seismographs there did not produce signals on the SOFAR hydrophone, which is situated a short distance northeast of the same island. Thus the island of Oahu casts a shadow for the T-phase from earthquakes exactly like that cast by Bermuda for SOFAR signals, as described by Ewing et al. (1946). This is additional evidence in support of the view that the T-phase is propagated as a compressional wave in the water."

Press et al. (1950) showed that the topography of the ocean floor at the epicenter is important in determining how efficiently the T-phase is generated by an earthquake. If the ocean bottom is horizontal at the epicenter, then the efficiency decreases with the increase of depth of focus. On the other hand an increasing ocean depth in the direction of propagation of the T-phase would allow more efficient entry of sound waves into the water and create suitable conditions for wave-guide propagation.

The authors attributed the differences between their results and those of Leet (1951) mainly to the effects of continental path and the corrections involved. In fact, Ewing et al. (1952, p. 49) emphatically stated this. (Table 3.4 summarizes the differences in the results of the Lamont school and Leet regarding T-phase.)

> "The consistency of our results ... and the excellent agreement of our results with the speed of sound in water, leaves little room for doubt that T is propagated as compressional waves in water; and the similarity between reception by SOFAR hydrophones of the T-phase and of signals from bombs exploded at the sound channel axis is additional strong evidence. Moreover, the hypothesis that T is transmitted as SH waves in ocean-bottom sediments is immediately ruled out since such waves could not enter the water for detection by the hydrophones."

Ewing et al. (1952) admitted that in their studies involving T-phase no destructive tsunamis occurred. As the whole purpose of tsunami warning service is to warn about destructive tsunamis (i.e. tsunamis capable of doing some damage), unless

TABLE 3.4. Properties of T-phase according to Lamont school and Leet.

Parameter	Lamont	Leet
Period	≤ 0.5 s	0.5–1.0 s
Required magnitude of earthquake	≥ 7.0	could be less than 7.0
Use for tsunami prediction in Atlantic	very definite	absurd
Velocity in Atlantic	velocity of sound in water	1.70–2.65 km/s
Velocity on land and in shallow water	3.75–5.5 km/s	1.46–1.53 km/s

T-phase studies are made involving large and destructive tsunamis, it is difficult to say how relevant the T-phase will be to tsunami warning. However, there has been considerable progress recently using T-phase for tsunami warning in French Polynesia (see Chapter 6).

Tsunami Travel on the Continental Shelf

In Chapter 1 the three ranges of the Ursell parameter and the relevant set of equations in each range were discussed. For small values of the Ursell parameter, phase dispersion is important and the linear set of equations is used. For large values of the parameter, amplitude dispersion is important and the nonlinear, long-wave equations are relevant. However, there is an intermediate zone (when the tsunami travels over the continental shelf) when the Boussinesq equations are relevant. Until recently this had not been done. Chen et al. (1975) used Boussinesq equations to develop a numerical model. They used the work of Peregrine (1967) who first developed the full Boussinesq approximation in two horizontal dimensions over variable depth.

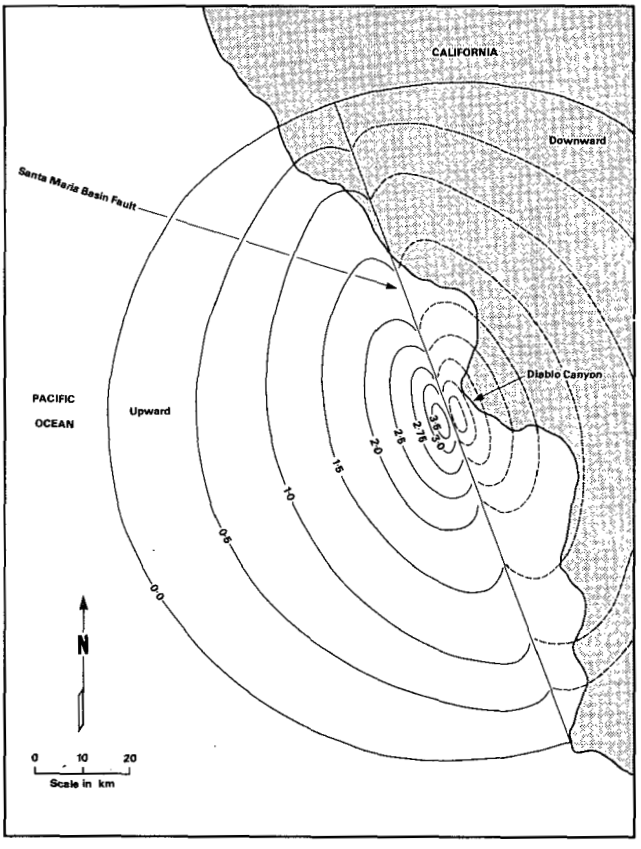


Fig. 3.20. General configuration of ground displacement in arbitrary units. (Chen et al. 1975)

This model has been applied to investigate tsunami behavior at the Diablo Canyon power plant in California (Fig. 3.20), associated with a strong earthquake at the Santa Maria Basin Fault. The assumed initial ground motion is also shown. The results showed that the Boussinesq model predicts a slightly lower maximum wave height of the tsunami.

Before concluding this section, one aspect of transmission of tsunami energy first considered by Yoshida (1959) will be discussed. According to him, the tsunami wave with the largest amplitude, hence the maximum energy, will occur earlier in the wave train for short travel distances but for larger travel distances it will occur later. To put this another way, the difference in the time of arrival at a given station between the first wave and the wave with the greatest energy increases with the travel distance.

Although Yoshida's surmise seems to be valid for Japanese data, the fact that it is not universally valid can be seen in Table 3.5. In this table, the period of the tsunami has been defined as the time interval between the arrival of the first and second crests at a given location. The observed periods have been compared with periods calculated from the following formula given by Stoneley (1963):

$$T = 0.03058 \left(\frac{x^2}{t}\right)^{\frac{1}{3}} \tag{3.154}$$

where x is the travel distance and t is the travel time (defined as the time taken by the first wave to arrive at the location under consideration). The proportionality constant is valid when x and t are in cgs units. Table 3.5 shows that Equation (3.154) underestimates the period of the tsunami by at least an order of magnitude. Of course, it is easy to understand why the calculated periods differ from the observed periods significantly, because (3.154) was derived from analytical theory by simple geometry.

TABLE 3.5. Observed data at stations on the west coast of Canada for the tsunami following the Alaskan earthquake of March 1964.

Station	Great circle distance from epicenter (*km*)	Obs. period of highest wave (*h*)	(*min*)	Calc. tsunami period (*min*)	Period of highest wave:travel time
Victoria	2056	0	16	7.1	0.06
Fulford Hbr.	2010	5	18	6.8	1.06
Vancouver	1995	1	45	6.4	0.31
Point Atkinson	1984	3	43	6.4	0.67
Port Alberni	1922	2	00	6.8	0.45
Tofino	1880	1	50	7.3	0.54
Alert Bay	1710	0	14	6.5	0.06
Ocean Falls	1530	0	25	5.8	0.09
Bella Bella	1523	0	31	6.4	0.16
Tasu	1304	0	19	6.9	0.16
Prince Rupert	1253	1	20	5.6	0.41

Yoshida (1959) distinguished between two types of stations; continental and oceanic. The first type is located along the continental edge of the ocean and the second is island stations. Based mostly on Japanese data, he deduced that when the period of the highest wave is plotted against the travel time, the slope of the approximate straight line is about $\frac{1}{3}$ for continental stations and $\frac{1}{10}$ for oceanic stations. Probably all Canadian stations listed in Table 3.5 are in the continental stations category. Column 5 shows there is a large scatter for this slope and it is doubtful that Yoshida's conjecture would hold generally.

3.4 Laboratory Experiments

Influence of Friction on Long-Wave Propagation

Harleman and Ippen (1963) considered the propagation of long waves and showed that inclusion of bottom friction leads to a velocity of propagation less than $\sqrt{gD}$ and, unlike the long-wave theory, the velocity of propagation depends on the wavelength, L, and a boundary resistance factor, μ. They also performed laboratory experiments to verify their theoretical prediction and their work will be considered briefly.

According to Harleman and Ippen, the effect of friction and energy dissipation is important for tsunami propagation, especially over continental shelves. They estimated that in water 6096 m deep a wave with an amplitude of 0.15 m and 161 km long would possess approximately a uniform maximum horizontal particle velocity of 0.006 m/s and a Reynolds Number of the order of 10^7.

Following Proudman (1953), Harleman and Ippen (1963) wrote the equation of motion for small-amplitude water waves with linear friction:

$$\frac{\partial u}{\partial t} = - g \left(\frac{\partial \eta}{\partial t} + \mathrm{M}u \right) \tag{3.155}$$

where u is the horizontal particle velocity, η is the wave height, and M is a linear resistance coefficient. In one wave period, the frictional work done is not much different either with linear or quadratic form of friction, hence, the use of the simple form is justified. The continuity equation is:

$$\frac{\partial \eta}{\partial t} = - \mathrm{D} \frac{\partial u}{\partial x} \tag{3.156}$$

where D is the water depth.

Equations (3.155) and (3.156) give:

$$c_0^2 \frac{\partial^2 \eta}{\partial x^2} = \frac{\partial^2 \eta}{\partial t^2} + g\mathrm{M} \frac{\partial \eta}{\partial t} \tag{3.157}$$

whose solution can be written as:

$$\eta = \mathrm{A}_0 \, \mathrm{e}^{-\mu x} \cos(\sigma t - kx) \tag{3.158}$$

where σ is the wave frequency, A_0 is the wave amplitude at $x = 0$, and μ is a damping coefficient.

From equations (3.157) and (3.158) the following two relations can be written:

$$c_0^2 (\mu^2 - k^2) + \sigma^2 = 0 \tag{3.159}$$

and

$$2 c_0^2 \mu k - g\mathrm{M}\sigma = 0 \tag{3.160}$$

Using the definition:

$$\sigma \equiv kc \tag{3.161}$$

in Equation (3.159):

$$c^2 = c_0^2 \left\{ 1 - \left(\frac{\mu}{k} \right)^2 \right\} \tag{3.162}$$

and Equation (3.160) becomes:

$$\mathrm{M} = \frac{2k\mathrm{D}}{c_0} \frac{\mu}{k\sqrt{1 - \left(\frac{\mu}{k} \right)^2}} \tag{3.163}$$

Equation (3.162) shows that inclusion of friction makes c depend on **L** and μ, in addition to D.

Harleman and Ippen (1963) then considered a channel communicating with a large basin. The wave in the channel is made up of two waves: an incident wave, $\eta_1(x,t)$, traveling in the positive x direction and a reflected wave, $\eta_2(x,t)$, traveling in the negative x direction given, respectively, by:

$$\eta_1 = \mathrm{A}_0 \mathrm{e}^{-\mu x} \cos(\sigma t - kx) \tag{3.164}$$

and

$$\eta_2 = \mathrm{A}_0 \mathrm{e}^{-\mu x} \cos(\sigma t + kx) \tag{3.165}$$

where σ is the frequency of natural oscillation of the basin, A_0 is the wave amplitude at the end of the channel ($x = 0$), and $t = 0$ corresponds to the time of maximum elevation at the closed end, $x = 0$.

The wave height, η, in the channel is given by:

$$\eta = \eta_1 + \eta_2 = \mathrm{A}_0 \left\{ \mathrm{e}^{-\mu x} \cos(\sigma t - kx) + \mathrm{e}^{\mu x} \cos(\sigma t + kx) \right\} \tag{3.166}$$

Maximum water level occurs at a given position in the channel when $\partial\eta/\partial t = 0$. The relative time, σt_{H}, of the maximum water elevation at any position with reference to the time of maximum water elevation at the end of the channel is given by:

$$\sigma t_{\mathrm{H}} = \tan^{-1} (-\tan kx \cdot \tanh \mu x) \tag{3.167}$$

Let η_H and η_{oH}, respectively, be the local wave amplitude at any given position and the wave amplitude at the end of the channel. Then from (3.156) and (3.157):

$$\frac{\eta_H}{\eta_{oH}} = \sqrt{\tfrac{1}{2}(\cos 2kx + \cosh 2\mu x)} \tag{3.168}$$

Let $\eta_H = a$ be the amplitude of the natural oscillation of the basin at the entrance, $x = -1$. Then:

$$\frac{a}{\eta_{oH}} = \frac{a}{2A_o} = \sqrt{\tfrac{1}{2}(\cos 2k + \cosh 2\mu)} \tag{3.169}$$

Harleman and Ippen assumed that k and μ could be treated as constant and wrote:

$$\mu = \frac{\Phi}{2\pi} k \tag{3.170}$$

where Φ is a constant of proportionality. From equations (3.167), (3.168), and (3.170):

$$\sigma t_H = \tan^{-1}\left\{-\tan kx \cdot \tanh\left(\frac{\Phi kx}{2\pi}\right)\right\} \tag{3.171}$$

and

$$\frac{\eta_H}{\eta_{oH}} = \sqrt{\tfrac{1}{2}\cos(2kx) + \cosh\left(\frac{\Phi kx}{\pi}\right)} \tag{3.172}$$

Harleman and Ippen (1963, p. 201) described their procedure to obtain μ and k as follows:

> "A plot of the amplitude ration η_H/η_{oH} versus the time angle of high water σt_H may therefore be made with the independent variables, Φ and kx, defining a family of curves. Thus, if the wave amplitude and time of high water are known at several points along the channel, these values when plotted in the manner suggested above, should fall along a curve of Φ = const. In principle, both μ and k could be determined by knowing the time and amplitude of the wave at the closed end of the channel and at only one other intermediate section. In practice, the method described above gives values of μ and k which are best fit for all of the available data."

The experiments were performed in a rectangular lucite flume 99.7 m long, 0.23 m wide, and water 0.15 m deep (average). Wave heights were recorded at nine stations along the length of the channel.

As an example of the orders of magnitude, k and μ, for test 1, k is 0.011 rad m^{-1} and μ is 0.005 rad m^{-1}. The energy dissipation due to molecular viscosity is several orders of magnitude lower than that by turbulent friction. Because of molecular viscosity, μ is about 10^{-10} rad m^{-1}.

Harleman and Ippen (1963, p. 204) summarized their conclusions:

> "(a) Friction influences the propagation characteristics of long, shallow-water waves. The celerity is shown to be function of water depth, wave length, and a parameter

depending upon the boundary roughness. The effect of boundary friction is to reduce the wave velocity below the value $c_0 = \sqrt{gD}$ for the frictionless case. A finite group of waves such as a tsunami may be expected to exhibit a dispersive character due to frictional effects.

"(b) The frictional effects on propagation appear to be independent of the wave period for a steady train of long oscillatory waves.

"(c) As the wave amplitude decreases, all other factors remaining constant, the wave celerity is less affected by friction and the celerity tends to increase toward the frictionless value $\sqrt{gD}$. This conclusion is probably only valid for fairly large-amplitude shallow-water waves. For waves of initially small amplitude-to-depth, the frictional effects should be essentially independent of wave amplitude.

"(d) A decrease in bottom roughness results in an increase in celerity toward the frictionless value $\sqrt{gD}$.

"(e) The observed rates of wave energy dissipation are clearly within the turbulent resistance regime. The damping modulus for wave amplitude is approximately 10^7 times greater than that due to molecular viscosity."

Recent Work

There is a great deal of literature concerning the problems of refraction. See Beitinjani and Brater (1965) for their description of experiments on refraction in prismatic channels.

Chao and Pierson (1972) performed laboratory experiments to study the refraction problems near a straight caustic. They also developed a linear theory. Their theoretical results compared favorably with their experimental results.

To perform experiments on the propagation of tsunami waves. Krivoshey (1970) used both laboratory models of real geometries and a hydraulic flume. The first laboratory model was developed to simulate a sector of the Pacific Ocean and investigate the influence of refraction, the location of the epicenter of the earthquake on the angle of wave approach to the coast, and the nature of the change of the wave form during its travel. The second was constructed to model a Pacific coastal region of USSR and investigate tsunami wave heights and run-up in coastal areas.

The horizontal scales used in these models were 1:65,000 and 1:5,000, respectively, and the vertical scales were 1:12,500 and 1:350. Modeling was based on the laws of gravitational similarity deduced from the equality of the Froude Number in the prototype and in the model.

Krivoshey used a hydraulic flume to study the following problems: the influence of scale distortion on the results of modeling, the laws of wave transformation at various bottom slopes of the shallow zone, and the formation and development of secondary waves (the so-called undulations on a long wave).

In the laboratory model used to study a sector of the Pacific Ocean, tsunami waves were produced by a pneumatic wave generator placed at the bottom and so arranged that the area of the generator agreed with the epicenter area, on the scale of the model. This generator created waves with periods ranging from 1.5 to 2.0 s corresponding to 15–20 min for the prototype. Electrical resistance sensors were used to record the vertical variations of water level at 25 positions in the model. Based on these, Krivoshey (1970, p. 353) came to the conclusions:

"1. Due to the decisive effect of refraction, the position of tsunami epicenter has no influence on the angle of wave approach to the coastline of the studied gulf.

2. When moving from the epicenter of tsunami towards the shore, the wave height at first diminishes due to energy dissipation and then increases due to the decrease of depth."

The second laboratory model was intended to simulate wave motion in a coastal area, and waves corresponding to periods of 10 min in the prototype were generated by placing the wave generator two wavelengths away from the shore. These experiments showed that the relative wave height of the crest, defined as the ratio of the height of the wave crest at a given point to the height of the wave crest near the generator, decreased from 1.0 to 0.6 during travel over a uniform depth of 200 m, whereas the relative wave period increased from 1.0 to 2.2 over the same travel path accompanied by a slight decrease of period in the gulf.

Krivoshey carried out four series of experiments in the hydraulic flume. The experiments under Series I were performed with the same horizontal and vertical scale of 1:200 and showed that (Krivoshey 1970, p. 355): "1. Modeling on spatial models with scale distortion has practically no effect on water level rise at the studied points. 2. Wavelength is of considerable importance for flooding depth."

Series II and III experiments were performed with variable bottom slope, and showed that the height of the wave crest changes very little during the propagation over uniform depth, but the slope of the front portion of the wave increases a little. An important feature is the occurrence of secondary oscillations (called "undulations") on the long waves. Krivoshey remarked that the undulations superimposed on a long wave are the first indication of wave breaking and might influence flooding on the shore due to tsunamis. According to him, the time, T, of the first appearance of these undulations is given for an ideal fluid by:

$$T = \frac{\pm \frac{2}{3} \sqrt{\frac{FB}{g} \cdot \frac{W}{a_0}}}{\left(1 - \frac{1}{3} \frac{F}{B} \frac{dB}{dH}\right)} \tag{3.173}$$

where F is the area of cross section of the stream; W is the velocity of propagation over uniform depth, H; B is the width of the channel; g is gravity; and a_0 is the rate of variation of discharge initially.

Krivoshey (1970, p. 359) stated that his experimental results agreed favorably with (3.173) and gave the following conclusions:

"1. Undulations in the zone of breaking may be regarded as independent waves; their breaking peculiarities depend on their slope in the deep zone.

2. With a decrease of the initial wave slope (in the beginning of the shallow zone) the breaking occurs in the deeper zone. In this case, longer undulations break before the shorter ones.

3. Earlier breaking of succeeding undulations of shorter length than the preceding ones may be explained also by a counter current which accelerates the wave overturn.

4. In the zone of breaking, the ratio of undulation length and depth of water is equal to 25 to 50."

Thus, based on his study of changes of undulation forms in shallow regions, Krivoshey (1970, p. 360) proposed the following tentative hypothesis:

"Undulations on shallow water may be regarded as independent long waves; their propagation is described by equations derived for long waves in shallow water (before the moment of breaking) and by equations derived for discontinuous waves (after breaking and propagation as a bore up to water edge)."

Series II and III experiments also revealed that features of wave breaking and run-up on dry coasts is different depending on whether the coast has a direct slope or an inverse slope. The wave propagation speed, V, is related to the wave height, η (above the dry bottom) in both cases. For a direct slope:

$$V = 1.8\sqrt{g\eta} \tag{3.174}$$

and for an inverse slope:

$$V = 2.54\sqrt{g\eta} \tag{3.175}$$

Hwang (1970) performed laboratory experiments on the wave set-up due to nonperiodic wave trains. He considered both breaking and nonbreaking waves. The nonperiodic wave train could set up shelf oscillations and characteristics of the oscillations would be related to the geometry of the shelf.

Chapter 4 Coastal Problems

4.1 Resonance

Resonance in Narrow Water Bodies

One-dimensional approach – For narrow water bodies the one-dimensional approach has been used extensively to determine natural free oscillations. There is a great amount of literature dealing not only with natural water bodies but also idealized situations such as rectangular basins. A few advances (preceded by a brief introduction) will be selected. See also the excellent books on oceanography by Sverdrup et al. (1942), Proudman (1953), Defant (1961), and Ippen (1966).

Merian (1828) developed a theory for free longitudinal oscillations in a nonrotating rectangular basin and gave the following formula for the period, T_n, of the n th mode.

$$T_n = \frac{1}{n} \frac{2L}{\sqrt{gD}} \tag{4.1}$$

where L is the length of the basin, D is the depth of the basin assumed to be uniform, and g is gravity. This formula holds when the bay is closed at both ends. On the other hand, for a rectangular bay of uniform depth, closed at one end and open at the other, the period of the first longitudinal mode is given by:

$$T_1 = \frac{4L}{\sqrt{gD}} \tag{4.2}$$

For this mode, there is a node at the mouth of the bay and an antinode at the head. In this situation, the length of the bay is $\frac{1}{4}$ the length of the standing wave that is excited.

The Merian formula gives a quick and rough estimation of the period of a bay. It can also be used to provide initial trial values for more accurate numerical calculations. Thorade (1931) stated that if the width of the bay is about $\frac{1}{10}$ the length, then a correction for the period could be applied by increasing the period (given by the Merian formula) by 10%. If the width is equal to the length then the period has to be increased by 32%. The Merian formula appears to consistently overestimate the periods compared to those determined by the more accurate numerical methods (Table 4.1).

An improvement over the Merian formula is the Defant method described by Neumann and Pierson (1966) and Defant (1961). For electrical analog methods to determine the free oscillations of one-dimensional systems see Defant (1961, vol. 2).

TABLE 4.1. Computed period, T_c, by numerical integration, of the first longitudinal mode of the five Great Lakes compared to periods, T_m, determined from Merian formula. (Rockwell 1966)

Lake	T_c (*h*)	T_m (*h*)
Superior	7.19	9.45
Michigan	8.83	10.53
Huron	6.49	9.77
Erie	14.08	16.76
Ontario	4.91	5.85

SYSTEMS WITH BRANCHES

Defant (1961) used the concept of electrical networks to describe procedures dealing with a system with branches (each assumed to have uniform depth). Occasionally the method of characteristics has been used to determine the characteristic oscillations of a basin with a branch (for example, see Horikawa and Nishimura 1968). However, these authors assumed uniform depth and a water body of regular shape. For this reason, although they give a rough estimate of the periods, these techniques cannot be used for accurate determination of the periods. Rao (1968) determined numerically free oscillations of the Bay of Fundy taking into account its two branches, Chignecto Bay and Minas Basin. Henry and Murty (1972) determined the resonance modes for a system with five branches. Rao (1968) also applied corrections for rotational and frictional effects in one-dimensional systems based on the work by Platzman and Rao (1964). Murty and Boilard (1970) used essentially the same technique to determine the free oscillations of an inlet on the west coast of Canada.

RESONANCE IN MULTIBRANCHED INLETS

Henry and Murty (1972) determined the resonant periods for a multi-branched inlet system on the west coast of Canada. Figure 4.1 shows the location of the Rivers Inlet complex treated in this study. Figure 4.2 schematically shows the five branches of this system with the grid scheme.

The finite-difference forms of the continuity equation and the momentum equation are for a variable grid size:

$$\frac{\eta_{i+1} - \eta_i}{\Delta x_i} = -\frac{\sigma(M_i + M_{i+1})}{g(A_i + A_{i+1})} \tag{4.3}$$

and

$$\frac{M_{i+1} - M_i}{\Delta x_i} = \sigma B_i \frac{(\eta_i + \eta_{i+1})}{2} \tag{4.4}$$

where M is the volume transport through a vertical cross section with area A and

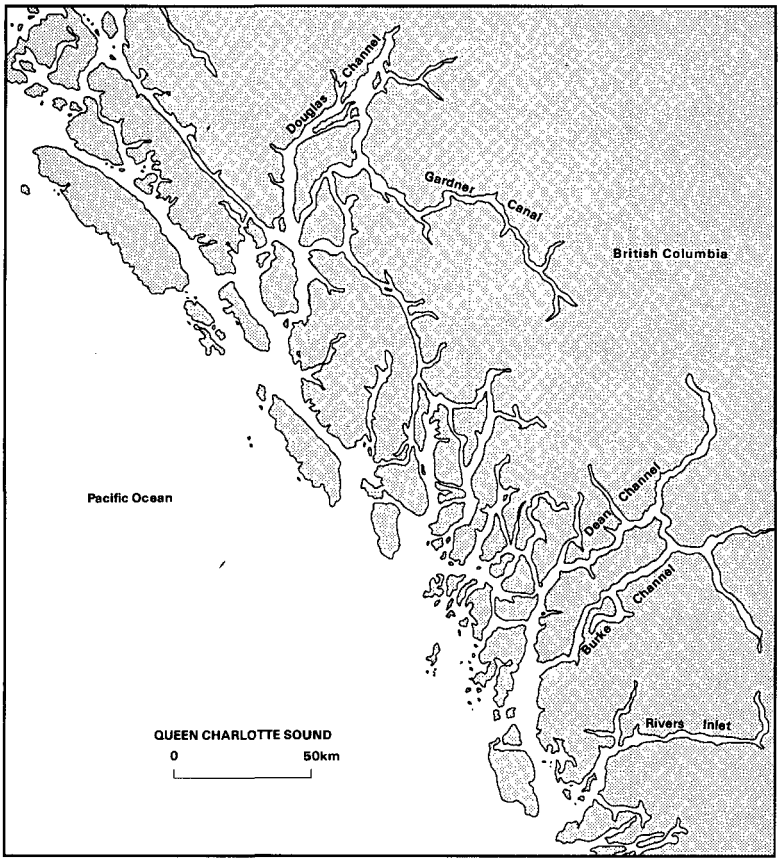


FIG. 4.1. Canadian west coast inlets.

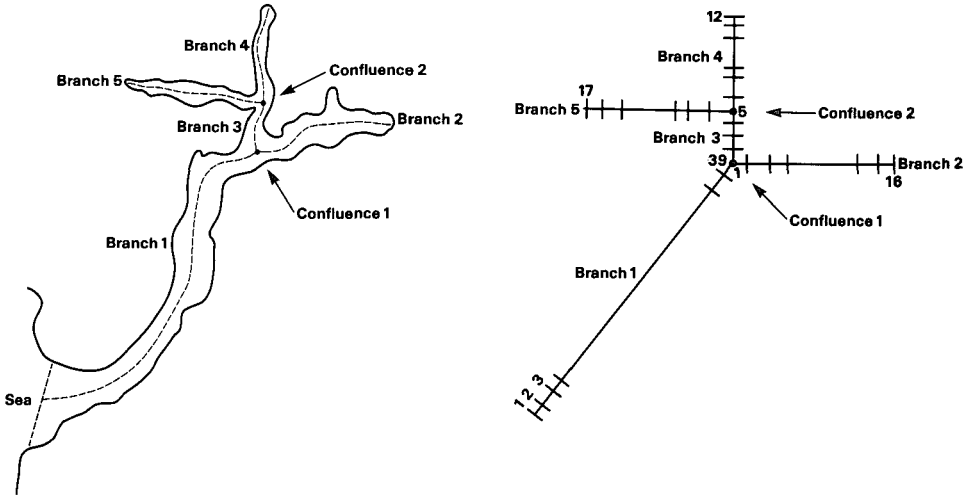


FIG. 4.2. Rivers Inlet on the west coast of Canada, map and schematic.

surface width B; η is the water-level deviation from the equilibrium position; g is gravity; Δx is the grid size at grid point, i; and σ is the frequency of oscillation. Frictional and Coriolis effects are ignored.

The conditions at confluence 1 are:

$$M_{39}^{(1)} = M_1^{(2)} + M_1^{(3)} \tag{4.5}$$

and

$$\eta_{39}^{(1)} = \eta_1^{(2)} = \eta_1^{(3)} \tag{4.6}$$

where superscript denotes the branch and subscript denotes the grid point in a given branch. At confluence 2 the following conditions have to be satisfied:

$$M_5^{(3)} = M_1^{(4)} + M_1^{(5)} \tag{4.7}$$

and

$$\eta_5^{(3)} = \eta_1^{(4)} = \eta_1^{(5)} \tag{4.8}$$

Branch 1 is open to the sea and has 39 grid points, branch 2 has 16, branch 3 has 5, branch 4 has 12, and branch 5 has 17. The boundary conditions of the problem are:

$$\eta_1^{(1)} = 0 \tag{4.9}$$

$$M_1^{(1)} \text{ is arbitrary} \tag{4.10}$$

and

$$M_{16}^{(2)} = M_{12}^{(4)} = M_{17}^{(5)} = 0 \tag{4.11}$$

A standard iteration technique described by Rao (1968) has been used to determine the resonance periods. (A) of Table 4.2 shows the periods determined by starting at sea and applying the final boundary condition at the head of branch 5. Although some modes are located with a few iterations, others took considerably more iterations. Let M^1 and M^2 denote the values of $M_{17}^{(5)}$ at the two values of bracketing the zero-crossing at the end of the fine search with frequency increment, $\Delta\sigma$.

Table 4.3 shows the zero-crossing behavior for a well-behaved and an ill-behaved mode for two different values of $\Delta\sigma$. This table shows that for a well-behaved mode, $M_{17}^{(5)}$ is a smooth function of σ near the zero-crossing and the values remain small. For an ill-behaved mode the values of M^1 and M^2 remain large. The authors ascribed this behavior to accumulation of numerical errors and called the ill-behaved modes false modes (these could be normal modes for a part of the system, however) and denoted them by F.

TABLE 4.2. Natural periods of Rivers Inlet computed by: (A) starting at sea and monitoring at head of branch 5, (B) starting at sea and monitoring at head of branch 2, (C) starting at head of branch 4 and monitoring at head of branch 2. Numerals denote genuine modes whereas the modes identified by F are spurious.

	(A)		(B)		(C)	
Mode No.	Period (*min*)	No. iterations	Period (*min*)	No. iterations	Period (*min*)	No. iterations
1	88.99	2	88.99	2	88.99	3
$F_{1,2}$	—	—	37.17	36	—	—
2	33.75	2	33.75	4	33.75	3
$F_{2,3}$	—	—	—	—	27.50	30
3	25.08	3	25.08	2	25.08	5
$F^1_{3,4}$	—	—	—	—	24.52	34
$F^2_{3,4}$	22.04	52	—	—	—	—
4	21.67	5	—	—	21.67	3
$F_{4,5}$	20.10	46	—	—	—	—
5	15.27	3	15.27	2	15.27	2
$F_{5,6}$	—	—	—	—	14.33	251
6	11.36	3	11.36	2	11.36	3
$F_{6,7}$	—	—	9.95	313	—	—
7	9.86	2	9.86	7	9.86	3

TABLE 4.3. The values $M^{(5)}_{1,7}$ (denoted by M^1 and M^2) at the two values of σ bracketing the zero-crossing in fine searches with two different frequency increments $\Delta\sigma$ for a well-behaved mode (number 4 for case A in Table 4.2) and for all ill-behaved mode (number $F^2_{3,4}$ for case A in Table 4.2).

	Values of $M^{(5)}_{1,7}$ ($cm^3\ s^{-1}$)			
	Well-behaved mode $\Delta\sigma = 10^{-10}$	Well-behaved mode $\Delta\sigma = 10^{-12}$	Ill-behaved mode $\Delta\sigma = 10^{-10}$	Ill-behaved mode $\Delta\sigma = 10^{-12}$
M^1	-2.138×10^{2}	-3.225×10^{1}	-2.463×10^{11}	-1.135×10^{13}
M^2	2.850×10^{-4}	2.625×10^{-6}	1.918×10^{9}	1.318×10^{12}

Table 4.2 also shows the modes, starting at sea (branch 1) and applying the final boundary condition at the head of branch 2 (i.e. monitoring in branch 2). Whereas the true modes denoted by numerals stay the same (the reason for the disappearance of genuine mode 4 will be considered below) an entirely different set of false modes appears, shown as (B). (C) shows the results from starting at the head of branch 4 and monitoring at the head of branch 2.

To understand this peculiar behavior of the modes, the nodal structures in terms of M and η were examined. Figure 4.3 shows the structures of modes 1 and 2 (both well behaved) and compares the well-behaved mode 3 with the false mode $F^2_{3,4}$.

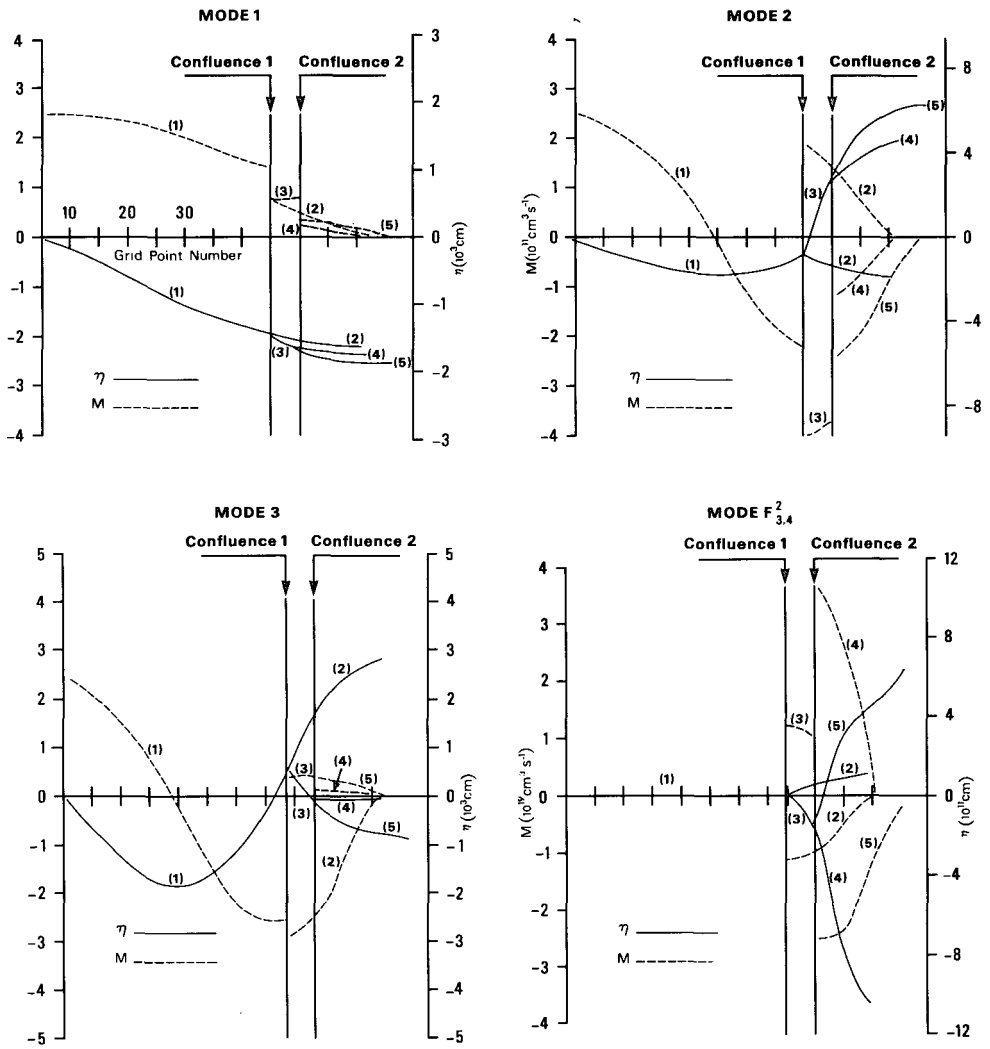


FIG. 4.3. Structure of modes 1, 2, 3, and $F^2_{3,4}$ in Rivers Inlet on the west coast of Canada in terms of volume transport (broken line) and water level (solid line).

An examination of the modal structures revealed the following important points: (1) when motion in the branch where the solution is begun is small compared to motion in the other branches, a false mode could occur, and (2) when the motion in both the starting and monitoring branches is small, a genuine mode could disappear.

Standard iteration technique is not suitable to determine free oscillations of multibranched inlets because all permutations and combinations of starting and monitoring must be used to eliminate the false modes. For a water body with n branches, n^2 separate calculations are necessary.

Henry and Murty (1972) used two alternate methods. In the first (the eigenvalue method), the partial differential equations were replaced by a set of difference-differential equations, i.e. discrete in space but continuous in time. The set of equations can be arranged in a matrix form where eigenvalues give the frequencies of natural oscillation of the system. This method causes neither spurious or false modes, nor misses any true modes. However, it suffers from the disadvantage that complex systems with many branch matrices of very large order have to be handled and computer storage limitations might not permit the matrix evaluation.

The second method is the impulse response method. In this method, the Green's function is used. Let $f_1(t)$ be the input at some point, x_1, in the system. Then the response, r_2, at some other point, x_2, in the system is given by:

$$r_2(x_1,t) = \int_{-\infty}^{\infty} K(x_1,x_2,t-\tau)\, f_1(\tau)\, d\tau \tag{4.12}$$

where K is a Green's function. For the tsunami problem, x_1 is at the mouth of the inlet. Hence, $K(x,t)$ expresses the response at any point, x, to a unit impulse (a unit delta function) imposed at the mouth.

Fourier Transform of (4.12) gives:

$$R_2(x,\omega) = K(x_1,x_2,\omega)\, F(\omega) \tag{4.13}$$

where $R(x,\omega)$ is the circular frequency. For the tsunami problem (4.13) simplifies to:

$$R(x,\omega) = K(x,\omega)\, F_1(\omega) \tag{4.14}$$

where $R(x,\omega)$ is the transform of the response at point, x, for input, $f_1(t)$, at the mouth, and $F_1(\omega)$ is the transform of $f_1(t)$.

If x does not coincide with a mode of any of the natural modes of the system, then $|K(x,\omega)|$ has vertical asymptotes at each of the resonant frequencies. Figure 4.4 shows this function for Rivers Inlet. Although the impulse response method is probably less accurate (Table 4.4) it is more practical than the other two methods.

TABLE 4.4. Comparison of period (min) for the first few genuine modes of Rivers Inlet computed by iterative method, direct eigenvalue method, and impulse response method.

Modal No.	Iterative method	Eigenvalue method	Impulse response method
1	88.99	88.97	87.38
2	33.75	33.79	36.69
3	25.08	25.06	24.82
4	21.67	21.68	21.35
5	15.27	15.25	15.38
6	11.36	11.36	–
7	9.86	9.86	–

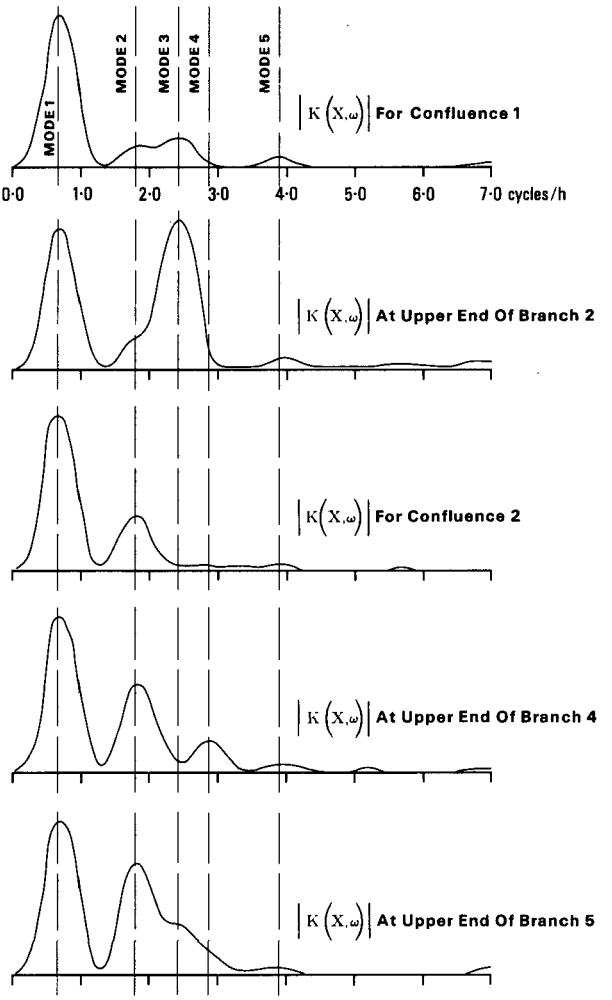


FIG. 4.4. Function $|K(X, \omega)|$ at 5 stations in Rivers Inlet on the west coast of Canada.

RESONANCE CALCULATIONS FOR IRREGULAR-SHAPED BASINS

Raichlen (1966a) calculated natural modes of basins of arbitrary shape and depth by what he called two-dimensional models. In fact, these are the so-called one-dimensional (only one horizontal dimension) models discussed in Section 1 of this chapter. Raichlen's three-dimensional model corresponds to the traditional two-dimensional model, and he simply outlines this model.

Lee and Raichlen (1971) developed a theory for calculating the resonant modes in harbors with arbitrary geometry but uniform depth. The solution of the two-dimensional problem is obtained in terms of an integral equation, later approximated into a matrix form. The area of study is divided into two regions, the region outside

the harbor mouth and the region inside the harbor. Boundary conditions at the harbor entrance are applied by matching the wave amplitude and its normal derivative for the exterior and interior solutions.

The authors examined the response of the harbor to incoming waves through an "amplification factor," defined (Lee and Raichlen 1971, p. 2169) as the ratio of the wave amplitude at any position inside the harbor to the sum of the incident and the reflected wave amplitude at the coastline (with the harbor entrance closed). They also performed some laboratory experiments to model Long Beach Harbor, Calif.

Clarke and Thomas (1972) calculated the normal modes of a spindle-shaped basin of uniform depth and applied the study to Port Kembla outer harbor on the east coast of Australia. This harbor, about 80 km south of Sydney, is well known for its seiche activity. Hidaka (1931) coined the name "spindle shape" to a basin whose perimeter at the surface can be defined as the intersection of two confocal parabolae.

The perimeter of a spindle-shaped basin can be defined by:

$$y^2 = \begin{cases} a(a-2x) \text{ for } x \geq 0 \\ a(a+2x) \text{ for } x < 0 \end{cases} \tag{4.15}$$

One interesting result from this case is that at the entrance to the harbor instead of a node (as is usually assumed in resonance calculations) an antinode was detected. This was a result of reflection off the harbor walls of the long waves which, as they emerge from the harbor entrance, will form a resonant standing-wave system outside the harbor. Only the symmetric modes will be excited when the standing-wave system is such that there is an antinode at the harbor entrance.

Olsen and Hwang (1971) calculated the resonant modes for a basin with arbitrary shape and variable depth. One new feature of this theory is that the boundary condition at the entrance to the basin need not be prescribed. The authors applied this study to Keauhou Bay, Hawaii.

Let $D(x,y)$ be the water depth and Φ the velocity potential. The linearized form of the long-wave equation is:

$$\frac{1}{g}\frac{\partial^2 \Phi}{\partial t^2} = \frac{\partial}{\partial x}\left(D\frac{\partial \Phi}{\partial x}\right) + \frac{\partial}{\partial y}\left(D\frac{\partial \Phi}{\partial y}\right) \tag{4.16}$$

Assume periodic excitation from outside that ultimately causes a steady periodic motion inside the harbor. For this write:

$$\Phi = \phi(x,y) \exp(-i\sigma t) \tag{4.17}$$

where σ is the frequency of periodic motion. Then from (4.16) and (4.17):

$$\frac{\partial}{\partial x}\left(D\frac{\partial \phi}{\partial x}\right) + \frac{\partial}{\partial y}\left(D\frac{\partial \phi}{\partial y}\right) + \frac{\sigma^2}{g}\phi = 0 \tag{4.18}$$

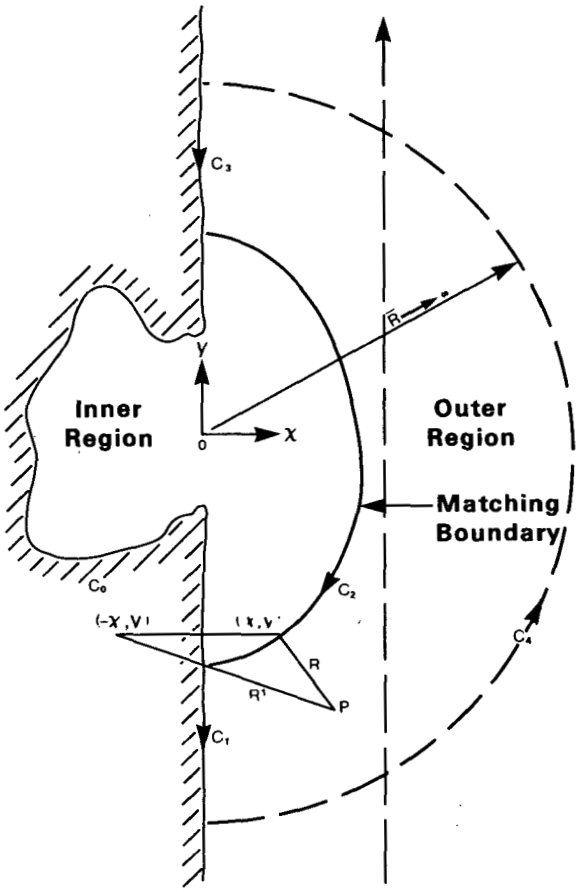


FIG. 4.5. Schematic diagram used to obtain boundary condition between inner and outer regions. (Olson and Hwang 1971)

Figure 4.5 shows that in the outer region a uniform depth (equal to depth at the matching boundary) will be assumed and an analytical solution will be obtained, whereas in the inner region a numerical solution will be given.

Because depth is uniform in the outer region the Helmholtz equation is:

$$\nabla^2 \phi + k^2 \phi = 0 \tag{4.19}$$

where

$$k^2 \equiv \frac{\sigma^2}{g\mathrm{D}} \tag{4.20}$$

The following boundary conditions should be satisfied. Along the shoreline:

$$\frac{\partial \phi}{\partial n} = 0 \tag{4.21}$$

and at ∞:

$$\phi = \phi_0 \tag{4.22}$$

Olsen and Hwang (1971) made some simplifications. They assumed a straight shoreline located at $x = 0$. Then, for a straight-crested standing wave with crest at an angle β to the x-axis:

$$\phi_0 = \cos(kx \cdot \cos\beta) \exp(-iky \sin\beta) \text{ for } 0 < \beta < \pi \tag{4.23}$$

However, if the wave front propagates parallel to the x-axis, then β is equal to zero and ϕ_0 reduces to:

$$\phi_0 = \cos kx \tag{4.24}$$

This condition is consistent with the assumption that the wave motion is the same on either side of the boundary.

Then:

$$\phi = \phi_0 + \phi' \tag{4.25}$$

where ϕ_0 is the contribution due to the incident waves and ϕ' is due to the presence of the harbor. Individually ϕ_0 and ϕ' satisfy Equation (4.19). However, the boundary condition (4.21) becomes:

$$\frac{\partial}{\partial n}(\phi_0 + \phi') = 0 \tag{4.26}$$

and this has to be satisfied on the shoreline C_1 and C_3.

The condition at the matching boundary is that ϕ_0 and ϕ' on one side of the boundary must be equal to ϕ_0 and ϕ' on the other side. Let G be a Green's function and S the contour of integration. Then, to determine the perturbation velocity potential Kernel ϕ', write:

$$\phi' = \int_S \left(\phi' \frac{\partial G}{\partial n} - G \frac{\partial \phi'}{\partial n}\right) ds \tag{4.27}$$

The contour integration is made around C_4, C_3, C_2, C_1 as shown in Fig. 4.6.

The Green's function, G, must satisfy the following conditions: (a) the Helmholtz Equation (4.19); (b) have a singularity at R = 0, and (c) vanish at ∞.

The Hankel function of the first kind and zero th order, $H_0^{(1)}(kR)$, could be chosen as the Green's function, because:

$$H_0^{(1)}(kR) \to \begin{cases} \frac{i}{\pi} \ln(kR) \text{ as } R \to 0 \\ -\frac{i}{\pi}\left[\frac{2\pi}{kR} \exp\left\{i\left(kR + \frac{\pi}{4}\right)\right\}\right]^{\frac{1}{2}} \text{ as } R \to \infty \end{cases} \tag{4.28}$$

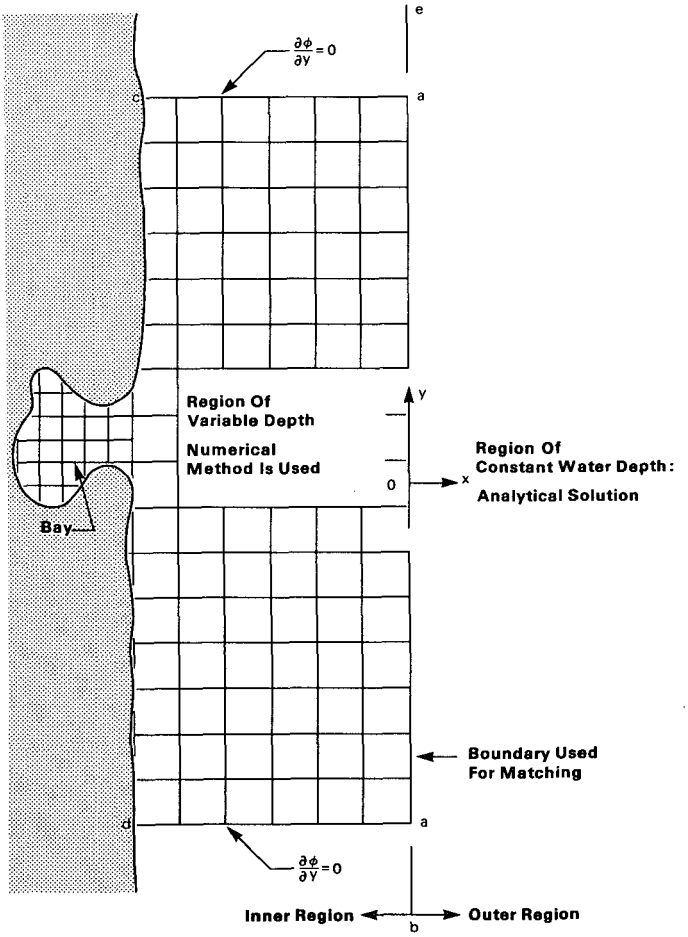


FIG. 4.6. Schematic diagram of the bay and method used in analysis. (Olson and Hwang 1971)

If the contour C_4 is extended to ∞ then $R \to \infty$, and (4.27) becomes:

$$\phi' = \int_{C_4} \left(\phi' \frac{\partial G}{\partial n} - G \frac{\partial \phi'}{\partial n} \right) ds \to 0 \text{ as } R \to \infty \tag{4.29}$$

For numerical evaluation purposes, Olsen and Hwang made further simplifications. As shown in Fig. 4.5, the boundaries C_1, C_2, C_3 are taken to be straight lines. Also the coordinate system is fixed as shown. This means at *d a b* and *c a* e, a rigid wall is assumed (Fig. 4.6).

Olsen and Hwang pointed out that the simplification will have little effect on the results for normal incident waves as long as *a* is large enough compared to the width at the mouth of the bay. They cautioned, however, that edge waves generated by obliquely incident waves will be affected.

Under these simplifications, Equation (4.27) becomes:

$$\phi'(x,y) = \int_{-\infty}^{\infty} \left(\phi' \frac{\partial G}{\partial x} - G \frac{\partial \phi'}{\partial x} \right) d\eta \tag{4.30}$$

Define:

$$R' \equiv \left\{ (x+\xi)^2 + (y-\eta)^2 \right\}^{\frac{1}{2}} \tag{4.31}$$

and

$$R \equiv \left\{ (x-\xi)^2 + (y-\eta)^2 \right\}^{\frac{1}{2}} \tag{4.32}$$

where ξ, η are the coordinates on the matching boundary. A choice of:

$$G = -\frac{i}{4} \left\{ H_0^{(1)}(kR) + H_0^{(1)}(kR') \right\} \tag{4.33}$$

satisfies not only the three conditions listed above but also the following condition:

$$\frac{\partial G}{\partial x} = 0 \tag{4.34}$$

along the y-axis. Then Equation (4.30) becomes:

$$\phi'(x,y) = -\frac{i}{2} \int_{-\infty}^{\infty} \frac{\partial \phi'(0,\eta)}{\partial x} H_0^{(1)}(k|y-\eta|)\, d\eta \tag{4.35}$$

As $a\,b$ and a e are assumed to be rigid walls, then:

$$\frac{\partial \phi'}{\partial x} = 0 \tag{4.36}$$

Also, if the incident wave is parallel to the y-axis, then Equation (4.24) holds and:

$$\phi(x,y) = \cos(kx) - \frac{i}{2} \int_{-a}^{a} \frac{\partial \phi(0,\eta)}{\partial x} H_0^{(1)}(k|y-\eta|)\, d\eta \tag{4.37}$$

The prime on ϕ in the integral is suppressed for convenience.

Next, Olsen and Hwang outlined a finite-difference procedure to obtain the solution of Equation (4.18) in the inner region under the boundary condition (4.37).

With reference to a rectangular grid system:

$$x_i = i\Delta x \text{ for } 0 \leq i \leq j$$
$$y_i = j\Delta y \text{ for } 0 \leq j \leq k \tag{4.38}$$

Equation (4.18) can be written as:

$$\frac{D_{i+\frac{1}{2},j}}{(\Delta x)^2}(\phi_{i+1,j} - \phi_{i,j}) - \frac{D_{i-\frac{1}{2},j}}{(\Delta x)^2}(\phi_{i,j} - \phi_{i-1,j}) + \frac{D_{i,j+\frac{1}{2}}}{(\Delta y)^2}(\phi_{i,j+1} - \phi_{i,j}) - \frac{D_{i,j-\frac{1}{2}}}{(\Delta y)^2}(\phi_{i,j} - \phi_{i,j-1}) = -\frac{\sigma^2}{g}\phi_{i,j} \tag{4.39}$$

Defining the following quantities:

$$B_{i,j} \equiv -D_{i,j-\frac{1}{2}}\frac{\Delta x}{\Delta y} \tag{4.40}$$

$$D_{i,j} \equiv -D_{i-\frac{1}{2},j}\frac{\Delta y}{\Delta x} \tag{4.41}$$

$$E_{i,j} \equiv D_{i+\frac{1}{2},j}\frac{\Delta y}{\Delta x} + D_{i-\frac{1}{2},j}\frac{\Delta y}{\Delta x} + D_{i,j+\frac{1}{2}}\frac{\Delta x}{\Delta y} + D_{i,j-\frac{1}{2}}\frac{\Delta x}{\Delta y} - \frac{\sigma^2}{g}\Delta x\,\Delta y \tag{4.42}$$

$$F_{i,j} \equiv -D_{i+\frac{1}{2},j}\frac{\Delta y}{\Delta x} \tag{4.43}$$

$$H_{i,j} \equiv -D_{i,j+\frac{1}{2}}\frac{\Delta x}{\Delta y} \tag{4.44}$$

From equations (4.39) to (4.44) then:

$$B_{i,j}\,\phi_{i,j-1} + D_{i,j}\,\phi_{i-1,j} + E_{i,j}\,\phi_{i,j} + F_{i,j}\,\phi_{i+1,j} + H_{i,j}\,\phi_{i,j+1} = 0 \tag{4.45}$$

This equation can be written in the following matrix form:

$$\mathbf{M}\,\phi = 0 \tag{4.46}$$

This square matrix, **M**, has a size $(j + 1)(k + 1)$.

The boundary condition (4.21) can be written as:

$$\left(\frac{\partial\phi}{\partial x}\right)_{i,j} = \frac{\phi_{i+1,j} - \phi_{i-1,j}}{2\Delta x} \tag{4.47}$$

with a similar expression for $\frac{\partial\phi}{\partial y}$.

The boundary condition (4.37) becomes singular at $y = \eta$. This is evaluated as follows:

$$\begin{aligned}\phi(x,y) &= \phi_0 - \frac{i}{2}\int_{-a}^{a} H_0^{(1)}(k\,|y-\eta\,|)\,\frac{\partial\phi}{\partial x}\,(0,\eta)\,d\eta \\ &= \phi_0 - \frac{i}{2}\int_{-a}^{y-\epsilon} H_0^{(1)}(k|y-\eta\,|)\,\frac{\partial\phi}{\partial x}\,d\eta \\ &\quad - \frac{i}{2}\int_{y+\epsilon}^{a} H_0^{(1)}(k|y-\eta|)\,\frac{\partial\phi}{\partial x}\,d\eta \\ &\quad - \frac{i}{2}\int_{y-\epsilon}^{y+\epsilon} H_0^{(1)}(k|y-\eta\,|)\,\frac{\partial\phi}{\partial x}\,d\eta\end{aligned} \tag{4.48}$$

The integral on the right side of this equation is singular, but if it is assumed that $\partial\phi/\partial x$ is uniform in the neighborhood of ϵ, then it can be evaluated analytically to give:

$$\begin{aligned}I_3 &= -\frac{i}{2}\int_{y-\epsilon}^{y+\epsilon} H_0^{(1)}(k|y-\eta|)\,\frac{\partial\phi}{\partial x}\,(0,\eta)\,d\eta = B\,\frac{\partial\phi}{\partial x} \\ &= -\frac{i}{2}\left[\begin{array}{l} -b\epsilon + \dfrac{ck^2}{3}\,\epsilon^3 + \dfrac{2\epsilon}{\pi}\left(\ln\dfrac{k\epsilon}{2} - 1\right) \\ + \dfrac{2ak^2\epsilon^3}{3\pi}\left(\ln\dfrac{k\epsilon}{2} - \dfrac{1}{3}\right)\dfrac{\partial\phi}{\partial x}\,(0,y)\end{array}\right]\end{aligned} \tag{4.49}$$

with $a = -0.2500000$, $b = 0.36746691$, $c = 0.06728818$.

By taking $\epsilon = \Delta y$, the first two integrals on the right side of Equation (4.48) can be evaluated by the trapezoidal quadrature technique. The numerical calculations for Keauhau Bay showed that the wave amplification inside the harbor was greater for shorter wave periods.

Loomis (1970) developed a technique to determine the normal modes of irregular shaped harbors with variable depth and applied this for several bays and harbors in Hawaii. He started with the linear shallow-water Equation (4.16).

In the numerical scheme, central finite differences were used and a function, K, was defined such that:

$$K_{i,j} \equiv \begin{cases} 0 \text{ if } i,j \text{ is outside the region} \\ 1 \text{ if } i,j \text{ is inside the region or on boundary} \end{cases} \tag{4.50}$$

Then the double indices, i,j, are mapped into a single index, I, using an index function, I(i,j). Reflecting boundaries are treated by hypothetical grid points outside the region.

The velocity potentials $\phi_{i,j}$ are identified as ϕ_I, I = 1, ... n, and define:

$$\vec{\phi} = \begin{bmatrix} \phi_1 \\ \phi_2 \\ \cdot \\ \cdot \\ \phi_n \end{bmatrix}$$

then

$$\frac{\partial \vec{\phi}}{\partial x} = D_x \vec{\phi} = \frac{1}{2\Delta x} \begin{bmatrix} 1 & 0 & -1 & 0 & \cdots & 0 \\ 0 & 1 & 0 & -1 & \cdots & -1 \\ \cdot & \cdot & \cdot & \cdot & \cdots & \cdot \\ \cdot & \cdot & \cdot & \cdot & \cdots & \cdot \\ \cdot & \cdot & \cdot & \cdot & \cdots & -2 \end{bmatrix} \begin{bmatrix} \phi_1 \\ \phi_2 \\ \cdot \\ \cdot \\ \phi_n \end{bmatrix}$$

and (4.51)

$$\frac{\partial^2 \vec{\phi}}{\partial x^2} = D_{xx} \vec{\phi} = \frac{1}{(\Delta x)^2} \begin{bmatrix} -2 & 1 & 0 & 1 & \cdots \\ 1 & -2 & 1 & 0 & \cdots \\ \cdot & \cdot & \cdot & \cdot & \cdots \\ \cdot & \cdot & \cdot & \cdot & \cdots \\ \cdot & \cdot & \cdot & \cdot & \cdots \end{bmatrix} \begin{bmatrix} \phi_1 \\ \phi_2 \\ \cdot \\ \cdot \\ \phi_n \end{bmatrix}$$

The finite-difference form of Equation (4.18) becomes:

$$\left[(D_x \vec{D}) * D_x + \vec{D} * D_{xx} + (D_y \vec{D}) * D_y + \vec{D} * D_{yy} \right] \vec{\phi} = \sigma \vec{\phi} \tag{4.52}$$

where the meaning of * is understood from:

$$\begin{bmatrix} a_1 \\ a_2 \\ \cdot \\ \cdot \\ \cdot \\ a_n \end{bmatrix} * \begin{bmatrix} b_1 \\ b_2 \\ \cdot \\ \cdot \\ \cdot \\ b_n \end{bmatrix} = \begin{bmatrix} a_1 & b_1 \\ a_2 & b_2 \\ \cdot & \cdot \\ \cdot & \cdot \\ \cdot & \cdot \\ a_n & b_n \end{bmatrix} \tag{4.53}$$

The eigenvalues were determined by the Hessenberg Method and the eigenvectors were determined from the set of homogeneous equations. Table 4.5 lists the results of the calculations by this method for several bays in Hawaii.

TABLE 4.5. Summary of calculated normal modes for bays and harbors on the Island of Hawaii. (Loomis 1970)

	No. grid pts.	Grid spacing (*m*)	Periods of normal modes (*min*)			
Hilo Harbor	63	365.6	20.6	11.8	8.83	7.16
Hilo Bay	70	$\Delta x = 507.9$ $\Delta y = 588.0$	26.16	14.6	12.55	11.56
Keauhou Bay	58	39.0	4.74	2.11	1.56	1.52
Kealakekua Bay (i)	97	169.2	4.80	3.16	2.87	2.43 1.41
Kealakekua Bay (ii)	51	253.9	5.10	3.34	3.19	2.42
Honaunau Bay	39	87.4	2.73	1.54	1.39	1.29

For some recent works on resonance calculations see Su (1975) and Larsen and Christiansen (1975). Lee and Hwang (1975) calculated the resonant oscillations in a partially open basin due to horizontal oscillation near the mouth, that could occur from an earthquake nearby.

Resonance Calculations with Two-Dimensional Models and Rotation

Computation of the free modes of oscillation of rotating two-dimensional basins with variable topography is difficult and, until recently, only an indirect method was available. In this crude method, the principle was to force the water body for a finite time, remove the forcing, and let the system oscillate. Then, by taking the power spectrum of the calculated water level, some idea of the free oscillations could be obtained. But there was no guarantee that all modes could be systematically excited or identified in this manner. However, if there is clear separation in the frequencies of the OFC and OSC for the water body under consideration, then the OFC can be determined (Murty and Taylor 1975).

Recently, Platzman (1971b, 1972), Rao (1972), and Hamblin (1972) developed techniques to calculate systematically the free oscillations of rotating basins with irregular geometry and applied their techniques to the Great Lakes.

The Platzman technique involved what he termed "resonance iteration" and can be used for fully closed as well as partially open water bodies. (In the latter case, there is an additional mode – the Helmholtz mode, which will be discussed.)

Rao approached the problem somewhat differently from Platzman. His approach involved the determination (once and for all) of the characteristic functions of a basin (in this study Rao assumed that the basin was completely closed) that depend only on the basin's topography. He did this by decomposing the vertically integrated flow into an irrotational and a solenoidal part. Through a solution of the relevant eigenvalue problem, the characteristic functions for the two parts could be determined. This procedure was used earlier by Proudman (1916) and Rao (1966).

Hamblin's (1972) work was similar to that of Platzman (1972) but more general, and he determined the frequencies of the modes of Lake Ontario. Hamblin com-

mented that the "resonance iteration method" used by Platzman suffered from computational inefficiency. Also, to achieve convergence, the matrix operator must be strictly Hermitian. Hamblin used another method (also used by Rao) he called "the exponential time factor method" whereby the time dependence was explicitly removed from the governing equations by an exponential time factor. Then the components of the horizontal transport were eliminated from the three equations (two equations of motion and a continuity equation). The single equation thus obtained was solved by some appropriate technique.

Helmholtz Mode

In the context of hydrodynamics the Helmholtz mode is a mode excited in a water body not completely closed. The period of this mode is greater than the slowest seiche-type mode and nodal points exist only at the openings (or "ports," a term used by Platzman (1971b)). There is much literature on this mode in the context of acoustics. Platzman (1971b) appears to be the first to systematically examine this mode taking the following factors into consideration: irregular shape and depth of water body, multiple openings, and effects of earth's rotation. He applied his study to the Gulf of Mexico which has two openings, the Yucatan Channel and the Straits of Florida.

A brief examination will be made of the nature of the Helmholtz mode or the cooscillating mode as referred to by Platzman (1971b). (Lee (1971) referred to this as the pumping mode.) The mode is formed by periodic transport through the openings and is thus analogous to the fundamental tone of an acoustic resonator (to be considered later). For a nonrotating rectangular bay of length, L, and uniform depth, D, the periods of free oscillation are given for two cases in units of $2L/\sqrt{gD}$ (g is gravity).

$$\text{mouth open: } 2, \tfrac{2}{3}, \tfrac{2}{5}, \tfrac{2}{7}, \ldots$$

$$\text{mouth closed: } -, 1, \tfrac{1}{2}, \tfrac{1}{3}, \ldots$$

With an adjustable barrier at the mouth, then from the state of completely open to the state of completely closed, modes having periods $\frac{2}{3}, \frac{2}{5}, \frac{2}{7}$, etc., are transformed continuously into modes with periods $1, \frac{1}{2}, \frac{1}{3}$, etc. However, the mode with period 2 degenerates into a mode of indefinitely large period.

Platzman also showed that earth's rotation reduces the period of the Helmholtz mode in contrast to increasing the period of the fundamental gravitational mode.

Acoustical Anology

In acoustics, a Helmholtz resonator is a rigid container with a small opening. For this system with single-degree of freedom the frequency of oscillation is given by (Seto 1971; Raichlen 1966b):

$$\omega = c\sqrt{\frac{A}{LV}} \tag{4.54}$$

Where V is the volume of the cavity, L is the length of the neck, and A is the cross-sectional area of the neck.

Where there is no neck but only an opening, an effective length, L, could be determined from (Seto 1971):

$$L_e = \frac{16}{3\pi} r \tag{4.55}$$

where r is the radius of the opening. For multiple openings, with areas of cross sections $A_1, A_2, \ldots$ and length $L_1, L_2, \ldots$ the frequency of the Helmholtz mode is given by:

$$\omega = \sqrt{\frac{g}{A}\left(\frac{A_1}{L_1} + \frac{A_2}{L_2} + \ldots\right)} \tag{4.56}$$

where A is the surface area of the basin.

Harbor Resonance

This discussion is based mostly on the paper by Miles (1971) who used the analogy with electrical circuits. Consider a narrow-mouthed harbor adjacent to a coastline as shown in Fig. 4.7. Miles cited several advantages of the equivalent circuit analysis over the traditional fluid mechanical approach. According to him, the problem of external radiation, coupling of channels, and resonance inside the harbor can be studied separately. Also the parameters for the equivalent circuit analysis can be expressed approximately without solving the complete boundary value problem.

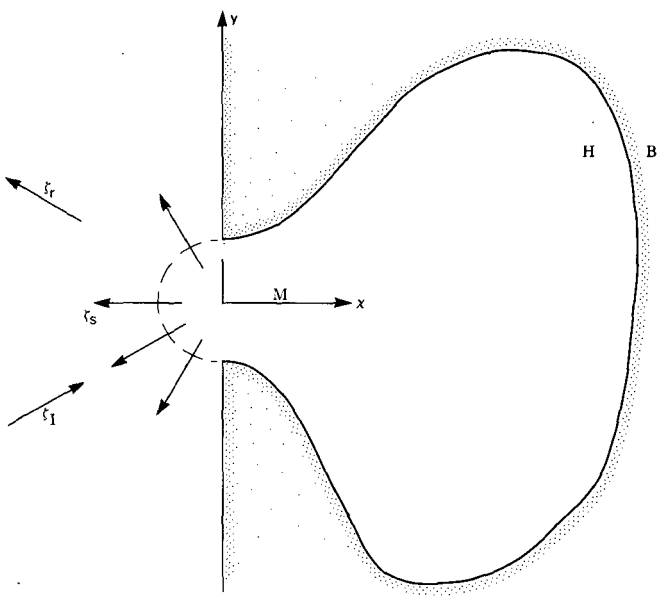


FIG. 4.7. Schematic diagram to determine resonant response of harbors. (Miles 1971)

In Fig. 4.7, a harbor, H, is connected to the sea through a narrow mouth, M, in a straight coastline. Take the origin of a Cartesian coordinate system, x, y, at the center of the mouth. let ζ_i and ζ_r given below represent the complex amplitudes of the incident wave and the specularly reflected wave from $x = 0$. Let ζ be the complex coamplitude of the free-surface displacement and assume monochromatic time dependence $\exp(j\omega t)$. Then:

$$\zeta_i(x,y) = \tfrac{1}{2} V_i \exp\left\{-jK(x \cos\theta_i + y \sin\theta_i)\right\} \tag{4.57}$$

and

$$\zeta_r = \zeta_i(-x,y)$$

Here K is the wave number, and V_i, a measure of the excitation of the harbor, is given by:

$$V_i = 2\zeta_i(0,0) \tag{4.58}$$

Let a be the width of the mouth and R be some representative dimension of the harbor. Then when:

$$\frac{a}{R} \ll 1 \text{ and } K\,a \ll 1 \tag{4.59}$$

the harbor mouth is considered to be narrow. These conditions imply that motion induced inside the harbor because of pressure, $\rho g\, V_i$ is small except for the natural modes of the harbor. The flow, I, through the mouth, M, must be proportional to V_i.

The analogous parameters to V_i and I in electrical circuits are voltage and current. The input impedance, Z_i, is given by:

$$Z_i \equiv \frac{V_i}{I} \tag{4.60}$$

This can be regarded as a series configuration of a radiation impendance, Z_M, given by:

$$Z_M = R_M + j\,X_m \tag{4.61}$$

and a harbor impendance Z_H:

$$Z_H = j\,X_H \tag{4.62}$$

The power radiated from H through M in the form of a scattered wave, ζ_s, is proportional to $R_M|I|^2$ whereas the nonradiated energy stored in the exterior half-space is proportional to $X_M|I|^2/\omega$. The energy stored in the harbor is proportional to $X_H|I|^2/\omega$. An empirical resistive component, R_H, in Z_H could be included to account for dissipation of energy proportional to $R_H|I|^2$.

Based on the solution of the analogous problem in acoustics (Miles 1948), both R_M and X_M are bounded and are positive definite functions of the frequency, ω. Miles interpreted these as single resistive and inductive elements. However, Z_H comprises an infinite sequence of parallel combinations of inductance, L_n, and capacitance, C_n, and there is a one-to-one correspondance between these and the modes of the harbor assumed to be closed, with frequencies given by:

$$\omega_n \equiv (L_n\, C_n)^{-\frac{1}{2}} \tag{4.63}$$

In addition there is a single capacitor, C_0, and this corresponds to the degenerate mode of uniform displacement with frequency given by $\omega_0 = 0$.

The solution inside the harbor may be expanded in the normal modes, so that the root mean square displacement and the kinetic and potential energies in the n th mode are proportional to the voltage across C_n and the energies stored in L_n and C_n. From these arguments it could be deduced that the individual nodal impedances are significant only near their respective resonant frequencies. This leads to the simplification that Z_H in the neighborhood of $\omega = \omega_n$ might be approximated by a lumped inductance, L_H, in series with either C_0 or in parallel combinations with L_n and C_n, so that the energy in all modes except the n th is proportional to $L_H |I|^2$.

The voltage amplification ratio A_n is given by:

$$A_n \sim \left| \frac{V_n}{V_i} \right| \tag{4.64}$$

which gives an estimate of the resonant response in the vicinity of $\omega = \omega_n$. For the zero th mode however, the harbor behaves like a Helmholtz resonator and the series circuit is a combination of R_M, $L_M + L_H$, and C_0. The resonant frequency $\tilde{\omega}_0$ for this mode is determined through a balance between the potential energy, $\frac{1}{2} C_0 |V_0|^2$, in the harbor and the kinetic energy, $\frac{1}{2} (L_M\, L_H)|I|^2$, in the neighborhood of the mouth.

For a rectangular harbor, Miles and Munk (1961) showed that the sharpness, δ, of the Helmholtz resonance is given by:

$$\delta = \frac{1}{\log\left(\frac{R}{a}\right)} \tag{4.65}$$

Let $\tilde{A}_n$ be the peak value of A_n and let Q_n represent the ratio of the resonant frequency to the half-power bandwidth of the resonance curve for the n th mode. Miles and Munk (1961) showed that:

$$\text{As } \frac{a}{R} \to 0$$

$$\tilde{\omega}_0 \equiv O(\delta^{\frac{1}{2}});\ \tilde{A}_0 \sim O\left(\frac{1}{\delta}\right) \text{ and } Q_0 \sim O\left(\frac{1}{\delta}\right) \tag{4.66}$$

An important result is that the resonant response in the higher modes is quite different from that of the simple resonant circuit. For the parallel resonant frequency, when $\omega = \omega_n$:

$$Z_i = \infty \tag{4.67}$$

And for the series resonant frequency when $\omega = \tilde{\omega}_n$

$$\begin{gathered} |Z_i| \text{ has a minimum} \\ \text{and} \\ A_n = \tilde{A}_n \text{ are both } \gg 1 \end{gathered} \tag{4.68}$$

It can be shown that:

$$\begin{aligned} \tilde{\omega}_n &= \omega_n + O(\delta) \\ \tilde{A}_n &= O\left(\frac{1}{\delta}\right) \\ Q_n &= O\left(\frac{1}{\delta^2}\right) \end{aligned} \tag{4.69}$$

An interesting consequence of (4.66) and (4.69) is that the mean square response to a random excitation in the vicinity of $\omega = \omega_n$ is not affected by narrowing the mouth of the harbor; except for the Helmholtz mode. The response in the neighborhood of $\omega = \omega_n$ is proportional to $\tilde{\omega}_n \tilde{A}_n^2 / Q_n$ provided the band width of the random input is large compared to $\delta\omega_n$. For the Helmholtz mode, the response of the harbor increased inversely as $\delta^{\frac{1}{2}}$.

This result contradicts the so-called "harbor paradox" postulated by Miles and Munk (1961). Miles (1971) pointed out that Miles and Munk (1961) overlooked the proximity of series and parallel resonance for the higher modes and arrived at the wrong result; that narrowing the mouth of the harbor would increase the value of $\tilde{\omega}_n \tilde{A}_n^2 / Q_n$ for all modes, rather than only for the Helmholtz mode.

Garrett (1970) showed that the qualitative aspects of the harbor paradox are not consistent with the quantitative results of Miles and Munk (1961) for a narrow rectangular harbor. He also showed that a similar result holds for a circular harbor through an open bottom.

Thus the harbor paradox of Miles and Munk (1961) only holds for the Helmholtz mode. Miles (1971) suggested a somewhat weaker paradox; that the mean square response of the higher modes in a harbor to random input is not affected by narrowing the mouth of the harbor. This is strictly true when friction is ignored because narrowing the mouth increases the friction leading to a decrease in the response. LeMéhauté (1962) and Wilson (1962) showed that the harbor paradox was due to neglect of friction and nonlinear effects.

Miles (1971) also developed an electrical analogy for the problem considered by Carrier et al. (1970) (see also Carrier and Shaw 1970). Carrier and Shaw included a narrow channel between the mouth and the harbor and showed that $\widetilde{A}_0$ and Q_0 are increased considerably because of the presence of the channel. Rayleigh (1945) had a similar result with the problem of Helmholtz resonance. Miles (1971) showed that a narrow channel such as that assumed by Carrier et al. (1970) is analogous to an electrical transmission line as long as it is restricted to excitation of plane waves in the channel. Actually this plane-wave approximation is quite satisfactory for channel widths less than half a wavelength.

The determination of Z_M and Z_H involves an integral equation for the normal velocity in the harbor mouth. When a canal is present there are two integral equations for the normal velocities at the two ends of the canal. For details see Miles (1946a, b, 1948, 1967).

During his detailed derivations, Miles (1971) established the correspondence between his work and those of Lee (1971), Sommerfeld (1949), Hwang and Tuck (1970a), and Bartholomeusz (1958). Lee (1971) considered a harbor of arbitrary shape and Hwang and Tuck (1970a) used a numerical technique to study similar problems. Lee and Raichlen (1972) considered harbors with connected basins and Su (1973) obtained asymptotic solutions of resonance in harbors with connected basins. Other important papers are Wilson (1972) and Miles (1974).

Miles and Lee (1975) extended the earlier work of Miles (1971) to include coupled basins (i.e. inner and outer harbors). Their calculation of the resonant frequency of the dominant mode for Long Beach Harbor, Calif., agreed within 1% of the observed value. They also showed that the influence of bottom friction is negligible.

4.2 Coastal Phenomena

Various coastal phenomena associated with tsunamis (tsunami forerunner, initial withdrawal of water, tsunami bore, and secondary undulations) will be considered. However, before proceeding to these topics, the concept of radiation stress, originally given by Longuet-Higgins and Stewart (1960, 1961, 1962, 1964), will be briefly discussed.

Radiation Stress

Longuet-Higgins and Stewart developed the concept of radiation stress by analogy with radiation pressure, a force produced on a surface on which electromagnetic radiation impinges. This force is in the direction of wave propagation and is not necessarily isotropic. In the context of fluid mechanics, the isotropic stress is usually referred to as pressure. Because the term pressure is associated with isotropy, Longuet-Higgins and Stewart coined the term "radiation stress" which does not have the connotation of isotropy.

For waves at the surface of water, for example, the momentum is directed parallel to the propagation direction and is proportional to the square of the amplitude. Suppose this wave train is reflected from an obstacle or a wall, then

the direction of momentum must reverse. Because of the requirements of conservation of momentum, a force equal to the rate of change of wave momentum acts on the obstacle. The excess flow of momentum from waves is referred to as the radiation stress.

Longuet-Higgins and Stewart (1960, 1961, 1962) used rigorous mathematical techniques to apply this concept to such physical phenomena as wave set-up due to storms, surf-beats, interaction of waves and steady currents, and steepening of short gravity waves on the crests of longer waves. In their 1964 paper, they gave a more physical interpretation and included the effect of capillarity.

When waves from deep water travel into shallow water and ultimately encounter a sloping beach, they become steep and could break. After breaking they could advance with reduced amplitudes. During this process, the radiation stress changes and this could lead to changes in the level of the water surface.

Longuet-Higgins and Stewart (1964) used radiation stress to explain the interaction of waves with currents. The principle is: in analogy with elasticity and rheology, the authors expressed the power-per-unit length and rate of strain. Suppose a fluid surface containing waves is acted on by some other flow (e.g. a current). This current will create a rate of strain which will oppose the radiation stress.

Longuet-Higgins and Stewart (1964, p. 556) expressed the relative importance of radiation stress and geometrical focusing effects as follows:

> "It should be emphasized that the changes in wave energy which are due to the non-linear interaction of waves with shear flow are of the same order of magnitude as those which occur due to the geometrical focussing effects produced by the currents. At first glance, this may seem surprising, since the radiation stresses are a second order phenomenon, while the focussing effects appear to be first order. The fact is, however, that the focussing effects are first order in the energy, i.e. of second order in the amplitude and comparable with the radiation stresses."

Tait (1972) used the concept of radiation stress to determine the wave set-up on coral reefs, such as Bikini Atoll. Munk and Sargent (1948) observed higher water levels on the reef flat of Bikini Atoll compared to the level of surrounding waters. Inman et al. (1963) reported a similar situation on the reef surrounding the island of Kauai. The models of Longuet-Higgins and Stewart (1962, 1963, 1964), Whitham (1962), and Lundgren (1963) predicted a set-down (lowering of water level) seaward of the breakers and a set-up shoreward of the breakers.

Jonsson et al. (1971) gave mathematical expressions to determine the wave set-up when a wave interacts with a current. This paper is important from a practical point of view as the authors gave the expressions in a convenient form as well as graphs and tables. They also used the concept of "mean energy level for a periodic irrotational flow" to determine "current wave set-down." Huang et al. (1972) generalized the study of interactions between steady nonuniform currents and gravity waves to include a random gravity wave field.

Loucks (1962) applied the concept of interaction of waves and currents developed by Longuet-Higgins and Stewart to explain the propagation of tsunami to Johnson Point through Slingsby Channel on the west coast of Canada. A very interesting observation during the 1960 Chilean earthquake tsunami was that the tsunami propagated through the narrows, channels, and rapids to arrive at Johnson

Point, and still retained an appreciable amplitude. The concept Loucks invoked to explain this was that the waves could extract energy from an opposing current and lose energy to a following current via Reynolds stresses. In the approaches to Johnson Point, the Reynolds stresses would be acting to increase the energy of the wave. Loucks stated that without the Reynolds stress effect, the wave would have arrived at Johnson Point with greater dissipation.

Tsunami Forerunners

Nakamura and Watanabe (1961) defined the tsunami forerunner as a series of oscillations of the water level preceding the arrival of the main tsunami waves (Fig. B). The forerunner, when it exists, has typically smaller amplitudes and periods than those of the main tsunami and could be easily distinguished. They stated that there has been no clear indication of tsunami forerunners on either the North or South American coasts.

Nakamura and Watanabe explained that absence of the forerunner on the coasts of North and South America was because of the oblique nature of the incidence of the initial wave on the coasts. They explained that the existence of the forerunner at other places (Japan, for example) was due to the resonance in bays and shelves that could occur before the arrival of the main tsunami.

If this is the correct explanation for the existence of the forerunner, then one can ask why the forerunner does not exist on the coasts of North and South America, as resonance indeed occurs there (see Henry and Murty 1972; Murty and Wigen 1976). This is still an unanswered question.

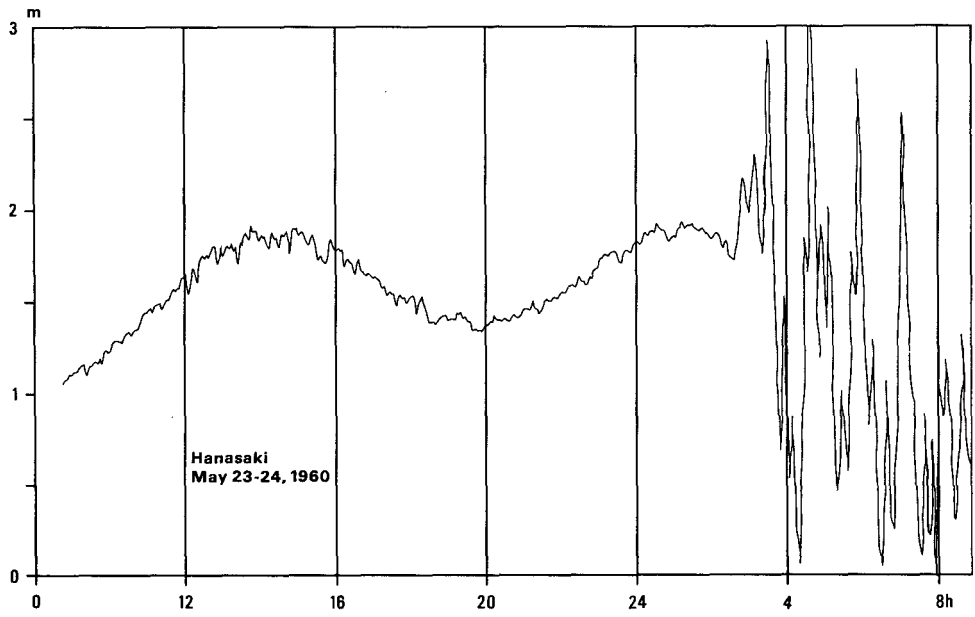


Fig. 4.8. Tsunami forerunner at Hanasaki for the Chilean earthquake tsunami May 1960. (Nakamura and Watanabe 1961)

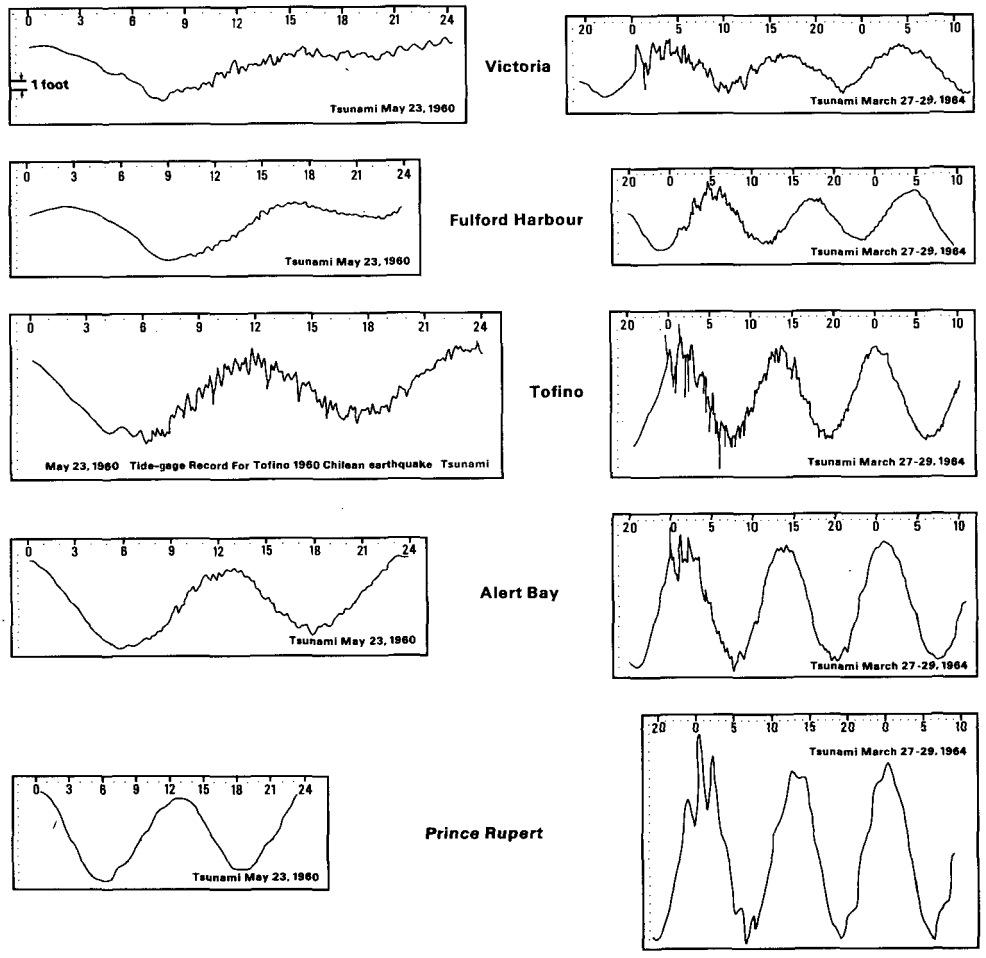


FIG. 4.9. Tidal records for the 1960 Chilean earthquake tsunami and the 1964 Alaskan earthquake tsunami showing no forerunner.

Nakamura and Watanabe (1961) studied the forerunners of the Chilean tsunami of May 1960. They remarked that no previous tsunamis on the Japanese coast showed forerunners and that the Chilean tsunami did not cause forerunners at any place other than Japan. These two statements are surprising and I am somewhat skeptical.

Figure 4.8 shows the forerunner at Hanasaki for the Chilean tsunami of May 1960. The authors attributed the forerunner to the motion of the water in the bays and along the coast before the arrival of the larger tsunami waves. If indeed this is the correct explanation, it is difficult to account for the following observations: (1) the Kamchatkan tsunami of November 1952 (Fig. B) showed a forerunner at Midway Island; (2) neither the Chilean earthquake tsunami of May 1960 nor the Alaskan earthquake tsunami of March 1964, showed any forerunners at stations on the west coast of Canada (Fig. 4.9).

Nakamura and Watanabe developed a simple theory to explain the occurrence of the forerunner and showed that, for large angles of incidence, the forerunner cannot be well developed. Also, for a forerunner to be produced, the tsunami period has to be considerably greater than the seiche period of the bay in which the tide gage is located.

Nakamura and Watanabe (1961) explained that the absence of forerunner at the Japanese coast associated with the Kamchatkan and Aleutian tsunamis was due to oblique incidence. They gave the same reason for the absence of the forerunner from the 1960 Chilean tsunami at stations other than Japanese.

Munk (1947) treated the problem of increase in the period of waves traveling over large distances and applied his general treatment to tsunamis, swell, and seismic surface waves. Although this work may not properly belong in this section, it was included because Munk's theory examined, as a by-product, the period of forerunner. The forerunners Munk dealt with were those observed at Pendeen, Eng., and Woods Hole, Mass. Nevertheless, his theory is sufficiently general to be of relevance to the tsunami forerunner problem. He applied his theory to three tsunamis, the Chilean earthquake tsunami of Nov. 10, 1922, the Kamchatkan earthquake tsunami of Apr. 13, 1923, and the Aleutian earthquake tsunami of Apr. 1, 1946. He found good agreement between the calculated and observed increase in period of the tsunami during propagation. The results showed that the period of the tsunami increases with the increase of travel distance but decreases with time at a given station.

Munk's theory showed that the period of the forerunner is proportional to I, where I is an integral defined below and inversely proportional to the square root of time

$$I = \frac{2\pi^2}{g^{\frac{3}{2}}} \int D^{\frac{1}{2}}\, dx \tag{4.70}$$

where g is gravity, $D(x)$ is the depth of the ocean, and x is the direction of tsunami travel.

Initial Withdrawal of Water

Much has been written in popular and scientific literature about the initial withdrawal of water before the arrival of a tsunami on a coast. After careful examination of hundreds of tsunami records, I concluded that, although many instances of initial withdrawal can be cited (e.g. Fig. B), there are many other instances where none occurred.

I am unable to form any particular opinion about this topic. However, a theory by Cherkesov (1966b) will be mentioned, where he showed that viscosity in the calculation of the form of the free surface produced a depression wave that arrived before the leading wave of the tsunami. Although the effect of viscosity on the main tsunami wave itself is rather small (it might reduce its amplitude by 2%), if the viscosity is ignored then there will be no depression wave before the main wave.

Spielvogel (1976) showed theoretically that in certain situations the run-up on a beach was caused by a leading negative wave followed by a positive wave.

Consider a two-dimensional flow on a sloping beach. Let V*, η^*, X*, and t^* be velocity, surface elevation, horizontal coordinate, and time (* denotes dimensional quantity).

Introduce nondimensional quantities through:

$$\begin{aligned} V^* &\equiv V_0 V \qquad & x^* &\equiv L\, x \\ \eta^* &\equiv \beta\, L \eta \qquad & t^* &\equiv T t \end{aligned} \tag{4.71}$$

where L is a typical length, g is gravity, β is the inclination of the beach, and:

$$\begin{aligned} T &\equiv \sqrt{\frac{L}{\beta g}} \\ V_0 &\equiv \sqrt{gL\beta} \end{aligned} \tag{4.72}$$

Spielvogel transforms the problem from the x, t plane to the σ, λ plane defined by:

$$V = \frac{1}{\sigma} \frac{\partial}{\partial \sigma} \phi(\sigma,\lambda) \tag{4.73}$$

$$x = \tfrac{1}{4} \frac{\partial}{\partial \lambda} \phi - \frac{V^2}{2} - \frac{\sigma^2}{16} \tag{4.74}$$

$$\eta = \tfrac{1}{4} \frac{\partial}{\partial \lambda} \phi - \frac{V^2}{2} \tag{4.75}$$

$$t = \frac{\lambda}{2} - V \tag{4.76}$$

where $\sigma \geq 0$. The significance of this transformation is that $\sigma = 0$ gives the instantaneous shoreline and $\lambda = 0$ gives the initial time.

The momentum equation valid for shallow water in the σ, λ plane becomes:

$$\left(\frac{\partial^2}{\partial \lambda^2} - \frac{\partial^2}{\partial \sigma^2} - \frac{3}{\sigma} \frac{\partial}{\partial \sigma} \right) V = 0 \tag{4.77}$$

or alternately

$$\frac{1}{\sigma} \frac{\partial}{\partial \sigma} \sigma \frac{\partial}{\partial \sigma} - \frac{\partial^2}{\partial \lambda^2} \phi = 0 \tag{4.78}$$

The following Jacobian has to be nonzero in the proper domain for transformation back to the x, t plane:

$$\frac{\partial(x,t)}{\partial(\sigma,\lambda)} = \frac{\sigma}{4} \left\{ V_\sigma^2 - (\tfrac{1}{2} - V_\lambda)^2 \right\} \tag{4.79}$$

Carrier and Greenspan (1958) gave the following solution for (4.78):

$$\phi = -\int_0^\infty \frac{1}{\tau} J_0(\tau\sigma) \sin(\tau\lambda) I(\tau) d\tau \tag{4.80}$$

with

$$I(\tau) = \int_0^\infty 4\sigma J_1(\sigma\tau) (\eta_0)_\sigma d\sigma \tag{4.81}$$

where

$$(\eta_0)_\sigma = \eta(\sigma,0) \tag{4.82}$$

gives the initial shape. The following formulae could be derived from above:

$$\eta_1(\sigma,\lambda) = -\tfrac{1}{4}\int_0^\infty J_0(\tau\sigma) \cos(\tau\lambda) I(\tau) d\tau \tag{4.83}$$

and

$$V(\sigma,\lambda) = \int_0^\infty \frac{1}{\sigma} J_1(\tau\sigma) \sin(\tau\lambda) I(\tau) d\tau \tag{4.84}$$

Spielvogel assumed run-ups of the form:

$$\tilde{\eta}(x,0) = A\, e^{16p(x-A)} \tag{4.85}$$

where A is positive and is the amplitude of run-up and is small enough to satisfy (4.79). Here p is also a positive quantity and is a measure of the width of the run-up and has to satisfy (4.79). To specify the initial condition as a function of σ, invert:

$$\sigma^2 = 16 [A e^{16p(x-A)} - x] \tag{4.86}$$

for $x(\sigma)$. However, instead of this, one can start with the following initial shape:

$$\eta_0 = \eta(\sigma,0) = A e^{-p\sigma^2}, A > 0 \tag{4.87}$$

Thus

$$x_0 = x(\sigma,0) = A e^{-p\sigma^2} - \frac{\sigma^2}{16} = \eta_0 + \frac{1}{16p} \ell n \left(\frac{\eta_0}{A}\right) \tag{4.88}$$

which gives:

$$\eta_0 = A e^{16p(x-\eta_0)} \tag{4.89}$$

as the initial condition. The fact that $p\mathrm{A}$ is small implies that η_0 obeys (4.85) except in a small area near $\sigma = 0$. Then:

$$x \sim -\frac{\sigma^2}{16} \tag{4.90}$$

$$\eta_0 \sim \mathrm{A}\, e^{16px} \tag{4.91}$$

and

$$0 < (\eta_0)_x = \frac{1}{1 + e^{p\sigma^2/(16p\mathrm{A})}} < 1 \tag{4.92}$$

if $16\,\mathrm{A}p \ll 1$, then:

$$(\eta_0)_x \approx 16\mathrm{A}p = \eta_x\big|_{\sigma=0} \tag{4.93}$$

Under this initial condition, (4.81) could be evaluated to give:

$$\mathrm{I}(\tau) = -\frac{2\mathrm{A}}{p}\, e^{-\tau^2/4p} \tag{4.94}$$

Then the solutions are:

$$\mathrm{V} = -\frac{2\mathrm{A}}{\sigma p} \int_0^\infty \tau\, e^{-\tau^2/4p} \mathrm{J}_1(\tau\sigma) \sin(\tau\lambda)\, d\tau \tag{4.95}$$

$$\eta_1 = \frac{\mathrm{A}}{2p} \int_0^\infty \tau\, e^{-\tau^2/4p}\, \mathrm{J}_0(\tau\sigma) \cos(\tau\lambda)\, d\tau \tag{4.96}$$

$$\eta = \eta_1 - \frac{\mathrm{V}^2}{2} \tag{4.97}$$

$$t = \frac{\lambda}{2} - \mathrm{V} \tag{4.98}$$

For numerical purposes it is convenient to write the solution in the following form:

$$\eta_1 = \mathrm{A} \sum_{k=0}^{\infty} \sum_{s=0}^{\infty} \frac{(-4p\lambda^2)^s\, (-p\sigma^2)^k\, (s+k)!}{2s!\; k!\; k!} \tag{4.99}$$

and

$$\mathrm{V} = -8p\mathrm{A}\lambda \sum_{k=0}^{\infty} \sum_{s=0}^{\infty} \frac{(-4p\lambda^2)^s\, (-p\sigma^2)^k\, (s+k+1)!}{(2s+1)!\; (k)!\; (k+1)!} \tag{4.100}$$

Both are convergent everywhere in principle. But in practice, their use is restricted because of round-off errors to the case of small $p\sigma^2$ and $p\lambda^2$.

Spielvogel represented the solution in another manner after defining:

$$g(\alpha^2) = \int_0^1 e^{-\alpha^2(1-y^2)}\, dy = \frac{\sqrt{\pi}\, i}{2\alpha} \operatorname{erf}(-i\alpha)$$
$$= \sum_{n=0}^{\infty} \frac{(-4\alpha^2)^n n!}{(2n+1)!} = e^{-\alpha^2} \sum_{n=0}^{\infty} \frac{\alpha^{2n}}{(2n+1)!\, n!} \tag{4.101}$$

and noting that:

$$\lim_{\alpha^2 \to \infty} \alpha^2 g(\alpha^2) = \tfrac{1}{2} \tag{4.102}$$

The solutions can be expressed in terms of $g(\alpha^2)$ as follows:

$$\eta_1 = \frac{A}{\pi} \int_0^{\pi} \left[1 - (\alpha_+^2)\, g(\alpha_+^2) - (\alpha_-^2)\, g(\alpha_-^2)\right] d\phi \tag{4.103}$$

$$V = \frac{4A}{\pi\sigma} \int_0^{\pi} \sin\phi \left[(\alpha_-^2)\, g(\alpha_-^2) - (\alpha_+^2)\, g(\alpha_+^2)\right] d\phi \tag{4.104}$$

Here:

$$(\alpha_+)^2 = p(\sigma \sin\phi + \lambda)^2 \tag{4.105}$$

$$(\alpha_-)^2 = p(\sigma \sin\phi - \lambda)^2 \tag{4.106}$$

The behavior on the shoreline could be inferred from (4.102). Then:

$$\eta_1(\lambda,0) = A[\,1 - 2\lambda^2\, pg(p\lambda^2) \tag{4.107}$$

$$V(\lambda,0) = -4A\lambda p\,[\,1 + (1-2\lambda^2 p)g(p\lambda^2)\,] \tag{4.108}$$

The last two equations show that the exponential run-up at the shoreline is caused by a leading negative wave, followed by a positive wave.

Tsunami Bore

The borelike behavior of tsunamis will be considered. It is increasingly realized that the tsunami wave resembles a bore more than a breaking wave. One of the earliest works on the bore is Nagoka (1907) who considered the bore on the shores of Odawara and Kozu in Japan. Although this work is usually included in tsunami literature, Nagoka mentioned meteorological disturbances as responsible for the bore.

Ishimoto and Hagiwara (1934) appear to be two of the few early authors who applied theoretical considerations to tsunami propagation viewed as sea water

overflowing the land. They studied the Sanriku tsunami of Mar. 3, 1933 and estimated the velocity with which the sea water overflowed the land, assuming that this overflow was simply due to the rise of water level at the shore. Let the slope of the land near the shore be θ. Also assume that the sea always maintains a horizontal level. Let dt be the time when the sea level rises through an amount, dh, and let v be the velocity of the water at distance, x, from the farthest arrival of the water from the shore. Then:

$$x\, dh = v\, dt\, x \tan\theta$$

Hence

$$v = \cot\theta \frac{dh}{dt} \tag{4.109}$$

Thus, the water velocity, v, is independent of x and is inversely proportional to θ.

Ishimoto and Hagiwara estimated that the slope of the waterfront near Kamaisi (one place affected by the Sanriku tsunami) was 1/50. Then taking appropriate values for dh and dt, it was deduced from Equation (4.109) that v was equal to one meter per second.

Next Ishimoto and Hagiwara removed the restriction that the water level be horizontal at all times. Including the bottom friction, they gave the following hydraulic formula:

$$v = \frac{87\sqrt{RI}}{1 + \frac{\gamma}{\sqrt{R}}} \tag{4.110}$$

where $R \equiv \frac{A}{S}$.

A is the sectional area of the water channel; S, the length along the bottom in the section normal to the flow which, of course, is the depth, H; I, the tilt of the water surface; and γ, a bottom friction coefficient (taken to be from 0.65 to 1.65). Ignoring $\gamma/\sqrt{R}$

$$v = 87\sqrt{HI} \tag{4.111}$$

If one puts $v = 1$ m/s and $H = 2$ m, then: $I \sim \frac{1}{15{,}000}$. Thus, for small velocities of the tsunami, the surface can be assumed as horizontal.

The Studies of Nasu

Nasu (1948) gave several formulae of practical interest to compute local characteristics of tsunamis. It should be cautioned that the basis for the expressions given by Nasu is not rigorously justifiable. He assumed that the earthquake motion is simple harmonic and the water motion is steady. He also assumed that the force acting on a coastal structure submerged by water varies as the square of the velocity of the water with which it strikes the body. Hence, knowing the strength of the structure and the damage caused, the water velocity could be estimated.

The first case considered by Nasu was a tsunami traveling through a curved river. According to him, the water level should be higher on the outer bank because

of centrifugal force and the differences of height between the outer and inner banks given by:

$$H = \frac{v^2}{g} \ln \frac{b}{a} \tag{4.112}$$

where v is the water velocity, g is gravity, and a and b are the radii of curvature of the inner and outer banks, respectively. Nasu cited a practical case — Yura Bay in Wakayama prefecture. Here $a = 50$ m, $b = 60$ m, and H was 0.19 m. Then Equation (4.112) gives $v = 2.26$ m/s. Another example was at Irami where $a = 140$ m, $b = 160$ m, H = 0.21 m, and $v = 3.16$ m/s. In the latter case, the speed was estimated independently from the overturning of a concrete wall at a distance of 50 m and the value turned out to be 3.0 m/s.

So far it has been assumed that velocity is uniform throughout a cross section. But in reality, the point of maximum velocity, somewhere in the middle of the river, is closer to the inner bank. Define:

$$\begin{aligned} h &\equiv \frac{b-a}{2} \\ \alpha &\equiv \frac{h}{a} \end{aligned} \tag{4.113}$$

From equations (4.112) and (4.113), the velocity at some point, with distance r from the imaginary center of the circles where the inner and outer banks are arcs, is given by:

$$v = -\frac{1}{2u}\frac{\partial p}{\partial \theta}\frac{h}{\alpha}\left\{\left[\frac{(1+2\alpha)^2 \ln(1+2\alpha)}{4\alpha + 4\alpha^2}\right]\left[1+\alpha+\frac{\alpha y}{h} - \frac{1}{\left(1+\alpha+\frac{\alpha y}{h}\right)}\right] - \left(1+\alpha+\frac{\alpha y}{h}\right)\ln\left(1+\alpha+\frac{\alpha y}{h}\right)\right\} \tag{4.114}$$

where:

$$y \equiv r - a - h \tag{4.115}$$

Here μ is the viscosity coefficient and $\partial p/\partial \theta$ is the pressure gradient along the river assumed to be uniform. The mean value of the velocity over a cross section is:

$$\bar{v} = -\frac{1}{4\mu}\frac{\partial p}{\partial \theta}\frac{h}{\alpha}\left\{\alpha + \alpha^2 - \frac{(1+2\alpha)^2}{4(\alpha+\alpha^2)}[\ln(1+2\alpha)]^2\right\} \tag{4.116}$$

The maximum value of v is 1.5 times $\bar{v}$.

Next, Nasu (1948) considered the rather fanciful case he called "a straight water course with a corrugated bottom." He considered the situation when the flow of water on a street is restricted by houses on either side. If the surface of the street is corrugated, there are noticeable water level changes. He assumed an inundated street as a straight canal with a rectangular cross section and a sinusoidal bottom of form:

$$y = a \sin(mx) \tag{4.117}$$

where x is along the length of the street. Let h be the mean depth of water on the street, a the amplitude ($a \ll h$), and m the wave number. The water level has the form:

$$y' = b \sin(mx) \tag{4.118}$$

for a given x:

$$\frac{y'}{y} = \frac{b}{a} = \frac{1}{\cosh(mh) - \frac{g}{mv^2} \sinh(mh)} \tag{4.119}$$

This formula could be derived from considerations of complex potential.

At this stage, Nasu assumed that the crests and troughs of the free surface and the bottom correspond to or oppose each other according to:

$$v^2 \gtrless c^2 \tag{4.120}$$

where

$$c \equiv \sqrt{\frac{g}{m} \tanh(mh)} \tag{4.121}$$

Here c is the propagation velocity of a wave $2\pi/\mathrm{m}$ long, in water depth, h. When $v = c$, $\frac{b}{a}$ is infinite and the calculation is meaningless because the assumption that the free surface could be represented by a plane surface is not valid.

Nasu cited an actual case where he applied this theory. At Kainan, $a = 0.35$ m, $b = 0.12$ m, and $v = 2.0$ m/s.

Nasu called the third case the "tsunami dissipation zone." He meant that the tsunami is dissipated when it enters a wider area from a narrow area. He calculated the reduction of the water level in the dissipation zone as follows:

Let b and b_1, respectively, be the widths in the narrow and wide parts of the channel, let v_0 and v be the velocities of an elemental volume of water, and z and z_1 be the respective water levels.

At this stage, Nasu made a rather dubious assumption – the change of pressure could be ignored. Then:

$$\tfrac{1}{2}\, dm\,(v^2 - v_0^2) = g\, dm\,(z - z_1) \tag{4.122}$$

If ρ is the density of water then:

$$dm = \frac{\rho}{g} b\, dz\, v_0\, dt = \frac{\rho}{g} b_1\, dz_1\, v\, dt \tag{4.123}$$

Hence:

$$b v_0\, dz = b_1\, v\, dz \tag{4.124}$$

Define:

$$a \equiv \frac{b_1}{v_0 b}$$

Then:

$$v \equiv \frac{1}{a} \frac{dz}{dz_1}$$

Hence, Equation (4.122) becomes:

$$\frac{dz}{dz_1} = a \sqrt{v_0^2 + 2g(z - z_0)} = a\, Z \tag{4.125}$$

Integration with respect to z gives:

$$a\,(agz_1 + v_0 - z) = \ln \left(\frac{a\,Z - 1}{av_0 - 1} \right) \tag{4.126}$$

Let D and D_1 be depths of water in the narrow and wider portions and h the decrease of height given by $D - D_1$. Then:

$$\begin{aligned} h &= \frac{b_1}{b} + \frac{b_1}{bv_0} \left[\frac{b_1 g}{bv_0} (t - h) - \sqrt{v^2 + 2gh} \right] \\ &= \ln \left\{ \frac{b_1 \sqrt{v_0^2 + 2gh} - bv_0}{v_0 (b_1 - b)} \right\} \end{aligned} \tag{4.127}$$

For a given value of $\frac{b_1}{b}$, (4.127) can be solved graphically. In the extreme case of $v \to \infty$, the decrease in height is given by:

$$h = \frac{(b_1 - b)}{b_1} \, D \tag{4.128}$$

For a fixed b_0/b the dissipation zone is more effective (in reducing the water level) for small v_0. Nasu (1948) stated he could not find a good example for this third case. He did find a decrease in height near the village Hiro in Wakayama prefecture during the 1946 tsunami. However, the velocity of the tsunami was too low to cause any damage and Nasu could not really apply his theory.

The fourth and final case considered by Nasu was referred to as "inclination of the ground and the decrease of the height of the tsunami." The pressure, P, exerted by the water on a coastal structure inundated by the water is:

$$P = \rho k S \frac{v^2}{2g} = K v^2 \tag{4.129}$$

where

$$K \equiv \rho k \frac{S}{2g} \tag{4.130}$$

Here ρ is the specific gravity of water, g is gravity, S is the cross-sectional area of the structure, and k is a constant depending on the shape of the structure. If ℓ was the length of the structure, then Nasu (1948, p. 33) gave the following values:

Dependence of k on the shape of the structure

$\ell/\sqrt{S}$	0.03	1	2	3
k	1.86	1.47	1.35	1.33

Let W be the weight of the wall (coastal structure) measured in the water and f a coefficient of friction between the base of the concrete wall and the rubble over which the wall is erected ($f \sim 0.6$ to 0.7). Nasu stated that:

$$\begin{aligned} &P \geq fW && \text{for sliding} \\ \text{and} \qquad & \\ &Ph \geq Wb && \text{for overturning} \end{aligned} \tag{4.131}$$

If ρ' is the specific gravity of the wall measured in water, then according to Nasu:

$$\begin{aligned} &v^2 \geq \frac{2f\rho' g b}{\rho_0 k} && \text{for sliding} \\ \text{and} \qquad & \\ &v^2 \geq \frac{2\rho' g b^2}{\rho_0 kh} && \text{for overturning} \end{aligned} \tag{4.132}$$

He took for a concrete wall submerged in water: $\rho_0 = 1.03$, $\rho' = 2.35 - 1.03 = 1.32$, $f = 0.65$, $k = 1.5$, and obtained:

$$\begin{aligned} &v^2 = 10.9\, b && \text{for sliding} \\ \text{and} \qquad & \\ &v^2 = 16.7\, \frac{b^2}{h} && \text{for overturning} \end{aligned} \tag{4.133}$$

Here v is in m/s and b and h are in meters. For a rubble mound he gave:

$$v^2 = \frac{h + 0.89\, b}{0.0358} \tag{4.134}$$

Nasu applied these formulae to estimate the water velocity during the Nankaido tsunami and found that water velocities estimated at Kainan and Yura agreed with the values determined by other techniques.

Freeman and LeMéhauté (1964) probably gave the best treatment of the general problem of wave breakers on a beach and surges on a dry bed. They considered several possible forms of a bore and covered topics such as long-wave deformation, wave breaking inception, spilling breakers, fully developed bores arriving at the shoreline, and waves rushing over a dry bed. They used the method of characteristics that was successfully used in many geophysical problems. For application of this

technique see Freeman (1951), Rao (1967, 1969), and Murty (1971). Other early works are Keller et al. (1960) and Ho and Meyer (1962) who considered the problem of a bore moving over a sloping beach.

One important result of the work of Freeman and LeMéhauté (1964) is their clarification of the hydrodynamic nature of the water surge on a dry bed. A tidal bore is analogous to a shock wave; when the water depth tends to zero the shock wave disappears. Thus, the surge that travels over a dry bed is not a bore but a "rarefaction wave." They also suggested the following terminology: the word "bore" might be used for the shock wave and "leading edge" is appropriate for the waterfront of the surge (part of the rarefaction wave) over a dry bed.

Neglect of the vertical acceleration in the long-wave equation leads to the so-called "Earnshaw paradox," that any finite-amplitude, shallow-water wave will either disappear or form a bore; the latter is more probable (see Rayleigh 1876). Based on this paradox, Ursell (1953) questioned the validity of the long-wave theory. Stoker (1957) and Laitone (1961) traced the paradox to the neglect of the vertical acceleration. When the vertical acceleration is included, a steady-wave profile such as a solitary wave or a cnoidal wave could result.

Water levels immediately behind and ahead of the bore determine its speed and are referred to as "preceding" and "following." The speed of the bore increases when the preceding height reduces. After a while, the speed of the bore exceeds the wave speed in the following water. However, the bore can sustain only if the speed of the following wave changes with time. This is accomplished through a decrease of the height of the bore and the generation of a rarefaction wave which adjusts the following flow.

Iwasaki and Togashi (1968, 1970) also applied the method of characteristics to study the tsunami bore. Two important results have emerged from this work. One is that the tsunami climbing a beach always has the form of a bore even if the beach slope tends to zero. Second, in the theory of Freeman and LeMéhauté (1964) there is a parameter, "A," that determines the length of the leading edge of the bore. Iwasaki and Togashi gave a hydraulic meaning to "A." They also considered the presence of a quay wall on the beach as a protective measure and treated the effects of both a perfect and a partial clapotis. Clapotis is a term referring to reflection of waves from a solid boundary.

A bore followed by a train of waves is called an undular bore (Johnson 1972). This is often observed in rivers, especially during flood tides. Benjamin and Lighthill (1954) studied the undular bore by treating it as a combination of a bore (with its discontinuity in the water level) and a cnoidal wave (a nonlinear oscillatory motion). They argued that if only a portion of the energy is dissipated at the bore front, the rest of the energy could be carried away by a cnoidal wave train.

Johnson (1972) showed that a single equation called the Kortweg-de Vries-Burgers Equation could explain the undular bore:

$$\frac{\partial \eta}{\partial T} + \frac{\partial^2 \eta}{\partial X^2} + \alpha \frac{\partial^3 \eta}{\partial X^3} = \beta \frac{\partial^2 \eta}{\partial X^2} \tag{4.135}$$

where η is the surface perturbation, T is time, X is a horizontal coordinate, and α and β, respectively, are dispersion and damping coefficients.

When $\alpha \to 0$ (4.135) reduces to the Burgers Equation (Burgers 1948) and when $\partial/\partial T \to 0$ the Taylor shock profile is obtained. In the limit $\beta \to 0$, (4.135) reduces to the equation of Kortweg and de Vries (1895).

Peregrine (1966) theoretically studied the development of an undular bore. He called a bore undular if the change in surface elevation was less than 0.28 of the undisturbed water depth. The numerical value of 0.28 was obtained from the laboratory experiments of Favre (1935). Miller (1968) studied through laboratory experiments the run-up due to undular as well as fully developed bores. Hawaleshka and Savage (1971) studied the development of undular bores theoretically as well as through laboratory experiments and emphasized the role of friction.

Secondary Undulations

Nakano (1932a) defined secondary undulations on tide-gage records as the peculiar zigzag parts of tidal curve. Omori (1906) investigated the secondary undulations on the Pacific coast of Japan. Honda et al. (1908) made a systematic study of the secondary undulations in 50 bays and coastal areas in Japan. These secondary undulations are essentially normal modes of oscillation of a bay and could be excited by several sources, such as passage of storms, squall lines, or coupling of the bay to wave motion outside the bay. Hence, tsunamis could excite secondary undulations.

Nakano (1932a) gave a tentative classification of the secondary undulations into types A, B, and C. Although this type of classification is not rigorous, it is included here because some type of classification of secondary undulations is useful.

In type A, the secondary undulations appear as coherent trains of waves with approximately the same form. In type B, the waves are not as regular and coherent as in type A, but are not completely irregular either. In type C, the secondary undulations are more or less irregular. The secondary undulations occur and persist after the passage of the main tsunami waves.

Nakano, in attempting to correlate the type of secondary undulation observed in a bay with the form of the bay, considered 16 bays in Japan (Table 4.6). In the final column the type indicated is based on the observed undulations in the bay under consideration.

Nakano plotted the data of this table with the depth, D, of the bay as ordinate and 10 S/b^2 as the abscissa where S is the area of the bay and b is the breadth (Fig. 4.10). The three types of secondary undulations appear distinct. Another result from Nakano's study is, in a U-shaped bay, the energy of the secondary undulations neither accumulates nor is dissipated as efficiently as in a V-shaped bay.

Nakano showed that the rate of accumulation of energy in a bay is proportional to: $\frac{S}{b^2}\frac{1}{D^{\frac{3}{2}}}$ where D is the (uniform) depth of the bay, S is the surface area, and b the width at the mouth. As the rate of accumulation of energy determines the secondary undulations, the above parameter is important in classifying bays for their resonant characteristics. The advantage of such a classification is that detailed

TABLE 4.6. Classification of secondary undulations in some Japan bays. (Nakano 1932a)

Bays	Mean depth (m)	Area $S(km^2)$	Breadth $b(km)$	S/b^2	Characteristic (class)
Otaru	9.1	7.19	4.84	0.367	C
Hamanaka	8.5	47.00	8.35	0.674	C
Hakodate	10.7	61.90	8.32	0.894	B
Turuga	28.5	67.62	7.22	1.297	B
Tonoura	11.6	0.54	0.83	0.784	B
Ryôisi	33.1	12.80	6.10	0.344	C
Ohunato	19.0	12.18	2.68	1.696	B
Ayukawa	12.7	1.42	1.98	0.362	C
Tôkyô	52.7	1622.10	22.08	8.327	A
Moroiso (Misaki)	3.0	0.36	0.30	4.000	A
Simoda	15.0	3.44	2.12	0.765	C
Kusimoto	5.0	11.06	3.83	0.754	C
Hososima	11.7	2.34	1.65	0.852	A
Kagosima	103.0	1220.15	24.45	2.041	B
Nagasaki	17.0	13.36	2.50	2.138	A
Hutami (Titijima)	23.9	4.04	1.57	1.639	B

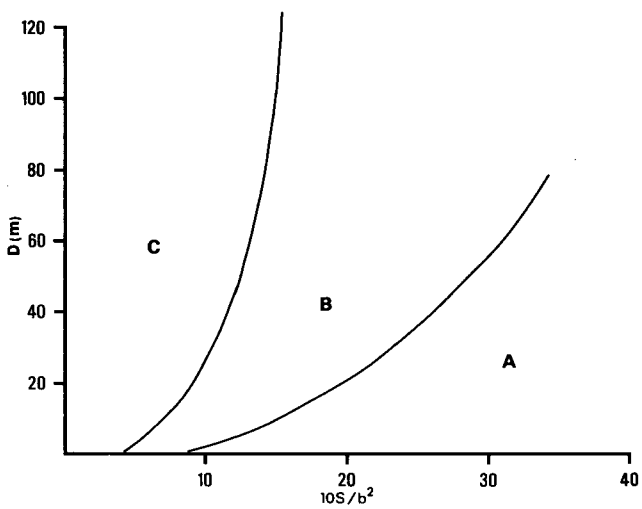


FIG. 4.10. Classification of secondary undulations. (Nakano 1932a)

numerical models can be constructed for only a few representative bays and the results for other bays can be deduced.

Nakano (1932b) also considered the secondary undulations in coupled bays. In this situation, the secondary undulations could exhibit a beat-type behavior, when the amplitude of the water level increases and decreases periodically. Figure 4.11A, B shows a coupled bay system in Japan and the mareograms recorded.

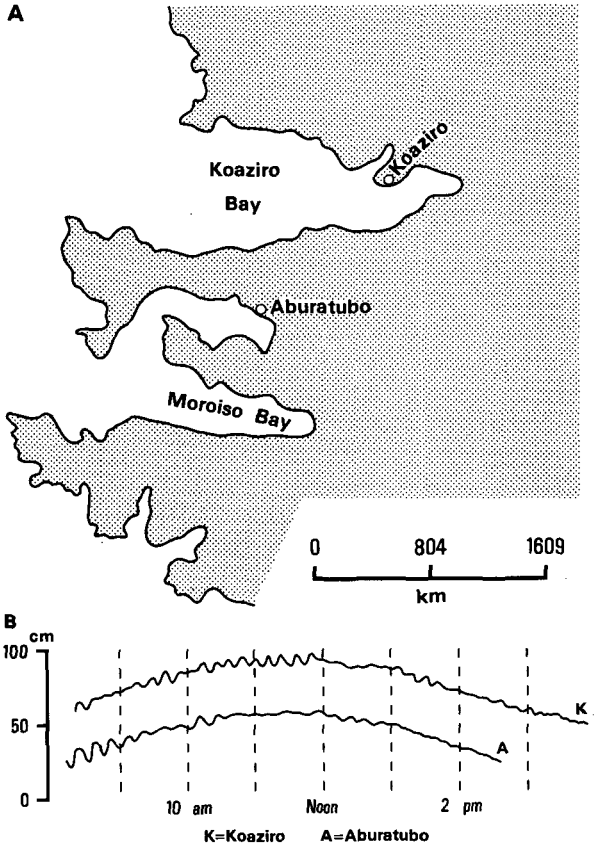


FIG. 4.11. (A) Two coupled days, shown in Fig. 4.12. on Japan coast and (B) secondary undulations in the bays. (Nakano 1932b)

Nakano (1932b) developed a theory for the oscillation of the coupled system. Consider a single rectangular bay and let the x-axis be in the direction parallel to the bay axis and let the y-axis be vertical. Let the origin be taken at the mouth of the bay at the bottom. Let L be the length, b the uniform breadth, and D the uniform depth of the bay, and ξ_i and ζ_i be the horizontal displacement of the water and the vertical motion of the free surface. Then:

$$\xi_i = \mathrm{B}\cos(\ell x)\sin(at+\alpha)$$

$$\zeta_i = \mathrm{B}h\ell\sin(\ell x)\sin(at+\alpha) \qquad (4.136)$$

The kinetic energy, K_i, and the potential energy, P_i, inside the bay are given by:

$$K_i = \frac{\rho b D}{2} \int_0^L \dot{\xi}_i^2 \, dx = \frac{\rho g D L}{4} \dot{\xi}_0^2$$
$$P_i = \frac{\rho b g}{2} \int_0^L \zeta_i^2 \, dx = \frac{\rho b g D^2 \ell^2 L}{4} \xi_0^2 \tag{4.137}$$

where ξ_0 is the value of ξ_i at $x = 0$, and the dot denotes differentiation with respect to time. The potential energy outside the bay is generally small and could be neglected but the kinetic energy outside the bay is given by:

$$K_a = \frac{\rho b D L Q}{4} \dot{\xi}_0^2 \tag{4.138}$$

where Q is a dimensionless quantity.

The kinetic and potential energies of the system consisting of regions inside as well as outside the bay are given by:

$$K = K_i + K_a = \frac{\rho b D L}{4} (1 + Q) \dot{\xi}_0^2$$
$$P = P_i + P_a = \frac{\rho b g D^2 \ell^2 L}{4} \xi_0^2 \tag{4.139}$$

Consider the situation where two bays exist side by side (Fig. 4.12). Let the depth of the ocean immediately outside the bay be uniform and equal to D. Let subscripts 1 and 2 denote the two bays and let:

$$X_{10} \equiv b D \xi_{10}$$
$$X_{20} \equiv b D \xi_{20} \tag{4.140}$$

Equations (4.139) and (4.140) then give:

$$K_1 = \frac{\rho L}{4 b D} (1 + Q) \dot{X}_{10}$$
$$K_2 = \frac{\rho L}{4 b D} (1 + Q) \dot{X}_{20}^2$$
$$P_1 = \frac{\rho g}{4} \frac{\ell^2 L}{b} X_{10}^2 \tag{4.141}$$
$$P_2 = \frac{\rho g \ell^2 L}{4 b} X_{10}^2$$

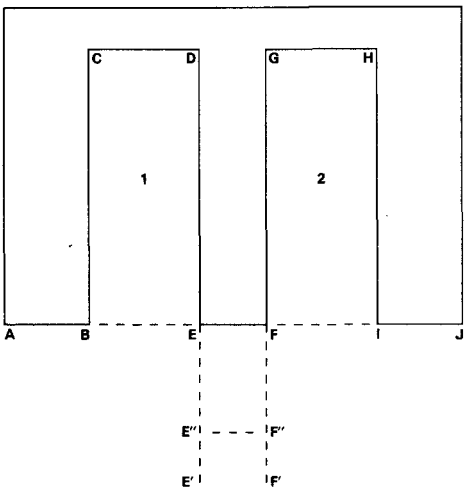


FIG. 4.12. Schematic diagram to compute secondary undulations in coupled bays. (Nakano 1932b)

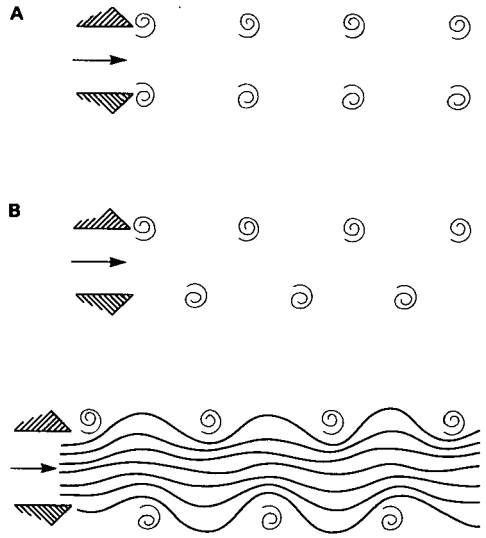


FIG. 4.13. Schematic diagram illustrating excitation of secondary undulations by currents. (Nakano 1933)

If there were no coupling between the two bays, they would oscillate independently and the nodes (for vertical motion) would be at BE and FI and the antinodes at CD and GH. (The water level will be increasing in the region EFE'F' when the water levels at CD and GH will be decreasing and vice versa.) However, the water near the shore, EF, creates a coupling between the two bays. Consider an imaginary barrier at E'' F'' at a distance of f from EF. Assume that beyond this barrier there is no coupling between the bays. Also assume there is a piston at EE'' and at FF'', both of which have no inertia, and that the vertical water motion over EFF'' E'' is uniform.

When a quantity of water, X_0, flows across BE or FI, some partakes in the coupling. Let the quantity, σX_0 (where $0 < \sigma < 1$), flow through the region EFF'' E''; this water moves the pistons at EE'' and FF''. Here σ can be treated as the coupling coefficient. Let d denote the distance between the points, E and F, and let z be the magnitude of vertical motion in EFF'' E''. Then:

$$bdz = -\sigma(X_{10} + X_{20}) \tag{4.142}$$

The potential energy associated with the vertical motion in EFF'' E'' is:

$$P_{12} = \int_0^z bd\,\rho g\, z\, dz = \frac{\rho g \sigma^2}{2bd}\,(X_{10} + X_{20})^2 \tag{4.143}$$

The kinetic energy of this portion of the water could be written as:

$$K_{12} = \frac{\mu_1}{2}\,\dot{X}_{10}^2 + \frac{\mu_2}{2}\,\dot{X}_{20}^2 + \mu\,\dot{X}_{10}\,\dot{X}_{20} \tag{4.144}$$

where μ_1, μ_2, and μ are functions of σ. If the two bays are identical, then:

$$\mu_1 = \mu_2 = \mu'$$

Hence, the kinetic, KE, and potential energies, PE, of the whole system are given by:

$$\begin{aligned} KE = K &= K_1 + K_2 + K_{12} \\ &= \frac{\rho L}{4bh}(1+Q)(\dot{X}_{10}^2 + \dot{X}_{20}^2) + \frac{\mu'}{2}(\dot{X}_{10}^2 + \dot{X}_{20}^2) + \mu \dot{X}_{10}\dot{X}_{20} \end{aligned} \tag{4.145}$$

$$\begin{aligned} PE = P &= P_1 + P_2 + P_{12} \\ &= \frac{\rho g \ell^2 L}{4b}(X_{10}^2 + X_{20}^2) + \frac{\rho g \sigma^2}{2bd}(X_{10} + X_{20})^2 \end{aligned} \tag{4.146}$$

From the Lagrangean equation:

$$\frac{d}{dt}\left(\frac{\partial K}{\partial \dot{X}_{k_0}}\right) - \frac{\partial K}{\partial X_{k_0}} = -\frac{\partial P}{\partial X_{k_0}}, \quad K = 1,2 \tag{4.147}$$

one obtains:

$$\left\{\frac{\rho L}{2bh}(1+Q) + \mu'\right\}\ddot{X}_{10} + \mu \ddot{X}_{20} + \left(\frac{\rho g \ell^2 L}{2b} + \frac{\rho g \sigma^2}{bd}\right)X_{10} + \frac{\rho g \sigma^2}{bd} X_{20} = 0 \tag{4.148}$$

$$\left\{\frac{\rho L}{2bh}(1+Q) + \mu'\right\}\ddot{X}_{20} + \mu \ddot{X}_{10} + \left(\frac{\rho g \ell^2 L}{2b} + \frac{\rho g \sigma^2}{bd}\right)X_{20} + \frac{\rho g \sigma^2}{bd} X_{10} = 0 \tag{4.149}$$

Nakano (1932b) solved these equations under certain assumptions. The details will be omitted but both bays execute oscillations with period: $\dfrac{T}{\left\{1 + \dfrac{(\delta_1 + \delta_2)}{2}\right\}}$ and their amplitudes vary as $\dfrac{2T}{|\delta_2 - \delta_1|}$

Here T, the period of each bay (assuming that the other bay does not exist), is given by:

$$T = \frac{4L}{\sqrt{gD}}(1+Q)^{\frac{1}{2}} \tag{4.150}$$

and

$$\delta_1 \equiv \frac{\nu}{N} - \frac{(\mu' + \mu)}{2M}, \qquad \delta_2 \equiv \frac{(\mu - \mu')}{2M} \tag{5.151}$$

with

$$\nu \equiv \frac{\rho g \sigma^2}{bd}$$

$$M \equiv \frac{\rho L}{2bD}(1+Q) \tag{4.152}$$

and

$$N \equiv \frac{\rho g \ell^2 L}{2b}$$

Because the phases of X_{10} and X_{20} corresponding to the period $2T/|\delta_2 - \delta_1|$ are always opposed, one bay oscillates vigorously, and the other more or less rests and vice versa (Fig. 4.11B).

Nakano (1933) considered the possibility of excitation of secondary undulations in bays by tidal or any other current. He stated that any current past the mouth of a bay could be a source of excitation of secondary undulation in the bay in analogy to a jet of air into the mouth piece of an organ pipe producing a standing oscillation of the air column in the pipe. Nakano concluded that such a generation of secondary undulations was observed at the Strait of Naruto in Japan.

Nakano (1933) used the concept of rows of vortices to give an explanation for coupling of the current to the bay. When a jet of water rushes through a narrow opening such as a strait (Fig. 4.13 shows the edges of the opening by the hatched areas) into a wider area such as a bay, either the symmetric system of vortices shown in (A) or the antisymmetric system of vortices shown in (B) are possible. It can be shown that only the antisymmetric system is stable. The lower part of Fig. 4.13 shows the streamline pattern for the stable system. The jet oscillates and let N be this frequency. Let ℓ be the distance between any two successive vortices on one side and u be the velocity of the vortices. Then:

$$N = \frac{u}{\ell} \tag{4.153}$$

If this frequency, N, agrees with the frequency of natural oscillation of the bay, then secondary undulations could be excited in the bay.

Although it is well known that the west coast of Canada is tsunami prone, it is not widely known that this is also true of the east coast. The only tsunami that caused multiple deaths in Canada occurred south of Newfoundland on Nov. 18, 1929. Thus, the problem of secondary undulations for the east coast of Canada is relevant. Honda and Dawson (1911) studied the secondary undulations in Sydney, Trepassey Harbor, Port aux Basque, Halifax, Southwest Point, and Anticosti harbors on the east coast of Canada.

Murty and Wigen (1976) applied Nakano's classification of secondary undulations to several bays on the rim of the Pacific Ocean, bays in Portugal and Newfoundland, and found that it was a useful classification. Care should be exercised in distinguishing between secondary undulations and secondary tsunamis. Royer and Reid (1971) observed so-called "secondary tsunamis" in the long-wave data record at Wake Island during the Aleutian earthquake tsunami in March 1957.

A variable period-band pass-filter of specified width was used to analyze the data. Waves that appeared in the record several hours after the main tsunami were deduced to be long surface gravity waves generated by aftershocks of the earthquake. Although the aftershocks did not produce permanent ground displacements, they did produce transient ground displacements that caused the secondary tsunamis.

4.3 Tsunami Response and Inundation of Specific Water Bodies

Isozaki and Unoki (1964) studied the tsunami response of Tokyo Bay by a two-dimensional numerical model. Figure 4.14 satisfactorily compares the observed and calculated water levels.

Street et al. (1970) described two numerical experiments to simulate tsunami behavior in shallow water. To obtain detailed information on the wave processes near the shore, nonlinear effects and finite-amplitude effects were included. The program for this, code name "Summac," is a modification of the MAC method developed at the Los Alamos laboratory (Welch et al. 1966). Another program, "Appsim," was used to make an approximate simulation. Mader (1974) also used numerical technique for simulation of tsunamis. Birchfield and Murty (1974) developed a "stretched coordinate system" to model water bodies joined by narrow straits where normal rectangular grids could not be used. Although this work was done in connection with storm surge studies, it could be adapted to tsunamis also.

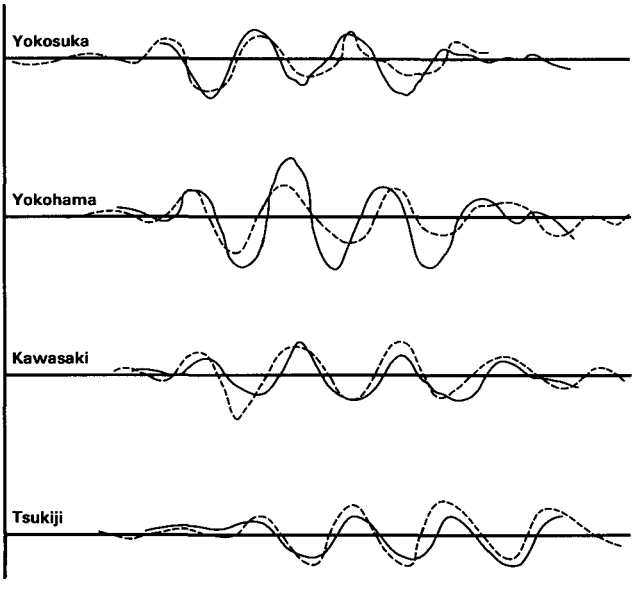


FIG. 4.14. Comparison between observed (broken lines) and computed elevations (solid lines) due to May 1960 Chilean earthquake. (Isozaki and Unoki 1964)

Nekrasov (1970) studied theoretically the transformation of a tsunami on the continental shelf, in particular the strong reflections that occur at the continental slope and the coastline. When a sequence of waves with successively decreasing amplitudes approach the coast, the record of these waves may not show the first wave as the highest. The second, or third, or even some later wave may be the highest. Thus, the record does not resemble the initial wave train and the distortion depends, among other things, on the nature of the continental shelf.

Murty and Henry (1972) studied the propagation of tsunami into a complex inlet system on the west coast of Canada (Fig. 4.15A).

The so-called river flow equations (Dronkers 1964) were used.

$$\frac{\partial Q}{\partial t} = -\frac{2Q}{A}\frac{\partial Q}{\partial x} + \frac{Q^2}{A^2}\frac{\partial A}{\partial x} - gA\frac{\partial \eta}{\partial x} - \frac{gBQ|Q|}{C^2 A}$$
$$\frac{\partial \eta}{\partial t} = -\frac{1}{B}\frac{\partial Q}{\partial x} \qquad (4.154)$$

where the x-axis is locally tangential to the axis of each branch of the system; Q is the volume transport through a vertical section of area A; B, the surface width; η, the deviation of the water level from its equilibrium position; C, Chezy coefficient; and g, gravity. The Chezy coefficient was taken as 55 $m^{\frac{1}{2}}/s$.

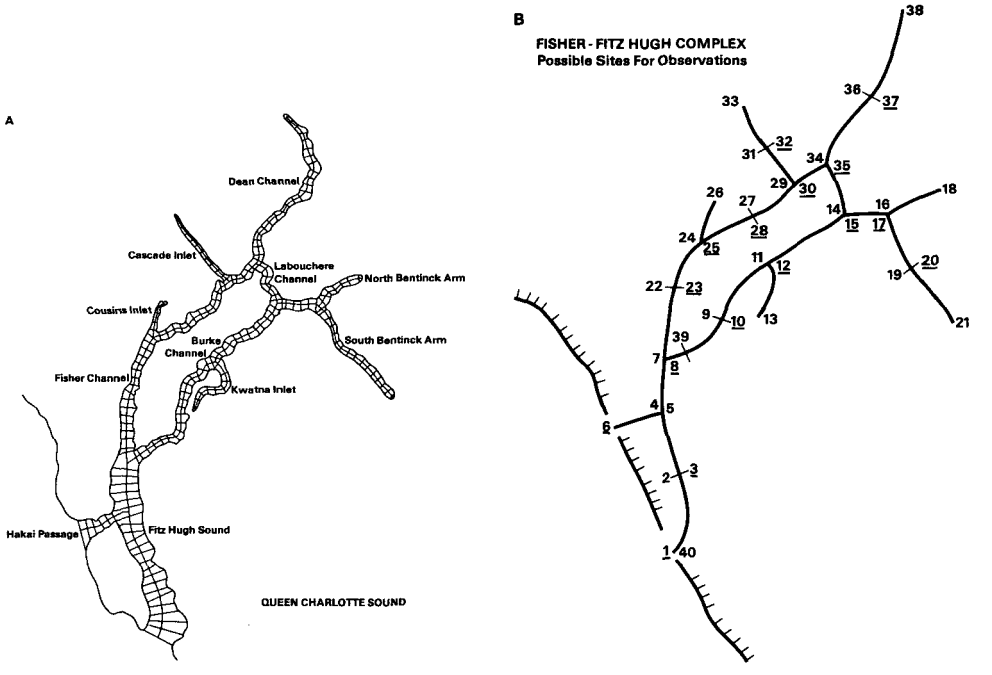


FIG. 4.15. The Fisher–Fitz Hugh inlet system on the west coast of Canada. (A) grid system, (B) schematic of Fisher–FitzHugh complex with 40 locations where output is taken from the computations. Volume transport, Q, is made available at the locations denoted by underlined numerals, other numerals denote locations at which the water level, η, is made available.

The above equations are integrated in time on a nonstaggered grid and the so-called "method of segments" developed by Henry (1971) was used. The principle of this method may be described as follows (Henry 1971):

> "A method is proposed which facilitates digital and hybrid computation of tidal motions for a coastal inlet or river system in which there are many bifurcations, confluences, islands, etc. The inlet is divided into overlapping segments and the tidal motion is computed for each segment separately over a time increment short enough to ensure that errors due to neglect of neighbouring segments are confined to the regions of overlap. The tidal motion for the whole inlet at the end of each time increment is found by discarding erroneous portions of the solutions for the various segments and piecing together the remaining parts.
>
> "This approach permits hybrid simulation of large inlet systems even when the amount of analog equipment available is limited. In purely digital computation of tidal motions, the difficulties of programming a single large difference scheme to cover a whole inlet system can be avoided by this proposed process of division into segments. The problem is reduced to linking standard subroutines representing commonly-encountered features such as bifurcations and confluences."

There were no observations against which this model could be tested. However, a recommendation is made (Fig. 4.15B) for locating tide gages (η stations) and current meters (Q stations) in case of a future tsunami.

Heitner and Housner (1970) used finite-element techniques to develop a numerical model to calculate tsunami run-up. The model uses what the authors referred to as "constrained flow," which means horizontal velocity is constant over the depth while the kinetic energy of the vertical velocity component is significant and is included. Because kinetic energy is included, solitary types of waves are permitted and this gives a better description of the wave-breaking process than the nonlinear long-wave theories which predict earlier breaking. Also, the introduction of an artificial velocity permits the formation of hydraulic shocks or bores.

Tsunami Response at Wake Island

Reid and Vastano (1966) developed an "island coordinate system" and used this system to calculate the tsunami response at Wake Island. They compared their numerical calculations satisfactorily with the laboratory experiments of Van Dorn (1970b).

The linearized form of the long-wave equation is:

$$\frac{\partial^2 \zeta}{\partial t^2} = g\nabla \cdot (D \nabla \zeta) \tag{4.155}$$

where ζ is the water surface deviation from its equilibrium position, t is time, g is gravity, ∇ is the horizontal gradient operator, and D is the variable water depth. At the shore of the island, the following boundary condition has to be satisfied:

$$(\hat{n} \cdot \nabla \zeta) D = 0 \tag{4.156}$$

where $\hat{n}$ is a unit horizontal vector perpendicular to the boundary.

Two possibilities exist for depth at the shore. If the depth $D = 0$ then Equation (4.156) requires that the normal derivative of ζ be finite at the boundary. On

the other hand, if $D \neq 0$, then (4.156) implies that the normal derivative of ζ be zero at the boundary. In either case, this condition (4.156) means the net flux of energy at the shoreline is zero and there is total reflection. Also solutions exist for ζ with a logarithmic singularity at the shore.

In the far field, i.e. for large r, it is required that the scattered part of the wave energy propagate outward. Then $r^{\frac{1}{2}}(\zeta - \zeta_i)$ is constant along the characteristic path:

$$\frac{dr}{dt} = (g\, D_\infty)^{\frac{1}{2}}, \quad \frac{d\theta}{dt} = 0 \tag{4.157}$$

where (r, θ) are the polar coordinates with reference to an origin located on the island, g is gravity, ζ_i is the incident wave field, and D_∞ is the far-field depth assumed to be uniform.

For ζ_i, a simple harmonic progressive wave of unit amplitude can be used. This is a solution of equation with $D = D_\infty$:

$$\zeta_i = \sin \Phi(r,t)$$

where (4.158)

$$\Phi = \omega \left[t + (r - R)(gD_\infty)^{-\frac{1}{2}} \cos(\theta - \theta_0) \right]$$

Here ω is the frequency, R is a constant reference radius, and θ_0 is the azimuth from which the incident waves arrive.

At this stage the so-called "island coordinate system" developed by Reid and Vastano (1966) (an orthogonal coordinate system) was employed and the equations were rewritten from polar coordinates into island coordinates. This system might be considered as a perturbed polar coordinate system (ρ, β) where the isolines of ρ are closed curves. The curve $\rho = 1$ represents the shape of the island. Further away from the island, the isolines become more and more circular. Equation (4.155) becomes in this coordinate system:

$$\frac{\partial^2 \zeta}{\partial t^2} = gS^2 \left[\rho \frac{\partial}{\partial \rho} \left(\rho D \frac{\partial \zeta}{\partial \rho} \right) + \frac{\partial}{\partial \beta} \left(D \frac{\partial \zeta}{\partial \beta} \right) \right] \tag{4.159}$$

Here S is a scale factor defined by:

$$S \equiv |\nabla \ell n \rho| = |\nabla \beta| \tag{4.160}$$

A variable grid spacing was used for the numerical integration. To calculate grid spacing for ρ, travel time, μ, was used for the propagation of long waves over the average depth profile starting at the island. If a grid of uniform $\Delta\mu$ is used, then the resolution increases in shallow water. The value of μ (referred to as the travel-time coordinate) could be determined from ρ by:

$$\mu = \int_1^\rho \frac{h(\rho)}{\rho}\, d\rho \tag{4.161}$$

where

$$h(\rho) \equiv \left[\bar{S}(g\bar{D})^{\frac{1}{2}}\right]^{-1} \tag{4.162}$$

The bar denotes an average over the full range of β for a given ρ.

In the (μ,β) coordinates the wave equation becomes:

$$\frac{\partial^2\zeta}{\partial t^2} = gS^2\left[h\,\frac{\partial}{\partial\mu}\left(hD\,\frac{\partial\zeta}{\partial\mu}\right) + \frac{\partial}{\partial\beta}\left(D\,\frac{\partial\zeta}{\partial\beta}\right)\right] \tag{4.163}$$

The boundary condition at the shoreline becomes:

$$\frac{\partial\zeta}{\partial\mu} = 0 \text{ at } \mu = 0 \tag{4.164}$$

The far-field condition becomes:

$$r^{\frac{1}{2}}\,(\zeta - \zeta_i) \text{ is constant} \tag{4.165}$$

along the path $\frac{d\mu}{dt} = 1$, $\frac{d\beta}{dt} = 0$.

Boundary conditions (4.164) and (4.165) were used to numerically integrate Equation (4.163). The results from the numerical model compared favorably with those from the laboratory experiments of Van Dorn (1970b).

Response of San Pedro Bay to Tsunamis

San Pedro Bay is located on the coast of California at approximately 33°45'N. Wilson (1971) modeled the continental shelf off San Pedro Bay by sectors of a cone, with uniformly sloping gradients starting at zero depth of water at the apex of the cone and maximum depth at the shelf. Two detailed models were developed. Model A (Fig. 4.16) treated the breakwater as a straight, rigid boundary with the sector angle, B, as 135° with the coast. In model B (Fig. 4.16) the irregular boundary was grossly approximated and B was taken to be 105°.

Solutions were obtained in terms of Bessel functions and the periods of free oscillation of the shelf off San Pedro Bay were determined. Wilson verified his calculations against the tidal records for the Chilean earthquake tsunami of Nov. 11, 1922; Aleutian earthquake tsunami of Apr. 1, 1946; Chilean earthquake tsunami of May 23, 1960; and Alaskan earthquake tsunami of Mar. 28, 1964. Figure 4.16 shows the tide-gage record and power spectrum in Los Angeles harbor for the Chilean earthquake tsunami of Nov. 11, 1922.

Tsunami Inundation of the Hawaiian Islands

Cox (1968) and Adams (1968) prepared potential tsunami inundation charts for the Hawaiian Islands, and Adams (1969) described how these were prepared. Some details of this important report are included because they deal with the tsunami inundation problems in a pragmatic way.

The principle underlying preparation of the charts is: even if there is only

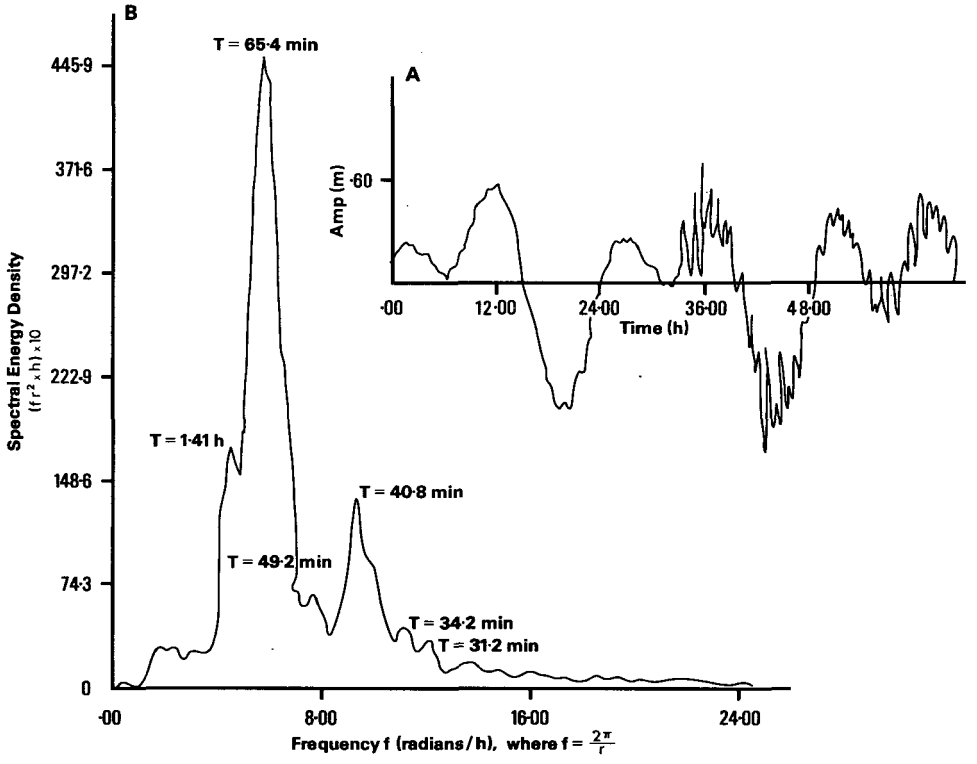


FIG. 4.16. Tide-gage record (A) and power spectrum (B) for Chilean tsunami Nov. 11, 1972, east channel, Los Angeles harbor. (Wilson 1971)

a slight possibility of tsunami inundation then people in the area should be evacuated. This means the value zero is ascribed to the disutility of a false tsunami warning and the value ∞ to even saving one life. Adams (1969) stated that it would be better to reduce the threshold above which a tsunami warning should be issued and at the same time to reduce the sizes of the evacuation areas.

The coefficients for a tsunami prediction algorithm were determined by Adams (1969, p. 18):

> "... we start with the historical observations of run-up and proceed to the source, using theory to estimate the appropriate functional relationships. In outline, we fit the historical observations for each tsunami to a cosine function centered on the azimuth of the earthquake and measured counter-clockwise about a center on the island. The ratio of the observed run-up to the 'best-fit' cosine function at the azimuth is taken as a local amplification factor. The cosine function at the azimuth of the station is called the shore amplitude. The set of observations for a given island for a given tsunami reduce to one number — the equivalent bow value. The equivalent bow value is then extrapolated to offshore deep water using the theoretical predictions relating amplification to island slope and the ratio of the island sea-level radius to the island base-radius. The offshore value of the tsunami for that island is propagated backwards to a canonical distance, 100.6 km, using both spreading and dispersion. The canonical values for the various islands and the same tsunami are then averaged

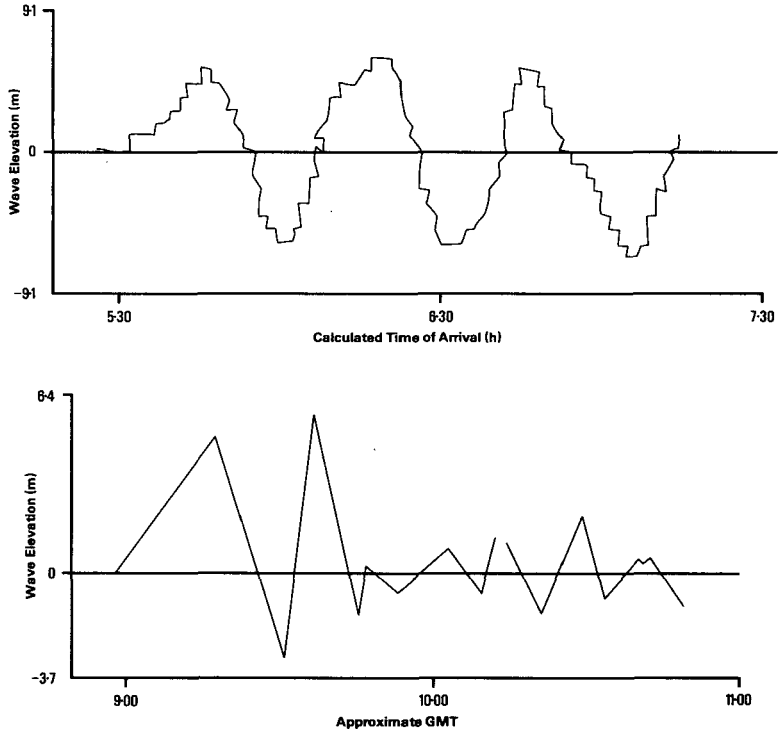


FIG. 4.17. Comparison of first 2 h of Hilo tide record with numerical prediction for Alaskan earthquake tsunami of March 1964. Calculated tsunami elevation (*top*), and observed elevation (*bottom*). (Hwang and Divoky 1975)

to give a mean, and if possible, a standard deviation. This mean is taken as a canonical tsunami index. By using the term index, we are admitting that the value may not be equal to the maximum wave amplitude, however, the value is still considered to be related to the tsunami run-up."

Thus, the scheme developed by Adams can estimate the tsunami run-up at any given location on the Hawaiian Islands coasts, provided magnitude of the earthquake, depth of focus, location of the epicenter, and depth of water at the epicenter are known.

Hwang and Divoky (1975) developed numerical models to compute the tsunami response at Hilo harbor for the 1960 Chilean and the 1964 Alaskan earthquake tsunamis. Figure 4.17 compares the numerically computed water level at Hilo with the observed level for the Alaskan tsunami.

For some simple but elegant models to determine tsunami response around islands, see Webster (1963), Arthur (1946), Vastano and Reid (1967), Summerfield (1972), and Vastano and Bernard (1973).

TSUNAMI RUN-UP PREDICTION FOR SOUTHERN CALIFORNIA

Garcia and Houston (1976) developed techniques to predict maximum run-up due to tsunamis of distant origin in southern California coastal communities, for

intervals of 100–500 yr, and flood hazard zones because of tsunami inundation could be determined. They used for the analysis data from the two largest tsunamis recorded in southern California, the 1960 Chilean and the 1964 Alaskan earthquake tsunamis.

To simulate tsunami generation, the general features of the permanent vertical displacement of the ocean floor were used as input into the numerical model. The Alaskan and Chilean earthquakes caused permanent ground displacements (parallel to the fault) in a distance of 804.5–965.4 km and about 161 km in a direction perpendicular to the fault. Thus, the ratio of length to width of the uplift area was about 6:1. The planform of the uplift area (with maximum displacements up to 9.1 m) could be considered an ellipse.

For simulation purposes, Garcia and Houston chose a hypothetical uplift area of elliptic plan view with a parabolic crest (concave downwards) parallel to the major axis. The tsunami wave generation and propagation to the edge of the continental shelf off southern California was done through a finite-difference model. The finite-difference grid was too coarse for propagation over the continental shelf, so an analytical method was used. In this method, the solution is in the form of a standing wave, following the work of Lamb (1945) on tides in canals.

Under variable depth, the two horizontal momentum equations together give:

$$\frac{\partial^2 \eta(x)}{\partial t^2} = g \frac{\partial}{\partial x} \left\{ d \frac{\partial \eta(x)}{\partial x} \right\} \tag{4.166}$$

For simple harmonic motion, such that $\eta \sim \cos(\omega t + \epsilon)$ the above equation becomes:

$$g \frac{\partial}{\partial x} \left[d \frac{\partial \eta(x)}{\partial x} \right] + \omega^2 \eta(x) = 0 \tag{4.167}$$

If it is assumed that the depth, d, increases linearly from the shoreline, $x = 0$, to the edge of the continental shelf, $x = a$, then:

$$d = d_0 \frac{x}{a}$$

$$k = \frac{\omega^2 a}{g d_0} \tag{4.168}$$

From (4.167) and (4.168):

$$\frac{\partial}{\partial x} \left[x \frac{\partial \eta(x)}{\partial x} \right] + k\eta(x) = 0 \tag{4.169}$$

The solution of this is:

$$\eta(x) = \mathrm{A} \mathrm{J}_0(2k^{\frac{1}{2}} x^{\frac{1}{2}}) \tag{4.170}$$

This solution is finite at $x = 0$. The solution for the water level is:

$$\eta(x,t) = AJ_0(2k^{\frac{1}{2}} x^{\frac{1}{2}}) \cos(\omega t + \epsilon) \tag{4.171}$$

For $x \geq a$, the oscillation is represented by:

$$\eta(x) = C \cos(\omega t + \epsilon) \tag{4.172}$$

From (4.171) and (4.172):

$$A = \frac{C}{J_0(2k^{\frac{1}{2}} a^{\frac{1}{2}})} \tag{4.173}$$

Hence:

$$\eta(x) = C \frac{J_0(2k^{\frac{1}{2}} x^{\frac{1}{2}})}{J_0(2k^{\frac{1}{2}} a^{\frac{1}{2}})} \cos(\omega t + \epsilon) \tag{4.174}$$

At $x = a$ (edge of the shelf) $\eta(a) = C \cos(\omega t + \epsilon)$. Hence: $C = \frac{\eta(a)}{\cos(\omega t + \epsilon)}$

Thus:

$$\begin{aligned} \eta(0) &= \frac{C}{J_0(2k^{\frac{1}{2}} a^{\frac{1}{2}})} \cos(\omega t + \epsilon) \\ &= \frac{\eta(a)}{J_0(2k^{\frac{1}{2}} a^{\frac{1}{2}})} \end{aligned} \tag{4.175}$$

This relation was used to determine the amplitude of the waves at the shoreline.

Table 4.7 compares the observed (1964 tsunami) and computed amplitudes of waves at five locations in California.

Garcia and Houston (1976) defined run-up as equal to the wave amplitude at the shoreline, for tsunamis with long periods. To determine the run-up in a

TABLE 4.7. Comparison of observed and computed amplitudes of tsunamis on the California coast. (Garcia and Houston 1976)

Location	Observed amplitude (*m*)	Computed amplitude (*m*)
Alamitos Bay	0.55	0.67
Santa Monica	0.79	0.70
Rincon Point	0.79	0.85
Avila Beach	1.34	1.13
Crescent City	2.44 (estimated)	2.23

bay where resonance is significant, either the amplitude of the first wave or the wave modified by resonance was used, depending on which was longer.

Garcia and Houston did a tsunami frequency analysis based on tsunami statistics. Let $n(i)$ be the probability of a tsunami with an intensity of i (see Chapter 2 for definition of tsunami intensity) generated during any given year. The statistics along the trench off the Chilian coast gives from least-square analysis

$$n(i) = (0.080 \pm 0.008)\, e^{-(0.63 \pm 0.10)\, i} \tag{4.176}$$

This equation predicts seven tsunamis with intensity greater than or equal to 3.5 during a 440-yr interval. During 1534–1973 (i.e. 440 yr), there were six tsunamis definitely with intensities exceeding 3.5 and one with intensity probably exceeding 3.5. For the Alaska Trench area, the following relation was obtained:

$$n(i) = 0.078\, e^{-0.71\, i} \tag{4.177}$$

In deriving these relations, it was assumed that the probability of tsunami occurrence was uniform along the Trench.

To relate the probability distribution of tsunami intensities to source characteristics, Garcia and Houston assumed that the ratio of the source uplift heights producing two tsunamis of different intensities was equal to the ratio of the average run-up heights produced on the coasts nearest these tsunami sources. This ratio is $2^{|i_1 - i_2|}$ for two tsunamis with intensities i_1 and i_2.

Let a and b be the lengths of the major and minor axes of the tsunami source area and let H_a and H_b be the wave heights in the directions of the major and minor axes, respectively. Hatori (1963) showed that $H_b/H_a = a/b$. Because a is 5 to 6 times b, H_b could be considerably larger than H_a. Thus, the run-up at a distant location due to one tsunami source cannot be taken as representative of all possible locations of the whole region of the trench. Based on this result, Garcia and Houston (1976) divided the Aleutian and Peru-Chile trenches into 12 segments and determined the run-up in southern California for a tsunami source located at the center of each segment.

Tsunamis with intensities in the range of 2 to 5 in steps of $\frac{1}{2}$ were considered. Tsunamis with intensities less than 2 will not produce significant run-up in southern California. The largest tsunami ever reported had intensity less than 5 so the upper limit of 5 is justified. For each of the 12 segments of the Aleutian Trench, a wave amplitude with an associated probability for each $\frac{1}{2}$ intensity step from intensity 2 to 5 was calculated for deepwater location near southern California. A cumulative probability distribution, $P_{AD}(z)$, was calculated from the wave amplitudes and their associated probabilities. $P_{AD}(z)$ gives the probability for a wave amplitude greater than or equal to a given value, and this includes such influences as propagation across the ocean, intensity of the source, and its orientation.

Garcia and Houston (1976) assumed that after the wave fronts of tsunamis generated by sources located in the 12 segments of the Trench passed over the abrupt change of depth at the Patton Escarpment, they had the same direction of approach relative to the continental shelf as they propagated over the continental

borderland off southern California. Let F_T be the transfer function for propagation over the continental borderland. Then:

$$F_T P_{AD}(z) = P_{AC}(z) \tag{4.178}$$

where $P_{AC}(z)$ is the cumulative probability distribution of tsunami amplitude equal to or greater than a given value, z, at a location on the continental shelf off southern California. At each site,

$$T_C P_{AC}(z) = P_{S1}(z) \tag{4.179}$$

where T_C is a transfer function for the propagation over the continental shelf and $P_{S1}(z)$ is the cumulative probability distribution for run-up greater than or equal to z at a site on the coast of southern California, due to tsunamis originating in the Aleutian Trench.

Let $P_{S2}(z)$ be the cumulative probability distribution for run-up greater than z at a site on the coast of southern California, due to tsunamis originating in the Peru–Chile Trench. This was calculated in a manner similar to that of $P_{S1}(z)$. Let $P_S(z)$ be the cumulative probability distribution for run-up at a site on the coast of southern California due to tsunamis generated in the Aleutian Trench and the Peru–Chile Trench. Then, because the tsunamis generated by earthquakes in the Aleutian and Peru–Chile trenches are statistically independent,

$$P_S(z) = P_{S1}(z) + P_{S2}(z) \tag{4.180}$$

Next, Garcia and Houston used a statistical approach to incorporate the effect of astronomical tides on tsunami run-up. They assumed that the variation of water level caused by tides was insignificant in the interval between the arrivals of the initial wave and the wave with maximum amplitude. Let z be the run-up at any time with reference to the local mean sea level. Let $P_S(z)$, $P_\beta(z)$, and $P(z)$, respectively, be the cumulative probability distribution for run-up at a given site equal to or greater than z, due to the maximum wave of the tsunami, tides, and the combined action of maximum tsunami wave and tides. Then:

$$P(z) = \int_{-\infty}^{\infty} f_\beta(\lambda)\, P_S(z-\lambda)\, d\lambda \tag{4.181}$$

where:

$$f_\beta(z) = -\frac{dP_\beta(z)}{dz} \tag{4.182}$$

If the highly unlikely case of two or more tsunamis arriving simultaneously at any site is excluded, the cumulative probability distribution, $P_S(z)$, can be written for the run-up at a given site to be equal to or greater than z due to tsunamis for N independent source regions.

$$P_S(z) = \sum_{n=1}^{N} P_{Sn}(z) \tag{4.183}$$

where $P_{Sn}(z)$ is the probability distribution corresponding to source region, n. Let:

$$P_{Sn}(z) = A_n e^{-\alpha_n z} \tag{4.184}$$

Then:

$$P_S(z) = \sum_{n=1}^{N} A_n e^{-\alpha_n z} \quad \text{for N sites} \tag{4.185}$$

If $P_\beta(z)$ follows a Gaussian distribution, then:

$$f_\beta(z) = \frac{1}{\sqrt{2\pi}\ \sigma} e^{-z^2/(2\sigma^2)} \tag{4.186}$$

Here the variance σ^2 is given by:

$$\sigma^2 = \sum_{m=1}^{\infty} C_m^2 \tag{4.187}$$

C_m being the m th tidal constituent.

From (4.185), (4.186), and (4.177):

$$P(z) = \sum_{n=1}^{N} A_n e^{-\left[\alpha_n z + \frac{\alpha_n \sigma^2}{2}\right]} \tag{4.188}$$

For the Aleutian and Peru–Chile trenches (4.185) can be written as:

$$P_S(z) = \sum_{n=1}^{2} A_n e^{-\alpha_n z} = A e^{-\alpha z} \tag{4.189}$$

Thus:

$$P(z) = Ae^{-\alpha(z - \frac{\alpha\sigma^2}{2})} \tag{4.190}$$

Define:

$$z' \equiv z - \frac{\alpha\sigma^2}{2} \tag{4.191}$$

Then:

$$P(z) = Ae^{-\alpha z'} \tag{4.192}$$

Hence, the tide produces a $P(z)$ similar to $P_S(z)$ except for a shift of z by $\alpha\sigma^2/2$. Knowing the tidal harmonic coefficients the variance of σ^2 can be determined. The exponential coefficient, α, in (4.189) can be obtained by a least-square exponential fit of $P_S(z)$.

Before concluding this section on the California coast's tsunami response, two interesting deductions will be discussed. First, the Aleutian earthquake tsunamis of Apr. 1, 1946, had a smaller amplitude on the coast of northern California than on the coast of South America, even though northern California was much closer to the epicenter. Sretenskiy and Stavroskiy (1961) stated that this was because of the directivity of the tsunami discussed earlier (i.e. the tsunami height is greater in a direction normal to the fault). Disastrous tsunamis have occurred mainly at Crescent City (on the California coast) because of the focusing effect and resonance.

The following explanation was given by Slatkin (1971, p. 90) to account for the large tsunami at Crescent City following the Alaskan earthquake of March 1964.

> "The important result is that a leading edge wave travels with the deep water wave speed and might not be distinguishable from the non-trapped waves by arrival time. This is a possible explanation for the unusually large response of the harbor in Crescent City, California, to the tsunami generated by the 1964 Alaska earthquake.
>
> "It is found that long waves can be trapped along the coast and travel with the deep water wave speed, $\sqrt{gD}$. The energy in these waves decays with $x^{-\frac{1}{2}}$ instead of x^{-1} so that more energy would be observed on this coast than expected on the basis of deep water wave amplitudes."

Tsunami Zonation for Kamchatka Coast and Kuril Islands

Soloviev et al. (1976) developed tsunami zonation for the Kamchatka coast and Kuril Islands. Figure 4.18A shows the generalized tsunami source used in the calculations. Figure 4.18B, C, respectively, show zonation based on tsunami amplitude and tsunami period. Figure 4.18D shows amplitude zonation for the northern part of Kamchatka Bay. Tsunami zonation is a concept useful for prediction of the amplitudes and periods of tsunamis.

4.4 Laboratory Experiments

Experiments on Resonance Amplification in Regular Geometries

Certain laboratory experiments dealing with resonance and amplification in regular geometries, which might be regarded as highly idealized (if not unrealistic) versions of real water bodies, will be considered first.

Nakano and Abe (1958) proposed that a tidal or any other oceanic current traveling past a bay laterally might create standing oscillation in the bay. In the literature such oscillations have been referred to as secondary undulations of tides. Nakano and Abe gave the example of a 2.5-min period oscillation in the Strait of Naruto (in the Seto Inland Sea) with a maximum amplitude of 18 cm. The observations showed that as the current increased, the amplitude of the oscillation also increased. They attributed this oscillation to the fundamental mode of Shioya-sumi Bay (a small bay).

Nakano and Abe (1958, p. 396) explained the mechanism of excitation of a standing oscillation by a current as:

> "... when the velocity of current exceeds a certain limit, periodic and unsymmetric Kármán vortices are formed on both sides of the jet of current and hence the jet

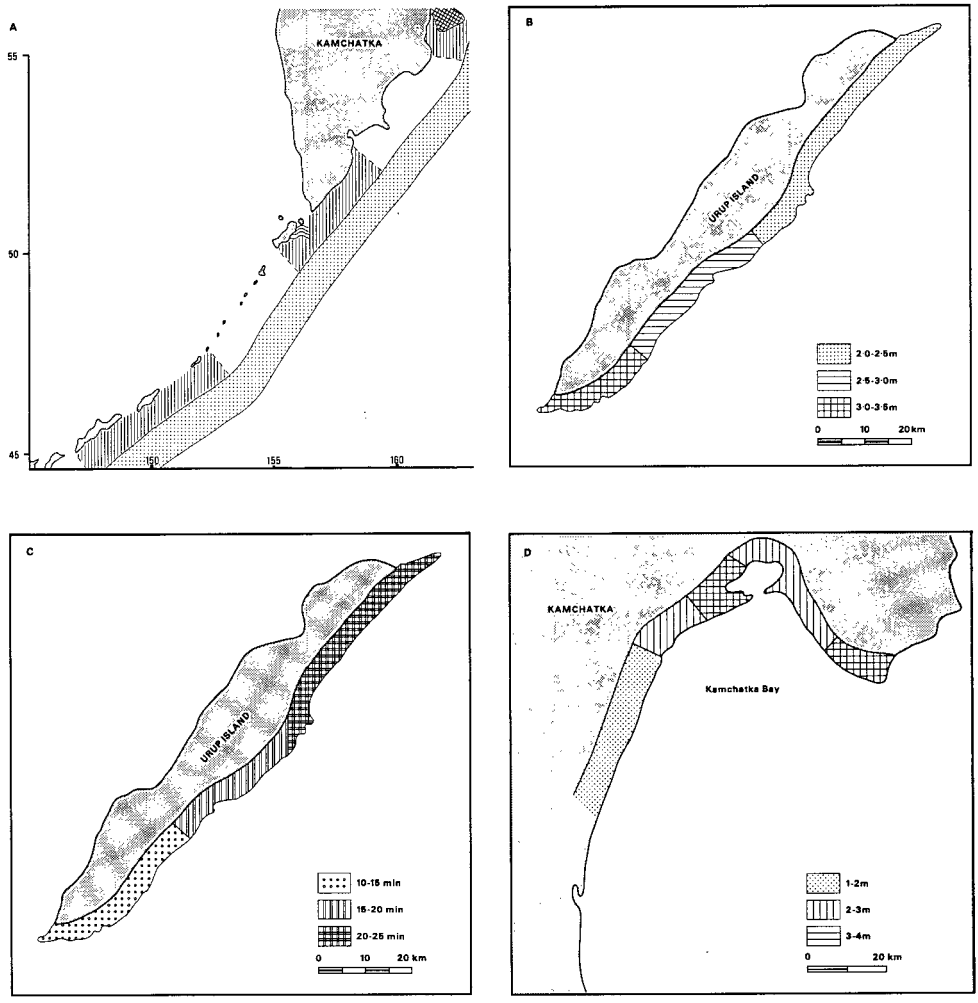


FIG. 4.18. (A) Generalized tsunami source (dotted area) adopted for calculations. Single-hatched area was studied through 1-D model and double-hatched area through 2-D model, (B) tsunami amplitude zonation of the Urup coast, (C) tsunami period zonation of the Urup coast based on tsunami period, (D) amplitude zonation of the northern part of Kamchatka Bay. (Soloviev et al. 1976)

tends to swing horizontally, causing a standing oscillation of bay water, and that when the period of swing of the jet coincides with the natural period of oscillation of bay water, vigorous oscillation of water are induced in the bay as the results of resonance."

Nakano and Abe performed experiments to verify their hypothesis. They showed that the following relation exists:

$$\frac{\ell}{u} = T \tag{4.193}$$

where ℓ is the mean distance between any two adjacent Kármán vortices on one

side of the current, u is the propagation velocity of the vortex system, and T is the period of standing oscillation in the bay.

I feel that, although the idea of Nakano and Abe is interesting, the experiments are inconclusive and further experiments are desirable.

Hwang and Lin (1970) investigated the influence of local geometry on wave run-up by performing three sets of experiments. The first was to study oscillation in a rectangular harbor under periodic wave excitation and the second under nonperiodic wave excitation. The third pertained to a three-dimensional bay.

The first two sets of experiments were performed in a rectangular harbor model and the third was in an idealized three-dimensional bay. The side walls of the harbor were vertical and fixed and the back wall could be adjusted to change the slope. At the harbor entrance, an adjustable vertical wing wall permitted the size of the opening to be changed. The run-up on the back wall was measured by resistance gauges. The three-dimensional bay was S-shaped with a beach slope of 1/5 and was perpendicular everywhere to the local shoreline. According to Hwang and Lin (1970, p. 412):

> "This arrangement, with a convex shoreline at the entrance and a concave region at the rear of the harbor, was adjacent to the tank wall and therefore, represents, by symmetry, half of a bay with general features similar to many natural bays. With such an arrangement, refractive effects were introduced with convergence of orthogonals at the entrance and divergence at the rear; in this way, general three-dimensional effects could be observed."

Height of the incident wave was interpreted as the average of the wave height, H_N, at a node and the wave height, H_A, at an antinode and it was arranged that these points were located in the region of uniform depth to minimize effects caused by shoaling.

For nonperiodic wave excitation, Hwang and Lin computed the maximum run-up from the following formula of Keller and Keller (1964, 1965):

$$\frac{R}{H} = \sqrt{\frac{\pi}{2\alpha}} \left[\tanh\left(\frac{2\pi d}{L}\right) \left\{ 1 + \frac{\left(\frac{4\pi d}{L}\right)}{\sinh\left(\frac{4\pi d}{L}\right)} \right\} \right]^{\frac{1}{2}} \tag{4.194}$$

where R is the run-up, α is the beach angle, H is the wave height at the reference depth, d is the reference water depth, and L is the wavelength at reference depth.

They compared their experimental values with those calculated from this formula and found that in most cases experimental values were substantially greater than computed values.

For the three-dimensional bay experiments, three different water depths were used and the periods and heights of the incident waves were varied over a wide range. These experiments showed that the run-up could vary by a factor of 20 from one location to the other. The authors attributed such large variations to refraction and resonance in the bay. The experiments also showed that at the same location, depending on the wave period, the run-up could vary by a factor of 7. Other important results were (Hwang and Lin 1970, p. 424):

"...the run-up appears to be larger inside the bay when the incident wave is long, and the run-up is larger at the entrance when the wave is short. In general, the run-up distribution tends to be more uniform for longer incident waves, while for short waves, the run-up distribution tends to be very nonuniform."

Williams and Kartha (1969) studied experimentally the amplification of long waves by circular islands. They performed the experiments in a ripple tank 5.2 m long, 1.4 m wide, and 0.15 m maximum depth. A hinged bulk head pivoted 0.45 m above the tank bottom served as the wave generator. To absorb the waves a beach with a slope of 1/6 was placed at the opposite end of the tank.

Two types of experiments were performed; (1) with straight circular cylinders and (2) model islands with shapes agreeing with Equation (4.194) and half islands.

$$h = h_0 \left(\frac{r}{r_b} \right)^{2\delta} \tag{4.195}$$

where h is the depth of water for $r_a \leq r \leq r_b$ and h_0 is the water depth for $r \geq r_b$. Here r is the radial coordinate, r_a is the radius of the cylindrical island cap, r_b is the radius of the seamount at its base, and the exponent, δ, can take any value from 0 to 1. This formula shows that at the island's coast $r = r_a$, water depth is $h_0 \ (r_a/r_b)^2$.

Although several theoretical studies were made on amplification of long waves around circular islands (e.g. Havelock 1940; Homma 1950; Yih 1953; Wong et al. 1963; Webster and Perry 1966) experimental studies have not kept up with them. Weiner (1947) and Laird (1955) performed experiments with circular cylinders and Wong et al. (1963) considered submarine topographies. Hence, the experiments of Williams and Kartha (1969) can be considered as the first comprehensive type of experiments on this problem.

Williams and Kartha (1969, p. 299) explained the types of island used in their experiments.

"... Five different seamount bases were used: one concave, two conical, and two convex. Three cylindrical caps were used with the parabolic convex seamount base, and five others were used with each of the other four seamount bases. The 'islands' were positioned in the ripple tank with the water depth adjusted to equal the height of the seamount base. The circular cylinders were tested in water depths which varied from one to six inches. Water surface fluctuations at several azimuth angles around the 'coastline' of the cylindrical cap and around the circular cylinders were recorded for a periodic wave input, and amplification factors were computed."

Some important conclusions reached by Williams and Kartha were: for the range of wave numbers, k, such that $kr_a \leq 3.0$ as predicted by Havelock's theory, the amplification factors do not depend on λ/h_0 where λ is the wavelength. Based on their group 2 experiments, Williams and Kartha arrived at the following conclusions:

"(1) The seamount base of an island focuses incident wave energy onto the cylindrical island cap, with the amount of focusing being less for a concave profile ($\delta < 0.5$) and greater for a convex profile ($\delta > 0.5$). For $\delta \leq 0.25$ and wavelengths equal to about three times the island-base diameters or larger, this focusing effect is negligible.

"(2) The amplification increases as the diameter of the seamount base increases with respect to wavelength – as relatively more of the seamount base is made available for focusing the wave energy.
"(3) Amplification factors vary around the island's cylindrical cap in a manner similar to that of a straight cylinder of the same radius. This similarity decreases as the island base becomes more convex and as r_a approaches zero.
"(4) The Webster and Perry theory is valid for long waves of lengths equal to or longer than the base diameter of the island, at least for the zero azimuth angle.
"(5) Homma's theory is valid at least for long waves whose length equals about two-thirds that of the base diameter of the island for all azimuth angles."

Iwasaki (1972) performed laboratory experiments to simulate resonance amplification of tsunami waves in harbors connected to the open sea through breakwaters with different sizes of gap. He found that when the breakwater was at the mouth of the bay, the peak of the first mode did not occur. When the gap ratio of the breakwater was less than 0.2, the peak of the second mode became sharper.

Resonance Amplification in Specific Water Bodies

Experiments for northern Honshu – Ogiwara and Ôkita (1951) studied tsunamis on the Pacific coast of northern Honshu in Japan through laboratory experiments. It is well known that this coast is very tsunami prone. The particular area modeled in these experiments was Shizukawa Bay, located in the southern part of the Sanriku district and connected to the Pacific Ocean through a relatively wide mouth. During the 1896 and 1933 tsunamis, the city Shizukawa-cho, situated in the inner part of the bay, was heavily damaged. These experiments studied the wave forms in the harbor, especially after the construction of the breakwaters following the 1933 tsunami.

A model of Shizukawa harbor on horizontal and vertical scales of 1:1500 and 1:125 was constructed in a wooden tank 240 × 120 × 60 cm deep. An iron plate hinged to one end served as the wave generator and special wave gauges measured the waves generated. Also, vertical water movement was recorded on paper on a rotating drum by a lamp arrangement. By pushing the iron gate, a wave of initial elevation was generated and by pulling it, a wave of initial depression was created.

The waves generated with an initial elevation were called "up waves" and those with initial depression were called "down waves." Travel time of the wave from the mouth to the interior was 1.25 times longer for the down waves than the up waves. If the ratios of the vertical and horizontal scales to those of nature are D and L, respectively, and if T denotes the ratio for the time scales of experiment to nature, then $T = L/\sqrt{D}$. As L = 1/1500 and D = 1/125, T = 1/134 is obtained. The process is speeded up 134 times in the experiment compared to nature.

The experiments showed that wave height increased at a faster rate in the inner part of the bay and could become as large as four times the wave height near the mouth. The progressive wave that invaded the bay gradually transformed to a stationary wave. Another interesting result of these experiments was that, because of construction of the breakwater following the 1933 tsunami, wave heights in the harbor were lowered while heights at the mouth of the Hachiman River were slightly raised.

Experiments to model Hebgen Lake – Wiegel and Camotim (1962) modeled the oscillation of Hebgen Lake, Mont., caused by the earthquake of Aug. 17, 1959. After the earthquake, the bottom of the lake at the Hebgen dam subsided by 3.0 m, and an oscillation with a period of approximately 17 min occurred for almost 12 h before it was damped.

The horizontal and vertical scales of the model were 1:8000 and 1:3500, respectively. The sudden dropping of the bottom at the dam end of the model simulated the earthquake. The water surface was monitored in time by wave meters. The water particle velocity wave in the experiments was approximately:

$$u_{\text{avg}} = \frac{\text{H}}{\pi}\sqrt{\frac{g}{d}} \simeq 0.03 \text{ m/s} \tag{4.196}$$

where H is the oscillation range and d is the average water depth. The relevant Reynolds Number is:

$$\text{R} = \frac{u_{\text{avg}}(4d)}{\nu} \approx 756 \tag{4.197}$$

As the Reynolds Number is too low, the influence of viscosity is too large in the model compared to the prototype and the authors attributed the disagreement between the observed and model results partly to this.

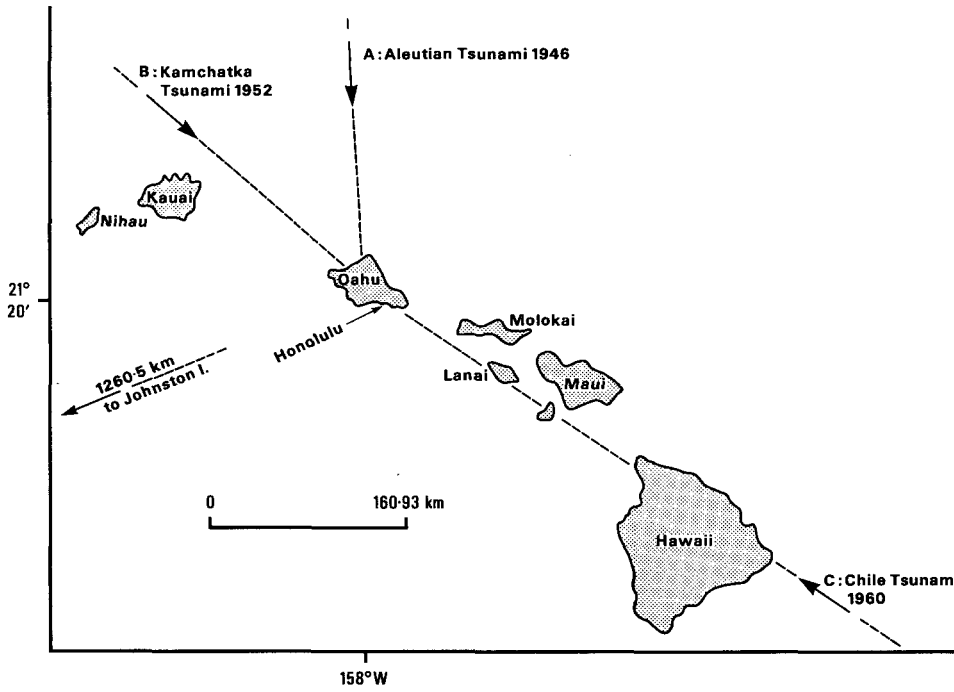


FIG. 4.19. Location plan showing Hawaiian Islands and directions at Oahu of large historical tsunamis. (Adams and Jordaan 1968)

Experiments to simulate tsunami amplification around Oahu Island, Hawaii – Adams and Jordaan (1968) studied the tsunami inundation on the coast of Oahu through models. Tsunamis originating in the circumpacific belt can approach the Hawaiian Islands from practically every direction (Fig. 4.19). Two different model studies were made; the first was to study the refraction of tsunamis by the Hawaiian Island group, which consists of eight major islands. The scale of this model was 1:247,500.

For a detailed study of Oahu Island, another model with horizontal and vertical scales of 1:20,000 and 1:2,000, respectively, was constructed. The models gave a

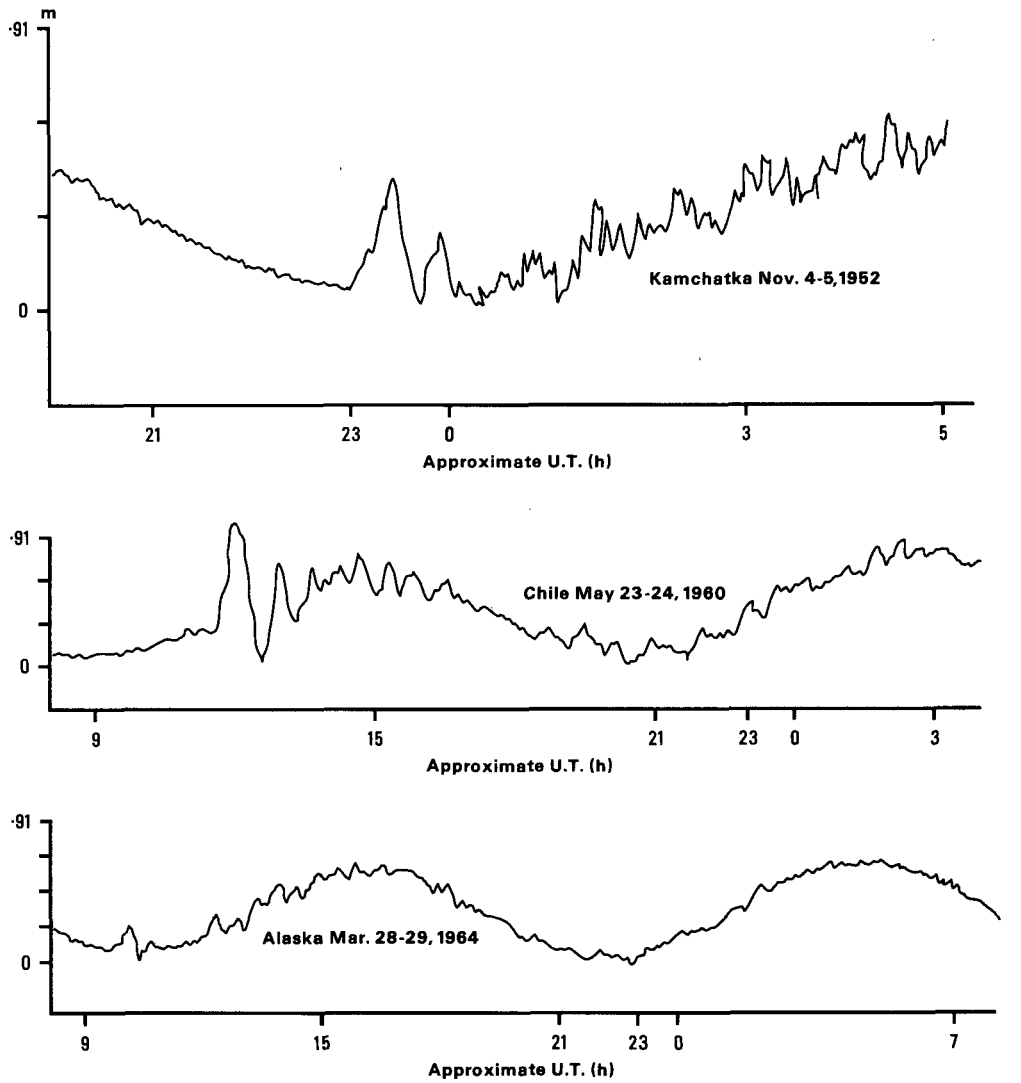


FIG. 4.20. Tsunami records at Johnston Island, 1126.5 km west-southwest of Hawaii. (Adams and Jordaan 1968)

scale of 1:141 for time and velocity. Provision was made to simulate tsunami approach to Oahu from any direction by allowing the model to rotate and present the desired angle to the wave generator. The tsunami record at Johnston Island, about 1126.3 km west-southwest of Oahu, was used as the deepwater tsunami record (Fig. 4.20). This assumption is probably satisfactory because Johnston Island is an atoll with an extremely small diameter compared to a tsunami wavelength. The authors attributed the similarity of the first crest of the three tsunamis shown in Fig. 4.20 to local effects.

The records at Johnston Island led Adams and Jordaan to adapt a few waves of equal period and amplitude to represent tsunamis approaching Oahu. The periods 18.8, 23.5, and 28.2 min of the modeled tsunamis in the experiments fall in the lower part of the observed range of 20–60 min for the Hawaiian Islands. Specifically, the Aleutian earthquake tsunami of 1946, the Kamchatkan earthquake tsunami of 1952, and the Chilean earthquake tsunami of 1960 were modeled in these experiments.

Figure 4.21 shows the phase lag of the waves in the model experiments compared to those in nature for the 1946 and 1960 tsunamis, and Fig. 4.22 shows the correlation of normalized heights of the first and third waves in the model with the normalized maximum run-up in nature. In these diagrams β is the angle between the direction of tsunami approach and the north.

The authors concluded that the experimental results did not correlate well enough with those of nature to allow quantitative prediction of tsunami inundation and they attributed the disagreement partly to the resonances between the model and the basin sides in the experiments, and to the fact that such topographic features as reefs were not included in the model.

Experiments to simulate tsunami response at Wake Island – Van Dorn (1970b) made a model study of the tsunami response at Wake Island. As there is no completely reliable theoretical method to predict refractive effects around islands, and Wake Island possesses unique characteristics and is a permanent observing station, Van Dorn felt that a suitably large laboratory model, if calibrated for the principally known directions of tsunami approach, could be used to interpret the tsunami records more accurately.

The experimental arrangement (Fig. 4.23A) consisted of a shallow basin 15 m long by 12 m wide. This had a beach with slope 1:8 around the sides for quick absorption of the waves in between runs. The basin represented a large sector of the northern part of the Pacific Ocean and the model itself represented Wake Island on a scale 1:57,500. The water depth of 9.4 cm in the model represented a real depth of 5.2 km. The wave generator was the vertical plunger type and, by adjusting the amplitude and speed of the generator, plane waves of desired frequency and amplitude could be generated.

The model of Wake Island consisted of a 60-km radius containing Wake Island and two seamounts near the island. To monitor the waves three sensors were used: two fixed at 1.5 m and 2.5 m from the generator on a line bisecting the island model and the generator; and the third mounted on a post that could be moved into any of the nine positions around the island shown in Fig. 4.23B.

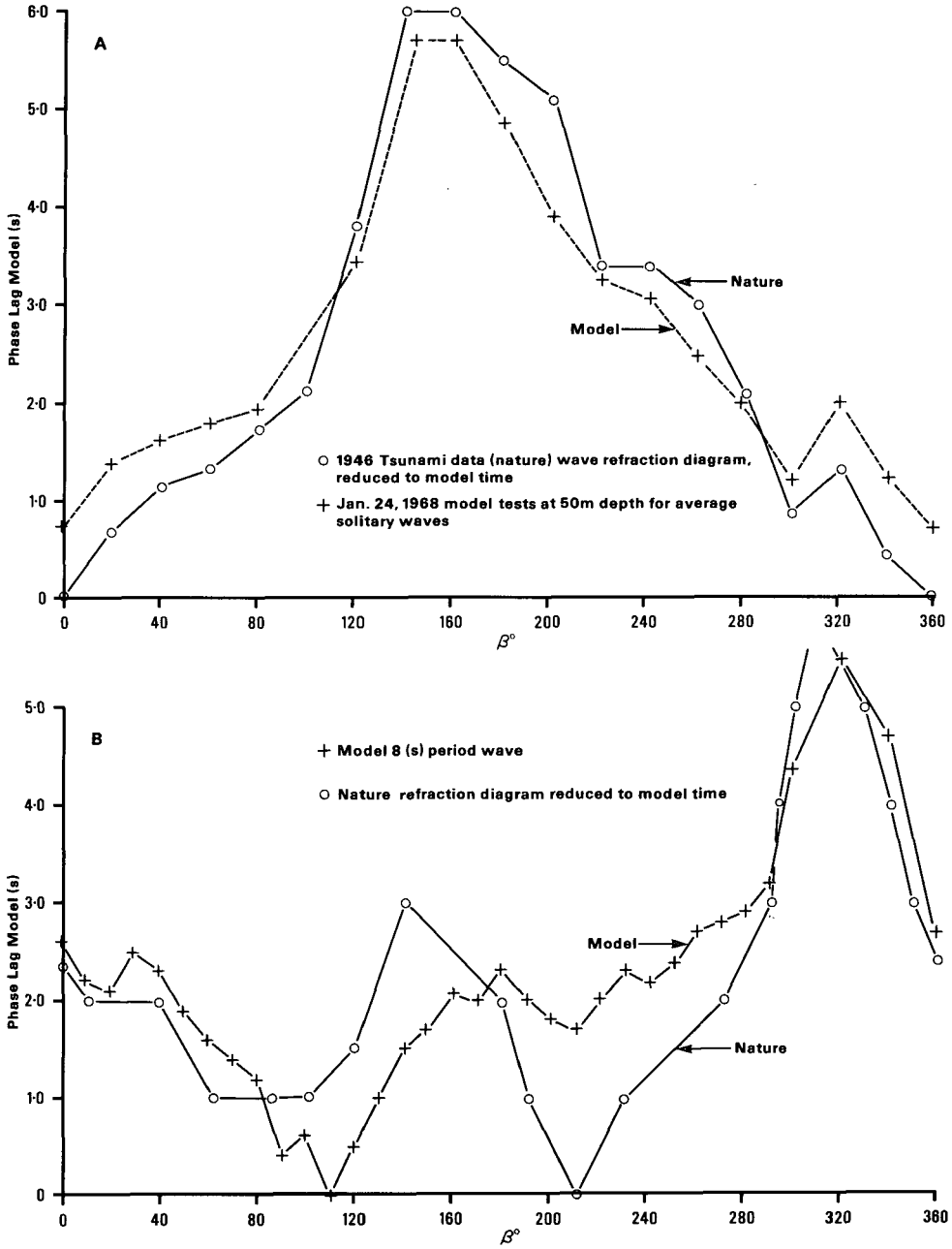


FIG. 4.21. (A) Phase lag of waves on model and for waves from (a) 1946 Aleutian tsunami, (b) 1960 Chilean tsunami as scaled to model time. (B) Phase lag of waves on model and for waves from 1960 Chilean tsunami, as scaled to model time. (Adams and Jordaan 1968)

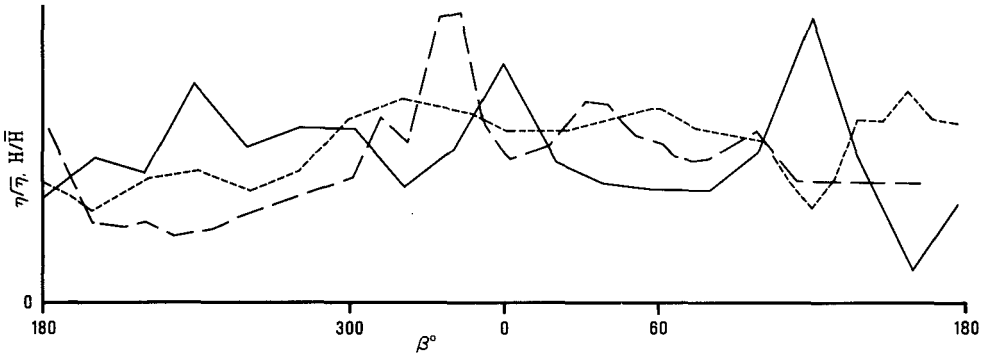


FIG. 4.22. Correlation of normalized first crest in model and normalized third wave height in model to normalized maximum run-up in nature (θ = 354°, 1946 Aleutian tsunami): — — model (third wave), ------ model (first wave), ——— nature (max. wave). (Adams and Jordaan 1968)

Waves were generated and the wave generator was operated until the waves traveled to the far end of the basin and were reflected. Then it was stopped and adjusted for the next run. The interval of 5–10 min was sufficient to damp out the waves before the plunger was operated for the next run.

Regarding the simulation of different approaches of tsunamis, Van Dorn stated (1970b, p. 339):

> "When all nine positions for the island sensor had been recorded, the entire island was rotated within the basin so that the new incident wave direction was 120° true north (simulating waves from Chile); 11 frequencies were run with the island sensor in position 2, which is the revised location of the tsunami recorder installed at Wake Island in 1960. Finally, the island was again rotated for incident waves from 320° true [north] (from Japan), and the same frequencies were rerun."

Caution was exercised in deducing the wave amplitudes from the oscillograph records by treating the uniform amplitude portion of the record between the wave build at the island initially and the arrival of the first reflected wave, as the respresentative record for steady state conditions. Van Dorn pointed out that whereas diffraction could, in principle, affect the wave record considerably, in practice this did not present any serious problem. Correction for the boundary dissipation was applied to wave records at the three stations. This correction was not uniform for all experiments but varied with the frequency of the waves, the distance traveled by them, water depth, and viscosity. For waves with the highest frequency used in the experiments it amounted to as much as $\frac{1}{5}$ of the wave record itself.

Let η and η_0 be the wave amplitude at the island and the average of the far field amplitudes, respectively, and τ' the least time required for a long wave to travel around an island with an i th contour, and depth, h_i, and circumference, C_i. Van Dorn defined the least time frequency ω' as: $\omega' \equiv \frac{2\pi}{\tau'} = \left\{ \frac{2\pi\sqrt{gh_i}}{C_i} \right\}_{\min}$ which could be minimized with iteration techniques. If $C_i/2\pi$ is interpreted as an effective radius, a', of an island in nature, then: $\frac{\omega}{\omega'} = ka'$ where k is the

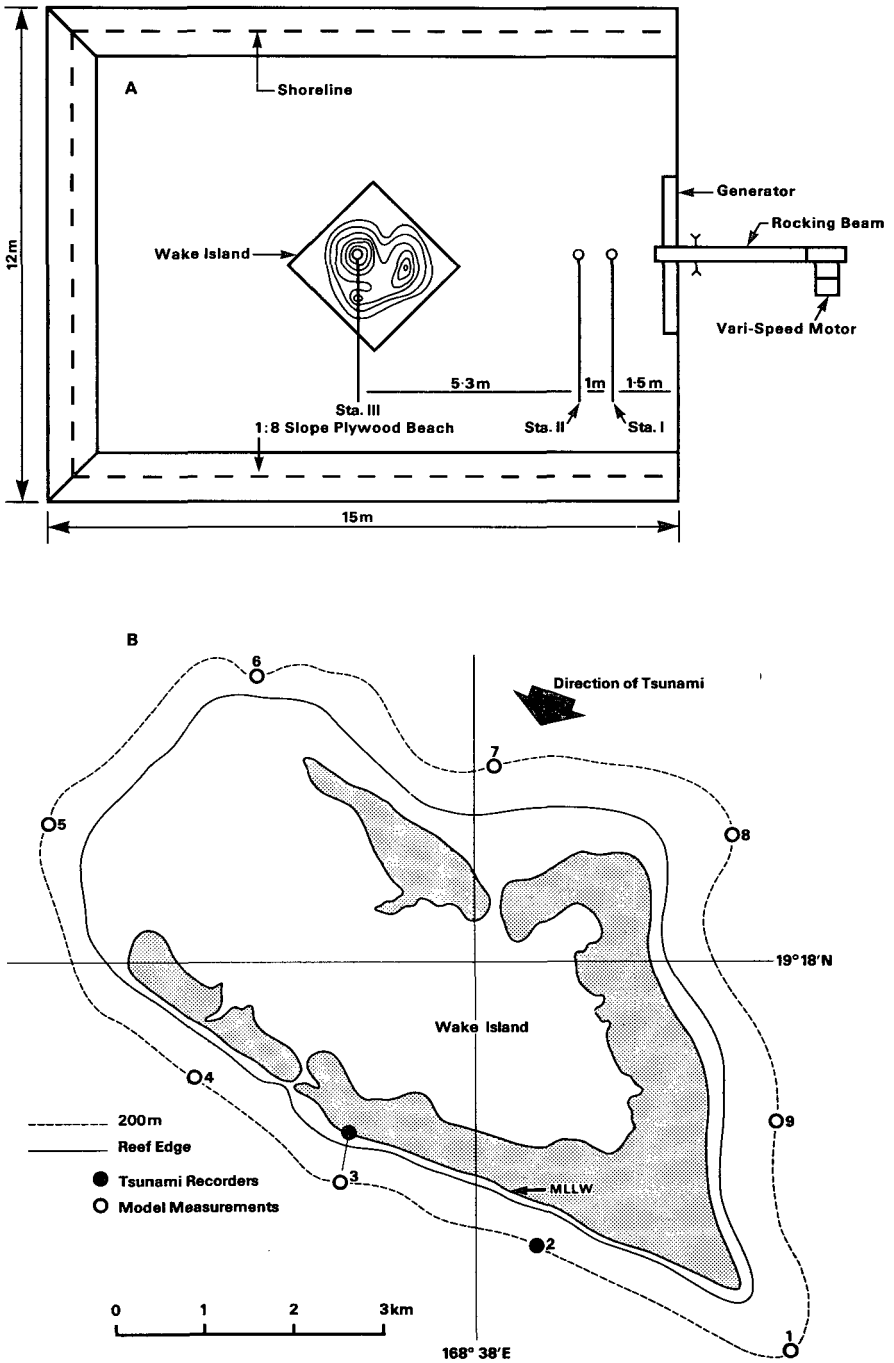


FIG. 4.23. Plan view of (A) the experimental basin, showing locations of wave generator, wave sensors, and model of Wake Island oriented to simulated waves from the tsunami Mar. 9, 1957, and (B) Wake Island, showing 9 sensor locations for recording waves. (Van Dorn 1970)

incident wave number. Van Dorn then made an analogy to scattering of sound waves by a cylinder and pointed out that ka' is analogous to the transition index from weak forward scattering corresponding to $ka' < 1$ and to strong back scattering followed by shadowing on the lee side corresponding to $ka > 1$.

One important result is that for $\omega/\omega' < 1$ there was no ambiguity in the Wake record anywhere and hardly any amplification. On the other hand, for $\omega/\omega' > 1$ large amplifications occurred on the incident side and some shadowing occurred on the leeward side. Figure 4.24 shows the amplitude responses deduced from the experiments at the tsunami station at Wake Island for tsunamis approaching from Chile, Japan, and the Aleutians. The largest amplifications occurred for waves correspond to $\omega/\omega' > 0.6$.

Experiments for Hilo Bay – Palmer et al. (1965) performed laboratory experiments to simulate tsunami amplification in Hilo Bay. They attributed the large tsunami amplification to a combination of three bathymetric features (Palmer et al., p. 30):

> "... First, the submarine ridge formations outside the bay mouth refracts the tsunami wave into the bay. Second, the triangular configuration of the bay, with Hilo at the apex, has a compressive effect on the wave. Third, the reflected wave off the cliffs superimposes on top of the incident wave in Hilo harbor..."

An area of about 77.7 km^2 was modeled on a horizontal scale of 1:600 and a vertical scale of 1:200. The tsunami bore in Hilo harbor was generated by a pneumatic wave generator. The model was calibrated by simulating the marigrams, inundation zones, and high-water marks observed during the 1946, 1952, 1957, and 1960 tsunamis.

One important deduction from these experiments was that the formation of the tsunami bore in Hilo harbor appeared to be caused by reflection of the incoming

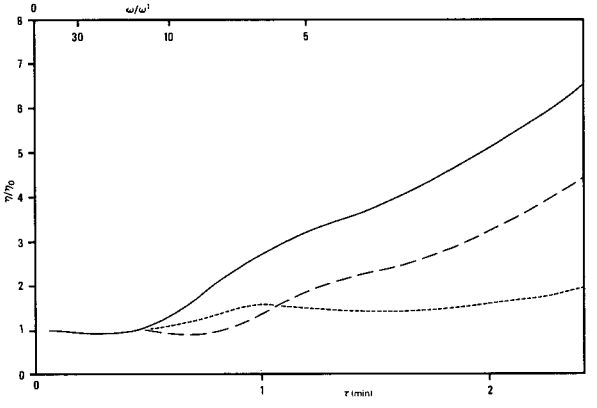


FIG. 4.24. Amplitude responses as a function of relative frequency ω/ω' (see top scale in abscissa) and prototype period T (see bottom scale in abscissa) at sensor station 2, site of the present tsunami recording station at Wake Island, for waves approaching from known tsunami generating region; ..... Aleutians, - - - - - Japan, —— Chile. (Van Dorn 1970b)

waves from the almost vertical Hamakua cliffs. Munk (1957) anticipated this earlier and stated that reflection off the Hamakua cliffs would increase tsunami wave heights. Another important result was that an approach of a tsunami with an incident angle of 80° might be critical by producing maximum wave heights inside the harbor. Palmer et al. (1965) mentioned some experiments by Wiegel (1963) on a Hilo model with a scale of 1:15,000 where the Mach stem phenomenon appeared to be important.

Experiments for Kochi harbor — Iwagaki et al. (1970) constructed a model of Kochi harbor on a horizontal scale of 1:250 and a vertical scale of 1:100. The current was modeled to 1:100 and the time 1:10 and bottom roughness was also considered. Data from the 1960 Chilean earthquake tsunami was used to calibrate the model. The tsunami response of the harbor was studied both for the present topography and for the topography that will exist after a proposed plan of dredging and land reclamation. The effect of breakwaters was also studied. Two important results of the experiments were: first, river flows into the harbor tend to decrease the amplitude of the waves in the harbor, and second, after dredging and the associated change of topography, a tsunami bore might be possible in Kochi harbor.

Experiments on bores — Krivoshey (1970) studied through laboratory experiments, the run-up of a bore on dry shores where, according to him, it loses its wave properties and becomes a jet of water.

Miller (1968) performed experiments in a wave tank 19.2 m high, 0.355 m uniformly wide, and 0.91 m deep; various bottom slopes were arranged in this tank. Waves were generated by a rigid vertical plate or a piston. The desired bottom roughness coefficients were achieved through coating the slope with glass beads of selected size (marine enamel coatings were used to create smooth surfaces).

The experiments showed that beach slope as well as bottom roughness influenced the run-up height and that the bore collapsed (only partially) in a limited range of Froude numbers, at the intersection of the undisturbed water level with the beach slope. Another interesting result was the existence of an inflection point in the run-up curves, attributed by Miller to the transition from an undular surge to a bore which happened as the piston velocity, u, increased.

Nakamura (1972) used a rectangular tank 30 m long, 0.5 m uniformly wide, and 0.5 m uniformly deep, to perform experiments on the hydraulic bore problem. The vertical movement of a steel plate through a system of pulleys and weights served as the generating mechanism. In the initial state (just at the instant of moving the steel plate) the bore can be visualized as consisting of a shallower region of depth, h_1, and a deeper region of depth, h_0. Nakamura's experiments showed that different initial ranges of h_1/h_0 resulted in different wave forms propagating in the tank.

Based on this ratio of h_1/h_0 Nakamura (1972, p. 4) identified essentially four patterns: "(i) $h_1/h_0 = 0$: a parabolic wave with a rounded front, (ii) $0 < h_1/h_0 < 0.4$: a uniformly progressive wave with a breaking front (moving hydraulic jump), (iii) $0.4 < h_1/h_0 < 0.56$: unstable undular bore with a front partly broken, and (iv) $0.56 < h_1/h_0 < 1.0$: stable undular bore."

Hawaleshka and Savage (1971) performed laboratory experiments on the influence of friction on the development of undular bores. Nakamura (1976) used the analogy between a bore caused by a dam breaking and a surging tsunami on a river mouth or a beach, to determine the shock pressure of tsunami surge on a wall, by laboratory experiments.

Chapter 5 Global Tsunamis

Some important tsunamis in various parts of the globe are cataloged and important deductions from the data are emphasized. In the first section the western part of the Pacific Ocean, specifically Japan, USSR, Australia, and New Zealand will be considered. In Section 2 the islands in the Pacific Ocean, such as Hawaii, Aleutians, Tahiti, and Alaska will be discussed. (Although Alaska is part of the North American continent, it is more convenient to study tsunamis of Alaska and the Aleutians together.) In the third section, the tsunamis on the west coasts of the North (excluding Alaska) and South American continents will be discussed. In Section 4, the Atlantic Ocean tsunamis and tsunamis in Europe, Middle East, and Asia will be treated.

5.1 Tsunamis in Japan, USSR, Australia, and New Zealand

Tsunamis in Japan

The Pacific coast of northeastern Japan has been referred to as the Sanriku coast because it contains the three Riku provinces – Rikuzen, Rikutyu, and Rikuoku. Table 5.1 lists 15 tsunamis that occurred in Japan from 869 to 1933 (Imamura 1934). In addition, information will be provided on some of the very destructive tsunamis, and on tsunamis subsequent to 1934.

The tsunami following the Sanriku earthquake of June 15, 1896, destroyed about 12,000 houses and affected 322–483 km of coastline north of Sendai. There were mainly three waves and the greatest amplitude was 15.2 m (Milne 1896). Practically every town and village between 30°15′N, 141°30′E and 40°30′N, 131°30′E was destroyed.

A major earthquake occurred in Sagami Bay on Sept. 1, 1923 (Shiratori 1925), and only 5 min after the earthquake a tsunami invaded Sagami Bay, Tokyo Bay, and the Pacific coast of Japan. Figure 5.1 shows the distribution of water level at various locations (Davison 1931). The tsunami attained maximum amplitude of 11 m, about 455 houses were destroyed, and about 160 persons killed.

The epicenter (38.2°N, 144.0°E) of the Sanriku earthquake of Mar. 3, 1933, was not on land, hence, destruction by the earthquake itself was small. Most of the destruction was caused by the tsunami and about 5000 houses were destroyed. At some places (Sirahama and Ryori) amplitudes as large as 28.7 m were attained.

Tsunamis rarely occur in the Sea of Japan (Kishinouye and Iida 1939). An insignificant tsunami occurred on May 1, 1939, in the Oga Peninsula following the Oga earthquake.

TABLE 5.1. List of tsunamis prior to 1934 on the Sanriku Coast. (Imamura 1934)

	Remarks
July 13, 869	epicenter under Pacific Ocean off Sanriku coast; about 1000 people killed
Dec. 2, 1611	epicenter under Pacific Ocean off Sanriku coast; about 3000 people killed; possible amplitude of 25 m
Sept. 9. 1616	epicenter under Pacific Ocean off Sanriku coast; tsunami probably small
July 3, 1640	following an eruption of the volcano Komagatake; tsunami killed about 700 people
Apr. 13, 1677	following an earthquake in Sanriku district; tsunami caused only property damage; people fled and no casualties
? ? 1689	following a Sanriku earthquake; probably small tsunami
Jan. 29, 1763	following an earthquake in the north Sanriku district; tsunami swept the coast
Feb. 17, 1793	following an earthquake near Rikutyu; tsunami killed 12 or 13 people
July 20, 1835	following an earthquake near Rikuzen; tsunami generated; casualties not known
Apr. 25, 1843	following an earthquake in east Hokkaido; details of tsunami not known
Aug. 23, 1856	following an eruption of the volcano Kamagatake; tsunami killed at least 21 people
June 15, 1896	following an earthquake in Sanriku; tsunami very destructive, killed at least 27,000 people
Mar. 22, 1894	following an earthquake in eastern Hokkaido; tsunami caused some damage
Aug. 5, 1897	following an earthquake in Rikuzen; tsunami was small
Mar. 3, 1933	following the Sanriku earthquake; tsunami very destructive, killed at least 2986 people

A severe earthquake occurred in western Hokkaido on Aug. 2, 1940. About 1 h after the earthquake a tsunami invaded the Hokkaido coast. Seven people were killed and about 1000 fishing boats were swept into the ocean (Miyabe 1940). Figure 5.2 shows tsunami amplitudes.

A severe earthquake occurred on Dec. 7, 1944, with epicenter at 34°N, 143°E. A tsunami of considerable amplitude was generated and effects were felt as far east as Simoda Harbor and as far west as Siworomsaki (Omote 1946). Along the coasts of Sima and the Kii Peninsula, heights were as large as 8 m; along the coasts of Ise Bay and Atumi Bay, the height was 2 m. Amplitudes were small along the Ensywnada coast but enormous heights were achieved in the bays of Owase, Atasika, Nisiki, and Yosizu.

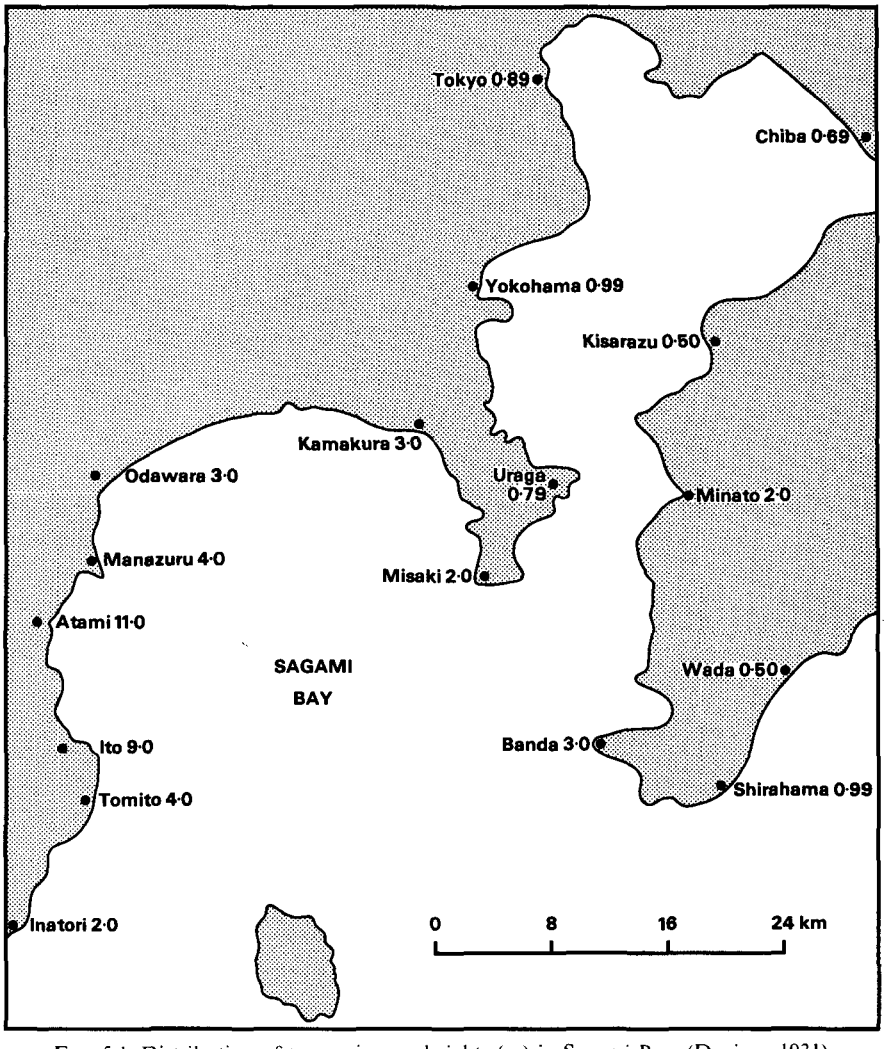


FIG. 5.1. Distribution of tsunami wave heights (m) in Sagami Bay. (Davison 1931)

On Dec. 21, 1946, a severe earthquake occurred in southwestern Japan with epicenter at 33.0°N, 135.6°E. The generated tsunami invaded the coasts of Shikoku and the Kii Peninsula. The largest amplitude was 6 m (Nagata 1950) and on the coast of the Kii Peninsula, initial withdrawal occurred. The most severe damage occurred on the coast of Kochi prefecture where 1451 houses were swept away (Nasu and Shirai 1947). The Nankai earthquake tsunami was studied in detail by Shimozuru and Akima (1952) and Rikitake and Murauchi (1947).

On Mar. 4, 1952, a severe earthquake (referred to as the Tokachi earthquake) occurred, followed by a tsunami, with epicenter at 42°N, 144°E, about 60 km east of Erimo-Misaki, at the southwestern tip of Hokkaido (Suzuki and Nakamura 1953; Suzuki et al. 1953; Yoshida et al. 1953; Kato et al. 1953; and Watanabe 1956).

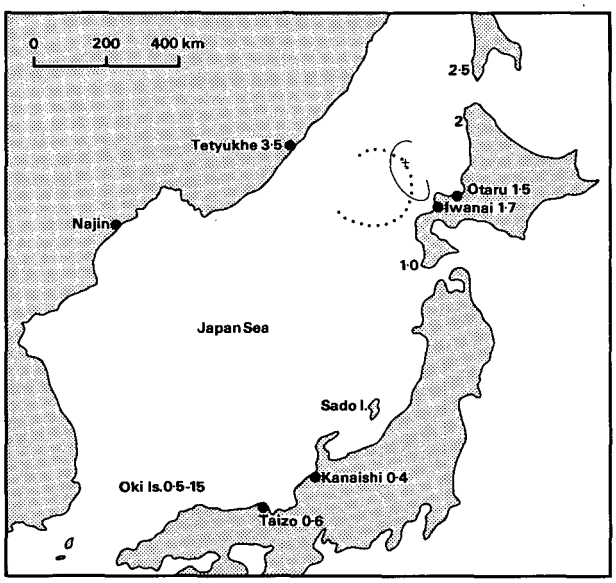


FIG. 5.2. Distribution of tsunami height (m) for 1940 tsunami. Tsunami sources inferred from the present (solid line) and Miyabe's analyses (dotted line). (Hatori 1969)

TABLE 5.2. Tsunami of Feb. 27, 1961, as recorded on tide gages (all times Japanese Standard Time). Wave originated at earthquake epicenter off the coast of Hiuganada (31.7°N, 131.7°E) at 03:11. (Takahasi and Hatori 1961)

Tide station	Arrival time (*h*)	(*min*)	Up, down	Max. amplitude time (*h*)	(*min*)	Max. amplitude (*cm*)	Period (*min*)
Naze	04	23	+	04	52	13	20
Nishino-omote	04	00	+	06	00	25	
Makurazaki	04	27	+	05	32	13	16
Namimi	03	30	+	04	20	12	
Suzureishi	03	30	+	04	18	12	
Aburatsu	03	14	+	03	51	45	22
Miyazaki	03	35	+	03	42	12	
Hosojima	03	22	+	05	22	78	20
Hosojima, (New Harbor)	03	25	+	05	55	124	
Tokai	03	35	+	03	42	13	18
Hebizak	04	00	+	05	10	10	19
Yavatahama	04	25	+	06	30	28	22
Uwajima	04	12	+	06	53	18	22
Hosogi	03	58	+	04	55	17	20
Misho	04	08	+	07	16	70	30
Tosa-Shimizu	03	42	+	04	12	96	22
Tosa-Shimoda	03	55	+	04	47	10	20
Urado	04	08	+	06	08	20	18
Kochi	04	15	+	06	05	17	20
Kushimoto	03	46	+	05	25	36	23
Aburatsubo	05	36	+	07	56	6	16
Mera	05	32	+	13	25	35	22
Hachijo Is.	05	10	?		?	3	?

TABLE 5.3. Tsunami of Mar. 28, 1964, as recorded by tide gages and tsunami recorders in Japan. (Hatori 1965c)

Tide station	Initial wave				Maximum wave			
	Travel time (*h*)	(*min*)	Height[b] (*cm*)	Period (*min*)	Travel time (*h*)	(*min*)	Height[b] (*cm*)	Period (*min*)
Wakkanai	6	39	6	50	39	09	34	35
Monbetsu	7	16	7	70	18	34	10	40
Abashiri	6	04	4	46	30	49	12	50
Hanasaki	6	34	8	60	15	04	36	10
Kushiro	6	55	20	45	45	40	40	42
Urakawa	7	12	5	40	18	14	25	28
Hakodate	7	34	11	150	22	17	33	35
Aomori	9	04	8	140	26	14	32	100
Asamushi	8	29	10	130	25	09	46	100
Hachinohe	7	24	18	50	26	44	60	30
Miyako	7	04	9	60	16	02	14	44
Kamaishi	6	44	15	30	16	34	38	22
Ofunato	7	14	18	40	12	44	75	40
Enoshima[a]	7	08	7	80	15	39	15	60
Onagawa	7	24	17	70	17	44	50	45
Onahama	7	29	7	50	16	34	35	23
Choshi	7	39	7	55	20	04	36	40
Mera	7	06	6	7	23	34	33	23
Kanaya[a]	7	30	7	70	21	14	17	35
Tokyo	9	02	4	65	22	59	10	56
Yokosuka	8	00	5	60	22	30	17	30
Aburatsubo	7	48	6	15	22	32	18	15
Hachijo Is.[a]	7	47	2	8	22	14	7	20
Uchiura	7	34	6	50	16	29	12	23
Shimizu	7	44	4	20	25	19	6	40
Omaezaki	7	04	3	18	22	12	30	22
Onizaki	9	41	6	25	19	54	10	35
Toba	11	24	4	50	18	24	15	15
Uragami	9	29	8	26	18	36	25	28
Kushimoto	9	14	6	15	26	24	45	28
Kainan	10	12	5	30	20	24	15	28
Kochi	11	06	8	40	25	04	20	20
Tosa-Shimizu	11	24	4	26	22	30	24	22
Hosojima	12	44	2	20	27	07	12	20
Aoshima[a]	10	44	2	—	26	57	15	30
Aburatsu	10	28	8	23	25	06	39	25
Naze	10	32	8	18	22	32	20	23

[a]Tsunami observatory.

[b]Crest height above the ordinary tide level.

An earthquake on Nov. 6, 1958, near Iturup Island, generated a tsunami. During the International Geophysical Year (IGY), special instruments were placed at Miyagi-Enoshima tsunami observatory. The tsunami occurred during this period (Takahasi et al. 1961).

Following a Chilean earthquake of magnitude 8.25–8.50 with epicenter at 38°S, 73.5°W, on May 22, 1960, a tsunami invaded Japan on May 24. The most

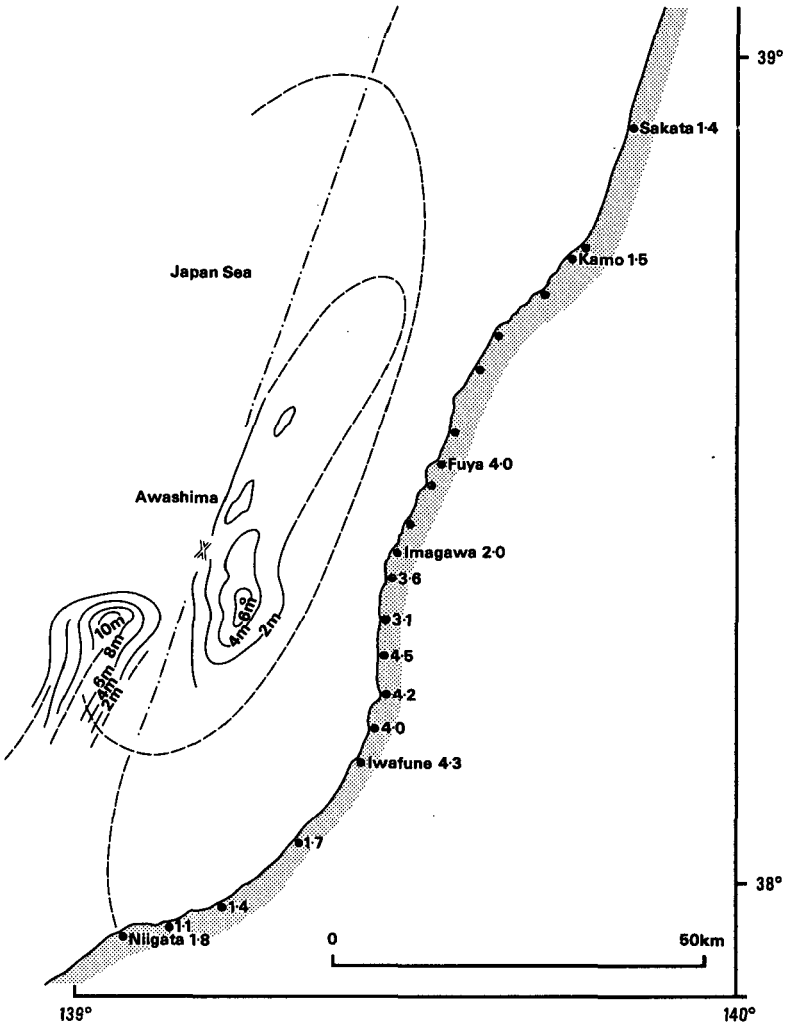


FIG. 5.3. Generating area of the tsunami which accompanied the 1964 Niigata earthquake. Bottom deformation (m) and inundation heights (m) are shown. (Hatori 1965b)

severe damage occurred in the districts of Tohoku and Hokkaido (Kato et al. 1961). This tsunami achieved amplitudes to 9 m and 180 people were killed. The Committee for Field Investigations of Chilean Tsunami (Anon. 1961) published a detailed account of this tsunami on the Japanese coast. Other references on the tsunami in Japan are Higuchi (1964), Nakamura and Emura (1961), and Takahasi (1961). Momoi (1963a, b) invoked the theory of diffraction to account for the large amplitude waves along the coast of Inubozaki in the Kanto district.

On Feb. 27, 1961, an earthquake occurred off the southeast coast of Kyushu. The magnitude of this earthquake was 7.2 and the epicenter was at 31.7°N,

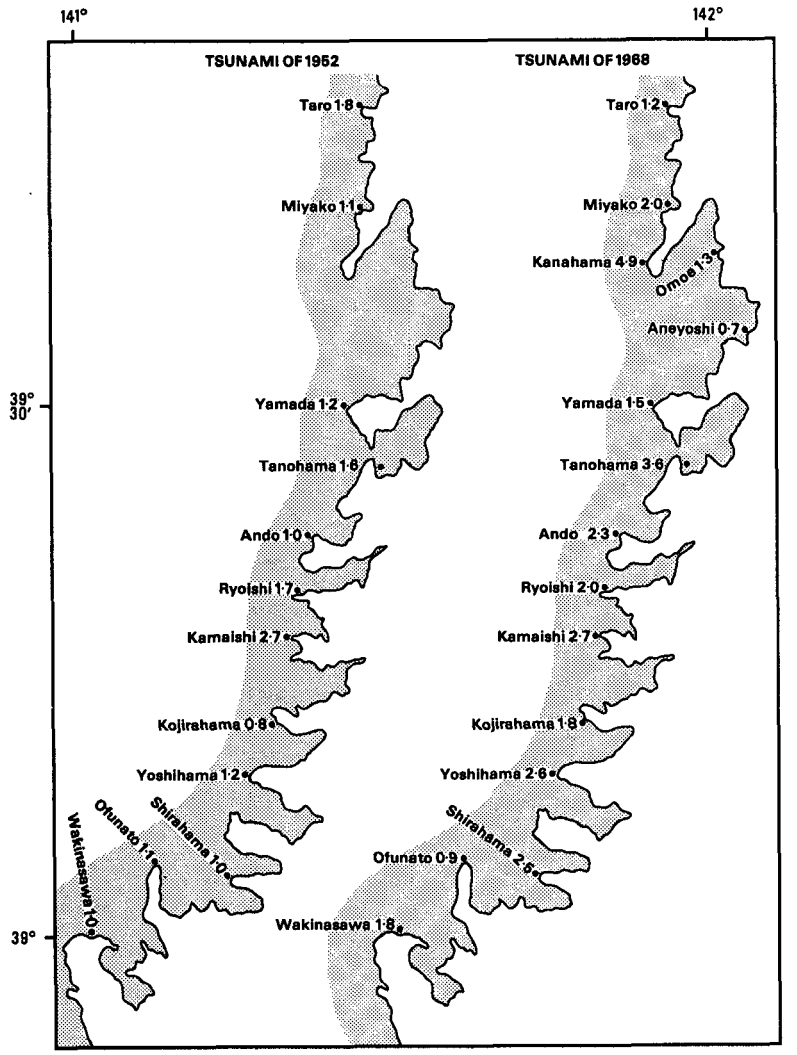


FIG. 5.4 Tsunami height (m) along Sanriku coast for the 1952 and 1968 Tokachi-Oki tsunamis. (Kajiura et al. 1968)

131.7°E. A tsunami of moderate amplitude was generated and was observed along the coasts of Kyushu and Shikoku (Takahasi and Hatori 1961). Table 5.2 lists pertinent information about the Hiuganada tsunami. No initial withdrawal of water was observed and the tsunami period was in the range of 16–30 min.

An earthquake of magnitude 7.9 occurred off Iturup Island (in the Kurils) on Oct. 13, 1963, with epicenter at 44.0°N, 150.0°E (Hatori and Takahasi 1964). The tsunami generated was observed all along the Pacific coast of Japan.

Hatori (1964) investigated the Alaskan earthquake tsunami of Mar. 28, 1964, along the Japanese coast. Table 5.3 lists the pertinent information. On June 16,

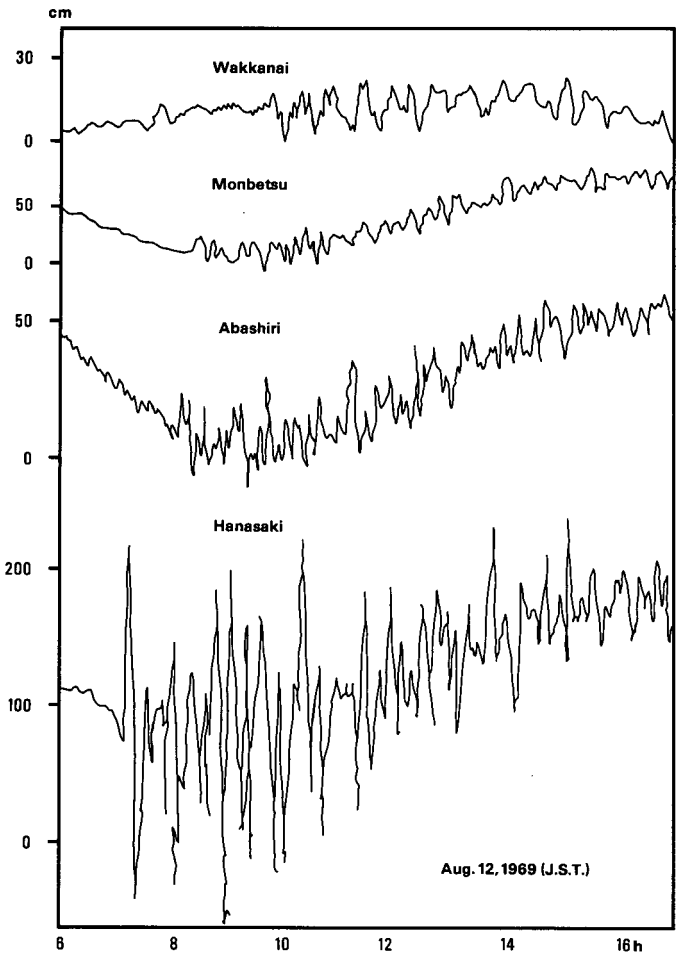


FIG. 5.5. August 1969 tsunami at 4 stations in Japan. (Hatori 1970a)

1964, an earthquake of magnitude 7.7 with epicenter at 38.4°N, 139.2°E occurred near Awashima Island (Hatori 1965a). Figure 5.3 shows the tsunami amplitudes along the coast. On May 16, 1968, an earthquake of magnitude 7.8 with epicenter at 40.7°N, 143.6°E occurred off the coast of Aomori prefecture in northeastern Japan (Suzuki 1970). Figure 5.4 compares the amplitudes of this tsunami with those of the 1952 Tokachi-Oki tsunami on the Sanriku coast. On Aug. 11, 1969, an earthquake of magnitude 7.8 with epicenter at 42°42′N, 147°37′E occurred off Shikotan Island in eastern Hokkaido (Hatori 1970a). The maximum height of this tsunami (1.5 m) was observed at Hanasaki. Figure 5.5 shows the distinctly different tsunami records at four stations.

Hatori (1965b) studied distribution of tsunami energy and travel times of tsunamis along the coast of Japan (that originated far from Japan). He studied seven tsunamis that originated in Alaska, Aleutians, Chile, Iturup, and Kamchatka.

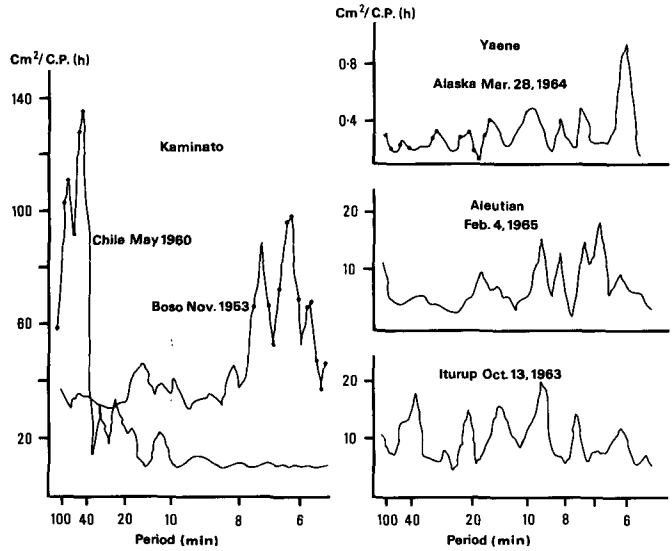


FIG. 5.6. Power spectra of different tsunamis observed at Hachijo Island. (Hatori 1969)

His study showed that the coasts of Sanriku and Kishu received a greater percentage of tsunami energy than other regions.

Iida (1956) studied the earthquakes that occurred under the sea off the islands of Japan, accompanied by tsunamis. He listed tsunamis from 684 to 1953 and his table has 136 entries. Figure 5.6 shows power spectra of the tsunami record at Kaminato for the Boso tsunami of November 1953, and at Yaene for three different tsunamis. The important periods are in the 5- to 150-min range.

Table 5.4 compares certain relevant parameters on the Japanese coast for the Alaskan earthquake tsunami of Mar. 28, 1964, and the Aleutian earthquake tsunami of Feb. 4, 1965. Generally, the period of the maximum wave was greater than the period of the initial wave and this was more true for the Alaskan earthquake tsunami than for the Aleutian earthquake tsunami. The generally held notion that the tsunami period increases with the travel distance does not seem to hold. Also, the amplitudes at various stations do not seem to bear any relation that is consistent for different tsunamis. In other words, amplitudes for the Alaskan earthquake tsunami were greater at certain stations than amplitudes at the same stations for the Aleutian earthquake tsunami, whereas the reverse situation occurred at other stations.

The effects of a distant tsunami on the Sanriku coast will be examined in detail. For this, an appropriate example is the Chilean earthquake tsunami of May 22, 1960. Although the tsunami was generated on the Chilean coast on May 22, 1960, it did not arrive on the Sanriku coast till May 24 because of the large travel distance (17,000 km). Kato et al. (1961) studied the distribution of the maximum amplitudes on the Sanriku coast and found some distinctive features attributable to the remote origin, as well as to the very long periods, of the Chilean tsunami.

TABLE 5.4. Comparison of periods and maximum amplitudes for the Alaskan earthquake tsunami of Mar. 28, 1964, and the Aleutian earthquake tsunami of Feb. 4, 1965, at selected tide stations.

Tide station	1964 Tsunami					1965 Tsunami				
	Travel time initial wave (*h*)	(*min*)	Max. amp. (*cm*)	Period of max. wave (*min*)	Period of initial wave (*min*)	Travel time initial wave (*h*)	(*min*)	Max. amp. (*cm*)	Period of max. wave (*min*)	Period of initial wave (*min*)
Aburatsu	10	28	39	25	23	5	47	32	16	28
Aburatsubo	7	48	18	15	15	4	15	28	14	14
Enoshima	7	08	15	60	80	3	49	12	32	14
Hachijo Is.	7	47	7	30	8	4	13	>23	7	7
Hachinohe	7	24	60	30	50	4	01	48	35	48
Hakodate	7	34	38	35	150	4	23	17	50	27
Hanasaki	6	34	36	10	60	3	29	21	20	40
Hosojima	12	44	12	20	20	5	54	7	18	15
Kainan	10	12	15	28	30	6	09	14	30	25
Kamaishi	6	44	38	22	30	3	43	40	25	30
Kanaya	7	30	17	35	70	4	23	13	30	13
Kochi	11	06	20	20	40	5	42	20	16	—
Kushimoto	9	14	45	23	15	5	18	55	15	18
Miyako	7	04	14	44	60	3	49	10	48	48
Monbetsu	7	16	10	40	70	3	59	9	33	20
Naze	10	32	20	23	18	6	12	40	20	22
Ofunato	7	14	75	40	40	3	59	38	24	20
Onagawa	7	24	50	45	70	4	07	28	46	35
Onahama	7	29	35	23	50	4	16	20	18	18
Onizaki	9	41	10	35	25	5	44	10	21	20
Tokyo	9	02	10	56	65	5	29	10	64	70
Tosa-Shimizu	11	24	24	22	26	5	39	36	23	30
Uragami	9	29	25	28	26	5	09	30	15	19
Urakawa	7	12	25	28	40	3	49	33	15	—
Yokosuka	8	00	17	30	60	4	43	12	25	20

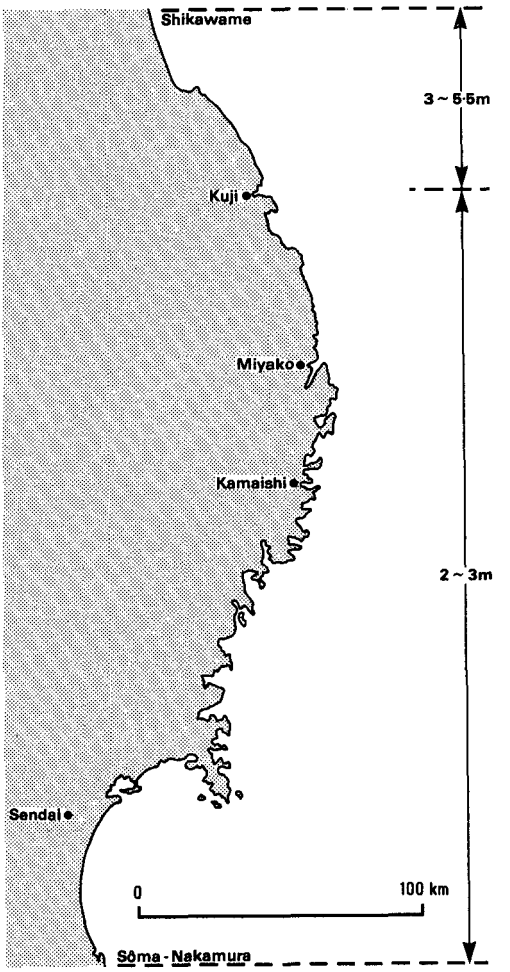


FIG. 5.7. Water-level distribution on a portion of the Sanriku coast associated with the May 1960 Chilean earthquake tsunami. (Kato et al. 1961)

The Chilean tsunami near the epicenter itself had periods of about 60 min whereas the 1933 Sanriku earthquake tsunami had periods of about 16 min.

On the Sanriku coast there are numerous bays with natural periods of oscillations in the range of 5–50 min. Because amplitudes of the tsunami waves were influenced by resonance in these bays, there was much more variation of water level along the coasts of the bays than along the shoreline outside the bays. Figure 5.7 shows the general distribution of the water level along the coastline. The average maximum amplitude south of Kuji was about 2.5 m whereas to the north of Kuji it was 5.5 m. The 1933 Sanriku earthquake tsunami did not show this type of water-level distribution.

Figure 5.8 shows the refraction diagrams for the Chilean earthquake tsunami of 1960 and the Sanriku earthquake tsunami of 1933. In the former case there is a convergence of orthogonals, whereas in the latter case there is no such convergence. This difference in convergence accounts for the difference in distribution of the water levels.

The water-level distributions also showed the effects of the tsunami diffraction by the Ojika Peninsula (see Fig. 5.9). The epicenter of the Sanriku earthquake was only 200 km from Miyako and the sea to the west of the Ojika Peninsula is in the shadow zone for the Sanriku tsunami but not for the Chilean tsunami. Observations confirm this and Fig. 5.9 shows the ratios of the amplitude of the tsunami at the east coast to that at the west coast at several locations along the length of the peninsula for both tsunamis. The ratios for the Chilean tsunami are about unity whereas for the Sanriku tsunami they are greater than unity, the maximum being about two.

Another interesting difference between the two tsunamis was the manner in which the water level varied from the mouth to the head of bays. For example, for Ofunato and Hirota bays (and several other bays on the Sanriku coast), the water level was amplified 2 to 3 times from the mouth to the head, whereas for the Sanriku tsunami it was reduced about 0.6 times. It is quite probable that the amplification in the case of the Chilean tsunami was due to resonance in the bay. Because the Chilean tsunami had long periods and consisted of several crests and troughs, it was favorable for resonance in the bays, whereas the short period and short duration of the Sanriku tsunami were unfavorable. The decrease of the tsunami amplitude from the mouth to the head in the case of the Sanriku tsunami was attributed to the influence of bottom friction and complicated shoreline configurations.

Tsunamis of USSR

Lavrentyev and Savarensky (1963) summarized the investigations on tsunamis in USSR until 1961. Soloviev (1970) discussed tsunamis in USSR as a part of a more general discussion of Pacific tsunamis. He periodically prepared summaries of the tsunami investigations in USSR and distributed them at periodic meetings of the tsunami committee of the International Union of Geodesy and Geophysics (e.g. Soloviev 1971). Several books on tsunamis were published in Russian (e.g. Interagency Geophysical Committee of USSR 1970).

The following is only a partial list of tsunamis that have been observed in the USSR. On Dec. 26, 1939, an earthquake occurred in Turkey at 39.5°N, 39.5°E at 23 h 57 min GCT (Grigorash and Korneva 1970). The epicenter was between Erzincan and Erzurum, about 160 km from the Black Sea coast. The magnitude of the main shock was 7.9 to 8.0 and tsunami amplitudes were larger on the Turkish coast of the Black Sea, and smaller on the USSR coast. Table 5.5 lists pertinent information on this tsunami.

Grigorash and Korneva (1972) constructed travel-time charts (they called them isochrone charts) and refraction diagrams for some Black Sea tsunamis, to examine the role of refractive focusing on the distribution of tsunami energy. For the tsunami

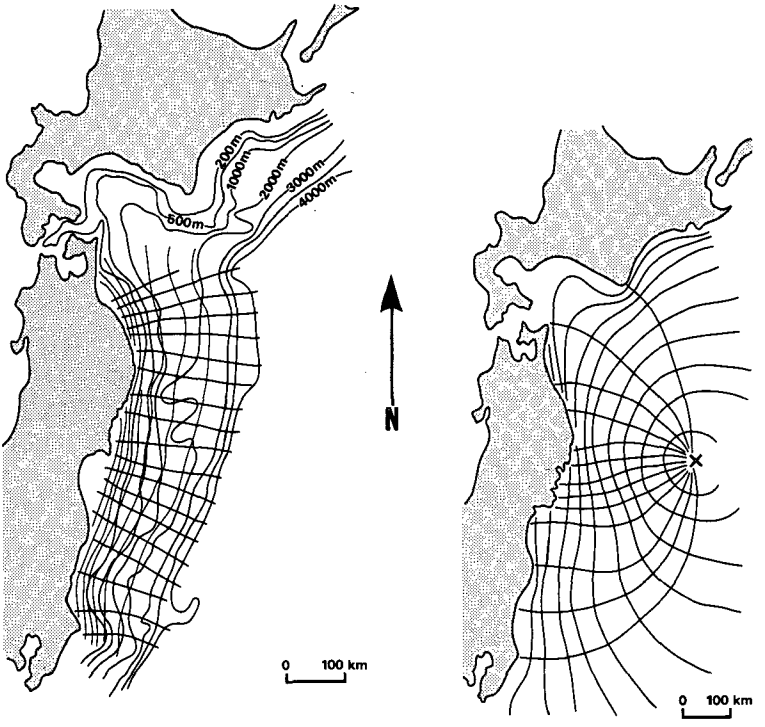


FIG. 5.8. Refraction diagrams for the Sanriku coast for 1960 Chilean earthquake tsunami (left) and 1933 Sanriku earthquake tsunami (right). (Kato et al. 1961)

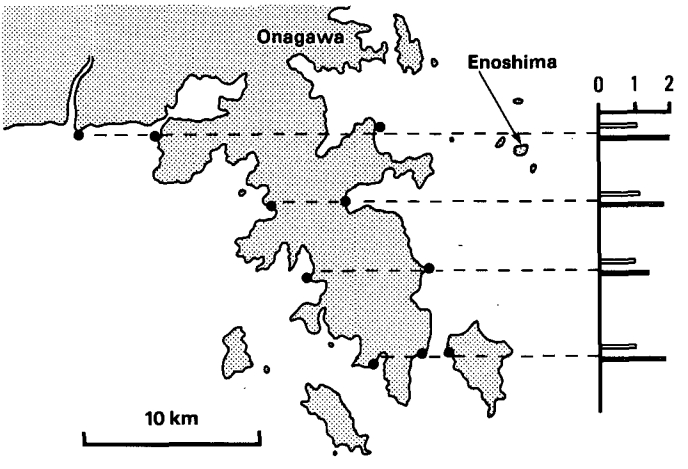


FIG. 5.9. Ratio of water level on the east coast to the west coast of Ojika Peninsula of Sanriku coast for 1960 Chilean earthquake tsunami (white column), and 1933 Sanriku earthquake tsunami (black column). (Kato et al. 1961)

TABLE 5.5. Tsunami of Dec. 27, 1939, as recorded by tide gages in USSR. (Grigorash and Korneva 1970)

Tide station	Initial rise (+) or fall (-)	No. max. ht. wave	Travel time Obs. (*min*)	Travel time Calc. (*min*)
Batumi	–		0	0
Poti				
Tuapse	+	1	50	53.7
Novorossiysk	+	1	73	60.0
Kerch	+	2	162	166.6
Feodosiya	+	3	80	84.0
Yalta	+	10	53	46.0
Sevastopol	+	7	135	132.0

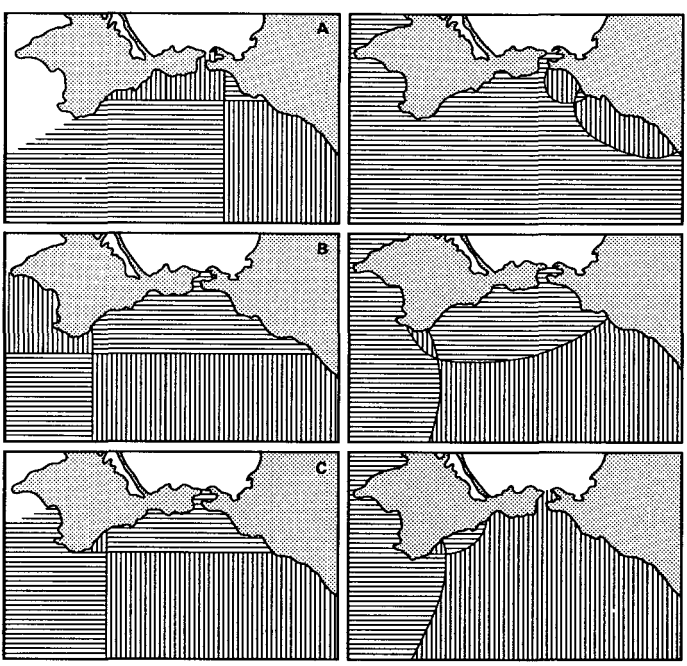


FIG. 5.10. Distribution of tsunami energy into 4 equal parts with radial rays for tsunamis of (a), July 12, 1966; (b), June 26, 1927; and (c), Sept. 11-12, 1927, without refraction (left) and with refraction (right). (Grigorash and Korneva 1972)

of June 26, 1972, the bulk of the energy traveled in three directions: (1) toward the southern coast of the Crimea; (2) into the area between Sudak and Anapa; (3) toward the southeast coast of the Caucasus and the northeast coast of Turkey. Very little energy reached the northwest coast of the Black Sea and the coast of Bulgaria.

Refractive focusing occurred on the south coast of Crimea where an increase in the tsunami amplitude could be expected. The pattern of the distribution of energy for the tsunami of Sept. 11–12, 1927 was quite similar to that of June 26, 1927.

The influence of refraction on the distribution of the tsunami energy can be seen more clearly in Fig. 5.10 where the total energy of the tsunami has been divided equally by rays 90° apart (corresponding to the four directions E, W, N, S). In the initial calculations it was assumed that the rays retain radial direction, and refraction was ignored (left side of Fig. 5.10). Calculation was made for the tsunamis of June 26, 1927; Sept. 11-12, 1927; and the Anapa earthquake tsunami of July 12, 1966.

To construct the right side of Fig. 5.10, refraction charts were used. The areas between the refracted rays (each contains one-fourth the tsunami energy) are shaded in the diagram. At the focus, the boundary rays of these areas take the same directions as those on the left side. Thus, the right side shows the deformation and rotation of the four energy zones because of refraction. The effect of the refraction can be best seen for the Anapa tsunami where three of the four areas point to the shores of the Caucasus.

The total tsunami energy at the focus can be computed, first approximately by ignoring refraction through Equation (2.14). Let this energy be denoted by E_t. Then the tsunami energy when refraction is taken into account can be expressed as:

$$E_{t_r} = K \cdot E_t \tag{5.1}$$

where

$$\frac{1}{K} = \frac{\partial \psi_r}{\partial \psi_0} = \text{coefficient of refraction} \tag{5.2}$$

Thus the left side of Fig. 5.10 shows the calculation with formula (2.14). Equation (5.1) was used along with the pattern on the right side of Fig. 5.10. However, $\Delta \psi_r$ in (5.2) was determined from detailed large-scale charts with several refracted rays moving from the focus to the observation point. The following table lists the energies of the tsunamis calculated with and without refraction (Grigorash and Korneva 1972).

	Earthquake magnitude (M)	E_t (*ergs*)	E_{t_r} (*ergs*)
June 12, 1966	5.25–5.5	6.5×10^{20}	2.0×10^{19}
June 26, 1927	5.5	2.5×10^{19}	2.25×10^{19}
Sept. 11, 1927	6.5	5.77×10^{19}	1.9×10^{20}

Thus, taking into account refraction of the tsunami waves, tsunami energy was lowered in the first case and increased in the third case. Grigorash and Korneva (1972) gave the following relation for energy of the Black Sea tsunamis.

$$\log E_{t_r} = -14.2 + 0.9\ M \tag{5.3}$$

Soloviev (1965a) described the tsunamis of Kamchatka and Kuril Islands. A devastating tsunami occurred on Nov. 4, 1952, following an earthquake in Kamchatka. The city of Severo-Kurilisk on the island of Maramushir was badly damaged. There was an initial withdrawal of water in the sea near this city and later the tsunami waves attained an amplitude of 10 m and many people were killed. Soloviev mentioned two similar tsunamis in 1737 and 1780.

Soloviev (1965b) described the tsunami following the Urup earthquake of Oct. 13, 1963. The tsunami attained amplitudes of 4–5 m and traveled east and south. There were several aftershocks, the strongest on Oct. 20, and a tsunami was generated by this aftershock also.

On July 12, 1966, an earthquake with epicenter in the Black Sea occurred near Anapa and the tsunami generated was the third known tsunami on the Black Sea coast of the Caucasus (Grigorash and Korneva 1969). The two earliest known cases are the Anapa earthquake tsunamis of Oct. 4, 1905, and Oct. 21, 1905, in the eastern part of the Black Sea. The following table compares the observed travel times of the tsunami with those calculated from the long-wave formula (Grigorash and Korneva 1969).

Grigorash and Korneva (1969) mentioned there were at least 115 earthquakes in the Crimea between 1292 and 1948 and, according to them, tsunamis definitely occurred on Oct. 11, 1869; May 31, 1908; Dec. 26, 1919; June 26, 1927; and Sept. 12, 1927. Tsunamis might have occurred also on July 25, 1875, and Jan. 8, 1902.

Tide station	Travel time (*min*)	
	Obs.	Calc.
Batumi	72	72
Feodosiya	109	120
Gelendzhik	27	42
Yalta	69	72

Figure 5.11 shows the epicenters of Crimean earthquakes. They were concentrated in a belt on the continental slope and their focal depths ranged from 10 to 40 km. The foci of the Crimean earthquakes are usually elongated; for example, for the earthquake of Dec. 26, 1919, the length of the focus was 40 km. Because the foci for the Crimean earthquakes are elongated, the tsunami source areas are also elongated.

According to Grigorash and Korneva, elongation of the focus can account for the difference between the observed travel time of a tsunami versus the travel time computed from the long-wave formula. If the tsunami generation area is elongated the computed travel time will be greater than the observed travel time.

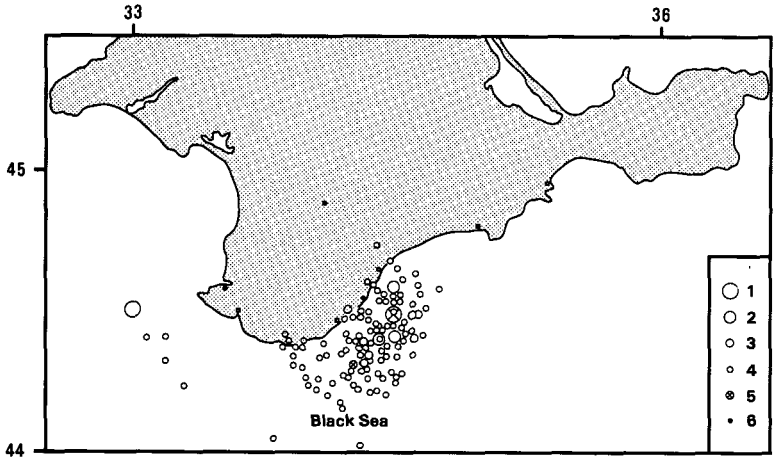


FIG. 5.11. Earthquake epicenters in the Crimea 1927–58: (1) $7.25 \geq M \geq 6.5$; (2) $6.25 \geq M \geq 5.25$; (3) $5 \geq M \geq 4.25$; (4) $M < 4.25$; (5) epicenters of June 26 and Sept. 12, 1927, earthquakes; (6) populated areas. (Grigorash and Korneva 1969)

This statement is supported by the following table, which shows the observed and calculated travel times for the tsunamis of June 26 and Sept. 12, 1927 (Grigorash and Korneva 1969).

Tide station	Travel time (*min*)			
	June 26 tsunami		Sept. 12 tsunami	
	Obs.	Calc.	Obs.	Calc.
Feodosiya	48	60	59	63
Yalta	76	90	35	60
Yevpatoriya	8	12	9	11

According to the authors, the distance covered by a tsunami in a time interval equal to the difference between the computed and observed time can be taken as an approximate measure of the linear dimension of the tsunami focus. The Crimean tsunami data also indicated that the linear dimension of the focus increases with the magnitude of the earthquake; the wavelength of a tsunami increases with the linear dimension of the focus.

Grigorash and Korneva also mentioned that the source areas of tsunamis generated in the Kamchatka region may have had linear dimensions ranging from 50 to 600 km. For example, for the tsunami of Nov. 4–5, 1952, in Kamchatka, the length of the focus was about 200 km.

There is little information on tsumamis on the Caucasian coast. The only one known with any certainty was on Oct. 4, 1905. Probably there was another on Oct. 21, 1905. In the literature mention was made of a Caucasian tsunami in the first century B.C. The most seismically active zone of the western Caucasus is the Anapa and Sochi areas (Fig. 5.12). The focal depths are small and range from 5 to 20 km. The eastern part of the Black Sea has also strong seismicity. A recent

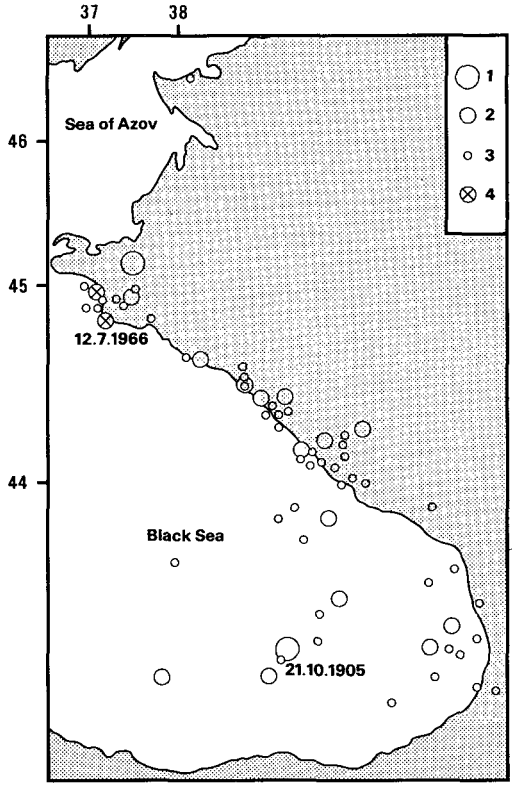


FIG. 5.12. Earthquake epicenters on Caucasian Black Sea coast and in eastern part of Black Sea 1834–1966; (1) $5 \leq M \leq 6.25$; (2) $4 < M < 5$; (3) $M < 4$; (4) epicenters of earthquakes accompanied by tsunamis. (Grigorash and Korneva 1969)

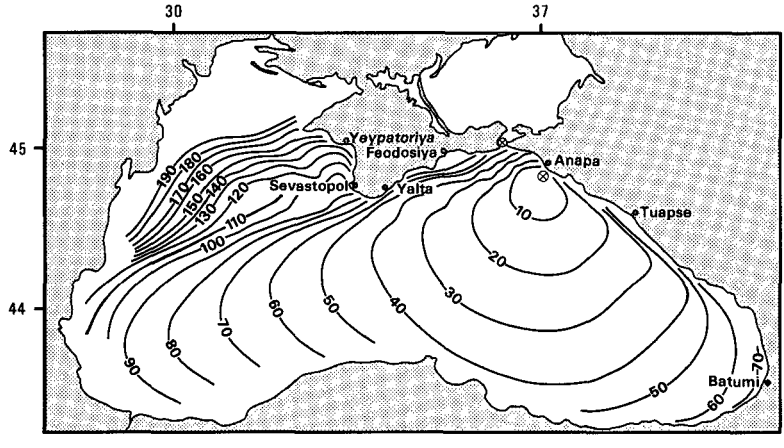


FIG. 5.13. Propagation of the July 12, 1966, tsunami in the Black Sea. (Grigorash and Korneva 1969)

TABLE 5.6. Tsunamis on the coast of New Zealand. (Laing 1954)

Date	Origin of tsunami	Remarks
Oct. 16, 1848	Wellington earthquake	abnormal sea level changes at Wellington, Nelson, and Wanganui
Jan. 23-24, 1855	Wellington earthquake	initial fall of 1.2 m followed by rise of 3.0 m at Wellington; similar occurrence at Nelson
Mar. 1856	–	large wave at Waiho River and Akaroa; tsunami observed at Awu Mar. 2 could have been same
May 11, 1877	probably Peru earthquake	tsunami originated in Peru; about 3.0 m amplitude in Waitangi River and .6 to .9 m at Gisborne; smaller amplitudes at Wellington and Fiji
Feb. 26, 1913	local earthquake	high water level at Westport
Nov. 11, 1922	probably Chilean earthquake	tsunami originated in Chile; observed at Port Chalmers and Timaru
Dec. 25, 1922	earthquake at Rangiora	several large waves at Castlecliff; amplitude of 38.1 cm at Leithfield Beach
Sept. 4, 1923	Kwanto earthquake in Japan Sept. 1 (Sept. 2 New Zealand time)	abnormal water level at Wellington on evening of Sept. 4 and morning of Sept. 5 (local time)
June 19, 1929	Westport earthquake	tsunami of 2.4 m amplitude at Karamla; no damage
Feb. 3, 1931	Napier earthquake	initial withdrawal of water at inner harbor at Napier
Sept. 16, 1932	local earthquake at Wairoa, Hawke's Bay	large wave (not verified) at Wairoa
Mar. 26, 1947	epicenter in the sea about 50 miles east of Gisborne	local tsunami; large waves on 12.9 km stretch between Whangara and Tatapouri; second wave highest with estimated amplitude of 9.1–10.7 m

tsunami was on July 12, 1966, following an earthquake at Anapa. This is the third known tsunami on the Black Sea coast of the Caucasus. Figure 5.13 shows the travel-time curves of this tsunami.

TSUNAMIS OF NEW ZEALAND AND AUSTRALIA

Laing (1954) described briefly the tsunamis that have been observed on the coast of New Zealand from 1848 to 1947. Table 5.6 is based on this list. Gilmour (1961) prepared a tsunami travel-time chart for New Zealand. Figure 5.14 shows the travel time of the tsunami originating at locations further than 1111.7 km from Wellington to reach a circle of 1111.7 km radius centered on Wellington. Figure 5.15 shows the travel time of a tsunami from a circle 1111.7 km radius from Wellington to the New Zealand coast. Gilmour (1967) gave a table of the time intervals between the time a tsunami propagating radially from a distant source

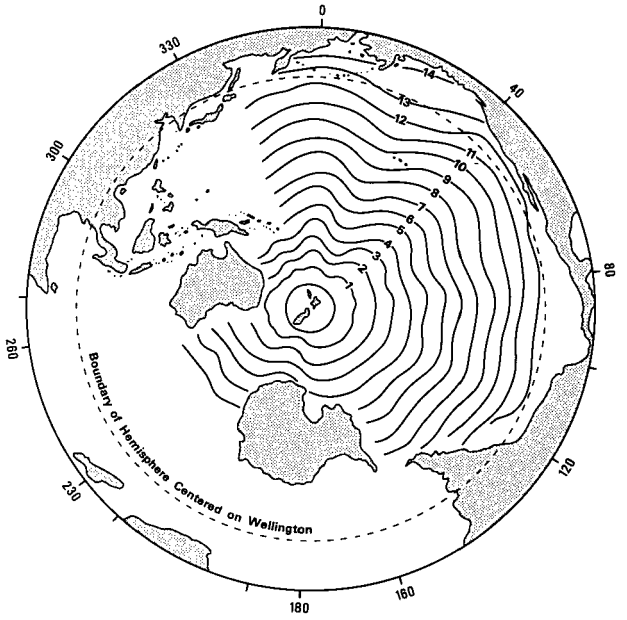


FIG. 5.14. Travel time (h) of tsunami waves originating at points further than 600 nautical miles from Wellington to reach a circle of 600 nautical miles radius centered on Wellington. (Gilmour 1961)

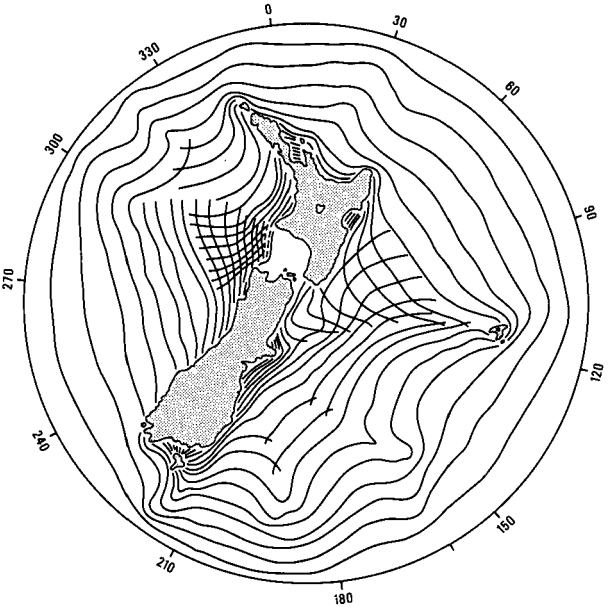


FIG. 5.15. Travel time of a tsunami wave from a circle 600 nautical miles radius from Wellington to the New Zealand coast, with successive positions of the wave at 10-min intervals from coincidence with the circle. (Gilmour 1961)

first reaches a position 1111.7 km from Wellington and the times when the tsunami first reaches any of the following selected places in New Zealand: New Plymouth, North Cape, Auckland, East Cape, Napier, Wellington, Lyttelton, Dunedin, Bluff, Milford Sound, and Westport.

The tsunami following the earthquake of May 9, 1877, on the Pacific coast of South America was observed in Australia at Sydney, Newcastle, Ballina, Richmond River, New South Wales, and Brisbane. The maximum amplitude in Sydney Harbor was 1.1 m, at Newcastle it was 0.8 m, and the period was 22 min. At Ballina the amplitude was 0.5 m. In the recorded history of Australia, the most damaging earthquake took place on Oct. 14, 1968 (Gordon 1970). The epicenter was near Meckering in the west part of Australia and the focal depth was only 8 km. The water-level records at Gnangara (19 km north of Perth) showed a forerunner.

5.2 Tsunamis in the Pacific Islands, Aleutians, and Alaska

Tsunamis in Hawaii

The following is a partial list of tsunamis that have done at least some damage in Hawaii. Following the earthquake of Nov. 7, 1837, off the Chilean coast, the tsunami generated was observed in the Hawaiian Islands with amplitudes to 2.4 m and periods of 15–30 min. The horizontal motion in Hilo Bay because of this tsunami was about 14.8 km/h (Jaggar 1931; Hitchcock 1911). The next observed tsunami was on May 17, 1841, and had a period of about 20 min. On Apr. 2, 1868, a tsunami accompanied a local volcanic earthquake; at least 46 people died and much destruction occurred along the shore from Kahuku to Kapopo. This tsunami had amplitudes of about 3.0 m at Hilo and 3.0–3.7 m at Kaupuna. There was a large negative amplitude (5.5 m) and the water level oscillated at least 8 times. At Lahaina on the island of Maui the tsunami period was 7–8 min and there were at least 13 waves. At Honolulu, the amplitude was 1.5 m.

Following an earthquake with epicenter near Arica, a tsunami was observed in Hawaii on Aug. 13, 1868. This tsunami took about 14 h to travel to Hawaii and although the amplitudes in Peru were 15.2–18.3 m, in Hawaii the maximum amplitude was 4.6 m. Considerable damage occurred at Waikea and Kapuhie.

After a volcanic eruption of the summit crater of Mauna Loa, a tsunami of about 1.2 m amplitude was observed at Hilo on Aug. 27, 1872. An earthquake occurred in Peru and Chile on May 9, 1877, and the tsunami generated arrived at Hilo on the morning of May 10 with an amplitude of over 3.7 m. Five people and 17 animals died.

The tsunami caused by an earthquake in the Gulf of Alaska arrived at Hilo on Feb. 3, 1923, 7 h after the earthquake. Destruction occurred at Hilo and Kahului. The amplitude at Hilo was greater than 6.1 m and one person died. It appears that from 1918 to 1929, at least another eight tsunamis occurred. Those definitely identified were: the Kamchatkan earthquake tsunami of Sept. 7, 1918, which did some damage at Hilo; the Chilean earthquake tsunami of Nov. 11, 1922; the Kamchatkan earthquake tsunami of Apr. 13, 1923; and the locally generated tsunami on Jan. 24, 1926.

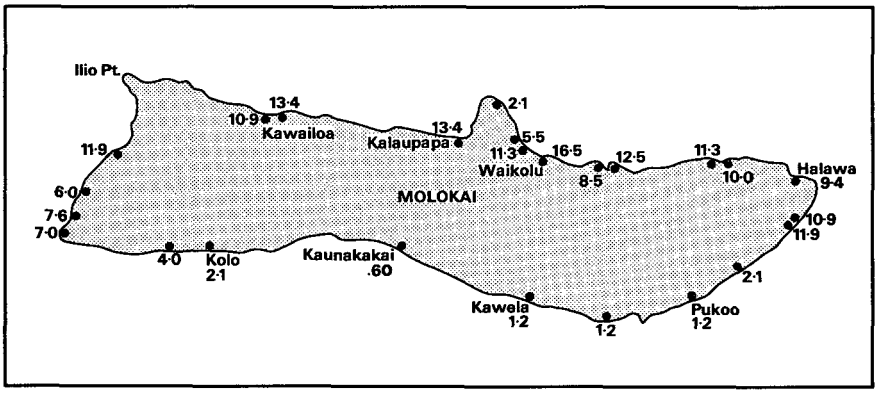


FIG. 5.16. Molokai Island, showing heights (m) above lower low water, reached during April 1, 1946, tsunami. (Macdonald et al. 1947)

The tsunami following an earthquake with epicenter roughly 161 km south of Amukta Island in the Aleutian Island chain attained an amplitude of about 41 cm and a period of about 15 min at Hilo (Jaggar 1929). Following an earthquake near Rennel Island (an island in the southernmost group of British Solomon Islands, southeast of New Guinea), a tsunami was generated. Fifty people died on the island of San Christoval. This tsunami was observed at Hilo with an amplitude of 0.3 m and period of 15 min.

The tsunami following the Aleutian earthquake of Apr. 1, 1946, killed 173 people and caused so much damage to property in Hawaii that the U.S. Coast and Geodetic Survey decided to establish a tsunami warning service based at Honolulu. Shepard et al. (1946) investigated this tsunami and found that the amplitude varied from 2.1 to 16.5 m in a distance of only 8 km. Figure 5.16 shows the tsunami amplitude distribution along the coast of Molokai.

Powers (1946) gave 10–15 min as the tsunami period at Hilo. The tsunami traveled to Hilo from the Aleutians (3910 km) with an average speed of 763 km/h. Green (1946) analyzed the tide-gage records of this tsunami for all tide stations between 57°N and 33°S and concluded that the observed travel times agreed fairly well with the travel times computed from the long-wave formula. He also stated that the initial rise was only about a third of the subsequent fall and this might be the reason why people usually speak of an initial withdrawal. The average tsunami period at stations closer to the epicenter was 15.6 min, whereas for stations farther away the period was 17.4 min.

The epicenter of the Kona earthquake was in the Island of Hawaii and most of the destruction occurred in the Kona area, on Aug. 21, 1951 (Macdonald and Wentworth 1951). At Napoohoo the water level fell by 1.2 m and then rose by 0.6 m. The negative and positive amplitudes at Milolui were, respectively, 0.9 and 1.1 m. The Kamchatkan earthquake tsunami arrived in Hawaii with amplitudes to 3.5 m and periods of about 17 min. Most damage occurred near Hilo. Figure 5.17 compares the tsunami amplitudes on the island of Hawaii of the 1946 Aleutian

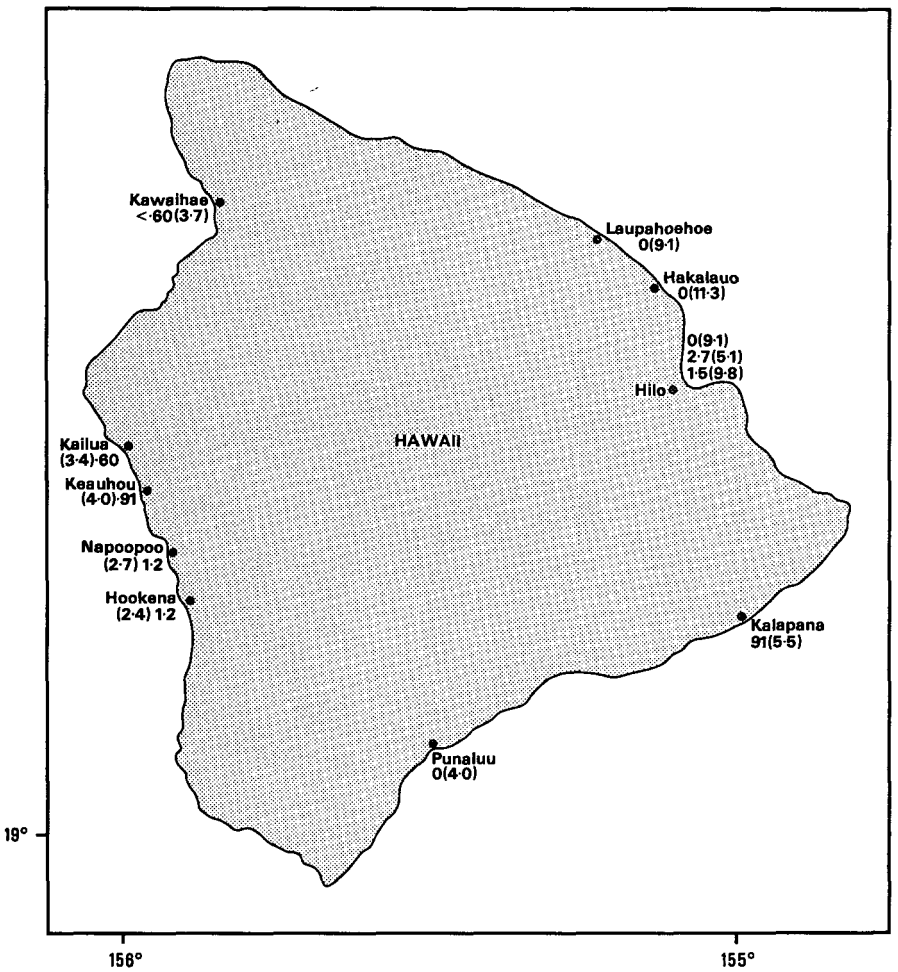


FIG. 5.17. Hawaii, showing heights reached by waves of tsunamis Nov. 4, 1952, and April 1, 1946. Larger numbers are heights of 1952 tsunami, smaller numbers in parentheses are heights of 1946 tsunami. Heights are in meters above lower low water. (Macdonald and Wentworth 1954)

earthquake tsunami and the 1952 Kamchatkan earthquake tsunami. This instance of the 1952 earthquake tsunami presented one of the few recorded instances of the simultaneous occurrence of a storm surge and a tsunami. This interaction occurred at Keaukou on the island of Hawaii.

The epicenter of the Aleutian earthquake of Mar. 9, 1957, was at 51.3°N, 175.8°W and the time was 14 h 22 min 27 s, GCT. The resulting tsunami caused great damage on the islands of Kaui and Oahu and slight damage in the other Hawaiian Islands. The amplitudes on Hawaii were somewhat intermediate to those of the Aleutian earthquake tsunami of Apr. 1, 1946, and the Kamchatkan earthquake tsunami of Nov. 4, 1952.

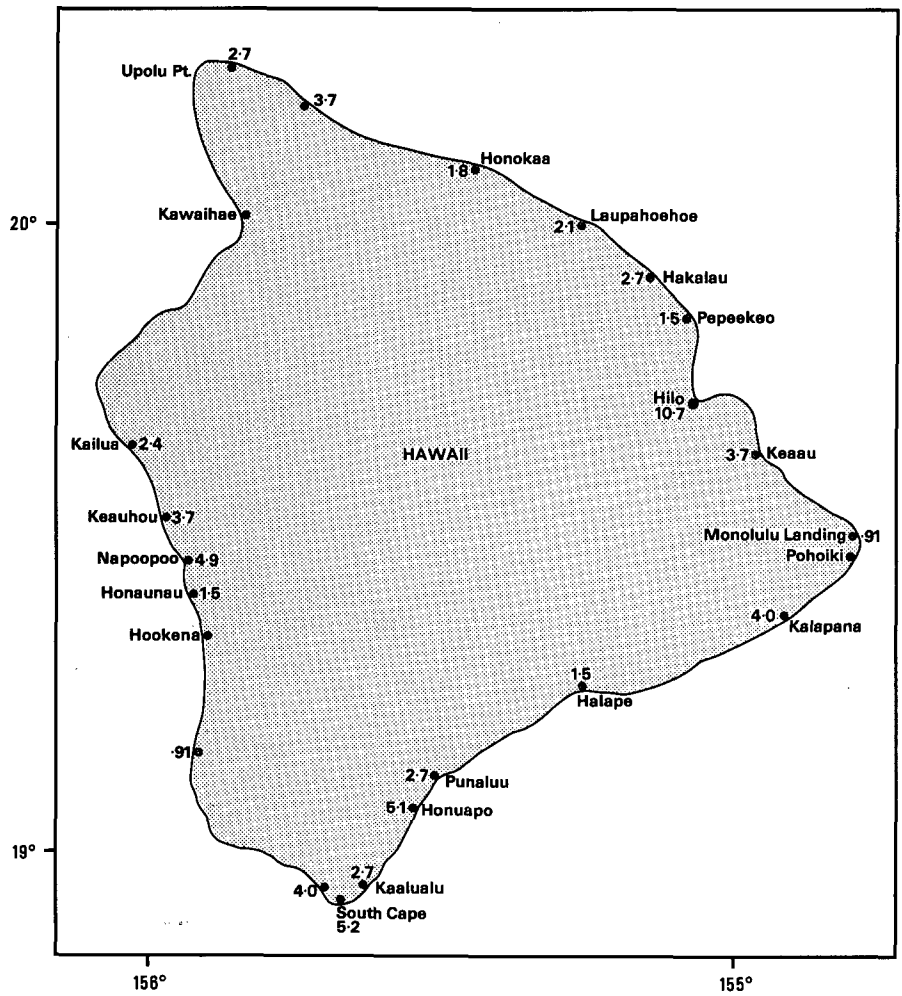


FIG. 5.18. Hawaii, showing run-up heights (m) above mean lower low water during 1960 tsunami. (Cox and Mink 1963)

The Chilean earthquake tsunami of May 22, 1960, arrived at the Hawaiian Islands May 23, at 0100 (Reese and Matlock 1968). Most damage occurred at Hilo and some at Kahului on the Island of Maui. According to Cox and Mink (1963) 61 people died and 282 were injured. This is rather strange because tsunami warning was given to the public 5 h in advance. This unfortunate instance shows the need to educate the public about the danger of tsunamis and to issue unambiguous warnings (see Chapter 6). Figure 5.18, 5.19, 5.20, respectively, show the tsunami amplitudes on the islands of Hawaii, Maui, and Kauai. Figure 5.21 compares the amplitudes along the island of Oahu for the 1946 Aleutian, for the 1952 Kamchatkan, for the 1957 Aleutian, and the 1960 Chilean earthquake tsunamis.

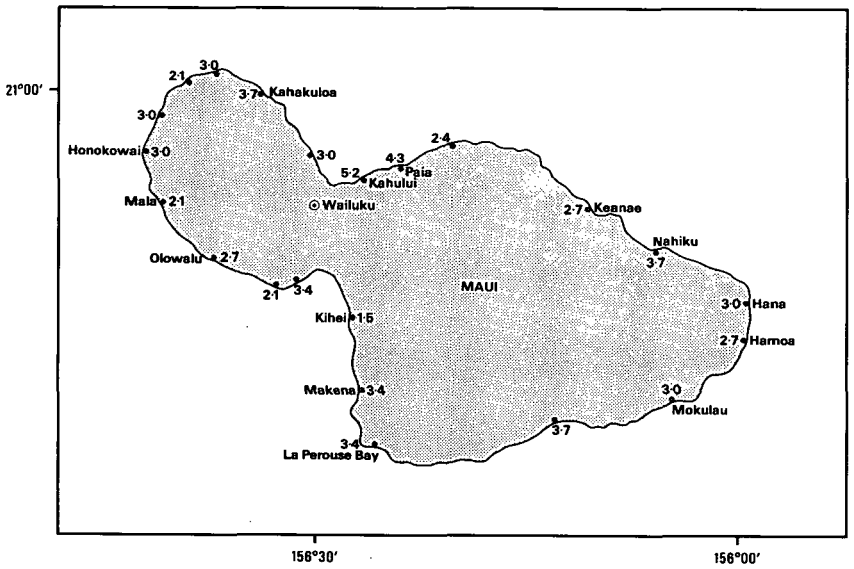


FIG. 5.19. Maui, showing run-up heights (m) above mean lower low water during 1960 tsunami. (Cox and Mink 1963)

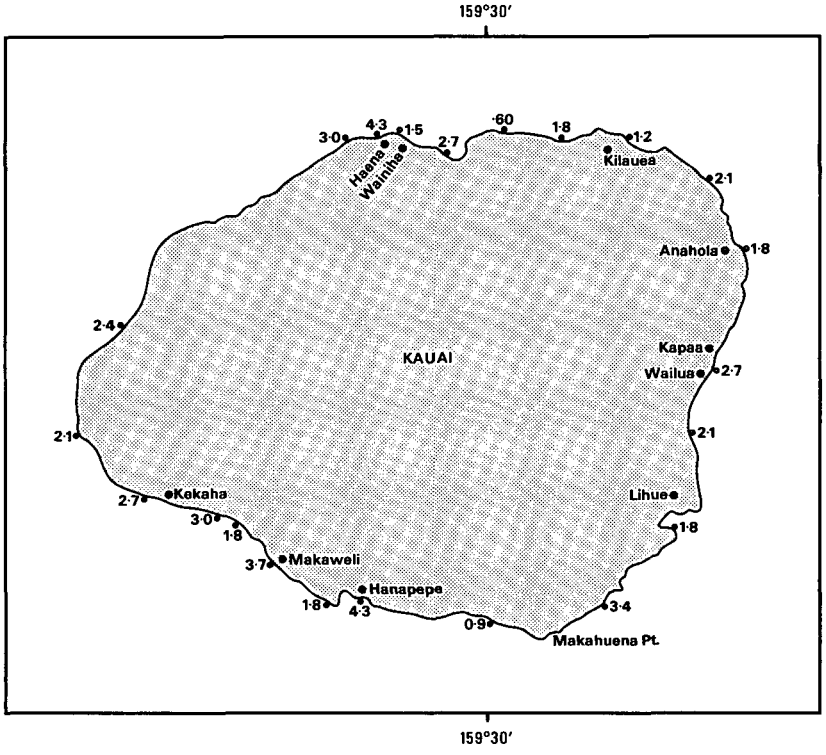


FIG. 5.20. Kauai, showing run-up heights (m) above mean lower low water during 1960 tsunami. (Cox and Mink 1963)

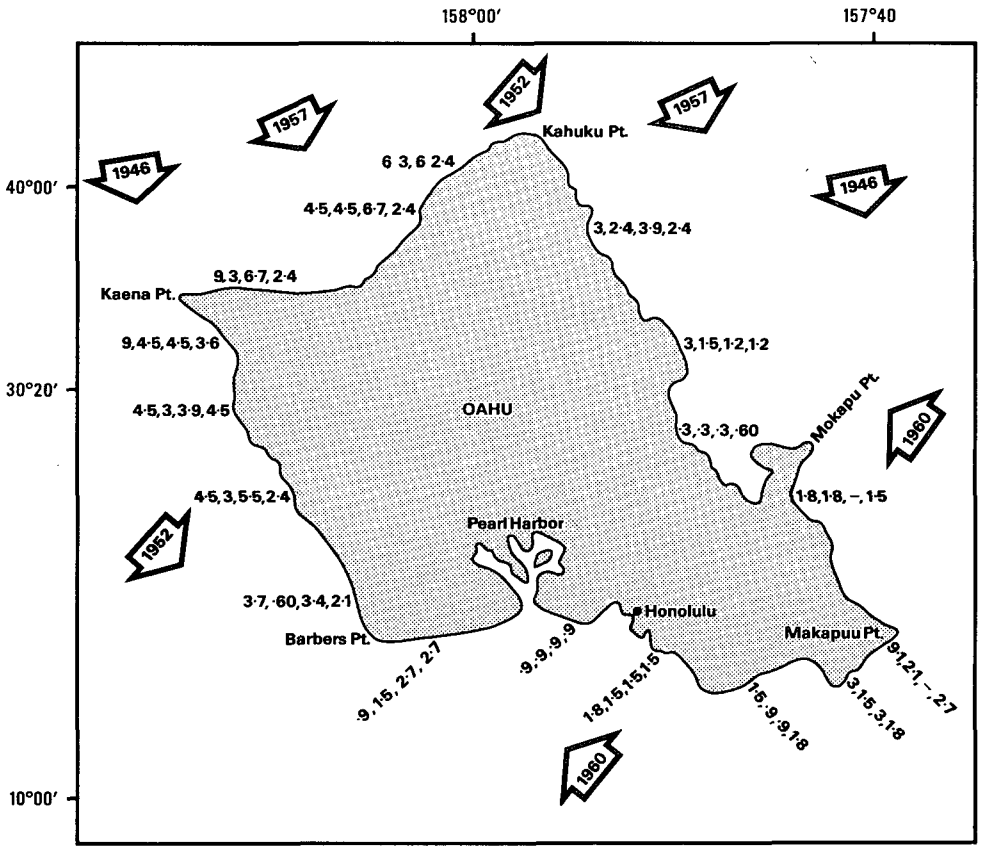


FIG. 5.21. Oahu, showing run-up heights (m) and directions of approach of 1946, 1952, 1957, and 1960 tsunamis, → direction of travel. (Cox and Mink 1963)

In concluding this subsection, Hawaiian tsunamis in general will be briefly discussed. According to Macdonald et al. (1947) the average frequency of tsunamis in Hawaii is more than one per year. However, not all cause damage. Between 1819 and 1947, 27 significant tsunamis occurred, but only 5 caused severe damage (Table 5.7). Hatori (1963) compared the tsunami amplitudes at several locations on the Hawaiian Islands for different tsunamis that originated elsewhere (Table 5.8).

Some specific points of relevance to tsunamis in Hawii will be briefly discussed. Adams (1973) developed the so-called "conditional expected tsunami inundation" (CETI) charts for the Hawaiian Islands. These maps are an improvement over the potential tsunami inundation charts used by the Hawaii Civil Defense to evacuate people from coastal areas in the event of a tsunami. The potential tsunami inundation is not a precisely defined upper bound, hence, tends to be on the conservative side. The additional information used in CETI is available during the course of an actual tsunami warning, i.e. the location of the epicenter and observations of the tsunami waves within a few hundred kilometers off Hawaii. Adams gave tables

TABLE 5.7. Hawaiian tsunamis during 1819–1946. (Macdonald et al. 1947)

Date	Source (nearest coast)	Damage in Hawaii	Avg. speed of waves (*km/h*)
Apr. 12, 1819	unknown	unknown	-
Nov. 7, 1837	South America	severe	-
May 17, 1841	Kamchatka	small	-
Apr. 2, 1868	Hawaii	severe	-
Aug. 13, 1868	South America	severe	-
July 25, 1869	South America (?)	moderate	-
Aug. 23, 1872	Hawaii	small	-
May 10, 1877	South America	severe	-
June 15, 1896	Japan	none	769.2
Aug. 9, 1901	Japan (?)	none	-
Jan. 31, 1906	unknown	none	-
Aug. 16, 1906	South America	small	-
Sept. 7, 1918	Kamchatka	small	733.8
Apr. 30, 1919	unknown (distant)	none	-
Nov. 11, 1922	South America	none	724.2
1923	Kamchatka	moderate	695.2
Apr. 13, 1923	Kamchatka	none	704.9
Nov. 4, 1927	California	none	743.5
Dec. 28, 1927	Kamchatka	none	704.9
June 16, 1928	Mexico	none	743.5
Mar. 6, 1929	Aleutian Is.	none	791.8
Oct. 3, 1931	Solomon Is.	none	719.4
Mar. 2, 1933	Japan	small	767.6
Nov. 10, 1938	Alaska	none	798.2
Dec. 7, 1944	Japan	none	684.0
Apr. 1, 1946	Aleutian Is.	severe	788.6

of the CETI for the islands of Hawaii, Kauai, Maui, Molokai, and Oahu. For each island, the CETI was given for a tsunami of magnitude 4 (Imamura–Iida scale) coming from any of the three sectors of the Pacific Ocean basin: northwest, northeast, and southeast. Adams (1967) also showed how the decision-making theory concepts and systems analysis could be profitably used in the tsunami warning service.

Loomis (1972) examined the water-level distribution on the coasts of the Hawaiian Islands following the 1964 Alaskan earthquake tsunami and offered the following comments: the tsunami caused little damage in Hilo because the successive crests of the tsunami rapidly became out of phase with the natural oscillations of the Hilo Bay. Low coherence of the tsunami at Midway Island, Honolulu, Kahului, and Hilo does not support the hypothesis that a coherent source of waves was emanating from the Gulf of Alaska. Reflections of the tsunami from North America, Kamchatka, Mexico, and Australia can be identified in the energy decay curve. These points need elaboration.

TABLE 5.8. List of the wave heights (meters) above mean low water for Hawaiian tsunamis. (Hatori 1963)

	Sanriku 1896	Sanriku 1933	Aleutian 1946	Kamchatka 1952	Aleutian 1957	Chile 1960
Hilo	2.4	.6～.9	8.5～9.1	0～2.7	2.4～4.0	4.0～5.8
Keaau			7.3	0	2.4	3.7
Honolulu landing						4.3
Cape Kumukahi					.9	.9
Pohoiki			2.7		2.1	1.8
Opihikrad						1.8
Kaimu			6.0		3.0	4.0
Kalapana			5.5	.9	2.1	2.1
Halape				0		1.5
Punaluu	3.7		4.0	0	2.1	3.4
Honuapo	3.7		4.3		2.1	5.1
Kaalualu	3.7					5.1
South Point			6.0		3.0	2.7～4.0
Milolii			6.1		1.5	.9
Hookena	2.4		2.4	1.2	2.1	2.1
Honaunau			2.1		1.8	1.5
Kauualoa	9.1					
Napoopoo	9.1	5.3	2.7	1.2	2.1	3.0
Keauhou	9.1		4.0	.9	2.1	3.7
Kahaluu						2.4
Kailua	2.4(9.1)		3.4	.6	1.5	2.4
Kawaihae			3.7	<.6	1.5	2.7
Mahukona			4.3		2.1	1.2
Upolu Point			6.0		2.4～3.4	2.1～2.7
Pololu Valley			10.4～16.8		4.6～9.8	3.0～3.7
Waipia Valley			12.2		7.0	2.4
Honokpa			8.5		3.0	1.8
Laupahoehoe			9.1		3.0	2.1
Hakalau			11.3		3.0	2.7
Honomu			11.3		3.4	3.7
Pepcekeo			8.2		3.7	1.5
Onomea			10.4		5.2	3.4
Papaikou			10.7		2.7	2.7

The tsunami record at Mokuoloe Island (on Oahu) showed five large waves with crests separated by an average period of 100 min. This can be interpreted as the low-pass filter effect of a large shallow bay enclosed by a reef. The tsunami waves arrived at Hilo, Honolulu, and Kahului with a period of 23 min. This period agreed with the period of natural oscillation at Kahului, hence, resonance amplification of the tsunami occurred. However, the period of natural oscillation of Hilo Bay was 30 min and as this did not agree with the incoming tsunami period, resonance amplification did not take place at Hilo.

Loomis stated that the data in Hawaii for this 1964 tsunami does not support the hypothesis of the "inverse tsunami problem" (Chapter 2) which assumes it is possible to determine the deepwater signature of a tsunami based on coastal records. Specifically, Loomis tested the hypothesis that the water in the Gulf of Alaska was set into oscillation following the earthquake and this oscillation in the Gulf fed energy into the Pacific Ocean at a constant frequency (or frequencies).

To test this coherent source hypothesis, the coherence and quadrature spectra between all pairs of the stations at Midway, Honolulu, Kahului, and Hilo were calculated from a 24-h record beginning 6 h after the first arrival of the tsunami. These spectra did not support the idea of a coherent source.

Figure 5.22 shows the energy decay curves for Hilo and Honolulu for the 1964 Alaskan earthquake tsunami. Loomis considered the tsunami energy in the 11- to 33-min band, for the following reasons. The lower limit of 11 min was set because both Honolulu and Hilo harbors have natural periods less than 11 min and sustained harbor oscillations could mask the tsunami energy. The upper bound of 33 min was set because this period is well removed from the tidal periods and is about the longest period that can be contained in a window of effective 1-h width, necessary to give the detailed time dependence of energy decay desired. For the first part of the decay curve, the decay constants for Honolulu and Hilo were, respectively, 12.5 h^{-1} and 12.2 h^{-1}.

Loomis attempted to identify the sources of some peaks in the energy decay curve. If the tsunami travel time from Honolulu to Hilo were about 1 h, reflections arriving on the Hilo–Honolulu axis would be separated by 1 h, whereas those arriving perpendicular to the axis would arrive simultaneously. Thus, the peak at Honolulu (0216 h) and at Hilo (0300 h) could have been reflections from the coast of Alaska. The following table summarizes the possible reflections.

Peak at Honolulu (*h*)	Peak at Hilo (*h*)	Coast producing reflection
0216 (Mar. 28)	0300 (Mar. 28)	Alaska
0530	0530	Washington–Oregon
0830	0900	Northern Japan and Kamchatka
1000	0900	Mexico
2000	2000	Australia–New Guinea
1600 (Mar. 29)	1600 (Mar. 29)	Antarctica

Loomis (1966) studied the spectra at several stations in Hawaii for the tsunamis of Oct. 13, 1963; Oct. 20, 1963; and Mar. 28, 1964. He found that a given tsunami produced spectra that were somewhat similar for the low frequencies (i.e. up to 1.6 C/KS) at nearby stations, but for stations as far apart as Hilo and Honolulu (338 km), this similarity disappeared. Only qualitative similarities can be seen in the spectra at a given station for different tsunamis. The time changes in the spectra at a given station do not appear to support the hypothesis of a simple local response function.

The Chilean earthquake tsunami of May 1960 produced bores on the Sanriku coast of Japan as well as in Hilo Bay. In fact, the greatest heights observed in Hawaii occurred at Hilo. The third wave was developed into a bore in the bay and attained horizontal velocities of 15 m/s and vertical amplitude of 10 m (Cox and Mink 1963). Figure 5.23, 5.24, and 5.25 show some damage done by this tsunami at Hilo.

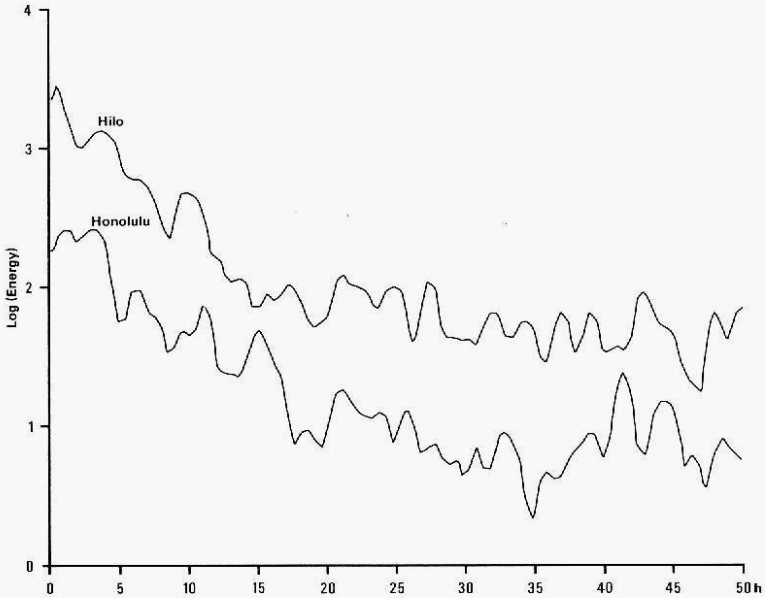


FIG. 5.22. Energy decay at Hilo and Honolulu for Alaskan earthquake tsunami March 28, 1964. Energy is in cm^2 in the frequency band of 0.03–0.09 cycle min^{-1}, averaged over a cosine window of effective width 1 h. (Loomis 1972)



FIG. 5.23. Chaotic mass of debris, including automobiles, houses, and machinery, left by May 23, 1960, Chilean earthquake tsunami at Hilo. (Cox and Mink 1963)



FIG. 5.24. Large building carried across a street by May 23, 1960, Chilean earthquake tsunami, in the Waiakea section of Hilo. (Cox and Mink 1963)



FIG. 5.25. Remains of a residential area in Hilo after May 23, 1960, Chilean earthquake tsunami. (Cox and Mink 1963)

Tsunamis of the Aleutian Islands and Alaska

Adams (1972) suggested that the Aleutian earthquake tsunami of Apr. 1, 1946, was a rare event and considered it to be at least a 1-in-2000 years event. This tsunami originated near the Unimak Island and traveled distances of 11,263 km and caused great damage.

The seismicity of the region consisting of Amchitka Island received considerable attention in the late 1960s and the early 1970s, because of the underground nuclear explosions "Milrow" and "Cannikan" conducted there (see Chapter 2). Hwang et al. (1970b) studied the tsunamis in the Amchitka Island region. In particular, they considered the tsunamis generated by the Andreanof earthquake of 1957, the Chilean earthquake of 1960, the Alaskan earthquake of 1964, and the Rat Island earthquake of 1965.

Cox and Pararas-Carayannis (1969) prepared a catalog of tsunamis in Alaska and Table 5.9 is based on this information (a recent revised edition prepared by Cox et al. 1976 is also available). Following the Alaskan earthquake of July 10, 1958, (GCT) a rockslide was triggered into the deep water in Gilbert Inlet, one of the two arms of Lituya Bay (a T-shaped tidal inlet on the northeast shore of the Gulf of Alaska). The rockslide with a volume of 3.06×10^7 m^3 caused the water to surge to an altitude of 530 m on a spur opposite the point of impact, and generated a gravity wave that swept 11.3 km to the mouth of the bay at a speed probably between 156 and 209 km/h. The surge and the wave destroyed the forest on the shores over an area of 10.4 km^2, sank two or three fishing boats, and took two lives (Miller 1960).

The earthquake of Mar. 28, 1964, with epicenter in Prince William Sound, Alaska, was one of the most damaging in the history of the North American continent. It had a magnitude of about 8.4 and the tsunami generated caused great damage, mostly in North America. Spaeth and Berkman (1967) described this tsunami and reproduced some tidal records. The number of casualties in Alaksa, Oregon, and California due to this tsunami was 122. Table 5.10 compares the maximum water level at several stations for different tsunamis. Wilson and Tørum (1968) made a thorough evaluation of this tsunami from an engineering point of view. The committee on Alaska earthquake of the Division of Earth Sciences, National Research Council of the U.S. National Academy of Sciences prepared several volumes dealing with all aspects of this earthquake and the resulting tsunami. Figure 5.26 to 5.33 show the damage in different locations.

Tsunamis in Other Pacific Islands

Repetti (1946) gave a list of Philippine earthquakes and tsunamis from 1589 to 1899. During this period there was hardly any instrumentation in use. Table 5.11 lists some tsunamis during this period and was prepared from the information in Repetti's paper. Masó (1918) described the destructive tsunami due to the earthquake of Aug. 15, 1918, in the island of Mindanao. The epicenter was in the Celebes Sea. The generated tsunami swept the coast between Lebak and Glan. Maximum height of the tsunami was 7.3 m at some locations; at Glan, its height was 5.5 m. Several people were killed in the Sarangani Bay area. At Port Lebak, the tsunami

TABLE 5.9. Some important tsunamis of Alaska.

	Origin of earthquake	Remarks
July 22, 1788	Alaskan Peninsula	tsunami at Shumagin Island, Kodiak Island, Three Saints Bay, Unga, Sanak, and Alaskan Peninsula; several persons drowned
?, 1827	Eastern Aleutians near Unimak	tsunamis at Chernabura Island
?, 1845	Yakutat Bay	tsunamis at Yakutat Bay; 100 people killed
Aug. 29, 1878	Eastern Aleutians near Unalaska	village of Makushin destroyed by earthquake and tsunami
Sept. 10, 1899 (Coffman and Von Hake (1973) gave date as Sept. 3)	Yakutat Bay	tsunami in Yakutat Bay, Disenchantment Bay; maximum height 10 m; perhaps an independent slump
July 4, 1905	Yakutat Bay	in Russelford wave height $4\frac{1}{2}$–6 m
Feb. 23, 1925	Port Valdez	in Valdez, boardwalk destroyed by waves
Dec. 7, 1944	Kii Peninsula (Japan)	tsunami height 0.3 m in Massacre Bay and 0.1 m in Sweeper Cove; tsunami caused 998 deaths in Japan
Apr. 1, 1946	Eastern Aleutians	tsunami amplitude in Unimak Island 30 m, 5 people killed; at Yakutat and Sitka maximum amplitudes 0.2 and 0.4 m; attained amplitudes of 3.5 m at Santa Cruz and Half Moon Bay, Calif.; 1 person killed
Nov. 5, 1952	East Kamchatka	tsunami attained amplitudes of a fraction of a meter in Kodiak, Women's Bay, Seward, Yakutat, Juneau, and Sitka; amplitude of 1.5 m observed in Aleutians
Mar. 9, 1957	Unimak Island	tsunami probably attained maximum amplitude of 15 m near Scotch Cap in Unimak Island; at Sweeper Cove maximum amplitude 4 m; at Massacre Bay and Dutch Harbour amplitudes of 0.6 and 0.7 m
July 9, 1958	Lituya Bay	wave amplitude 525 m (a splash of water); 2 deaths
May 22, 1960	South Chile	at Sitka, Yakutat, and Kodiak amplitudes were 0.6, 0.9, 0.7 m; amplitude greater than 1.8 m at Massacre Bay; at Dutch Harbour and Sweeper Cove, 0.8 and 1.5 m, respectively
Mar. 27, 1964	Prince William Sound	in Valdez amplitude more than 6 m, 31 deaths; Passage Canal, at Whittier, maximum amplitude 9.2 m, 13 deaths; Chenega, Prince William Sound, amplitude 16.6 m, 23 deaths; Seward, amplitude 7.0 m, 12 deaths; Alaska, 20 deaths, Kodiak Island, amplitude about 20 m; about 9 m at Old Harbour and Kaguyak; about 6 m at Kodiak and Women's Bay; about 4 m at Cordova and Cape Yakatag; over 2 m at Yakutat and Sitka; about 1 m at Juneau and Seldoval
Feb. 3, 1965	Rat Island (Aleutians)	tsunami of 3.2 m at Massacre Bay and 0.2 m at Dutch Harbour

TABLE 5.10. Comparison of maximum recorded rise or fall (meters) at selected stations for Alaskan earthquake tsunami of Mar. 28, 1964, and earlier tsunamis, (Spaeth and Berkman 1967)

	1946	1952	1957	1960	1964
Massacre Bay, Alaska		2.4	1.2	3.4	8.5
Sweeper Cove, Alaska		2.1		2.1	.58
Yakutat, Alaska		.55	.67	1.6	2.3
Sitka, Alaska	.79	.46	.79	.91	4.4
Prince Rupert, B.C.				.12	2.7
Tofino, B.C.	.58	.61		1.4	2.5
Neah Bay, Wash.	.37	.46	.30	.73	1.4
Crescent City, Calif.	1.8	2.0	1.3	3.3	4.0
San Francisco, Calif.	.52	1.0	.52	.88	2.3
Santa Monica, Calif.		1.1	.91	2.8	2.0
Los Angeles, Calif.	.76	.61	.64	1.5	.97
La Jolla, Calif.	.43	.24	.61	1.0	.67
San Diego, Calif.	.37	.70	.46	1.4	1.1
Ensenada, Mexico			1.0	2.5	2.4
Salina Cruz, Mexico		1.2	.36	1.6	.85
La Libertad, Ecuador		1.9	1.0	1.9	1.3
La Punta, Peru		1.9	.27	2.2	1.9
Antofagasta, Chile	1.8	1.4	.91	1.4	1.0
Valparaiso, Chile	1.5	1.8	2.0	1.7	1.9
Talcahuano, Chile		3.7	1.4	5.1	1.6
Hilo, Hawaii		2.4	2.7	3.0	3.8
Honolulu, Hawaii	1.2	1.3	.97	1.7	.82
Midway Island		2.0	.82	.60	.27
Johnston Atoll		.43	.21	1.0	.30
Pago Pago Harbor, Amer. Samoa		1.8	.43	1.6	.40
Wake Island		.52	.73	1.0	.15
Ft. Denison, Sydney Harbour, Aust.				.82	.30
Coffs Harbour, N.S.W., Aust.				1.0	.06
Miyako Jima, Japan				3.1	.33
Aburatsu, Japan				2.0	.73
Shimizu (Tosa) Japan				2.7	.55
Kushimoto, Japan				3.2	.79
Toba Ko, Japan				1.8	.24
Mera, Japan				2.4	.58
Hanasaki, Japan				2.5	.67



FIG. 5.26. View of part of Kodiak City showing destruction caused by March 1964 Alaskan earthquake tsunami. (Wilson and Tørum 1968) (Photo by Alf Madsen)



FIG. 5.27. Damaged road bridge on the Deltaic area at the southwest head of Women's Bay, following March 1964 Alaskan earthquake tsunami. (Wilson and Tørum 1968) (Photo by U.S. Navy)

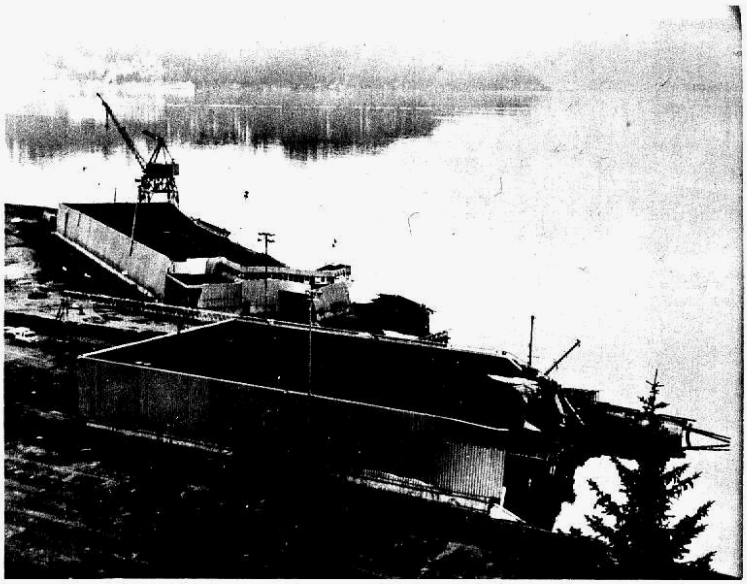


FIG. 5.28. Remains of the Alaska railroad docks at south end of Seaward after earthquake and seismic sea waves March 1964. (Wilson and Tørum 1968) (Photo by Irvin Cook, Anchorage)

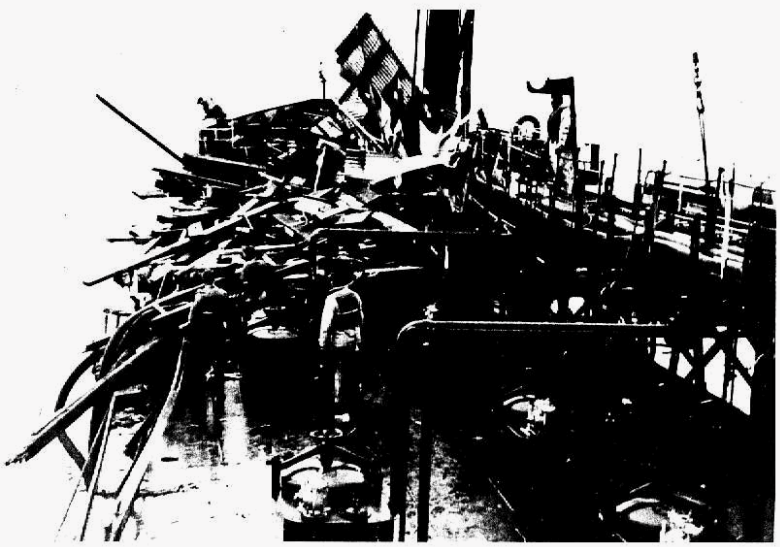


FIG. 5.29. Deck of tanker *Alaska Standard* with wreckage from Standard Oil Company dock at Seaward, Alaska, following March 1964 tsunami. (Wilson and Tørum 1968) (Photo by Standard Oil Company of California)

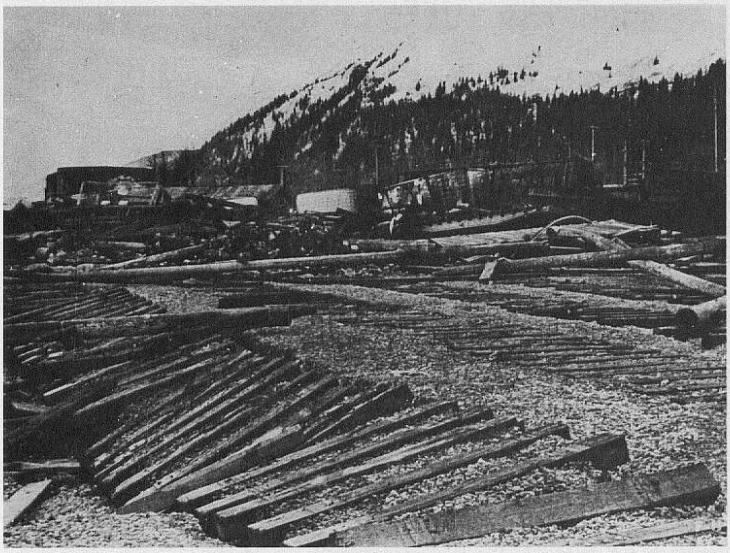


FIG. 5.30. Part of the Alaska railroad freight yard showing tracks stripped of rails following 1964 Alaskan earthquake tsunami. (Wilson and Tørum 1968) (Photo by Dave Thompson, Seward)

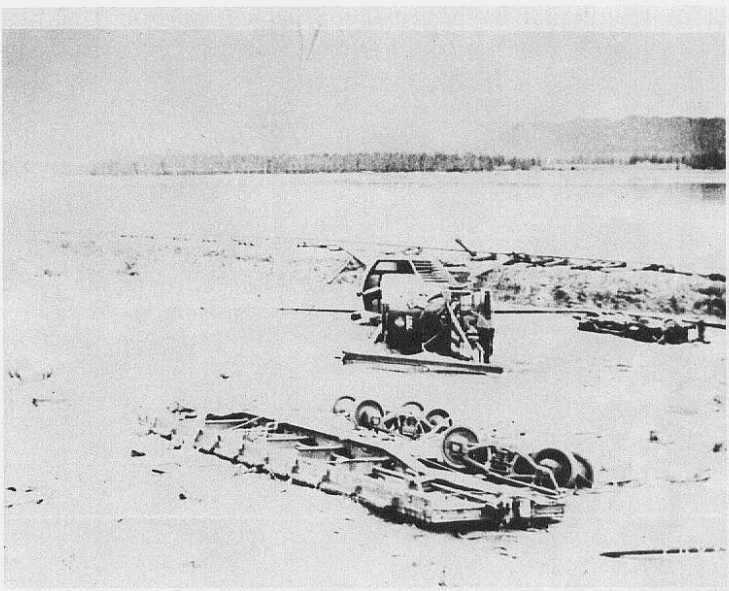


FIG. 5.31. One hundred and fifteen ton locomotive transported and overturned by March 1964 tsunami. (Wilson and Tørum 1968) (Photo by Dave Thompson, Seward)



FIG. 5.32. Chaos of wreckage left by 1964 Alaskan earthquake tsunami at the northwest end of head of Resurrection Bay (Wilson and Tørum 1968) (Photo by U.S. Army)



FIG. 5.33. View of Alaska Ave., Valdez after March 1964 tsunami. (Wilson and Tørum 1968) (Photo by U.S. Army)

TABLE 5.11. Philippine tsunamis during the period 1589–1899.

	Remarks
Sept. 1627	earthquake in Province of Cagayan; in Camarines a tsunami caused some destruction
Dec. 21, 1636	earthquake in western Mindanao near Punta Flecha; a mountain fell into the sea
July 1653	earthquake in island of Mindora; tsunami observed in Straits of San Bernardino
? 1744	earthquake in northern Luzon; a tsunami mentioned
Nov. 9, 1825	earthquake near Manila; water level fluctuations observed in a river
Sept. 16, 1830	earthquake at Manila; overflowing occurred in a river
Sept. 21, 1897	earthquake at Mindanao, Sulu Archipelago, and southern Visayan Islands; sea rose and fell near Zamboanga; tsunami also observed at Jolo, Isabela, San Roman, Recodo, Sibuguey Gulf

amplitude was 1.8–2.4 m and six people were killed. Truby (1971) described the areas affected by the tsunami following the Krakatoa eruption of August 1883.

The Suvan earthquake of Sept. 14, 1953, had its epicenter at 18°30′S, 178°30′E. The tsunami caused by the earthquake itself was small but the tsunami created by the landslide following the earthquake attained amplitudes to 1.8 m (Houtz 1962). The pattern of cable breaks at the bottom of the sea gave credence to the argument that the tsunami was caused by a landslide following the earthquake and not directly by the earthquake itself.

Keys (1963) described the Chilean earthquake tsunami of May 22, 1960, as observed in the Samoa and Cook islands. There are three main islands in the Samoan Archipelago, Savaii (Western Samoa), Upolu (Western Samoa), and Tutuila (American Samoa). Table 5.12, 5.13, and 5.14, respectively, give some information on the tsunami as observed on the islands of Upolu, Savaii, and Tutuila. Table 5.15 lists some tsunamis in the Samoa Islands area from 1917 to 1959. This table based on information contained in Keys (1963).

Vitousek (1963a) described the 1960 Chilean earthquake tsunami as observed in French Polynesia. Figure 5.34 shows the tsunami height distribution along the coast of Tahiti.

On July 14, 1971, an earthquake of magnitude 7.9 occurred at 5°30′S, 153°54′E. Many aftershocks followed this and a second major earthquake occurred on July 26, 1971, with epicenter at 4°54′S, 153°12′E. Table 5.16 summarizes the pertinent information on the tsunamis that followed the two earthquakes.

TABLE 5.12. Tsunami of May 23, 1960, at Upolu in the Samoa and Cook islands. (Although the tsunami originated in Chile May 22 it was May 23 in Samoa and Cook islands.) (Keys 1963)

	Time (GMT)	Range (*m*)	Period (*min*)	First feature	Remarks
Observatory tide-gage record	0750	.15	30	crest	first arrival
Fagaloa Bay	0815 ±	1.8 ±	10 ±	-	observed by Samoans
Sataoa	0915 ±	2.4 ±	20	-	3 large waves at this time, second and third largest; max. crest 1.5 m; report reliable; reef offshore
Fagaloa Bay	1045 ±	4.9 ±	10 ±	trough	observed by Samoans; major wave in Samoa; subsequent crest caused minor damage to buildings; 44 gal drums gasoline carried 73.1 m inland; probably correlation between this and similar wave in Rarotonga at approx. 0930 GMT; no indication of series of crests
Lalomanu	1045 ±	1.8 ±	-	crest	range refers to half amplitude; wave appears to be same as crest at Fagaloa Bay, possibly preceded by trough, no conclusive verification; 2 fishermen in canoes 1.6 km from shore, but inside reef, swept ashore; one major wave only
Poutasi	1100 (?)	1.8–2.1	5 (?)	-	report sketchy; reef well offshore
Apia Harbor	1100	1.2 ±	8 ±	-	prominent continuous surge but no sinusoidal wave form observed; no damage at any stage
Upolu south coast beaches, e.g. Lepa	1430–1600	Approx. 1.2–1.8	5–6	-	continuous short-period surges
Malaela	1730	1.8 ±	4	-	successive crests advancing and retreating across lagoon for about 1.6 km as long, straight lines
Fagaloa Bay	1930	1.2 ±	3	-	sinusoidal waves coming up bay seen from Fagaloa saddle
Apia Harbor	2345	5	-	trough	sea retreated in harbor and returned several minutes later; eyewitness accounts not consistent; one wave only, but no sign on tide-gage record
Observatory tide-gage record	to May 29	-	-	-	tsunami can be identified to this time; no indication of new onset corresponding to sea wave of May 25; no reports of second wave in Samoa

TABLE 5.13. Tsunami of May 23, 1960, at Savii. Although tsunami originated in Chile on May 22, it was May 23 in Samoa and Cook islands. (Keys 1963)

	Time (GMT)	Range (*m*)	Period (*min*)	Remarks
Falelima	0800 ±	2.4–2.7	30 ±	3 large waves; reef very close to shore
Neiafu	–	3.0 (?)	–	1 large wave; max. crest +2.1 to +2.4 m
Tufutafoe	0900 ±	3.0 (?)	15 ±	reef terminates 45.7 m offshore; 2 major crests observed, max. +1.8 to +2.1 m
Tuasivi	during night	1.2–1.5	short	short period surges; shallow lagoon screened by reef at about 457 m
Sasina	1600	1.5	30 ±	waves over road at head of bay; bay enclosed by reef

TABLE 5.14. Tsunami of May 23, 1960, at Tutuila. (Keys 1963)

	Time (GMT)	Range (*m*)	Period (*min*)	First feature	Remarks
Pago Pago tide gage (Goat Island)	0735	.23	15	crest	crest amplitude of first arrival
One-half mile up bay from Goat Island	0900 (?)	3.0–3.7	–	–	max. crest 1.8–2.1 m, probably same as on marigram at 0845
Tafuna	0840	–	–	–	not observed, loud rumble for about 1 min
One mile up bay from Goat Island	0815	2.4–3.0	20 ±	–	series of 5 large waves identifiable on marigram
Pago Pago village	–	4.6–4.9	20 ±	–	village at head of bay; estimated $50,000 property damage
Fagaalu	during night	1.2 ±	–	–	located immediately inside harbor entrance, debris on road
Pago Pago tide gage	May 29, 0100	–	–	–	tsunami identifiable to this time

TABLE 5.15. Some previous tsunamis in Samoan Islands.

	Epicenter
May 1, 1917	Kermadec Islands
June 25, 1917	Samoa Islands
Sept. 7, 1918	Kuril Islands
Apr. 30, 1919	Tonga Islands
Sept. 20, 1920	New Hebrides Islands
Nov. 11, 1922	Chile
Feb. 3, 1923	Hawaii
June 17, 1928	Mexico
June 3, 1932	Mexico
Mar. 2, 1933	Japan
Dec. 7, 1944	Japan
Apr. 1, 1946	Aleutian Islands; also reflection
Nov. 4, 1952	Aleutian Islands
Mar. 9, 1957	Aleutian Islands
Nov. 6, 1958	Kuril Islands

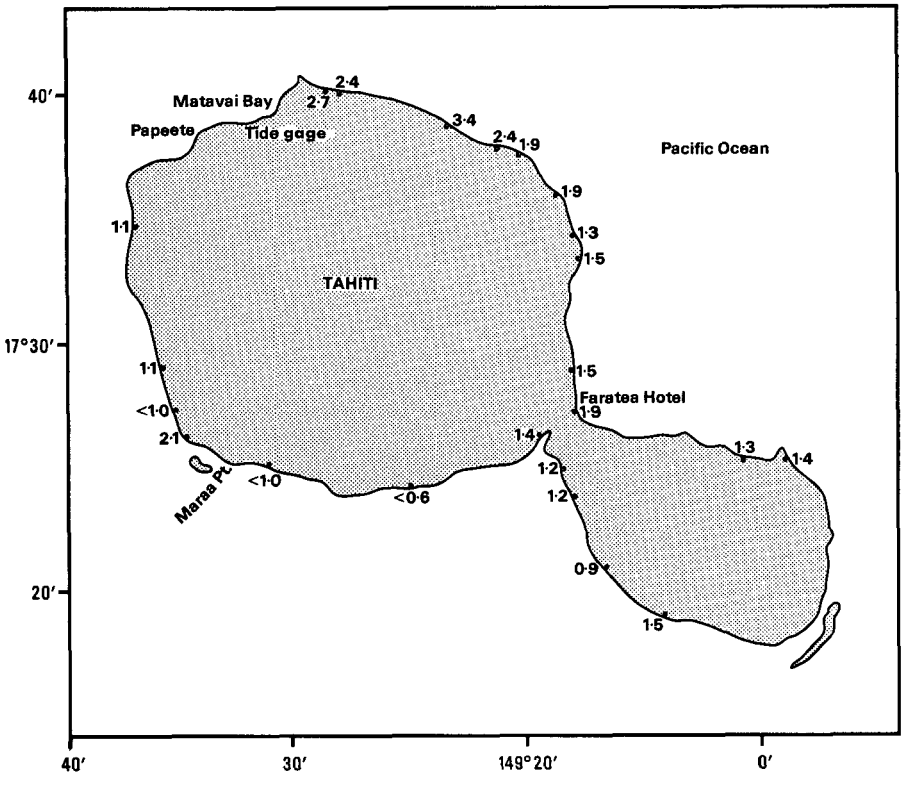


FIG. 5.34. Tahiti, showing locations mentioned in text and run-up heights (m) during tsunami May 22, 1960. (Vitousek 1963a)

TABLE 5.16. Relevant information on the Solomon Sea tsunamis of July 1971. (Braddock 1973)

Tide station		Period (*min*)	Initial wave initial rise (*m*)	Following fall (*m*)	Max. elevation (*m*)	Greatest amplitude crest to trough (*m*)	Arrival time (EST)	Approx. distance from epicenter (*km*)	Travel time (*min*)	Avg speed (*km/h*)
Rabaul	July 14	26	.54	.54	1.3	.79	1703	241.4	52	273.6
40°12′S, 152°12′E	July 26	30	.49	1.1	1.4	1.3	1151	144.8	28	305.8
Aitape	July 14				recorder not operational					
30°07′S, 142°24′E	July 26			uncertain			1520	1207.0	249	305.8
Alotau	July 14			uncertain			1740	659.8	89	442.6
10°17′S, 150°25′E	July 26	27	.09	.12	tidal effects dominate	.18	1245	708.1	82	515.0
Anewa Bay	July 14	10.5	.20	.24	1.6	.48	1646	201.1	35	346.0
6°11′S, 155°33′E	July 26	10	.12	.06	tidal effects dominate	.43	1209	297.7	46	386.2

TABLE 5.17. Tsunamis on west coast of South America from 1562 to 1960. (Based on Beringhausen 1962)

	Epicenter	Remarks
Oct. 28, 1562	between 37° and 39°S	about 1448.4 km of coastline affected
Feb. 8, 1570	near Concepcion, Chile	great damage
Dec. 16, 1575	between 39° and 41°S	intense tsunamis at Valdivia (Bahia Corral); no tsunamis at Bahia de Arabco or Concepcion
July 9, 1586	near Lima, Peru	tsunami amplitude 25.6 m
Nov. 24, 1604	near Arequipa, Peru	tsunami felt along more than 1448.4 km of coastline; Arica inundated
? ? 1615	in Chile	tsunami Arica
Mar. 15, 1657	between 36° and 39°S	tsunami along considerable length of coastline; Concepcion inundated
June 17, 1678	near Sante Fe, Peru	tsunami observed
? ? 1686	in Chile	tsumami observed
Oct. 20, 1687	in Peru	destruction at Callao
Nov. 26, 1705	?	tsunami observed in Arequipa
? ? 1724	near Lima	24.4 m tsunami at Callao caused damage
July 8, 1730	near Rio Aconcaqua	tsunami affected 965.6 km of coastline; inundations at Valparaiso and Concepcion
Oct. 28, 1746	in Peru	24.4 m tsunami at Callao; about 4800 people killed; damage at Cavallos, Cuanape, Changay, Gaura
May 25, 1751	near Concepcion, Chile	tsunamis inundated Concepcion; also at Islas Juan Fernandez
Apr. 11, 1819	near Copiapo, Chile	tsunami destroyed Caldera
Nov. 19, 1822	15 miles north of Valparaiso, Chile	tsunami caused damage along coast from Rio Copiapo to Valdivia
Nov. 11, 1922	near Coquimbo	hundreds of people killed; 5.2 m waves at Coquimbo; 6.4 m waves at Caldera; at Chanaral 9.14 m tsunami
Nov. 21, 1927	44°40′S, 73°00′W	tsunami observed along 40.2 km of coastline near Rio Aisen
Mar. 31, 1928	Antofagasta, Chile	huge tsunami near port of Molito
Apr. 26, 1928	in Peru	tsunami observed
Dec. 28-30, 1930	in Chile	tsunami along 482.8 km of coast; large amplitude at Coquimbo
July 13, 1936	24°S,70°W	small tsunami
Aug. 24, 1942	near Pisco, Peru	tsunami observed at Callao and Matarani
Apr. 6, 1943	33°01′S,71°38′W	.91 m tsunami at Valparaiso
Apr. 1, 1946	53°30′N,163°W	destructive tsunami at Iquique, Isla Juan Fernandez; 1.5 m or more at Matarani, Antofagasta, Valparaiso; .97m at Talara
Nov. 5, 1952	52°30′N,159°E	light tsunami damage at Callao; damage at Valparaiso, Punta, Coquimba; 1.8 m tsunami at La Libertad and Callao, Valparaiso; about 2.3 m at Arica; over 2.8 m at Caldera, and about 3.7 m at Talcahuano
Apr. 19, 1955	30°S,72°W	.91 m tsunami at Coquimbo, Tongay, La Serena
Mar. 9, 1957	51°18′N,175°48′W	tsunami of about .76 m at Talara, Chimbote; about .91 m at Arica: 1.1 m at La Libertad: 1.3 m at Matarani, Caldera: 1.4 m at Talcahuano, and 2.0 at Valparaiso
Jan. 19, 1958	01°30′N,70°30′W	large tsunami at Las Esmeraldas and Guayaquil
Feb. 7, 1959	4°S,81.5°W	small tsunami at Talara
May 22, 1960	41°S,73.5°W	tsunami about 5.0–7.4 m, eastern Chiloe, record indicates one of the large tsunamis of the past century; tide gages gave following maximum oscillations: Matarani 1.2 m, San Juan .914 m, La Punta (Callao) 2.2 m, Chimbote 1.2 m, Talara 1.7 m, La Libertad 1.9 m, San Cristobal (Galapogos Is.) 1.2 m, Tumanco small wave, Buenaventura, small wave

5.3 Tsunamis in South and North America (Excluding Alaska)

South American Tsunamis

Berninghausen (1962) gave a list of 49 tsunamis on the west coast of South America from 1562 to 1960. Table 5.17 summarizes the pertinent information contained in this paper. Lomnitz (1971) listed and described the tsunamis on the coast of Chile from 1535 to 1955. Neither list appears to be complete and there are some disagreements as to dates in the two lists. Figure 5.35 compares the amplitudes on the South American coast from the tsunamis of May 9, 1877, and May 22, 1960.

Hatori (1968) discussed tsunamis (generated by earthquakes in South America) that occurred along the Japanese coast. Yumura (1961) gave a list of tsunamis in Japan due to distant earthquakes, especially from Peru and Chile. A very important reference for tsunamis in the Pacific Ocean is the catalog prepared by Iida et. al. (1967). According to Hatori, in waters near the South American coast about 52 tsunamis were documented from 1562 to 1966. Of these, 15 tsunamis arrived at the Japanese coast, and of the 15, only 5 had amplitudes in excess of 2 m and caused damage on the Sanriku coast. Table 5.18 lists South American earthquakes, classified according to magnitude, which generated tsunamis observed in Japan.

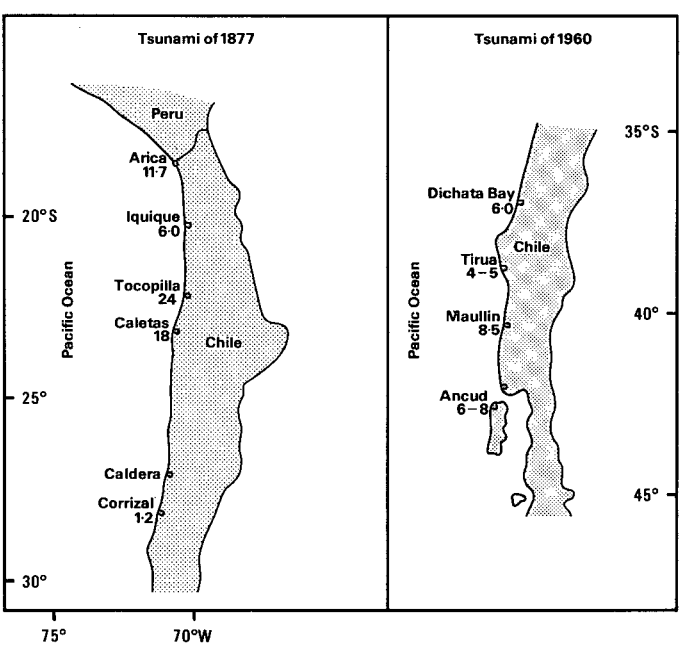


FIG. 5.35. Distribution of tsunami height (m) for tsunamis of 1877 and 1960. (Hatori 1968)

TABLE 5.18. (A) Number of earthquakes, (B) tsunamigenic earthquakes near the Pacific coast of South America, and (C) tsunamis observed in Japan from 1900 to 1966. (Hatori 1968)

Earthquake magnitude (M)	A	B	C
<6.9	–	1	1
7.0 ~ 7.2	49	3	0
7.3 ~ 7.5	22	3	1
7.6 ~ 7.8	9	3	0
7.9 ~ 8.1	4	2	1
8.2 ~ 8.4	2	2	2
8.5 ~ 8.6	2	2	2

Figure 5.36 shows the relation between tsunami amplitudes in Japan and Hawaii and earthquake magnitudes in South America.

Tsunamis from South American earthquakes were observed in Australia and New Zealand also. In Australia, at least two observations were made for the tsunami following the May 9, 1877, earthquake with epicenter at Iquique, Peru. The tsunami amplitude at Sydney was 0.6 m whereas at Newcastle the water level fell by 6.1 m. In New Zealand there were several observations of this tsunami. Tsunami amplitudes of 0.9–2.4 m with periods of 15–60 min were observed at several locations. At Samoa

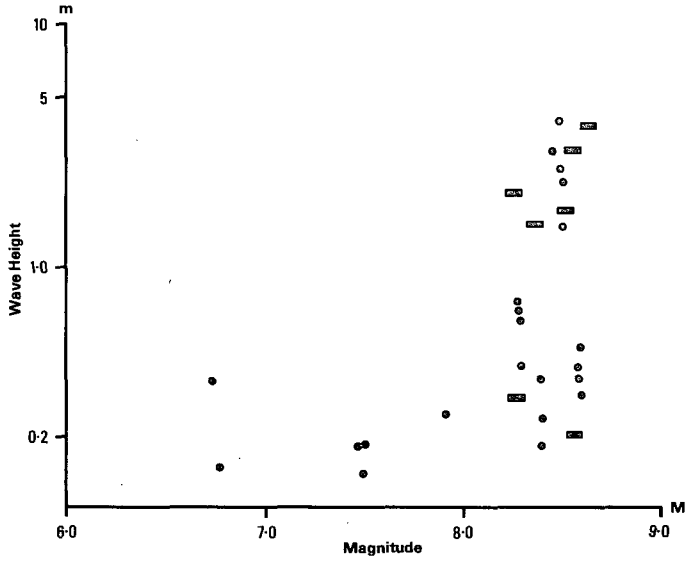


FIG. 5.36. Relation between wave heights at several places in Japan and Hawaii and magnitude of South American earthquake, ● Japan, ■ Hawaii. (Hatori 1968)

Islands, Apia (13°49′S, 171°41′W) the maximum amplitude of the tsunami was 3.7 m with a period of 10 min (Milne 1880).

The Chilean earthquake tsunami of May 1960 observed along the coast of Chile will be described briefly. An excellent source of reference for this is Sievers et al. (1963). The earthquake occurred at 1510 h Chilean time (GCT + 4) and damage from the earthquake and the tsunami was widespread in the provinces between Concepción and Chiloé. The cities most affected were Puerto Montt, Valdivia, Ancud, Castro, and Corral. In this zone, all the ports were destroyed by the tsunami. Figure 5.37, 5.38, and 5.39 show the destruction in three locations.

Tsunami heights to 20 m were observed. One significant point is that the tsunami entered the harbors of Ancud and Punta Corona as a bore. Another important observation was that from Valparaiso northward the tsunami waves of greatest amplitude occurred on May 24 and not on May 22 as would be expected. One explanation might be the influence of new earthquakes in this region or a little to the south. A more plausible explanation is that the greatest amplitudes occurred because of superposition of the tsunami waves reflected from the coast of Asia.

Murty and Wigen (1975) studied the tsunami water-level spectra for several stations on the coast of Peru (Fig. 5.40). Table 5.19 lists the significant periods at these stations for three different tsunamis. At Matarani, the period 9.5 min appeared in the tsunamis of 1966 and 1968 but not in 1964. An examination of the table shows that, although some periods were repeated, there were differences also.

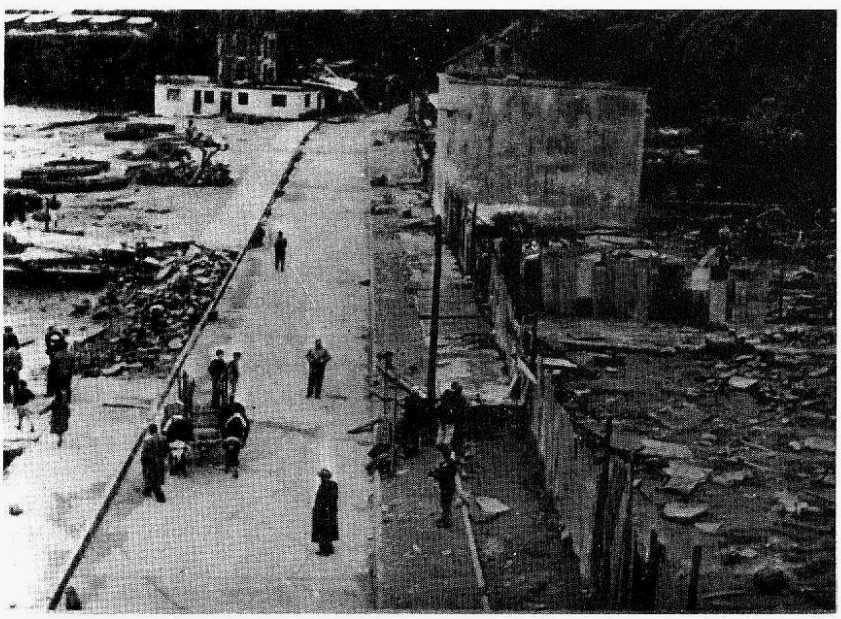


FIG. 5.37. Main street of Corral following May 1960 Chilean earthquake tsunami. (Sievers et al. 1963)



FIG. 5.38. Destruction at Corral Bajo by May 1960 Chilean earthquake tsunami. (Sievers et al. 1963)

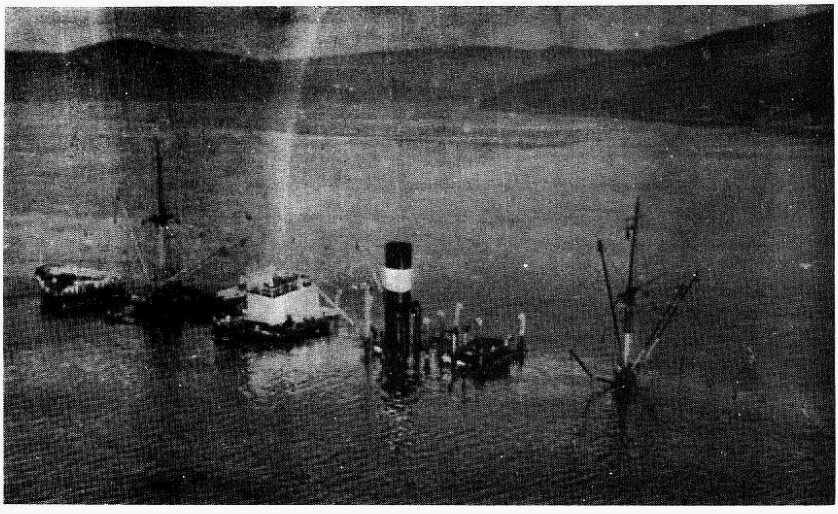


FIG. 5.39. Aerial view of the ship *Carlos Haverbeck* after May 1960 Chilean earthquake tsunami. (Sievers et al. 1963)

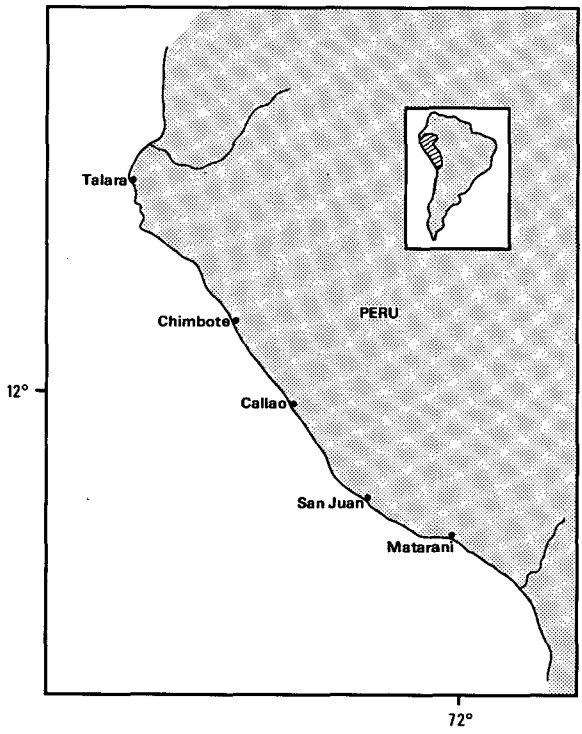


FIG. 5.40. Tide stations on the coast of Peru.

TABLE 5.19. Significant periods in the spectra of Peru tsunamis.

	Tide station	Significant periods (*min*)
May 27–30, 1964	Chimbote	–
"	Callao	–
"	Matarani	33
Oct. 17–19, 1966	Talara	18
"	San Juan	22, 13
"	Chimbote	50, 22, 14
"	Callao	–
"	Matarani	6, 9.5, 66
May 15–18, 1968	Talara	18, 10, 29
"	San Juan	22, 17
"	Chimbote	18
"	Callao	40
"	Matarani	9.5

Tsunamis in North America

The tsunamis of continental USA (excluding Alaska) are almost exclusively confined to the California coast with some activity on the coasts of Oregon and Washington. Table 5.20 lists some tsunamis in USA and is based on Coffman and Von Hake (1970), Anon. (1940), Anon. (1946a, b), Munk (1953), Murphy and Cloud (1954), Von Hake and Cloud (1965, 1966, 1968), Coffman and Cloud (1970), Byerly (1930), Magoon (1965), and O'Brien and Kuchenreuther (1957).

On Aug. 17, 1959, an earthquake of magnitude 7.1 occurred in Montana. Although no tsunami was generated, some unusual water-level activity occurred. Following the earthquake, seiches were set up in Hebgen Lake and new lakes formed (Steinbrugge and Cloud 1962).

Miller et al. (1962) studied the tsunami in California following the 1960 Chilean earthquake. Their study was based on digital tsunami data recorded every 15 s

Table 5.20. Tsunamis of continental USA (excluding Alaska but including Puerto Rico).

	Epicenter	Remarks
Dec. 16, 1811	New Madrid, Mo.	large waves generated on Mississippi River; several persons drowned
Nov. 18, 1867	Virgin Islands between St. Thomas and St. Croix	southeastern Puerto Rico tsunami generated with initial withdrawal of water; observed at Fajarado
Aug. 31, 1886	15 miles NW Charleston, S.C.	vicinity Charleston, unusual water-level activity; significant wave in the Cooper River
Nov. 4, 1927	California	local tsunami
Mar. 22, 1938	Queen Charlotte Is., B.C.	small tsunami observed at Santa Monica
May 19, 1938	1°N, 119°E	tsunami of 7.6 cm amplitude at Santa Monica
Nov. 10, 1938	South coast Alaska	small tsunami at Santa Monica
Apr. 1, 1946	Aleutian Islands	some tsunami damage on California coast at Santa Cruz, San Pedro, San Luis, Obispo, Princeton, Port Arenas, Santa Barbara, Coos Bay, Sinshaw, and Depoe Bay; only moderate waves at Golden Gate, San Diego, Sharp's Park; little activity at San Francisco, Monterey Bay, Eureka, Crescent City, and Newport
Mar. 4, 1952	Hokkaido, Japan	tsunami of 36.6 cm at Crescent City
Nov. 4, 1952	Kamchatka	waves 2.1–2.9 m on California coast
Mar. 9, 1957	Aleutian Islands	water-level disturbances on California coast; amplitude in Port Hueneme Harbor 53.0 cm
Oct. 13, 1963	Kuril Islands	.91-m tsunami at Crescent City and Avila
Mar. 27, 1964	Alaska	11 persons killed at Crescent City and 4 at Newport (Ore.); amplitude at San Diego 1.1 m
Oct. 17, 1966	Peru	amplitude at Crescent City and at Los Angeles outer harbor 30.5 cm
May 16, 1968	Honshu, Japan	tsunami amplitudes at several California stations: Alameda 6.0 cm, Avila Beach 6.0 cm, Crescent City 1.2 m, La Jolla 6.0 cm, Long Beach 21.3 cm, Los Angeles 15.2 cm, Newport Bay 6.0 cm, Rincon Island 6.2 cm, San Diego 15.2 cm, Neah Bay (Wash.) 9.1 cm

at La Jolla by a low-frequency recorder. These observations showed that the energy of the tsunami was greater than the background for as long as a week. These authors estimated the total energy of the tsunami to be 3×10^{23} ergs and the e-folding time to be half-day.

Miller (1964) studied the departures in the spectra of tsunamis at a fixed station, compared to the normal tsunami spectrum at that station. Through an examination of the spectral ratios, he removed the influence of the local resonances, and arrived at the so-called generating spectra. His study showed that tsunamis generated in shallow water are relatively rich in low frequencies. This could be because a given dimension in shallow water is associated with lower frequencies than the same dimensions in deeper water.

Miller also examined the decay of tsunami energy as a function of time and location. Figure 5.41 and 5.42, respectively, show the total tsunami energy recorded at La Jolla and Santa Monica as a function of time for several tsunamis. He compared these with the energy decay curves for Honolulu and Hilo and concluded that, although to a first approximation the energy decays exponentially with time, there are significant variations. The time required for the energy to drop to 1/e is 1.3 days along the California coast, and 0.4 days in Hawaii. For the astronomical tides the decay time is 0.22 days. Thus, along the California coast, because of the long decay time, tsunami energy can be trapped on the continental shelf. Miller

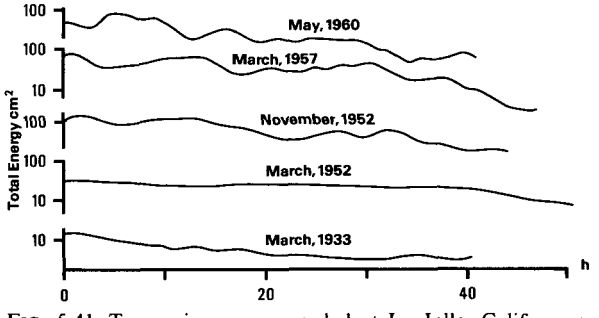


FIG. 5.41. Tsunami energy recorded at La Jolla, Calif., as a function of time. Zero time is not the arrival time of first tsunami wave. (Due to smoothing and filtering, plots do not start until several hours after the initial arrival.) (Miller 1964)

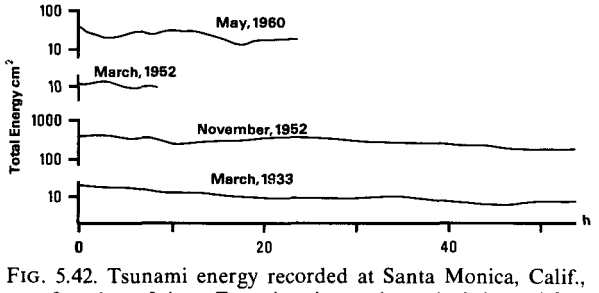


FIG. 5.42. Tsunami energy recorded at Santa Monica, Calif., as a function of time. Zero time is not the arrival time of first tsunami wave (see legend Fig. 5.41). (Miller 1964)

also showed that the frictional dissipation of tsunami energy in the Pacific Ocean is more important than the leakage out of the Pacific Basin.

Characteristics of tsunami damage on the California coast (Magoon 1965; Wilson and Tørum 1968) in the last 30 yr or so will be discussed. Magoon summarized the water levels associated with tsunamis on the northern California coast. With the exception of two locations (mouths of the Noyo and Albion rivers) the tsunami characteristics are quite similar. The tsunami records consisted of rapid changes of the water level with a maximum rate of change of 0.3–0.7 m/min, for a duration of 5–10 min. Almost always the initial waves were the major ones, especially along the outer coast. Usually the tsunami waves became insignificant after one day but could be detected up to a week.

With the exception of Crescent City in 1964 and possibly Half Moon Bay in 1946 (Aleutian earthquake tsunami), all damage had been confined to commercial fishing or pleasure boats and shore facilities, because of the unusually strong horizontal movements associated with the tsunami (e.g. Santa Cruz Harbor). Inside San Francisco Bay, both the Chilean earthquake tsunami of May 1960 and the Alaskan earthquake tsunami of March 1964 were greatly attenuated after passing through the Golden Gate.

The Noyo and Albion rivers enter the Pacific Ocean at the landward end of relatively deep bays. The Alaskan earthquake tsunami of March 1964 entered these rivers in the form of a bore. At Noyo, the speed of propagation of the bore was estimated to be about 32 km/h.

At Noyo Harbor, both the harbor and its entrance are restricted and the tsunami effects were felt over the entire reach of the harbor. The first wave of the Alaskan earthquake tsunami of March 1964 rose relatively slowly and exhibited the characteristics observed elsewhere along the coast. However, the second wave came 15 min later, formed a bore with a height of about 2.3 m, and consisted of a series of steplike jumps.

At Crescent City in 1964, the third wave appeared to be the highest with amplitudes to 7 m, over a length of the shoreline that included 3.2 km southwest of Crescent City and 1.6 km northeast. However, a departure from this run-up pattern was noticed wherever the ground elevation decreases seaward from the coast and either decreases or remains uniform landward from the coast. The severe structural damage in Crescent City was because the majority of buildings were of wooden frame construction (due to local lumber industry) and very old.

In Canada, tsunamis have occurred on the west and east coasts. On June 23, 1946, at about 1015 (Pacific Standard Time) an earthquake occurred on the east coast of Vancouver Island, B.C. This is one of the few documented cases (Hodgson 1946) where a tsunami was generated following a British Columbia earthquake. Telegraph cables at the ocean bottom broke in several places following the earthquake. In the Alberni Canal near the Franklin River, the water level was 6.1–9.1 m above average. At Sisters Rock on Texada Island, the tsunami amplitude was 2.1–2.4 m. A second wave had an amplitude of 1.2–1.5 m and one person died near Maple Guard spit.

S. O. Wigen (unpublished data) described the tsunami on the west coast of Canada generated by the Chilean earthquake of May 22, 1960. The tsunami arrived on the B.C. coast at 0421 (Pacific Standard time) on May 23, thus the travel time was over 17 h. The maximum amplitude of the tsunami at Tofino was 1.3 m, whereas at Shields Bay it could have been 2.1 m. Loucks (1962) studied this tsunami on the Canadian coast by spectrum analysis of observed records.

Following the Alaskan earthquake of Mar. 28, 1964, at 0336:13, GCT, the tsunami generated attained large amplitudes on the west coast of Canada (S. O. Wigen and W. R. H. White unpublished data). The maximum amplitude at Port Alberni exceeded 5.2 m. Murty and Boilard (1970) studied this tsunami through analytical and numerical models.

Contrary to popular belief, the eastern part of Canada is also seismic and has indeed produced tsunamis. Milne (1967) stated that severe earthquakes can occur in the St. Lawrence Valley, in the arctic, and near Newfoundland. The so-called Grand Banks earthquake occurred on Nov. 18, 1929, in the Atlantic Ocean, southeast of Newfoundland. The epicenter was at 44°30′N, 57°15′W and the time of occurrence was 0432:8 (Newfoundland Standard Time). The turbidity currents following this earthquake caused numerous cable breaks in the Atlantic Ocean.

This earthquake generated a tsunami with amplitudes to at least 12.2 m (Johnstone 1930) in Burin Inlet on the south coast of Newfoundland and killed 26 people. Gregory (1929) gave 30.5 m as the maximum amplitude in Burin Inlet. McIntosh (1930) gave a value of 4.6 m for the tsunami amplitude at Lamaline. According to Johnstone, no tsunami was observed at Sable Island, probably because the island was well protected by sandbanks. Although the tsunami waves were considerably amplified in a northerly direction (i.e. in the direction of Newfoundland), they were not significantly amplified in a westerly direction as can be seen from the water-level records on the Canadian and U.S. east coasts. At Halifax, the amplitude was only 0.5 m and at Atlantic City the amplitude was 0.3 m. Murty (1975) explained the nonamplification westward as due to the orientation of the fault in a east–west direction. Murty and Wigen (1976) studied this tsunami in detail and showed that resonance in the V-shaped Burin Inlet accounts for the great amplification of the tsunami in that inlet. Figure 5.43 shows the travel-time curves for this tsunami and it can be seen that the tsunami energy traveled preferentially toward the south coast of Newfoundland.

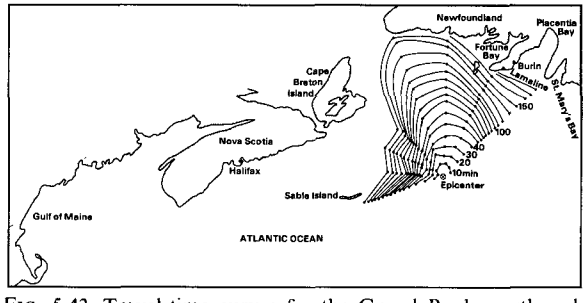


FIG. 5.43. Travel-time curves for the Grand Banks earthquake tsunami of Nov. 18, 1929.

5.4 Tsunamis in the Atlantic Ocean, Europe, Middle East, and Asia

Tsunamis in the Atlantic Ocean

It is not widely known that tsunamis do occur in the Atlantic Ocean, although the frequency and destruction are considerably less than that caused by Pacific tsunamis. Berninghausen (1964) briefly described tsunamis for the Eastern Atlantic south of the Bay of Biscay from 1531 to 1960. He cautioned that this is not a comprehensive list of tsunamis, and some cases might be storm surges and not tsunamis. Table 5.21 is prepared from this paper.

Tsunamis in the Virgin Islands area will now be considered. A destructive tsunami occurred on Nov. 18, 1867, in the Virgin Islands. Several shocks occurred from this date till early 1868, and the series of shocks ended on Mar. 17, 1868 (Reid and Taber 1920). The tsunami height in the harbor of St. Thomas was between 4.6 and 6.1 m. There were at least four waves and they approached the harbor from the southeast between the islands of St. Thomas and St. Croix. In Frederiksted harbor on the west coast of St. Croix Island, the tsunami height was between 7.6 and 9.1 m. Tsunami waves invaded Saba Island, and high water occurred at St. Christopher. In St. John harbor on the west coast of Antigua Island, the tsunami height was 2.4–3.0 m.

On the island of Guadeloupe, several interesting phenomena took place. At Basseterre, there was a withdrawal of the sea and the subsequent range (trough to crest) was only 2 m. In the northwestern part of the island, at Deshayes and Saint-Rose, the tsunami amplitude was said to have exceeded 18.3 m, but according to Reid and Taber, this is an overestimation. On the south side of the island at Point-a-Pitre, the tsunami was small because of the protection at the head of the Petit Cul de Sac. No details were available about the tsunami at Martinique. At St. Vincent the tsunami was small but at Becquia Island, 16.1–24.1 km to the south, the height was 1.8 m. At St. George on Grenada Island, the water level went down by 1.2–1.5 m and then rose to the same height above the average level. The vertical oscillation of the water level took place 6 times. At Gouyave the range of vertical oscillation was said to be 6.1 m (another overestimation according to Reid and Taber). A large tsunami occurred on the south side of Viequez Island. The tsunami was also observed on the southeast coast of Puerto Rico.

A series of earthquakes occurred in Puerto Rico during October–November 1918. Following the earthquake of Oct. 11, 1918, the generated tsunami had an amplitude of 6.1 m. Several people died at Aquadilla and property damage occurred at Mayaguez.

Tsunamis of the Dominican Republic are of interest also. Following the earthquake on Aug. 4, 1946, the generated tsunami caused destruction at several locations in the Dominican Republic. The epicenter was to the northeast of Julia Molina and about 64.4 km offshore (Lynch and Bodle 1948). The tsunami height at Julia Molina was estimated to be about 4–5 m. The town of Matanzas was totally destroyed by the tsunami and abandoned. About 100 people died. The water level fluctuated in Samana Bay but no damage occurred.

TABLE 5.21. Tsunamis in the eastern Atlantic south of Bay of Biscay from 1531 to 1960.

	Epicenter	Remarks
Jan. 26, 1531	near Lisbon, Portugal	several ships destroyed by waves; flood on banks of Tagus River
July 26, 1591	Azores	waves damaged several ships
Dec. 21,1641	Azores	inundation of Port Velas, Ilha de Sao Jorge
? 1653	Azores	destruction on coast off Ilha Terceira
Nov. 23, 1668	Azores	Calheta and Ilha de Sao Jorge flooded
? 1676	Azores	destruction of Praia da Victoria
May 6, 1706	Canary Islands	tsunami caused by volcanic eruption; destruction at Garachico and Isla de Tenerife
Dec. 26, 1746	Lisbon, Portugal	tsunami observed
Apr. 28, 1752	near Buarcos and Aveiro, Portugal	tsunami observed
Mar. 29, 1756	Lisbon	high water in Tagus River
July 9, 1757	Azores	large waves on coasts of Ilha de Sao Jorge, Ilha de Pico, and Ilha Graciosa
Mar. 31, 1761	off coast of Portugal	tsunami at Lisbon 2.4 m; tsunami also at Cabo Finisterre (Spain), Madeira, Ilha de Fayal, Ilha Terceira, Portorico, U.K., Barbados
Dec. 27, 1772	Portimao, Portugal	tsunami observed near Cabode Sao Vicente
Nov. 1, 1775	38°N, 10°W	so-called infamous Lisbon earthquake; 3 tsunamis waves from 4.6 to 12.2 m caused destruction at Lisbon; at Cadiz waves were 5.5 m, at Gibraltar 2.1 m; large waves at Tangier, Agadier, Madeira, Funchal, Azores
? 1787	Azores	destructive tsunami
Jan. 23, 1792	Azores	tsunami at Velas and Ilha de Sao Jorge
July 4, 1809	no earthquake listed	sea disturbed at Lisbon
Dec. 4, 1809	Cape of Good Hope	large wave in Table Bay
Feb. 17, 1855	Azores	tsunami of 10 m amplitude at Ilha Terceira
Jan. 6, 1856	Azores	large tsunami at Velos and Ilha de Sao Jorge
Aug. 27-28, 1883	Krakatoa (volcanic) eruption in Sundra Strait, Indonesia	about 15.2 cm amplitude waves in Table Bay, English Channel
Feb. 3, 1899	Azores	destruction at Velas and Ilha de Sao Jorge; one death
May 11, 1911	Gold Coast	destruction at Lome
Aug. 22, 1926	Azores	tsunami of 60.9 cm amplitude on Ilha de Fayal and Ilha de Pico
Dec. 19, 1926	Lisbon	high water in the Tagus River
Nov. 19, 1929	40°N, 56°W	tsunami at Azores due to the Grand Banks earthquake
Aug. 31, 1931	Azores	destruction at Horta, Feteira, Ilha de Fayal
June 22, 1939	Gold Coast	tsunami at Labadi and Tishi
Feb. 29, 1960	Agadir, Morocco	tsunami existence, not confirmed

A strong earthquake occurred in Jamaica on June 7, 1692, and there is some confusion in the descriptions of damage attributed to land subsidence caused by the tsunami (Taber 1920). Initial withdrawal of water was reported at Liganee and at Yallhouse. At Port-Royal the tsunami ampltiude was 1.8 m and 13 people were killed. At St. Ann's, on the north coast of the island, a tsunami arrived almost immediately after the earthquake. There were seven waves at St. Ann's, due to the reflections between the coasts of Jamaica and Cuba. The tsunami amplitude was greater on the north coast of the island (which is less densely populated) and insignificant on the south coast.

The earthquake of Oct. 3, 1790, created a large tsunami on the west coast of Jamaica and swept away the town of Savanna La Mar. There is a possibility that the devastation was due to a storm surge and not a tsunami. About 300 people died. The earthquake of Jan. 14, 1907, occurred near Kingston and a large tsunami wave arrived at the north coast of the island. The amplitude of the tsunami on the south coast was insignificant.

Tsunamis of Europe

Although not as frequent and devastating as Pacific tsunamis, tsunamis in the European and Mediterranean Sea areas do exist and have killed many people. Ambraseys (1964) listed some important tsunamis from 1900 to 1960 for Europe and North Africa (Table 5.22). For details on the seismic seawave intensity scale,

Table 5.22. Tsunamis of Europe. (Ambraseys 1964)

	Epicenter	Magnitude (M)	Max. amplitude (*m*)
July 5, 1902	40N, 23.25E	6.6	.60
Dec. 28, 1908	38N, 15.50E	7.5	5.4
May 11, 1911	6N, 1W	6.6	3.0
Nov. 27, 1914	38.50N, 20.50E	6.2	3.3
Aug. 7, 1915	38.50N, 20.50E	6.2	1.5
Dec. 18, 1920	41N, 29E	6.2	3.0
Aug. 22, 1926	38.50N, 28.50W	?	.60
Sept. 11, 1927	44.50N, 34.50E	6.5	1.5
Mar. 31, 1928	?	?	.60
May 3, 1928	?	?	.91
Sept. 26, 1932	40.50N, 23.75E	6.9	.91
June 22, 1939	6N, 1W	6.5	1.2
Nov. 25, 1941	–	–	.60
Nov. 27, 1945	24.50N, 63E	8.2	1.4
Oct. 6, 1947	37N, 22E	7.0	1.2
Feb. 9, 1948	35.50N, 27E	7.1	2.4
Apr. 22, 1948	38.50N, 20.25E	6.4	.91
June 29, 1953	–	–	2.1
Aug. 20, 1953	–	–	.30
July 9, 1956	37N, 26E	7.8	30.5
Nov. 2, 1956	39.50N, 23E	5.7	1.2
Jan. 22, 1957	4.50S, 28.50E	6.3	3.0

see Ambraseys (1964, p. 80). Kárník (1971) gave a diagram of epicenters of earthquakes that have generated significant tsunamis in this area (Fig. 5.44). Kárník (1971, p. 203) considered the following regions as tsunami prone: certain coastal regions of the Mediterranean Sea and the Atlantic (only some specific regions are subject systematically to the effects of seismic sea waves). The most prominent regions are the Aegean and Adriatic coasts, the Ionian Sea coasts, and the eastern Mediterranean coast of North Africa and Portugal. On the eastern Mediterranean coast the following regions are subject to tsunamis: the Gulf of Corinth; the Euboean Gulf; the area between Himara and Durres; the Sea of Marmara; the area between Cyprus, Jubeli, and Acre; the area between Chios and Izmir; and south of the Greek Archipelago.

Ambraseys (1962) gave a detailed list of tsunamis for the eastern Mediterranean. In preparing this list, he omitted irrelevant and incorrect statements from the original sources. Moreira (1970) stated that since the middle of the 18th century, the most destructive tsunamis on European coasts were due to the Lisbon earthquake, Nov. 1, 1755; the Sicily and Calabria earthquake, Feb. 5, 1783; and Sicily and Calabria earthquake, Dec. 28, 1908; and the Aegean Sea earthquake, July 9, 1956.

European tsunamis are usually local, but some spread over great distances. Examples of great tsunamis are the Lisbon earthquake tsunami of 1755 and probably the one on July 21, 365, in the Mediterranean Sea. The latter tsunami occurred following an earthquake on Crete Island, and the tsunami reached Alexandria, Egypt; Sicily; Calabria, Italy; and probably the Mediterranean coast of Spain.

Earthslides appear to be sources of at least some tsunamis in Greece (e.g. tsunamis of July 9, 1956, and July 6, 1965). However, the earthslide itself might

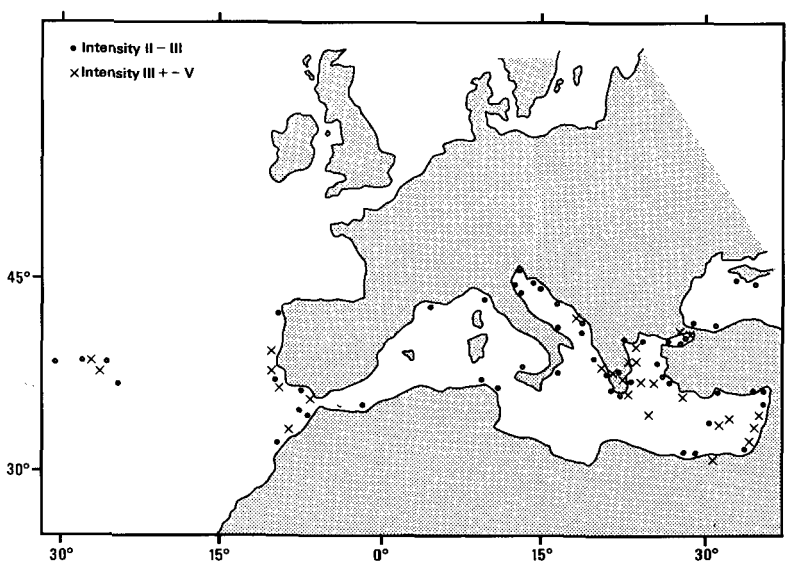


FIG. 5.44. Observations of tsunamis in the European area. (Kárnik 1971)

occur following an earthquake. Moreira (1970) stated that faulting accompanied by earthslides appears to have been responsible for the following tsunamis: Apr. 27, 1894, in the Gulf of Euboea; Sept. 8, 1905, in Sicily and Calabria; and Dec. 28, 1908, in Sicily and Calabria. Cable breaks occurred with the 1905 and 1908 tsunamis and earthslides and turbidity currents must have occurred. Cable breaks also occurred following the earthquakes of Nov. 25, 1941, and Sept. 9, 1954.

The following tsunamis were associated with earthquakes whose epicenters were certainly located on land: in 1638 near Pizzo, Italy; 1694 near Brindisi, Italy; Feb. 2, 1703, in the Tiber River, following a series of earthquakes in the Aquila region of Italy; Feb. 1783 in Calabria, Italy; Dec. 26, 1939, in the Black Sea following an earthquake in Anatolia, Turkey.

On Feb. 28, 1969, an earthquake occurred at 36.2°N, 10.5°W, southwest of the Cape of St. Vincent (Fig. 5.45). A small tsunami was generated and was recorded on the coasts of Portugal, Spain, Morocco, Madeira, Azores, and Canary Islands. On the Portugese coast the amplitude was 0.8 m and at Casablanca it was 1 m. The tsunami also penetrated the Tagus River. Figure 5.45 also shows the travel-time curves of this tsunami.

The tsunami of July 9, 1956, in the Greek Archipelago will be discussed in detail (Ambraseys 1960). This tsunami was probably triggered by landslides which followed a violent earthquake on the same date. The coasts of the Greek islands and Asia Minor are abundant in narrow passages and V-shaped bays. The severity

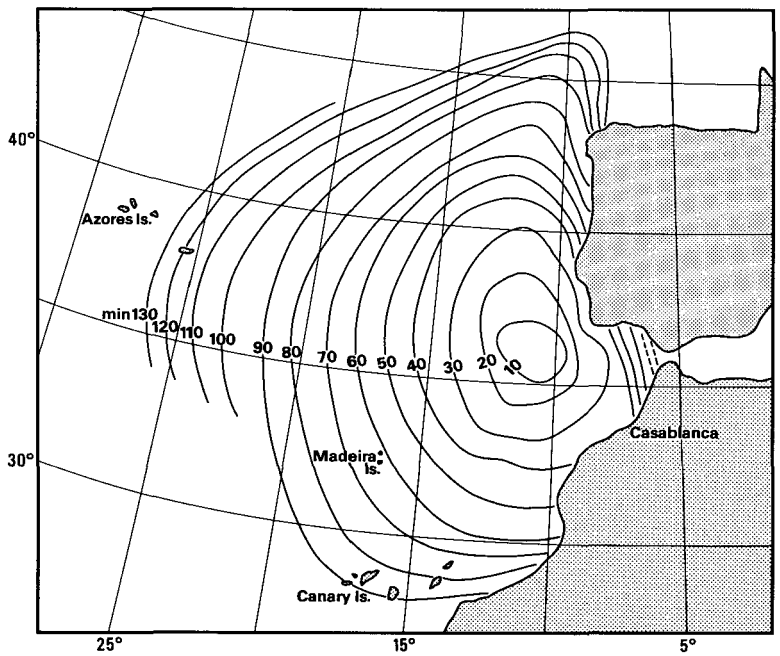


FIG. 5.45. Travel-time curves of Feb. 28, 1969 tsunami near Portugal. (Moreira 1970)

of the tsunami varied from place to place and amplitudes to 30 m were attained. The area affected by the tsunami exceeded 100,000 km^2 and the disturbance lasted one day. The epicenter of the main shock was at 36°54′N, 26°00′E and the time was 0311:38 GCT. The magnitude was 7.5 and the focal depth was shallow. At 0324:05 GCT an aftershock with a magnitude of 7 occurred at 36°48′N, 25°12′E. Figure 5.46 shows the travel-time curves of this tsunami.

Table 5.23 lists maximum positive and negative amplitudes, the period of the tsunami, and the nature of initial motion at 33 locations in the Greek Archipelago. Table 5.24 lists the tsunamis in the Greek Archipelago and adjacent seas from 1400 B.C. to 1956 A.D. Figure 5.47 shows the locations of these tsunamis.

Pararas-Carayannis (1973) described the tsunami caused by the eruption of the volcanic island Santorin, which occurred between 1450 and 1480 B.C., the precise time is difficult to estimate (Fig. 5.48). The eruption of Santorin (also called Thera) created a large tsunami and statements have been made to the effect that this tsunami destroyed, for all practical purposes, the Minoan empire. Although Pararas-Carayannis (1973) and Bolt et al. (1975) agreed that disastrous tsunamis might have occurred following the volcanic explosion, they doubted whether the volcanic eruption and the tsunamis alone caused the collapse of the empire. It is more probable that these natural disasters were a contributing cause, and possibly made the empire weak and vulnerable to invasion by Mycenaeans or others.

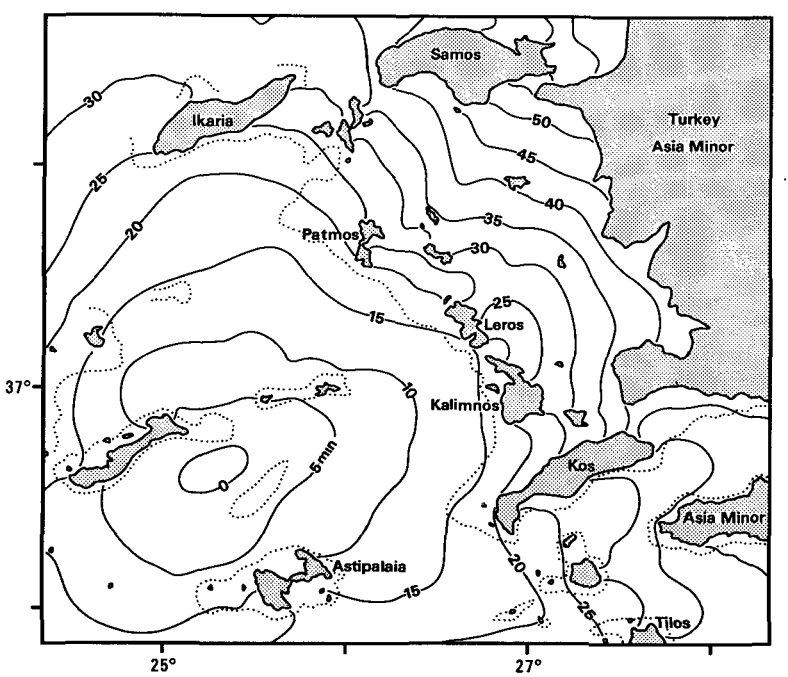


FIG. 5.46. Travel-time curves of July 9, 1956 tsunami in the Greek Archipelago. (Ambraseys 1960)

TABLE 5.23. Characteristics of the seismic sea wave of July 9, 1956. (A) reported initial movement of water level. (B) max. amplitude of crest (m), (C) max. amplitude of trough (m), (D) avg period of water (min). (Ambrasays 1960)

Station	A	B	C	D
Amorogos	–	30.48		
Katapola	+	2.74	3.04	
Astipalaia	–	20.42		
Porto-Scala	–	4.87	5.18	10
Cos	+	.91	.60	
Kalimnos	–	3.66	5.18	
Pothea	–	2.44	2.44	
Leros, Laki	–	1.22	1.22	
Patmos, Scala	–	3.96	15.24	
Samos				
Marathokambos	–	2.13	2.13	8
Tigani	–	.91	1.52	8
Vathi	–	.60	.91	10
Kassos,				
Ag. Marina	–	1.22	1.52	5
Nisyros, Mandraki	(?)	2.74		
Kimolos	–	1.22	1.52	
Folegandros	–	10.05	7.92	
Paros, Parikia	–	1.21	1.52	
Ios	+	1.52	3.04	15
Ermioni	(?)	.91	.91	8
Kythira,				
Kapsalos	+		.91	5
Serifos	+	.91	.60	5
Naxos	+	1.22	.91	
Skopelos	(?)	.30	.30	8
Crete, Sitia	+	1.52	1.52	5
Ag. Nikolaos	–	.91	1.22	6
Palaiokastro	+	3.66	3.96	
Heraclion	+	2.13		
Souda	–	1.22	.91	6
Chania	(?)	.91	.60	
Rethymnon	(?)	1.22	1.82	10
Attica, Voula	–		.30	5
Tinos	(?)	3.04		
Poros	(?)			10

The tsunami following the Lisbon earthquake of Nov. 1, 1755, caused great damage in Europe. There were many widely held misconceptions about this earthquake and tsunami and Reid (1914, p. 79) corrects some of the ridiculous claims made earlier. He concluded that the tsunami waves approached the shores of southwestern Europe, northwestern Africa, southern England and Ireland, and the West Indies; and that they may have appeared in the western part of the Mediterranean; but there was no evidence they entered the North or Baltic seas and only a hint that they were observed on the coast of America. At Lisbon there appears to have been three waves with heights between 4.6 and 12.2 m. The amplitudes in the region south of Lisbon were greater than those in the region north of Lisbon.

TABLE 5.24. Seismic sea waves in the Greek Archipelago and adjacent seas. (Ambraseys 1960)

	Location
1400 B.C.	Santorin, Crete, Amnisos, Knossos
1300 B.C.	Troad
479 B.C.	Chalcidice, Potidaea
426 B.C.	Maliacos, Opuntian gulfs, Atalanta, Peparathos Is.
373 B.C.	Gulf of Corinth, Helice
222 B.C. (227?)	Rhodes Is., Tilos Is., Carian and Lycian towns
62 A.D. (65?)	Crete
77 A.D.	Cyprus, Episkopi
July 21, 365	Crete, Asia Minor
Sept. 6, 543	Asia Minor, Kyzicos
July 7 or 9, 551	Maliacos Gulf
554	Cos Is., Dodecanese Is.
Dec. 14, 558	Marmara Sea, Constantinople
Oct. 26, 740	Marmara Sea, Constantinople
1050	Cyclades Is., Santorin
Dec. 25, 1222	Cyprus, Paphos
Oct. 14, 1344	Constantinople
Mar. 20, 1389	Chios Is., Lesvos Is., Smyrna
May 3, 1481	Rhodes Is., Dodecanese Is.
Sept. 14, 1509	Bosporus Sea, Constantinople
Nov. 8, 1612	Sea of Crete, Crete
May 5, 1622	Ionian Is., Zante
Apr. 5, 1646	Constantinople
Sept. 29, 1650	Santorin
May 14, 1748	Gulf of Corinth, Aiyion
Jan. 8, 1805	Gulf of Patras, Patras
Aug. 23, 1817	Gulf of Corinth, Aiyion
Jan. 9, 1821	Ionian Is., Zante
Nov. 13, 1856	Aegean Is., Chios
Oct. 20, 1859	Pireaus
Dec. 26, 1861	Gulf of Corinth
Jan. 22, 1866	Chios
Jan. 28, 1866	Santorin
Oct. 1866	Mirtoon Sea, Kithera Is.
Apr. 10, 1867	Lixouri
Sept. 20, 1867	Ionian Is., Syros
Oct. 5, 1871	Gulf of Corinth
Apr. 15, 1878	Nikomedia, Prussa
Jan. 28, 1893	Samothrace Is.
Apr. 16, 1894	Skiathos Is., Atalanti Is.
Nov. 27, 1914	Ionian Is., Lefkas
Apr. 25, 1928	Piraeus
Sept. 26, 1932	Gulf of Strimon, Ierissos
Apr. 23, 1933	Cos Is., Dodecanese Is.
Feb. 9, 1948	Karpathos Is., Dodecanese Is.
Apr. 22, 1948	Ionian Is., Lefkas
July 9, 1956	Aegean Is., Crete

Hamilton (1783) described the tsunami generated by the earthquake of Feb. 5 1783, at Calabria and Messina in Italy. At Scilla, 2473 people drowned and at Faro, 24 people died. The tsunami following the earthquake at Calabria on Dec. 28, 1908, attained large amplitudes on the Italian mainland and Sicilian coasts

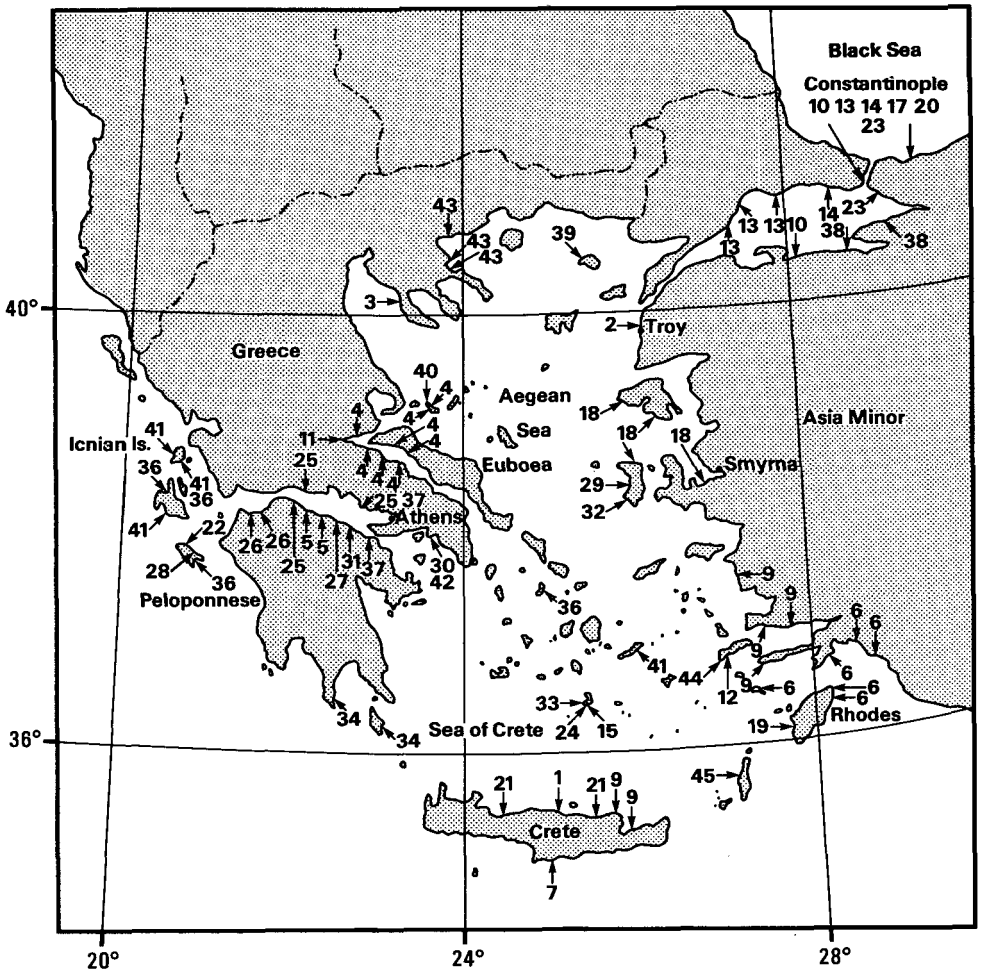


FIG. 5.47. Locations of tsunamis that occurred in the Greek Archipelago and adjacent seas. (Ambraseys 1960)

of the Straits of Messina. The tsunami was observed (Anon. 1909) all along the north coast of Sicily as far west as Termini. It was reported that no tsunami was noticed north of Cannitello, near the entrance to the straits.

The tsunami amplitude varied from 2.7 m at Messina to 8.4 m at Giordini and Ali, and 8.5 m at Briga Marina. The tsunami was also noticed at Naples, Ischia, Civitavecchia, Porto Corsini, near Ravenna, and Mazzara. Wright (1909) mentioned that the tsunami was not particularly destructive. He gave an amplitude of 2.4 m at Messina and 3.7–4.6 m at Reggio. Oldham (1909, p. 288) stated that the sea wave washed the shores of the Straits of Messina and the Tyrrhenian Sea, swept over Messina and Reggio with a height of 9.1 m, caused three deaths at Catania, and reached at least as far as Malta.

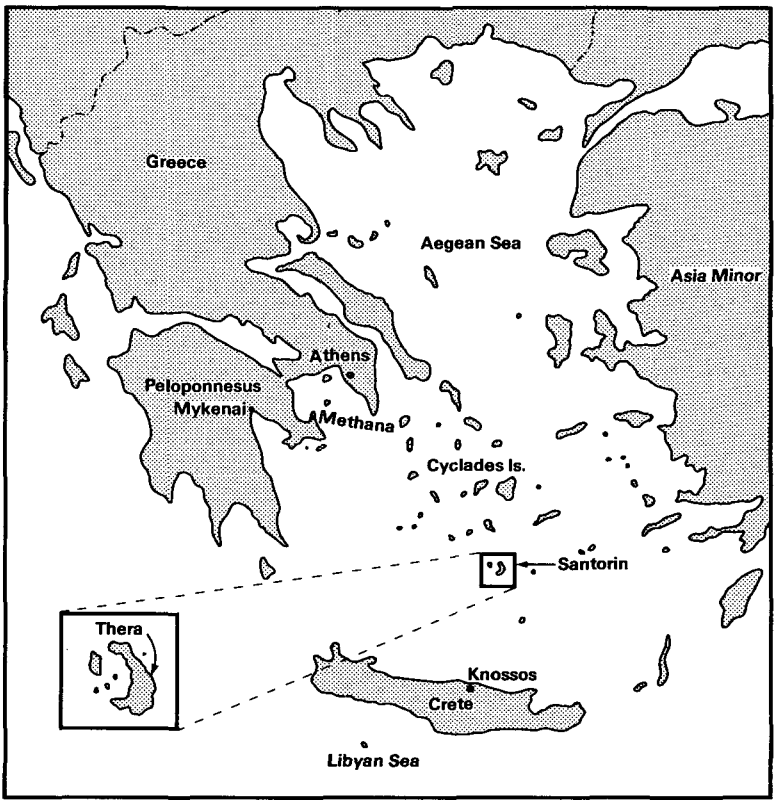


FIG. 5.48. Location of the volcanic island Santorin (Thera). (Bolt et al. 1975)

According to Omori (1910) maximum height of the waves (6–10 m) on the Calabria coast was reached between Pellaro and Lazzaro, but for the opposite coast, at Platania, the height was 11.7 m. All along the east coast of Sicily the waves were perceptible, although at the northern point (Torre di Faro) they attained a height of only 0.8 m, and at the southern point (Capo Passero) of 1.5 m. Along the north coast they were observed as far as Termini, and along the south coast as far as Porto Empedocle. In the Lipari Islands they passed unnoticed, but were conspicuous at Malta. At Catania the mareograph was inundated, but good records were available at Malta, Palermo, Mazzara, Cagliari, Ischia, Naples, Civitaveechia, Livorno, and Ravenna. Heezen (1957) discussed the turbidity currents in the Straits of Messina following this earthquake.

The Assam earthquake of Aug. 15, 1950, with epicenter near 28.6°N, 96.5°E caused seiches in many fjords and lakes in Norway and the U.K. (Kvale 1955). One important recent tsunami (after World War II) was generated by the Aegean Sea earthquake of July 9, 1956, with epicenter at 36°24′N, 25°26′E (Anon. 1956). The tsunami had a maximum amplitude of 4.6 m and was observed as far away as Kalymnos, Astipalaia, Andiparus, and Iraklion. On Feb. 7, 1963, a tsunami occurred in Europe, and was observed on the coast of the Gulf of Corinth from Patras

to Aiyion (Ambraseys 1963). Belated submarine landslides due to a series of light shocks on Feb. 2, 1963, caused the tsunami that attained amplitudes to 2.1–2.4 m with periods between 1 and 2 min. Ambraseys mentioned that local tsunamis due to submarine landslides are not infrequent here.

Tsunamis in the Middle East and Asia

I found only one instance of a tsunami in the Holy Land. This occurred in 1837 (correct details on the date are not known). The earthquake was felt in Syria,

Table 5.25. Tsunamis in Indonesia.

	Epicenter	Remarks
Feb. 2, 1648	?	tsunami at Ambona, perhaps storm surge
Nov. 11, 1659	?	tsunami at Ambona
Dec. ?, 1659	?	tsunami at Buru
May 20, 1673	?	tsunami at Ternate
? 1690	?	tsunami at Banda Islands reported, confirmed
Mar. 6, 1710	?	tsunami at Banda Neira
Aug. 24, 1757	?	tsunami at Djakarta
? 1773	?	tsunami on Borneo coast
? 1814	?	tsunami at Timor
Apr. 11, 1815	?	tsunami at Madura and Sumbawa
? 1818	?	tsunami at Bima, Sumbawa
Sept. 9, 1823	Buitenzorg (Bogor), Java	tsunami presumbly at Batava (Djakarta)
Nov. 28, 1836	?	tsunami at Bima, Sumbawa
Nov. 17, 1857	?	tsunami at Kema, North Celebes
Nov. 18, 1857	?	another tsunami at Kema
July 20, 1859		tsunami at Banda
Oct. 6, 1860		tsunami at Halmahera
May 23, 1864		tsunami at Geelvink Bay, New Guinea
Aug. 26–27, 1883	Sunda Strait	five tsunamis, the last one biggest
Aug. 15, 1968		tsunami in Makassar Strait
Feb. 23, 1969		tsunami in Makassar Strait

Palestine, and the Jordan Valley (Willis 1928). According to him, the Sea of Galilee was thrown into violent commotion following the earthquake. Again I found only one instance of a tsunami in Iran (McEvilly and Razani 1973). This tsunami occurred sometime between April 1 and May 9, 1008, following an earthquake in southern Iran.

The tsunami following the Krakatoan eruption in August 1883 was recorded at many stations in India and Arabia. The amplitude varied from 0.6 m at Negapatam to 0.2 m at Aden. The earthquake of Nov. 27, 1945, in the Arabian Sea (with epicenter 290 km from Karachi) generated a tsunami that killed several people and caused property damage at Bombay, coast of Mahran, Baluchistan, and Pasni. Walker (1884) briefly described two tsunamis on the coast of India. The first occurred following an earthquake in the western part of the Bay of Bengal. Tsunamis were observed at Port Blair in the Andaman Islands, and at Dublet near the mouth of Hooghly River.

Cox (1970) modified the list of tsunamis given by Beringhausen (1969) for Southeast Asia. Table 5.25 lists some tsunamis in Indonesia, based on Cox. Table 5.26 is based on Cox (1970) and lists some tsunamis in China and Taiwan.

TABLE 5.26. Tsunamis in China and Taiwan.

	Remarks
Aug. ?, 173	earthquake in sea adjacent to northern China; tsunami in Laichow Bay, Po-hai, and Shantung
Oct. 31, 1076	tsunami in Kwantung (not confirmed)
Summer, 1509	earthquake felt at Woosong (near Shanghai); commotion in sea
Sept. ?, 1640	shocks felt near Shantow (Kwantung) followed by tsunami
Aug. 19, 1670	earthquake felt in Soochow Fu area; many people killed by tsunami
May 22, 1782	tsunami in Taiwan Strait (perhaps storm surge)
Dec. 18, 1867	earthquake near Kilong (Taiwan); tsunami caused property damage and several hundred people drowned
?, 1882	tsunami in Kansu province in north central China (not confirmed)

Chapter 6 Tsunami Warning Systems Past, Present, and Future

Tsunami warning systems of the past and present are based on seismographic and tide-gage information. Recently it has been realized that tsunami detection and warning might be based on the effects created in the ionosphere by a propagating long wave such as tsunami. In the first three sections the instrumentation, warning systems, and sociological problems will be discussed and in the final three sections the concept of a future tsunami warning service based on atmospheric detection of tsunamis will be included.

6.1 Seismic and Tsunami Instrumentation

Seismic Instrumentation

The basic principle of a seismograph and then some recent developments will be considered. In this discussion, the books by Richter (1958) and Hodgson (1964) are followed closely. Although seismic waves lose much of their energy during propagation, they may still be detected by a sensitive instrument called a seismometer. When a recording system is added to the seismometer it becomes a seismograph. Thus, a seismograph is an instrument that records the nature of the earth's movement caused by an earthquake or any other disturbance. The most general movement consists of translation, rotation, and strain. Our interest is in the translation movement due to an earthquake at a distance, and rotational effects that may be important only close to the epicenter (Bullen 1963).

The earliest seismograph appears to have been invented in China in the year 132. This instrument consisted of a ring in which several dragon mouths, each holding a ball, were arranged. When an earthquake occurred, depending on the direction of movement, a particular ball would drop into the mouth of a dragon. By mid-19th century, Italy had seismographs that recorded the time of the earthquake by making a mark on a rotating chronograph drum. Present seismographs, based on the principle of the pendulum, were developed in Japan around 1880; then in Italy, and later in other European countries.

The principle of a pendulum-type seismograph is: in an ideal situation a heavy mass, because of its inertia, would not move at all, while the ground would move following the earthquake. As this cannot be realized in practice, the mass is restrained by a spring or some other restoring force, to return the mass to its original position relative to the ground. The spring should not be strong enough to alter the motion significantly.

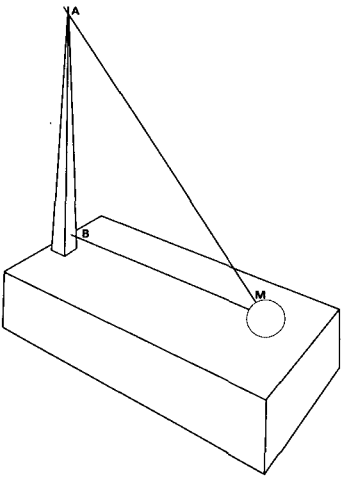


FIG. 6.1. Schematic diagram of a horizontal pendulum, the simplest form of seismometer. (Hodgson 1964)

The horizontal pendulum is shown in Fig. 6.1. A large mass, M, is held in position by a wire, AM, and a strut, MB, pivoted at B; A and B are points near the top and bottom, respectively, of a vertical support, AB (Hodgson 1964). By embedding this vertical support in a concrete pier in the ground a seismometer may be obtained. In the ideal case of zero friction at B, when an earthquake occurs the pier and the upright support will move in response to the incoming seismic waves; however, the inertia of M will tend to keep it from moving. The differential motion between M and the pier is the earthquake signal at this seismometer.

In practice, improvements had to be made to this simple system. Once the pendulum starts to swing because of an earthquake, it will continue to do so, and its motion as time goes on will be unrelated to the actual ground movement. Hence, the pendulum must be stopped after it has recorded the initial ground motion. There are several ways of doing this; a paddle attached to the strut, BM, moves in a pool of oil, which will quickly damp the motion, or alternately a copper vane on the strut moves between the pole pieces of a magnet. The motion of the strut in the vane sets up eddy currents that oppose the motion and thereby bring the pendulum to rest.

The motion can be recorded in several different ways: a pen attached to the strut would draw a straight line on a moving paper roll, but when an earthquake occurs this line would zigzag. A system of levers could be used to magnify the motion of the strut from 10^2 to 10^5 times so that distant earthquakes could be recorded. A mirror and light arrangement for magnification with recording on photographic paper is an alternative. At present it is common to record electromag-

netically by attaching a coil to the strut and making this coil move in a magnetic field, and thereby generate a current, operate a galvanometer on this current, and record on a moving paper roll either by pen and ink or photographically. To conserve paper, it is wound round a rotating drum and the paper moves sideways as it rotates, so when it is removed from the drum, the record appears in the form of a number of parallel lines.

Knowledge of arrival time of different waves at the station is necessary to determine the time of the earthquake. This can be obtained by providing a time scale, as marks at every minute or so, on the record. Because these times must be accurate, crystal clocks are used at present. The site for a seismograph has to be selected carefully because extraneous factors such as microseisms might mask the true record. It is advisable to locate the seismograph in hardcore rock rather than in soft ground.

To describe the translational movement of the ground due to the earthquake three separate components have to be measured; the east-west component, the north–south component, and the vertical component. Thus, at a given seismographic station a complete set of seismographs consists of two horizontal seismographs and a vertical seismograph.

Seismic waves have periods ranging from a fraction of a second to several minutes, and no single instrument can give a uniform response over such a range. Thus, different instruments are needed for different ranges: short-period seismographs are used for the period range of 0.2–2 s, and long-period seismographs for the 15–100 s, intermediate seismographs cover the range of 2–15 s, and ultralong-period instruments for periods over a minute.

Near earthquakes, with predominant periods of a fraction of a second, could be recorded by short-period seismographs whereas distant earthquakes, usually with surface waves with periods of more than 2 s, could be recorded through long-period seismographs. Bullen (1963) mentioned that if the station has only one instrument, usually a seismograph with good response over the range 6–8 s is used. The important observatories contain three seismographs to cover three ranges. If the observatory is located in a seismically active region, then it has, in addition to these, a low-sensitive, strong-motion seismograph that cannot be knocked out by a strong earthquake locally.

The following three parameters specify a simple seismometer (Richter 1958): the free period, the damping constant, and the static magnification. Another parameter called dynamic magnification is the amount by which the magnitude of the ground motion is magnified. A seismometer of free period much shorter than the periods of the waves it records is called an accelerometer, whereas in the reverse situation, it is called a displacement meter.

In the presence of damping, the free period, τ, is modified to τ/j where j is a constant that satisfies the relation $h^2 + j^2 = 1$, h being an instrumental constant. To determine τ, the damping part of the instrument is removed and the free oscillations are timed, or the period of a damped oscillation is timed and corrected. Although the instrumental constant, h, could be used to specify the damping, in practice another constant, ϵ, related to h through $\epsilon = e^{-\pi h/j}$, is used. Thus ϵ is the

ratio of two successive swings (in opposite directions) of the motion given by $h^2 + j^2 = 1$. The static magnification, V, of the instrument can be understood if T is the period and A is the amplitude of the simple harmonic motion in the ground at the seismograph station. If the pendulum performs an oscillation with period, T, and amplitude, B, then the seismogram gives a period, T, and amplitude, VB.

Until the beginning of the 1920s, the important consideration in seismograph design was to lengthen the period of the pendulum so that the dynamical magnification was nearly uniform. According to the formula $T = 2\pi \sqrt{L/g}$ which gives the period, T, of a simple pendulum of length, L, under the action of gravity, g, a pendulum with a period of 10 s needs a cumbersome length of 25 m.

In the Milne-Shaw seismograph, a period of 12 s was achieved by designing the instrument so that only a small part of g is used to control a horizontal bracket pendulum. The restoring force for the inverted pendulum is a heavy mass balanced on a knife edge coupled with springs. Recording is done photographically on smoked paper. A seismograph weighing 22,353 kgm was built in Zurich (Richter 1958). Actually, the tiny torsion seismometers developed by Anderson and Wood in 1922 are much more effective than these cumbersome seismographs.

Bilham and King (1970) discussed the recent advances in strainmeters and compared their advantages and disadvantages with other geophysical instruments. They considered the frequency response and amplitude response of strainmeters. Laser interferometers were also included in their discussion. For recent advances in seismic instrumentation, see Plesinger (1970), Vogel (1970), Willmore (1970), Berckhemer (1970), Husebye (1970), Bonjer and Mueller (1970), Husebye and Bungum (1970), Weichert (1970), and Smith (1975).

A submarine seismograph developed by Koresawa (1963) will be described briefly. As shown in Fig. 6.2, this system consists of an electrodynamic transducer of vertical component, a transistorized amplifier, an oscillograph, a clock, a galvanometer, and a photographic recording apparatus driven by a small motor. This whole assembly is enclosed in an iron case to which heavy ballasts (to put the

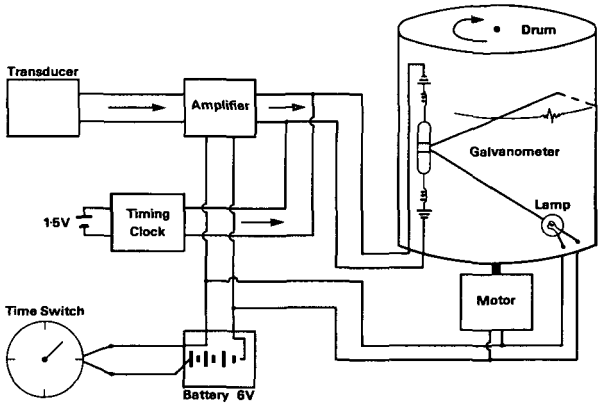


FIG. 6.2. Submarine seismograph. (Koresawa 1963)

seismograph at the ocean bottom) are attached, as well as a float and an arrangement for refloating the seismograph after the ballasts are detached. When the observation is made and the instrument rises to the sea surface, an alarm attached to the system serves as a warning.

Nagumo et al. (1965) described the details of such an ocean-bottom seismograph. Kishinouye (1966) described a modification to the earlier ocean-bottom seismograph. In the latter version, not only the vertical motion at the sea bottom, but also the other components (east–west and north–south) of the motion could be recorded.

Ewing and Ewing (1961) described a telemetering ocean-bottom seismograph that will rest either on the ocean bottom or planted in the sediments. Arnett and Newhouse (1965) described an ocean-bottom seismograph developed as a part of the project "vela uniform" at the Air Force Cambridge Research Laboratories by Texas Instruments. This was used to study the acoustic wave energy generated either by earthquakes or by explosions at the interface of the solid earth with the water. Another important paper dealing with ocean-bottom seismographs is that of Sutton et al. (1965), who described seismic and geophysical measurements at the ocean bottom through seismic observatories.

Bradner et al. (1965, p. 1906) discussed the reliability of seismic measurements made at the ocean bottom and described a technique of improving the reliability. "Motion of the seismometer cases and seismometers due to ocean currents, thermal convection, or mechanical motions of parts in the seismometer package could be responsible for details in the apparent seismic spectra. Thermal convection can be caused, for example, by heat dissipation in the instrument electronics. The validity of the spectra can be most easily checked by making detailed digital analyses of simultaneous spectra from two proximate three-component ocean-bottom instruments."

Tsunami Gauges

The Hawaiian Institute of Geophysics has developed sophisticated gauges to record tsunamis in the deep ocean. Some important papers are Vitousek (1963b), and Vitousek and Miller (1970). It was claimed that tsunamis in the open ocean at depths to 6 km could be measured. Filloux (1970a, b) described Bourdon tube deep-sea gauges. Homma et al. (1966) described the response characteristics of underwater gauges.

Benioff and Gutenberg (1939) described a portable tsunami recorder; Snodgrass (1958) discussed a shore-based recorder of low-frequency ocean waves; Van Dorn (1960a) described a long-period wave recorder for the range of $10–10^5$ s; and Larsen (1971) discussed the electromagnetic field of long and intermediate water waves.

Microbaragraphs and Aerological Data for Tsunami Prediction

The aerological aspects of the tsunami and related problems will be discussed in subsequent sections. Some microbarographs that could be used to record pressure fluctuations in the atmosphere due to any perturbation will be briefly described.

Van Dorn (1960b) described a low-frequency microbarograph that was used by the Scripps Institution of Oceanography, La Jolla, Calif. A hydraulic

resistance-capacitance filter network attenuates the high-frequency gusts and atmospheric tide. The resolution of the instrument was ± 0.05 mb and the instrument could attain sensitivities up to 0.1 mb. Donn (1958) described a microbarovariograph with a maximum resolution of 0.002 mb.

Hines (1972, p. 78) proposed that atmospheric internal gravity waves might be used for tsunami prediction.

> "Tsunamis have their origins in major earthquakes beneath the ocean floor or at its verge. A tsunami rises to rampaging amplitudes only in shallow waters, typically at the coasts themselves, where its energy must be carried by relatively small masses of water. In the open ocean, a tsunami is very tame indeed, producing, perhaps, a few meters' rise or fall of water, and that spread over a horizontal peak-to-trough distance of many km. Tsunamis are therefore virtually undetectable in the open ocean, and the prediction of their appearance on shore is most difficult. But a tsunami must displace the atmosphere as it propagates and the displaced atmosphere must respond by generating a gravity wave. The parameters are such that these waves will be of the internal type, and so will grow exponentially with height. A rise of a few meters at the surface of the water might well amplify to a few km at ionospheric heights, and that sort of amplitude could hardly escape detection if it were sought. We arrive then, at this speculative question: if we wish to keep track of the progress of a tsunami, and so predict with some assurance the onslaught of its destructive force, might we not serve our interests best by keeping watch on the ionosphere?"

One interesting phenomenon to briefly consider is the biological precursors to tsunamis. Musya (1934), Terada (1934), and Adams (1974) discussed the luminous phenomena associated with the Sanriku earthquake tsunami of 1933. Adams (1974, p. 65) states:

> "There have been numerous reports on lights accompanying earthquakes. Since these reported lights were usually observed concomitant with the earthquakes, they are of no predictive value.
>
> "In the case of tsunamis, the light seems to often occur from the direction of the sea. One possible explanation is that the light is generated by luminiscent plankton excited by the tsunami. If this explanation is correct, then the light provides a natural signal of the impending tsunami (Terada, 1934) ... other observers of light associated with a tsunami attributed it to luminiscence of the animals on the sea bottom, exposed during ebbing of the tsunami. This would be of value to a warning system only if the tsunami began as a withdrawal."

Adams mentions that the 1933 tsunami–earthquake pair exhibited anomalous behavior of fishes several hours before the event and gave two specific examples (surface fish feeding on ocean-bottom diatoms and migration of deepwater fish).

6.2 Tsunami Protection Measures

It is obvious there is no foolproof method to protect against tsunami damage to property; nevertheless, breakwaters might offer some protection. There is an enormous amount of literature on breakwaters for protection against short-period waves, but it will not be included in this Bulletin.

Numerical Experiments

Itô (1970, 1971) gave some interesting results on tsunami waves in Ofunato Harbor with and without a breakwater (Fig. 6.3). The tsunamis of 1896, 1933,

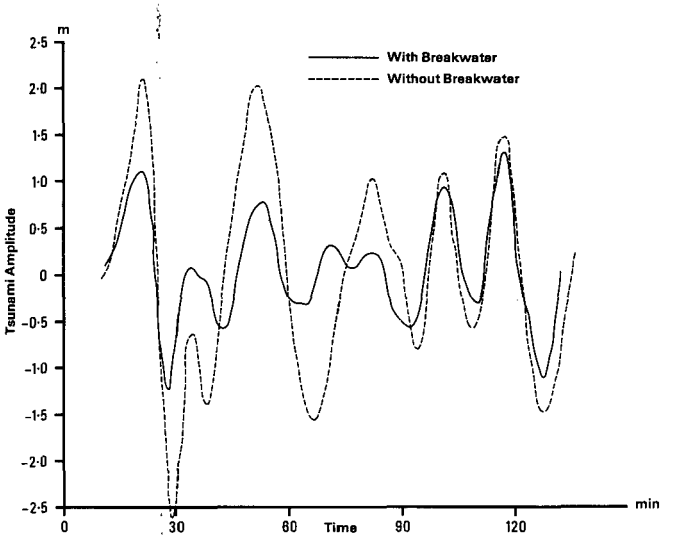


FIG. 6.3. Water-level variation inside a harbor, with and without a breakwater. (Itô 1971)

and 1960 caused heavy damage in Ofunato Bay. A breakwater was constructed in 1967 and a year later, another tsunami occurred. Thus, this case provides an opportunity to examine tsunami waves with and without a breakwater.

Ito used a numerical model to compute the amplitude of the tsunami inside the harbor with and without a breakwater. Figure 6.3 shows that the breakwater indeed damps the tsunami inside the harbor. Murty and Boilard (1970) calculated the effect of a hypothetical breakwater on the tsunami amplitude in Alberni Inlet on the west coast of Canada and their results are in general agreement with those of Ito.

LABORATORY EXPERIMENTS

Kamel (1970) described hydraulic model experiments specifically to understand design criteria for breakwaters to protect Hilo from incoming tsunamis. The experiments were performed in a steel flume 148.1 m long, 1.8 m wide, and 1.2 m deep. The ratio of the model to prototype was 1:50. Some preliminary experiments were made in a three-dimensional model to simulate the tsunami bore, and the data obtained on the height and shape of the bore as well as the height and duration of the overtopping above the barrier were used in the flume experiments.

Based on these experiments, Kamel concluded that efforts to develop an overtopping rubble-mound tsunami barrier with a steep harborside slope were not successful. Wiegel (1960) studied theoretically and through laboratory experiments the wave transmission past a thin rigid barrier, extended above the water surface and to some distance below the water surface. The aim of Wiegel's study was to determine the depth to which such a barrier (realized in practice by mounting a siding on a pile structure) had to be immersed for effectively stopping the waves.

Wiegel concluded that a rigid barrier extending only a short distance below the surface is not useful as a protection measure.

Force of Tsunami Surge on a Structure

Fukui et al. (1963) showed that the maximum pressure, p_{max}, by a tsunami on a vertical (or nearly vertical) wall is

$$p_{max} = \frac{K\gamma u^4}{g^2 D} \tag{6.1}$$

where K is a constant empirically determined to be 0.5, γ is the specific weight of water, g is gravity, D is the height of the bore, and u is the velocity of the tsunami advancing as a bore over dry bed and is given by:

$$u = 1.83\sqrt{gD} \tag{6.2}$$

The pressure is maximum at the bottom of the wall and decreases linearly to zero at a height of 1.5 D.

Matlock et al. (1962) studied the structural damage at Hilo due to the 1960 Chilean earthquake tsunami. The pressure on the structures was estimated as the sum of the hydrostatic pressure and the dynamic pressure, p_D, given by:

$$p_D = \tfrac{1}{2}\rho C_D u^2 \tag{6.3}$$

where ρ is the density of water and the drag coefficient, C_D, was taken as 1.2.

Cross (1967) studied, both theoretically and through laboratory experiments, tsunami surge force due to the propagation of tsunami as a bore over drybed. Cross assumed that the shape of the front portion of the tsunami bore is determined mainly by friction and hydrostatic pressure gradient induced by the surface slopes. Another assumption is that the velocity and acceleration at the front are mainly determined by factors external to the region of the tip of the surge and these were assumed to be known. The present problem is in several respects very similar to the turbidity current problem discussed in Chapter 2.

Cross used momentum considerations to arrive at the following relation for the force, F, on the wall:

$$F = \tfrac{1}{2}\gamma D^2 + C_F \rho u^2 D \tag{6.4}$$

where C_F is a force coefficient defined by:

$$C_F = \frac{F_D}{\rho u^2 D} \tag{6.5}$$

where F_D is the dynamic force on the wall. Equations (6.4), (6.5) can be used to calculate the force exerted by the tip of the tsunami surge on a vertical wall. Cross's laboratory experiments agreed fairly well with his theoretical results. The discrepancies were attributed to the neglect of convective accelerations in the tip region.

6.3 Tsunami Warning Systems of the Past and Present

It is difficult to allocate a date when the idea of tsunami warning systems was conceived. Following the Aleutian earthquake of Feb. 3, 1923, Finch (1924) suggested the possibility of tsunami prediction for warning purposes. However, he stated that his idea was not new and as early as 1904 speculation was made on the possibility of warning against tsunamis. Before the development of seismic instruments, the occurrence of a major earthquake was taken as the first indication of a tsunami.

For a continuously evolving problem such as tsunami warning service, any descriptions of the existing system are likely to become out-dated. Nevertheless, in the following pages, how the tsunami warning service came into existence and how it functions at present will be described.

The U.S. Coast and Geodetic Survey's Tsunami Warning System

Following the disastrous Aleutian earthquake tsunami of Apr. 1, 1946, which killed 173 people and caused property damage of about $25 million in Hawaii, a group of scientists in the U.S. Coast and Geodetic Survey conceived the idea of a tsunami warning service for the Pacific Ocean by seismographs to detect the earthquakes, and tide gages to observe the tsunami. However, in 1946, seismographic recording was done photographically and photographs were not developed until the following day. Other difficulties were: neither the tide gages were suitable to distinguish between tsunamis and any other type of wave, nor were there any communication circuits for rapid transmission of messages.

By 1948, a functional tsunami warning service was achieved. Seismographs with continuous and visible records were developed and installed at Hawaii and other stations in the Pacific. These were equipped with automatic alarm signals. A seismic seawave detector (that could filter out tides and wind waves but leave the tsunami) had been developed and installed at several locations.

Better tsunami travel-time charts were prepared with accuracy of $\pm$ 1.5 min for every hour of travel. Communication channels were established through the Federal Aviation Agency (at that time it was referred to as the Civil Aeronautics Administration) and through U.S. military services. Later National Aeronautics and Space Administration (NASA) and the U.S. Weather Bureau joined the communication network.

The Seismic Sea Wave Warning System (SSWWS) started operating in 1948 at the Honolulu Magnetic and Seismological Observatory, where a 24-h watch was maintained on large earthquakes and tsunamis. Although originally it was intended to provide tsunami warning for Hawaii, later its role was expanded to include several other nations bordering the Pacific.

Figure 6.4 shows the seismograph stations and tide-gage stations on which SSWWS was based. When an earthquake of magnitude large enough to generate a tsunami occurs, the automatic seismic alarm of each seismograph station responds at once and the seismograph stations report arrival times of P and S waves to Honolulu. Based on this data, Honolulu determines the epicenter and if the focus falls in or near the ocean, it issues an advisory bulletin. This bulletin is given

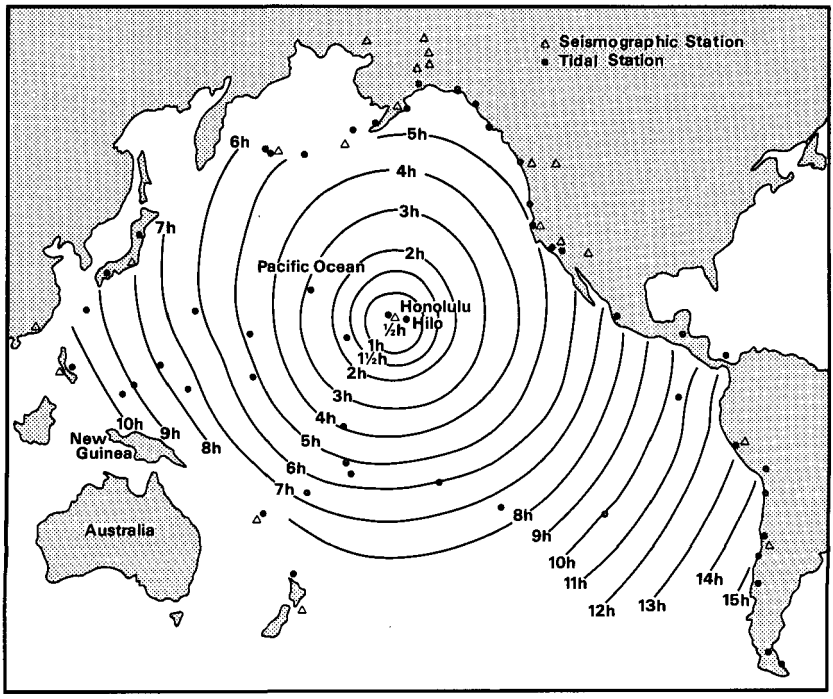


FIG. 6.4. Tsunami warning system showing seismic seawave travel times to Honolulu; tidal (●), and seismographic (△) stations. (International Tsunami Information Center Honolulu)

to SSWWS participants and contains information on the earthquake epicenter and the possibility of tsunami generation. Also, estimated time of arrival (ETA) to each participating station is given, based on the tsunami travel-time curves.

The next step in the SSWWS involves interrogation of the tide stations, especially those closer to the epicenter, to detect any unusual activity, in which case Honolulu issues a tsunami warning. However, local warning and evacuation of people is up to the designated agencies of the participating countries.

The chronological events associated with the SSWWS activities during the 1964 Alaskan earthquake tsunami are taken from Anon. (1965, p. 13–24).

0336:13 (Greenwich Mean Time, March 28, 1964) Earthquake strikes the northern shore of Prince William Sound, Alaska. This disturbance at 8.5 on the Pasadena scale (Richter scale) of earthquake magnitude is the most severe ever reported for North America. (In Alaska, where it is Good Friday afternoon, the earthquake is called the Good Friday Earthquake by the press). The warning alarm sounds at Honolulu Observatory and at four other participating seismograph stations. The SSWWS begins its race with time.

0344. Seismic seawave warning alarm sounds at Honolulu Observatory. Requests issued for immediate readings from seismograph stations at College, Alaska; Sitka, Pasadena, Berkeley, Tucson, Tokyo, and Guam.

0452 Honolulu Observatory completes preliminary determination of location of earthquake epicenter: 61N, 147.5W.

0502 Honolulu Observatory issues first advisory via FAA and Defense Communications network:

> THIS IS A TIDAL WAVE ADVISORY. A SEVERE EARTHQUAKE HAS OCCURRED AT LAT. 61N, LONG. 147.5W, VICINITY OF SEWARD, ALASKA, AT 0336Z, 28 MAR. IT IS NOT KNOWN, REPEAT NOT KNOWN, AT THIS TIME THAT A SEA WAVE HAS BEEN GENERATED. YOU WILL BE KEPT INFORMED AS FURTHER INFORMATION IS AVAILABLE. IF A WAVE HAS BEEN GENERATED, ITS ETA FOR THE HAWAIIAN ISLANDS (HONOLULU) IS 0900Z, 28 MARCH...

0530 Communications inoperative on Alaskan mainland. Honolulu Observatory issues second bulletin. This is an information bulletin, stating that it is not yet known whether a seismic sea wave has been generated, but providing all participants in the SSWWS with estimated times of arrival. The observatory also requests inspection of tide records by observers at Unalaska, Kodiak, Adak, Sitka, Alaska; and Crescent City, Calif.

0555 Kodiak replies:

> EXPERIENCE SEISMIC SEA-WAVE AT 0435Z. WATER LEVEL 10-12 FT ABOVE MEAN SEA LEVEL. WILL ADVISE.

0630 Another message from Kodiak tide observer confirms existence of seismic sea wave. Honolulu Observatory issues third bulletin:

> THIS IS A TIDAL WAVE/SEISMIC SEA-WAVE WARNING. A SEVERE EARTHQUAKE HAS OCCURRED AT LAT. 61N, LONG. 147.5W, VICINITY OF SEWARD, ALASKA, AT 0336Z, 28 MAR. A SEA WAVE HAS BEEN GENERATED WHICH IS SPREADING OVER THE PACIFIC OCEAN. THE ETA OF THE FIRST WAVE AT OAHU IS 0900Z, 28 MARCH.
> THE INTENSITY CANNOT, REPEAT, CANNOT BE PREDICTED. HOWEVER, THIS WAVE COULD CAUSE GREAT DAMAGE IN THE HAWAIIAN ISLANDS AND ELSEWHERE IN THE PACIFIC AREA. THE DANGER MAY LAST FOR SEVERAL HOURS...

(estimated times of arrival are repeated).

0700 Tsunami reaches Tofino, B.C.

0708 Kodiak reports series of waves:

> SEA WAVES AT 0435Z, 32 FT AT 0540Z; 35 FT AT 0630Z; 9.0 m SEAS DIMINISHING WATER RECEDING. EXPECT 6 MORE WAVES.

0739 First wave arrives at Crescent City. The wave is 0.9 m high. Some evacuees return to danger area.

0750+ Four persons drown at DePoe Bay, Oreg.

0900 Tsunami reaches Hawaiian Islands. Damage slight at Hilo, with three restaurants and a house inundated; at Kahului, a shopping center is flooded.

0920 A 3.7-m wave – probably the fourth – sweeps into Crescent City. This wave, and its successors, destroy or displace more than 300 buildings; 5 bulk gasoline storage tanks explode; 27 blocks are substantially destroyed; there are casualties.

1020 Tsunami reaches east coast of Hokkaido, Japan.

1038 Tsunami reaches northeast coast of Honshu, Japan.

1100 Honolulu Observatory sends final bulletin. It is an all-clear for Hawaii;

other participants in the SSWWS are advised to assume all-clear status 2 h after their tsunami ETA unless local conditions warrant continuation of alert.

1355 Tsunami reaches Kwajalein.

1910 Tsunami reaches La Punta, Peru.

The tsunami does much damage along the coasts of Alaska, Canada, and Crescent City, Calif. Minor damage is reported from the coasts of Washington, Oregon, and the Hawaiian Islands. There are casualties in Alaska, Oregon, and California, but the number is in tens, not hundreds and not thousands.

The following is a reproduction from Anon. (1965, p. 24–25) on reminders to population living on coastal areas.

> ***The warning and evacuation of personnel in endangered areas is the job of designated agents participating in the SSWWS. The agent in your location will know what measures to take — and will take them, with your cooperation. You can help him, and yourself, by remembering these facts:***
>
> ***1. All earthquakes do not cause tsunamis, but many do; when you hear that an earthquake has occurred in the Pacific Ocean area, stand by for possible communications from your local emergency headquarters.***
>
> ***2. An earthquake in your immediate area should be interpreted as a natural seismic sea-wave warning; do not stay in low-lying coastal areas after a local earthquake has occurred.***
>
> ***3. A tsunami is not a single wave, but a series of waves. If you have been evacuated as a result of a SSWWS warning, stay out of the danger area until the entire wave-series has passed.***
>
> ***4. Approaching tsunamis are sometimes heralded by a noticeable rising or falling of coastal water. This is nature's seismic sea-wave warning; it should be heeded by those in low-lying coastal areas.***
>
> ***5. There is at present no way to determine in advance the amplitude, or size, of tsunamis in specific locations. A small tsunami at one beach can be a giant a few miles away; don't let the modest size of one make you lose respect for all.***
>
> ***6. The SSWWS does not issue false alarms. When a warning is issued, a seismic sea-wave exists. The tsunami of May 1960 killed 61 persons in Hilo, Hawaii, who thought it was "just another false alarm."***
>
> ***7. All tsunamis — like hurricanes — are potentially dangerous, even though they may not strike each Pacific coastline or do damage at each coastline they strike.***
>
> ***8. Never go down to the beach to watch for a tsunami; when you see the wave you are too close to escape it.***
>
> ***9. Sooner or later, tsunamis visit every coastline in the Pacific. This means that SSWWS warnings apply to you if you live in any Pacific coastal area.***
>
> ***10. During a tsunami emergency, your local Civil Defense, police and other disaster organizations will try to save your life. Give them your fullest cooperation.***

Member nations of SSWWS (USA, American Samoa, Canada, Chile, Fiji Islands, French Polynesia, Hong Kong, Japan, New Zealand, Philippines, Taiwan, and Western Samoa) prepared Anon. (1965).

Alaska

Some details of tsunami information dissemination are provided. Tsunami bulletins and warnings are sent to (1) FAA station at Anchorage, (2) U.S. Air Force weather relay facility at Elmendorf Air Force Base, and (3) Alaska Civil Defense, Anchorage. The Civil Defense Headquarters contacts district or area directors of civil defense, mayors, municipal police departments, radio and television stations, newspapers, and wire services. The U.S. weather bureau uses its facilities

through Alaskan weather stations located at Barrow, Barter Island, Kotzebue, Nome, Fairbanks, Bethel, St. Paul Island, King Salmon, Cold Bay, Shemya, Anchorage, Cordova, Yakut, Juneau, and Annette, and California, Oregon, and Washington states.

Bulletins and warnings are sent via FAA or defense communications system to Hamilton Air Force Base, Calif. This center sends the messages to various places in the three states via the National Warning System (NAWAS). For California, the responsible agencies are the California Disaster Office (CDO) in Sacramento, and the California Highway Patrol in Sacramento. Tsunami alerts are issued usually in the following counties: Alameda, Contra Costa, Del Norte, Humboldt, Los Angeles, Marin, Mendocino, Monterey, Orange, San Diego, San Luis Obispo, San Mateo, San Francisco, Santa Barbara, Santa Clara, Santa Cruz, Solaro, and Sonoma.

In Oregon, tsunami bulletins are received by the NAWAS district warning point in Salem or the State Police duty officer. Tsunami warnings are disseminated to counties Clatsop, Coos, Curry, Douglas, Lane, Lincoln, and Tillamook.

In Washington, messages are received at the Washington State Patrol radio dispatch office in Olympia.

In Hawaii, messages are received at the Honolulu police department dispatch bureau which disseminates the information to the State Civil Defense Agency and Civil Defense agencies in Oahu, Kauai, Maui, and Hawaii.

In American Samoa, messages are received via the Defense Communication network by the office of the Governor of Pago Pago.

Various U.S. governmental agencies receive tsunami messages and bulletins. In the Pacific Islands, the U.S. Naval Station at Guam, the U.S. Naval Station at Midway Island, and the U.S. Weather Bureau stations at Johnston Island and Marshall Island receive the bulletins.

Tsunami messages for Canada are sent to the U.S. Navy Communications in Seattle via the Defense Communications network. From Seattle, the messages are sent to the Canadian Armed Forces naval base in Victoria, B.C. This agency disseminates the warnings to the RCMP and the B.C. Civil Defense.

Tsunami bulletins for Chile are sent through the Defense Communications system to Green Belt, Md., and from there, to NASA Minitrack Station in Santiago, Chile. The station relays the information to the Departamento de Navegacion e Hidrografia in Valparaiso, at the same time the messages are sent to the U.S. Navy Communications Station in Balboa (Canal Zone) and from Balboa to Valparaiso. Alerts are given to various stations and messages could also be sent to Chilean light houses.

Tsunami messages for Fiji Islands are sent via FAA Communications to the Aeronautical Communications Station in Nandi and relayed to the Royal New Zealand Air Force Station in Lawthala Bay. From this station, the message is telephoned to the harbor master in Suva.

Tsunami messages for French Polynesia are sent via FAA communications to the Aeronautical Communications Station in Nandi, and from there to the Aeronautical Communications Station in Papeete, Tahiti, via radio telegraph. This station notifies the Chief of the Mission hydrographique in Papeete.

Tsunami messages for Hong Kong are sent via FAA Communications to the Philippine CAA Communications Station in Manila and then relayed to the Royal Air Force Communications Center in Hong Kong, then the Director of the Royal Observatory is notified.

Tsunami bulletins for Japan are sent through the Defense Communications system to the Japan Meteorological Agency.

Tsunami messages for New Zealand are sent via FAA network to the Aeronautical Communications Station in Nandi, Fiji Islands, or via the U.S. Navy Communications to Christchurch, N.Z. From Fiji or Christchurch, the messages are transmitted to Wellington and then relayed to the Civil Defense Officer.

Tsunami bulletins for the Philippines are sent via the FAA Communications to the Philippine CAA Communication Station in Manila and then relayed to the weather bureau.

Tsunami bulletins for Taiwan are sent via the Defense Communications network to Taiwan Defense Command Communications Center in Taipei and then telephoned to the weather bureau.

Tsunami messages for Western Samoa are sent via FAA Communications to the Aeronautical Communication Station in Nandi, Fiji Islands, and then relayed by radio telegraph to Faleolo Airport. The information is then sent to the APIA Observatory.

Further Developments in Pacific Tsunami Warning System

Murphy and Eppley (1970) discussed developments and plans for the Pacific tsunami warning system since its inception in 1948. Originally it was organized with four seismological stations at College, Sitka, Tucson, and Honolulu, and tide stations at Attu, Adak, Dutch Harbor, Sitka, Palmyra, Midway, Johnston Island, Hilo, and Honolulu. At present all these stations except Palmyra are still part of the warning system.

As of October 1969, there were 21 seismic stations and 41 tidal stations participating in the tsunami warning system (TWS). Eleven nations bordering the Pacific are members.

The following seismic stations recently joined the TWS: Wellington, Port Moresby, Suva, Tacubaya, Antofagasta, and Easter Island. The inclusion of these will provide quicker and more accurate epicenter determinations in certain areas. The tide stations that plan to join the TWS are Galapagos, Marsden Point (New Zealand), Gambier Island, Tuamotu Arch, Okinawa, Amchitka, Salina Cruz and Manzanillo (Mexico), and Talara (Peru).

For locally generated tsunamis in Hawaii, an experimental tsunami warning system is operational. This system consists of seismic and tide-gage stations on the Hawaiian Islands. All data are transmitted to Honolulu Observatory (HO), and recorded there as visual display. Within 10–15 min potential earthquakes capable of generating tsunamis can be identified. The hydraulic gauge data can then be used to supplement the warning.

The Alaska Regional Warning System (ARWS) has been in existence in Alaska since 1967. The observatory at Palmer is the center for ARWS, and Adak, one

of the Aleutian Islands, is responsible for local warnings within 300 km of Adak.

Tsunami Warning System of Canada

Dohler (1970) described a tide-gage data telemetry system that has been developed for tsunami warning in Canada. Starting in 1966, Canada installed equipment at three selected stations, Tofino, Victoria, and Langara Island, to supply water-level data, mainly to the Pacific Tsunami Warning System (PTWS) at Honolulu, to assist in decision making. Special equipment at the three locations is supplemented with ordinary tide-gage functions. The equipment also has a dialing unit which automatically calls a predetermined party in the event of an unusual water-level condition. The equipment is so instructed that any disturbances in excess of specified conditions, and different from normal tidal oscillations, will be interpreted as a tsunami.

Some instrumentation involved in these operations will be briefly described. For details see Dohler (1970). At the Tofino and Victoria stations, the conventional-type tide gages involving a float and a counterweight are used. At the third station on Langara Island a potentionmeter-type, absolute pressure transducer is used. The pressure recording system consists of a pressure head, a three-conductor connecting cable, and a recorder unit. The principle involved here is determination of the height of a water column by measuring the hydrostatic pressure with a resistance potentionmeter-type, absolute pressure transducer. Atmospheric pressure changes that affect the total pressure, measured by the submerged pressure transducer, are compensated in the recorder unit.

Tsunami Warning Service in Japan

The Japanese cabinet approved the tsunami warning system on Dec. 2, 1949, and it came into existence on Apr. 1, 1952 (Anon. 1972). The tsunami warning service in Japan consists of three parts: (1) tsunami forecast system – Japan Meteorological Agency (JMA) is responsible; (2) dissemination system for sending messages to the coastal areas – civil and public organizations; (3) terminal systems to evacuate the people – local authorities.

The tsunami warning system of JMA is based on seismic and tidal monitoring stations and analysis centers. If land communication lines are broken for any reason, wireless communication will be used. Figure 6.5 shows the 17 divisions of the Japanese coast, each region under the jurisdiction of one of the five regional tsunami centers.

If the epicenter is more than 600 km from the Japanese coast, then JMA Tokyo headquarters has the responsibility of analyzing the earthquake. For nearby earthquakes, the regional centers are responsible. At headquarters two persons are on watch 24 h a day, and at the regional centers one person is on watch round the clock.

Japan Meteorological Agency had 106 seismic stations. The four seismic stations at Okinawa joined the JMA network on May 15, 1972, bringing the total to 110. Of these, 69 stations are designated as seismic stations for tsunami warning. Of the 69, 13 are selected for distant earthquakes and are called teleseismic stations for tsunami warning.

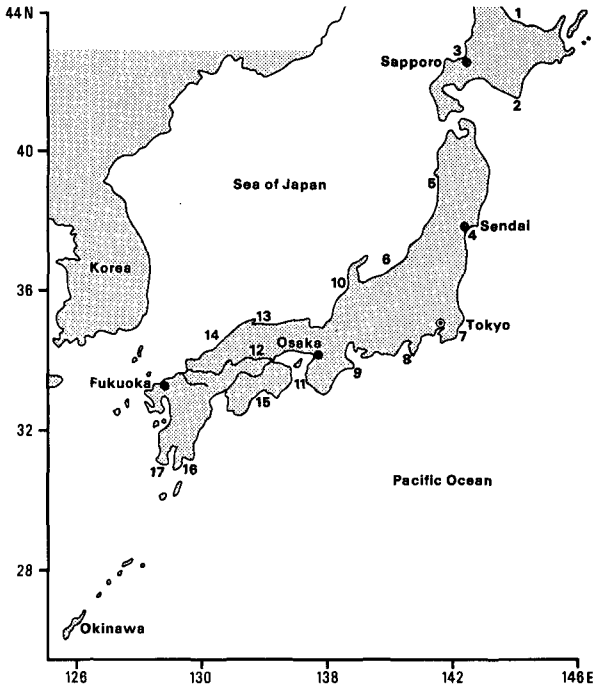


FIG. 6.5. Japan Meteorological Association network for tsunami warning. Numbers show divisions of coasts assigned to respective tsunami centers; Sapporo, 1, 2, 3; Sendai, 4, 5; Tokyo, 6, 7, 8, 9, 10; Osaka, 11, 12, 13, 14, 15; Fukuoka, 16, 17; ● regional tsunami centers; ◉ national tsunami center. (Japanese National Report)

When an earthquake occurs, a seismic station immediately interprets the seismogram and sends the results by telegram to its tsunami center. This telegram is referred to as "seismic-telegram."

Japan Meteorological Agency operates 53 tide-gage stations and 11 are equipped with telemetering devices.

When the alarm bell rings at the regional tsunami centers, the location of the epicenter is first determined by the S–P times. The second step is determination of the grade magnitude of the tsunami. The grade magnitude works on a 3-grade scale; grade 1 means major tsunami, grade 2 signifies a minor tsunami, and grade 3 means no tsunami. The grade magnitude is determined by the amplitudes reported in the seismic-telegram (Fig. 6.6).

The third step is preparation of the warning message. Five degrees are used for this purpose. In these messages, the tsunami height refers to the amplitude above the normal tide level. First degree means, no tsunami; second degree refers to a tsunami of unknown amplitude; third degree refers to a minor tsunami (not exceeding 2 m); fourth degree refers to a major tsunami (heights from 1 to 3 m); and fifth degree means the warning is cancelled and there is no more danger.

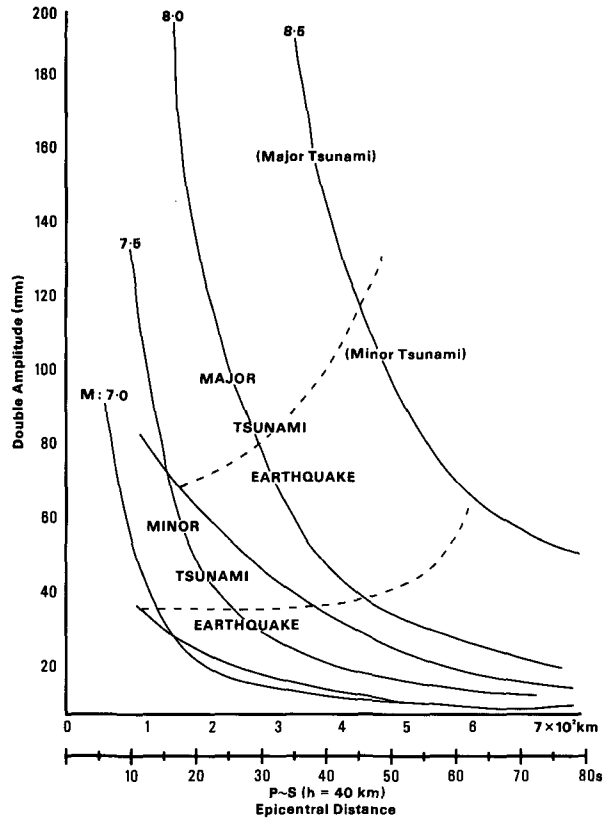


FIG. 6.6. Japan Meteorological Association tsunami forecasting chart. (Japanese National Report)

For tsunamis originating at distances greater than 600 km from the Japanese coast, the National Center in Tokyo is responsible for warning the public. This warning is based on bulletins issued by the Honolulu Warning Center. Since October 1963, the Soviet Union has been issuing tsunami broadcasts in English from Khabarovsk. For tsunamis originating in the northern Pacific, Japan uses these broadcasts.

Nakayama (1972) described the tide telemetering system employed by JMA for warning of tsunamis and storm surges.

TSUNAMI WARNING SERVICE IN SOUTH PACIFIC

The tsunami warning system for New Caledonia and Tahiti is somewhat different from the others and is based on T-phase (see Chapter 3). Actually, this system is applied for Tahiti only because barrier reefs protect the New Caledonia shoreline and no tsunami warning is needed there.

This warning system will be briefly described, based on a paper by Talandier (1966). Five short-period, vertical seismographs were established in the island group

of Tahiti and Moorea. The separation between these seismographs varies from 15 to 50 km and they are equipped with filters to eliminate background noise due to swell. Based on the difference in arrival times of seismic waves at these stations, a rough but instantaneous idea of the distance of the earthquake and location is obtained.

If two of the five stations report P waves with sufficient amplitude, then an initial alarm is given. Experience shows that any earthquake followed by a tsunami produces large amplitude T waves which travel slower than P waves, but (as sound waves in the water) faster than swell or tsunami. Although the warning time is much shorter than that of Honololu, the Tahiti warning system is much more reliable for that area. However, this statement should not be interpreted as a criticism of the SSWWS, whose purpose is general warning over the whole Pacific area.

Tsunami Warning Service for USSR

Abouziyarov (1970) described problems of the tsunami warning service in the Soviet Union. The main tsunami threat is from the seismic areas over the continental slope of the deepsea Kuril-Kamchatka trough. Sometimes the tsunamis take only 20–30 min to arrive at the nearest shore.

Based on past history, the Kuril-Kamchatka region has been divided into three zones: (1) the most violent tsunami zone on the east coast of Kamchatka between Cape Lopatka and Cape Kamchatka, and the Komandor Islands; (2) moderate tsunami zone opposite the South Kuril Islands beginning at Urup; (3) no tsunamis in the area opposite the middle Kuril Islands (i.e. between the Straits of Krwenstern and the Strait of Boussol).

Two types of tsunami sources exist in the far eastern region of USSR. The sources at depths of 5–6 km near the deepsea trough at the positions of the longitudinal breaks could cause large tsunamis affecting distances to 1000 km. On the other hand, sources near the shore associated with lateral faults could cause tsunamis affecting 300–400 km.

The tsunami warning service was established following the Kamchatkan tsunami in 1952. Three tsunami warning centers were located at Petropavlovsk-on-Kamchatka, Kurilsk, and Uthno-Sakhalinsk. Table 6.1 summarizes the activities of the tsunami warning service between 1958 and 1965. Special seismographs called UBOPE were developed to quickly determine the epicenters of earthquakes in the magnitude range of 7.0–8.5 and at distances of 150–2000 km.

The Kuril-Kamchatka coast is divided into six regions, according to the predicted intensity of tsunami (using statistical relations based on past data): (1) Kamchatka and Kronoki Bay; (2) the Cape of Shipunsky; (3) southern Kamchatka; (4) northern Kuril; (5) Rashuwa, Ketoi, and Simushir Islands; and (6) southern Kuril.

Sociological Problems

Few scientific studies have been made on human behavior during a tsunami warning evacuation and the study by Lachman et al. (1961) points to the necessity of unambiguous warning procedures. The authors conducted a survey on human behavior in Hilo, Hawaii, during the 1960 Chilean earthquake tsunami and dis-

TABLE 6.1 Activity of the tsunami warning service in the Far East from 1958 to 1965. (Abouziyarov 1970)

	Organization reporting, data used	Processing time of seismic data (*min*)	Tsunami characteristic
Nov. 7, 1958	Sakhalinsk Administration of Hydrometeorological Service on basis of broadcast by Japan Meteorological Agency	–	moderate tsunami south of Kuril Islands
May 4, 1959	seismic station Petropavlovsk	5	weak tsunami area Cape Shipunsky and Bay of Avachinsk
Mar. 20, 1960	tsunami station Uthno-Sakhalinsk	10	no tsunami
May 24, 1960	Sakhalinsk Administration of Hydrometeorological Service on basis of information from a man on port post duty Sevezo-Kurilsk	–	destructive tsunami on Pacific coast of Kamchatka and Kuril Islands
July 29, 1960	tsunami station Uthno-Sakhalinsk	10	no tsunami
Feb. 13, 1961	tsunami station Uthno-Sakhalinsk	7	very weak tsunami south of Kuril Islands
Oct. 13, 1963	seismic tsunami station Uthno-Sakhalinsk	10	destructive tsunami on Pacific coast of Urup and Iturup islands

cussed the consequences of an ambiguous tsunami warning system. Some highlights are (Lachman et al. 1961, p. 1405):

> "... Despite at least 10 hours of warning, the wave killed 61 persons, injured several hundred more, and completely destroyed an estimated 500 dwellings. A study group was organized by the Hawaii Division of the Hawaiian Academy of Science to objectively examine the human element in the disaster. The objectives of the research, subsequently undertaken, were to study the subjective interpretations of the warnings and the resulting behaviour. A questionnaire was prepared to be administered to a cross section of the adult population of the affected area."

Characteristics of the sample – Composition of the sample of 327 individuals in terms of sex, age, race, and education is summarized in Table 6.2. The sample included 28 persons who had lost one or more members of their immediate family in the disaster. Also, 50 persons in the sample (15% of those interviewed) had suffered injuries. Of the 50, 47 had not left their homes, the 3 injured among the evacuees either (i) left but later returned to their homes or (ii) sought safety in another stricken area.

Preimpact period – The Siren Signal: The tidal wave warning siren sounded for a 20-min period, more than 4 h prior to the impact of the wave, yet only 40% of the sample evacuated, and presumably this was the percentage of the entire population of the devastated areas who evacuated. Therefore, the question was

TABLE 6.2. Sample of human behavior during the tsunami of May 1960. (Lachman et al. 1961)

	Total sample		Nonevacuees		Evacuees	
	No.	%	No.	%	No.	%
Sex						
Male	140	42.8	88	44.7	52	40.0
Female	187	57.2	109	55.3	78	60.0
Age						
18–27	59	18.0	29	14.7	30	23.1
28–37	76	23.2	41	20.8	35	26.9
38–47	77	23.5	45	22.8	32	24.6
48–57	64	19.6	45	22.8	19	14.6
58–67	33	10.1	25	12.7	8	6.2
68 or older	18	5.5	12	6.1	6	4.6
Race						
Caucasian	8	2.4	3	1.5	5	3.8
Filipino	33	10.1	23	11.7	10	7.7
Hawaiian	74	22.6	23	11.7	51	39.2
Japanese	178	54.4	123	62.4	55	42.3
Portuguese	15	4.6	14	7.1	1	0.8
Other	19	5.7	11	5.5	8	6.1
Education						
Grade, intermediate school	151	46.2	100	50.8	51	39.1
High school	152	46.4	81	41.1	71	54.6
College	24	7.3	16	8.1	8	6.2

TABLE 6.3. Various interpretations of the siren from individuals interviewed following the tsunami of May 1960. (Lachman et al. 1961)

	Total sample		Nonevacuees		Evacuees	
Interpretation	No.	%	No.	%	No.	%
Alert	14	4.8	10	5.9	4	3.3
Warning	13	4.5	8	4.7	5	4.0
Preliminary signal preceding evacuation signal	71	24.4	55	32.4	16	13.2
Evacuation signal	84	28.9	10	5.9	74	61.2
Signal to await further information	26	8.9	24	14.0	2	1.7
Signal to make preparations	18	6.2	12	7.1	6	5.0
Subjective meaning not ascertainable	65	22.3	51	30.0	14	11.6
Total	291	100.0	170	100.0	121	100.0

posed. "Did you hear the 8:30 siren on Sunday, May 22?" Of those interviewed, 309 (95%) said they had heard the siren; 18 (5%) said they had not. Of those who heard the siren, 127 (41%) evacuated and 182 (59%) did not.

The 309 individuals who had heard the siren were asked further if they knew what it meant. Only 18 individuals (6%) said they did not. However, in the course

of analyzing the data, it became obvious that not all the 291 persons who said they knew what the siren meant had the same understanding of its significance.

Table 6.3 summarizes the various meanings the siren had for the 291 individuals who heard it. As the siren meant so many different things to different people, one wondered just what it was meant to signify officially. Consulting the telephone directory (presumably the official medium for disseminating this information), the siren signal was characterized as an "alert," with no indication as to what behavioral response was expected of the public on hearing it. Responses to the siren are shown in Table 6.4. The disaster victims are classified according to their immediate response to the siren – whether they continued their normal routine, evacuated, or waited for information and instructions. Table 6.5 lists sources of information other than the siren.

TABLE 6.4. Relation between ultimate evaluation and immediate response to the siren. (Lachman et al. 1961)

	Total sample		Nonevacuees		Evacuees	
Immediate response	No.	%	No.	%	No.	%
Did nothing (continued normal routine)	44	15.0	40	23.3	4	3.3
Evacuated	94	32.0	12	7.0[a]	82	67.2
Waited (for advice, information, etc.)	131	44.5	100	58.1	31	25.4
Other (returned home, etc.)	25	8.5	20	11.6	5	4.1
Total	294	100.0	172	100.0	122	100.0

[a] Represents individuals who evacuated when they heard the siren but returned home prior to time of impact.

TABLE 6.5. Information source concerning the May 1960 tsunami, other than the siren. (Lachman et al. 1961)

	Individuals reporting	
Information source	No.	%
Relatives, friends	45	17.2
Radio, TV	178	68.2
Government (police, firemen, civil defense)	8	3.1
Radio, TV, relatives, friends	22	8.4
Radio, TV, government	6	2.3
Relatives, friends, government	1	0.4
No answer	1	0.4
Total	261	100.0

6.4 Acoustic and Internal Gravity Waves in the Atmosphere

Structure of the Atmosphere

Dobson (1963) gave a comprehensive view of the atmosphere in his book; the frontispiece depicts its structure (Fig. 6.7). The nomenclature of different regions of the atmosphere is confusing at present because too many names are used to designate the same region.

One important characteristic of the atmosphere is the change of temperature with height. As the temperature reverses several times with height there are three warm and two cold regions. The warm regions are near the earth's surface, at a height between 40 and 60 km and above 150 km (more or less the top of the atmosphere). The first cold region extends from about 10 to 35 km, whereas the second is around 80–90 km. The exact distribution of temperature with height depends on latitude and to some extent on time of year.

Figure 6.7 shows that the temperature decreases upward from the earth's surface as far as the level called the tropopause. The atmosphere below the tropopause is the troposphere and the region above the tropopause is the stratosphere.

Deductions from meteor observations showed that the temperature at about 50 km is approximately equal to that at the surface of the earth. A small amount of ozone is present in the atmosphere, and because the ozone is opaque to ultraviolet light it absorbs solar radiation, and this creates the warm region around the 50-km level.

The air generally conducts electricity and conductivity above the 80-km level is much greater than at lower levels, especially during sunlight hours. This region of the atmosphere, called the ionosphere, is basically responsible for allowing radio waves to propagate over great distances. Electrical currents of the region are related to variations of the earth's magnetic field. At least four regions exist in the ionosphere, known as the D, E, F_1, and F_2 layers, with heights above the earth's surface varying roughly from 70 km to 400 km.

Ionization (when a molecule either gains or loses an electron) in the lower layers of the atmosphere is mainly produced by cosmic radiation. The intensity of ionization in the ionosphere is much greater than in the troposphere or stratosphere, and has an entirely different origin. The higher levels of the atmosphere contain little air and absorb only small amounts of solar short-wave radiation; consequently the ionization is small. When solar radiation reaches lower levels, the abundance of air absorbs the radiation strongly, producing greater ionization. Because of absorption when passing through these layers, the intensity of solar radiation is reduced greatly, and little ionization takes place further down. Thus, there will be some level where the rate of ionization is a maximum.

Another important difference between ionization of air in the ionosphere and that in the troposphere and lower stratosphere is that ions are found in abundance in the lower regions, whereas electrons mainly give the ionosphere its characteristics.

Acoustic and Internal Gravity Waves in the Atmosphere

Two major mechanisms appear to generate waves in the atmosphere (Hines 1960): one is tidal oscillations of the atmosphere, and the second is tropospheric

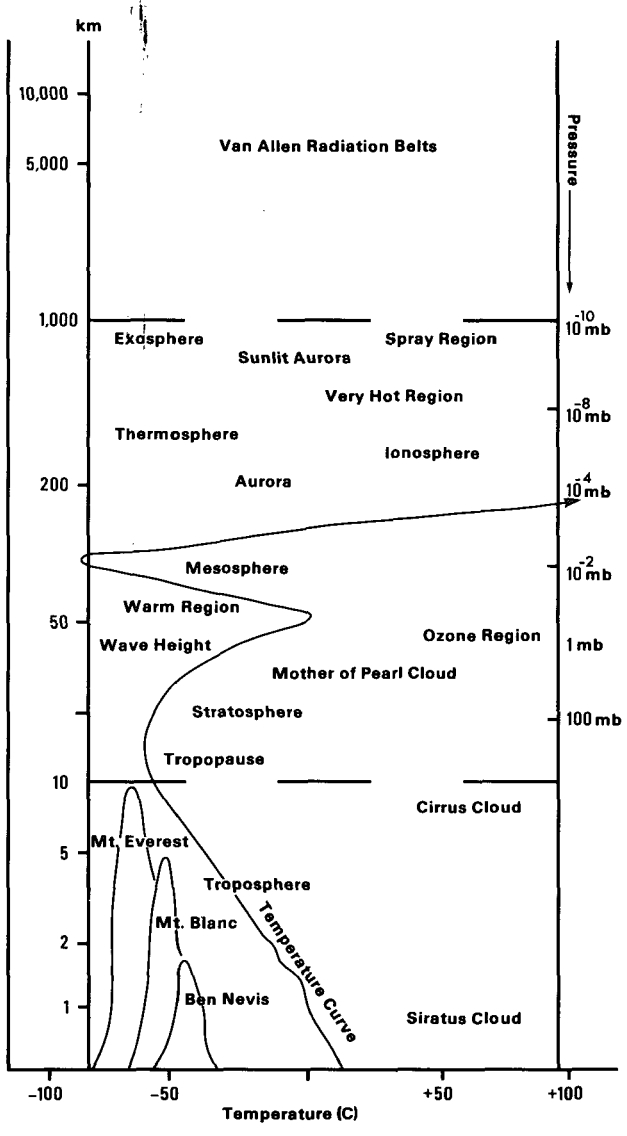


FIG. 6.7. Vertical structure of the atmosphere. (Dobson 1963)

wind systems. In considering any wave motion in the atmosphere, both gravitational and compressional forces must be considered. Hines showed that even a simple model of the atmosphere (which is stationary and of uniform temperature and composition) can produce two distinct classes of wave motion with one feature in common; in the absence of dissipative forces both are unattenuated in the horizontal direction. However, in their vertical behavior they differ drastically. The class identified as surface waves, although having an exponential variation vertically,

cannot support any phase propagation in the vertical direction. The class identified as internal waves can support significant phase propagation in the vertical direction.

The internal atmospheric waves are of two types (Obayashi 1963). In the high-frequency range they are acoustic (sound waves in the atmosphere), whereas in the low-frequency range they are internal gravity waves. Low frequency refers to a period of several minutes when gravitational forces introduce a profound anisotropy.

Two characteristic frequencies separate the two limiting cases. One is the Brunt-Vaisala frequency, ω_g, also called the gravitational stability frequency, and the other is the modified acoustic stability frequency, ω_a. For an atmosphere in hydrostatic equilibrium, the two frequencies are given by:

$$\omega_g^2 = -g\left(\frac{g}{c^2} + \frac{1}{\rho}\frac{\partial\rho}{\partial z}\right) = \frac{g}{H}\left(\frac{\gamma-1}{\gamma} + \frac{\partial H}{\partial z}\right) \tag{6.6}$$

and

$$\omega_a^2 = \left(\frac{c}{2\rho}\frac{\partial\rho}{\partial z}\right)^2 = \frac{\gamma g}{4H}\left(1 + \frac{\partial H}{\partial z}\right)^2 \tag{6.7}$$

Here g is acceleration due to gravity, $\rho(z)$ is the density of the atmosphere, $c(z)$ is the speed of sound, γ is the ratio of specific heats, and H is the scale height (scale height, H, is the equivalent height of a homogeneous, isothermal atmosphere and is given by $\frac{K\theta_A}{mg}$ where K is Boltzmann's constant, θ_A is the absolute temperature, g is gravity, and m is the mean molecular mass) of the atmosphere (a function of the vertical coordinate, z). The phase-velocity, V, of the waves is given by:

$$\left(\frac{V}{c}\right)^2 = \frac{1 - Y\sin^2\theta}{1-X} \tag{6.8}$$

where

$$X \equiv \left(\frac{\omega_a}{\omega}\right)^2$$

and

$$Y \equiv \left(\frac{\omega_g}{\omega}\right)^2 \tag{6.9}$$

and θ is the angle between the field of gravity and the wave normal. Here ω is frequency and $T = 2\pi/\omega$ is the period. Waves with periods less than T_a are acoustic waves; those with periods greater than T_g are gravity waves. In the period range, $T_a < T < T_g$, no internal atmospheric waves exist. For acoustic waves (with periods less than T_a), the phase velocity is approximately equal to the velocity of sound but tends to ∞ as the periods approach T_a. For gravity waves, the phase

as well as the group velocities are zero at $T = T_g$, and the velocities increase with increasing T and approach $\frac{Y}{X} \sin \theta$ for longer periods. The acoustic waves more or less propagate isotropically whereas the gravity waves propagate mainly in a horizontal direction and exhibit strong anisotropy.

Hines' Theory for Acoustic and Gravity Waves

Hines (1960) developed a theory in connection with his interpretation of the irregular motions in the upper atmosphere in terms of internal atmospheric gravity waves. He used a simple model of the atmosphere and brought forth some important features. In the absence of waves, his model atmosphere is stationary and has uniform temperature and composition. As all three assumptions are drastic, further improvements of the theory are considered. Temperature varies in a complex manner in the atmosphere, as opposed to an isothermal state. The atmosphere, of course, is not stationary; an important force is the Coriolis force due to earth's rotation. The assumption of uniform composition, although far from the truth, nevertheless is not as drastic as the others for this particular problem.

Hines assumed that the superimposed wave motion on the atmosphere has only perturbation magnitude (i.e. second and higher order terms for the amplitude of oscillation in the equations of motion are ignored) and occurs adiabatically. Forces taken into account are gravity, inertia, and pressure gradients. The gravity field is assumed to be constant in magnitude as well as direction. Details of the mathematics leading to the existence of acoustic and internal gravity waves is omitted here but can be found in Hines (1960).

Next Hines examined the problem of dissipation. The two basic causes of energy dissipation are molecular viscosity and thermal conduction. Hines also considered the nonlinear effects and concluded that in certain parts of the spectrum and at certain heights, the nonlinearities could be important.

Further Theoretical Developments

Although Hines' original work involved only an isothermal atmosphere, subsequent models used many layers to model realistically the variation of temperature with height. For example, Harkrider (1964) used 40 layers, each a thin isothermal layer. Many numerical studies have been made for the wave-guide modes of acoustic and internal gravity waves for different atmospheric models, all more or less derived from the Air Research and Development Command (ARDC) standard atmosphere (see Fig. 6.8). For periods ranging from a few seconds to a few minutes, these studies were satisfactory in the sense that the calculated values agreed well with observed values.

Several authors introduced wind structure and considered its effects on the gravity wave. The work of Weston and vanHulsteyn (1962) is typical. They showed that wind increases the phase velocity of the gravity wave mode. Some important results of the theoretical studies are: in the long-period wave range of 10–100 min, propagation is mainly in the form of gravity waves. There has been some confusion in the atmospheric propagation problems because the distinction between acoustic

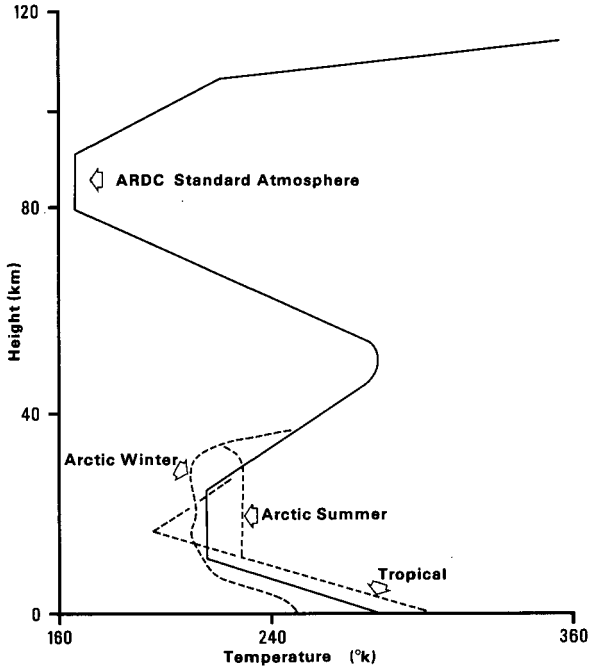


FIG. 6.8. Standard and extreme ARDC atmospheres. (Harkrider 1964)

modes influenced by buoyancy effects, and internal gravity wave modes influenced by compressibility effects, has not been clear in the commonly used term acoustic-gravity wave propagation. Actually, as far as the lower 100 km or so of the atmosphere is concerned, the behavior of gravity and acoustic modes is sufficiently different that no confusion arises. The difference in behavior could be easily visualized in terms of the two limiting frequencies already introduced; the acoustic low-frequency cutoff, ω_a, and the Brunt-Vaisala frequency or the internal gravity wave, high-frequency cutoff, ω_g. In the literature several notations have been used for these; Tolstoy and Pan (1970) used ω_0 and N.

In the regions where $\omega_a > \omega_g$, there is no ambiguity in the two types of modes. However, centered at about 120 km in the atmosphere there is an anomalous zone in which $\omega_g > \omega_a$. This anomalous zone is probably important for ground-level detection of surface gravity waves excited by atmospheric nuclear explosions as will be shown later.

Tolstoy and Pan (1970) showed that simple models involving two to four layers in the atmosphere, can be used to determine the propagation and dispersion of the lowest two to three gravity modes of the atmospheric wave guide. Two important facts brought out by this paper are: these simple models could explain the long-period portion of the 300 m/s group velocity plateaus in terms of coupling effects of the internal gravity wave guide. Tolstoy and Pan cautioned that, as this result is is obtained from an atmospheric model with two incompressible layers, the 300 m/s

value is somewhat fortuitously related to the velocity of sound in air. Also, surface gravity-wave modes of the atmosphere are better understood by this approach.

Another concept introduced pertains to the top boundary condition in the atmosphere. For example, Pfeffer and Zarichny (1962), Press and Harkrider (1962), Harkrider (1964), Daniels (1967), and Harkrider and Wells (1968) used a free-surface condition, at several heights arbitrarily, to compute surface modes of the atmosphere, but did not explain the logic of this.

Tolstoy (1967) showed that it is indeed impossible to justify the use of a free-surface boundary condition, and thereby make the selection of H, the effective atmospheric wave height, less arbitrary. For this he used the concept of vacuum, i.e., at heights where the mean free path, ℓ, of the neutral gas molecules exceeds the wavelength, L, of the disturbance, the medium is considered to be vacuum. Hence, for heights where $\ell \ll L$, the usual continuum equations apply. Then the effective free surface of the atmosphere is at height, $z = H$, where $\ell = L$. This means the effective height of the atmosphere depends on the wavelength of the disturbance.

However, the region, $Z = H$, at which $\ell \simeq L$ is not infinitesimal, but is a transitional layer of thickness, d (say). In this transition layer, strictly speaking, Boltzmann's equations must be applied. For $d \ll L$, the layer mainly behaves as a region with large viscosity and strongly attenuates waves with periods less than 10 min. Another consideration is that (at the heights relevant here) because of large ionization, hydromagnetic interactions could occur. However, Dungey (1954), Fejer (1960), and Hines (1955) showed that these interactions are effective only for periods greater than or equal to 3 h. Hence, it can be assumed that the atmosphere acts as a window for surface gravity waves, with periods between 10 and 200 min.

Tolstoy and Pan's Mathematical Model

The simple mathematical model of Tolstoy and Pan (1970) for wavelengths $L > 300$ km will now be discussed, with particular attention to aspects of the propagation directly relevant to recent observations with microbarographs. They showed motions with 600 m/s and energy concentrated around the 15-min period.

The logic behind using a simple model is given by Tolstoy and Pan (1970, p. 35):

> "Since in the present study we are interested chiefly in internal and surface gravity modes with periods > 10 min and wavelengths > 200 km, a small number of layers provides adequate approximations for discussing the propagation properties of atmospheric waves. One must remember that the frequency-wave number relationship and the group velocity may be written as quotients of two quadratic forms in the wave amplitudes (Boit, 1957). These are stationary with respect to variations of the amplitude, so that in most calculations relatively large errors in the amplitude distribution of the displacement field can be tolerated, without appreciably affecting the eigenvalue and propagation velocity calculations. Thus, even though the amplitude of the vertical displacement predicted by an oversimplified model may be in error, the characteristic curve calculations can be quite accurate.
>
> "We have limited ourselves to calculations on two and four-layer models, illustrating the effects of compressibility, of the upper boundary condition, of the earth's

rotation, and of layering upon the propagation of long periods. Within the limitations imposed by the small number of layers, we have used models that represent fits to the Vaisala frequency, the density, and sound velocity functions in the earth's atmosphere."

Tolstoy and Pan's model allows interpretation of recent observations by microbarographs. Tolstoy and Herron (1970) also gave a new interpretation of the traveling disturbances in the ionosphere due to nuclear explosions. This is possible because in the moderately long-period range of 10–30 min there is considerable separation between the velocities of surface and internal gravity waves.

The main difficulty appears to be in the magnitude of the pressure signal. Harkrider and Wells (1968) showed that the observed pressure amplitudes from peak to trough of 10–100 μb would require unrealistically large vertical displacements of the atmosphere above 100 km. Other calculations with simple models essentially confirm their result. Tolstoy and Pan (1970) attributed this to ignoring the anomalous zone between 110 and 200 km, and ignoring the influence of the winds at high altitudes. When these are taken into account the difficulty disappears. That is, the vertical displacements of the atmosphere above 100 km need not be ridiculously large to be consistent with ground-level pressure amplitudes in the range of 10–100 μb.

Next Tolstoy and Pan considered the question of the attenuation of the surface gravity waves and showed that generally the attenuation is small for periods greater than 10 min for the modes m = 0 and 1.

Liu and Yeh (1971) studied the excitation of acoustic–gravity waves in an isothermal nonrotating atmosphere; because their model is highly idealized it is not included here. Yeh and Liu (1972) gave a good review of the propagation of waves in the ionosphere.

6.5 Atmospheric Nuclear Explosions

Before discussing the acoustic–gravity waves that could be generated by nuclear explosions in the atmosphere, some general effects of atmospheric nuclear explosions are described. The release of a large amount of energy in a small volume in a short time interval is referred to as an explosion (Glasstone 1962). This quick release of energy, whether from conventional chemical explosives or from nuclear materials, produces a great increase in temperature and pressure, so that all materials in the immediate vicinity are transformed into hot and compressed gaseous forms. At high temperatures and pressures these gases expand rapidly and cause a pressure wave, generally called a shock wave. However, this term is used only for underground and underwater tests, whereas for explosions in the atmosphere the term used is blast wave.

Two factors primarily determine the amount of energy (in proportion to the total energy) that will arrive as thermal energy at a given point at some distance from the site of the explosion; the nature of the nuclear device and the nature of the surroundings. At higher levels in the atmosphere there is little air to interact with the energy of the explosion and the proportion of the fission energy converted into the blast wave is small in comparison with the portion that goes into thermal

energy. On the other hand, at a relatively low level of 30.5 km, about 50% of the energy goes into blast, 35% into thermal energy, 5% into the initial nuclear radiation, and the rest (i.e. 10%) is accounted for by residual nuclear radiation. In the extreme case of an underground explosion that is confined, little thermal radiation escapes into the atmosphere.

Glasstone (1962) identified five types of explosions: air burst, high altitude burst, underwater burst, underground burst, and surface burst. He used the differences in the nature of the accompanying fireball to set them apart. The fireball is a hot and luminous mass (roughly spherical) created from the residues of the exploded nuclear device as well as from the surroundings. An explosion at a level in the atmosphere not greater than 30.5 km, followed by a fireball that does not touch the ground surface at the time of its maximum brilliance, is called an air burst. Glasstone stated that a 1.02×10^9 kgm device would cause a fireball with a radius of 0.88 km.

If the device is exploded at an altitude greater than 30.5 km it is called a high-altitude burst. A surface burst is when the weapon is exploded either at or just above land or water. If the explosion occurs beneath the ground, it is called an underground burst, and beneath water it is called an underwater burst; these can be called subsurface bursts.

Certain terms will now be defined following Glasstone (1962). The overpressure in the blast wave is the excess over the atmospheric pressure of 101.4 kN/m^2 (6.895 kN/m^2 = 1 psi) at standard sea-level conditions. Most material damage from a nuclear explosion is caused by the shock or blast wave. A difference of air pressure on different surfaces of a building, for example, will produce a force on the building. The so-called overpressure should be considered when estimating the destructive effects of a blast wave. The overpressure is maximum at the shock front and this value is called the peak overpressure. As the blast wave moves away from the origin, the overpressure at the front decreases steadily and after a short time (when the shock front has traveled some distance from the fireball) the pressure behind the front becomes less than that of the atmosphere. This is the so-called negative phase of the blast wave. That is, in this region the air pressure is less than the ambient atmospheric pressure, and an underpressure exists. Another important parameter is the dynamic pressure, proportional to the square of the wind velocity and the density of the air behind the shock front.

Effects of Nuclear Explosions on Atmosphere Ionization

Ionization is the phenomenon when ion pairs of separated electrons and positive ions are formed in the ionosphere. There are mainly three regions in the ionosphere – D, E, and F regions. In the daytime, and especially in summer, the F layer splits in two, F_1 and F_2. The electron density is a maximum in each region. However, the electron density increases generally with altitude, i.e. it is greater for the F region than for the E region, which has greater electron density than the D region.

In the lower part of the atmosphere, i.e. below 48.3–56.3 km, the air is dense and the probability of collisions between free electrons and atmospheric atoms and molecules is great. Because of this, electrons are rapidly attached to the neutral particles and ionization cannot be produced. Even if it is produced, it is destroyed

immediately because, on the average, the life span of a free electron in this part of the atmosphere is less than a microsecond.

In the ionosphere, electrons and ions are produced by interaction of solar radiation with atoms and molecules of the atmospheric constituents. They are destroyed by combining either with neutral particles or positive ions. Of the two destructive processes, the former dominates at lower levels where air density is greater, whereas the latter dominates at higher levels where electron density is greater.

The effect of a nuclear explosion on atmospheric ionization is mainly because of an increase in electron density in the surrounding region. The added electrons can affect all electromagnetic communication, either by attenuating the signal or by changing its direction of propagation through refraction.

Acoustic-Gravity Waves from Atmospheric Nuclear Explosions

Donn and Shaw (1967) studied the atmospheric nuclear tests conducted by the USA and USSR during 1952–62 and, based on data recorded by a global network of stations maintained by the Lamont Geological Observatory of Columbia University, they arrived at interesting conclusions about pressure waves due to these explosions.

In fact, effects of the high-yield atmospheric nuclear explosions are comparable to those of the enormous Krakatoa eruption of 1883 (see Chapter 2) and the impact of the Siberian meteor in 1908, when pressure waves in the atmosphere traveled round the globe more than once, with appreciable amplitudes.

Donn and Shaw used the data from sensitive microbarographs at 15 recording stations, and acquired 208 records of 45 nuclear explosions. The dispersion relations of the acoustic-gravity waves in the atmosphere were used to analyze the records and the authors concluded that:

> "The initial spherical wave at the source, which is modified into a cylindrical wave by the layered structure of the atmosphere, is composed of a broad spectrum of pressure waves whose frequencies, which propagate away at about the speed of sound in air, range from audible sound to about 0.002 cps. At distances of a thousand or more kilometers, the spectrum becomes considerably narrowed, with the highest frequency detectable being about 0.03 cps (30 sec in period). It is more convenient to refer to period rather than frequency for these infrasonic waves. Such waves are also referred to as acoustic-gravity waves, since their propagation characteristics are controlled by both gravity and the acoustic properties of the atmosphere.
>
> "Because the atmosphere is a dispersive medium for the long waves within this period range (30 to 500 sec), the initial impulse becomes dispersed into a train of waves. The exact character of the period-velocity dispersion is a function of the temperature and wind stratification of the atmosphere along the propagation path."

Daniels et al. (1960) studied vertically traveling shock waves in the ionosphere caused by nuclear explosions at the surface of the earth. They interpreted the distortions in ionosphere recordings as the result of retarded sound waves.

Daniels and Harris (1961) reinterpreted the record (because the velocity of the shock wave was 115 m/s) as an ordinary hydrodynamic shock wave. They also mentioned that the pressure amplitude of this upward traveling shock wave was large enough to be detected by acoustic methods at ground level.

Webb and Daniels (1964) reported ionospheric oscillations following the Soviet atmospheric nuclear test of Nov. 1, 1962. They measured the rotation of the polarization plane of the radio waves during their travel through the ionosphere, and this parameter was proportional to the electron density. They used a 151-MC/S transmitter at Fort Monmouth, N.J., to reflect signals from the moon. The signals were received at the University of Illinois at Danville, between 1100 and 1800 CST on Nov. 1, 1962. Thus, the signals traveled twice through the ionosphere.

From newspaper and other reports it was known that the Soviet Union had conducted a nuclear test in the atmosphere a few hours earlier. The record at Danville showed an oscillation with 30-min period, larger than the period recorded by ground-level microbarographs. Webb and Daniels attributed the oscillation to acoustic waves in the atmosphere caused by the explosion. These acoustic waves are expected by theory to have a group velocity of about 730 m/s, but the authors were unable to check this from the oscillations that may have started before the record began. Long-period ionospheric oscillations have been known to continue for several hours following a nuclear explosion (Daniels and Harris 1958).

Tolstoy and Herron (1970) studied the atmospheric gravity waves excited by nuclear explosions during 1967–68. The data used were from the large aperture, i.e. a 250 km × 200 km array of 6–12 low-frequency microbarographs with period pass-band 1–60 min, in the New York–New Jersey area.

The spectra of these gravity waves showed peaks at 15-min periods and the average group velocity was approximately 600 m/s. The authors deduced that these were indeed atmospheric surface-gravity waves, based on agreement of the dispersion and attenuation of the recorded waves with expected theoretical relations. Tolstoy and Herron (1970, p. 59) concluded that the 600m/s, 15-min period arrivals were probably surface gravity waves traveling along what is effectively the top of the atmosphere. The height, H, of this "effective free surface" depends on the wavelength, L, as it corresponds approximately to the region where the mean free path, ℓ, of air molecules is of the order of L (indeed, the condition explicitly applied in making calculations is $2\pi\ell/L = 1$).

They thought that a number of published ionospheric observations of fast-traveling disturbances generated by U.S. and USSR thermonuclear tests in the early 1960s could probably be explained in a similar way. It appears that reported ionospheric disturbances with horizontal group velocities $\gtrsim$ 500 m/s are surface gravity waves, whereas lower velocities correspond to internal gravity waves (Hines 1967). Acoustic modes of propagation (Wickersham 1966) are possible for spectral components with periods shorter than 10 min.

Earlier, the problem of the pressure amplitude of atmospheric gravity waves was mentioned. To be consistent with the pressure amplitudes at the ground, it appeared at the outset that unrealistically large vertical displacements of the atmosphere above 100 km altitude would be needed. Later the problem was explained as neglect of an anomalous zone. Tolstoy and Herron (1970, p. 60) proposed that:

> "A much oversimplified one-layer model of the atmosphere (Tolstoy, 1967) can be used to give peak-to-trough pressure perturbations at ground level of 2 μb km^{-1} displacement at these heights, a result which would be quite adequate were it not

for the fact that a more realistic two-layer model decreases this estimate to 0.2 μb or less. Proper inclusion of the effects of a layer between altitudes of 110 and 150 km, in which the acoustic cut-off frequency of the medium is lower than the Vaisala frequency, might eliminate the discrepancy; the problem is discussed in more detail elsewhere (Tolstoy and Pan, 1970)."

Hines (1967) clarified some confusion that arose in connection with the ionospheric disturbances caused by the Soviet upper atmospheric nuclear test over Novaya Zemlaya on Oct. 30, 1962. Obayashi (1962, 1963) attributed these perturbations in the F-layer critical frequency to atmospheric surface gravity waves with periods in excess of 10 min. Wickersham (1966) differed and proposed that the ionospheric disturbances were due to fully ducted acoustic-gravity waves in the atmosphere. Hines showed that Wickersham's interpretation is not well founded and Obayashi's original interpretation is correct.

6.6 Atmospheric Disturbances Generated by Earthquakes and Volcanic Explosions

Benioff et al. (1951) presented data on atmospheric sound waves generated by an earthquake. A microbarograph at Pasadena recorded a train of waves with periods ranging from $\frac{3}{4}$ to 1 s, attributed by the authors to an earthquake that occurred Jan. 24, 1951. Donn and Posmentier (1964) studied the ground-coupled air waves from the Alaskan earthquake of March 1964, by the micropressure fluctuations recorded on microbarovariographs at Honolulu, Berkeley, and Palisades. The microbarovariographs have a sensitivity in the range of a few to several hundred microbars and a flat response up to 300 s.

The authors indicated that atmospheric pressure oscillations due to earthquakes may be produced by three mechanisms in the region directly surrounding the recording station, the epicentral region, and a region where there is resonant ground–air coupling. Rayleigh waves emanating from the epicentral area can generate large pressure fluctuations in the atmosphere by impulsive effect, provided their vertical displacement is large. The following relation holds between the air-pressure perturbation, p; density of air, ρ; velocity of sound in air, c; and velocity of the vertical ground motion, $\dot{v}$ (Donn and Posmentier 1964):

$$p = \rho c \dot{v} \tag{6.10}$$

The formula assumes that the interference from sound waves in adjacent regions is negligible. This condition is met, provided resonant coupling between ground and air is not appreciable and wavelengths of the Rayleigh waves are much greater than the height of the receiver (microbarograph) above the ground.

If $\rho = 1.19 \times 10^{-3}$ g/cm and C = 330 m/s, the above equation becomes:

$$p = 247 \frac{a}{t} \tag{6.11}$$

where p is peak-to-peak pressure in microbars, a is the double amplitude of ground motion in centimeters, and t is the period of motion in seconds.

In the second region the vertical displacement of the ground near the epicenter will generate atmospheric acoustic waves. Donn and Posmentier (1964) visualized this mechanism as somewhat analogous to generation of acoustic-gravity waves from nuclear explosions.

In the third region, vertical displacement of the earth's surface far from the epicenter might generate acoustic waves that could be detected at distances of a few hundred km, provided the appropriate conditions for ground-air coupling exist. It is this type of mechanism that accounted for the ground-coupled air waves reported by Benioff et al. (1951) for the Imperial Valley earthquake of Jan. 24, 1951.

Donn and Posmentier estimated from the seismograms that the maximum vertical ground motion at Palisades was 4.2 cm, attained by the initial Rayleigh wave. The observed maximum pressure fluctuation at Palisades was 40 μb, and from Equation (6.11) (assuming a period for local vertical ground motion as 23 s, the period of strongest pressure waves) one gets 3.72 cm for the required vertical motion. Because this value approximates the observed value of 4.2 cm, it was concluded that the main source for the pressure fluctuations was indeed the local vertical ground displacement due to the earthquake.

Donn and Posmentier concluded that dispersion curves for Palisades and Honolulu showed typical continental and oceanic Rayleigh waves, respectively, and the record for Berkeley showed both; mechanism 2 seemed to have worked only at Berkeley. The Berkeley record showed large-amplitude, long-period waves in the period range of 3–5 min. The superimposed smaller waves were continuations for earlier ground-coupled air waves. The structure of the initial long-period waves is different from that of the background gravity waves. Donn and Posmentier attribute the dissimilarity between these waves and those caused by nuclear explosions (those due to earthquakes show clearer dispersion) to the fact that in earthquakes the generation area is large, whereas an explosion is a point source.

Ionospheric Effects Due to Earthquakes

Davies and Baker (1965) detected ionospheric disturbances associated with the Alaskan earthquake of March 1964. They made observations at Boulder, Colo., on frequencies of 4 and 5 Mc/s with vertical propagation, and on 10 Mc/s at WWVH in Hawaii, 5000 km from Boulder. During 4 years of observation, they recorded only one other such incident; that was due to the July 9, 1962, nuclear explosion at Johnston Island.

Soviet Work on Vertical Propagation of Acoustic Waves Due to an Earthquake

Important contributions were made by Romanova (1970) and Petukhov and Romanova (1971) to understand generation and vertical propagation of acoustic waves in the atmosphere due to an earthquake, and subsequent heating in the atmosphere at different levels, caused by these waves. The earlier paper deals mainly with development of the theory, the later paper with its application. Results of the second paper are summarized here.

Petukhov and Romanova applied Romanova's theory to calculate the dissipation of infrasonics from earthquakes in the atmosphere in the form of heat. In

particular they estimated the rate and amount of atmospheric heating due to acoustic waves traveling upward from two great earthquakes, the Alaskan earthquake of 1964 and the Katinoko, Japan, earthquake of 1968. This atmospheric heating had a significant role in the observed ionospheric disturbances.

The authors essentially started with the same initial conditions as Donn and Posmentier (1964), i.e. with Equation (6.10) or (6.11). This means the Rayleigh waves from the epicenter propagate over the earth's surface with a velocity of roughly 3 km/s, which is supersonic for air. The vertical motion of the Rayleigh waves produces a vertical impulse effect in the atmosphere, and produces pressure perturbations. The relation between the pressure perturbation, p, and the displacement, a, of the ground surface is given (as in Donn and Posmentier's work) by (6.10).

Under the linear theory for small amplitude oscillations, the Stokes–Kirchoff equation for the attentuation coefficient, α, of acoustic waves is given by:

$$\alpha = 260 \frac{2\pi\omega^2}{\gamma P} \left(\frac{\rho\mu_a}{\gamma n}\right)^{\frac{1}{2}} \left(\frac{4}{3} + \frac{\gamma - 1}{P_n}\right) \tag{6.12}$$

where ω is the frequency expressed in Hertz, ρ is air density, γ is ratio of specific heats, μ_a is the molecular weight of air, n is density of air molecules, and P_n is the Prandtl Number (0.7 for air).

The equation used for atmospheric heating is:

$$\frac{\partial \bar{\theta}_a}{\partial t} = -\overline{\frac{\partial}{\partial z}(cE)} \tag{6.13}$$

where θ_a is the absolute temperature, E is the wave energy, c is the velocity of sound, and bar denotes averaging over a period. After some algebra (6.13) becomes:

$$\frac{\partial \bar{\theta}_a}{\partial t} = 2c\alpha(z)\,(c_p\rho)^{-1} \exp\left[-2\int_0^z \alpha(z)\,dz\right] \tag{6.14}$$

where c_p is the specific heat at constant pressure. This formula was used to calculate the temperature change for the atmosphere over Berkeley, Boulder, and Palisades for the 1964 Alaskan earthquake and for the atmosphere over Maui for the 1968 Katinoko earthquake. The calculations showed that maximum heating occurred in altitudes of 170–190 km. At this altitude, the atmosphere over Berkeley was heated by 900°. Although this value appears large, the peak-to-peak amplitude of the ground motion with a period of 23 s was 12.6 cm.

Ionospheric disturbances were observed associated with this earthquake (i.e. 1964 Alaskan earthquake). An important method of identifying these disturbances was an increase of about 20 km in the altitude of the critical reflecting layers. The role of atmospheric heating in this could be significant, because, when the 170–190 km altitude layer (with maximum heating) expands with heat, it disturbs the layers above it. Under the assumption of an isobaric process, the rise in the

critical layer $z = z_0$ caused by heating and expansion of the underlying layers can be computed from the following relation:

$$\Delta z(z_0) = \int_0^{z_0} \frac{\Delta\theta_a(z)}{T_0(z)}\, dz \tag{6.15}$$

Here $T_0(z)$ is temperature at height, z, in the atmosphere before heating starts, and $\Delta\bar{\theta}_a = (\partial\theta_a/\partial z)\,\Delta t$; $\partial\bar{\theta}_a/\partial z$ is calculated from Equation (6.14). This calculation gives a rise of 20 km for the layer at 240 km altitude over Boulder and the observed rise is of the same order. Over Maui, the 200-km altitude layer theoretically should rise 15 km, although it was observed to rise only 5–6 km.

In contrast to the linear theory, the nonlinear theory shows that lower atmospheric layers are heated more and higher layers are heated less, thus the nonlinear theory gives a smaller rise of the critical layers. Another important point Petukhov and Romanova (1971) emphasized is that because of the decrease of atmospheric density with altitude, temperature fluctuations will mainly travel upward, and a new isothermal condition is rapidly established in the atmosphere above the heat source at the ground. To obtain this isothermal condition at the 170–200-km level would only take about 3 h.

Seismic Wave Coupling to the Ionosphere

Details on analysis of ionospheric disturbances due to seismic waves are presented. Yuen et al. (1969) studied the May 16, 1968, Hachinohe, Japan, earthquake and analyzed and compared the seismic, atmospheric, and ionospheric data. Some important results are: acoustic waves generated in the atmosphere by seismic waves due to the earthquake traveled to 300 km altitude and created oscillatory disturbances in the ionosphere. Acoustic waves in the period range of 20–25 s were attenuated more strongly than those with longer periods of the order of 2 min. Value of the results lies in the fact that the observed pressure changes, determined from Doppler records, agreed well with theoretically expected values. Donn and Posmentier (1964), for the Alaskan earthquake of March 1964, could not directly compare the seismograms with microbarograms because the vertical component seismograms were illegible, due to large ground displacements.

For the Hachinohe earthquake, the average double amplitude of the Rayleigh wave was 0.28 cm, as shown by the seismograph at the Hawaiian Institute of Geophysics (HIG). The average Rayleigh wave period was taken as 25 s, and this gives from Equation (6.11) a value of 2.8 μb for the average peak-to-peak pressure variation, an order of magnitude less than the pressure variations associated with the 1964 Alaskan earthquake. The pressure fluctuations for the Hachinohe earthquake were too small for the microbarographs at Honolulu to record. However, Yuen et al. (1969, p. 2258) were able to deduce the pressure changes from the ionospheric Doppler records. They described the HF Doppler technique, where the instantaneously received frequency of a highly stable ionospherically reflected signal is measured. The Doppler frequency shifts indicate changes in the ionosphere caused by movements of the reflecting layer or by variations in the electron concentration below the point of reflection.

A few minutes after the Rayleigh waves reached Hawaii, short-period oscillations were produced at heights near 200 km and long-period oscillations were produced near 300 km.

The Faraday rotation of the polarization of CW signals, transmitted from geostationary satellites, were measured to continuously obtain total electron content data. The period after the earthquake showed no unusual behavior. This indicated that no significant net production or loss of electrons were associated with disturbances on the Doppler and ionogram records, and implied that these disturbances were produced by electron concentration pressure waves in the ionosphere.

According to Yuen et al. (1969):

> "An acoustic longitudinal pressure wave with a vertical velocity component would be expected to move the contours of constant electron concentration up and down with an oscillatory motion similar to the pressure wave itself. This would mean that the height of reflection for HF radio signals such as those used in the Doppler system would also move up and down with an oscillatory motion. The pressure wave at ground level generated by a Rayleigh wave would be proportional to the seismic motions at the earth's surface. Thus similar shapes would be expected on the seismic and Doppler records."

To support their contention that the ionospheric disturbances shown on the Doppler recordings were caused by acoustic waves generated by Rayleigh waves from the earthquake, Yuen et al. used ray tracing, and calculated the attenuation by the 1966 U.S. standard atmosphere. In this calculation, the exospheric temperature was taken to be 1200° k over Hawaii at the time of the earthquake. Assuming adiabatic conditions, Yuen et al. (1969) calculated the pressure change from the change in the electron concentration.

Atmospheric Disturbances Due to Volcanic Explosions

The effects of the Krakatoan eruption of August 1883, and the atmospheric disturbances on the water-level changes that occurred globally were treated in Chapter 2, but information on the observed atmospheric pressure disturbances is presented here.

Scott (1883) described the atmosphere pressure fluctuations observed following the Krakatoan eruption, and Strachey (1883) made deductions based on this work. Scott mentioned that the volcanic explosion probably occurred between 1600 on Aug. 26, and 0500 Aug. 27, 1883, local time (in Greenwich time, between 0900 and 2200 Aug. 27). The pressure disturbances discussed by Scott are summarized in Table 6.6. On the average, the pressure wave took 36 h 37 min to travel around the earth from east to west, and 35 h 17 min from west to east. By working back with this data, Strachey deduced that the Krakatoan eruption occurred at 0224 GCT (or 0924 local time) Aug. 27, 1883. The atmospheric pressure wave on the average traveled 674 mph from east to west and 706 mph from west to east.

TABLE 6.6. Start of barometrical oscillations Aug. 27, 28, and 29, 1883. (Scott 1883)

Stations	Aug. 27 (1st)			Aug. 28 (2nd)		Aug. 29 (3rd)		Aug. 29 (4th)		Oscillation amplitude			
	PM	PM	PM	AM	AM	AM	AM	PM	PM	1st (*cm*)	2nd (*cm*)	3rd (*cm*)	4th (*cm*)
St. Petersburg	1105	1135	0000	0440	0515	0020	0100	0300	0335	0.101	0.060	0.030	.086
	AM	AM											
Brussels	0033	0058	0130	0348	0428	0143	0208	0223	0243	0.129	0.099	.099	.043
Geldeston	0042	0112	0140	0310	0407	0140	0202	0214	0244	0.152	.102	.089	.025
Kew	0050	0110	0147	0310	0405	0145	0213	0200	0243	.124	.129	.061	.028
Oxford	0053	0123	0150	0300	0357	0155	0215	0153	0240	.076	.076	.038	.038
Aberdeen	0100	0125	0153	0310	0352	0150	0233	0153	0230	.157	.132	.117	.091
Stonyhurst	0100	0128	0155	0257	0345	0200	0227	0148	0233	.157	.162	.074	.127
Glasgow	0058	0135	0205	0300	0345	0210	0237	0142	0227	.116	162	.127	.071
Falmouth	0107	0135	0205	0257	0345	0205	0225	0120	0228	.127	.203	.076	.076
Armagh	0113	0145	0212	0253	0333	0230	0245	0146	0222	.048	.157	.074	.091
Valencia	0120	0148	0225	0230	0320	0228	0250	0127	0210	.060	.178	.102	.025
Coimbra		0150	0220	0305	0315	0210	0215	0210	0235	.152	0.046	.109	.045

References

ABOUZIYAROV, Z. K. 1970. Problems of the tsunami warning service in the USSR, p. 271–282. *In* W. M. Adams [ed.] Tsunamis in the Pacific Ocean. East West Center Press, Honolulu, Hawaii.

ADAMS, J. K., AND V. T. BUCHWALD. 1968. The generation of continental shelf waves. J. Fluid Mech. 35: 815–826.

ADAMS, W. M. 1958. A study of earthquake mechanism using S wave data. Bull. Seismol. Soc. Am. 48: 201–219.

1967. Analysis of a tsunami warning system as a decision-making process. Proc. Symp. Tsunami and Storm Surges, 11th Pac. Sci. Congr., Tokyo. p. 1–22.

1968. Potential tsunami inundation zones for the islands of Molokai and Lanai, Hawaiian Islands. Univ. Hawaii Inst. Geophys. Rep. HIG-68-15: 13 p.

1969. Prediction of tsunami inundation from current real-time seismic data. Univ. Hawaii Inst. Geophys. Rep. HIG-69-9: 57 p.

1972. The rarity of the 1 April, 1946, tsunami. J. Phys. Oceanogr. 2: 199–201.

1973. Expected tsunami inundation for the Hawaiian Islands. J. Mar. Technol. Soc. 7: 551–556.

1974. Tsunami anomalies and precursory phenomena having potential value as predictors. Proc. 5th World Conf. Earthquake Eng. 11: 2754–2762.

ADAMS, W. M., AND A. S. FURUMOTO. 1970. Features of tsunamigenic earthquakes, p. 57–68. *In* W. M. Adams [ed.] Tsunamis in the Pacific Ocean. East West Center Press, Honolulu, Hawaii.

ADAMS, W. M., AND J. M. JORDAAN JR. 1968. Model study of tsunami amplification around the island of Oahu, Hawaii. Univ. Hawaii Cent. Eng. Res. 58 p.

AIDA, I. 1967. Water level oscillations on the continental shelf in the vicinity of Miyagi-Enoshima. Bull. Earthquake Res. Inst. 45: 61–78.

1969a. Numerical experiments for the tsunami propagation – the 1964 Niigata tsunami and the 1968 Tokachi-Oki tsunami. Bull. Earthquake Res. Inst. 47: 673–700.

1969b. Numerical experiments for tsunamis caused by moving deformations of the sea bottom. Bull. Earthquake Res. Inst. 47: 849–862.

1972. Estimation of the offshore form of tsunami waves. J. Oceanogr. Soc. Jpn. 28: 220–227.

AIDA, I., T. HATORI, M. KAYAMA, AND K. KAJIURA. 1968. A model experiment on long-period waves travelling along a continental shelf. Bull. Earthquake Res. Inst. 46: 707–739. (In Japanese)

AIRY, G. B. 1845. Tides and waves. Encycl. Metropol., London.

AKI, K. 1960a. The use of Love waves for the study of earthquake mechanism. J. Geophys. Res. 65: 323–331.

1960b. Study of earthquake mechanism by a method of phase equilization applied to Rayleigh and Love waves. J. Geophys. Res. 65: 729–740.

1960c. Interpretation of source functions of circumpacific earthquakes obtained from long period Rayleigh waves. J. Geophys. Res. 65: 2405–2417.

1966. Earthquake generating stress in Japan for the years 1961–1963 obtained by smoothing the first motion radiation patterns. Bull. Earthquake Res. Inst. 44: 447–471.

ALLEN, J. H., AND L. E. BAILEY. 1970. Earthquake and nuclear detonations. Science 167: 1011–1014.

AMBRASEYS, N. N. 1960. The seismic sea wave of July 9, 1956, in the Greek Archipelago. J. Geophys. Res. 65: 1257–1265.

1962. Data for the investigation of the seismic sea waves in the eastern Mediterranean. Bull. Seismol. Soc. Am. 52: 895–913.

1963. Seismic sea wave in the Gulf of Corinth. Bull. Seismol. Soc. Am. 53: 849.

1964. Data for the investigation of seismic sea-waves in Europe. 1963–1964 European Seismol. Comm. Budapest, Prog. Rep. 1: 78–80.

ANDERSON, D. L. 1971. The San Andreas fault. Sci. Am. p. 52–68.

Anon. 1909. The Italian earthquake of December 28, 1098. Nature 80: 445.

1940. United States earthquakes, 1938. U.S. Dep. Comm. Geod. Surv. p. 32–33.

1946a. Seismic sea wave of April 2, 1946. Nature 157: 474.

1946b. The earthquake and seismic sea wave of April 1, 1946. Earthquake Notes 18: 10–11.

1956. Earthquake in the Aegean Sea. Nature 178: 125.

1961. The Chilean tsunami of May 24, 1960. Committee for field investigation of the Chilean tsunami of 1960. p. 397.

1965. The story of the seismic sea-wave warning system. U.S. Dep. Comm. Coast Geod. Surv. 46 p.

1972. Tsunami warning service and its system in Japan. 3rd Sess. Int. Coord. Group for Tsunami Warning Syst. in the Pacific. Jpn. Meteorol. Agency, Tokyo. 21 p.

ARNETT, R. A., AND T. W. NEWHOUSE. 1965. Ocean-bottom seismograph. Proc. Inst. Eng. Electron. Eng. 53: 1899–1905.

ARTHUR, R. S. 1946. Refraction of water waves by islands and shoals with circular bottom contours. Trans. Am. Geophys. Union 27: 168–177.

1951. The effects of islands on surface waves. Bull. Scripps Inst. Oceanogr. 6: 1–26.

BACKUS, G. E. 1962. The effect of the earth's rotation on the propagation of ocean waves over long distances. Deep-Sea Res. 9: 185–197.

BAIRD, A. W. 1884. Report on the tidal disturbances caused by the volcanic eruptions at Java, Aug. 27 and 28, 1883 and propagations of the supertidal waves. Proc. R. Soc. London Ser. A, 36: 248–253.

BALAKINA, L. M. 1970. Relationship of tsunami generation and earthquake mechanism in the northwestern Pacific, p. 47–55. *In* W. M. Adams [ed.] Tsunamis in the Pacific Ocean. East West Center Press, Honolulu, Hawaii.

BALL, F. K. 1965. Second-class motions of a shallow liquid. J. Fluid Mech. 23: 545–561.

1967. Edge waves in an ocean of finite depth. Deep-Sea Res. 14: 79–88.

BARTHOLOMEUSZ, E. F. 1958. The reflection of long waves at a step. Proc. Cambridge Philos. Soc. 54: 106–118.

BASSET, A. B. 1888. A treatise on hydrodynamics. Vol. II. Dover Publishing, Inc., New York, N.Y. 328 p.

BEITINJANI, K. I., AND E. F. BRATER. 1965. A study on refraction of waves in prismatic channels. Proc. Am. Soc. Civ. Eng. 91: 37–64.

BENIOFF, H., M. EWING, AND F. PRESS. 1951. Sound waves in the atmosphere generated by a small earthquake. Proc. U.S. Natl. Acad. Sci. 37: 600–603.

BENIOFF, H., AND B. GUTENBERG. 1939. Waves and currents recorded by electromagnetic barographs. Bull. Am. Meteorol. Soc. 20: 421–426.

BENJAMIN, T. B. 1968. Gravity currents and related phenomena. J. Fluid Mech. 31: 209–248.

BENJAMIN, T. B., AND M. J. LIGHTHILL. 1954. On cnoidal waves and bores. Proc. R. Soc. London Ser. A, 224: 448–460.

BEN-MENAHEM, A., AND M. ROSENMAN. 1972. Amplitude patterns of tsunami waves from submarine earthquakes. J. Geophys. Res. 77: 3097–3128.

BERCKHEMER. H. 1970. Mars 66 – a new portable system for explosion seismometry. Obs. R. Belg. Comm. Ser. A, 101: 288 p.

BERG, G. V., AND G. W. HOUSNER. 1961. Integrated velocity and displacement of strong earthquake ground motion. Bull. Seismol. Soc. Am. 51: 175–189.

BERNINGHAUSEN, W. H. 1962. Tsunamis reported from the west coast of South America, 1562–1960. Bull. Seismol. Soc. Am. 52: 915–921.

1964. Tsunamis and seismic seiches reported from the eastern Atlantic south of the Bay of Biscay. Bull. Seismol. Soc. Am. 54: 439–442.

1969. Tsunamis and seismic seiches of southeast Asia. Bull. Seismol. Soc. Am. 59: 289–297.

BILHAM, R., AND G. KING. 1970. Strain-gauges for geophysics. Obs. R. Belg. Comm. Ser. A, 101: 258–278.

BIRCHFIELD, G. E., AND T. S. MURTY. 1974. A numerical model for wind-driven circulation in lakes Michigan and Huron. Mon. Weather Rev. 102: 157–165.

BLUME, J. A. 1970. An engineering intensity scale for earthquakes and other ground motion. Bull. Seismol. Soc. Am. 60: 217–229.

BOLT, B. A. 1974. Earthquake studies in the People's Republic of China. Trans. Am. Geophys. Union 55: 108–117.

BOLT, B. A., W. L. HORN, G. A. MACDONALD, AND R. F. SCOTT. 1975. Geological hazards. Springer-Verlag, New York, N.Y. 328 p.

BONJER, K. P., AND S. MUELLER. 1970. The prototype of a mobile seismic station. Obs. R. Belg. Comm. Ser. A, 101: 291–292.

BOUTELLE, C. O. 1884. Water waves from Krakatoa. Science 3: 777.

BRADDOCK, R. D. 1970. Tsunami propagation over large distances, p. 285–303. *In* W. M. Adams [ed.] Tsunamis in the Pacific Ocean. East West Center Press, Honolulu, Hawaii.

1973. The Solomon Sea tsunamis of July 1971,. p. 9–14. *In* Oceanography of the South Pacific. N.Z. Natl. Comm. UNESCO.

BRADDOCK, R. D., AND P. VAN DEN DRIESSCHE. 1971. Tsunami generation. Univ. Queensland, Dep. Math., Appl. Math. Reprint 45: 13 p.

BRADNER, H., J. DODDS, AND R. FOULKS. 1965. Coherence measurements with time sampling ocean-bottom seismometers. Proc. Inst. Eng. Electron. Eng. 53: 1906–1908.

BRANDSMA, M., D. DIVOKY, AND L.-S. HWANG. 1975. Sea wave – a revised model for tsunami applications. U.S. Natl. Sci. Found. by Tetra Tech. Inc., Pasadena, Calif. 45 p.

BROER, L. J. F. 1964. On the interaction of non-linearity and dispersion in wave propagation I. Boussinesq's equation. Appl. Sci. Res. Sect. B, 2: 273–285.

BRUNE, J. N. 1961. Radiation pattern of Rayleigh waves from the southeast Alaska earthquake of July 19, 1958. Can. Dep. Mines Tech. Surv. Publ. 24: 373–383.

BRUNE, J. N., J. E. NAFE, AND J. E. OLIVER. 1960. A simplified method for the analysis and synthesis of dispersed wave trains. J. Geophys. Res. 65: 287–304.

BUCHER, W. H. 1940. Submarine valleys and related geologic problems of the North Atlantic. Geol. Soc. Am. Bull. 51: 489–512.

BUCHWALD, V. T. 1969. Long waves on oceanic ridges. Proc. R. Soc. London Ser. A, 308: 343–354.

BUCHWALD, V. T., AND J. K. ADAMS. 1968. The propagation of continental shelf waves. Proc. R. Soc. London Ser. A, 305: 235–250.

BUDDEN, K. G. 1961. The wave-guide mode theory of wave propagation. Logos Press, London. 325 p.

BULLEN, K. E. 1963. An introduction to the theory of seismology. Univ. Cambridge Press, London. 381 p.

BURGERS, J. M. 1948. A mathematical model illustrating the theory of turbulence. Adv. Appl. Mech. 1: 171–199.

BUTLER, J. P. 1967. Double-humped waves on a sloping beach. Univ. Hawaii. Inst. Geophys. Rep. HIG-67-16. ESSA-JTRE-2: 28 p.

BYERLY, P. 1930. The California earthquake of Nov. 4, 1927. Bull. Seismol. Soc. Am. 20: 53–66.

1942. Effects of earthquakes from seismology. Prentice-Hall, Inc., New York, N.Y. p. 72–73.

CANNON, W. 1971. The Amchitka affair: why it shows the need for a nuclear test moratorium. Sci. Forum 4: 3–8.

CARDER, D. S. 1945. Seismic investigations in the Boulder Dam area, 1940–1944, and the influence of reservoir loading on local earthquake activity. Bull. Seismol. Soc. Am. 35: 175–192.

CARRIER, G. F. 1966. Gravity waves on water of variable depth. J. Fluid Mech. 24: 641–659.

1970. The dynamics of tsunamis. Lect. Notes. Rensselaer Polytech. Inst. Rep. p. 1–49.

1971. The dynamics of tsunamis, p. 157–187. *In* Mathematical problems in the geophysical sciences. Lect. Appl. Math. Am. Math. Soc. 14.

CARRIER, G. F., AND H. P. GREENSPAN. 1958. Water waves of finite amplitude on a sloping beach. J. Fluid Mech. 4: 97–109.

CARRIER, G. F., AND R. P. SHAW. 1970. Response of narrow mouthed harbors to tsunamis, p. 337–398. *In* W. M. Adams [ed.] Tsunamis in the Pacific Ocean. East West Center Press, Honolulu, Hawaii.

CARRIER, G. F., AND R. P. SHAW, AND M. MIYATA. 1970. Response of narrow-mouthed harbors with an entrance channel to periodic incident waves. Univ. Hawaii, Inst. Geophys. Rep. HIG-70-21: 35 p.

CARTER, L. J. 1969. Earthquakes and nuclear tests: playing the odds on Amchitka. Science 165: 773–776.

CHAMBERS, L. G. 1964. Long waves on a rotating earth in the presence of a semi-infinite barrier. Proc. Edinburgh Math. Soc. 14: 25–31.

CHAO, Y. Y. 1970. The theory of wave refraction in shoaling water including the effects of caustics and the spherical earth. Univ. New York, Dep. Meteorol. Oceanogr., Geophys. Sci. Lab. Tech. Rep. 70-7: 70 p.

CHAO, Y. Y., AND W. J. PIERSON. 1972. Experimental studies of the refraction of uniform wave trains and transient wave groups near a straight caustic. J. Geophys. Res. 77: 4545–4554.

CHEN, M., D. DIVOKY, AND L.-S. HWANG. 1975. Near-field tsunami behaviour. U.S. Natl. Sci. Found. by Tetra Tech. Inc., Pasadena, Calif. 49 p.

CHERKESOV, L. V. 1965. On the tsunami problem in a nonhomogeneous sea. Atmos. Oceanic Phys. 1: 498–503. (Transl. from Russian by D. Barcilon and V. Barcilon)

1966a. Tsunami in a heterogeneous sea. Oceanology 6: 615–622.

1966b. The influence of viscosity on the propagation of tsunami type waves. Atmos. Oceanic Phys. 2: 793–797. (Transl. from Russian by F. Goodspeed)

1968. On the problem of tsunamis in a sea with continuously varying density. Atmos. Oceanic Phys. 4: 1101–1106. (Transl. from Russian by F. Goodspeed)

1970. Influence of viscosity on tsunami waves in a basin of variable depth. Atmos. Oceanic Phys. 6: 86–91. (Transl. from Russian by K. Syers)

CHU, H. L. 1975. Numerical model for wave refraction by finite amplitude wave theories. Symposium on modeling techniques. 2nd Annu. Symp. Waterways, Harbors Coastal Eng. Div. San Francisco, Calif. Am. Soc. Civ. Eng. 2: 1082–1100.

CLARKE, D. J., AND N. D. THOMAS. 1972. The two-dimensional flow oscillations of a fluid in a spindle-shaped basin; application to Port Kembla outer harbour N.S.W. Australia. Aust. J. Mar. Freshwater Res. 23: 1–9.

COCHRANE, J. D., AND R. S. ARTHUR. 1948. Reflection of tsunamis. J. Mar. Res. 7: 239–251.

COFFMAN, J. L., AND W. K. CLOUD. 1970. United States earthquakes 1968. U.S. Dep. Comm. Coast Geod. Surv. p. 72–73.

COFFMAN, J. L., AND C. A. VON HAKE. 1970. Earthquake history of the United States. U.S. Dep. Comm. Natl. Oceanic Atmos. Adm. 208 p.

COX, D. C. 1968. Performance of the seismic sea wave warning system 1948–67. Univ. Hawaii Inst. Geophys. Rep. HIG-68-2: 69 p.

1970. Discussion of "Tsunamis and seismic seiches of southeast Asia" by W. H. Berninghausen. Bull. Seismol. Soc. Am. 60: 281–287.

COX, D. C., AND J. F. MINK. 1963. The tsunami of 23 May, 1960 in the Hawaiian Islands. Bull. Seismol. Soc. Am. 53: 1191–1209.

COX, D. C., AND G. PARARAS-CARAYANNIS. 1969. Catalog of tsunamis in Alaska. U.S. Dep. Comm. Coast Geod. Surv., World Data Cent. A. WDCA-T 69-1: 39 p.

COX, D. C., G. PARARAS-CARAYANNIS, AND J. P. CALEBAUGH. 1976. Catalog of tsunamis in Alaska. Rev. ed. World Data Cent. Publ., Asheville, N.C. 43 p.

CREASE, J. 1956. Long waves on a rotating earth in the presence of a semi-infinite barrier. J. Fluid Mech. 1: 86–96.

CROSS, R. H. 1967. Tsunami surge force. J. Waterways, Harbors Coastal Eng. Div., Proc. Am. Soc. Civ. Eng. 93: 201–231.

DANIELS, F. B., S. J. BAUER, AND A. K. HARRIS. 1960. Vertically travelling shock waves in the ionosphere. J. Geophys. Res. 65: 1848–1850.

DANIELS, F. B., AND A. K. HARRIS. 1958. Some effects of strong blast waves upon the ionosphere. Paper presented at URSI meeting, Pennsylvania State Univ., University Park, Penn., Oct. 22.

1961. Note on vertically travelling shock waves in the inosphere. J. Geophys. Res. 66: 3964.

DANIELS, G. M. 1967. Acoustic-gravity waves in model thermospheres. J. Geophys. Res. 72: 2419-2428.

DANTZIG, G. B. 1960. Management on the shortest route through a network. Science 6: 187-190.

DAS, M. M., AND R. L. WIEGEL. 1972. Water waves generated by horizontal motion of a vertical wall. Univ. California, Berkeley, Tech. Rep. HEL-16-7: 16 p.

DAVIDSON, G. 1884. Notes on the volcanic eruption of Mount St. Augustine, Alaska on October 6, 1883. Science 3: 186-189.

DAVIES, K., AND D. M. BAKER. 1965. Ionospheric effects observed around the time of the Alaskan earthquake of March 28, 1964. J. Geophys. Res. 70: 2251-2253.

DAVISON, C. 1931. The Japanese earthquake of 1923. Thomas Murby and Co., London. p. 100-105.

DEFANT, A. 1961. Physical oceanography. Pergamon Press, Inc., New York, N.Y. 598 p.

DERR, J. S. 1970. Discrimination of earthquakes and explosions by the Rayleigh wave spectral ratio. Bull. Seismol. Soc. Am. 60: 1653-1668.

DOBSON, G. M. B. 1963. Exploring the atmosphere. Clarendon Press, Oxford, U.K. 209 p.

DOHLER, G. 1970. The tide-gauge data telemetry between the tsunami warning center at Honolulu, Hawaii and selected stations in Canada, p. 191-206. *In* W. M. Adams [ed.] Tsunamis in the Pacific Ocean. East West Center Press, Honolulu, Hawaii.

DONN, W. L. 1958. The microbarovariograph: a new instrument for measuring minute atmospheric pressure variations. IGY Bull. U.S. Natl. Acad. Sci. 39: 366-368.

1959. The Great Lakes storm surge of May 5, 1952. J. Geophys. Res. 64: 191-198.

DONN, W. L., AND M. EWING. 1956. Stokes' edge waves in Lake Michigan. Science 124: 1238-1242.

DONN, W. L., AND E. S. POSMENTIER. 1964. Ground-coupled airwaves from the Great Alaskan earthquake. J. Geophys. Res. 69: 5357-5361.

DONN, W. L., AND D. M. SHAW. 1967. Exploring the atmosphere with nuclear explosions. Rev. Geophys. 5: 53-82.

DORRESTEIN, R. 1960. Simplified method of determining refraction coefficients for seawaves. J. Geophys. Res. 65: 637-642.

DRONKERS, J. J. 1964. Tidal computations in rivers and coastal waters. North Holland Publishing Co., Amsterdam, Holland. 518 p.

DUNGEY, J. W. 1954. The propagation of Alfven waves through the ionosphere. Pennsylvania State Univ., Ionosphere Res. Lab. Sci. Rep. 57: 19 p.

EATON, J. P., D. H. RICHTER, AND W. U. AULT. 1961. The tsunami of May 23, 1960 on the island of Hawaii. Bull. Seismol. Soc. Am. 51: 135-157.

ECKART, C. 1950. The ray-particle analogy. J. Mar. Res. 9: 139-144.

EMILIANI, C., C. G. A. HARRISON, AND M. SWANSON. 1969. Underground nuclear explosions and the control of earthquakes. Science 165: 1255-1256.

EVANS, D. M. 1966. The Denver area earthquakes and the Rocky Mountain arsenal disposal. Mt. Geol. 3: 23-26.

EVISON, F. F. 1963. Earthquakes and faults. Bull. Seismol. Soc. Am. 53: 873-891.

EWING, J., AND M. EWING. 1961. A telemetering ocean-bottom seismograph. J. Geophys. Res. 66: 3863-3878.

EWING, M., AND F. PRESS. 1953. Tide gauge disturbances from the great eruption of Krakatoa. Lamont Geol. Obs., Columbia Univ., Palisades, N.Y., Tech. Rep. 27: 10 p.

1955. Tide gauge disturbances from the great eruption of Krakatoa. Trans. Am. Geophys. Union 36: 53-60.

EWING, M., F. PRESS, AND J. L. WORZEL. 1952. Further study of the T-phase. Bull. Seismol. Soc. Am. 42: 37-51.

EWING, M., I. TOLSTOY, AND F. PRESS. 1950. Proposed use of the T-phase in tsunami warning systems. Bull. Seismol. Soc. Am. 40: 53-58.

EWING, M., G. P. WOOLLARD, A. C. VINE, AND J. L. WORZEL. 1946. Recent results in submarine geophysics. Geol. Soc. Am. Bull. 57: 909-934.

FAVRE, H. 1935. Étude des ondes de translation. Publ. Lab. Rech. Hydraul. Annexe École Polytech. Féd. Zurich., Dunod, Paris. p. 140-163.

FEDOSENKO, V. S., AND L. V. CHERKESOV. 1968. Internal waves from submarine earthquakes. Atmos. Oceanic Phys. 4 (11): 1197-1203. (Transl. from Russian by J. Buchner)

FEDOTOV, S. A. 1968. Long-term seismic predictions for the Kurile-Kamchatka zone. Tsunami problem. Nauka Publ. House, Moscow. p. 121-139. (Transl. from Russian by U.S. Dep. Comm. Tech. Inf. Serv.)

FEJER, J. A. 1960. Hydromagnetic wave propagation in the ionosphere. J. Atmos. Terr. Phys. 18: 135-146.

FILLOUX, J. H. 1970a. Bourdon-tube, deep-sea tide gauges, p. 223-238. *In* W. M. Adams [ed.] Tsunamis in the Pacific Ocean. East West Center Press, Honolulu, Hawaii.

1970b. Deep-sea tide gauge with optical readout of Bourdon tube rotations. Nature 226: 935-937.

FINCH, R. H. 1924. On the prediction of tidal waves. Mon. Weather Rev. 52: 147-148.

FITCH, T. J. 1970. Earthquake mechanisms in the Himalayan, Burmese and Andaman regions and continental tectonics in central Asia. J. Geophys. Res. 75: 2699-2752.

FREEMAN, J. C. 1951. The solution of nonlinear meteorological problems by the method of characteristics, p. 921-933. *In* Compendium of meteorology. Am. Meteorol. Soc.

FREEMAN, J. C., AND B. LÉMEHAUTÉ. 1964. Wave breakers on a beach and surges on a dry bed. J. Hydraul. Div., Proc. Am. Soc. Civ. Eng. 90: 187–216.

FREEMAN, N. G., AND T. S. MURTY. 1972. A study of a storm surge on Lake Huron. Proc. 15th Conf. Great Lakes Res. Int. Assoc. Great Lakes Res., Ann Arbor, Mich. p. 565–582.

FUKUI, Y., M. NAKAMURA, H. SHIRAISHI, AND Y. SASAKI. 1963. Hydraulic study on tsunami. Coastal Eng., Jpn., Jpn., Soc. Civ. Eng. 6: 67–82.

FURUMOTO, A. S. 1970. Ionospheric recordings of Rayleigh waves for estimating source mechanisms, p. 119–133. *In* W. M. Adams [ed.] Tsunamis in the Pacific Ocean. East West Center Press, Honolulu, Hawaii.

GARCIA, A. W., AND J. R. HOUSTON. 1976. Tsunami run-up predictions for southern California, coastal communities USA. Proc. IUGG Conf. tsunamis, tsunami Res., Jan. 29–Feb. 1, 1974, Wellington, N.Z., R. Soc. N.Z., Bull. 15: 5–17.

GARCIA, W. J., JR. 1972. A study of water waves generated by tectonic displacements. Univ. California, Hydraul. Eng. Lab. Rep. HEL-16-9: 114 p.

GARIPOV, R. M. 1965. Nonsteady waves above and under water ridge. Sov. Phys. Dokl. 10: 194–196.

1967. On the linear theory of gravity waves: the theorem of existence and uniqueness. Arch. Ration. Mech. Anal. 24: 352–362.

GARRETT, C. J. R. 1969. The fundamental mode of acoustic gravity wave propagation in the atmosphere. Fluid Dyn. Trans. 4: 707–719.

1970. Bottomless harbors. J. Fluid Mech. 43: 433–449.

GILL, D. 1883. The great tidal wave – South Africa. Nature 28: 626–627.

GILMOUR, A. E. 1961. Tsunami warning charts. N. Z. J. Geol. Geophys. 4: 132–135.

1967. Tsunami travel times to New Zealand. N.Z. J. Mar. Freshwater Res. 1: 139–142.

GLASSTONE, S. 1962. Effects of nuclear weapons. Rev. ed. USAEC. 730 p.

GORDON, F. R. 1970. Water level changes preceding the Meekering Western Australia earthquake of October 14, 1968. Bull. Seismol. Soc. Am. 60: 1739–1740.

GREEN, C. K. 1946. Seismic sea wave of April 1, 1946 as recorded on tide gauges. Trans. Am. Geophys. Union 27: 490–500.

GREEN, R. 1961. The sweep of long waves across the Pacific. Aust. J. Phys. 14: 120–128.

GREENSPAN, H. P. 1956. The generation of edge waves by moving pressure distributions. J. Fluid Mech. 1: 574–592.

GREGORY, J. W. 1929. The earthquake south of Newfoundland and submarine canyons. Nature 124: 945–946.

GRIGORASH, Z. K., AND L. A. KORNEVA. 1969. Tsunami waves accompanying the Anapa earthquake of July 12, 1966. Oceanology 9: 793–798.

1970. An estimation of tsunami energy during the Anapa earthquake of July 12, 1966 taking wave refraction into consideration. Atmos. Oceanic Phys. 6: 715–719.

1972. Wave-field charts and energy of tsunamis in the black Sea. Atmos. Oceanic Phys. 78: 320–323. (Transl. from Russian by Am. Geophys. Union)

GRISWOLD, G. M. 1963. Numerical calculation of wave refraction. J. Geophys. Res. 68: 1715–1723.

GUTENBERG, B., AND C. F. RICHTER. 1954. Seismicity of the earth and associated phenomena. 2nd ed. Princeton Univ. Press, Princeton, N.J. 273 p.

1956. The energy of earthquakes. Q. J. Geol. Soc. London 112: 1–14.

HAMBLIN, P. F. 1972. Some free oscillations of a rotating natural basin. Ph.D. Thesis, Univ., Washington, Seattle, Wash. 97 p.

HAMILTON, W. 1783. Of the earthquakes in Italy, from February to May 1783. Philos. Trans. R. Soc. London 15: 373–386.

HAMMACK, J. L. JR., AND F. RAICHLEN. 1972. Tsunami generation and near-field propagation. 13th Int. Conf. Coastal Eng., July 10–14, 1972, Vancouver, B.C. p. 401–404. (Abstract)

HAMMOND, A. L. 1973. Earthquake predictions: breakthrough in theoretical insight. Science 180: 851–853.

HAMON, B. V. 1962. The spectrums of mean sea level at Sydney, Coff's Harbor, and Lord Howe Island. J. Geophys. Res. 67: 5147–5155.

1963. Corrections to: the spectrums of mean sea level at Sydney, Coff's Harbor, and Lord Howe Island. J. Geophys. Res. 68: 4635.

1966. Continental shelf waves and the effects of atmospheric pressure and wind stress on sea level. J. Geophys. Res. 71: 2883–2893.

HARKRIDER, D. G. 1964. Theoretical and observed acoustic-gravity waves from explosive sources in the atmosphere. J. Geophys. Res. 69: 5295–5321.

HARKRIDER, D. G., AND F. PRESS. 1966. Air sea waves from the explosion of Krakatoa. Science 154: 1325–1327.

1967. The Krakatoa air sea waves: an example of pulse propagation in coupled systems. J. R. Astron. Soc. Can. 13: 149–159.

HARKRIDER, D. G., AND F. J. WELLS. 1968. The excitation and dispersion of the atmospheric surface wave. Proc. Symp. Acoustic-Gravity Wave. Boulder, Colo. p. 299–313.

HARLEMAN, D. R. F. 1961. Stratified flow, p. 1–21. *In* V. L. Streeter [ed.] Handbook of Fluid Dynamics. McGraw-Hill, Inc. New York, N.Y.

HARLEMAN, D. R. F., AND A. T. IPPEN. 1963. Friction and energy dissipation in long wave hydrodynamics, p. 198–205. *In* D. C. Cox [ed.] Proc. tsunami meetings associated 10th Pac. Sci. Congr. Honolulu, Hawaii. Union Geod. Geophys. Monogr. 24.

HART, P. J. [ED.] 1969. The earth's crust and upper mantle. Am. Geophys. Union Monogr. 13: 735 p.

HATORI, T. 1963. Directivity of tsunamis. Bull. Earthquake Res. Inst. 41: 61-81.

1964. A study of the damage to houses due to a tsunami. Bull. Earthquake Res. Inst. 42: 181-191.

1965a. Study on distant tsunamis along the coast of Japan. Part I. Distribution of tsunami energy and travel time. Bull. Earthquake Res. Inst. 43: 499-508.

1965b. On the tsunami which accompanied the Niigata earthquake on June 16, 1964 — source deformation propagation and tsunami run-up. Bull. Earthquake Res. Inst. 43: 129-148.

1965c. On the Alaska tsunami of March 28, 1964, as observed along the coast of Japan. Bull. Earthquake Res. Inst. 43: 399-407.

1967. The wave form of tsunami on the continental shelf. Bull. Earthquake Res. Inst. 45: 79-90.

1968. Study on distant tsunamis along the coast of Japan. Part II. Tsunamis of South American origin. Bull. Earthquake Res. Inst. 46: 345-359.

1969. Analyses of oceanic long-period waves at Hachijo Island. Bull. Earthquake Res. Inst. 47: 863-874.

1970a. An investigation of the tsunami generated by the East Hokkaido earthquake of August, 1969. Bull. Earthquake Res. Inst. 48: 399-412.

1970b. Dimensions and geographic distribution of tsunamis sources near Japan, p. 69-83. *In* W. M. Adams [ed.] Tsunamis in the Pacific Ocean. East West Center Press. Honolulu, Hawaii.

1970c. Vertical crustal deformation and tsunami energy. Bull. Earthquake Res. Inst. 48: 171-188.

HATORI, T., AND M. KOYAMA. 1971. Travel times of tsunamis and refraction diagrams. Bull. Earthquake Res. Inst. 49: 127-142.

HATORI, T., AND R. TAKAHASI. 1964. On the Iturup tsunami of Oct. 13, 1963 as observed along the coast of Japan. Bull. Earthquake Res. Inst. 42: 543-554.

HAVELOCK, T. H. 1940. Pressure of water on a fixed obstacle. Proc. R. Soc. London Ser. A, 175: 409-421.

HAWALESHKA, O., AND S. B. SAVAGE. 1971. The development of undular-bores with friction. Proc. 12th Conf. Coastal Eng. Washington, D.C., 1970. Am. Soc. Civ. Eng. 1: 461-472.

HECK, N. H. 1947. List of seismic sea waves. Bull. Seismol. Soc. Am. 37: 269-286.

HEEZEN, B. C. 1957. 1908 Messina earthquake, tsunami, and turbidity current. Part II. Geol. Soc. Am. Bull. 68: 1743. (Abstract)

1963. Turbidity currents, p. 742-771. *In* M. N. Hill [ed.] The Sea. Interscience Publishers Inc., New York, N.Y.

HEEZEN, B. C., D. B. ERICSON, AND M. EWING. 1954. Further evidence for a turbidity current following the 1929 Grand Banks earthquake. Deep-Sea Res. 1: 193-202.

HEEZEN, B. C., AND M. EWING. 1952. Turbidity currents and submarine slumps and the 1929 Grand Banks earthquake. Am. J. Sci. 250: 849-873.

1955. Orléansville earthquake and turbidity currents. Bull. Am. Assoc. Pet. Geol. 39: 2505-2514.

HEITNER, K. L., AND G. W. HOUSNER. 1970. Numerical model for tsunami run-up. J. Waterways, Harbors Coastal Eng. Div., Proc. Am. Soc. Civ. Eng. 96: 701-719.

HENRY, R. F. 1971. Simulation of tidal motion in complex river systems and inlets by a method of overlapping segments. Dep. Energy, Mines Resour., Mar. Sci. Branch, MS Rep. 17: 30 p.

HENRY, R. F., AND T. S. MURTY. 1972. Resonance periods of multi-branched inlets with tsunami amplication. Dep. Environ. Mar. Sci. Div., MS Rep. 28: 47-79.

HIDAKA, K. 1931. The oscillations of water in spindle-shaped and elliptic basins as well as the associated problems. Mem. Mar. Obs. Kobe. 4: 99-219.

HIGUCHI, H. 1964. On the behaviour of Chilean tsunami in the Seto Inland Sea. Geophysics papers dedicated to Prof. Kenzo Sassa. Kyoto Univ. Geophys. Inst. Kyoto, Japan. p. 49-57.

HINES, C. O. 1955. Hydromagnetic resonance in ionospheric waves. J. Atmos. Terr. Phys. 7: 14-27.

1960. Internal atmospheric gravity waves at ionospheric heights. Can J. Phys. 38: 1441-1481.

1967. On the nature of travelling ionospheric disturbances launched by low altitude nuclear explosions. J. Geophys. Res. 72: 1877-1882.

1972. Gravity waves in the atmosphere. Nature 239: 73-78.

HITHCOCK, C. H. 1911. Earthquake waves and earthquake wave of 1868, p. 291-295. *In* Hawaii and its volcanoes. 2nd ed. Hawaiian Gazette Co. Ltd., Honolulu, Hawaii.

HO, D. V., AND R. E. MEYER. 1962. Climb of a bore on a beach. Part I. Uniform beach slope. J. Fluid Mech. 14: 305-318.

HODGSON, E. A. 1946. British Columbia earthquake, June 23, 1946. J. R. Astron. Soc. Can. 40: 285-319.

HODGSON, J. H. 1964. Earthquakes and earth structure. Prentice-Hall Inc., Englewood Cliffs, N.J. 166 p.

HODGSON, J. H., AND A. E. STEVENS. 1964. Seismicity and earthquake mechanism, p. 27-59. *In* H. Odishaw [ed.] Research in geophysics. Vol. II. Mass. Inst. Technol. Press, Cambridge, Mass.

HOMMA, M., K. HORIKAWA, AND S. KOMORI. 1966. Response characteristics of underwater wave gauge. Coastal Eng. Jpn., Jpn. Soc. Civ. Eng. 9: 45-54.

HOMMA, S. 1950. On the behaviour of seismic sea waves around a circular island. Geophys. Mag., Tokyo 21: 199-208.

HONDA, H. 1961. The generation of seismic waves, p. 329-334. *In* J. H. Hodgson [ed.] Symposium earthquake mechanism Can. Dep. Mines Tech. Surv.Publ. 24.

HONDA, K., AND W. B. DAWSON. 1911. On the secondary undulations of the Canadian tides. Sci. Rep. Tohoku Imp. Univ. Sendai 1(1): 61–66.

HONDA, K., T. TERADA, Y. YOSHIDA, AND D. ISITANI. 1908. Secondary undulations of oceanic tides. Publ. Earthquake Invest. Comm. Foreign Lang. 26: 1–110.

DE HOOP, A. T. 1958. Presentation theorems for the displacement in an elastic solid and their application to elastodynamic diffraction theory. Doct. Diss. Delft. 84 p.

HORIKAWA, K., AND H. NISHIMURA. 1968. Characteristic oscillation in a basin with a branch. Coastal Eng. Jpn., Jpn. Soc. Civ. Eng. 11: 59–68.

HOUTZ, R. E. 1962. The 1953 Suva earthquake and tsunami. Bull. Seismol. Soc. Am. 52: 1–12.

HUANG, N. E., D. T. CHEN, C. C. TUNG, AND J. R. SMITH. 1972. Interactions between steady nonuniform currents and gravity waves with applications for current measurements. J. Phys. Oceanogr. 2: 420–431.

HUSEBYE, E. S. 1970. The Norwegian seismic array. Obs. R. Belg. Comm. Ser. A, 101: 289 p.

HUSEBYE, E. S., AND H. BUNGUM. 1970. Seismic arrays and data handling problems. Obs. R. Belg. Comm. Ser. A, 101: 293–296.

HWANG, L.-S. 1970. Wave set-up of nonperiodic wave train and its associated shelf oscillation. J. Geophys. Res. 75: 4121–4130.

HWANG, L.-S., H. L. BUTLER, AND D. DIVOKY. 1972a. Tsunami model: generation and open-sea characteristics. Bull. Seismol. Soc. Am. 62: 1579–1596.

1972b. Tsunami generation and propagation. 13th Int. Conf. Coastal Eng. July 10–14, 1972, Vancouver, B.C. p. 397–400. (Abstract)

HWANG, L.-S, AND D. DIVOKY. 1970. Tsunami generation. J. Geophys. Res. 75: 6802–6817.

1971. Tsunamis. Reprint from: Underwater J. p. 207–219.

1972. A numerical model of the major tsunami. The great Alaska earthquake of 1964. U.S. Natl. Acad. Sci. p. 191–200.

1975. Numerical investigations of tsunami behavior. U.S. Natl. Sci. Found., by Tetra Tech. Inc., Pasadena, Calif. 37 p.

HWANG, L.-S., D. DIVOKY, AND L. BUTLER. 1970a. Numerical studies of surface wave generation by bottom motion. Tetra Tech. Inc., Pasadena, Calif. Rep. TC-174-3: 52 p.

HWANG, L.-S., D. DIVOKY, AND A. YUEN. 1970b. Amchitka tsunami study. Tetra Tech. Inc., Pasadena, Calif. Rep. TC-177: 84 p.

HWANG, L.-S., AND A. C. LIN. 1970. Experimental investigations of wave run-up under the influence of local geometry, p. 407–425. *In* W. M. Adams [ed.] Tsunamis in the Pacific Ocean. East West Center Press, Honolulu, Hawaii.

HWANG, L.-S., AND E. O. TUCK. 1970a. On the oscillations of harbors of arbitrary shape. J. Fluid Mech. 42: 447-464.

1970b. Wave generation by beach displacement. Tetra Tech. Inc., Pasadena, Calif. Rep. TC-174-2: 86 p.

ICHIKAWA, M. 1969. Mechanism of earthquakes in and near Japan and related problems, p. 160–165. *In* P. J. Hart [ed.] The earth's crust and upper mantle. Am. Geophys. Union Monogr. 13.

IIDA, K. 1956. Earthquakes accompanied by tsunamis occurring under the sea off the islands of Japan. J. Earth Sci., Nagoya Univ. 4: 1–43.

1958. Magnitude and energy of earthquakes accompanied by tsunami and tsunami energy. J. Earth Sci., Nagoya Univ. 6: 101–112.

1963a. A relation of earthquake energy to tsunami energy and the estimation of the vertical displacement in a tsunami source. J. Earth Sci., Nagoya Univ. 7: 49–67.

1963b. Magnitude, energy and generation mechanisms of tsunamis and a catalogue of earthquakes associated with tsunamis, p. 7–18. *In* D. C. Cox [ed.] Proc. tsunami meetings associated 10th Pac. Sci. Congr., Honolulu, Hawaii. Union Geod. Geophys. Monogr. 24.

1963c. On the estimation of tsunami energy, p. 167–173. *In* D. C. Cox [ed.] Proc. tsunami meetings associated 10th Pac. Sci. Congr., Honolulu, Hawaii. Union Geod. Geophys. Monogr. 24.

1970. The generation of tsunamis and the focal mechanism of earthquakes, p. 3–18. *In* W. M. Adams [ed.] Tsunamis in the Pacific Ocean, East West Center Press, Honolulu, Hawaii.

IIDA, K., D. C. COX, AND G. PARARAS-CARAYANNIS. 1967. Preliminary catalog of tsunamis occurring in the Pacific Ocean. Univ. Hawaii, Inst. Geophys. Data Rep. 5 HIG-67-10.

IMAMURA, A. 1934. Past tsunamis of the Sanriku coast. Jpn. J. Astron. Geophys. 11: 79–93.

1949. List of tsunami in Japan. Zisin. Ser. 2, 2: 23–28.

INGRAM, R. E. 1957. Statistics and the fault plane, a conjecture, p. 263–265. *In* J. H. Hodgson [ed.] The mechanics of faulting, with special reference to the fault-plane work. Symposium on earthquake mechanism. Can. Dep. Mines Tech. Surv. Publ. 20. [Ingram 1959 in Appendix should read Ingram 1957.]

1961. Generalized focal mechanism, p. 305–308. *In* J. H. Hodgson [ed.] Symposium on earthquake mechanism. Can. Dep. Mines Tech. Surv. Publ. 24.

INMAN, D. L., W. R. GAYMAN, AND D. C. COX. 1963. Littoral sedimentary processes on Kauai, a subtropical high island. Pac. Sci. 17: 106.

IPPEN, A. T. [ED]. 1966. Estuary and coastline hydrodynamics. McGraw Hill, New York, N.Y. 258 p.

ISACKS, B., J. OLIVER, AND L. R. SYKES. 1968. Seismology and the new global tectonics. J. Geophys. Res. 73: 5855–5899.

ISACKS, J. D., E. A. WILLIAMS, AND C. ECKART. 1951. Total reflection of surface waves by deep water. Trans. Am. Geophys. Union 32: 37–40.

ISHIMOTO, M., AND T. HAGIWARA. 1934. The tsunami considered as a phenomenon of sea water overflowing the land. Bull. Earthquake Res. Inst. Suppl. 1: 17-24.

ISOZAKI, I., AND S. UNOKI. 1964. The numerical computation of the tsunami in Tokyo Bay caused by the Chilean earthquake in May, 1960, p. 389-402. *In* K. Yoshida [ed.] Studies in oceanography. Univ. Washington Press, Seattle, Wash.

ITÔ, Y. 1970. On the effect of tsunami breakwater. Coastal Eng. Jpn. Jpn. Soc. Civ. Eng. 13: 89-102.

1971. Head loss at tsunami breakwater opening. Proc. 12th Conf. Coastal Eng. Washington, D.C., Am. Soc. Civ. Eng. 3: 2123-2131.

IWAGAKI, Y. Y. TSUCHIYA, AND S. NAKAMURA. 1970. On a tsunami generator. Bull. Disaster Prev. Res. Inst. 19: 57. (Abstract)

IWASAKI, T. 1972. Laboratory study on harbor oscillations due to tsunami waves. 13th Int. Conf. Coastal Eng., July 10-14, 1972, Vancouver, B.C. p. 389-392. (Abstract)

IWASAKI, T., AND H. TOGASHI. 1968. On the overland flow of tsunami and effectiveness of wall as a counter measure. Coastal Eng. Jpn., Jpn. Soc. Civ. Eng. 11: 69-83.

1970. On the shoreline and leading front conditions of tsunami waves in the light of the method of characteristics. Coastal Eng. Jpn., Jpn. Soc. Civ. Eng. 13: 113-125.

JACOBS, J. A., R. D. RUSSEL, AND J. T. WILSON. 1959. Physics and geology. McGraw-Hill Book Company Inc., New York, N.Y. 424 p.

JAEGAR, J. C., AND L. READ. 1969. Seismicity of southeast Australia, p. 145-147. *In* P. J. Hart [ed.] Earth's crust and upper mantle. Am. Geophys. Union Monogr. 13.

JAGGAR, T. A. 1929. Seismic sea waves on March 6, 1929. The Volcano Letter 220. Hawaiian Volcano Res. Assoc., U.S. Geol. Surv. p. 1.

1931. Hawaiian damage from tidal waves. The Volcano Letter 321. Hawaiian Volcano Res. Assoc. U.S. Geol. Surv. p. 1-3.

JARLAN, G. E. 1965. The application of acoustic theory to the reflective properties of coastal engineering structures. Nat. Res. Counc. Can. Lab., Div. Mech. Eng. Tech. Rep. p. 24-63.

JEFFREYS, H. 1952. The earth, its origin, history and physical constitution. 3rd ed. Cambridge Univ. Press, New York, N.Y. 392 p.

JEFFREYS, H., AND B. S. JEFFREYS. 1946. Methods of mathematical physics. Rev. ed. 1965, 1960. Cambridge Univ. Press, New York, N.Y. 679 p.

JOHNS, B. 1965. Fundamental mode edge waves over a steeply sloping shelf. J. Mar. Res. 23: 200-206.

JOHNSON, J. W. 1947. The refraction of surface waves by currents. Trans. Am. Geophys. Union 28: 867-874.

JOHNSON, R. H. 1970. Estimating earthquake rupture length from T-waves, p. 253-259. *In* W. M. Adams [ed.] Tsunamis in the Pacific Ocean. East West Center Press, Honolulu, Hawaii.

JOHNSON, R. H., AND R. A. NORRIS. 1968. T-phase radiators in the western Aleutians. Bull. Seismol. Soc. Am. 58: 1-10.

JOHNSON, R. S. 1972. Shallow water waves on a viscous fluid — the undular bore. Phys. Fluids 15: 1693-1699.

JOHNSTONE, J. H. L. 1930. The Acadian-Newfoundland earthquake of November 18, 1929. Proc. Trans. N.S. Inst. Sci., Halifax, N.S. 17: 223-237.

JONSSON, I. G., C. SKOUGAARD, AND J. D. WANG. 1971. Interaction between waves and currents. Proc. 12th Conf. Coastal Eng., Washington, D.C., Am. Soc. Civ. Eng. 1: 489-507.

KACHADOORIAN, R. 1965. Effects of the earthquake of March 27, 1964 at Whittier, Alaska. Geol. Surv. Prof. Pap. 542-B: 439-460.

KAILA, K. L., V. K. GAUR, AND H. NARAIN. 1972. Quantitative seismicity maps of India. Bull. Seismol. Soc. Am. 62: 1119-1132.

KAILA, K. L., N. M. RAO., AND H. NARAIN. 1974. Seismotectonic maps of southwest Asia region comprising eastern Turkey, Caucasus, Persian Plateau, Afghanistan and Hindukush. Bull. Seismol. Soc. Am. 64: 657-669.

KAJIURA, K. 1958. Effects of Coriolis force on edge waves (II). Specific examples of free and forced waves. J. Mar. Res. 16: 145-157.

1961. A note on the partial reflection of long waves passing through a submarine ridge. Comm. Field Invest. Chilean Tsunami. p. 100-102.

1963. The leading wave of a tsunami. Bull. Earthquake Res. Inst. 41: 535-571.

KAJIURA, K., T. HATORI, I. AIDA, AND M. KOYAMA. 1968. A survey of the tsunami accompanying the Tokachi-Oki earthquake of May 1968. Bull. Earthquake Res. Inst. 46: 1373-1382. (In Japanese)

KAMEL, A. M. 1970. Laboratory study for design of tsunami barrier. J. Waterways, Harbors Coastal Eng. Div., Proc. Am. Soc. Civ. Eng. 96: 767-779.

KANAMORI, H. 1970. Synthesis of long-period surface waves and its application to earthquake source studies: Kurile Islands and earthquake of Oct. 13, 1963. J. Geophys. Res. 75: 5011-5027.

KARNIK, V. 1969. Seismicity of the European area. Part I. D. Reidel Publishing Co., Dordrecht, Holland. 364 p.

1971. Seismicity of the European area. Part II. D. Reidel Publishing Co., Dordrecht, Holland. 218 p.

KATO, Y. ET AL. 1961. The Chile tsunami of 1960 observed along the Sanriku Coast of Japan. Sci. Rep. Tohoku Univ. 13: 107-125.

KATO, Y., K. NORITOMI, J. OSSAKA, AND A. TAKAGI. 1953. Report of tsunami in Shizugawa harbour accompanying Tokachi earthquake on March 4, 1952. Sci. Rep. Tohoku Univ. 4: 143-145.

KATZ, E. J. 1963a. Statistical model of the oceans' variable depth. Deep-Sea Res. 10: 11–16.

1963b. A ray theory for wave propagation in a non-uniform medium. J. Fluid Mech. 16: 343–356.

KELLEHER, J. A. 1970. Space-time seismicity of the Alaska–Aleutian seismic zone. J. Geophys. Res. 75: 5745–5756.

KELLEHER, J. A., L. R. SYKES, AND J. OLIVER. 1973. Possible criteria for predicting earthquake locations and their application to major plate boundaries of the Pacific and the Caribbean. J. Geophys. Res. 78: 2547–2585.

KELLER, J. B. 1963. Tsunami water waves produced by earthquakes, p. 154–166. *In* D. C. Cox [ed.] Proc. tsunami meetings associated 10th Pac. Sci. Congr., Honolulu, Hawaii. Union Geod. Geophys. Monogr. 24.

KELLER, J. B., AND H. B. KELLER. 1964. Water wave run-up on a beach. Service Bureau Corp. Res. Rep. prepared for Off. Naval Res. Contract 3828.

1965. Water wave run-up on a beach. Service Bureau Corp. Res. Rep. prepared for Off. Naval Res. Contract 3828.

KELVIN, W. 1887. On the waves produced by a single impulse in water of any depth or in a dispersive medium. Proc. R. Soc. London 42: 80–83.

KEULEGAN, G. H. 1958. The motion of saline fronts in still water. 12th Prog. Rep. on model laws for density currents. U.S. Natl. Bur. Stand. Rep. 5831.

KEULEGAN, G. H., AND J. HARRISON. 1970. Tsunami refraction diagrams by digital computer. J. Waterways, Harbors Coastal Eng. Div., Proc. Am. Soc. Civ. Eng. 96: 219–233.

KEYLIS-BOROK, V. I. 1956. Methods and results of the investigations of earthquake mechanisms. Bur. Cent. Inst. Seismol. Travaup. Sci. Ser. A, 19: 383–394.

KEYS, J. G. 1963. The tsunami of May 22, 1960, in the Samoa and Cook islands. Bull. Seismol. Soc. Am. 53: 1211–1227.

KINSMAN, B. 1965. Wind waves, their generation and propagation on the ocean surface. Prentice-Hall, Inc., Englewood Cliffs, N.J. 655 p.

KISHINOUYE, F. 1966. The submarine seismograph; the second paper. Bull. Earthquake Res. Inst. 44: 1443–1447.

KISHINOUYE, F. AND K. IIDA. 1939. The tsunami that accompanied the Oga earthquake of May 1, 1939. Bull. Earthquake Res. Inst. 17: 733–740.

KISHINOUYE, F., Y. YAMAZAKI, H. KOBAYASHI, AND S. KORESAWA. 1963. A submarine seismograph; the first paper. Bull. Earthquake Res. Inst. 41: 819–824.

KISSLINGER, C. 1974. Earthquake prediction. Phys. Today. 27: 36–42.

KNOPOFF, L. 1961. Analytical calculation of the fault-plane problem, p. 309–315. *In* J. H. Hodgson [ed.] Symposium earthquake mechanism. Can. Dep. Mines Tech. Surv. Publ. 24.

KNOPOFF, L., AND F. GILBERT. 1959. Radiation from a strike-slip fault. Bull Seismol. Soc. Am. 49: 163–178.

1960. First motions from seismic sources. Bull. Seismol. Soc. Am. 50: 117–134.

KNOWLES, C. E., AND R. O. REID. 1970. The inverse tsunami problem for symmetric islands of simple shape. Texas A and M Univ. Dep. Oceanogr., College Geo-Sci., Tech. Rep. 69 p.

KORESAWA, S. 1963. A submarine seismograph; the first paper. Bull. Earthquake Res. Inst. 41: 819–824.

KORTWEG, D. J., AND G. DE VRIES. 1895. On the change of form of long waves advancing in a rectangular canal, and on a new type of long stationary waves. Philos. Mag. 5(39): 422–443.

KRANZER, H. C., AND J. B. KELLER. 1955. Water waves produced by explosions. New York Univ. Inst. Math. Sci. p. 222–226.

1959. Water waves produced by explosions. J. Appl. Phys. 30: 398–407.

KRIVOSHEY, M. I. 1970. Experimental investigations of tsunami waves, p. 351–365. *In* W. M. Adams [ed.] Tsunamis in the Pacific Ocean. East West Center Press, Honolulu, Hawaii.

KUENEN, PH. H. 1952. Estimated size of the Grand Banks turbidity current. Am. J. Sci. 250: 874–884.

1956. The difference between sliding and turbidity flow. Deep-Sea Res. 3: 134–139.

KVALE, A. 1955. Seismic seiches in Norway and England during the Assam earthquake of August 15, 1950. Bull. Seismol. Soc. Am. 45: 93–113.

LACHMAN, R., M. TATSOUKA, AND W. J. BONK. 1961. Human behaviour during the tsunami of May, 1960. Science 133: 1405–1409.

LAING, A. C. M. 1954. Note on tsunamis reaching New Zealand. N.Z. J. Sci. Technol. p. 470–472.

LAIRD, A. D. K. 1955. A model study of wave action on a cylindrical island. Trans. Am. Geophys. Union 36: 279–285.

LAITONE, E. V. 1961. Higher approximations to nonlinear water waves and the limiting heights of cnoidal, solitary and Stokes' waves. Univ. California, Berkeley, Inst. Eng. Res., Tech. Memo 133: 106.

LAMB, H. 1945. Hydrodynamics. 6th ed. Dover Publishing, Inc., New York, N.Y. 738 p.

LANE, F. W. 1965. Earthquakes from "the elements rage." Chilton Co., Philadelphia, Pa. 280 p.

LARSEN, J., AND P. L. CHRISTIANSEN. 1975. Computations of harbor oscillations by ray methods. Symposium on modeling techniques. 2nd Annu. Symp. Waterways, Harbors Coastal Eng. Div. San Francisco, Calif., Am. Soc. Civ. Eng. 2: 888–906.

LARSEN, J. C. 1971. The electromagnetic field of long and intermediate water waves. J. Mar. Res. 29: 28–45.

LAUTENBACHER, C. C. 1970. Gravity wave refraction by islands. J. Fluid Mech. 41: 655–672.

LAVRENTYEV, M. A., AND E. F. SAVARENSKY. 1963. On the results of investigations of tsunamis in the USSR, p. 36–38. *In* D. C. Cox [ed.] Proc. tsunami meetings associated 10th Pac. Sci. Congr., Honolulu, Hawaii. Union Geod. Geophys. Monogr. 24.

LEE, J. J. 1971. Wave-induced oscillations in harbors of arbitrary geometry. J. Fluid Mech. 45: 375–394.

LEE, J. J., AND F. RAICHLEN. 1971. Resonance in harbors of arbitrary shape. Proc. 12th Conf. Coastal Eng., Washington, D.C., Am. Soc. Civ. Eng. 3: 2163–2180.

1972. Oscillations in harbors with connected basins. J. Waterways, Harbors Coastal Eng. Div., Proc. Am. Soc. Civ. Eng. 98: 311–332.

LEE, Y. K., AND L.-S. HWANG. 1975. Waves generated by horizontal oscillations. U.S. Natl. Sci. Found. by Tetra Tech. Inc., Pasadena, Calif. 72 p.

LEENDERTSE, J. J. 1967. Aspects of a computational model for long period water-wave computation. Rand Corp. Memo RM-5294-PR: 165 p.

LEET, L. D. 1951. Discussion of proposed use of the T-phase in tsunami warning systems. Bull. Seismol. Soc. Am. 41: 165–167.

LEMÉHAUTÉ, B. 1962. On the nonsaturated breaker theory and the wave run-up, p. 77–92. *In* 8th Conf. Coastal Eng., Mexico City, Mexico. Am. Soc. Civ. Eng.

1969. An introduction to hydrodynamics and water waves. Vol. II. Water wave theories. Env. Sci. Serv. Admin. Tech. Rep. 118-POL 3-2: 507–725.

1971. Theory of explosion-generated water waves, p. 1–77. *In* V. T. Chow [ed.] Advances in hydroscience. Vol. VI. Academic Press, Inc. New York, N.Y.

LENSEN, G. J. 1961. Principal horizontal stress directions as an aid to the study of crustal deformation, p. 389–397. *In* J. D. Hodgson [ed.] Symposium on earthquake mechanism. Can. Dep. Mines Tech. Surv. Publ. 24.

LEVY, D. M., AND J. B. KELLER. 1963. Water wave production by point sources and extended sources. Appendix to J. B. Keller's 1963 article, p. 162–166. *In* D. C. Cox [ed.] Proc. tsunami meetings associated 10th Pac. Sci. Congr. Honolulu, Hawaii. Union Geod. Geophys. Monogr. 24.

LIGHTHILL, M. J. 1958. River waves. Proc. 1st Symp. Naval Hydrodynamics, Washington, D.C. 1956, U.S. Natl. Res. Counc. p. 17–44.

LINEHAN, D. 1940. Earthquakes in the West Indian region, Trans. 21st Annu. Meet., Am. Geophys. Union. p. 229–232.

LIU, C. H., AND K. C. YEH, 1971. Excitation of acoustic-gravity waves in an isothermal atmosphere. Tellus 23: 150–163.

LOMNITZ, C. 1971. Grandes terremotos y tsunamis en Chile durante el periodo 1535–1955. Geofis. Panam. 1: 151–178.

LONGUET-HIGGINS, M. S. 1964. Planetary waves on a rotating sphere. Proc. R. Soc. London Ser. A, 279: 446–473.

1965. Planetary waves on a rotating sphere II. Proc. R. Soc. London Ser. A, 284: 40–68.

1967. On the wave-induced difference in the mean sea level between the two sides of a submerged breakwater. J. Mar. Res. 25: 148–153.

1968. On the trapping of waves along a discontinuity of depth in a rotating ocean. J. Fluid Mech. 31: 417–434.

1974. On the mass momentum, energy and circulation of a solitary wave. Proc. R. Soc. London Ser. A, 337: 1–13.

LONGUET-HIGGINS, M. S., AND J. D. FENTON. 1974. On the mass, momentum, energy and circulation of a solitary wave. II. Proc. R. Soc. London Ser. A, 340: 471–493.

LONGUET-HIGGINS, M. S., AND R. W. STEWART. 1960. Changes in the form of short-gravity waves on long waves and tidal currents. J. Fluid Mech. 8: 565–583.

1961. The changes in amplitude of short-gravity waves on steady non-uniform currents. J. Fluid Mech. 10: 529–549.

1962. Radiation stress and mass transport in gravity waves with application to surf-beats. J. Fluid Mech. 13: 481–504.

1963. A note on wave set up. J. Mar. Res. 21: 4–10.

1964. Radiation stress in water waves; a physical discussion, with applications. Deep-Sea Res. 11: 529–562.

LOOMIS, H. G. 1966. Spectral analysis of tsunami records from stations in the Hawaiian Islands. Bull. Seismol. Soc. Am. 56: 697–713.

1970. A method of setting up the eigenvalue problem for the linear shallow water-wave equation for irregular bodies of water with variable water depth and application to bays and harbors in Hawaii. Univ. Hawaii, Inst. Geophys., Rep. HIG-70-32: 9 p.

1972. The major tsunami in the Hawaiian Islands, p. 181–190. *In* The great Alaska earthquake of 1964: oceanography and coastal engineering. U.S. Natl. Acad. Sci.

LOUCKS, R. H. 1962. Investigation of the 1960 Chilean tsunami on the Pacific coast of Canada. M.Sc. Thesis, Univ. British Columbia, Vancouver, B.C. 21 p.

LOVE, A. E. H. 1892. A treatise on the mathematical theory of elasticity. Cambridge University Press, New York, N.Y. 1: 428.

LUDWIG, D. 1965. Wave propagation near a smooth caustic. Bull. Am. Math. Soc. 71: 776–779.

1966. Uniform asymptotic expansions at a caustic. Comm. Pure Appl. Math. 19: 215–250.

1968. Strength of caustics. J. Acoust. Soc. Am. 43: 1179–1180.

LUNDGREN, H. 1963. Wave thrust and energy level. Proc. Int. Assoc. Hydraul. Res. Congr. London. p. 147–151.

LYNCH, J. J., AND R. R. BODLE. 1948. The Dominican earthquakes of August, 1946. Bull. Seismol. Soc. Am. 38: 1–17.

MACDONALD, G. A., F. P. SHEPARD, AND D. C. COX. 1947. The tsunami of April 1, 1946, in the Hawaiian Islands. Pac. Sci. 1: 21–37.

MACDONALD, G. A., AND C K. WENTWORTH. 1951. The Kona earthquake of August 21, 1951. The Volcano Letter 513. U.S. Geol. Surv. p. 1–4.

1954. The tsunami of November 4, 1952, on the island of Hawaii. Bull. Seismol. Soc. Am. 44: 463–469.

MADER, C. L. 1974. Numerical simulation of tsunamis. J. Phys. Oceanogr. 4: 74–82.

MAGOON, O. T. 1965. Structural damage by tsunamis. Coastal Eng. Spec. Conf., Santa Barbara, Calif. Oct. 1965. Am. Soc. Civ. Eng. p. 35–68.

MANSINHA, L., AND D. E. SMYLIE. 1971. The displacement fields of inclined faults. Bull. Seismol. Soc. Am. 61(5): 1433–1440.

MARINATOS, S., AND O. IMBODEN. 1972. Thera key to the riddle of Minoan. Natl. Geogr. 141: 702–726.

MASÓ, M. S. 1918. Great earthquake and tidal wave in Southern Mindarao, P.I. Bull. Seismol. Soc. Am. 8: 125–126.

MATLOCK, H., L REESE, AND R. MATLOCK. 1962. Analysis of structural damage from the 1960 tsunami at Hilo, Hawaii. Rep. Def. At. Support Agency – 1268. Univ. Texas, Struct. Mech. Res. Lab., Contract DA-49-146-XZ-028: 95 p.

MCCOWAN, J. 1894. On the highest wave of permanent type. Philos. Mag. 38: 351–358.

MCEVILLY, T. V., AND R. RAZANI. 1973. A preliminary report: the Qir, Iran earthquake of April 10, 1972. Bull. Seismol. Soc. Am. 63: 339–354.

MCGOLDRICK, L. F. 1968. Long waves over wavy bottoms. Univ. Chicago, Dep. Geophys. Sci., Tech. Rep. 1: 64 p.

MCINTOSH, D. S. 1930. The Acadian-Newfoundland earthquake. Proc. Trans. N.S. Inst. Sci. 17: 213–222.

MERIAN, J. R. 1828. Über die Bewegung. Tropfbarer Flussigkeiten in Gebässen (Basle).

MIDDLETON, G. V. 1966a. Small scale models of turbidity currents and the criterion for auto-suspension. J. Sediment. Petrol. 36: 202 p.

1966b. Experiments on density and turbidity currents. (I) Motion of the head. Can. J. Earth Sci. 3: 523–546.

MILES, J. W. 1946a. The analysis of plane discontinuities in cylindrical tubes. Part I. J. Acoust. Soc. Am. 17: 259–271.

1946b. The analysis of plane discontinuities in cylindrical tubes. Part II. J. Acoust. Soc. Am. 17: 272–284.

1948. The coupling of a cylindrical tube to a half infinite space. J. Acoust. Soc. Am. 20: 652–664.

1967. Surface-wave scattering matrix for a shelf. J. Fluid Mech. 28: 755–767.

1968. The Cauchy–Poisson problem for a viscous liquid. J. Fluid Mech. 34: 359–370.

1971. Resonant response of harbors: an equivalent circuit analysis. J. Fluid Mech. 46: 241–265.

1974. Harbor seiching. Annu. Rev. Fluid Mech. 6: 17–35.

MILES, J. W., AND Y. K. LEE. 1975. Helmholtz resonance of harbors. J. Fluid Mech. 67: 445–464.

MILES, J. W., AND W. H. MUNK. 1961. Harbor paradox. J. Waterways, Harbors Coastal Eng. Div., Proc. Am. Soc. Civ. Eng. 87: 111–130.

MILLER, D. J. 1960. The Alaska earthquake of July 10, 1958: giant wave in Littuya Bay. Bull. Seismol. Soc. Am. 50: 253–266.

MILLER, G. R. 1964. Tsunamis and tides. Ph.D. Thesis, Univ. California, San Diego, Calif. 120 p.

MILLER, G. R., W. H. MUNK, AND F. E. SNODGRASS. 1962. Long-period waves over California's continental borderland. Part II. Tsunamis. J. Mar. Res. 20: 31–41.

MILLER, R. L. 1968. Experimental determination of run-up of undular and fully developed bores. J. Geophys. Res. 73: 4497–4510.

1970. An experimental study of form and transitions in impulse waves, p. 15. *In* Proc. Symp. Long Waves, Sept. 10–11, 1970, Univ. Delaware, Newark, Del.

1971. Prediction curves for waves near the source of an impulse. Proc. 12th Conf. Coastal Eng., Washington, D.C., Am. Soc. Civ. Eng. 1: 609–624.

MILLER, R. L., AND R. V. WHITE. 1966. A single impulse system for generating solitary, undulating surge and gravity shock waves in the laboratory. Univ. Chicago, Fluid Dyn. Sediment Trans. Lab., Dep. Geophys. Sci., Tech. Rep. 5: 48 p.

MILNE, J. 1880. The Peruvian earthquake of May 9, 1877. Trans. Seismol. Soc. Jpn. 2: 50–96.

1896. The great seismic wave of Japan. Nature 54: 449–450.

MILNE, W. G. 1967. Earthquake epicenters and strain release in Canada. Can. J. Earth Sci. 4: 797–814.

MIYABE, N. 1940. Tsunami associated with the earthquake of August 2, 1940. Bull. Earthquake Res. Inst. 19: 104–114.

MIYOSHI, H. 1954. Efficiency of the tsunami. J. Oceanogr. Soc. Jpn. 10: 11–14.

1955. Directivity of the recent tsunamis. J. Oceanogr. Soc. Jpn. 11: 151–155.

MIZOUE, M. 1967. Variation of earthquake energy release with depth [I]. Bull. Earthquake Res. Inst. 45: 679–709.

MOGI, K. 1968. Development of aftershock areas of great earthquakes. Bull. Earthquake Res. Inst. 46: 175–203.

MOMOI, T. 1963a. Tsunami in a T-shaped canal. Bull. Earthquake Res. Inst. 41: 357–373.

1963b. Tsunami in a canal of varying width. Bull. Earthquake Res. Inst. 41: 375–389.

1964. Construction of refraction diagrams of tsunami [I]. Bull. Earthquake Res. Inst. 42: 729–739.

1967a. A long wave around a breakwater (case of perpendicular incidence) [I]. Bull. Earthquake Res. Inst. 45: 91–136.

1967b. A long wave around a breakwater (case of perpendicular incidence) [II]. Bull Earthquake Res. Inst. 45: 749–783.

1968a. A long wave around a breakwater (case of perpendicular incidence) [III]. Bull Earthquake Res. Inst. 46: 125–135.

1968b. A long wave around a breakwater (case of lateral incidence) [IV]. Bull. Earthquake Res. Inst. 46: 319–343.

1968c. A long wave around a breakwater (case of perpendicular incidence) [V]. Bull. Earthquake Res. Inst. 46: 889–899.

1969a. A long wave around a breakwater (case of lateral incidence) [VI]. Bull. Earthquake Res. Inst. 47: 165–184.

1969b. A long wave in the vicinity of an estuary [VI]. Bull. Earthquake Res. Inst. 47: 487–521.

1969c. A long wave around a breakwater (case of normal incidence) [VII]. Bull. Earthquake Res. Inst. 47: 701–719.

1969d. A long wave around a breakwater (case of oblique incidence) [VIII]. Bull. Earthquake Res. Inst. 47: 875–890.

MOOERS, C. N. K., AND R. L. SMITH. 1968. Continental shelf waves off Oregon. J. Geophys. Res. 73: 549–557.

MOREIRA, S. 1970. Tsunamis observed on the coasts of Europe, North Africa and Middle East, p. 113–114. *In* J. M. Van Gils [ed.] Gén. Comm. Seismol. Eur., Luxembourg, 12th Assem., Sept. 21–29, 1970. Obs. R. Belg. Comm. Ser. A,13.

MORROW, C. T. 1966. Diffraction of ocean waves about a breakwater. J. Waterways, Harbors Coastal Eng. Div., Proc. Am. Soc. Civ. Eng. 92: 25–44.

MUGA, B. J., AND J. F. WILSON. 1970. Surface gravity water waves, p. 20–67. *In* Dynamic analysis of ocean structures. Plenum Press, New York, N.Y.

MULLER, L. 1964. The rock slide in the Vajont Valley. J. Intr. Soc. Rock Mech. 2: 3–4.

MUNK, W. H. 1947. Increase in the period of waves travelling over large distances: with applications to tsunamis, swell, and seismic surface waves. Trans. Am. Geophys. Union 28: 198–217.

1953. Small tsunami waves reaching California from the Japanese earthquake of March 4, 1952. Bull. Seismol. Soc. Am. 43: 219–222.

1957. Hilo seawall, Island of Hawaii. Territory of Hawaii. Appendix I to review report on survey of Hilo harbor. Scripps Inst. Oceanogr., Univ. California, Berkeley.

1963. Some comments regarding diffusion and absorption of tsunamis, p. 53–72. *In* D. C. Cox [ed.] Proc. tsunami meetings associated 10th Pac. Sci. Congr. Honolulu, Hawaii. Union Geod. Geophys. Monogr. 24.

MUNK, W. H., AND R. S. ARTHUR. 1952. Wave intensity along a refracted ray, p. 95–108. *In* Proc. Symp. Gravity Waves. U.S. Natl. Bur. Stand. Circ. 521.

MUNK, W. H., G. R. MILLER, AND F. E. SNODGRASS. 1962. Long-period waves over California's continental borderland. Part III. The decay of tsunamis and the dissipation of tidal energy. J. Mar. Res. 20: 119–120.

MUNK, W. H., AND M. C. SARGENT. 1948. Adjustment of Bikini Atoll to ocean waves. Trans. Am. Geophys. Union 29: 855–860. (Abstract)

MUNK, W. H., F. E. SNODGRASS, AND G. CARRIER. 1956. Edge waves on the continental shelf. Science 123: 127–132.

MUNK, W. H., F. E. SNODGRASS, AND F. GILBERT. 1964. Long waves on the continental shelf: an experiment to separate trapped and leaky modes. J. Fluid Mech. 20: 529–554.

MURPHY, L. M., AND W. K. CLOUD. 1954. Tidal disturbances of seismic origin for 1952. U.S. Earthquake Notes 773: 1–50.

MURPHY, L. M., AND R. A. EPPLEY. 1970. Developments and plans for the Pacific tsunami warning system, p. 261–270. *In* W. M. Adams [ed.] Tsunamis in the Pacific Ocean. East West Center Press, Honolulu, Hawaii.

MURTY, T. S. 1971. The response of a lake with a depth-discontinuity to a time-dependent wind-stress. Arch. Meteorol. Geophys. Bioklamatol. Ser. A, 20: 55–66.

1975. The dynamics of tsunamis. Proc. 1975 Conf. Ocean Mar. Tech. Soc. p. 1–8.

MURTY, T. S., AND L. BOILARD. 1970. The tsunami in Alberni Inlet caused by the Alaska earthquake of March, 1964, p. 165–187. *In* W. M. Adams [ed.] Tsunamis in the Pacific Ocean. East West Center Press, Honolulu, Hawaii.

MURTY, T. S., AND N. G. FREEMAN. 1973. Applications of the concepts of edge waves and numerical modeling to storm surge studies on Lake Huron. Proc. 16th Conf. Great Lakes Res. Int. Assoc., Great Lakes Res. Ann Arbor, Mich. p. 533–548.

MURTY, T. S., AND R. F. HENRY. 1972. Some tsunami studies for the west coast of Canada. Dep. Environ., Mar. Sci. Dir., MS Rep. 28: 1–46.

MURTY, T. S., AND J. D. TAYLOR. 1975. Free oscillations in bays and harbors. Symposium on modeling techniques. 2nd Annu. Symp. Waterways, Harbors. Coastal Eng. Div., San Francisco, Calif. Am. Soc. Civ. Eng. 2: 874–887.

MURTY, T. S., AND S. O. WIGEN. 1975. Tsunami water levels and spectra for Peru. Newsl., Tsunami Inf. Cent. 8: 2–17.

1976. Tsunami behavior on the Atlantic coast of Canada and some similarities to the Peru coast. Proc. IUGG Symp. tsunamis and tsunami Res. Jan. 29–Feb. 1, 1974. Wellington, N.Z., R. Soc. N.Z. Bull. 15: 51–60.

MUSYA, K. 1934. On the luminous phenomena that accompanied the great Sanriku tsunami in 1933. Part I. Bull. Earthquake Res. Inst. Spec. 1: 87–111.

MYSAK, L. A. 1966. Continental shelf waves. Ph.D. Thesis, Harvard Univ., Cambridge, Mass. 69 p.

1967a. On the theory of continental shelf waves. J. Mar. Res. 25: 205–227.

1967b. On the very low frequency spectrum of the sea level on a continental shelf. J. Geophys. Res. 72: 3043–3047.

1968a. Edge waves on a gently sloping continental shelf of finite width. J. Mar. Res. 26: 24–33.

1968b. Effects of deep-sea stratification and current on edge waves. J. Mar. Res. 26: 34–42.

MYSAK, L. A., AND B. V. HAMON. 1968. Low-frequency sea level behaviour and continental shelf waves of North Carolina. Trans. Am. Geophys. Union 49: 212 p. (Abstract)

NABARRO, F. R. N. 1951. The synthesis of elastic dislocation fields. Philos. Mag. 7: 1224–1231.

NAGATA, T. 1950. Summary of the geophysical investigations on the great earthquake in southwestern Japan on December 21, 1946. Trans. Am. Geophys. Union 31: 1–6.

NAGOKA, H. 1907. Note on the bore in Odawara. Proc. Tokyo Math. Phys. Soc. 4: 210–212.

NAGUMO, S., H. KOBAYASHI, AND S. KORESAWA. 1965. Construction of ocean bottom seismograph. Bull. Earthquake Res. Inst. 43: 671–683.

NAKAMURA, K. 1961. Velocity of long gravity waves in the ocean. Sci. Rep. Tohoku Univ. Ser. 5, 13: 164–173.

1962. The generation of edge waves by cylindrical waves impinging from the outer sea. Sci. Rep. Tohoku Univ. Ser. 5, 14: 27–40.

NAKAMURA, K., AND K. EMURA. 1961. Maximum water height at bay head in case of tsunami invasion. Sci. Rep. Tohoku Univ. Ser. 5, 13: 32–42.

NAKAMURA, K., AND H. WATANABE. 1961. Tsunami forerunners observed in the case of the Chilean tsunami of 1960. Rep. Chilean Tsunami May 24, 1960 as observed along the coast of Japan. Comm. Field Invest. Chilean Tsunami 1960. p. 379.

1966. Edge waves and tsunamis. Proc. 11th Pac. Sci. Congr., Tokyo, Jpn. 1–4: 163 p.

NAKAMURA, S. 1972. On hydraulic bore and its application – tsunami generation and propagation, p. 1–13. *In* Proc. Tsunami Symp. Associated with 14th General Assembly of IUGG, Moscow, 10–12 Aug., 1971. (In Russian)

1976. Shock pressure of tsunami surge on a wall. Proc. IUGG Conf. tsunamis and tsunami Res., Jan. 29–Feb. 1, 1974. Wellington, N.Z., R. Soc. N.Z., Bull. 15: 177–190.

NAKANO, M. 1932a. Preliminary note on the accumulation and dissipation of energy of the secondary undulations in a bay. Proc. Phys. Math. Soc. Jpn. Ser. 3: 44–56.

1932b. The secondary undulations in bays forming a coupled system. Proc. Phys. Math. Soc. Jpn. Ser. 3: 372–380.

1933. Possibility of excitation of secondary undulations in bays by tidal or oceanic currents. Proc. Imp. Acad. Jpn. 9: 152–155.

NAKANO, M., AND T. ABE. 1958. Standing oscillation of bay water induced by currents. Geophys. Mag. 28: 375–397.

NAKANO, M., S. UNOKI, M. HANZAWA, R. MARUMO, AND J. FUKUOKA. 1954. Oceanographic features of a submarine eruption that destroyed the Kaiyo-Maru No. 5. J. Mar. Res. 13: 48–66.

NAKAYAMA, M. 1972. On the PCM-FS-FM tide telemetering system for warning of tsunamis and storm surges. Oceanogr. Mag. 23: 59–67.

NASU, N. 1948. Local phenomena of tsunami. Part II. Bull. Earthquake Res. Inst. 26: 27–35.

NASU, N., AND T. SHIRAI. 1947. Local phenomena of tsunami. Part I. Bull. Earthquake Res. Inst. 25: 81–84.

NEKRASOV, A. V. 1970. Transformation of tsunamis on the continental shelf. p. 337–350. *In* W. M. Adams [ed.] Tsunamis in the Pacific Ocean. East West Center Press, Honolulu, Hawaii.

NEUMANN, G., AND W. J. PIERSON. 1966. Principles of physical oceanography. Prentice-Hall Inc. Englewood Cliffs, N.J. 545 p.

NIAZI, M. 1964. Partition of energy in the focal region of earthquakes. Bull. Seismol. Soc. Am. 54: 2175–2183.

NIKITIN, A. K., AND E. N. POTETYUNKO. 1967. Cauchy-Poissons spatial problem of waves on the surface of a viscous liquid of finite depth. Doklady Acad. Sci. USSR. 1974: 50–52.

NODA, E. N. 1970. Water waves generated by landslides. J. Waterways, Harbors Coastal Eng. Div., Proc. Am. Soc. Civ. Eng. 96: 835–855.

NOMURA, Y. 1938. On the waves of water of finite depth due to disturbances on the surface. Sci. Rep., Tohoku Univ. Ser. 1, 26: 687–713.

NOWROOZI, A. A. 1972. Focal mechanism of earthquakes in Persia, Turkey, West Pakistan, and Afghanistan and plate tectonics of the Middle East. Bull. Seismol. Soc. Am. 62: 823–850.

NUR, A. 1972. Dilatancy, pore fluids and premonitory variations of ts/tp travel times. Bull. Seismol. Soc. Am. 62: 1217–1222.

OBAYASHI, T. 1962. Wide-spread ionospheric disturbances due to nuclear explosions during Oct. 1961. Jpn. Ionosphere Space Res. Rep. 16: 334–340.

1963. Upper atmospheric disturbances due to high altitude nuclear explosions. Planet. Space Sci. 10: 47–63.

O'BRIEN, J. T., AND D. I. KUCHENREUTHER. 1957. Waves in and around Port Hueneme, California, associated with the tsunami of 9 March, 1957. U.S. Naval Civ. Eng. Res. Eval. Lab. Rep. LR-R-015: 13 p.

OGIWARA, D., AND T. ÔKITA. 1951. Studies on tsunami on the Pacific coasts of northern Honshû (I – the model experiment of tsunami in Shizukawa Harbor). Sci. Rep. Tohoku Univ. Ser. 5, 2: 58–65.

OLDHAM, R. D. O. 1909. The Italian earthquake. Nature 79: 287–288.

OLSEN, K., AND L.-S. HWANG. 1971. Oscillations in a bay of arbitrary shape and variable depth. J. Geophys. Res. 76: 5048–5064.

OMER, G. C., AND H. H. HALL. 1949. The scattering of a tsunami by a cylindrical island. Bull. Seismol. Soc. Am. 39: 257–260.

OMORI, F. 1906. Note on the tidal waves caused by the Great Krakatoa eruption of 1883. Proc. Tokyo Math. Phys. Soc. 2: 455–457.

1910. Seismic experiments on the fracturing and overturning of columns. Bull. Imp. Earthquake Invest. Comm. 4: 99 p.

OMOTE, S. 1946. The tsunami: the earthquake sea waves that accompanied the great earthquake of Dec. 7, 1944. Bull. Earthquake Res. Inst. 24: 31–57.

PAGE, R. 1968. Focal depths of aftershocks. J. Geophys. Res. 73: 3897–3903.

PAKISER, L. C., J. P. EATON, J. H. HEALY, AND C. B. RALEIGH. 1969. Earthquake prediction and control. Science 166: 1467–1474.

PALMER, R. Q., M. E. MULVIHILL, AND G. T. FUNASAKI. 1965. Hilo harbor tsunami model-reflected waves superimposed. Proc. 10th Conf. Coastal Eng., Am. Soc. Civ. Eng. p. 21–31.

PARARAS-CARAYANNIS, G. 1967. A study of the source mechanism of the Alaska earthquake and tsunami of March 27, 1964. Part I. Water waves. Pac. Sci. 21: 301–310.

1973. The waves that destroyed the Minoan Empire. Sea Frontiers 19: 94–106.

PEKERIS, C. L. 1948. Theory of propagation of explosive sound in shallow water, p. 1–117. *In* Propagation of sound in the ocean. Geol. Soc. Am. Mem. 27.

PENNY, W. G., AND A. T. PRICE. 1944. Diffraction of sea waves by breakwaters — artificial harbors. Dir. Misc. Weapon Dev. Tech. Hist. 26.

PEREGRINE, D. H. 1966. Calculations of the development of an undular bore. J. Fluid Mech. 25: 321–330.

1967. Long waves on a beach. J. Fluid Mech. 27: 815–827.

PETUKHOV, V. K., AND N. N. ROMANOVA. 1971. Effects caused by acousto-gravitational waves in the upper atmosphere. Atmos. Oceanic Phys. 7: 219–223.

PFEFFER, R. L., AND J. ZARICHNY. 1962. Acoustic-gravity wave propagation from nuclear explosions in the earth's atmosphere. J. Atmos. Sci. 19: 256–263.

PLAFKER, G., AND J. C. SAVAGE. 1970. Mechanism of the Chilean earthquakes of May 21 and 22, 1960. Geol. Soc. Am. Bull. 31: 1001–1030.

PLAPP, J. E., AND J. P. MITCHELL. 1960. A hydrodynamic theory of turbidity currents. J. Geophys. Res. 65: 983–992.

PLATZMAN, G. W. 1971a. Ocean tides and related waves — mathematical problems in the geophysical sciences. Lect. Appl. Math. Am. Math. Soc. 14: 239–291.

1971b. Two-dimensional free oscillations in natural basins. Univ. Chicago, Dep. Geophys. Sci. Tech. Rep. 23: 106 p.

1972. Two-dimensional free oscillations in natural basins. J. Phys. Oceanogr. 2(2): 117–138.

PLATZMAN, G. W., AND D. B. RAO. 1964. The free oscillations of Lake Erie, p. 359–382. *In* K. Yoshida [ed.] Studies of oceanography. (Hidaka volume) Univ. Washington Press, Seattle, Wash.

PLESINGER, A. 1970. Theory and realisation of broad-band feed back seismographs. Obs. R. Belg. Comm. Ser. A, 101: 279–284.

PODYAPOLSKY, G. S. 1970. Generation of the tsunami wave by the earthquake, p. 19–32. *In* W. M. Adams [ed.] Tsunamis in the Pacific Ocean. East West Center Press, Honolulu, Hawaii.

POWERS, H. A. 1946. The Aleutian tsunami at Hilo, Hawaii, April, 1946. Bull. Seismol. Soc. Am. 36: 355–356.

PRANDTL, L. 1952. Essentials of fluid dynamics. Hafner Publishing Co., New York. 452 p.

PRESS, F., AND M. EWING. 1948. A theory of microseisms with geological applications. Trans. Am. Geophys. Union 29: 163–174.

PRESS, F., M. EWING, AND I. TOLSTOY. 1950. The airy phase of shallow focus submarine earthquakes. Bull. Seismol. Soc. Am. 40: 111–148.

PRESS, F., AND D. HARKRIDER. 1962. Propagation of acoustic-gravity waves in the atmosphere. J. Geophys. Res. 67: 3889–3908.

1966. Air-sea waves from the explosion of Krakatoa. Science 154: 1325–1327.

PRINS, J. E. 1956. Characteristics of waves generated by a local surface disturbance. Univ. California, Wave Res. Lab. Inst. Eng. Res., Ser. 99.

1958a. Water waves due to a local disturbance. Proc. 6th Conf. Coastal Eng. Counc. Wave Res. Eng. Found., Berkeley, Calif. p. 147–162.

1958b. Characteristics of waves generated by a local disturbance. Trans. Am. Geophys. Union 39: 865–874.

PROUDMAN, J. 1916. On the dynamical theory of tides. Part II. Flat seas. Proc. London Math. Soc. Ser. 2: 21–50.

1953. Dynamical oceanography. John Wiley and Sons, Inc., New York, N.Y. 409 p.

RAICHLEN, F. 1966a. Long period oscillations in basins of arbitrary shape. Coastal Eng. Spec. Conf. Santa Barbara, Calif., 1965. Am. Soc. Civ. Eng. Part I. p. 115–145.

1966b. Harbor resonance, p. 281–340. *In* A. T. Ippen [ed.] Estuary and coastline hydrodynamics. McGraw-Hill, Inc. New York, N.Y.

RAMIREZ, J. E. 1971. The destruction of Bahia Solano, Colombia, on Sept. 26, 1970 and the rejuvenation of a fault. Bull. Seismol. Soc. Am. 61: 1041–1049.

RANDALL, M. J. 1964a. On the mechanism of earthquakes. Bull. Seismol. Soc. Am. 54: 1283–1289.

1964b. Seismic energy generated by a sudden volume change. Bull. Seismol. Soc. Am. 54: 1291–1298.

1966. Seismic radiation from a sudden phase transition. J. Geophys. Res. 71: 5297–5302.

RAO, D. B. 1966. Free gravitational oscillations in rotating rectangular basins. J. Fluid Mech. 25: 523–555.

1967. Response of a lake to a time dependent wind stress. J. Geophys. Res. 72: 1697–1708.

1968. Natural oscillations of the Bay of Fundy. J. Fish. Res. Board Can. 25: 1097–1114.

1969. Effect of travelling disturbances on a rectangular bay of uniform depth. Arch. Meteorol. Geophys. Bioklimatol. Ser. A, 18: 171–190.

1972. Transient response of shallow enclosed basins. Univ. Wisconsin, Cent. Great Lakes Stud. Tech. Rep. 59 p.

RAYLEIGH, LORD 1876. On waves. London Philosoph. Mag. Ser. 5,1: 257–279.

1914. Further applications of Bessel's functions of high order to the whispering gallery and allied problems. Philos. Mag. 27: 100–109.

1945. The theory of sound. Dover Publishing Inc., New York. 984 p.

REESE, L. C., AND H. MATLOCK. 1968. Structural damage from tsunami at Hilo, Hawaii. J. Hydraul. Div. Proc. Am. Soc. Civ. Eng. 94: 961–982.

REID, H. F. 1914. The Lisbon earthquake of November 1, 1755. Bull. Seismol. Soc. Am. 4: 53–80.

REID, H. F., AND S. TABER. 1920. The Virgin Islands earthquakes of 1867–1868. Bull. Seismol. Soc. Am. 10: 9–30.

REID, R. O. 1958. Effect of Coriolis force on edge waves. Part I. Investigation of the normal modes. J. Mar. Res. 16: 109–144.

REID, R. O., AND C. E. KNOWLES. 1970. An inverse tsunami problem, p. 399–406. *In* W. M. Adams [ed.] Tsunamis in the Pacific Ocean. East West Center Press, Honolulu, Hawaii.

REID, R. O., AND A. C. VASTANO. 1966. Orthogonal coordinates for the analysis of long gravity waves near islands. Coastal Eng. Spec. Conf. Santa Barbara, Calif., 1965. Am. Soc. Civ. Eng. Part I. p. 1–20.

REPETTI, W. C. 1946. Catalogue of Philippine earthquakes, 1589–1899. Bull. Seismol. Soc. Am. 36: 133–322.

RHINES, P. B. 1969a. Slow oscillations in an ocean of varying depth. Part I. Abrupt topography. J. Fluid Mech. 37: 161–189.

1969b. Slow oscillations in an ocean of varying depth. Part II. Islands and seamounts. J. Fluid Mech. 37: 191–205.

RICHTER, C. F. 1958. Elementary seismology. W. H. Freeman and Company, San Francisco, Calif. 768 p.

RIKITAKE, T., AND S. MURAUCHI. 1947. Tsunami in Tsubaki-Tomari Bay. Bull. Earthquake Res. Inst. 25: 21–25.

RINGWOOD, A. E. 1962. A model for the upper mantle. J. Geophys. Res. 67: 857–867.

RITSEMA, A. R., AND J. VELDKAMP. 1960. Fault plane mechanisms of southeast Asian earthquakes. Meded. Verhand. Koninklijk Nederlands Meteor. Inst. 76: 7 p.

ROBINSON, A. R. 1964. Continental shelf waves and the response of sea level to weather systems. J. Geophys. Res. 69: 367–368.

ROCKWELL, D. C. 1966. Theoretical free oscillations of the Great Lakes. Great Lakes Res. Div. Univ. Michigan, Ann Arbor, Mich. 15: 352–368.

RODRIGUEZ, A., J. S. STEINHART, AND T. ASADA. 1962. The San Agustin fault system of southern Peru. Bull. Seismol. Soc. Am. 52: 793–805.

ROMANOVA, N. N. 1970. The vertical propagation of short acoustic waves in the real atmosphere. Atmos. Oceanic Phys. 6: 134–145.

ROYER, T. C., AND R. O. REID. 1971. The detection of secondary tsunamis. Tellus 22: 136–142.

RUSSEL, J. S. 1844. Report of the committee on waves. Meet. Br. Assoc. Adv. Sci.

SANTO, T. 1969. Characteristics of seismicity in South America. Bull. Earthquake Res. Inst. 47: 635–672.

SATO, Y. 1955. Analysis of dispersed surface waves I and II. Bull. Earthquake Res. Inst. 33: 33–48, 34: 9–18.

SAVARENSKY, E. F., AND N. V. GOLUBEVA. 1969. Seismicity of continental Asia and the Sea of Okhotsk, 1953–1965, p. 134–139. *In* P. J. Hart [ed.] The earth's crust and upper mantle. Am. Geophys. Union Monogr. 13.

SCHEIDEGGER, A. E. 1964a. The tectonic stress and tectonic motion direction in Europe and western Asia as calculated from earthquake fault plane solutions. Bull. Seismol. Soc. Am. 54: 1519–1528.

1964b. On the possibility of the seismic detection of explosions from the signs of first onsets. Bull. Seismol. Soc. Am. 54: 1529–1535.

SCHOLTZ, C. H., L. R. SYKES, AND Y. P. AGGARWAL. 1973. Earthquake prediction: a physical basis. Science 181: 803–810.

SCOTT, R. H. 1883. Note on a series of barometrical disturbances which passed over Europe between the 27th and 31st of August, 1883. Proc. R. Soc. London, Ser. A, 36: 139–143.

SEKERZH-ZEN'KOVICH, S. YA. 1968. Diffraction of plane waves by a circular island. Atmos. Oceanic Phys. 4: 35–40.

SETO, W. W. 1971. Theory and problems of acoustics. Schaum's Outline Series. McGraw-Hill Inc., New York, N.Y. 195 p.

SHEPARD, F. P., G. A. MACDONALD, AND D. C. COX. 1946. Recent tsunami in the Hawaiian Islands. Geol. Soc. Am. Bull. 57: 1230.

1950. The tsunami of April 1, 1946. Bull. Scripps Inst. Oceanogr. 5: 391–528.

SHIMOZURU, D., AND T. AKIMA. 1952. Reflections on the tsunami of Dec. 21, 1946. Bull. Earthquake Res. Inst. 30: 223–230.

SHIRATORI, K. 1925. Notes on the destructive earthquake in Sagami Bay on the 1 September, 1923. Jpn. J. Astron. Geophys. 2: 178–192.

SHOJI, D. 1955. On the variations of daily mean sea level and the Kuroshio from 1954–1955. Proc. UNESCO Symp. Phys. Oceanogr., Tokyo. p. 130–136.

1961. On the variations of the daily mean sea levels along the Japanese islands. J. Oceanogr. Soc. Jpn. 17: 141–152.

SIEVERS, H. A., G. VILLEGAS, AND G. BARROS. 1963. The seismic sea wave of May 22, 1960 along the Chilean coast. Bull. Seismol. Soc. Am. 53: 1125–1190. (Transl. from Spanish by P. St. Amand)

SKJELBREIA, L. 1959. Gravity waves, Stokes' third order approximation, tables of functions. Univ. California Counc. Wave Res., Eng. Found. p. 1–337.

SKJELBREIA, L., AND J. HENDRICKSON. 1962. Fifth order gravity wave theory and tables of functions. Natl. Eng. Sci. Co.

SLATKIN, M. W. 1971. Long waves generated by ground motion. J. Fluid Mech. 48: 81–90.

SMITH, S. W. 1975. Progress in seismological instrumentation. Rev. Geophys. Space Phys. 13: 311–312.

SNODGRASS, F. E. 1958. Shore-based recorder of low-frequency ocean waves. Trans. Am. Geophys. Union 39: 109–120.

SNODGRASS, F. E., W. H. MUNK, AND G. R. MILLER. 1962. Long-period waves over California's continental borderland. Part I. Background spectra. J. Mar. Res. 20: 3–30.

SOKOLOWSKI, T., AND G. MILLER. 1970. Identification of source region from a single seismic record, p. 135–147. *In* W. M. Adams [ed.] Tsunamis in the Pacific Ocean. East West Center Press, Honolulu, Hawaii.

SOLOVIEV, S L. 1965a. Seismicity of Sakhalin. Bull. Earthquake Res. Inst. 43: 95–102.

1965b. The Urup earthquake and associated tsunami of 1963. Bull. Earthquake Res. Inst. 43: 103–109.

1970. Recurrence of tsunamis in the Pacific, p. 149–163. *In* W. M. Adams [ed.] Tsunamis in the Pacific Ocean. East West Center Press, Honolulu, Hawaii.

1971. A report on scientific investigations upon the tsunami problem in the USSR 1967–1970. Acad. Sci. USSR. Inter-Dep. Counc. Seismol. Earthquake Eng. Comm. Tsunami. 7 p.

SOLOVIEV, S. L., A. V. NEKRASOV, V. G. BUKHTEEV, AND R. V. PYASKOVSKY. 1976. Materials for preliminary tsunami. Zonation of Kurile Kamchatka coast based on hydrodynamical calculations. Proc. IUGG Symp. tsunamis and tsunami Res., Jan. 29–Feb. 1, 1974, Wellington, N.Z. R. Soc. N.Z. Bull. 15: 29–38.

SOMMERFELD, A. 1896. Théorie mathematique de la diffraction. Math. Ann. 47: 317–374.

1949. Partial differential equations in physics. Pure Appl. Math. 1: 335 p.

SPAETH, M. G., AND S. C. BERKMAN. 1967. The tsunami of March 28, 1964 as recorded at tide stations. Coastal Geod. Surv. Tech. Bull. 33: 86 p.

SPIELVOGEL, L. Q. 1976. Run-up of single waves on a sloping beach. Proc. IUGG Symp. tsunamis and tsunami Res., Jan. 29–Feb. 1, 1974, Wellington, N.Z. R. Soc. N.Z. Bull. 15: 113–119.

SRETENSKIY, L. 1941. Concerning waves on the surface of a viscous fluid. Tr. Tsentr. Aèrol. Gidrodinam 541: 1–34. (In Russian)

SRETENSKIY, L. N., AND A. S. STAVROSKIY. 1961. Computation of height of tsunami waves along the coast. Trans. Mar. Hydrol. Inst. Acad. Sci. USSR 24: 23–43.

STAUDER, W. 1962. The focal mechanism of earthquakes, p. 1–76. *In* H. E. Landsberg and J. Van Meighem [ed.] Advances in geophysics. Academic Press, Inc., New York, N.Y.

STEINBRUGGE, K. V., AND W. K. CLOUD. 1962. Epicentral intensities and damage in Hebgen Lake, Montana, earthquake of August 17, 1959. Bull. Seismol. Soc. Am. 52: 181–234.

STEVENS, A. E. 1964. Earthquake mechanism determination by S-wave data. Bull. Seismol. Soc. Am. 54: 457–474.

1967. S-wave earthquake mechanism equations. Bull. Seismol. Soc. Am. 57: 99–112.

STOKER, J. J. 1957. Water waves: the mathematical theory with applications. Pure Appl. Math. Intersci. 567 p.

STOKES, G. G. 1846. Report on recent researches in hydrodynamics. Br. Assoc. Rep. 1846: 167 p.

1847. On the theory of oscillatory waves. Trans. Cambridge Philos. Soc. 8: 441.

STONELEY, R. 1963. The propagation of tsunamis. J. R. Astron. Soc. Can. 8: 64–81.

STRACHEY, R. 1883. A note on barometrical disturbances. Proc. R. Soc. London 36: 139–151.

STREET, R. L., R. K. C. CHAN, AND J. E. FROMM. 1970. The numerical simulation of long water waves: Progress on two fronts, p. 453–473. *In* W. M. Adams [ed.] Tsunamis in the Pacific Ocean. East West Center Press, Honolulu, Hawaii.

SU, C. L. 1973. Asymptotic solutions of resonances in harbors with connected basins. J. Waterways, Harbors Coastal Eng. Div. Proc. Am. Soc. Civ. Eng. 99: 375–392.

1975. Resonances in harbors with variable depths. Symposium on modeling techniques. 2nd. Annu. Symp. Waterways, Harbors Coastal Eng. Div. San Francisco, Calif. Am. Soc. Civ. Eng. 3: 803–815.

SUMMERFIELD, W. C. 1969. On the trapping of wave energy by bottom topography. Flinders Univ., South Australia, Horace Lamb Cent. Oceanogr. Res., Res. Pap. 30: 214 p.

1972. Circular islands as resonators of long-wave energy. Philos. Trans. R. Soc. London Ser. A, 272: 361–402.

SUN, T. 1959. On a wave guide of surface gravity waves. Izv. Sib. Otd. Akad. Nauk SSSR 5: 20–25. (In Russian)

SUTTON, G. H., W. G. MCDONALD, D. D. PRENTISS, AND S. N. THANOS. 1965. Ocean-bottom seismic observatories. Proc. Inst. Electr. Eng. 53: 1909–1921.

SUZUKI, Z. 1970. The tsunami accompanying the Tokachi-Oki earthquake, 1968, p. 85–97. *In* W. M. Adams [ed.] Tsunamis in the Pacific Ocean. East West Center Press, Honolulu, Hawaii.

SUZUKI, Z., AND K. NAKAMURA. 1953. On the heights of the tsunami on March 4, 1952 in the district near Erimo-Misaki. Sci. Rep. Tohoku Univ. Ser. 5, 4: 139-143.

SUZUKI, Z., K. NORITOMI, J. OSSAKA, AND A. TAKAGI. 1953. On the tsunami in Sanriku district accompanying the Tokachi earthquake, March, 4, 1952. Sci. Rep. Tohoku Univ. Ser. 5, 4: 134-139.

SVERDRUP, H. U., M. W. JOHNSON, AND R. H. FLEMING. 1942. The oceans, their physics, chemistry and general biology. Prentice-Hall, Inc., Englewood Cliffs, N.J. 1087 p.

SYKES, L. R. 1969. Seismicity of the mid-oceanic ridge system, p. 148-153. *In* P. J. Hart [ed.] The earth's crust and upper mantle. Am. Geophys. Union Monogr. 13.

1970. Seismicity of Indian Ocean and a possible Nascent Island arc between Ceylon and Australia. J. Geophys. Res. 75: 5041-5055.

1971. After-shock zones of great earthquakes, seismicity gaps, and earthquake predictions for Alaska and the Aleutians. J. Geophys. Res. 76: 8021-8041.

SYMONS, G. J. [ED.] 1888. The eruption of Krakatoa and subsequent phenomena. Triibner and Co., London. 494 p.

TABER, S. 1920. Jamaica earthquakes and the Bartlett trough. Bull. Seismol. Soc. Am. 10: 55-89.

TAIT, R. J. 1972. Wave set-up on coral reefs. J. Geophys. Res. 77: 2207-2211.

TAKAHASI, R. 1934. A model experiment on the mechanism of seismic sea wave generation. Part I. Bull. Earthquake Res. Inst. 12: 152-178.

1951. An estimate of future tsunami damage along the Pacific Coast of Japan. Bull. Earthquake Res. Inst. 29: 71-95.

1961. Report on the Chilean tsunami of 1960. Proc. 2nd World Conf. Earthquake Eng. p. 639-647.

1963. On some model experiments on tsunami generation, p. 235-247. *In* D. C. Cox [ed.] Proc. tsunami meetings associated 10th Pac. Sci. Congr., Honolulu, Hawaii. Union Geod. Geophys. Monogr. 24.

TAKAHASI, R., AND T. HATORI. 1961. On the tsunami which accompanied the Hiuganada earthquake of Feb. 27, 1961. Bull. Earthquake Res. Inst. 39: 561-577.

TAKAHASI, R., K. HIRANO, I. AIDA, T. HATORI, AND S. SHIMIZU. 1961. Observations at Miyagi-Enoshima tsunami observatory during the IGY period. Bull. Earthquake Res. Inst. 39: 491-521.

TALANDIER, J. 1966. Contribution to tsunami forecasting. C. R. Acad. Sci., Paris 263: 940-942. (Transl. from French by H. Bureau)

TERADA, T. 1934. Luminous phenomena accompanying destructive sea-waves (tsunami). Bull. Earthquake Res. Inst. 1: 26-35.

TERAZAWA, K. 1915. On deep-sea water waves caused by a local disturbance on or beneath the surface. Proc. R. Soc. London Ser. A, 92: 57-81.

1917. On the oscillations of the deep-sea surface caused by a local disturbance. Sci. Rep. Tohoku Imp. Univ. 6: 169-181.

THIRLAWAY, H. 1968. Seismic methods for monitoring underground explosions. Stockholm Int. Place Res. Inst. Rep.

THORADE, H. 1931. Probleme der wasserwellen. Probleme der Kosmischen Physik. Hamburg 13-14: 219 p.

TOLSTOY, I. 1967. Long period gravity waves in the atmosphere. J. Geophys. Res. 72: 4605-4622.

TOLSTOY, I., AND M. EWING. 1950. The T-phase of shallow-focus earthquakes. Bull. Seismol. Soc. Am. 40: 25-51.

TOLSTOY, I., AND T. J. HERRON. 1970. Atmospheric surface gravity waves from nuclear explosions. J. Atmos. Sci. 27: 55-61.

TOLSTOY, I., AND P. PAN. 1970. Simplified atmospheric models and the properties of long-period internal and surface gravity waves. J. Atmos. Sci. 27: 31-50.

TRUBY, J. D. 1971. Krakatoa, the killer wave. Frontiers 17: 130-139.

TRYGGVASSON, E. 1970. Surface deformation and fault displacement associated with earthquake swarm in Iceland. J. Geophys. Res. 75: 4407-4422.

UENO, T. 1965. Numerical computations for the Chilean earthquake tsunami. Oceanogr. Mag. 17: 87-94.

UNITED STATES COAST AND GEODETIC SURVEY. 1965. Tsunami travel-time charts for use in the seismic sea wave warning system. U.S. Dep. Comm. 32 charts.

UNITED STATES NATIONAL OCEAN SURVEY. 1971. Tsunami travel-time charts for use in the seismic sea wave warning system. U.S. Dep. Com. 50 charts.

UNNA, P. J. H. 1942. Waves and tidal streams. Nature 149: 219.

UNOKI, S., AND M. NAKANO. 1953a. On the Cauchy-Poisson waves caused by the eruption of a submarine volcano. Part I. Oceanogr. Mag. Biol. Annu. Rev. 4: 119-141.

1953b. On the Cauchy-Poisson waves caused by the eruption of a submarine volcano. Part II. Oceanogr. Mag. Biol. Annu. Rev. 5: 1-13.

URSELL, F. 1951. Trapping modes in the theory of surface waves. Proc. Cambridge Philos. Soc. 47: 347-358.

1952. Edge waves on a sloping beach. Proc. R. Soc. London Ser. A, 214: 79-97.

1953. The long wave paradox in the theory of gravity waves. Proc. Cambridge Philos. Soc. 49: 685-694.

UTSU, T., AND A. SEKI. 1955. Relation between the area of aftershock region and the energy of main shock. Zisin, Ser. 2: 233-250. (In Japanese)

VAN DORN, W. G. 1960a. A new long-period wave recorder. J. Geophys. Res. 65: 1007-1012.

1960b. A low-frequency microbarograph. J. Geophys. Res. 65: 3693-3698.

1961. Some characteristics of surface gravity waves in the sea produced by nuclear explosions. J. Geophys. Res. 66: 3845-3862.

1963. The source motion of the tsunami of March 9, 1957 as deduced from wave measurements at Wake Island, p. 39–48. *In* D. C. Cox [ed.] Proc. tsunami meetings associated 10th Pac. Sci. Congr., Honolulu, Hawaii. Union Geod. Geophys. Monogr. 24.

1964. Source mechanism of the tsunami of March 28, 1964, in Alaska. Proc. 9th Conf. Coastal Eng., Lisbon. p. 166–190.

1966. Theoretical and experimental study of wave enhancement and run-up on uniformly sloping impermeable beaches. Scripps Inst. Oceanogr., Univ. California, Berkeley, S10-66-11: 101.

1968a. Tsunamis. Contemp. Phys. 9: 145–164.

1968b. Tsunamis on the moon. Nature 220: 1102–1107.

1970a. A model experiment on the generation of the tsunami of March 28, 1964, in Alaska, p. 33–45. *In* W. M. Adams [ed.] Tsunamis in the Pacific Ocean. East West Center Press, Honolulu, Hawaii.

1970b. Tsunami response at Wake Island: a model study. J. Mar. Res. 28: 336–344.

VASTANO, A. C., AND E. N. BERNARD. 1973. Transient long-wave response for a multiple-island system. J. Phys. Oceanogr. 3: 406–417.

VASTANO, A. C., AND R. O. REID. 1966. A numerical study of the tsunami response at an island. Texas A and M Univ. Proj. 471 Ref. 66-26T: 129–139.

1967. Tsunami response for islands: verification of a numerical procedure. J. Mar. Res. 25: 129–139.

VERBEEK, A. D. M. 1884. The Krakatoa eruption. Nature 30: 10–15.

VITOUSEK, M., AND G. MILLER. 1970. An instrumentation system for measuring tsunamis in the deep ocean, p. 239–252. *In* W. M. Adams [ed.] Tsunamis in the Pacific Ocean. East West Center Press, Honolulu, Hawaii.

VITOUSEK, M. J. 1963a. The tsunami of 22 May, 1960 in French Polynesia. Bull. Seismol. Soc. Am. 53: 1229–1236.

1963b. Proposed mid-ocean tsunami gauge and oceanography instrument system, p. 131–133. *In* D. C. Cox [ed.] Proc. tsunami meetings associated 10th Pac. Sci. Congr., Honolulu, Hawaii. Union Geod. Geophys. Monogr. 24.

VOGEL, K. A. 1970. A horizontal pendulum station with tilt compensation. Obs. R. Belg. Comm. Ser. A, 101: 285.

VON HAKE, C. A., AND W. K. CLOUD. 1965. United States earthquakes – 1963. U.S. Coast Geod. Surv. p. 46.

1966. United States earthquakes – 1964. U.S. Coast Geod. Surv. p. 68–72.

1968. United States earthquakes – 1966. U.S. Coast Geod. Surv. p. 72–73.

VON KÁRMÁN, T. 1940. The engineer grapples with non-linear problems. Bull. Am. Math. Soc. 46: 615.

VVEDENSKAYA, A. V. 1958. Displacement in the surface of a fracture accompanied by slip. Am. Geophys. Union. p. 102.

1959. The displacement field associated with discontinuities in an elastic medium. Am. Geophys. Union p. 357.

WADA, A. 1965. On a method of solution of diffraction problems. Coastal Eng. Jpn., Jpn. Soc. Civ. Eng. 8: 1–19.

WALKER, J. T. 1884. Earthquake disturbances of the tides on the coasts of India. Nature 29: 358–360.

WARD, P. L., AND S. BJÖRNSSON. 1971. Microearthquakes, swarms, and the geothermal areas of Iceland. J. Geophys. Res. 76: 3953–3981.

WATANABE, H. 1956. Studies on the tsunamis on the Pacific coast of northern Japan. Geophys. Mag. 27: 61–75.

1970. Statistical studies of tsunami sources and tsunamigenic earthquakes occurring in and near Japan, p. 99–117. *In* W. M. Adams [ed.] Tsunamis in the Pacific Ocean. East West Center Press, Honolulu, Hawaii.

WEBB, H. D., AND F. B. DANIELS. 1964. Ionospheric oscillations following a nuclear explosion. J. Geophys. Res. 69: 545–546.

WEBSTER, D. L. 1963. The mathematics of tsunamis at small islands, p. 249. *In* D. C. Cox [ed.] Proc. tsunami meetings associated 10th Pac. Sci. Congr., Honolulu, Hawaii. Union Geod. Geophys. Monogr. 24.

WEBSTER, D. L., AND B. PERRY. 1966. Amplification of tsunamis by oceanic islands. Hawaii Inst. Geophys. Rep. HIG-66-11. Issued as Stanford Univ. Tech. Rep. 67.

WEGENER, A. L. 1928. The theory of continental drift. Symp. on the origin and movement of land masses both inter-continental and intracontinental. Bull. Am. Assoc. Pet. Geol. 240 p.

WEICHERT, D. H. 1970. The general purpose digital processing system for seismic data in Ottawa. Obs. R. Belg. Comm. Ser. A. 101: 297.

WEINER, F. 1947. Sound diffraction by rigid spheres and circular cylinders. J. Acoust. Soc. Am. 19: 444–451.

WELCH, J. E., F. H. HARLOW, J. P. SHANNON, AND B. J. DALY. 1966. The MAC method, a computing technique for solving viscous, incompressible, transient fluid-flow problems involving free surfaces. Univ. California Los Alamos Sci. Lab., Rep. LA-3425: 144 p.

WESTON, V. H., AND D. B. VANHULSTEYN. 1962. The effects of winds on the gravity waves. Can. J. Phys. 40: 797–804.

WHALIN, R. W. 1965. Water waves produced by underwater explosions: propagation theory for regions near the explosion. J. Geophys. Res. 70: 5541–5549.

WHITCOMB, J. H., J. D. GARMANY, AND D. L. ANDERSON. 1973. Earthquake prediction: variation of seismic velocities before the San Francisco earthquake. Science 180: 632–635.

WHITHAM, G. B. 1961. A note on group velocity. J. Fluid Mech. 9: 347–352.

1962. Mass, momentum and energy flux in waterwaves. J. Fluid Mech. 12: 135–147.

1974. Linear and nonlinear waves. John Wiley and Sons, Inc., New York, N.Y. 636 p.

WICKERSHAM, A. F., JR. 1966. Identification of acoustic-gravity wave modes from ionospheric range-time observations. J. Geophys. Res. 71: 4551-4555.

WIEGEL, R. L. 1954. Laboratory studies of gravity waves generated by the movement of a submerged body. Trans. Am. Geophys. Union 36: 759-774.

1955. Laboratory studies of gravity waves generated by the movement of a submerged body. Trans. Am. Geophys. Union 36: 759-774.

1960. Transmission of waves past a rigid vertical thin barrier. J. Waterways, Harbors Coastal Eng. Div., Proc. Am. Soc. Civ. Eng. 86: 1-12.

1963a. Memorandum to members. Hilo Tsunami Advisory Council. Univ. Calif. Berkeley, Publ. Eng.

1963b. Research related to tsunamis performed at the hydraulic laboratory, University of California, Berkeley, p. 174-197. *In* D. C. Cox [ed.] Proc. tsunami meetings associated 10th Pac. Sci. Congr. Honolulu, Hawaii. Union Geod. Geophys. Monogr. 24.

1964. Oceanographical engineering. Prentice-Hall Inc., Englewood Cliffs, N.J. 532 p.

WIEGEL, R. L., AND D. CAMOTIM. 1962. Model study of oscillations of Hebgen Lake. Bull. Seismol. Soc. Am. 52: 273-277.

WIEGEL, R. L., E. K. NODA, E. M. KUBA, D. M. GEE, AND G. F. TORNBERG. 1970. Water waves generated by landslides in reservoirs. J. Waterways, Harbors Coastal Eng. Div., Proc. Am. Soc. Civ. Eng. 96: 307-333.

WILLIAMS, J. A., AND J. M. JORDAAN JR. 1970. A laboratory model of a double-humped wave impingent on a plane sloping beach, p. 367-376. *In* W. M. Adams [ed.] Tsunamis in the Pacific Ocean. East West Center Press, Honolulu, Hawaii.

WILLIAMS, J. A., AND R. KARTHA. 1966. Model studies of long wave amplification by circular islands and submarine seamounts. Univ. Hawaii, Inst. Geophys. Rep. HIG-66-19: 46 p.

1969. Model study of long wave amplification by circular islands. Bull. Seismol. Soc. Am. 59: 299-316.

WILLIAMS, W. E. 1964. Note on the scattering of long waves in a rotating system. J. Fluid Mech. 20: 115-119.

WILLIS, B. 1928. Earthquakes in the Holy Land. Bull. Seismol. Soc. Am. 18: 73-103.

WILLMORE, P. L. 1970. The IGS-thermionic portable seismic system. Obs. R. Belg. Comm. Ser. A, 101: 286.

WILSON, B. W. 1962. The nature of tsunamis. Natl. Eng. Sci. Co., Tech. Rep. SN-57-2. (Abstract)

1971. Tsunami-responses of San Pedro Bay and Shelf, California. J. Waterways, Harbors Coastal Eng. Div., Proc. Am. Soc. Civ. Eng. 97: 239-258.

1972. Seiches. Adv. Hydrosci. 8: 1-94.

WILSON, B. W., AND A. TØRUM. 1968. The tsunami of the Alaskan earthquake, 1964: engineering evaluation. U.S. Army Corps. Eng. Coastal Eng. Res. Cent. Tech. Memo 25: 401 p.

WILSON, J. T. 1969. Earthquake. Coliers's Encyclopedia 8: 486-489.

WONG, K. K., A. T. IPPEN, AND D. R. F. HARLEMAN. 1963. Interaction of tsunamis with oceanic islands on submarine topographies. Mass. Inst. Tech. Hydrodyn. Lab. Rep. 62, R63-47.

WOOLARD, G. P. 1969. Tectonic activity in North America as indicated by earthquakes, p. 125-133. *In* P. J. Hart [ed.] The earth's crust and upper mantle. Am. Geophys. Union.

WORZEL, J. L., AND M. EWING. 1948. Explosive sounds in shallow water, p. 1-53. *In* Propagation of sound in the ocean. Geol. Soc. Am. Mem. 27.

WRIGHT, C. W. 1909. The world's most cruel earthquake. Natl. Geogr. Mag. 20: 373-396.

YEH, K. C., AND C. H. LIU. 1972. Propagation and application of waves in the ionosphere. Rev. Geophys. Space Phys. 10: 631-709.

YIH, C. S. 1953. On tides in estuaries and around small islands. Trans. Am. Geophys. Union 34: 389-393.

YOSHIDA, K. 1959. A hypothesis on transmission of energy of tsunami waves. Rec. Oceanogr. Works Jpn., Sci. Counc. 5: 14-37.

1960. The oceanic waves of days' to months' periods. Rec. Oceanogr. Works Jpn., Sci. Counc. 5: 11-24.

YOSHIDA, K., K. KAJIURA, AND H. MIYOSHI. 1953. On the tsunamis of March 4, 1952. Tokyo Univ., Geophys. Inst. Notes 6: 99-104.

YUEN, P. C., P. F. WEAVER, R. K. SUZUKI, AND A. S. FURUMOTO. 1969. Continuous traveling coupling between seismic waves and the ionosphere evident in May, 1968, Japan earthquake data. J. Geophys. Res. 74: 2256-2264.

YUMURA, T. 1961. List of tsunamis which accompanied distant earthquakes. Jpn. Met. Agency Tech. Rep. 8: 247 p. (In Japanese)

ZERBE, W. 1953. The tsunami of November 4, 1952 as recorded at tidal stations. U.S. Coast Geod. Surv. Spec. Publ. 300: 62 p

ZETLER, B. D. 1947. Travel times of seismic sea waves to Honolulu. Pac. Sci. 1: 185-188.

APPENDIX A SEISMOLOGY

A.1 Structure of the Earth and the new Global Tectonics

The shallow and deep structures of the earth are outlined and the new global tectonics, which have revolutionized thinking in many branches of geology, is discussed.

STRUCTURE OF THE EARTH

The outermost shell of the earth is called the crust and is thin compared to earth's radius (Fig. A.1, not drawn to scale). The crust has a thickness of only 4.8-8.0 km under the oceans, 19.3-90.1 km under the continents, and an average thickness of about 32.2 km (Wilson 1969). Next is the mantle, composed of magnesium and iron silicates. The boundary between the crust and the mantle is called the Mohorovicic discontinuity (presently referred to as Moho or simply M). The outer core and the inner core, respectively, consist of molten iron and iron plus nickel. The boundary between the lower mantle and the outer core is called the Gutenberg-Weichert discontinuity.

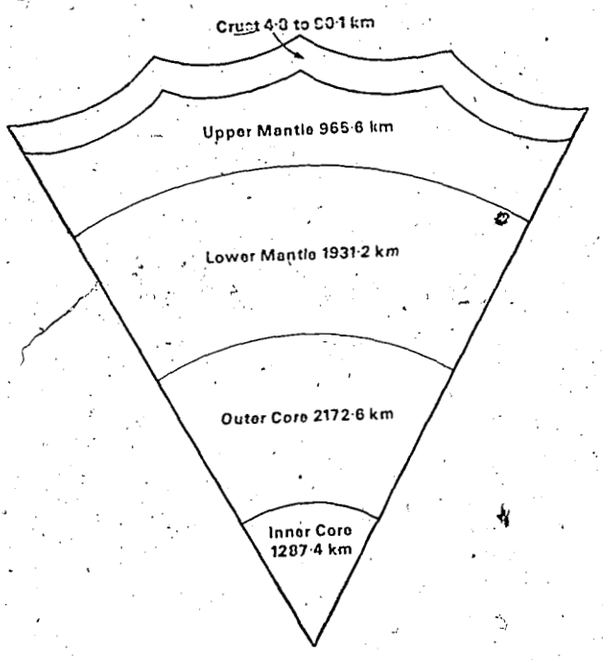


Fig. A.1. Structure of the earth.

The earth's crust is divided into two layers: (1) sial consists of silica and aluminum, usually occurs as granite, and forms the continental crust; (2) sima consists of silica and magnesium, occurs as basalt, and forms the oceanic crust mainly. However, this may underlie parts of the continental crust also. Recent studies indicate that in certain transitional regions of the earth's crust, the oceanic crust is slowly being converted into the continental crust, or vice versa.

Mohorovicic was the first to infer the existence of the crust when he prepared travel-time curves for the Oct. 8, 1909, Kulpa Valley (Croatic) earthquake in the Balkans. Later, other seismologists constructed similar travel-time curves for other earthquakes; to account for all the different phases, they postulated the existence of additional layers in the crust. There was considerable disagreement as to the exact number, but most seismologists felt there were at least two. As the velocity of seismic waves in the upper layer is similar to that in granite, it was called the granite layer, and the second was called the basaltic or intermediate layer. The boundary between the two was called the Conrad discontinuity. After World War II experiments with controlled energy sources greatly helped scientists to understand the structure of the earth. The term lithosphere is understood to comprise the crust and top portion of the mantle.

NEW GLOBAL TECTONICS

Isacks et al. (1968) introduced the term "New Global Tectonics" (NGT) to refer in a general manner to current concepts of large-scale tectonic movements within the earth, based on the concepts of continental drift, seafloor spreading, transform faults, and underthrusting of the lithosphere at island arcs. A brief summary of the developments that led to the concept of NGT is in order here. The idea of continental drift, originally proposed by Wegener (1928), did not gain acceptance until recently, mainly because no satisfactory mechanism was proposed to explain the movement of the continents through the oceanic crust and upper mantle without a great change in form.

New data from the fields of marine geology and geophysics made possible the proposal that the seafloor is spreading at the ocean ridges, and that new crust is being created there while older crust is disappearing into the mantle at trenches in the oceans. Convection in the earth's mantle is thought to be the driving mechanism for this. The hypothesis of seafloor spreading has gained great acceptance because it satisfactorily explains observations on the topography of the ocean floor, distribution and configuration of continental margins and other land patterns, patterns of deepsea sediments, and magnetic anomalies in the ocean.

Isacks et al. (1968) distinguished three regions: the strong top layer is the lithosphere and includes the crust and upper portion of the mantle and is 100 km thick on the average. In the middle, the asthenosphere extends from the bottom of the lithosphere to a depth of several hundred km; on the appropriate time scale this layer has no strength. The bottom layer, the mesosphere may have some strength and

is the inner portion of the mantle. Current thinking is that the mesoscale is probably not involved in tectonic processes.

In the context of seismology, the lithosphere and mesosphere do not significantly attenuate seismic waves which have relatively high velocities through these layers, whereas the asthenosphere corresponds more or less to the low velocity layer for seismic waves and causes strong attenuation.

Figure A.2 shows the world-wide distribution of all earthquake epicenters for 1961-67, concentrated in narrow belts, more or less continuous. If global tectonics can be modeled by the interaction of a few large plates of lithosphere, this model can account for most of the world's seismic activity as effects at or near the edges of the plates. The distribution shows that earthquakes occur much more frequently in zones of convergence (arcs and arclike features) than in the zones of divergence (ocean ridges). Along the ridges, where the less complicated processes of tectonics apparently occur, the zones are narrow; on the continents, where the processes are apparently more complex, the zones are broad.

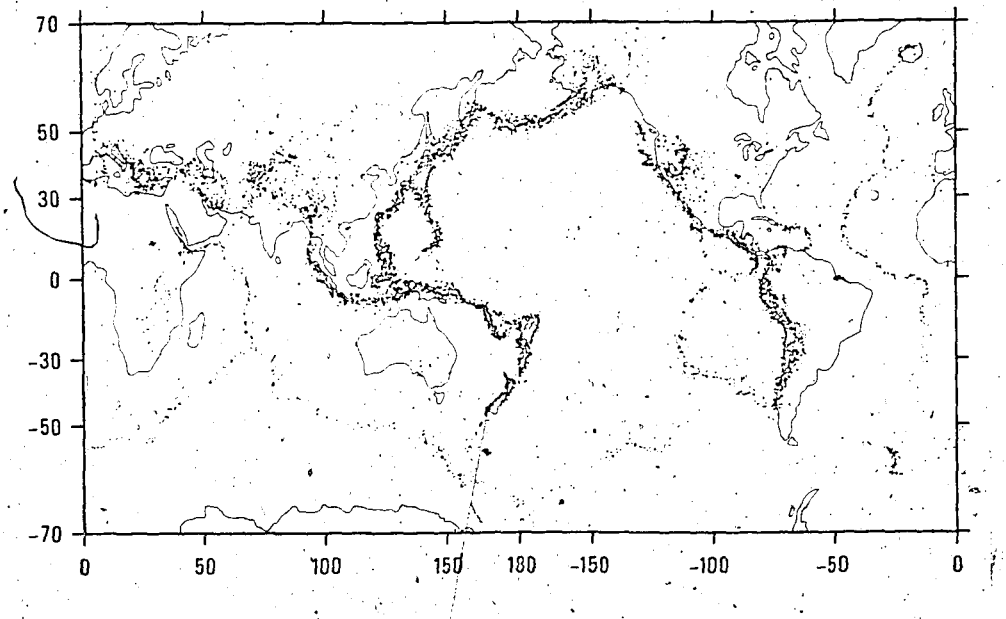


Fig. A.2, Worldwide distribution of earthquake epicenters 1961-67, by U.S. Coast and Geodetic Survey. Continuous narrow, major seismic belts outline aseismic blocks; very narrow, sometimes steplike pattern of belts of only moderate activity along zones of spreading; broader very active belts along zones of convergence; diffuse pattern of moderate activity in certain continental zones. (Isacks et al. 1968)

It is not intended to give the feeling that the global tectonics can account for all the observations. For example, the patterns of minor seismicity, including an occasional large earthquake in certain continental areas such as the St. Lawrence Valley and the Rocky Mountains, and broad regional scattering of epicenters as in East Africa are not explained as yet, nor is the almost complete lack of earthquakes in the oceanic lithosphere, which presumably can and does transmit stress over large distances.

A.2 Seismic waves and concepts of intensity and magnitude

As the earth's material is elastic, the waves associated with earthquakes can be understood in terms of the concepts of the theory of elasticity. The discussion here follows the arguments of Richter (1958), Byerly (1942), Bullen (1963), Jacobs et al. (1959), and Hodgson (1964).

BODY WAVES: P AND S WAVES

The concepts of stress and strain are fundamental to the theory of elasticity, hence, to the theory of seismic waves. Stress at any point in a body is the force acting on unit area of the body, whereas strain is the resulting deformation. It can be shown that (see Richter 1958) in an ideal, elastic, homogeneous isotropic medium of infinite extent, there are only two possible plane waves, referred to as the P (primary) and S (secondary) waves. The velocity of propagation of these given by:

$$C_P = \sqrt{\frac{L_F + 2L_S}{\rho}} \qquad (A.1)$$

$$C_S = \sqrt{\frac{L_S}{\rho}} \qquad (A.2)$$

where ρ is the average density of the medium and L_F and L_S are the first and second Lamé constants. The constant, L_S, expresses the resistance of an elastic solid to shearing stress and is called the modulus of rigidity. The other Lamé constant, L_F, is related to the Bulk modulus B_m and L_S through

$$L_F = B_m - \frac{2}{3} L_S \qquad (A.3)$$

The P wave is a compressional-rarefactional wave and is longitudinal and irrotational. It is called primary wave because it is the first to be recorded at seismograph stations following an earthquake. The

secondary wave, unlike the P-wave, is a vector wave. It is a transverse wave and the deformation is of a shear type. Waves of the S-type can exist only in solids. The ratio of the speed of propagation of the P-wave to that of the S-wave is approximately $\sqrt{3}$. If boundaries and discontinuities are introduced into the medium, then other types of wave motion are possible.

SURFACE WAVES - RAYLEIGH AND LOVE WAVES

Rayleigh (1914) showed theoretically that a special type of elastic wave that propagates along the earth's surface or along the surfaces of a bounded elastic solid could exist. He started with a simple model where the earth's curvature effects were ignored, the wave front was plane, an infinite train of sinusidal waves propagated along a flat surface, and the amplitude of the displacement decreased exponentially with depth. He showed that the speed of propagation depends on the Poisson's ratio, P_r, given by:

$$P_r = \frac{L_F}{2(L_F+L_S)} \qquad (A.4)$$

These waves have no transverse vibration and the displacements are purely vertical and in the propagation direction.

Although waves of the type described by Rayleigh were actually recorded on the seismograms, they showed transverse motion also. This means Rayleigh waves are not the only possible surface waves, but other types of surface waves that allow transverse motion must occur. Love (1892) developed the theory for these and found waves (now referred to as Love waves) that have only transverse components (without any longitudinal or vertical components); these were the first of the general group of guided waves discovered.

For Poisson's ratio $P_r = \frac{1}{4}$, the speed of the Rayleigh wave is 0.9194 that of the S-wave along the earth's surface. For the Rayleigh wave (R-wave), the planes of wave propagation and particle oscillation are the same. The motion is retrograde and decays exponentially with depth. The horizontal part of the motion becomes zero at a depth of 0.192 of the wavelength. The sign of the vertical motion is the same at all depths. Love waves have no vertical component, but only have transverse motion.

DISPERSION, REFLECTION, AND REFRACTION OF SEISMIC WAVES

The dependence of the velocity of propagation on wavelength is called phase dispersion (see Chapter 1). Body waves P and S suffer extremely small phase dispersion, and for all practical purposes can be treated as nondispersive. On the other hand, surface waves exhibit strong dispersive properties. This is quite significant, and one has to understand the dispersive characteristics of the surface waves to interpret

seismograms properly. Although the R-wave that emerges from the ideal theory should be nondispersive, in practice it suffers dispersion because the elastic properties of the earth change with depth.

When a body wave of either the P- or S-type strikes an interface between two elastic layers, in general, reflected or refracted P or S waves could develop. Subject to the possibility that in particular cases some resulting waves may be excluded, either by total reflection or by the nature of the incident wave, it is possible for the incident wave to become four different types of waves. However, if a P-wave is incident normal to a discontinuity, it cannot introduce any component of shear normal to the boundary and cannot be transformed into an S-wave. Similarly, if the plane of vibration of the S-waves is parallel to the plane of the boundary, it cannot introduce any dilatation component at the boundary because there is no motion normal to the boundary.

EARTHQUAKE INTENSITY

"Intensity" is one way to grade the strength of an earthquake by observing the earthquake effects. De Rossi of Italy and Forel of Switzerland proposed one of the earliest intensity scales in 1883, now referred to as the Rossi-Forel scale and abbreviated as RF. This concept can be used to express earthquake intensity at any given point on the globe using a 10-point scale (see Richter 1958, p. 650).

With subsequent growth of science and technology, the RF scale became outdated. Also, it was more relevant to European countries, and its maximum scale, X, encompassed a large range of intensity.

In 1902, Mercalli proposed an improved scale based on 10 grades and later, on a suggestion by Cancani, he changed this to a 12-grade scale. Wood and Neumann modified this scale in 1931 and referred to this as the Modified-Mercalli (MM) scale. Two forms of the MM scale appear in the literature: a complete version and an abridged version (Richter 1958).

In spite of the elaborate descriptions involved in these intensity scales, their use is somewhat limited. Hodgson (1964, p. 57) stated:

> "... The description 'many frightened' does not mean very much; a shock which would alarm the residents of Toronto or Cleveland would pass unnoticed in Tokyo. The damage to buildings varies so much with soil conditions, and to some extent with the standard of 'good' building in the particular country involved that the intercomparison of earthquakes in different countries obviously does not mean very much. But, when the scale is applied uniformly over an area to describe the effects of a single earthquake, it has a good deal of value. Usually, in such cases it is possible to contour the intensity map. The contours on such maps - seismologists call them isoseismals - usually enclose the epicenter and their irregularities serve to point up areas of poor soil or of poor building ..."

Other intensity scales are the Japan Meteorological Agency (JMA) scale and the Medvedev, Sponheuer, and Karnik (MSK) scale. For specific purposes special scales were also designed. For example, Blume (1970) devised an engineering e intensity scale.

EARTHQUAKE MAGNITUDE

The concept of earthquake magnitude developed from the necessity to measure any earthquake in an absolute sense, rather than describe it based simply on human experience. This can be done by instruments called seismographs that measure and record the ground motion (see Chapter 6). Some readers might wonder whether two different concepts are needed to describe an earthquake. Richter (1958, p. 354) pointed out that it has been said that the double use of magnitude and intensity is confusing, and seismologists should stick to one; this is like saying that a police description of a thief is confusing because it gives both his height and weight.

Suppose that around the epicenter of an earthquake there is a network of identical seismographs, not necessarily distributed uniformly. Records of ground motion because of the earthquake need not be identical at all stations, the closer stations may record a larger amplitude than farther stations. Amplitudes of the ground motion can be plotted against the distance of the stations from the epicenter, and a curve fitted to the series of points. A similar plot could be made for another earthquake with its epicenter somewhere in the center of this group of stations. A difference in the levels of the two curves represents the difference between the absolute sizes of the two earthquakes. However, a basic curve is needed to which other curves, due to different earthquakes, can be referred. To obtain this reference curve, imagine a zero earthquake (Hodgson 1964), the smallest earthquake that could be recorded in the area under consideration. The average height of the curve for a given earthquake above this zero curve is called the magnitude, M, of the earthquake and is represented by:

$$M = \log A - \log A_0 \qquad (A.5)$$

where A and A_0 are, respectively, the amplitudes (or average heights) of the curves for the particular earthquake and the zero earthquake.

The necessity for the logarithm of the amplitude came about as follows. Wadati (quoted by Richter 1958) plotted the amplitude of ground motion versus epicentral distance. The curves for different earthquakes were approximately parallel, and the bigger the earthquake, the higher the position of the curve in the plot. In 1931, Richter made similar plots for southern California earthquakes, but was forced to use logarithms of the amplitudes rather than the amplitudes themselves because of the wide range in the recorded amplitudes. It is evident that if the zero curve is once established so it is truly representative of the decrease in energy with increasing distance, then to determine the magnitude of an earthquake, no further plots are necessary. If the logarithm of the zero earthquake is subtracted from the logarithm of the amplitude record (at a given seismograph station), then

the earthquake can be said to have that magnitude at that station.

The development of this concept of magnitude and the so-called Richter scale (named after C. F. Richter) was a fundamental breakthrough in seismology, and, for the first time, provided an accurate scale to express the absolute size of an earthquake. Richter originally constructed the scale for near earthquakes, i.e. for short epicentral distances. Richter and Gutenberg extended the scale to distant earthquakes also. They used the same principle, namely the amplitude of the largest movement of the record. For distant earthquakes, the largest movement on the record is associated with surface waves. However, deep-focus earthquakes do not generate surface waves; hence, another scale is necessary. There are three scales, one for near earthquakes, a second for distant shallow earthquakes, and a third for deep-focus earthquakes.

Richter (1958) gave the following relations between the magnitudes m and M derived from body and surface waves respectively:

$$m = 2.5 + 0.63\ M$$
$$M = 1.59\ m - 3.97 \qquad \text{(A.6)}$$

The two values agree at $m = M = 6.75$. Above this value, magnitude determined from surface waves is larger than that derived from body waves and the opposite result holds below this value.

ENERGY

Hodgson (1964) gave the following relation between magnitude, M, and energy, E, (in ergs) released by an earthquake:

$$\log E = 11.4 + 1.5\ M \qquad \text{(A.7)}$$

Although in principle, it would be better to derive the magnitude from the energy released, in practice this is not done. Instead, the energy is calculated from relations identical or similar to (A.7). Gutenberg and Richter (quoted by Bullen 1963) gave the following relation between E and M:

$$aM = \log_{10} \frac{E}{E_0} \qquad \text{(A.8)}$$

with $a = 1.5$ and $E_0 = 2.5 \times 10^{11}$ ergs. This formula gives an energy increase of 30 times per-unit-increase of M.

FREQUENCIES

Gutenberg and Richter (quoted by Bullen 1963) gave the following empirical relation for the frequencies of earthquakes of different magnitudes:

$$\log_e N = A - BM \qquad (A.9)$$

Here N is the average number of earthquakes per year with magnitudes between M and M + 0.1. For shallow earthquakes, the values for the coefficients A and B were: for $M > 7.3$, $A = 8.2$, $B = 1.1$; for M between 5.8 and 7.3, $A = 4.6$, $B = 0.6$. The authors estimated that the number of earthquakes per year strong enough to be felt is of the order of 10^5, and the total number that could be recorded by instruments is of the order of 10^6, and that the total energy released in all earthquakes annually is of the order of 10^{25} ergs. About 80% of the energy is due to earthquakes with $M \geq 7.9$. Richter stated (1958, p. 367):

> "... Although the frequency of earthquakes increases rapidly with decreasing magnitude, the energy released in the individual shocks, computed by any of the formulas in the preceding subsection, decreases yet more rapidly. In consequence, if the earthquakes of any given area, or of the world, are examined for a limited time interval, it is generally found that the release of energy takes place principally in the relatively few shocks of largest magnitude. This has a practical bearing on the popular idea that small earthquakes may operate as a 'safety valve' to release harmlessly the energy which might otherwise express itself in a large earthquake.
>
> "Strictly on an energy basis, such reassurance is doubtful, and it does not fit very well with the history of large and small earthquakes in areas where information is adequate. The energy relations suggest that major strains are released only in major earthquakes, and that minor earthquakes are rather incidental indications of the accumulation of regional strain.
>
> "Benioff points out that if strains are compared directly, instead of by way of the energy, this no longer necessarily holds. The strains are taken as proportionate to the square roots of the energies; if these quantities are then combined linearly, the total contribution from smaller shocks is often of the same order as that of the comparatively few large shocks."

BASIS FOR CLASSIFICATION OF EARTHQUAKES

The basis for classification of earthquakes into shallow, intermediate, and deep (given earlier) was explained by Jacobs et al. (1959, p. 36):

> "... When the total annual increment in energy of strain release for earthquakes occurring within certain levels is plotted, it is found that graphs of strain release against time plotted for a series of different depths fall into three groups. For each group of shallow, intermediate, and deep earthquakes, the curves have a characteristic pattern showing that, although they may be subject to the same stresses, the three levels react independently but within each level earthquakes all over the world are closely con-

nected with one another. This relationship confirms the division of earthquakes into shallow, intermediate and deep groups, which had already been devised on the basis of distribution ..."

Gutenberg and Richter (quoted by Bullen 1963) stated that 12% of earthquake energy released annually comes from intermediate earthquakes, 3% from deep earthquakes, and the rest from shallow earthquakes. The frequency appears to decrease rapidly with increasing focal depth in the intermediate range. In the deep-focus levels, the frequency distribution with depth is fairly uniform until the greatest focal depths of about 700 km are approached. The circumpacific belt almost entirely accounts for the deep earthquakes.

FORESHOCKS, AFTERSHOCKS, AND EARTHQUAKE SWARMS

On the basis of observational data, Page (1968) concluded that well-defined aftershocks occur only at shallow depths not exceeding 20 km, i.e. in the earth's crust. The sequence of aftershocks exhibits two important properties: the frequency of aftershocks decays in time according to an inverse power law with an exponent of about 1.1; and distribution with respect to magnitude is according to the following relation: $n(m) = a - b \cdot m$. Here $n(m)$ is the number of shocks with magnitudes between m and $m + dm$, and a and b constants.

Utsu and Seki (1955) gave the following relation between the area, S, of aftershocks and the magnitude, M, of the principal shock: $\log_{10} S = cM + d$. These authors gave the following values for the nondimensional constants, c and d:

$c = 0.9$	$d = 6.8$ (for submarine earthquakes)
$c = 0.85$	$d = 6.95$ (for land earthquakes)
$c = 1.0$	$d = 6.0$ (for land and submarine earthquakes)

A.3 Epicenter Determination and Travel-Time Curves

The books of Richter (1958), Hodgson (1964), Bullen (1963), and Jacobs et al. (1959) were followed in this section. A fundamental problem in seismology is the location of the epicenter of an earthquake. The P-waves travel faster than S-waves and as a consequence, become more separated with increasing distance. Suppose the travel-time of the P and S waves is related by curves to the distance traveled. Then, knowing the separation in time between the P and S waves at a given seismographic station, the distance of the epicenter of the earthquake from the station can be calculated. The next question is how to obtain these so-called travel-time curves.

Suppose a particular earthquake was recorded at a number of seismograph stations around the epicenter. Based on the observed damage or some other descriptive parameter, an epicentral position could be assumed temporarily and the distances of each station from this assumed epicenter could be determined. Travel-times to each station could be computed by propagation velocities for P and S waves, and compared with observed travel-times. Then by trial, the best epicentral position that would give calculated travel-times that agree closely with

the observed travel-times could be determined. By repeating this procedure with several earthquakes, an average set of travel-time curves can be obtained. Over the last several decades several authors have constructed such curves, and Fig. A.3 shows one such set.

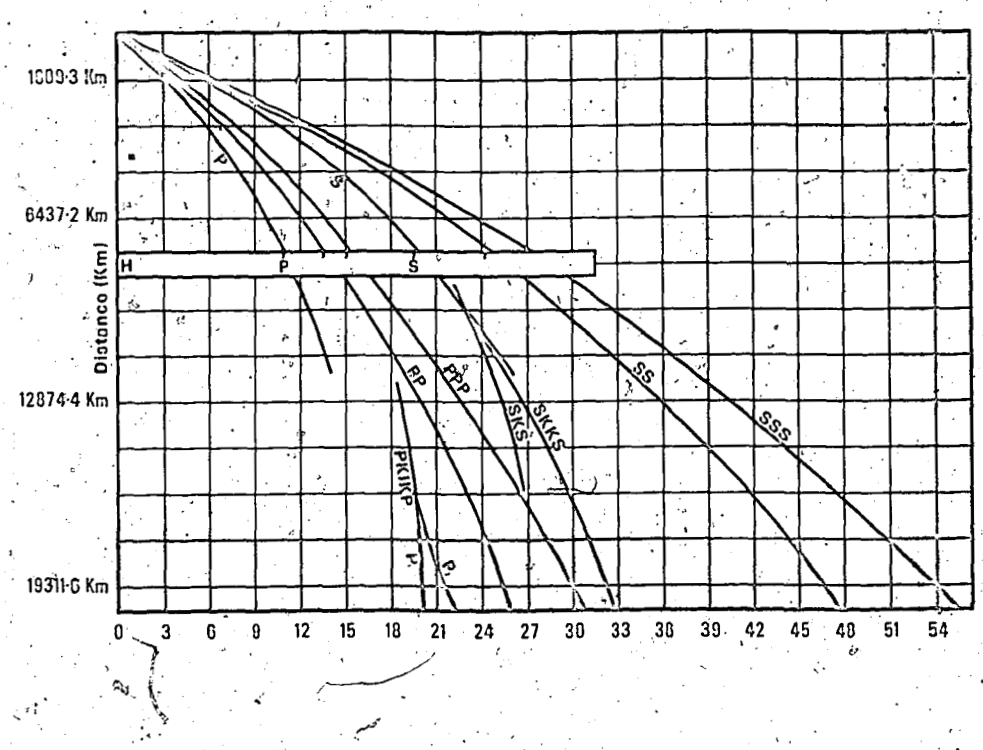


Fig. A.3. Modern travel-time curves, showing how they may be used to determine the distance and origin time of an earthquake (after Jeffrup and Bullen). (Hodgson 1964)

In Section A.1, the shallow structure of the earth was discussed briefly and the concept of the Moho discontinuity introduced. However, for greater distances simple travel-time curves based on travel through the earth's crust are not sufficient, because the waves penetrate deeper and deeper into the earth. Curves shown in Fig. A.3 should be used. Actually these curves are not completely smooth but are made up of different segments because velocity of the waves changes with depth. To account for the inhomogeneous nature of the earth, one might at the outset assume that the earth consists of two layers, that allow a given seismic wave to travel with a velocity V_1 in top layer and V_2 in the bottom layer, and let $V_2 > V_1$. Also, make the hypothetical assumption that there are seismograph stations spaced at equal distances. The energy released by the earthquake in the form of waves travels to nearby stations by the direct path, and, as the stations are assumed to be at equal intervals of distance, the waves take equal time intervals to travel between the stations. For a distant station from the earthquake the direct path need not be the path of fastest travel although it is the shortest route, because the wave may take less time by traveling with the high-velocity, V_2, in the

bottom layer after being refracted at the boundary of the two layers, than it loses by traveling down to the bottom layer and up again. There will be a distance, Δ, when the time taken by the direct as well as the refracted rays will be the same (Hodgson 1964):

$$\Delta = 2d\sqrt{\frac{v_2 + v_1}{v_2 - v_1}}$$

where d is the thickness of the top layer.

In reality there are more than two layers, hence, with increasing distance of the station, the first phase to reach the station might be one that traveled through a third layer and the travel-time curve will have a third segment. As there are many layers in the earth, the travel-time curves have different segments and together they may still look like a smooth curve. In the above discussion it is assumed that the velocity of seismic waves increases with increasing depth. Although this statement is somewhat an oversimplification (Hodgson 1964), nevertheless, it is true for depths as far as the rays penetrate.

The significance of the qualified statement "as far as the rays penetrate" can be understood in Fig. A.3. The travel-time curves for P and S waves stop abruptly at distances of 11,745.7 and 11,906.6 km, respectively, and a station even slightly farther away would not receive these initial waves. Gutenberg explained this was due to a central core in the earth at a depth of 2896.2 km, which acts as a spherical lens and refracts the rays, and more or less blocks the passage of seismic waves, creating a shadow zone.

However, better seismographs developed later showed the presence of weak and delayed P-waves, but not of S-waves in the shadow zone. This was explained by postulating an inner core that could reflect the waves back into the shadow zone. Thus, broadly speaking, the earth has a thin crust, a thick mantle (where both P and S wave velocities increase generally with increasing depth), an outer core, and an inner core.

One important difference between solids and liquids is that solids, because of their finite rigidity, can support shear stresses, but fluids cannot. The core of the earth must be a fluid because shear waves (S waves) are not observed to travel through it.

Oldham in 1900 was among the first to distinguish among P, S, and surface waves in actual seismograms (quoted by Jacobs et al. 1959). At a given station the initial indication of an earthquake is the sudden arrival of P-waves. Subsequently the S-waves arrive, with amplitudes usually larger than P-waves, and the surface waves (Rayleigh and Love waves) arrive even later. In travel-time curves it is customary to measure the distance along the surface of the earth in degrees. As would be expected, graphs for surface waves will be straight lines whereas those for P and S waves are curves with downward concavity.

The shadow zone for P and S waves starts at distances of 105° and ends at 142°. However, P-waves are found again in the range of 142-180°.

Following an earthquake, the seismogram at any station is complicated in appearance. In the early portion of the record, body waves that have traveled various routes are present, whereas the latter part shows surface waves. As the amplitude decay with distance is smaller for surface waves, except close to the epicenter, surface waves have larger amplitudes than body waves, generally speaking. However, for deep earthquakes the amplitudes of surface waves are very small.

Many phases other than the simple P, S, Rayleigh (L_r), and Love waves (L_q) are possible. In general, the amplitude of the P-wave may be much smaller than that of the S-wave at the focus (Bullen 1963). Then the S-wave may travel upward from the focus to epicenter and be reflected there, creating both P and S waves that might be recorded at a seismograph station. The P and S waves thus generated are called *s*P and *s*S. Similar arguments lead to *pp* and *ps* phases. If both P and *pp* (or S and *s*S) are recorded at a station then the difference in arrival times could be used to determine the focal depth accurately.

Waves emanating from the focus and reflected either at the earth's surface or at some discontinuous surface in the crust could cause a different set of phases. For example, a P-wave could create PP or PS, and an S-wave create SS or SP. These are due to single reflection. Two reflections could cause phases such as PPP, SSS, PPS, etc. A combination of these phases with those described above could become PPP, SPP, SPS, etc.

The next set of phases is due to upward reflection (denoted by *c*) at the mantle-outer core boundary, and phases such as P*c*P, P*c*S, S*c*S, and S*c*P can easily be visualized. Bullen (1963, p. 168) mentioned that a phase such as S*c*SP would correspond to reflection into the P type, at (or near) the outer surface of a wave that had, before reflection, approached the outer surface as S*c*S. Phases such as *p*S*c*S are also significant, the symbol *p* corresponds as before to an initial ascent to the outer surface in the P type.

Another type of phase (denoted by K) is due to penetration of the P-wave into the core. Thus, phases such as PKP, PKS, etc., can easily be visualized. A phase such as PKKP results from an internal reflection at the core boundary. Some phases such as PKP have two branches, thus the travel-time curve is a two-valued function of the distance (Bullen 1963). Then subscript 2 is used to denote the upper branch (PKP_2 for the upper branch of PKP).

Further types of phases are due to existence of the inner core, with symbols *i* and I used for reflection at the outer core-inner boundary and for penetration into the inner core. Only the P-wave can travel inside the core. Bullen (1963, p. 170) stated that phases PKP, PK*i*KP, and PKIKP need to be discriminated; the first corresponds to a wave that has entered the outer and not reached the inner core, the second to one that has been reflected upward at the boundary between the two

portions, and the third to one that has penetrated into the inner portion. By combining *p*, *s*, P, S, *c*, K, *i*, I in various ways, notation for all the main phases associated with body waves can be written. The symbol J represents S-waves in the inner core.

Early surface waves with long periods of 1-4 min are the Love type, designated as L_q or G (named after Gutenberg). Instruments that measure the horizontal component will record the Rayleigh wave denoted by L_r. Both Rayleigh and Love waves suffer dispersion. The dispersion relations differ for oceanic and continental paths. The fastest Love and Rayleigh waves have velocities of the order of 4.5 and 4.2 km/s^{-1} respectively. An L_g phase is a short-period wave, guided in the continental crust. This can propagate over continental paths without much dissipation but cannot propagate through oceanic paths. The T phase is a seismic wave that propagates as a sound wave in the ocean paths.

EPICENTER DETERMINATION

In the nomenclature on epicenter determination, the symbol Δ denotes the distance of the epicenter to the station. Actually, Δ is the angle at the center of the earth between radii to the epicenter and the station. This parameter can be determined from knowledge of the geocentric latitude and longitude. On ordinary maps, the geodetic latitude is used, not the geocentric latitude. The geodetic latitude is the angle between the equatorial plane and the normal to the earth's spheroidal surface. The geocentric latitude, Ψ, is related to the geodetic latitude, ϕ, through the relation (Richter 1958):

$$\tan \psi = (1-f)^2 \tan \phi = 0.993277 \tan \phi \qquad \text{(A.10)}$$

where f is the flattening of the earth, which is 1/279.

Jeffreys (1952) described the following procedure for the determination of Δ. Let ϕ_0' and λ_0 be the geocentric latitude and longitude of the epicenter and ϕ' and λ those of the station. Then the following formula holds:

$$\cos \Delta = \sin \phi_0' \sin \phi' + \cos \phi_0' \cos \phi' \cos(\lambda-\lambda_0) \qquad \text{(A.11)}$$

However, when many stations are involved, this formula is rather cumbersome and Turner (quoted by Jeffreys 1952) gave the following procedure. With reference to a rectangular coordinate system at the center of the earth, with x pointing toward 0°N, 0°E, y toward 0°N, 90°E, and z toward 90°N, the direction cosines (A,B,C) of the epicenter and the direction cosines (a,b,c) of the station are:

$$(A,B,C) = (\cos \phi_0' \cos \lambda_0, \cos \phi_0' \sin \lambda_0, \sin \phi_0')$$

$$(a,b,c) = (\cos \phi' \cos \lambda, \cos \phi' \sin \lambda, \sin \phi') \qquad \text{(A.12)}$$

Then (A.11) becomes:

$$\cos \Delta = aA + bB + cC$$

Two formulas equivalent to A.12 that could be derived from geometrical considerations are:

$$2(1-\cos\Delta) = (A-a)^2 + (B-b)^2 + (C-c)^2$$
$$2(1+\cos\Delta) = (A+a)^2 + (B+b)^2 + (C+c)^2 \qquad (A.13)$$

The three formulas given by (A.12, A.13) can be used to check each other over the full range of $0 < \Delta < 180°$. Define, following Jeffreys:

$$D \equiv \tfrac{1}{2}(A^2 + B^2 + C^2 - 1)$$
$$d \equiv \tfrac{1}{2}(a^2 + b^2 + c^2 - 1)$$

Then it can be shown that:

$$Aa + Bb + Cc = D + d + 1 - \tfrac{1}{2}[(A-a)^2 + (B-b)^2 + (C-c)^2]$$
$$= -D - d - 1 + \tfrac{1}{2}[(A+a)^2 + (B+b)^2 + (C+c)^2]$$

With an epicenter, two orthogonal directions given by $(0, \lambda_0, -\frac{\pi}{2})$, and $(\phi_0', -\frac{\pi}{2}, \lambda_0)$ were associated within Turner's procedure, and the direction cosines of these were denoted by (D,E,O) and (G,H,K). Thus, the azimuths also can be found, noting that: $Da + Eb = -\sin\Delta\cdot\sin AZ$; $Ga + Hb + Kc = -\sin\Delta\cdot\cos AZ$.

GENERAL METHOD TO DETERMINE EPICENTER

If clock times are accurate at each station, then, from arrival times of the P-waves (as their propagation velocity is known), the distance of the epicenter from each station could be determined and using several stations, the position of the epicenter could be deduced. If clock times are not accurately known, the time difference between the arrivals of P and S waves at each station can be used. However, the difficulty with the second method is identifying the beginning of the S-phase, especially because the S-waves have a multiplicity.

For this reason, usually P-wave arrivals are used for accurate determination of the epicenter. To determine the depth of focus for deep-focus earthquakes, some phase that is reflected near the epicenter must be used. A few methods Byerly (1942) are described:

Geiger method - First, the time difference in arrival of S and P phases at several different stations and travel-time data from the appropriate tables are used to determine an approximate epicenter. This approximate epicenter is then located on a large terrestrial globe and its latitude and longitude are denoted as ϕ^* and λ^*. From this approximation, the distance to each station is subtracted from the arrival time of P at that station, and the difference gives the time of occurrence of the earthquake as computed for that particular station. In a similar manner, times of occurrence are computed at all

stations and their mean value t_0^* is the assumed time of occurrence.

With reference to this approximate epicenter and the assumed travel-time computed, let t_n^* be the computed arrival time at each station and t_n the corresponding observed arrival time. Let $F_n \equiv t_n - t_n^*$, and if F_n is small, one can write:

$$\begin{aligned} t_n &= t_n^* + F_n \\ &= t_n^* + \frac{\partial t_n^*}{\partial \lambda_0^*} d\lambda_0^* + \frac{\partial t_n^*}{\partial \phi_0^*} d\phi_0^* + \frac{\partial t_n^*}{\partial t_0^*} dt_0^* \end{aligned} \qquad \text{(A.14)}$$

Shift the epicenter slightly, compute the corresponding change in epicentral distance, and use the tables, then the change in travel-time of P phase is found and t_n^* is determined. Thus, at each station $\partial t_n^*/\partial \lambda_0^*$ and $\partial t_n^*/\partial \phi_0^*$ can be deduced. Then the set of equations (A.14) can be solved by least squares method. The correct position of the epicenter is given by the first two equations of:

$$\begin{aligned} \lambda_0 &= \lambda_0^* + d\lambda_0^* \\ \phi_0 &= \phi_0^* + d\phi_0^* \\ t_0 &= t_0^* + dt_0^* \end{aligned} \qquad \text{(A.15)}$$

and the third equation gives the correct time of occurrence.

Spherical trigonometry method - Let e be the colatitude of a station, S the colatitude of the epicenter, and p the polar angle between the meridians of the station and epicenter. Colatitude is equal to 90° ± latitude (- sign is used if south). Then:

$$\cos \Delta = \cos e \cdot \cos S + \sin e \cdot \sin S \cdot \cos p \qquad \text{(A.16)}$$

Let ϕ_0 be the latitude of the epicenter and E the bearing of the station at the epicenter, taken as a positive angle between 0° and 180°. Then the following relations are obtained:

$$\begin{aligned} \frac{\partial \Delta}{\partial \phi_0} &= -\cos E \\ \text{and} \qquad \qquad & \qquad \text{(A.17)} \\ \pm \frac{\partial \Delta}{\partial \lambda_0} \cdot \sin \Delta &= \frac{\partial \Delta}{\partial p} = \cos \phi_0 \sin E \end{aligned}$$

The sign of the term in the second equation of (A.17) depends on the relative longitudes of the station and the epicenter. The following three equations can be derived from (A.16, A.17) and used to determine Δ, E, and S, noting that geocentric latitudes should be used (Byerly 1942).

$$\log \tan \frac{E+S}{2} = \log \cot \frac{p}{2} + \log \cos \frac{e-S}{2} + \operatorname{colog} \cos \frac{e+S}{2}$$

$$\log \tan \frac{E-S}{2} = \log \cot \frac{p}{2} + \log \sin \frac{e-S}{2} + \operatorname{colog} \sin \frac{e+S}{2}$$

$$\log \tan \frac{\Delta}{2} = \log \sin \frac{E+S}{2} + \operatorname{colog} \sin \frac{E-S}{2} + \log \tan \frac{e-S}{2}$$

Straight-line method - For Δ in the range of 0-18°, and possibly to 20°, the P-wave travel-time curve is almost a straight line. Also, if the station is close to the epicenter, then for the phase $\bar{P}$ ($\bar{P}$ is a p wave traveling completely through the granite layer) the travel-time curve is a straight line for epicentral distances larger than the depth of focus. Then the travel-time curve could be represented by:

$$t = \frac{\Delta}{v} + I \qquad \text{(A.18)}$$

where v is the apparent surface speed and I is the time intercept of the branch of the curve. The epicenter and I should be determined under the condition that, for each station the following relation is satisfied:

$$t_n - \left(\frac{\Delta n}{v} + I\right) = 0$$

subscript n denotes the station.

The time difference in arrival times of the S and P waves (called the S-P intervals) is used to deduce approximate values for the epicenter, v, and I. Let the assumed epicenter have latitude and longitude ϕ_0^* and λ_0^*; let I* and v* be the assumed values of I and v, and let Δn^* be the distance of a given station to this assumed epicenter. To find corrections for these in the least squares sense, if the corrections are small, write (Jeffreys 1952):

$$(t_n - I^* - dI)\ (v^* + dv) - \frac{\partial \Delta}{\partial \phi_0} d\phi_0 - \frac{\partial \Delta}{\partial \lambda_0} d\lambda_0 = \Delta n^*.$$

To first order in small quantities, this becomes:

$$(t_n - I^*)\, dv - v^*\, dI - \frac{\partial \Delta}{\partial \phi_0} d\phi_0 - \frac{\partial \Delta}{\partial \lambda_0} d\lambda_0 = \Delta n^* - (t_n - I^*)\, v^*$$

An adequate number of equations are used to solve the four unknowns in this equation, namely dv, dI, $d\phi_0$ and $d\lambda_0$.

The station pair method - This method is of an approximate nature, but is worthy of attention. Suppose two stations receive P-waves at the same time. Then the epicenter must lie on a great circle joining the stations and is normal to it at the intersection. Of course, it is assumed that P-waves travel with the same speed in all directions, which is not strictly true because of inhomogeneities in the earth. If two such pairs of stations are found, then the epicenter must be at an intersection of the two great circles. More station pairs and other data such as S-P intervals will indicate which intersection is correct. As it is highly unlikely to find two stations at which P-waves arrive exactly at the same time, in practice the stations selected are those at which arrival times of P-waves are approximately the same.

Interval method - S-P intervals could be used to make a quick determination of the epicenter. In a tsunami prediction problem, this quick determination of the epicenter (even if it is not accurate) is highly desirable. The epicenter can be determined approximately by the S-P intervals from three stations. Byerly (1942) cautions that after the P and S phases are identified, one should check the interval between S and surface waves that arrive after the S-waves. However, a close check is not possible because surface waves exhibit a considerable scatter (a check within a few minutes is probably adequate). It is precisely because of this scatter that surface waves cannot be used in this interval method for epicenter determination.

If the check is not satisfactory, then it is probable that P and S waves are not properly identified. Byerly gave an example when the Berkeley seismograph records from earthquakes originating in India showed PP and SKS which looked like P and S from a closer epicenter. Thus, if the other phases such as PP and SKS can be correctly identified, the intervals of these phases also could be used for quick epicenter determination. In practice, most of the time the S-P interval is used.

Method of direction (Byerly 1942, p. 224) - P-waves are the first to arrive at a station and when they reach the surface they get reflected. Since the surface motion is determined from both the incident and reflected waves, the apparent angle of incidence at the surface (determined as the $\tan^{-1}$ of the ratio of the recorded horizontal amplitude to the vertical amplitude) does not provide the direction of approach of the wave as the horizontal amplitude lies in the great circle joining the station with the epicenter. Its direction can be determined by compounding as vectors the first P-wave amplitudes on the E-W and N-S component seismograms. After determining the great circle, the vertical component is examined. If the motion is upward, the first wave was compression and the horizontal motion was away from the epicenter. Thus, after the direction of the epicenter is obtained, the distance to the station can be computed from the S-P interval at the station, and the epicenter can be approximately located.

A.4. Earthquake Mechanism

Reid's elastic rebound theory was originally developed in connection with the San Francisco earthquake of 1906. In Fig. A.4, let 0' 0" represent a fault and A 0 B be a line normal to the fault (Hodgson 1964). This diagram is distorted because the vertical dimension is about 6.1 m, whereas the horizontal dimension is about 32.2 km. The line A 0 B gradually distorts itself into A' 0 B'. At the instant when the strength of the fault no longer exceeds the stresses set up, it will break and A' 0 suddenly assumes the position A' 0' and 0 B' becomes 0" B'. This sudden movement toward equilibrium relieves the strain and produces the earthquake, In reality, the fault does not break at a single point. In the San Francisco earthquake, the movement in the San Andreas fault occurred over 402 km (Hodgson 1964). In this situation the focus must be defined as the point at which the fault broke first.

However, Hodgson (1964) cautioned that the initial break may be minor, although this is infrequent, whereas the second break may be major. In such a situation, sensitive seismographs close to the earthquake might identify the first break as the focus, although distant seismographs might identify the major break as the focus. To understand what happens in the immediate vicinity of the focus, Fig. A.5 shows F as the focus, and 0' 0" as the fault. Any observers in quadrants A and B would feel an initial compression, whereas those in quadrants C and D would feel an initial dilatation (Hodgson 1964). Thus, in the vicinity of the epicenter there will be four quadrants which are alternately compressional and dilatational.

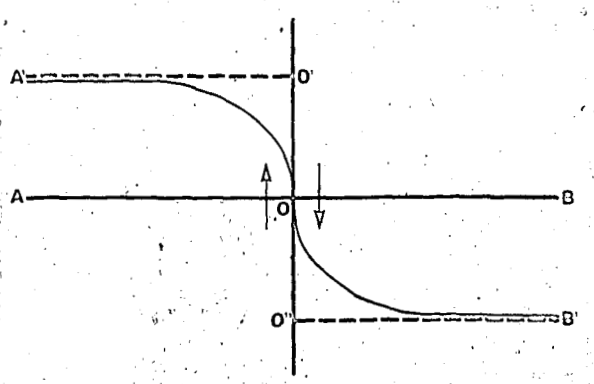


Fig. A.4. Reconstruction of the regional displacements preceding the San Fransisco earthquake and their release in the sliping of the fault. This reconstruction provides the basis for the elastic-rebound theory of earthquakes. (Hodgson 1964)

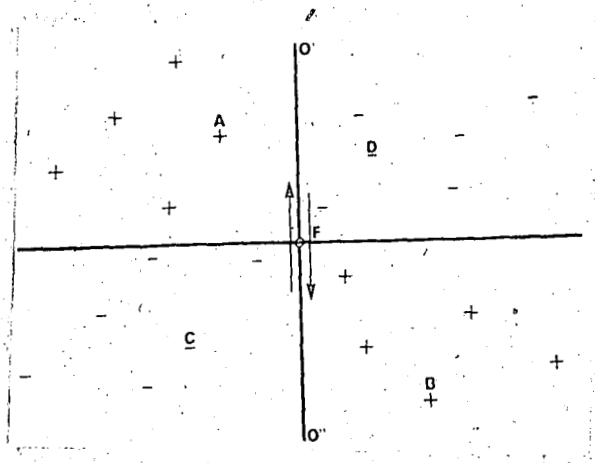


Fig. A.5. Separation of compressions from dilatations by the nodal planes. (Hodgson 1964)

The more interesting problem is the converse where knowing the initial motions at several points around the epicenter, one could separate the regions of compressions from those of dilatations by means of a pair of straight lines. One line is the trace of the fault. In nature, the situation is often much more complicated, because the faults are usually not vertical and the motion in the fault during the earthquake is not purely horizontal.

However, if the fault model of the earthquake mechanism is accepted, then the general model described by Hodgson and Stevens (1964) (a pair of orthogonal planes, i.e. fault plane and an auxiliary plane at right angles to it) can be adapted. Because the direction of motion changes as it passes through these planes, it must be zero on them. Hence, they are called nodal planes.

The important question is whether the fault model of the earthquake mechanism is general enough to be universally applicable to all earthquakes. Several major earthquakes have occurred that were not associated with any faulting. Richter (1958) appears to subscribe to the fault plane model of earthquakes and gives a table of earthquakes with known faulting. Adams and Furumoto (1970, p. 58) take an opposing view, because of what they consider to be a notable lack of direct evidence. Hodgson (1964) stated that stresses associated with an earthquake develop through a finite volume and not just across a plane. He noted that some seismologists think regional forces cause earthquakes, and that the fault, if it exists, is an effect and not a cause.

Byerly (quoted by Hodgson and Stevens 1964) first considered the problems in using observed data from world-wide distribution of stations, and tried to overcome the problem from the curvature of the seismic ray. A station to the right of the fault plane EF (Fig. A.6) receives its initial motion from a ray originating to the left of the fault. To maintain proper polarity, in Byerly's method the tangent for the ray is used, which locates the station at a virtual position S' instead of at the true position S.

The second problem concerned mapping. Byerly used the property that the fault plane and the auxiliary plane which meet the earth in circles will project as circles in stereographic projection. In Fig. A.7 the station, S, considered at the virtual position S', is plotted at B, O B is called the extended distance (Hodgson and Stevens 1964). That is, stations are plotted at their measured azimuth from the epicenter and at the extended distance corresponding to their distance from the epicenter. A diagram prepared by Stauder (1960) for an Alaskan earthquake separated compressions and dilatations by means of two circles drawn to represent orthogonal planes (Fig. A.8). Although such a diagram could be prepared with sufficient reliable data, Hodgson and Stevens (1964) estimated that because of background noise, weak first motion, and instrument defects, about 15% of the data was inaccurate and complicated construction of the circles, and the data were also insufficient.

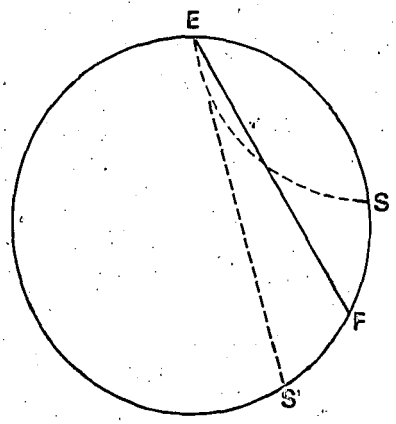


Fig. A.6. True position S of a station versus its virtual position S^1. (Hodgson and Stevens 1964)

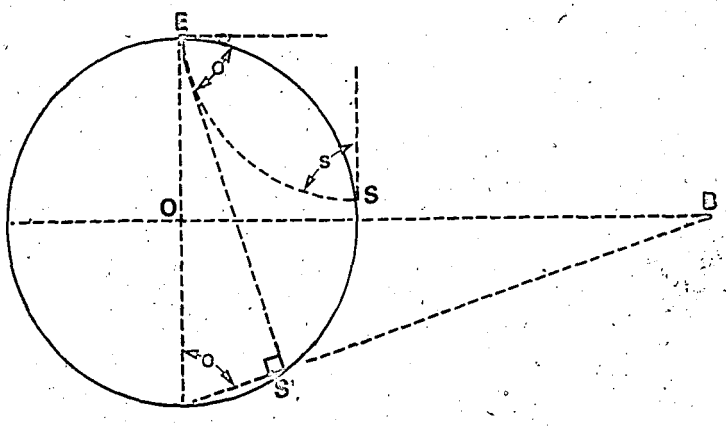


Fig. A.7. Geometry of the Byerly projection. (Hodgson and Stevens 1964)

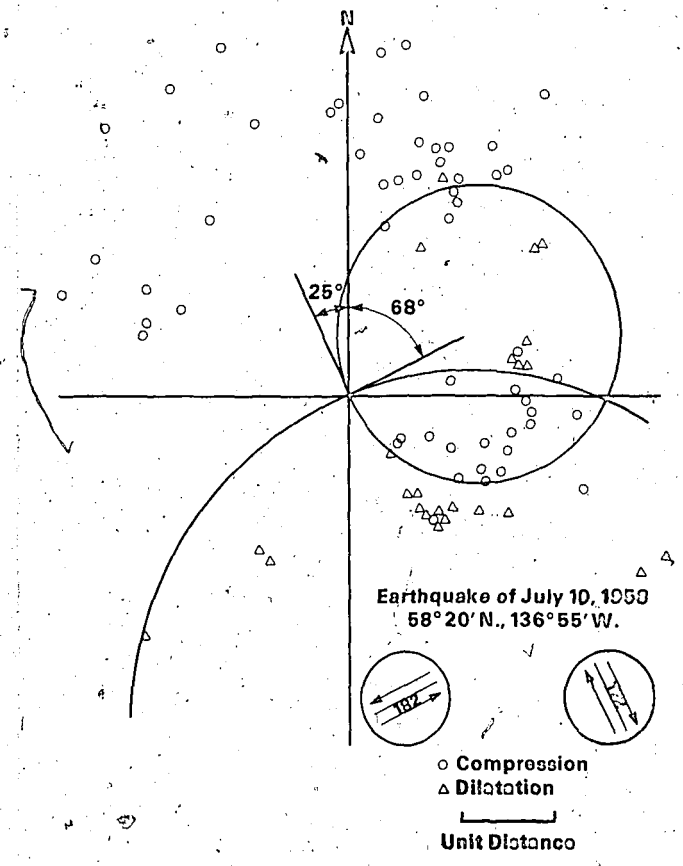


Fig. A.8. P nodal solution for the earthquake July 10, 1958. (Hodgson and Stevens 1964)

In contrast to Byerly's method, the focus can be surrounded with a unit sphere, called the focal sphere (Fig. A.9). As above, the tangent of the ray gives the virtual position S' for the station.

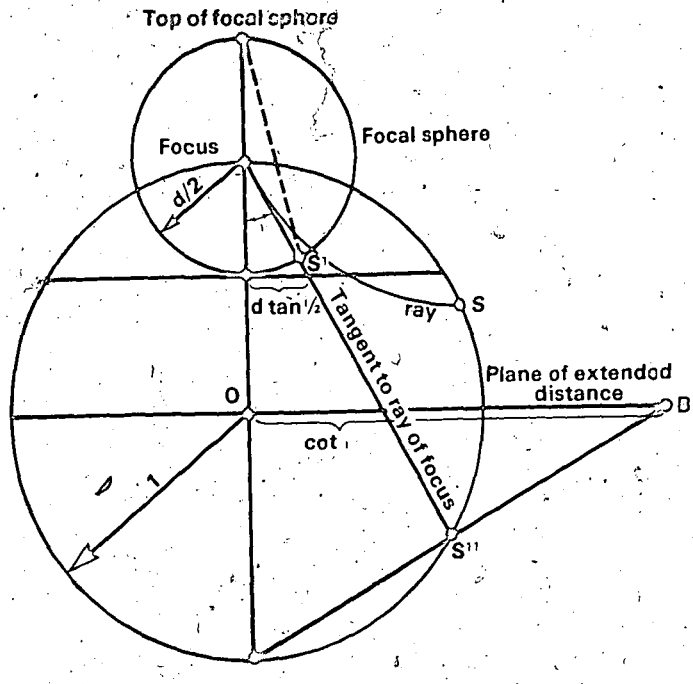


Fig. A.9. Diagram showing the various projections used in determining P nodal solutions. (Hodgson and Stevens 1964)

Figure A.10a shows the projection of the focal sphere as a Wulff projection, and Fig. A.10b shows it on a central projection. All projections react similarly to either incorrect data or lack of data. Hodgson and Stevens (1964) point out that these fault plane diagrams do not tell which plane represents the fault, and that many seismologists think they do not represent the fault at all.

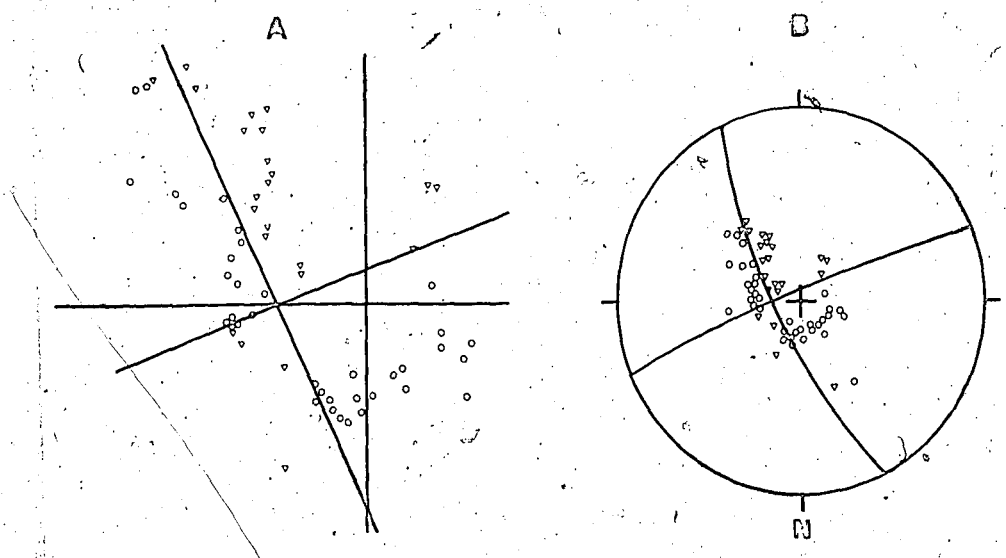


Fig. A.10. P nodal solution for the earthquake July 10, 1958, as it appears (a) in the Wulff projection and (b) in the central projection. (Stauder 1960)

In principle, the S-wave pattern could be used to resolve the question of which plane represents the fault. Figure A.11 shows the theoretically calculated radiation patterns for P and S waves resulting from a single couple shown on the left. Although the P-pattern offers no insight as to which line represents the fault, the S-pattern offers a clue, because the amplitude is zero on the plane of the fault and is maximum on a line at right angles to it.

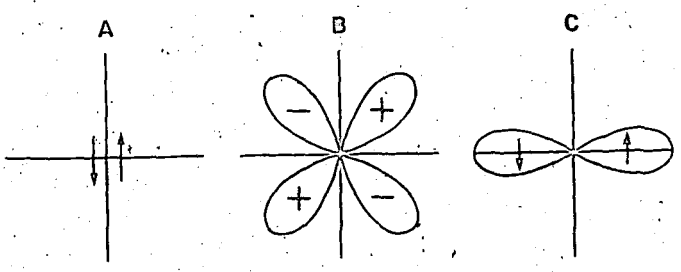


Fig. A.11. Theoretical radiation pattern for (b) P-waves and (c) S-waves from a single couple oriented as in (a). (Hodgson and Stevens 1964)

Honda (1961) was among the first to study the S-wave radiation patterns in detail. In particular, he examined 10 deep-focus earthquakes from data taken close to the epicenter. In the S-radiation pattern, he found maxima along each P-nodal plane; these two maxima could be accounted for by two couples acting along orthogonal directions, as shown in Fig. A.12. In seismological literature the models in Fig. A.11; A.12 were, respectively, called models I and II.

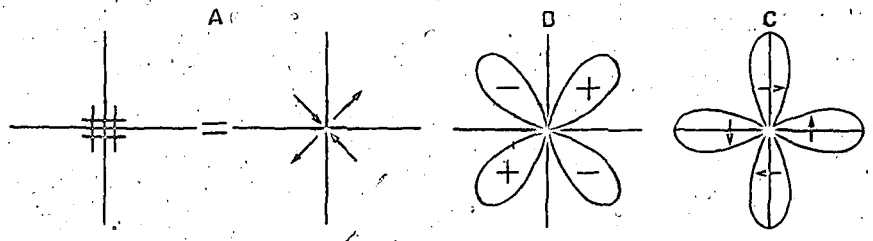


Fig. A.12. Theoretical radiation pattern for (b) P-waves and (c) S-waves from double couple or equal deviatoric stresses oriented as in (a). (Hodgson and Stevens 1964)

Model I was developed originally in connection with the San Francisco earthquake of 1906, and later applied to other earthquakes. Regarding model II, Hodgson and Stevens (1964, p. 37) pointed out that the stresses within the earth could be reduced to an orthogonal triad of principal stresses. For shallow earthquakes one of these is likely to be vertical and represent hydrostatic stress. Subtracting the

hydrostatic stress from the other two gives the so-called deviatoric stresses. These are closely analogous to the forces postulated in model II. Failure occurs by collapse of a volume of rock or by faulting on one or both of a pair of conjugate planes, and the impulsive release of stress sets up the seismic wave. This model has the attraction of being related to the regional stresses.

Hodgson and Stevens summarized briefly the important features of the theoretical models available until 1963 and raised some questions. The first was in connection with model II, where the deviatoric stresses are considered, instead of the three principal stresses at a point. They asked, "What was the justification for assuming that these deviatoric stresses are equal in magnitude?" They pointed to the work of Ingram (1961), who examined the situation when the three principal forces were unequal and concluded that quadrant distribution does not occur, and that the surfaces separating compressions from dilatations were not orthogonal planes but became cones.

They also noted that, as the energy released in an earthquake must have been stored in a volume, the concept of a point focus is unrealistic. As a result, several authors considered an ellipsoidal source and produced a quadrant pattern in P and a distorted (relative to model II) S-radiation pattern, the amount of distortion depends on the fault length. Hodgson and Stevens (1964) cited the work of Vvedenskaya (1958, 1959) who used the dislocation theory and showed that when a fault occurs the stresses relieved are those bearing on the fault at the moment of failure. Knopoff and Gilbert (1959, 1960) treated the earthquake as the result of the sudden disappearance of accumulated strain along a fault plane and took into account the finite propagation rate of faulting.

Knopoff and Gilbert compared their calculations with observations and showed that only three of the possible models are likely to be valid physically. They disregarded the other models because they do not produce the quadrant distribution of P. At this stage, the quadrant distribution of P has not been defined. Hodgson and Stevens (1964, p. 38) briefly summarized the three models arrived at by Knopoff and Gilbert as follows:

> "... the first corresponds to rigid body motion, dislocation or fault fling, the faulting proceeding in two directions from the focus. This produces a radiation pattern the same as model II, except that one of the P nodal planes represents the fault. The second mechanism corresponds to a sudden discontinuity in the shear strain between two sides of a fault. This produces a simple radiation pattern; instead of a quadrant distribution of P, there should be only two zones, one compressional and one dilatational."

The third mechanism is provided by the sudden release of shear strain in a laminar region. This produces a radiation pattern identical to that of model I. Of the P nodal planes, the one representing the orientation of the long axis of the laminar region is identified by the S-pattern.

Hodgson and Stevens stated that there have been four schools of thought on earthquake mechanism, broadly speaking - that of Japan, Holland (Netherlands), USSR, and followers of Byerly. In contrast to the techniques of the other three groups, in Japan only the data from nearby stations were mostly used so there was no necessity to employ any projection. Data on the compressions and dilatations of P were plotted simply on a map, and either arcs or straight lines were used to separate the compressions from dilatations. Then the S-amplitudes were looked at for various azimuths relating to the P nodal planes. Honda (1961) used this technique for 10 earthquakes to show that the S-radiation pattern corresponded to that of model II.

The other three schools also used data from distant stations. In the Soviet Union, data on the first motions of P, SH, and SV were plotted on a Wulff projection. Additional data on PP, SS, *pP*, *sS*, etc., have also been utilized. There appears to be a controversy in the Soviet Union on the validity of models I and II. The group directed by Keylis-Borok appears to favor model I, whereas Vvedenskaya favors model II. To summarize, the Soviet observations are based on the direction motion of S rather than the amplitude.

Stauder (1962) appears to be one of the few in the USA who has used techniques analogous to those in USSR. He made considerable use of the S-radiation patterns; instead of dealing with initial amplitudes or first motion, he plotted the particle motions. From these plots, the angle of polarization was measured at each station, plotted on a map projection, and compared with the patterns deduced from models I and II.

Some of his results supported model I, but others supported model II. Hodgson and Stevens mentioned that Ritsema and Veldkamp (1960) followed a procedure somewhat similar to that of Stauder, except they simplified the procedure by avoiding the particle motion diagram to obtain the polarization angles, and instead estimated them approximately from the reported data.

Adams (1958) derived a set of equations to calculate the direction of motion at the focus for model I, knowing the polarization angles of the S-radiation. Stevens (1964) extended Adam's method to include three unequal principal forces originally proposed by Ingram (1961). Hodgson and Stevens (1964) concluded that use of the particle motion diagrams, from which S-polarization angles could be determined, was the most satisfactory method to select the model. In fact, in a given area both models may be applicable. There has been considerable work on the use of surface waves (Rayleigh and Love waves) instead of body waves P and S, for mechanism studies.

Hodgson and Stevens discussed available earthquake mechanism solutions and their reliability. Some theoretical models call for a quadrant distribution of compressions and dilatations whereas others do not. The resulting confusion was summarized by Hodgson and Stevens (1964, p. 49). If a quadrant distribution is typical, interpretation is considerably simplified. There are only two possibilities: one

of the two nodal planes represents the fault, or the bisector of the dilatational quadrant represents the direction of maximum pressure. Either model might apply to a particular region. But at present many reliable P-solutions exist without any corresponding S-data. To plot the strikes and dips or the directions of displacement would be to assume that a fault exists; to plot the directions of pressure would seem to assume it does not.

Hodgson and Stevens (1964) pointed out that probably the direction of the principal pressure determined from the fault model and the pressure model would agree closely. They used the following formula after Lensen (1961) which relates the angle, α, between the fault strike and the principal horizontal stress, to the components, DH and DV, of the displacement in the direction of the strike and in the vertical direction:

$$\tan 2\alpha = \frac{DH}{DV} \qquad (A.19)$$

In a given nodal diagram, two possibilities for the fault exist. If one is selected as the fault, then the other is the auxillary plane; this enables the computation of DH and DV, then α, and finally the direction of the principal horizontal stress. According to the fault interpretation, this is the direction and as there are two possible faults, there are two possible directions for the pressure. Hodgson and Stevens computed α for the good computer solutions available for some earthquakes and compared these directions with those obtained by bisecting the dilatational quadrant, following Honda (1961) or Vvedenskaya (1958, 1959). They agreed with each other closely (the difference amounted to an rms value of less than 10°).

Hodgson and Stevens then plotted a series of maps showing the direction of pressure determined from the Honda-Vvedenskaya method and referred to these directions as "pressure directions," with the understanding that they represent the best determinations in an average sense under either interpretation (fault or no fault). The differences in patterns among the Kamchatka, Kurils, Japan, and the islands south of Japan, can be interpreted in terms of differences in faulting as follows: thrust-faulting is mainly responsible for Kamchatkan earthquakes, whereas slip-faulting is predominant in Kurils and Japan, and normal faulting occurs in the islands south of Japan. Hodgson and Stevens pointed out that the earthquakes of the oceanic systems are too small to yield any solutions.

MATHEMATICAL MODELS

There is controversy as to the relative validities of models I and II and to resolve this problem, S-radiation data are being used in addition to P-data. Stauder (1962) contends that the use of S-radiation data depends on a fuller use of the theory of point sources and he found the work of Keylis-Borok and Kagan (1957) particularly relevant in this context.

The point source is of course not a good representation of a focus. Instead, for use in fault-plane solutions one needs a model for the focus, so that the calculated distribution of amplitudes and first motions of P and S waves from this model agree with those caused by an earthquake. This is the so called "principle of equivalence." Keylis-Borok (1956) treated the movement at the source as inelastic. He avoided the issue of the form of movement in the immediate vicinity of the focus by assuming that the elastic waves are generated either by body forces acting in a small volume surrounding the focus, or by small mass movement of rock in this volume.

Consider a plane within an elastic body and assume that a cut is made over a finite area of the plane. Let an applied force displace the two faces of the cut relative to each other and later let the two faces be brought back together. Volterra (see Stauder, 1962) described the resulting deformation as the simplest case of a dislocation. This concept is particularly useful in defining the static displacement field set up in an elastic body. Instantaneous displacement because of a moving dislocation is studied by Nabarro (1951).

Stauder concluded that the fault plane method is quite successful in predicting the first motion of P, so the quadrant distribution must be correct. However, instead of a unilateral faulting, Knopoff and Gilbert (1959, 1960) assumed a bilateral faulting, when the fault propagated in two opposite directions from the focus.

The use of surface waves for focal mechanism studies is a significant advance. Brune (1961) suggested that an azimuthal variation in the ratio of the amplitudes of Love and Rayleigh waves can be used to determine the orientation of a fault. Sato's (1955) method can be applied for focal mechanism studies even when considerations of stationary phase do not apply. In this method, the record is subjected to Fourier analysis, and a correction is applied for the phase factor of each component for the delay involved in propagation. From these component waves, the source function is determined.

Aki's (1960a, b, c) method has an important difference from that of Sato. Whereas, Sato obtains the source function from the component waves, Aki computes the impulse response of the medium and then determines the source function by cross-correlation with the seismogram.

A completely different approach has been suggested by Ingram (1959). As the focal mechanism studies involved graphical methods of separating a given displacement field consisting of compressions and rare-fractions, this problem may be solved by statistical methods to determine orientation of the straight lines that give the best separation of compressions from rare-factions. Following Ingram's suggestion, Knopoff (1961) developed mathematical techniques reported there and in later papers (see various issues of Bulletin of the Seismological Society of America subsequent to that work).

Randall (1964a) introduced new concepts and techniques in earthquake mechanism studies by a better use of the elastic wave concepts. In a sense he deviated from earlier studies, in that he viewed an earth-

quake as the result of a disturbance to the elastic equilibrium of the earth (the elastostatic problem) and the wave motion as caused by finite elastic forces resulting from this disturbance. He considered the displacements, velocities, and wave motion as effects rather than causes. In this paper, Randall considered only the dynamic problem and showed that only certain aspects of the change of equilibrium are relevant. The problem Randall posed is how to solve the elastic wave equation, knowing the initial displacement from equilibrium. He also allowed for displacement fields which may be discontinuous across surfaces within the medium. One of Randall's important results is that the disturbance at a given point does not commence until a longitudinal wave arrives from the nearest point of discontinuity of the initial displacement field or its gradient. In this sense, he views the discontinuity surfaces as sources of seismic waves.

Randall (1964b) also tackled the elastostatic problem. He examined mathematically the concept that a sudden phase transition could provide a mechanism for earthquakes. By examining the simpler case of a sudden volume change, he showed that even a small change in density can provide a much more concentrated source of energy than is provided by sudden faulting. Evison (1963) suggested (on the basis of Ringwood's (1962) theoretical work) that the cause of earthquakes may be phase transition ... that faulting may be an effect of earthquakes and not a cause (Ringwood hypothesized that one fundamental cause for tectonic activity in the mantle is phase instability).

Randall (1966) extended his earlier work to include change of shape during the phase transition which, in contrast to his 1964 models, created transverse waves also. He obtained the following expression for the seismic energy carried by the longitudinal and transverse waves respectively:

$$E_L = \frac{4\rho k^2 \, V \, V_T^4}{15 \, V_L^2}$$

$$E_T = \frac{\rho k^2 \, V_T^2 \, V}{5} \qquad \text{(A.20)}$$

where ρ is the density of the spherical volume, V (i.e. volume of the source) in the final equilibrium state, k is a parameter used by Randall to define the strain tensor, and V_L and V_T are the velocities of longitudinal and transverse waves, respectively. When the change of shape is ignored, the seismic energy is carried only by the longitudinal wave, as no transverse wave exists then.

Niazi (1964) studied the energetics involved in fault plane models. He showed that only a fraction of the stored shear energy is released at the time of rupture: for the three-dimensional model developed by

him, this is about $\frac{1}{2}$. About $\frac{1}{3}$ of this fraction is converted into dilatational energy to be retained in the focal region. On the average, only about $\frac{1}{3}$ the original stored strain energy is released in the form of seismic waves.

For mathematical studies on radiation patterns from strike-slip and dip-slip faults, see Knopoff and Gilbert (1959), Knopoff (1956, 1958), de Hoop (1958), and Mansinha and Smylie (1971).

A.5 Regional Seismicity

Gutenberg and Richter (1954) is an excellent work on this topic and should be consulted for the concepts of regional seismicity as existed in the early 1950s. For more recent developments, see Hart (1969).

SEISMICITY IN AND AROUND JAPAN

Ichikawa (1969) discussed the seismicity in and around Japan by considering more than 150 nodal plane solutions for large earthquakes. He found that although the distribution of the pressure directions of stresses producing the earthquakes is regular, the tension directions in the upper mantle are distributed irregularly. Aki (1966) arrived at the same conclusion from his statistical study of small earthquakes.

Ichikawa's study also showed that most earthquakes in central and southwestern Japan are shallow (foci are in the crust) but the foci for the northern Japanese earthquakes are in the upper part of the mantle. Other regions of shallow earthquakes are the areas between Shikoku and Kyushu in western Japan, the Ku Peninsula, and the area southeast of Kwanto in central Japan.

SEISMICITY OF SOUTHEAST AUSTRALIA

Jaegar and Read (1969) described the seismicity of southeast Australia (which has the greatest density of seismic stations in that country) through a study mostly of micro-earthquakes (i.e. earthquakes with Richter magnitudes between 1 and 3).

One seismic area is the region of Dalton-Gunning to the north of Canberra; another region is east of Melbourne. The seismic activity near Snowy Mountains appears to be associated with the Crackenback Fault, a high-angle reverse fault reaching the surface at Crackenback Valley in the Snowy Mountains. Part of the seismic activity might be due to the Murrumbidgee Fault. The edge of the Sydney Basin also appears to be seismically active.

INDIAN OCEAN

Sykes (1970) studied about 900 earthquakes in the Indian Ocean and determined their epicenters more accurately than earlier determinations. He reported a possible nascent island arc between Ceylon and Australia.

According to Sykes, this region is the most seismically active area in the world oceans, excluding those clearly identified as ridges or transform faults.

SEISMICITY OF NORTH AMERICA

Wollard (1969) described the seismicity of continental North America. The west coast of North America is considered part of the Pacific Seismic Belt; however, it is not a continuous belt and the following branches exist: (a) a belt that includes the Aleutian Island Arc and Trench and terminates in central Alaska; (b) a belt that extends from about 140°W on the southern coast of Alaska to the boundary between the states of Washington and Oregon; (c) a belt that starts approximately at the boundary between Oregon and California. This belt has two branches; one branch is associated with the San Andreas Fault and follows the coast of California, the second branch extends inland and follows the eastern flank of the Sierra Nevada Mountains and then joins the first branch in northern Baja California (both branches terminate here); and (d) the seismicity around the Gulf of California is minor. The Middle America Trench starts at about 20°N and terminates near the boundary between Costa Rica and Panama.

There is a seismic belt that follows more or less the Appalachian Mountains from Alabama to New Brunswick, Canada, through Maine. This belt is not continuous but has the following segments: (a) in the southern part, the seismicity is associated with faulting in the region of Piedmont, Ga.; (b) in the northern part, the belt splits into two branches; one branch is associated with the Taconic Fault in the western part of Vermont, and the other branch follows the boundary between Vermont and New Hampshire; and (c) a third segment extends from the central part of Maine to the tip of Long Island in New York.

There is a seismic belt extending from the South Carolina coast to the Appalachians. A seismic belt which caused some major earthquakes in the past extends from northern Arkansas to eastern Quebec. This belt includes the fault system of the St. Lawrence River Valley. Two examples of major earthquakes in this belt are the 1663 Trois Rivières, Que., earthquake, and the 1811 New Madrid, Mo., earthquake.

There are scattered areas of seismicity in the midwestern states of South Dakota, Nebraska, and Kansas. Parts of the Texas-Oklahoma boundary region are also seismic. An important paper was written by Anderson (1971) on the San Andreas Fault.

SEISMICITY OF CONTINENTAL ASIA AND THE SEA OF OKHOTSK REGION

Savarensky and Golubeva (1969) used instrumental data to study the seismicity of this area from 1953 to 1965. The seismicity as inferred from the distribution of epicenters generally agreed with that deduced earlier by Gutenberg and Richter (1954).

The following seismic regions could be recognized from their work: (a) the Asian Mediterranean seismic belt begins in the eastern part of Asia and is quite wide there; epicenters are mainly along mountain ridges; width decreases in the region of the Pamir and Hindu-Kush

mountains, (b) the Burma Arc is a curved chain of mountain ridges, (c) seismic belt widens west of Hindu-Kush, and (d) he belt is narrow in the region of Caucasus, Asia Minor, and in Europe.

Deep focus earthquakes occur in the central parts of the Sea of Okhotsk, with focal depths of 300-650 km. Focal depths west of the Kuril Ridge are in the range of 100-160 km, and east of Kuril Islands and Kamchatka are in the range of 30-60 km. The seismicity of Sakhalin is less, comparatively.

Soloviev (1965a) discussed the seismicity of Sakhalin from 1909 to 1963. Kanamori (1970) discussed the technique of synthesizing long-period surface waves to determine earthquake source parameters, and applied his technique to the Kuril Islands earthquake of Oct. 13, 1963. Fedotov (1968) described the techniques for long-term as well as short-term seismic predictions.

SEISMICITY OF EUROPE

The formation of the European Seismological Commission in 1951 enabled a systematic investigation of the seismicity of Europe (Kárník 1969). From 1901 to 1955, data on about 5500 earthquakes were gathered.

The study showed that although most seismic activity can be related to faulting, all the epicenters could not be identified with faulting. The Anatolian fault system, the largest strike-slip fault in the region under consideration, affords a good example for close relation between seismicity and faulting.

Some important seismic regions are: (1) a seismic belt which starts at the western edge of the Carpathian Mountains and follows the Vah, Leitha, and Mur River valleys, crosses the Carnic Alps in northeastern Italy, and has highest seismicity at its southwest tip; (2) a belt which starts at the eastern end of the Adriatic Sea and extends toward Rhodes through Greece and Crete; (3) probably a narrow seismic belt joining Lisbon Bay with the mid-Atlantic Ridge; and (4) seismic belts of limited extent in Crimea, in the region southest of Shabla in Bulgaria, in Libya, Iceland, and Jan Mayen.

For details on the seismicity of Iceland, see Tryggvason (1970) and Ward and Bjornsson (1971).

SEISMICITY OF MIDOCEAN RIDGES

In the last 2 decades, much work has been done on the seismicity of midocean ridge systems. According to Sykes (1969) midocean ridges and their continental extensions account for only about 5% of the shallow earthquakes on the globe.

Well-developed oceanic ridge systems exist in the Atlantic, Pacific, Indian, and Arctic oceans. In the oceanic parts of the ridge systems, the seismicity is confined to narrow belts of the order of 10 km and

in the continental extensions of the ridge systems, the seismic belt has widths of 100 km or more. However, in both situations, intermediate and deep focus earthquakes are absent.

SEISMICITY OF SOUTH AMERICA

Santo (1969) studied the seismicity of South America from August 1960 to September 1968. On Sept. 26, 1970, three main earthquakes and over 300 aftershocks occurred in Columbia, and Ramirez (1971) stated that an old fault in Columbia was rejuvenated. Figure A.13 shows the location of the Bahia Solano-Ibague Fault.

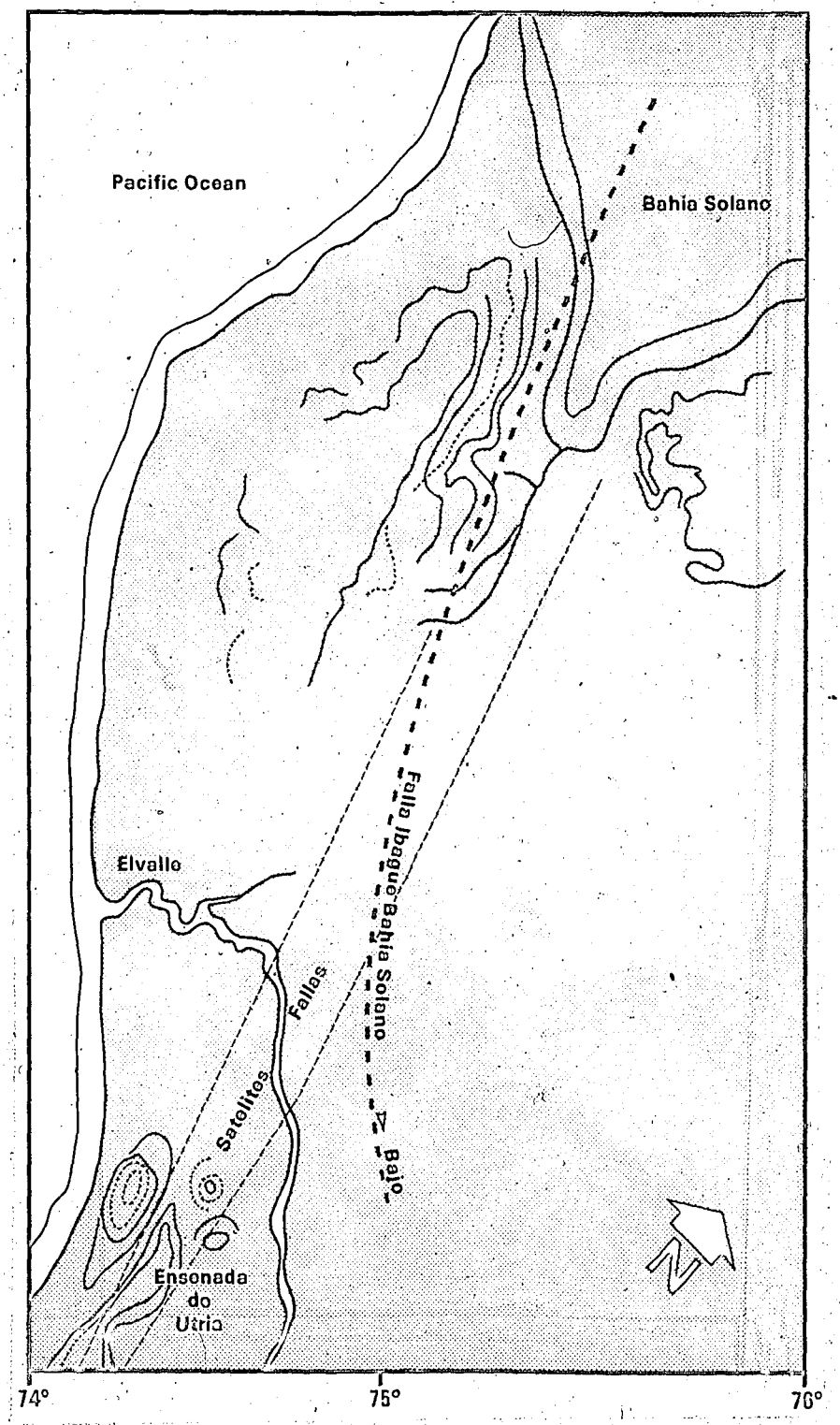


Fig. A.13. Location of the Bahia Solano-Ibaque Fault. (Ramirez 1971)

Rodriguez et al. (1962) discussed the San Augustin Fault system of southern Peru and the associated earthquakes (epicenters are shown in Fig. A.14). Figure A.15 shows the distribution of epicenters of normal, intermediate, and deep earthquakes (W. Stauder unpublished data).

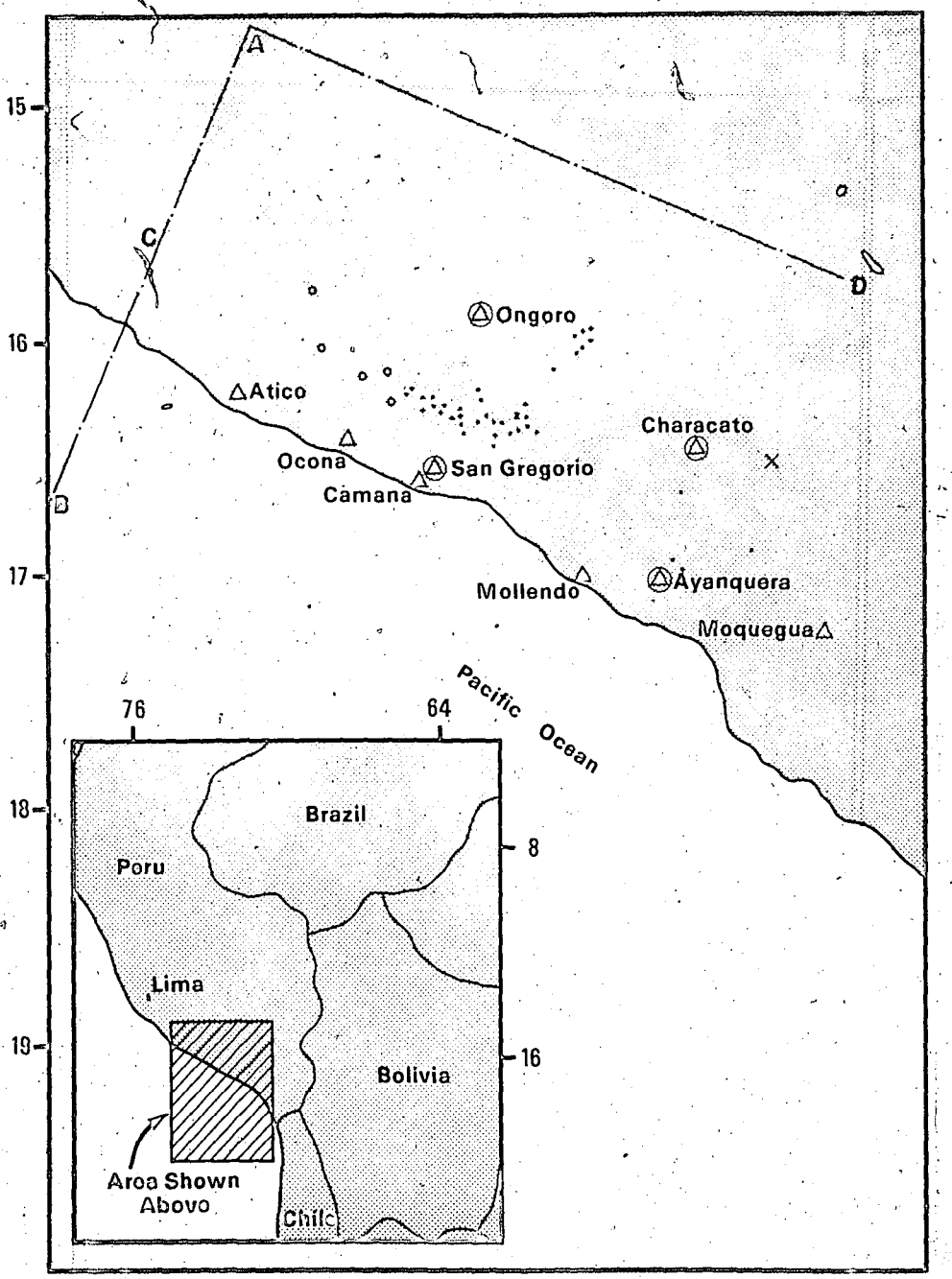


Fig. A.14. Index map and locations of epicenters (solid dots) determined from four stations: San Gregorio, Ongoro, Characato, and Ayanquera. Crosses show epicenters of recent destructive earthquakes in the area. (Rodriguez et al. 1962)

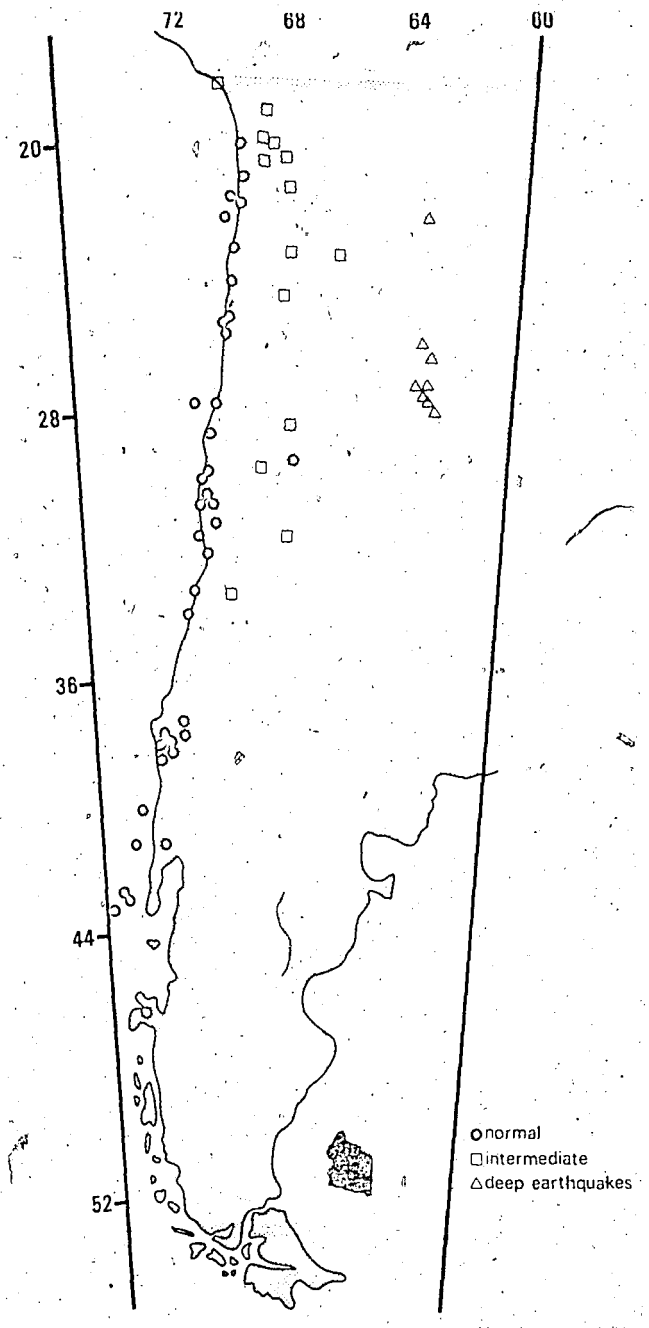


Fig. A.15. Epicenter distribution in South America o normal, □ intermediate, Δ deep earthquakes. (Stauder 1972)

SEISMICITY OF ASIA AND MIDDLE EAST

The zone of seismicity in Burma is considered to be the northern extension of the trench-islands arc system which runs along Java, Sumatra, Nicobar Islands, and Andaman Islands region (Santo 1969). However, characteristics of the Burmese seismic zone are quite different

from those of the oceanic seismic zone. For a discussion of the earthquake mechanisms in the Himalayan, Burmese, and Andaman regions, see Fitch (1970).

Kaila et al. (1972) prepared quantitative seismicity maps of India, and stated (p. 1119):

> "... India can be divided into two broad seismic zones, the northern seismically highly active zone and the southern moderately active zone. In the northern active zone, a number of seismic highs have been delineated such as the Pamir high, the northwest-southeast trending Srinagar-Almora high, the Shillong massif high, the Arakan Yoma high and the West Pakistan highs. These seismic highs are consistent with the Himalayan tectonic trends. Contrary to this, two seismic highs fall in the Tibet plateau region which align transversely to the main Himalayan trend. In the southern moderately active zone, two seismic highs are clearly discernible, the east and the west coast high, the latter being seismically more active than the former. The least active zone encompasses the Vindhyan syncline and the areas of Delhi and Aravalli folding. Between this zone and the east coast high lies another moderately active zone which encloses the Godavari graben, western part of the Mahanadi graben, and the Chattisgarh depression."

Santo (1969) discussed the seismicity of the Hindu Kush region. Stevens (1967) discussed the S-wave focal mechanisms of the Hindu Kush earthquakes.

Nowroozi (1972) described the seismicity of western India, Pakistan, Afganistan, and Middle East. Figure A.16 shows the epicenter distribution in this area. For seismicity maps of eastern Turkey, Caucasus, and Persian Plateau, see Kaila et al. (1974).

Bolt (1974) described the seismicity of China. Figure A.17 shows the distribution of epicenters from data since 780 B.C.

A.6 Earthquake Prediction and Control

EARTHQUAKE PREDICTION

The first systematic attempt at earthquake prediction appears to be an outline prepared by a research group in Japan in 1962. After the great destruction in Japan by the Niigata earthquake of 1964, the Japanese government supported a 5-year study on earthquake prediction. After the 1964 Alaskan earthquake, an ad hoc committee was organized by the U.S. government. This committee recommended a 10-year study that involves new instrumentation for monitoring faults in Alaska and California, and extensive geological and geophysical surveys. At the same time, laboratory and theoretical studies were proposed on rock failure and earthquake engineering. The U.S. National Science Foundation and the Japanese Society for the Promotion of Science jointly sponsored several symposia on earthquake prediction.

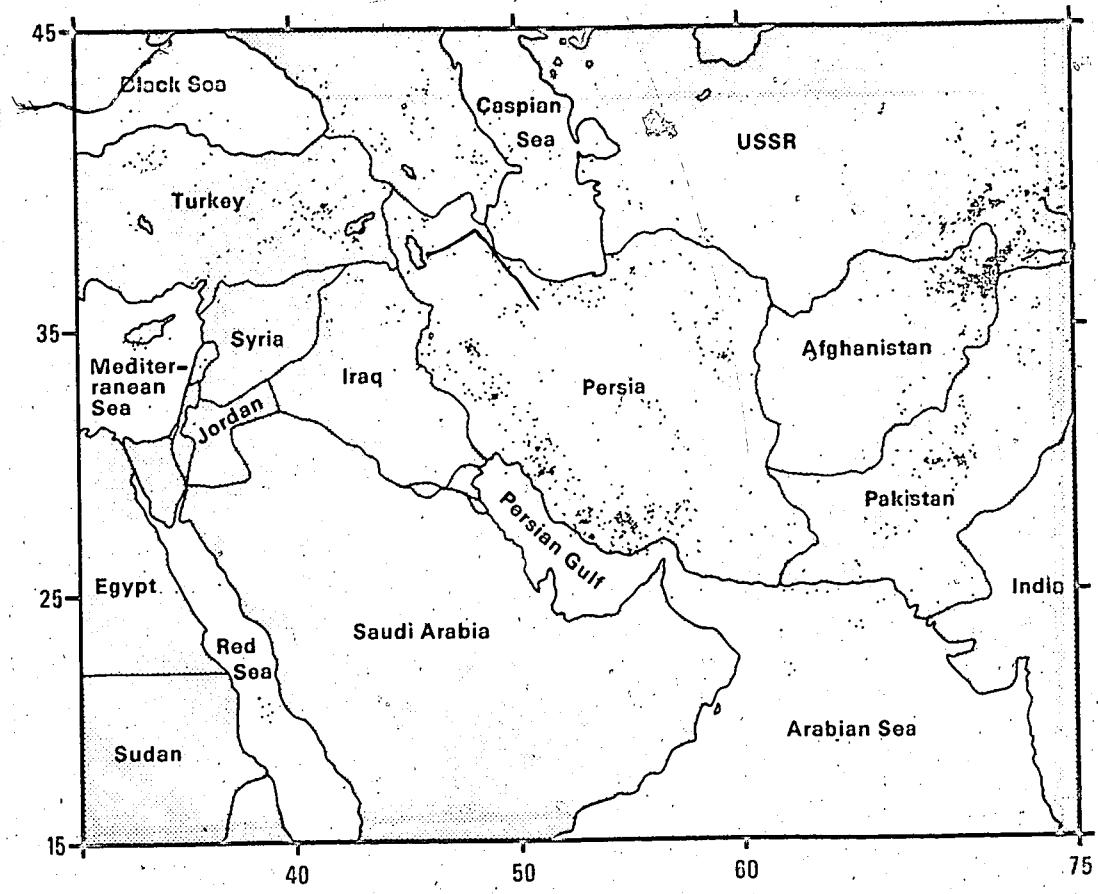


Fig. A.16. Seismicity of the mideast region during 2 decades. (Nowroozi 1972)

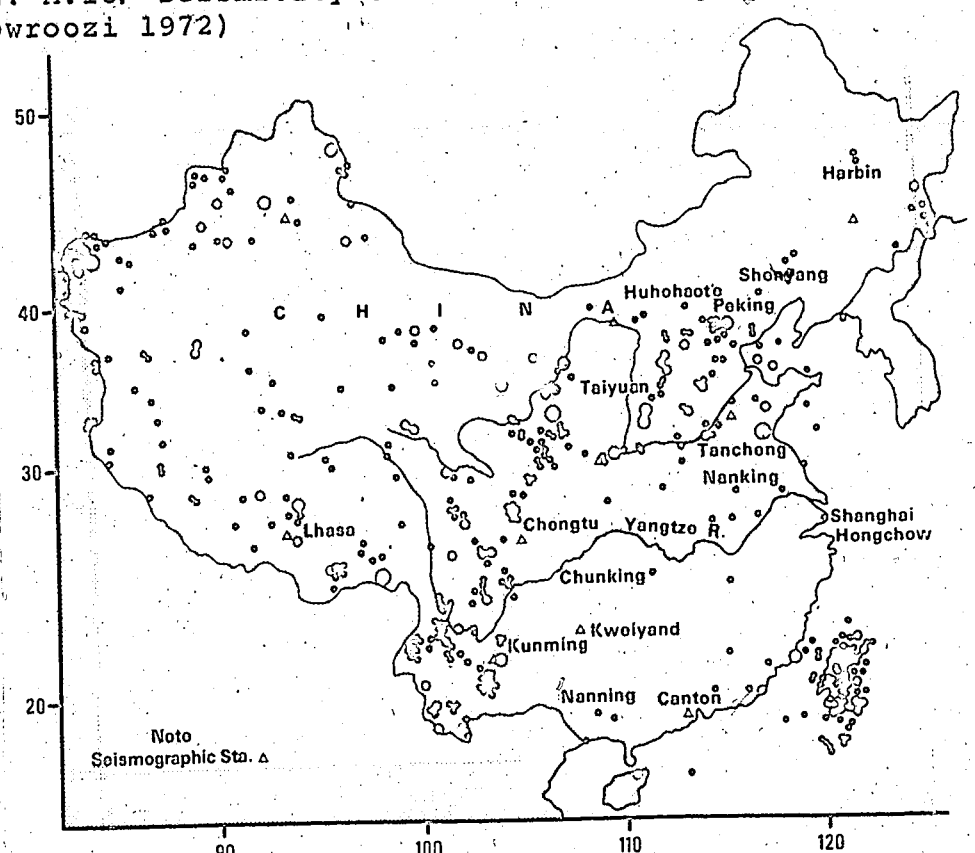


Fig. A.17. The seismicity of China as represented by damaging earthquakes (magnitude above 6) since 780 B.C. (Bolt 1974)

Kisslinger (1974) summarized techniques for predicting earthquakes, and this paper is a main source for the following discussion, based on the distribution of epicenters for about 42,000 quakes between 1961 and 1969. The earthquake belts are not continuous but have several gaps. Before the postulation of the "New Global Tectonics," these seismic gaps were regarded as earthquake-free zones. However, at present some gaps are viewed as potential future earthquake zones. The seismicity gaps were used as predictive tools by the Lamont-Doherty Geological Laboratory, by Japan and USSR. Fedotov (quoted by Kisslinger) developed a basis for predicting the location of some major earthquakes in Kamchatka.

The main criteria of the Lamont-Doherty group (e.g. Kelleher 1970; Sykes 1971; Kelleher et al. 1973) for delineating zones of "special seismic potential" are that the zone must be part of a major shallow seismic belt with predominant strike-slip or thrust faulting, and that it has not ruptured in the last 30 years. Many regions satisfy these primary criteria, hence they used secondary criteria based on regional seismic history to identify the important zones.

The seismic gap approach does not give any indication of the expected time of future earthquakes unless other criteria are used. Mogi (1968) and Kelleher et al. (1973) suggested that major earthquakes may migrate along the major seismic belts. A more objective approach is to estimate earthquake recurrence rates from strain rates or from analysis of past data. A linear relation appears to hold between log N and M, where N is the number of earthquakes that have magnitudes greater than M, and this relation applies on all space scales from local quakes to global. The slope of this relation, referred to as b, varies from -0.5 to -1.5 and is about -1. The value of b in a given region varies with time and this could be indicative of a future earthquake. Rikitake (quoted by Kisslinger) estimated, on the basis of rate of strain accumulation, that the probability of an 8-magnitude earthquake in Sagami Bay (where a great earthquake occurred in 1923) is only 0.2 for 1980 and will be 0.8 around 2080.

Considerable effort is directed to discovering premonitory phenomena for earthquakes to provide a basis for earthquake prediction. Some precursors are: unusual increase in microearthquake activity, anomalous patterns in the geomagnetic field, and changes in the chemical composition of ground water (especially, increase in radon content). The search for precursors has been generally in the context of the Elastic Rebound theory. Two classes of observations (Kisslinger 1974) provide evidence that a volume of rock is in a strained state. The first class is direct observation, when variations in the relative positions of points on the earth's surface is measured, by either geodetic measurements or point measurements of strain and tilt. The indirect approach is observation of strain-dependent physical properties of the local rocks, either by direct measurement or by observing the local values of force fields that depend on these properties. Some properties that have been examined so far are velocities of elastic waves, electrical conductivity, and magnetic properties.

Japan has used observation of changes in the bench marks as a major earthquake precursor (e.g. great changes were observed before the Niigata earthquake of June 16, 1964). About 20,000 km of first-order levelling routes are established in Japan, and are surveyed at least once every 5 years. Equation (A.21) expresses the relation between magnitude, M, of an expected earthquake and radius, r, of the region of anomalous elevation change.

$$M = 1.96 \log r + 4.45 \qquad (A.21)$$

Several authors reported measurements of accumulated strain at selected points through use of tilt meters and strain meters. Some success was reported when such measurements were used to predict earthquakes. However, the relations between these near-surface measurements and the tectonic processes at the depths where earthquakes originate are not adequately established.

Probably the most significant discovery in earthquake prediction research is the work of Semenov and Nersesov (quoted by Hammond 1973). Their studies in the Garm region of Tadzhik, USSR, showed that anomalies in observed velocities of elastic waves occur prior to an earthquake. Specifically, the ratio of the velocity V_p of P-waves to the velocity V_s of S-waves decreased from its normal value several weeks or months before a quake, and then increased gradually to its normal value just prior to the occurrence of the quake. Although the extent of the decrease of this ratio appears to be independent of the magnitude of the quake that followed later, the longer the ratio continues to decrease, the larger the quake.

The relation between duration of the anomaly and the size of the quake is linear with a slope of about 0.7 (Kisslinger 1974). The following table shows the expected earthquake magnitude versus the duration of the V_p/V_s anomaly (Kisslinger 1974).

Duration	Magnitude (M)
30 days	4
90 days	5.5
3.5 years	6.5
10.0 years	7.5
no data available	8.0 or greater

The original discovery of this anomaly in V_p/V_s in the Soviet Union was confirmed in other regions also: northern New York State, California, and central islands of the Aleutian Chain. Whitcomb et al. (1973) found that this anomaly is due to a decrease in V_p rather than an increase in V_s. Nur (1972) proposed a model based on "dilatancy" to account for this anomalous behavior (dilatancy means an inelastic volumetric increase in the rock prior to failure).

In the rocks during dilatancy, new cracks develop and porosity increases; this makes rocks that are initially saturated with water less saturate, and as V_p is more sensitive to the degree of saturation than V_s, the ratio V_p/V_s decreases. To account for the return of V_p/V_s to

normal value just prior to the occurrence of an earthquake, Nur proposed that ground water from surroundings enters the new cracks and V_p increases again. The resaturation of the medium weakens its resistance to slippage, thus, when the rock becomes fully saturated, an earthquake occurs.

Brady (mentioned by Kisslinger 1974, p. 42) proposed an alternate view for the return of V_p/V_s to its normal value:

> "... the interval of wide-spread dilatancy throughout the volume of rock is followed by a period of very strong dilatancy in the immediate neighborhood of the incipient fracture. The nascent source zone acts as an inhomogeneity in the medium, with corresponding strong stress concentrations around it and a reorientation of the principal stress axes in the immediate neighborhood. The substantial volume increase in the neighborhood of the fault surface is accommadated by a closing of the cracks in the region into which the fracture will extend next, causing the velocities in this zone to return to their predilatancy values."

Scholtz et al. (1973) showed that the dilatancy model can account for other premonitory phenomena as well. As the dilatancy model is based on limited data to date, dilatancy has not yet been accepted by all seismologists (Hammond 1973) as the chief cause of earthquake precursors. At least three objections have been raised about this model: (1) the V_p/V_s anomaly has only been observed on thrust faults where one crystal block pushes under another and not along strike-slip faults such as the San Andreas fault; (2) the determination of V_s is not precise enough to rule out the possibility that V_p/V_s anomaly is due to this lack of precision; (3) dilatancy model requires physical changes over huge regions (order of 100 km or more) and so far there are no data to support this.

NUCLEAR EXPLOSIONS VS EARTHQUAKES

Underground nuclear explosions and how they could be distinguished from earthquakes is considered here, whereas, atmospheric and underwater explosions were considered in chapters 2 and 6. The U.S. Atomic Energy Commission (AEC) has conducted many underground nuclear explosions in Nevada, the two biggest were "Box Car" (1.22×10^9 kgm) in April 1968, and "Benham" (1.12×10^9 kgm) in December 1968: These tests caused linear fracturing approximately 8 km long (Carter 1969) and the displacement appears to have occurred within a few seconds after the explosion. However, the seismic activity continued for many weeks and thousands of aftershocks were recorded.

The AEC shifted the tests to Amchitka Island in the Aleutians and conducted two bigger tests: "Milrow" (about 2×10^9 kgm) in 1969 and "Cannikan", (about 5.08 kgm) in 1971. On Dec. 22, 1971, the Soviet Union conducted a large underground test (about 10.16 to 12.19×10^9 kgm) supposedly for diverting a river in Siberia.

The systematic starting point for the seismological research on under-

ground nuclear explosions was the 11th general assembly of the International Union of Geodesy and Geophysics held at Toronto, Canada, in September 1957 (Hodgson 1964), where suggestions were made to set up special seismic networks. It was also proposed that methods be developed to detect underground nuclear tests. Initially it was felt that the distinction between earthquakes and underground nuclear explosions was clear, because the former cause quadrant distributions of compressions and rarefactions, whereas, the latter show only compressions due to radiation of energy outwards. But closer examination revealed that the distinction is not that simple.

Some available techniques to distinguish earthquakes and underground nuclear explosions are: (1) fault-plane studies, (2) the Rayleigh wave spectral ratio, and (3) the ratio of the body-wave magnitude to surface-wave magnitude.

Fault-plane studies showed that, although there may not be any distinct pattern to the orientation of the fault planes, the pattern of the orientation of the null axis is quite regular. Based on this regularity, the type of first motions from earthquakes and underground explosions could be established (Scheidegger 1964a, b).

Derr (1970) suggested that the spectral ratio of short- to long-period Rayleigh waves is systematically larger for underground explosions than for shallow earthquakes. His technique was successful in western USA, but failed in the Aleutians for the "Milrow" test. Thirlaway (1968) showed that the ratio of the body-wave magnitude m_b to the surface-wave magnitude m_s distinguishes earthquakes from explosions, provided $m_b > 4.75$.

LARGE RESERVOIRS AND RESULTING EARTHQUAKES

In the decade following the construction of the Hoover Dam in 1935 and the subsequent formation of Lake Mead in Arizona and Nevada, several hundred minor earthquakes occurred whose magnitudes did not exceed 5.0 (Carder 1945). He said these quakes were due to the reactivation of local faults by the weight of the water. In early 1962, a strong correlation was noticed between the rate of injection of waste liquids of an arsenal into the ground and earthquake frequency near Denver, Colo. (Evans 1966). The sump was 3.8 km deep, and foci of the quakes were in the range of 4-6 km deep; the seismic activity was limited to a linear zone about 8 km long (Pakiser et al. 1969).

The fluid injection was stopped in February 1966, and the earthquake frequency decreased. The increase of earthquake frequency in late 1966 through 1967 was never properly accounted for. From the first motions on the seismograms, it was inferred that the fractures parallel to the seismic zone were characterized by right-lateral strike-slip motion; the increasing pore pressure reduced the frictional resistance to faulting, thus initiated the earthquakes. Another instance of similar seismic activity in the USA was near the Rangeley oil field in Colorado, the site of a secondary recovery operation involving the injection of water under pressure (Pakiser et al. 1969).

Similar instances were reported in Zambia following the construction of dams for hydroelectric power. The most devastating man-made earthquake occurred on Dec. 10, 1967, near Koyna (India) with a magnitude of 6.5. It caused great destruction and killed 200 people.

EARTHQUAKE CONTROL

From the above discussions, the possibility emerges of controlling earthquakes through liquid injection into deep wells or through underground explosions, thereby releasing the strain gradually, and through small nondestructive earthquakes (Emiliani et al. 1969). This suggestion was criticized by Allen and Bailey (1970):

> "... the man-induced earthquakes might be only due to the superficial adjustments of near-surface stress, whereas large earthquakes might result from those depths that are not influenced by these artificial inducements and thus nothing would really be achieved. Some seismologists take the view that large underground explosions might lead to major earthquakes and thus one might generate destructive earthquakes in trying to control them."

Cannon (1971) presented the view that earthquakes and underground nuclear explosions are not similar as is believed but are thermodynamically inverse processes. According to him, earthquakes are a relaxation process whereas underground explosions are a stimulation process. Earthquakes do not impose any strain on the crust because they are an adjustment of the crust to a new set of relaxed constraints and the total strain energy of the crust decreases after an earthquake. On the other hand, an underground explosion imposes new strains on the crust and is similar to the tectonic processes that cause earthquakes.

Tadepalli S. Murty was born August 5, 1937 in Rambhotlapalem, India. He received his B.S. in physics in 1955 and M.S. in Meteorology and Oceanography in 1959, from Andhra University, Waltair, India. In October 1960 he joined the Hydrodynamics Laboratory, Department of Geophysical Sciences at the University of Chicago, Chicago, Ill., as a graduate student-research assistant and received his M.S. and Ph.D. degrees in 1962 and 1967, respectively. Since immigrating to Canada in August 1967 he has been working as a senior research scientist with the Department of Fisheries and the Environment, Ottawa, Ontario.

Dr. Murty's interests lie in mathematical modeling of physical oceanographic problems. Since 1971 he has been a member of the Tsunami Committee of the International Union of Geodesy and Geophysics and served as secretary from 1975 to 1977. At present he is vice-chairman of the Committee. He served with the Intergovernmental Oceanographic Commission (IOC) of UNESCO, Paris, 1972-74, on Integrated Global Ocean Station System (IGOSS), a joint project between IOC and World Meteorological Organization (WMO). He is married and has one daughter.